FORSCHUNGSZENTRUM ROSSENDORF FZR

WISSENSCHAFTLICH-TECHNISCHE BERICHTE
FZR-287
Februar 2000
ISSN 1437-322X

Workshop on X-rays from electron beams

Editor: Harald Prade

Herausgeber:
FORSCHUNGSZENTRUM ROSSENDORF
Postfach 51 01 19
D-01314 Dresden
Telefon +49 351 26 00
Telefax +49 351 2 69 04 61
http://www.fz-rossendorf.de/

Als Manuskript gedruckt

FORSCHUNGSZENTRUM ROSSENDORF
WISSENSCHAFTLICH-TECHNISCHE BERICHTE
FZR-287
Februar 2000

Workshop on X-rays from electron beams

with special emphasis on possible developments at ELBE

Transparencies of the Workshop

Forschungszentrum Rossendorf, February 24 - 26, 2000

Editor: Harald Prade

Workshop on X-rays from electron beams

with special emphasis on possible developments at ELBE

Presently, at the Forschungszentrum Rossendorf (FZR) the ELBE facility - a superconducting **E**lectron accelerator of high **B**rilliance and low **E**mittance (ELBE) with a maximum electron energy of 40 MeV and a beam current of up to 1 mA - is under construction. The electron beam of ELBE is intented to drive different facilities for producing secondary radiation of various modalities as infrared photons, quasimonochromatic X-rays, polarized bremsstrahlung and photoneutrons. One of the main research objectives at ELBE will be dealing with the development of novel non-conventional X-ray sources for radiobiological applications.

Therefore, in the first part of the workshop latest investigations in the field of X-ray sources based on the electron-solid interaction like channeling, parametric X-ray and transition radiation, the influence of acoustic waves on the X-ray production and aspects of X-ray optics as well as the possibility of Compton backscattering off the ELBE electron beam have been discussed. The second part of the workshop has mainly been devoted to radiobiological investigations with monochromatic X-rays, but also the actual status of medical imaging with monochromatic X-rays has been presented.

Responsible for the scientific program and the local organization were W. Enghardt, E. Grosse, U. Lehnert, J. Pawelke, H. Prade and W. Wagner. The work in the Workshop Office including culinary service was done by Mrs. D. Hachenberger, J. Kerber and H. Römer.

The organizers have to thank their sponsors, the German Research Community (DFG), the Saxon State Ministry for Science and Art (SMWK) as well as the Executive Board of the Forschungszentrum Rossendorf for its essential financial support, which was very important for the success of the workshop.

On behalf of the Organizing Committee, Harald Prade

Workshop on X-rays from electron beams

Forschungszentrum Rossendorf (FZR)
Institute of Nuclear and Hadron Physics

February 24 - 26, 2000
Auditorium, Building 120, FZR

Programme

Thursday, February 24

11:30 Registration and visits to ELBE (under construction)

(Chairman: H. Prade)

13:30	F. Pobell (FZR)	Welcome
14:00	N. F. Shulga (Kharkov)	Mechanism of coherent radiation by relativistic electrons
14:50	W. Wagner (FZR)	Quasi-monochromtic X-rays from ELBE
15:40	*Coffee break*	
16:10	H. Backe (Mainz)	X-ray research with the 855 MeV electron beam at MAMI
17:00	P. Rullhusen (Geel)	Radiation produced by electrons interacting with flat and modulated surfaces
17:50	I. G. Grigorieva (Moscow)	Highly oriented pyrolytic graphite for X-ray bending and focusing

Friday, February 25

(Chairman: A. P. Potylitsin)

09:00	A. R. Mkrtchyan (Yerevan)	Investigation of channeling radiation under the influence of acoustic waves
09:25	A. H. Mkrtchyan (Yerevan)	Investigation of PXR under the influence of acoustic waves
09:50	H. W. Barz (FZR)	Compton backscattering of laser light off the ELBE electron beam
10:40	*Coffee break*	
11:10	M. A. Piestrup (Stanford)	Compound refractive lenses for X-ray sources

12:00	H. Genz (Darmstadt)	Channeling radiation as a probe in the solid state plasma accelerator regime
13:00	*Lunch*	

Friday, February 25

(Chairman: W. Enghardt)

14:00	D. Frankenberg (Göttingen)	Relative biological effectiveness of X-rays for mammography
14:50	D. Harder (Göttingen)	Chromosome aberrations by soft and ultrasoft X-rays: Microdosimetric and radiobiological aspects
15:40	*Coffee break*	
16:10	M. Hill (Oxfordshire)	Radiobiological investigations with mono-chromatic soft X-rays
17:00	B. D. Michael (Middlesex)	A focused soft X-ray microbeam for investigating the radiation responses of individual cells
17:50	W. Mondelaers (Gent)	Application of X-rays for medical purposes
18:45	*Buffet*	

Saturday, February 26

(Chairman: E. Grosse)

09:00	K. Kobayashi (Ibaraki)	Radiation biology at the KEK Photon Factory
09:45	W. Thomlinson (Grenoble)	Synchrotron medical imaging: From amplitude to phase
10:30	*Coffee break*	
10:50	S. Fiedler (Grenoble)	Current status of the coronary angiography project at ESRF
11:20	D. Hermsdorf (Dresden)	Biological experiments with low energy charged particles
11:50	A. Panteleeva (FZR)	Cell survival studies with X-rays
12:10	J. Pawelke (FZR)	A device for cell irradiation with low energy quasi-monochromatic photons at ELBE
12:30	H. Backe/D. Harder/ W. Thomlinson/W. Enghardt	Closing remarks

Lunch

Production of Quasi-Monochromatic X-Rays from Electron Beams

N. F. Shulga:

Mechanism of coherent radiation by relavistic electrons in crystals

SLAC experiment 1994.

1978

in amorphous media

PROCESSES

Migdal (1954)

Landau, Pomeranchuk (1953)

PROCESSES in crystals

CB at regular and chaotic motion (1992, ...)

dynamical chaos (1986, ...)

Baier et al, 1983.
Kimball, Cue, 1983
Baryshevskii, Tikhomirov } 1982
Shul'ga, 1980.

Const. field approx. (synchrotron approx)

above-barrier, Chenneling } radiation (Akhiezer et al 1977; Kiemakhov, 1976)

1975 ÷ 1979

e^+, e^- { 1970

Morokhovskii et al (1972)
Bermann et al (1970, 1972)
Akhiezer, P. Fomin, N. Shul'ga

experiments

1960 1956 Überall
1953 Ter-Mikaelian (l_{coh}) } $d\sigma_{coh}$
1950 Ferretti

1933 Bethe - Heitler ($d\sigma_{BH}$)

Coherent length
(Ter-Mikaelian 1952)

$$d\sigma \sim \int_{\delta}^{\sim 2\delta} \frac{dq_{\parallel}}{q_{\parallel}^2} \int d^2 q_{\perp}\ \vec{q}_{\perp}^{\,2}\ |U_q|^2$$

$$u(r) = \frac{Ze^2}{r} e^{-r/R} \qquad q_{\parallel} \geq \delta = \frac{\omega m^2}{2\varepsilon\varepsilon'}$$

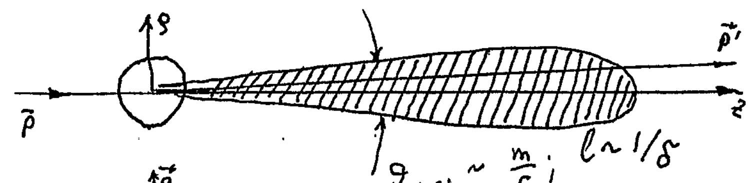

$\vartheta_{\gamma\,eff} \sim \frac{m}{\varepsilon}; \quad l \sim 1/\delta$

$$\left.\begin{array}{l} z_{eff} \cdot q_{\parallel\,eff} \sim 1 \\ q_{\parallel\,eff} \sim \delta \end{array}\right\} \qquad z_{eff} \approx \delta^{-1} = \frac{2\varepsilon\varepsilon'}{m^2\omega}$$

$$\left.\begin{array}{l} \rho_{eff}\, q_{\perp\,eff} \sim 1 \\ mc \geq q_{\perp\,eff} \geq \hbar/R \end{array}\right\} \qquad \rho_{eff} \leq R_{T-F}$$

for high energy ($\varepsilon \to \infty$)

$$z_{eff} \sim \frac{2\varepsilon\varepsilon'}{m^2\omega} \gg \rho_{eff} \sim R_{T-F}.$$

$$\boxed{l_c = \frac{2\varepsilon\varepsilon'}{m^2\omega}}$$ - Coherent length

Coherence length.

(Ter-Mikaelian (1953) — crystal
Landau-Pomeranchuk (1953) — amorphous media)

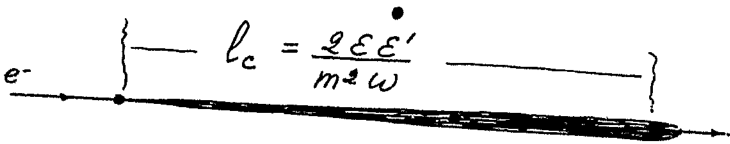

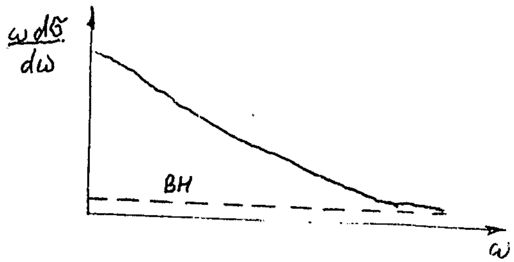

coherent effect.

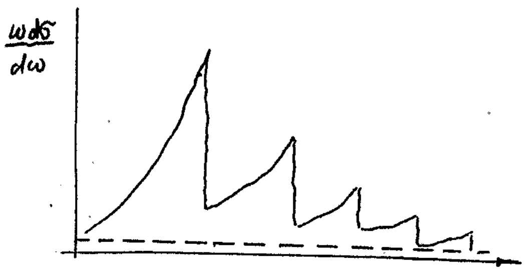

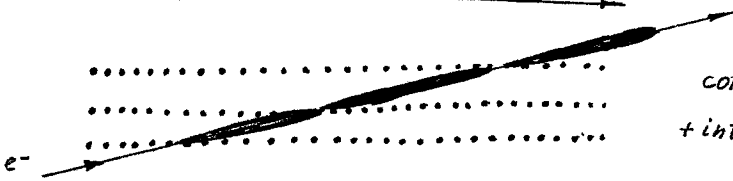

coherence + interference.

At $\mathcal{E} = 500$ Gev for $\omega \sim \frac{\mathcal{E}}{2}$

$\ell \sim 10^{-4}$ ///

Radiation

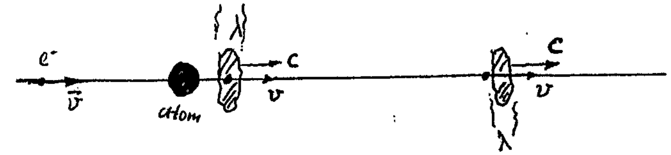

$v_{relat.} \sim c - v$

$\lambda = \Delta t \cdot v_{relat.} = \Delta t (c - v) = \frac{\Delta t\, c}{2\gamma^2}$

$$\boxed{\ell_c = c\Delta t \sim \lambda \cdot 2\gamma^2}$$

Pair production

$\hbar\omega = \mathcal{E}_+ + \mathcal{E}_-$

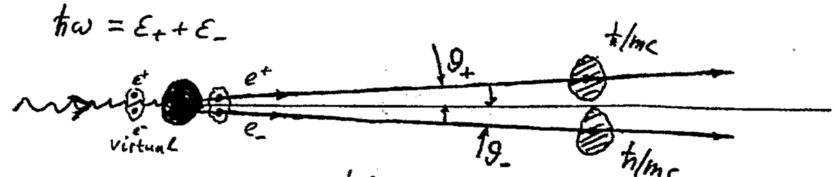

$\mathcal{E}_+ \sim \mathcal{E}_- \sim \frac{\hbar\omega}{2}$

$\vartheta_\pm \sim \frac{mc^2}{\mathcal{E}_\pm}$

$2\frac{\hbar}{mc} \sim \ell_\pm(\vartheta_+ + \vartheta_-) \sim \ell_\pm \frac{mc^2\hbar\omega}{\mathcal{E}_+\mathcal{E}_-}$

$$\boxed{\ell_\pm \sim \frac{2\mathcal{E}_+\mathcal{E}_-}{m^2c^3\omega} \sim \frac{\omega}{m^2}}$$

Frish, Olsen. Phys. Rev. Lett. 3 (1959) 396
Akhiezer, Shul'ga. Sov. Phys. Usp. 30 (1987) 197

Coherent Bremsstrahlung

(Ferretti 1950, Ter-Mikaelian 1952, Überall 1956, 1960)

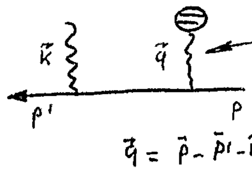

$\vec{q} = \vec{p} - \vec{p}' - \vec{k}$

$$U(\vec{r}) = \sum_n u(\vec{r} - \vec{r}_n)$$

$$d\sigma_{atom} \sim \dots \int d^3q \dots \longrightarrow d\sigma_{crystal} \sim \dots \sum_{\vec{g}} \dots$$

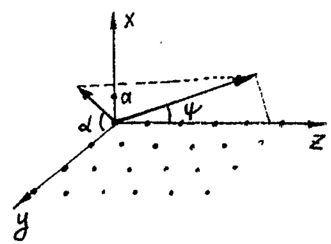

A.I. Akhiezer, N.F. Shul'ga
High Energy Electrodynamics in matter.
Gordon and Breach (1996)
(Nauka, Moscow, 1993).

$l_{coh} = \frac{2\varepsilon(\varepsilon-\omega)}{m^2\omega}$

$\psi \ll R/a$

$\alpha \ll 1$

$\varepsilon \sim 1$ GeV

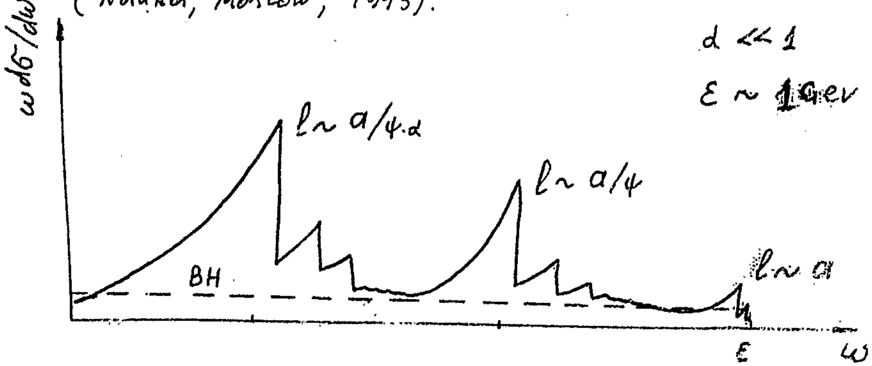

Akhiezer, Shul'ga, Sov. Phys. Usp., 1982.

$$l_{coh} = \frac{2\varepsilon\varepsilon'}{m^2\omega} \sim a$$

CB – type B

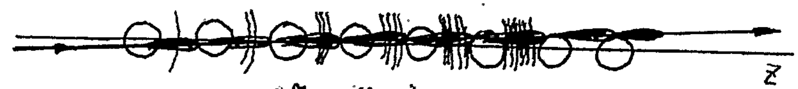

$$g_z = \frac{2\pi}{a} = \frac{\omega m^2}{2\varepsilon\varepsilon'}$$

$$l_{coh} \sim \frac{a}{\psi}$$

CB – row effect

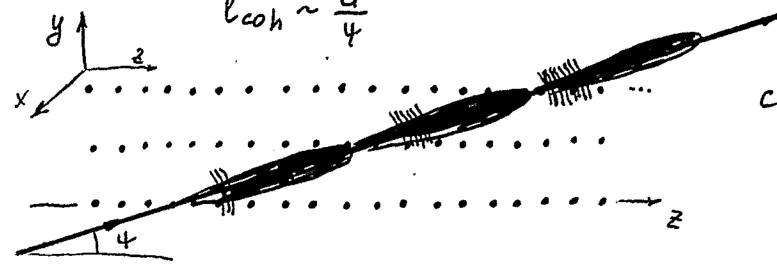

$$\psi g_y = \psi \cdot \frac{2\pi}{a} = \frac{\omega m^2}{2\varepsilon\varepsilon'}$$

$$l_{coh} \sim \frac{a}{\Theta}$$

CB – point effect

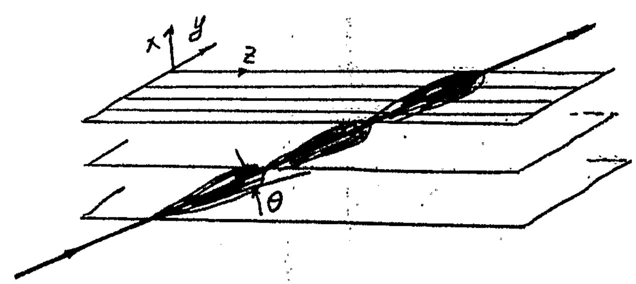

$$\Theta g_x = \Theta \frac{2\pi}{a} = \frac{\omega m^2}{2\varepsilon\varepsilon'}$$

$\Theta \approx \psi \cdot \alpha \ll \psi$

Types of coherent bremsstrahlung

$$\frac{d\sigma_{coh}}{d\omega} = \frac{2e^2}{m^2}\frac{\delta}{\Delta}\frac{\varepsilon'}{\varepsilon}\sum_{\vec g}\frac{g_\perp^2}{g_{\parallel}^2}\left[1+\frac{\omega^2}{2\varepsilon\varepsilon'}-2\frac{\delta}{g_{\parallel}}\left(1-\frac{\delta}{g_{\parallel}}\right)\right]|u_g|^2 e^{-\overline{u^2}g^2},$$

$g_{\parallel} \geqslant \delta$

Positions of coherent maxima.

$$g_{\parallel} = g_z + \psi\left(g_y \cos\alpha + g_x \sin\alpha\right) = \delta = \frac{\omega m^2}{2\varepsilon(\varepsilon-\omega)}.$$

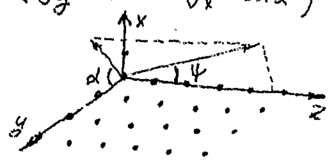

$g_{z,y,x} = \frac{2\pi}{a} n_{z,y,x}$

1. $g_z = \frac{2\pi}{a} n_z \neq 0$ CB type A $g_z = \delta$

1. $g_z = 0$, $g_y \neq 0$, $\alpha \ll 1$ the row effect $\psi g_y = \delta$

$g_z = 0$, $g_y = 0$, $\alpha \ll 1$ the point effect $\psi\alpha g_x = \delta$

1. thin structure of CB.

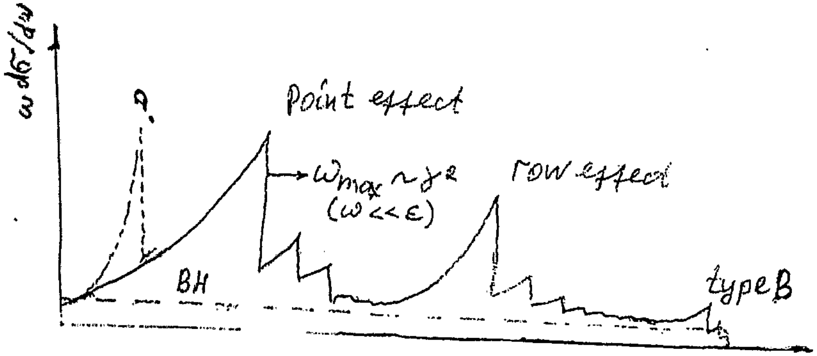

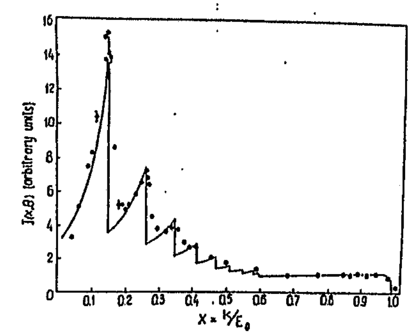

Fig.3.7. Bremsstrahlung intensity spectrum in a diamond crystal measured by the Frascati group ($E_0 = 1$ GeV, $\theta = 4.6 \pm 0.1$ mrad, $\alpha = 0°$). The *solid curve* is the calculated spectrum

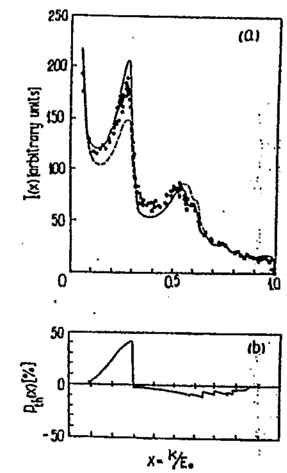

Fig.3.8

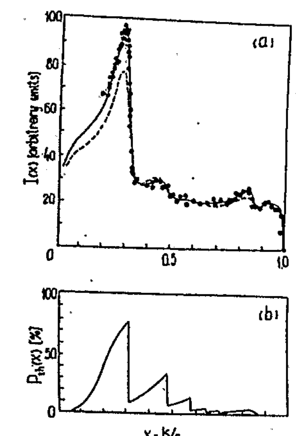

Fig.3.9

Fig.3.8a,b. CB intensity (a) and polarization (b) in a diamond crystal for $E_0 = 4.8$ GeV, $\theta = 3.44$ mrad, $\alpha = 0°$ (DESY data). Theoretical spectra were calculated with a Hartree screening potential (——) and an exponential potential (----)

Fig.3.9a,b. The same as in Fig.3.8a,b for diamond-crystal orientation angles $\theta = 50$ mrad, $\alpha = 1.5°$

e^+, e^- – dependence of CB
(1969 – 1972)

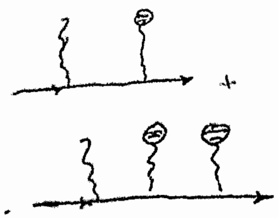

Theory

• A. Akhiezer, P. Fomin, N. Shul'ga
(JETP Lett. 1970)

$$\frac{Ze^2}{\hbar c}$$

$$d\sigma_{coh} = d\sigma_{coh}^{(Born)} \cdot \left(1 + \frac{e}{|e|}\, z\, \frac{R}{a}\, \frac{Ze^2}{\varepsilon a \theta^2} + \dots\right)$$

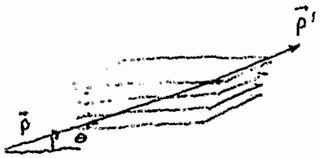

$$z \frac{R}{a} \frac{Ze^2}{\varepsilon a \theta^2} \sim \frac{\theta_{ch}^2}{\theta^2} \quad !!!$$

Experiment:

• R. Walker, B. Bermann et al.
(PRL, 1970; Phys. Rev. A 11, 1972)

• V. L. Morokhovskii, G. Kovalenko et al.
(JETP Lett. 1972)

CHANNELING OF POSITRONS OF 1 GeV ENERGY

V.L. Morokhovskii, G.D. Kovalenko, I.A. Grishaev, A.N. Fisun, V.I. Kasilov, B.I. Shramenko, and A.N. Krinitsyn
Physico-technical Institute of the Ukrainian Academy of Sciences
Submitted 30 June 1972
ZhETF Pis. Red. 16, No. 3, 162 - 164 (5 August 1972)

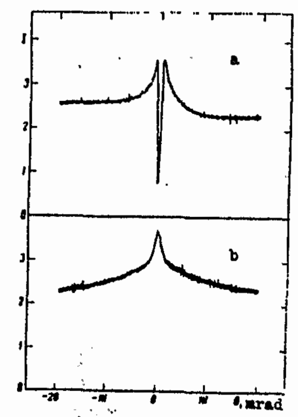

Fig. 1. Bremsstrahlung energy flux vs. angle between the direction of the beam and the silicon [110] crystal axis: a - positrons, b - electrons.

CHANNELING AND COHERENT BREMSSTRAHLUNG EFFECTS FOR RELATIVISTIC POSITRONS AND ELECTRONS*

R. L. Walker
Department of Applied Science, University of California, Davis, California 95616

and

B. L. Berman, R. C. Der, T. M. Kavanagh, and J. M. Khan
Lawrence Radiation Laboratory, University of California, Livermore, California 94550
(Received 10 December 1969; revised manuscript received 27 April 1970)

VOLUME 25, NUMBER 1 PHYSICAL REVIEW LETTERS 6 JULY 1970

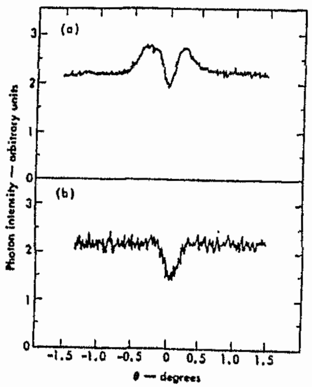

FIG. 2. (a) Forward (±0.1 deg) bremsstrahlung detected by the ionization chamber, for 28-MeV positrons incident on a 53-μm silicon crystal. θ is the angle between the beam axis and the (110) crystallographic direction. (b) Similar data, but with a ½-in. lead absorber between the crystal and the detector. Curves are normalized to equal off-channel values.

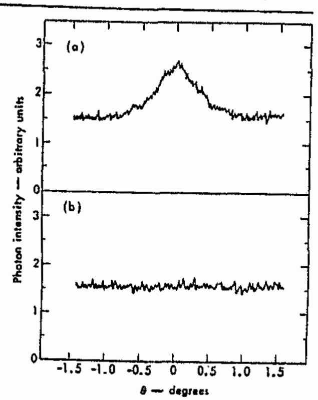

FIG. 3. (a) Forward (±0.1 deg) bremsstrahlung detected by the ionization chamber, for 28-MeV electrons incident on a 53-μm silicon crystal. θ is the angle between the beam axis and the (110) crystallographic direction. (b) Similar data but with a ½-in. lead absorber between the crystal and the detector. Curves are normalized to equal off-channel values.

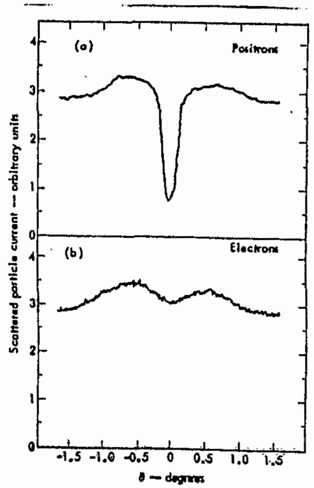

FIG. 1. Scattering of 28-MeV (a) positrons and (b) electrons into an angular range 0.9 to 1.0 deg with respect to the beam. Data are for a 42-μm silicon crystal, and θ is the angle between the (111) crystallographic direction and the beam axis. Curves are normalized to equal off-channel values. Our best scattering data, for the (111) direction of a 19-μm silicon crystal, showed a channeling minimum that was ~¼ the off-channel value.

Semiclassical theory of CB

(eikonal, WKB approx.)

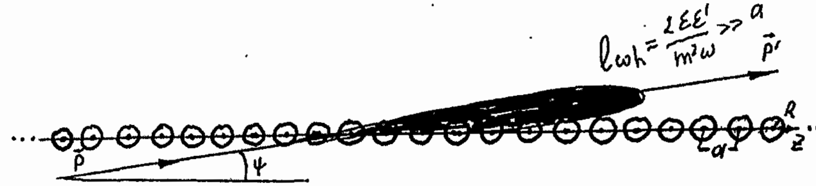

$$Z|e| \to Q_{eff} \sim N_c Z|e|$$

$$N_c \sim \min\left(\frac{l_{coh}}{a}, \frac{R}{4a}\right)$$

$$\frac{Ze^2}{\hbar c} \ll 1 \longrightarrow \boxed{N_c \frac{Ze^2}{\hbar c} \sim \frac{R}{4a}\frac{Ze^2}{\hbar c} \ll 1}$$

The validity condition of Born approx. was not fulfilled in a number of experiments, which was performed to verify the Born theory of Coherent radiation.

But the prediction of the Born theory CB were in good agreement with experiments when !!!

$$\boxed{\frac{R}{4a}\frac{Ze^2}{\hbar c} \gtrsim 1}.$$

Why?

A. Akhiezer, V. Boldyshev. N. Shul'ga (1975).

Eikonal, quasi-classical, classical approximation

$$\boxed{\frac{RZe^2}{4\psi a\hbar c} \gg 1} \longrightarrow \psi \ll 10^{-2}\,\text{rad}$$

$\hbar \to 0!$

$$\boxed{d\sigma_{coh}^{(WKB)} \approx d\sigma_{coh} \cdot \left(1 + O\left(\frac{\psi_c^2}{\psi^2},\ \gamma\cdot\vartheta\right)\right)}$$

$$\begin{cases} 1.\ \ \psi \gg \psi_c \longrightarrow \text{trajectory is close to rectilinear} \\ 2.\ \ \gamma\vartheta \ll 1 \longrightarrow \text{dipole approximation.} \end{cases}$$

$\psi \lesssim \psi_c$ — channeling (finite) or above-barrier (infinite) motion particles in the field of atomic strings.

$\gamma\vartheta \gg 1$ ⟶ $l_c \ll \frac{R}{\psi}$ — synchrotron approximation

$\gamma\vartheta \gg 1$ ⟶ $l_c \gg \frac{R}{\psi}$ — velocity changes in jump approxim.

N. Shul'ga
JETP Lett. 1980, v.32, p.166.

$$\frac{d\vec{p}}{dt} = -\vec{\nabla}\, U(\vec{r})$$

$$U(\vec{r}) \to U(x,y) = \frac{1}{L_z}\int_{-\infty}^{\infty} dz \sum_n u(\vec{r}-\vec{r}_n)$$

J. Lindhard (1965)

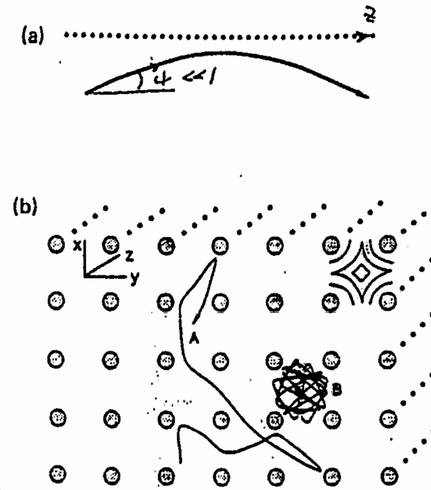

Fig. 4. Motion of a fast positively charged particle (a) in the field of a single atom string and (b) in the periodic field of atom strings of a diamond crystal in the plane orthogonal to the ⟨100⟩ axis.

$$\frac{d\vec{p}}{dt} = -\nabla U(x,y)$$

$$\begin{cases} p_z = \text{const} \\ \ddot{\vec{\rho}} = -\frac{1}{\varepsilon}\vec{\nabla} U(x,y) \\ p_z \gg p_\perp \end{cases}$$

Continuous string potential in the theory of coherent radiation.

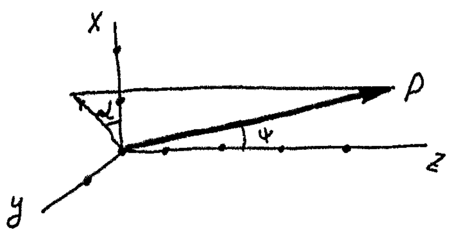

$$g_{\parallel} \approx g_z + \psi\left(g_x \cos\alpha + g_y \sin\alpha\right).$$

for $\psi \ll 1$ only $g_z = 0$! give the major contribution in $d\sigma_c$

$$d\sigma_c \sim \frac{d\omega}{\omega} \sum_{g_x, g_y} \frac{g_\perp^2}{g_\parallel^2} |u_g|^2 \left(1 + \dots\right)$$

Reviews: G. Diambrini (1968)
M. Ter-Mikaelyan (1969)
U. Timm (1971)

$\boxed{g_z = 0}$

$$U(x,y) = \frac{1}{L_z} \int dz \sum_n u(r - r_n)$$

Continuous string potential. !

A. Akhiezer, N. Shul'ga
Sov. Phys. Usp. 30(1986)19...

M. Ter-Mikaelian (1952) JETP v. 25.
H. Überall (1960) Z. Naturforsch. A 17.

Überall (1956) Phys. Rev. v. 103.

$$d\sigma_{coh} \to \dots \sum_{\vec{g}} \dots$$

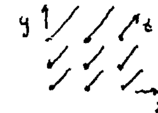

periodic

$$d\sigma_{coh} \to \dots \sum_{g_z} \int dq_x dq_y \dots$$

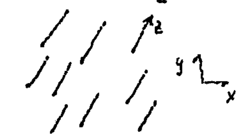

random

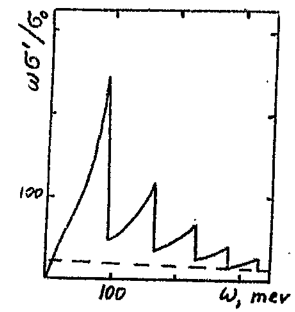

$g_z = 0$

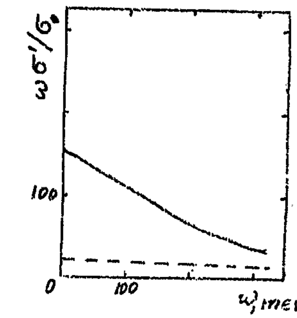

$g_z = 0$

$\varepsilon = 1$ Gev, Si, $\langle 100 \rangle$, $\psi = 2 \cdot 10^{-3}$ rad.

. Born approxim.

Semiclassical and classical CB

$$d\sigma_{coh} \{\vec{r}(t)\}$$

. Regular motion

. Dynamical chaos
. Random string approx...

Akhiezer et al. Sov. Phys. Usp. (198.2); Phys. Rep. (198...

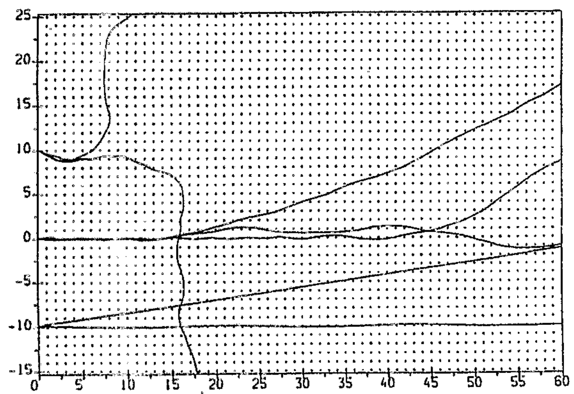

Character of the particle motion in crystal.

- Regular motion
- Dynamical chaos phenomenon

Let us consider the motion in continuous string potential.

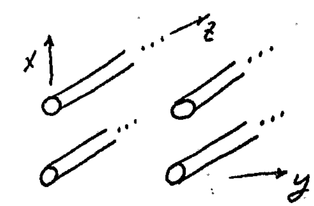

$U(x,y)$ – two-dimentional periodic field.

$$\ddot{\vec{\rho}} = -\frac{1}{E}\frac{\partial}{\partial\vec{\rho}}U(\vec{\rho}) \,, \qquad p_z \gg p_\perp .$$

The character of motion is determined by a number of integrals of motion.

The motion can be regular and chaotic.

Dynamical chaos phenomenon ...
A.I. Akhiezer, N.F. Shuliga, V.I. Truten'
Phys. Rep. 1990, v. 203, p.289 - 343.

Poincare map for above-barrier motion.

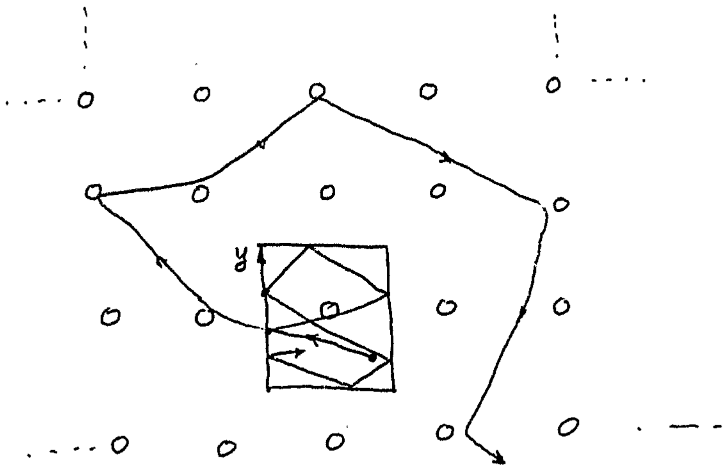

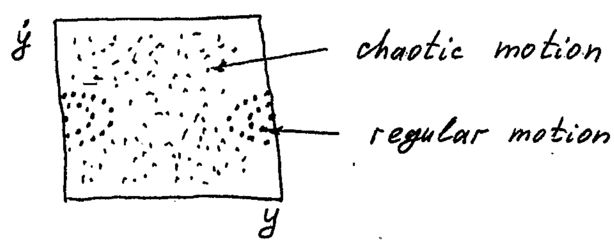

Results:

character of motion (regular or chaotic) being appreciably dependent on

a) initial conditions,
b) charge sign,
c) relation between ψ and ψ_c ($\varepsilon_\perp$ and V_0)

Measurement of the linear polarization of channeling radiation in silicon and diamond

M. Rzepka, G. Buschhorn, E. Diedrich, R. Kotthaus, W. Kufner, W. Rößl, K. H. Schmidt

Max-Planck-Institut für Physik (Werner-Heisenberg-Institut), 80805 München, Germany

P. Hoffmann-Stascheck, H. Genz, U. Nething, A. Richter

Institut für Kernphysik, Technische Hochschule Darmstadt, 64289 Darmstadt, Germany

J. P. F. Sellschop

University of the Witwatersrand, 2050 Johannesburg, South Africa

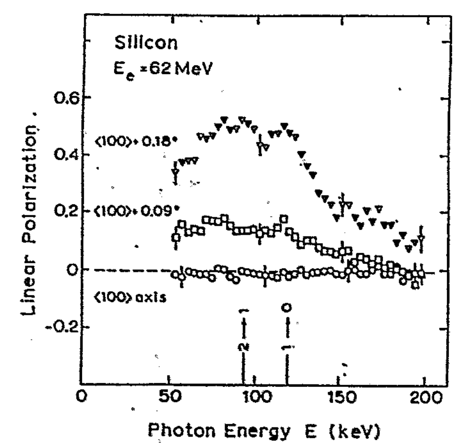

b)

FIG. 9. a) Azimuthal distributions of the integral yield of $\Theta = 90°$ Compton scattered axial channeling radiation produced with the silicon ⟨100⟩ axis exactly aligned (circles) and for two different tilt angles (0.09° and 0.18°) in the (110) plane. The curves show fits of $\cos^2\varphi$-distributions to the data. b) Energy dependence of the linear polarization of axial channeling radiation for the ⟨100⟩ axis exactly aligned (circles) and tilted by 0.09° and 0.18°.

Picture 9

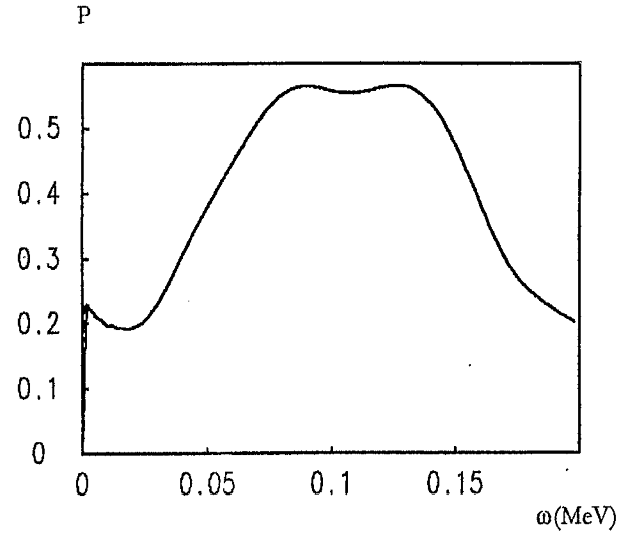

Si Ψ=2Ψc to <100> aligned to (110) E=62MeV

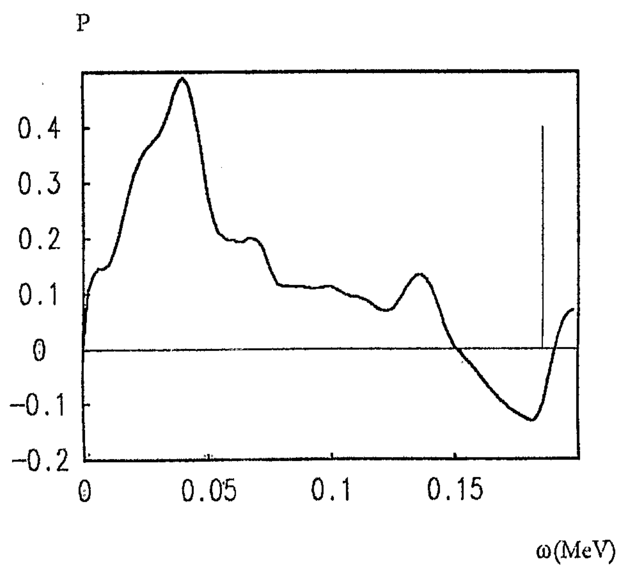

Si Ψ=2.42Ψc to <100> aligned to (100) E=32MeV

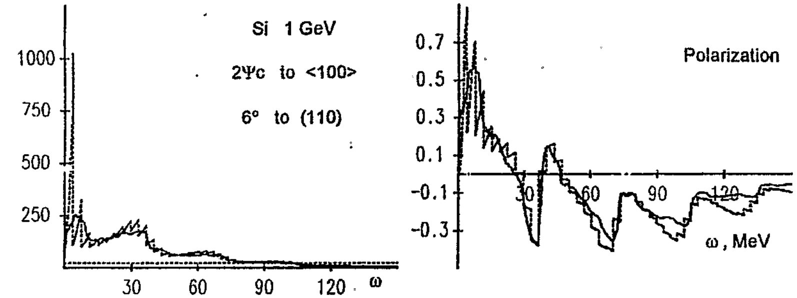

Fig. 3

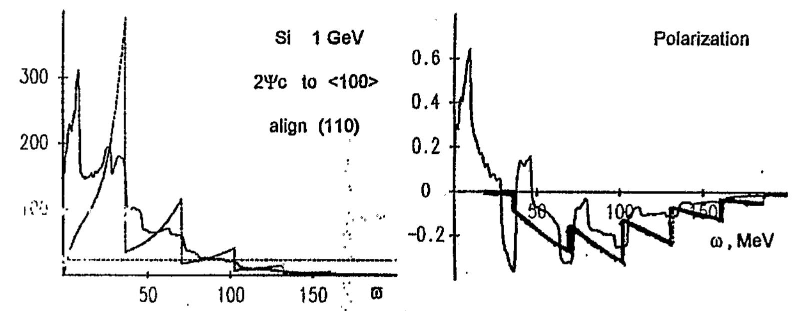

Fig 4

NiM B (1998)

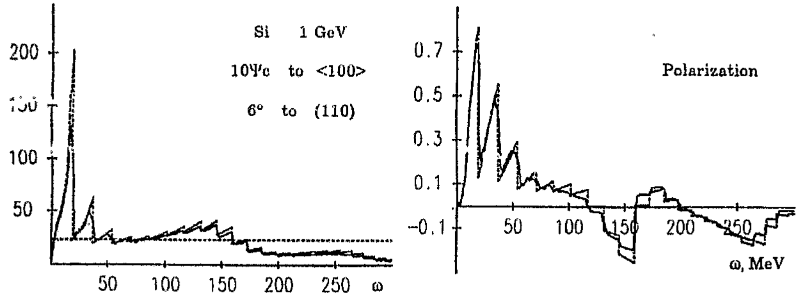

Fig. 1

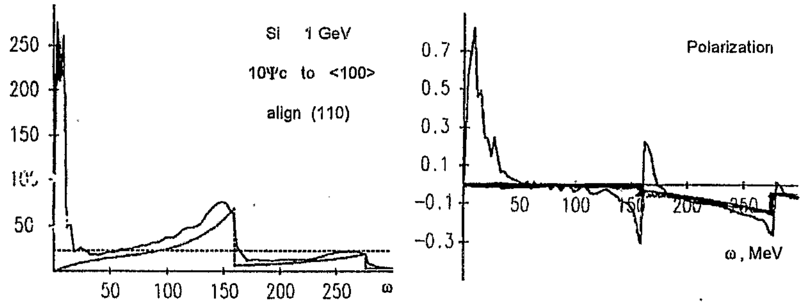

Fig. 2

— CB
— simulatio

- all ω $\quad \left(\frac{2R}{\psi} \not\gg l_c = \frac{2\gamma^2}{\omega} \right)$
- polarization and spectrum
- averaged on different trajectories
- test

$$\frac{dE}{d\omega} = 2\pi e^2 \omega \int_\delta^\infty \frac{dq}{q^2} \left[1 - 2\frac{\delta}{q}\left(1 - \frac{\delta}{q}\right)\right] \left(|W_x|^2 + |W_y|^2 \right),$$

$$P = \frac{1}{dE/d\omega}\, 2\pi e^2 \omega \int_\delta^\infty \frac{dq}{q^2} \frac{\delta^2}{q^2} \left(|W_x|^2 - |W_y|^2 \right).$$

$$\vec{W}_{x,y}(q) = \int_{-\infty}^{\infty} dt\, \dot{\vec{v}}_{\perp x,y}\, e^{iqt} \longrightarrow$$

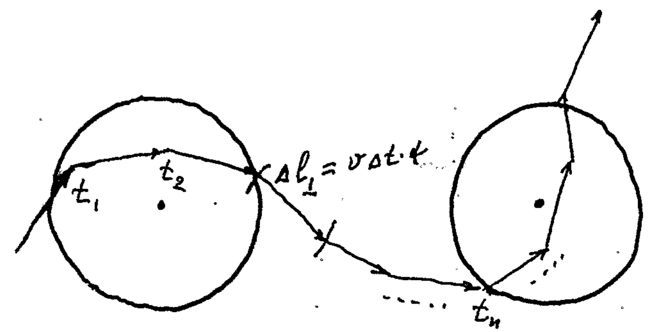

$$\Delta l_\perp \ll l_{coh} = 2\gamma^2/\omega$$

$$\longrightarrow \sum_n \Delta t_n\, \dot{\vec{v}}_{\perp,n}\, e^{iqt_n}.$$

Fine structure of CB spectra

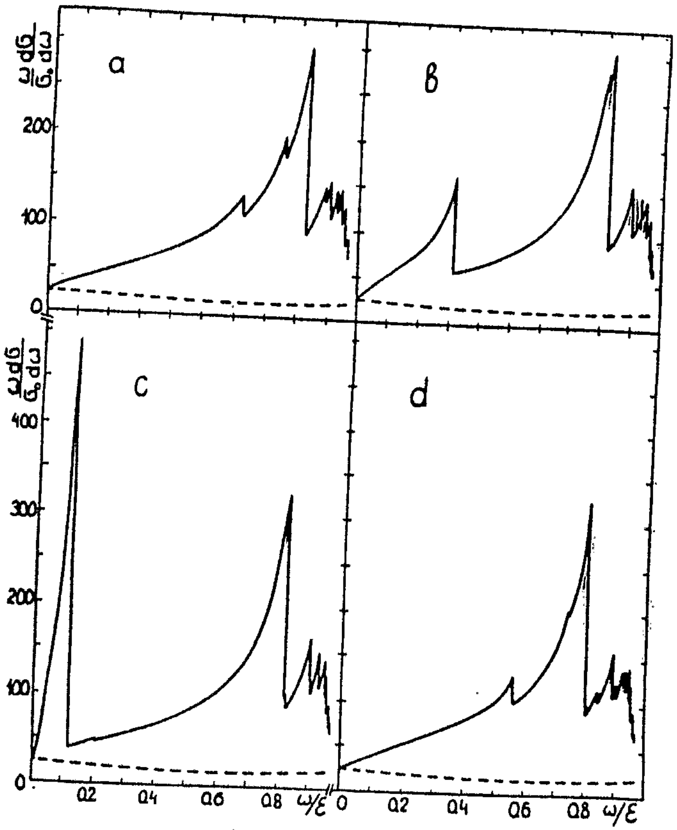

Fig. 1. Coherent radiation spectrum of 150 GeV electrons in a diamond crystal at $\psi = 10^{-3}$ rad and $\sin\alpha = 0.21$ (a), $\sin\alpha = 0.2$ (b), $\sin\alpha = 0.195$ (c), $\sin\alpha = 0.185$ (d), ($\sigma_0 = Z^2 e^6/m^2$).

The types of CB.

$$g_{\parallel} = g_z + \psi(g_y\cos\alpha + g_x\sin\alpha) = \delta = \frac{\omega m^2}{2E(E-\omega)}.$$

1. $g_z = 0.$
2. $g_z = 0, \quad g_y \neq 0.$
3. $g_z = g_y = 0, \quad g_x \neq 0, \quad \alpha \ll 1.$
4. Large value of the $|\vec{g}|$,

$$g_z = 0, \quad g_y = -\frac{2\pi}{a}, \quad g_x = 5\cdot\frac{2\pi}{a}, \quad \alpha \approx \frac{1}{5} + \beta.$$

$$g_{\parallel} = \psi(g_y + \alpha g_x) = \delta$$

$$g_{\parallel} = \psi\left(\cancel{-\frac{2\pi}{a}} + \left(\cancel{\frac{1}{5}} + \beta\right)\cdot 5\frac{2\pi}{a}\right) \approx \boxed{\psi\beta g_x = \delta}$$

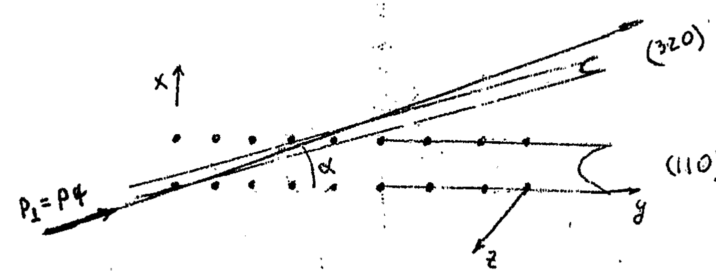

' *Meth. in Phys. Res. B 119 (1996) 55–58*

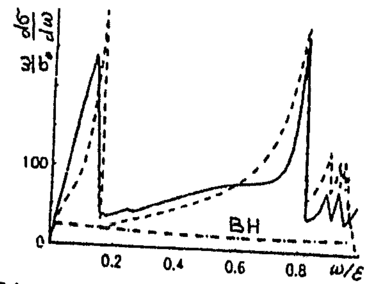

Fig. 1. Coherent radiation spectrum of 150 GeV electrons in a diamond crystal at $\psi = 2\times10^{-3}$ rad and $\alpha = 0.199$. Solid line – simulations results; dashed line – calculations by Eq. (1); $\sigma_0 = Z^2 e^6 m^{-2}$.

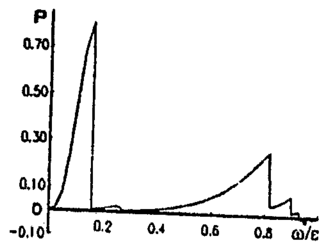

Fig. 2. Polarization of coherent radiation of 150 GeV electrons in a diamond crystal at $\psi = 2\times10^{-3}$ rad and $\alpha = 0.199$.

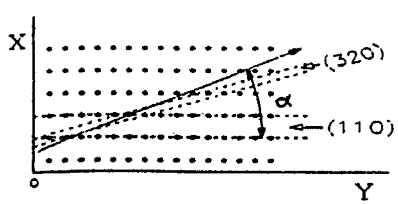

Fig. 3. Trajectory of 150 GeV electrons in a diamond crystal in the plane orthogonal to the < 001 > axis.

Picture 5

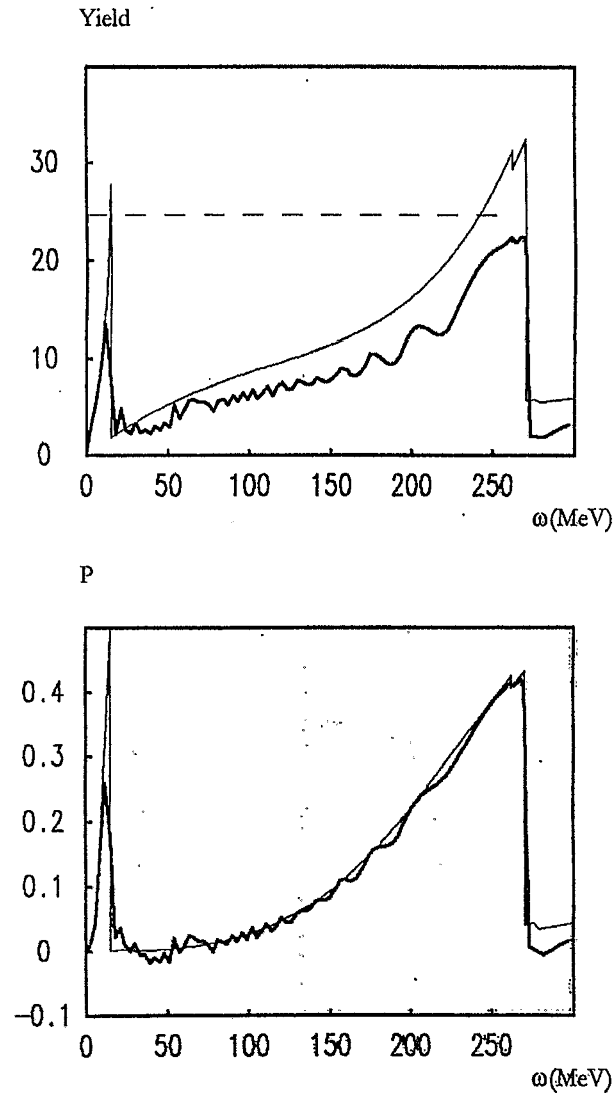

Si Ψ=80Ψc to <100> α=199mrad to (110) E=1GeV
without thermal vibrations

Picture 1

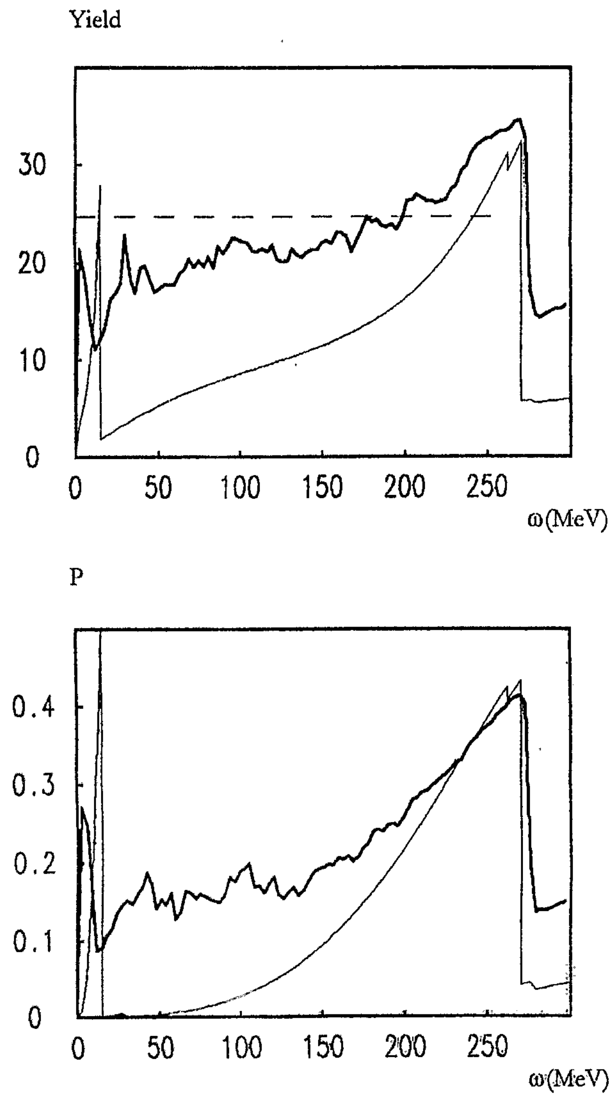

Si $\Psi=80\Psi_c$ to <100> α=199mrad to (110) E=1GeV
with thermal vibrations

Picture 6

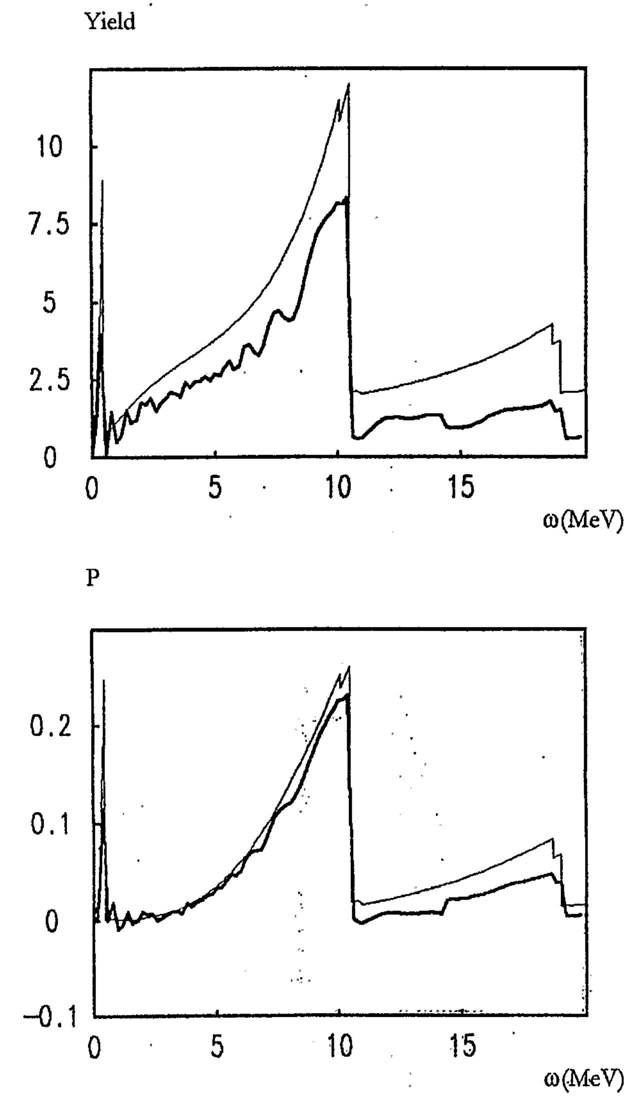

Si $\Psi=80\Psi_c$ to <100> α=199mrad to (110) E=100MeV
without thermal vibrations

Picture 2

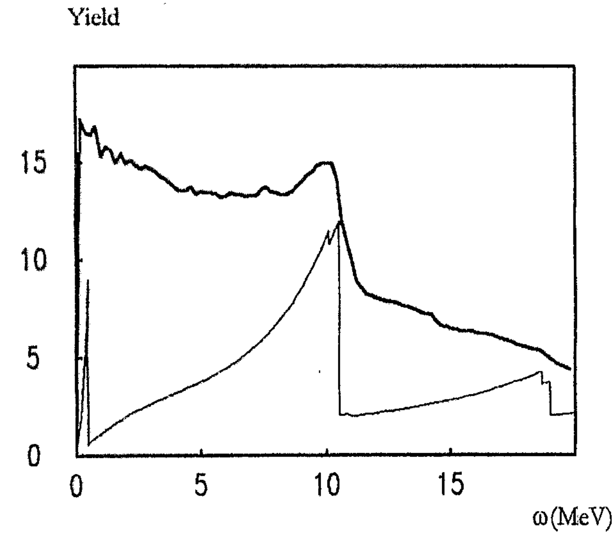

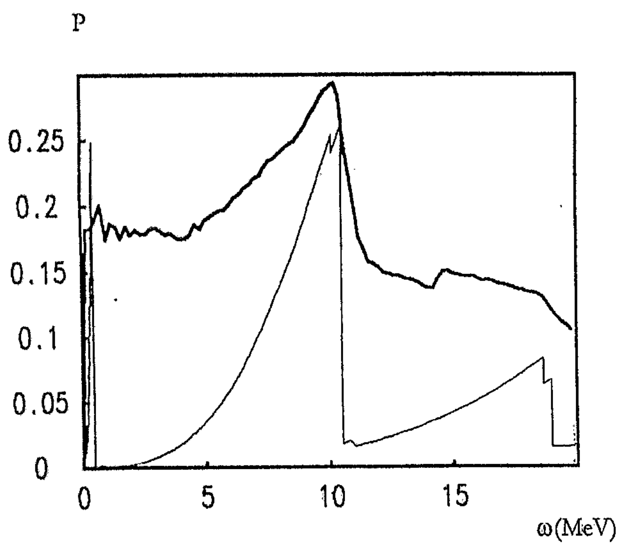

Si Ψ=80Ψc to <100> α=199mrad to (110) E=100MeV
with thermal vibrations

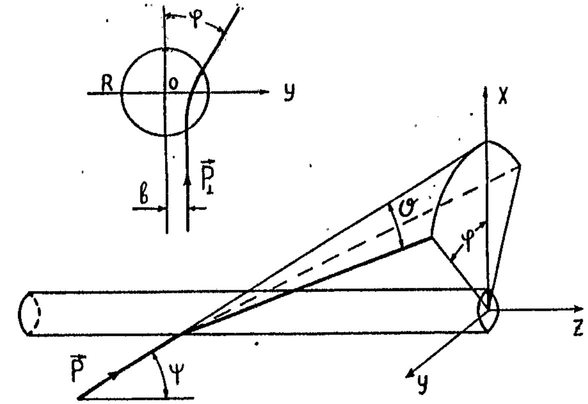

$$\vartheta = \psi \cdot 2\sin\left(\frac{\varphi(b)}{2}\right)$$

$$\varphi(b) = \pi - 2b\int_{\rho_0}^{\infty} \frac{d\rho/\rho^2}{\sqrt{1-\frac{U_r(\rho)}{\varepsilon_\perp}-\frac{b^2}{\rho^2}}}, \quad \varepsilon_\perp = \frac{\varepsilon\psi^2}{2}$$

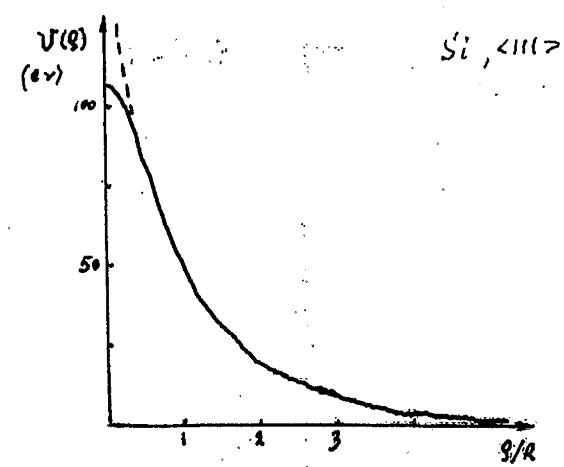

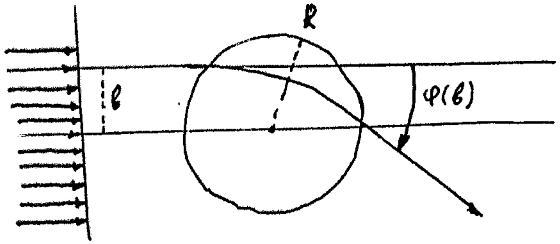

$$U(\rho) = \begin{cases} -\dfrac{\alpha}{\rho} + \dfrac{\alpha}{R}, & \rho \le R \\ 0, & \rho > R \end{cases}$$

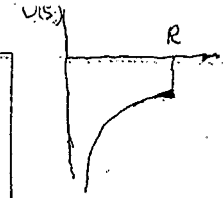

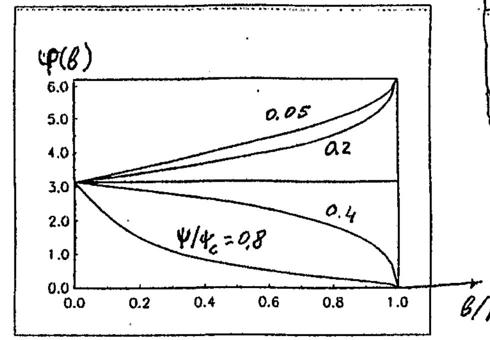

Classical theory

$$\varphi(\ell) = \pi - 2b \int_{\rho_0}^{\infty} \frac{d\rho}{\rho^2} \frac{1}{\sqrt{1 - \frac{U(\rho)}{\varepsilon_\perp} - \frac{b^2}{\rho^2}}}$$

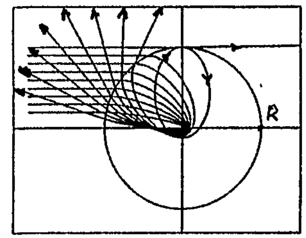

$\psi = 0.2\,\psi_c$

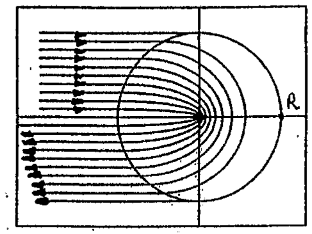

$\psi \approx 0.3\,\psi_c$

$$\frac{d\sigma_{cl}}{d\varphi} = L\psi \left| \frac{d\varphi}{db} \right|^{-1}$$

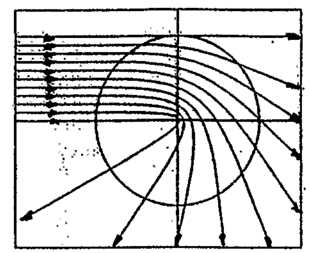

$\psi = 0.8\,\psi_c$

$$\psi_c = \sqrt{\frac{4Ze^2}{\varepsilon a}}$$

Quantum theory

$$\frac{d\sigma_q}{d\varphi} = \frac{L\psi}{2\pi p_\perp} \left| \sum_{l=-\infty}^{\infty} e^{il\varphi} \left(e^{2i\eta_l} - 1 \right) \right|^2 ,$$

$$\eta_l^{(WKB)} = \int_{\rho_0}^{\infty} d\rho \sqrt{p_\perp^2 - 2\varepsilon U(\rho) - \frac{l^2}{\rho^2}} - \int_{\rho_0'}^{\infty} d\rho \sqrt{p_\perp^2 - \frac{l^2}{\rho^2}} ,$$

$$\sigma_{tot} = \frac{4L\psi}{p_\perp} \sum_{l=-\infty}^{\infty} \sin^2 \eta_l .$$

$\varepsilon = 10$ mev, $Si, \langle 100 \rangle$

$\psi = 0{,}2\,\psi_c$ $\qquad$ $\psi = 0{,}8\,\psi_c$

$\frac{1}{LR\psi}\frac{d\sigma}{d\varphi} = F$

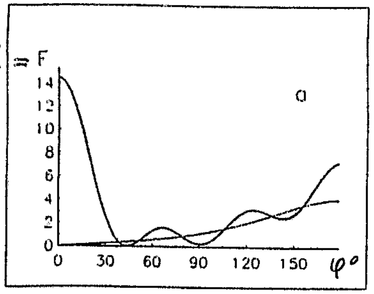

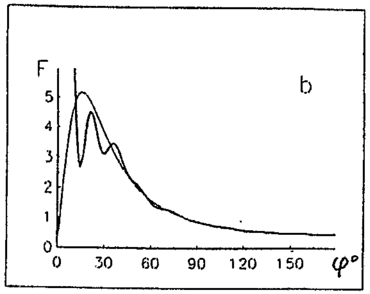

$\frac{1}{2LR\psi}\cdot\sigma^e_{tot} = F$

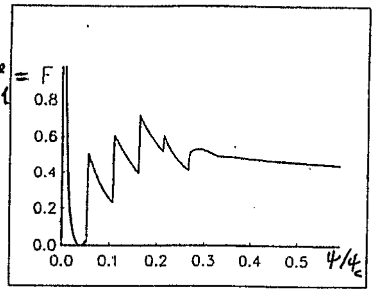

Mechanisms of CB

$$g_{\parallel} = g_z + \psi\left(g_x \cos\alpha + g_y \sin\alpha\right) \geq \delta = \frac{\omega m^2}{2\varepsilon(\varepsilon-\omega)}$$
$\psi \ll 1$

- CB type B $\qquad g_z \neq 0$
- row effect $\qquad g_z = 0,\ g_x \neq 0\ ,\quad \alpha = 0$
- point effect $\qquad g_z = g_x = 0\ ,\ g_y \neq 0 \quad 0 < \alpha \ll 1$
- fine structure of CB $\qquad$ two $\vec{g}$ important for CB
- CB for real traject.
  - dynamical chaos
  - splitting of CB maxima
  - simulation of CB
  - different E_-
  - e^-, e^+
  - ⋮

- CB and channeling rad.
- quantum effects at low E.
- LPM-effect for CB
- CB and synchrotron rad.
- CB and parametric rad
- ⋮

W. Wagner:

Quasi-monochromatic X-rays from ELBE

Quasi- monochromatic X-Rays from the ELBE Radiation Source

W. Wagner

W. Enghardt A. Panteleeva
U. Lehnert J. Pawelke
B. Naumann H. Prade
W. Neubert

Collaboration partners

Technical University Darmstadt
Johannes-Gutenberg-University Mainz
ROBL ESRF Grenoble, France
Institute of Applied Problems of Physics, Yerevan, Armenia
Yerevan Physics Institute, Armenia

"Workshop on X-rays from electron beams"
Rossendorf, February 24 - 26, 2000

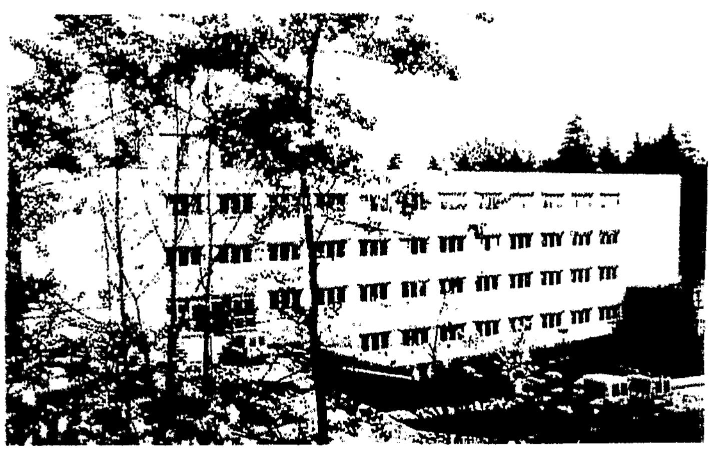

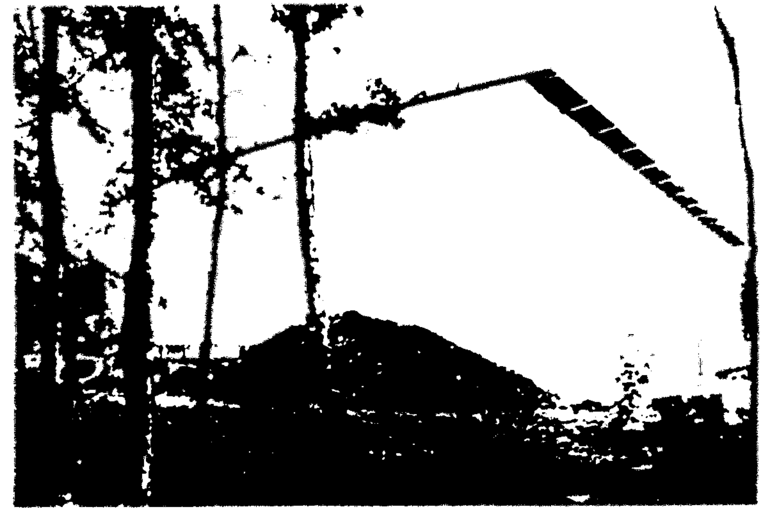

View of the new building for the ELBE radiation source at the FZR

ELBE

is a new superconducting Electron accelerator of high Brilliance and low Emittance developed and presently under construction in Rossendorf near Dresden

This facility will deliver secondary beams of different kinds

- High-brilliant infrared radiation coming from different free-electron lasers (FEL)
- Intensive bremsstrahlung γ-rays for nuclear spectroscopy
- Quasi-monochromatic X-rays
- Neutrons via (γ,n) in the 0.1 - 10 MeV range (10^{6}/s cm²)
- Positrons via e^+e^--pair production (10^{8}/s cm²)

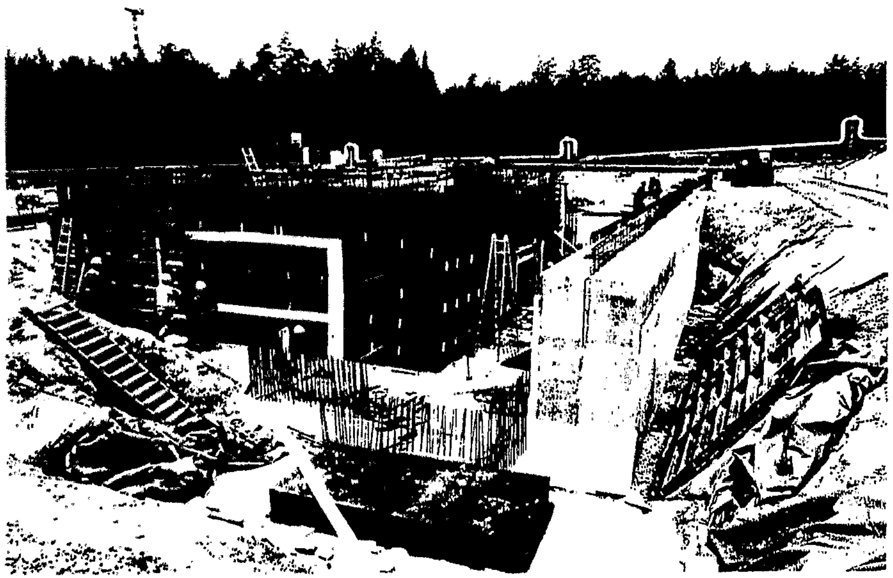

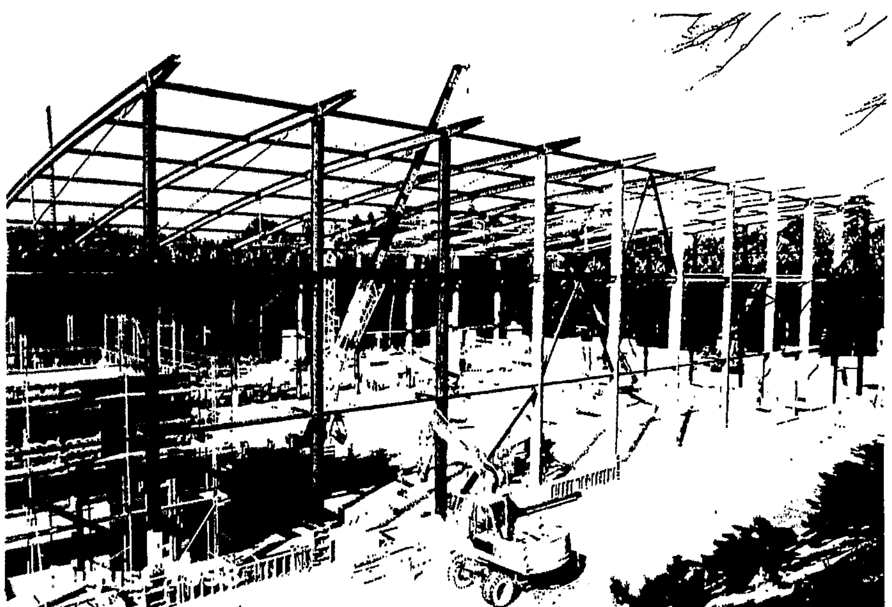

W. Wagner@fz-rossendorf.de

FZR
Postfach 51 01 19
D - 01314 Dresden

September 1998

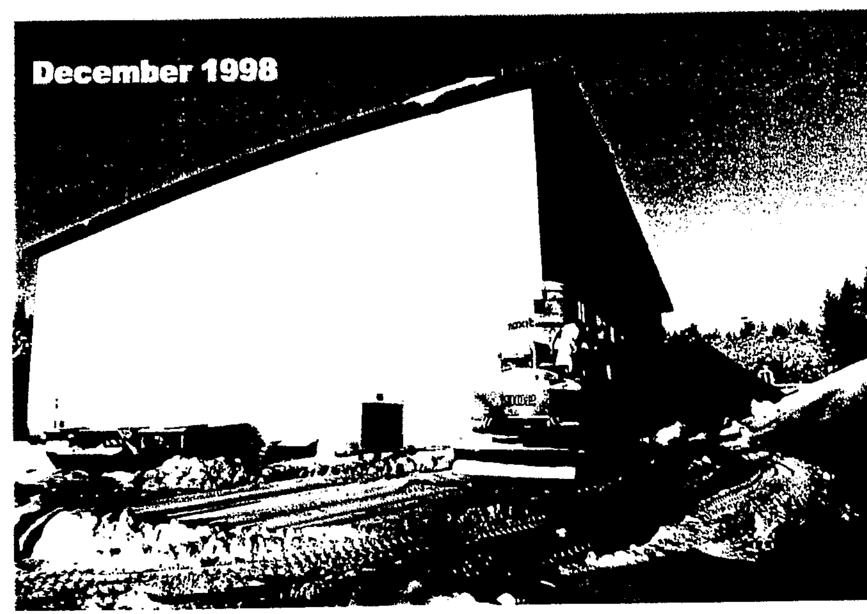

December 1998

W. Wagner@fz-rossendorf.de

FZR
Postfach 51 01 19
D - 01314 Dresden

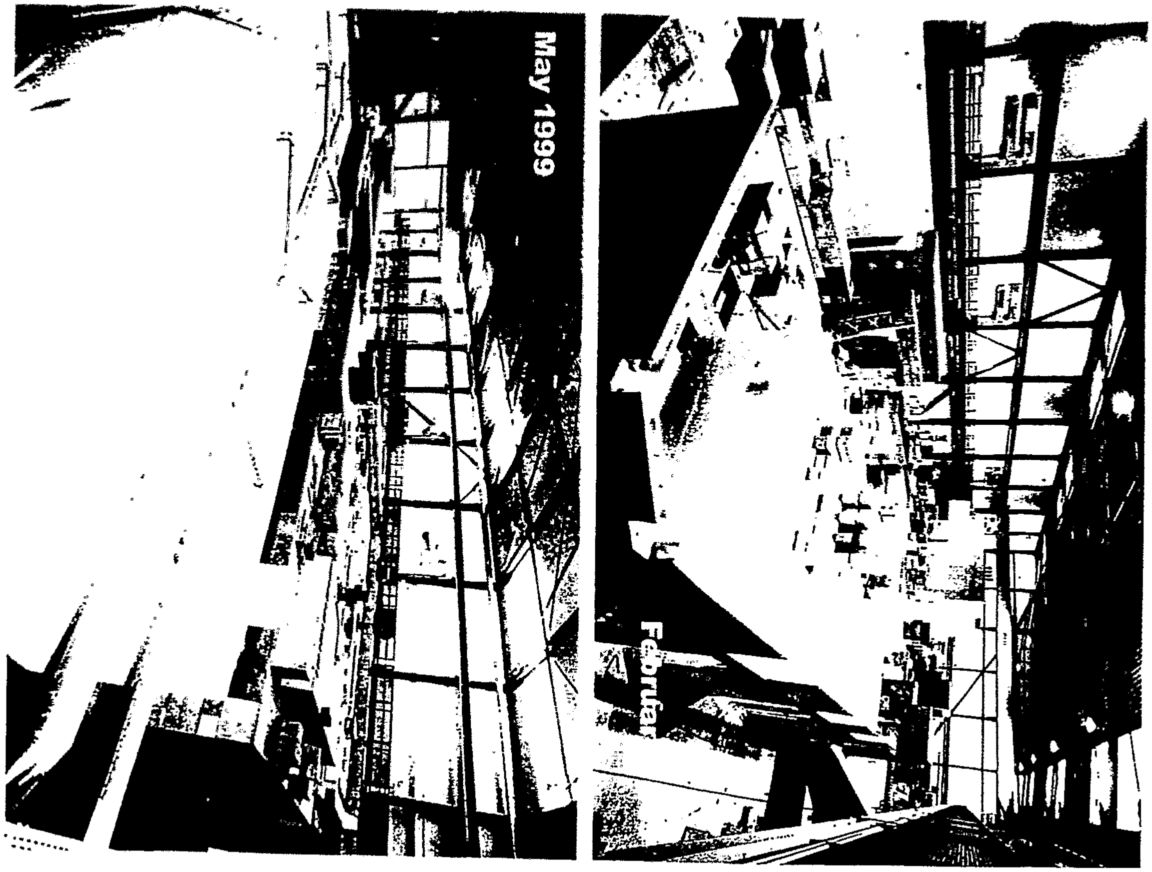

W.Wagner@fz-rossendorf.de
FZR
Postfach 51 01 19
D-01314 Dresden

FORSCHUNGSZENTRUM ROSSENDORF
Institut für Kern- und Hadronenphysik

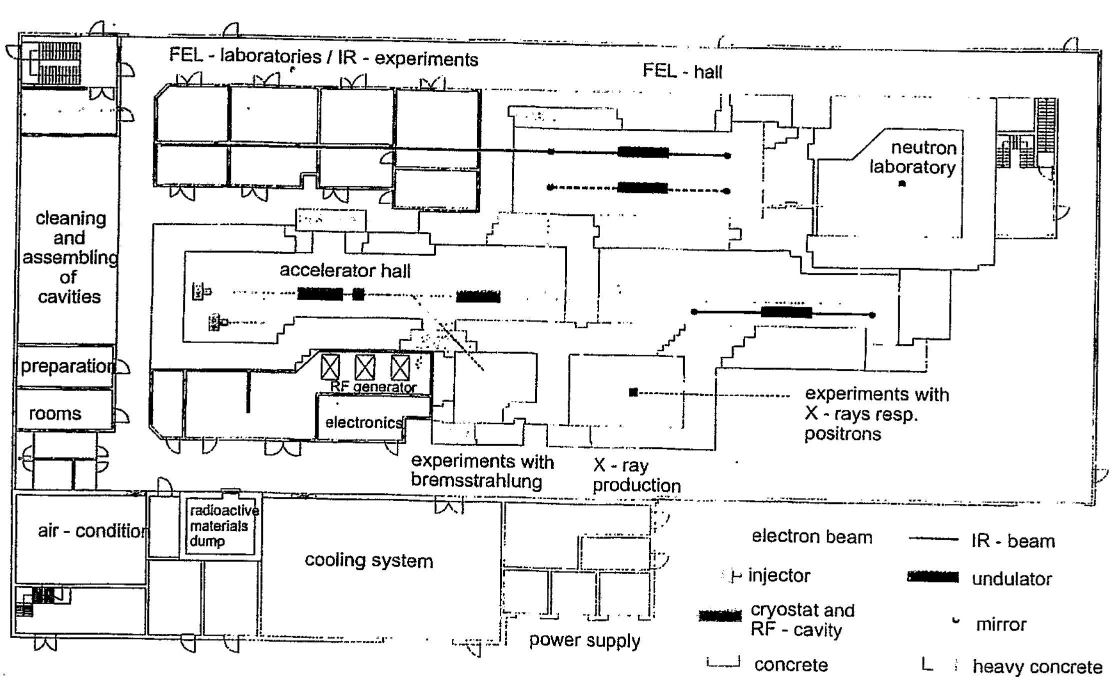

Floorplan of the new building for ELBE

W.Wagner@fz-rossendorf.de
FZR
Postfach 51 01 19
D-01314 Dresden

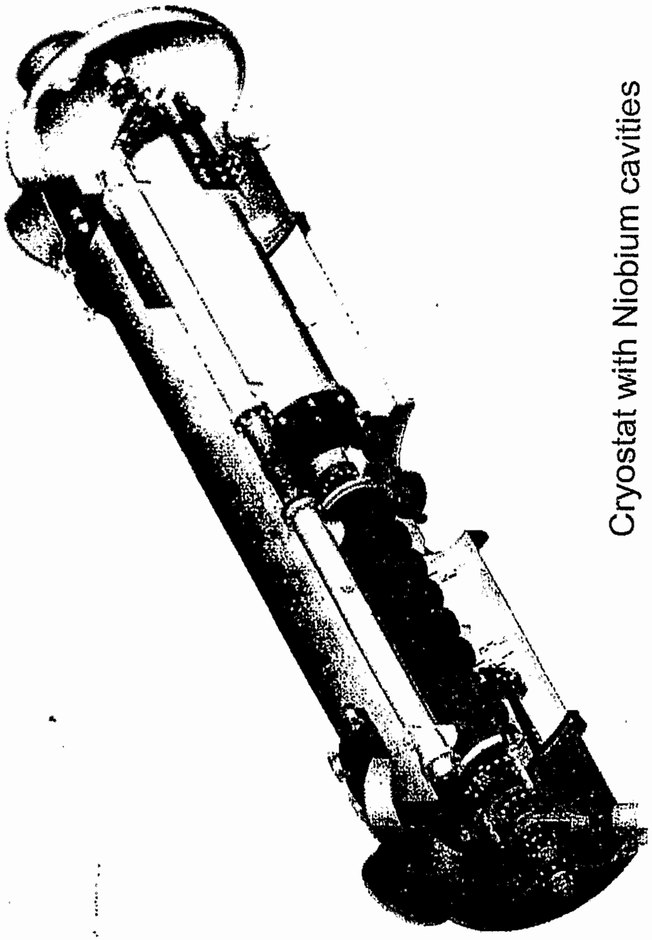

Cryostat with Niobium cavities

Superconducting Acceleration Structure

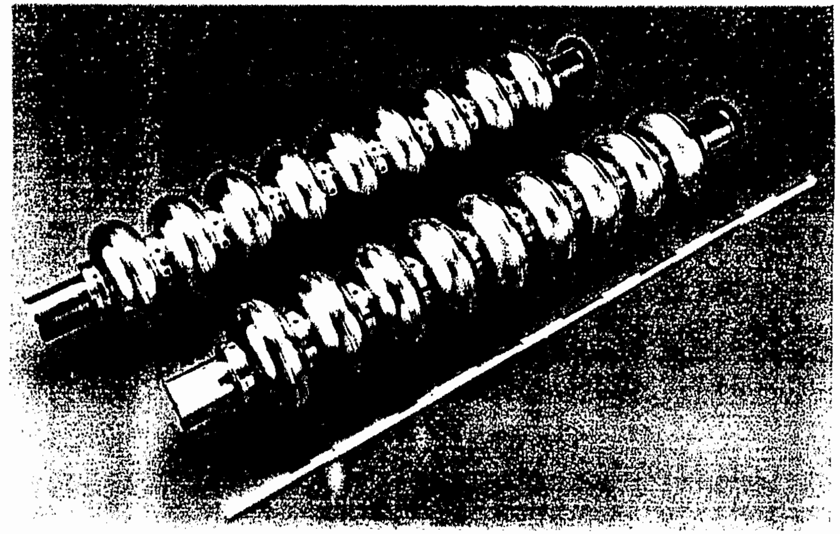

The acceleration structure consists of two nine-cell RFcavities made of Nb.

The cavities have been developed at DESY in Hamburg for the TESLA (Tera Electron Volt Superconducting Linear Accelerator) test facility.

First successful tests at DESY showed that acceleration gradients up to about 20 MV/m can be achieved.

The ELBE design is based on the rather conservative value of 10 MV/m.

Technical parameters

-Operation temperature	1.8 K
-Operation frequency	1.3 GHz
-Resonator quality	10^{10}

First electron injector for ELBE

FEL - high bunch charge
short bunchlength (ps)
lower micropulse repetition rate due to HF power
two bunchers for injection (260 MHz and 1.3 GHz)

X-ray source - low-emittance beam
small beam divergence
moderate bunch charge
large micropulse repetition rate (cw - beam)

In the first stage of ELBE (20 MeV) an injector based on a thermionic triode gun, as used for the FEL at HEPL Stanford, will be available.

This injector was optimized for the formation of a low -emittance beam with a maximum average currentof 0.1 mA for radiation physics.

Furthermore, design work has been initiated for a laser-driven superconducting RF-gun of high brilliance as needed to perform Compton backscattering studies.

Gun	thermionic triode gun		s.c. RF gun
Values	design	measured	design
Micropulse repetition rate	11.8	(13) MHz	1.3 GHz / 650 MHz
Maximum bunch charge / pC	85 (77) / 8.5		85 (1) / 1000
Maximum average current / mA	1 / 0.1		100 / 650
Transverse emittance (rms) / π mm mrad	7 / 1.2	9.4 / 5.4	0.77 (0.06) / 1.25
Norm. trans. emittance (rms) π mm mrad (20 MeV)	4 / 0.75	10.9	
Bunch lenght (90 %) / ps	5.1	2.9	
Energy width (rms) / keV	33	64	

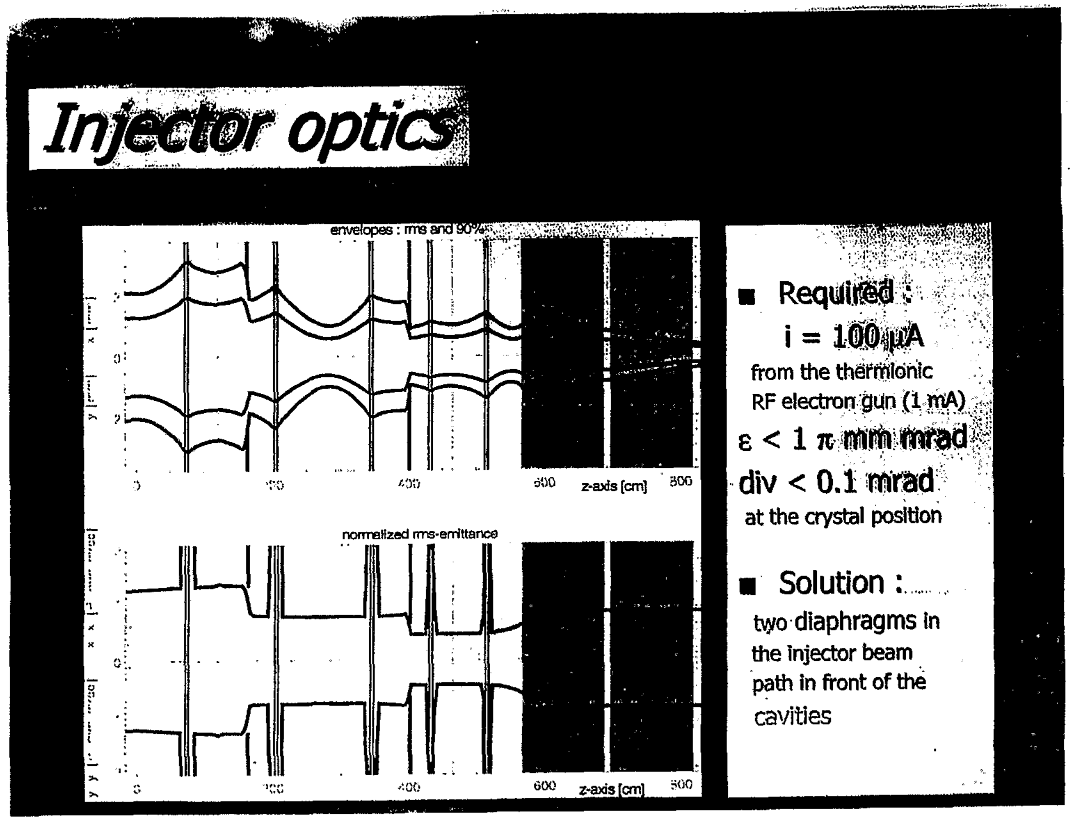

Beam to cave

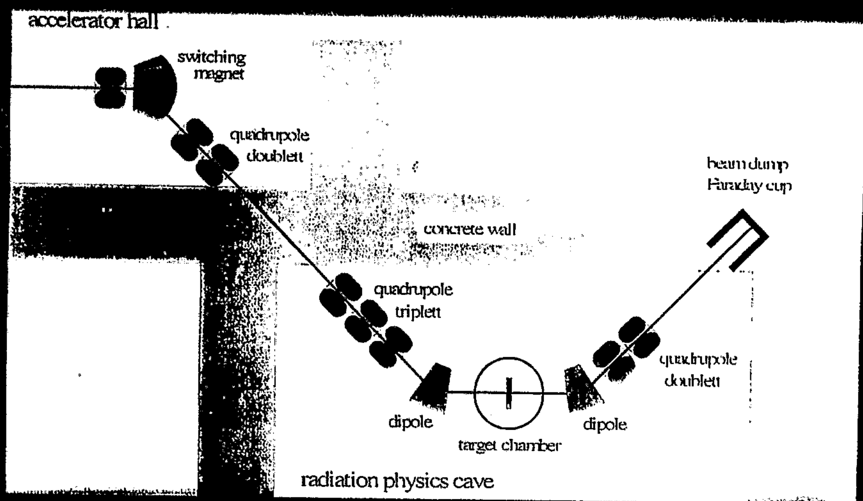

Electron optical elements on the radiation physics beamline

Geometry

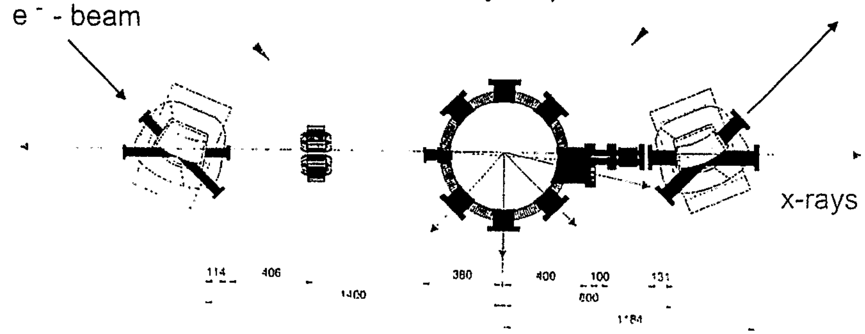

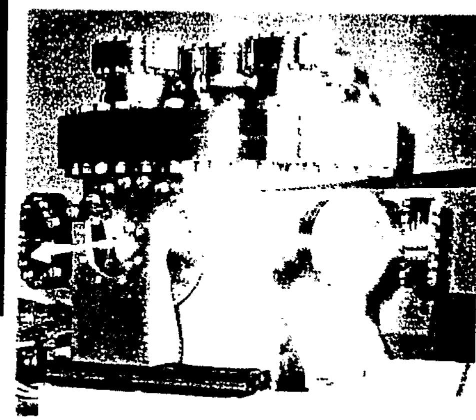

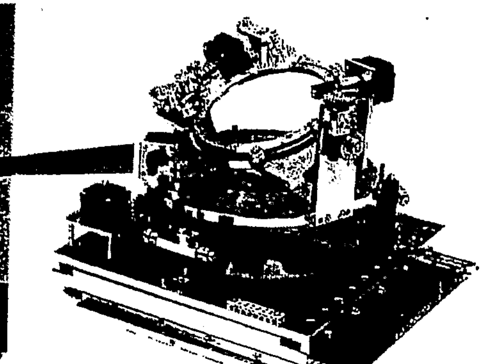

6-axes goniometer

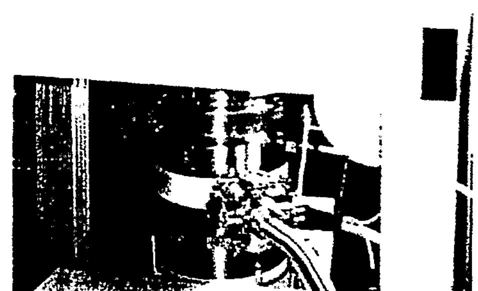

UHV goniometer chamber

$p < 10^{-9}$ mbar

W.Wagner@fz-rossendorf.de

FZR
Postfach 51 01 19
D - 01314 Dresden

Non-conventional sources of quasi-monochromatic X-rays

Channeling radiation

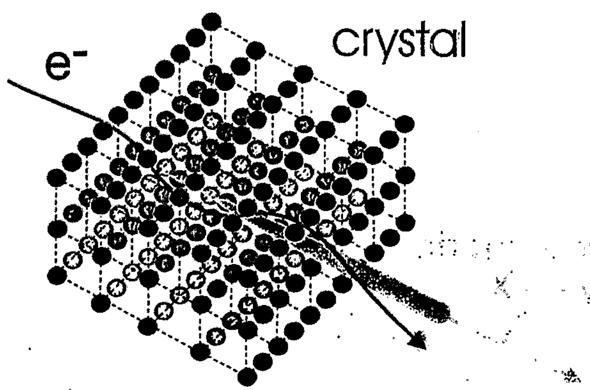

PXR

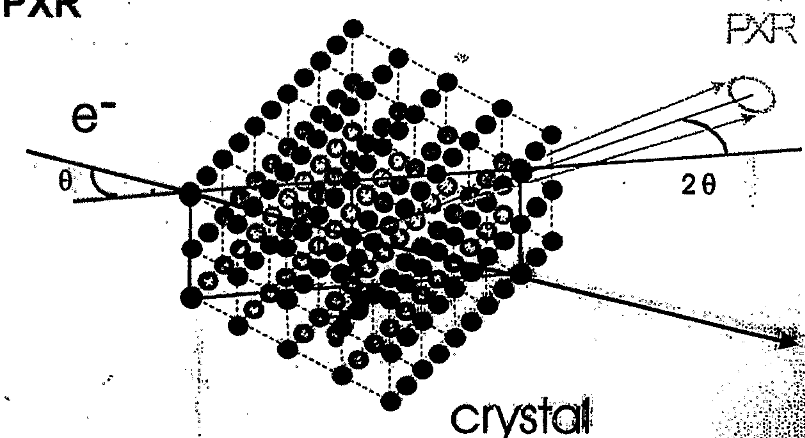

W.Wagner@fz-rossendorf.de

Characteristics of X-ray sources

Photon number

intensity	$I = P_R = dE / dt = dN_x \cdot h\omega / dt$	[MeV / s]
flux	$\phi = dN_x / dt$	[ph / s]
spectral flux	$\phi_S = d^2N_x / dt\ (\Delta h\omega / h\omega)$	[ph / s 0.1% BW]
flux density	$d\phi / d\Omega = d^2 N_x / dt\, d\Omega$	[ph / s sr]
radiance	$R = d^2N_x / dt\, dA$	[ph / s mm²]
fluence	$F = dN_x / dA$	[ph / mm²]

Source quality

- divergence (focussing)
- spatial resolution

brightness	$S = \phi_S / 2\pi\, \sigma_{x'} \sigma_{y'}$	[ph / s mrad² 0.1% BW]
brilliance	$B = \phi_S / 4\pi^2\, \sigma_x \sigma_y \sigma_{x'} \sigma_{y'} = \phi_S / 4\pi^2\, \varepsilon_x \varepsilon_y = \phi_S / 2\pi\, \sigma_r \sigma_{r'}$	
	$B = \phi_S / 2\pi\, \varepsilon_t$	[ph / s mm² mrad² 0.1% BW]

Radiation production efficiency

yield	$Y = d^2N_x / dN_e\, d\Omega$	[ph / sr per e⁻]
efficiency	$\eta = P_R / P_{beam}$	(W_R / W_{beam}) [%]

spec. brilliance $B_S = B\, e / i\, E_e = B\, e / mc^2\, i\, \gamma$
[ph / mm² mrad² 0.1% BW MeV$_e$]

Chromaticity

Tunability

W.Wagner@fz-rossendorf.de
FZR Postfach 51 01 19 D-01314 Dresden

X-ray sources with a continuous spectrum

Bremsstrahlung (BS) and characteristic X-rays (CX)
(**medium** : X-ray tubes)

$B_T = 10^{6-9}$ ph / s mm² mrad² 0.1%BW i = $(10^{-2} - 1)$ A; 10-100 kV

Synchrotron radiation (SR, WR, UR)
(dipol **magnets**, wiggler, undulator ; electron or positron beams)

$E_c = 3\,ch\,\gamma^3 / 4\pi R = 10$ keV $\gamma = (7\text{-}9)\,10^3$ $E_e = 4\text{-}5$ GeV

$B_S = 10^{13-15}$ ph / s mm² mrad² 0.1%BW i = 100 mA

Transition radiation (TR)
(**medium boundary**, foil stacks-RTR ; electron beams)

$E_{cut} = \gamma\,h\,\omega_p / 2\pi = 10$ keV $\gamma = 350$ $E_e = 150\text{-}170$ MeV

$B_{5\,keV} = 10^{13}$ ph / s mm² mrad² 0.1%BW i = 100 μA; 855 MeV

Quasi-monochromatic X-ray sources

Channeling radiation (CR)
(**crystalline medium** : electron beams)

$E_x = 30$ keV $\gamma = 40$ $E_e = 20$ MeV i = 100 μA

$B_{CR} = 3\;10^6$ ph / s mm² mrad² 0.1%BW ($B_{CR}^{5\%BW} = 10^8$)

Parametric X-rays (PXR)
(**crystalline medium** : electron beams)

$B_{CR} = 10^5$ ph / s mm² mrad² 0.1%BW low background

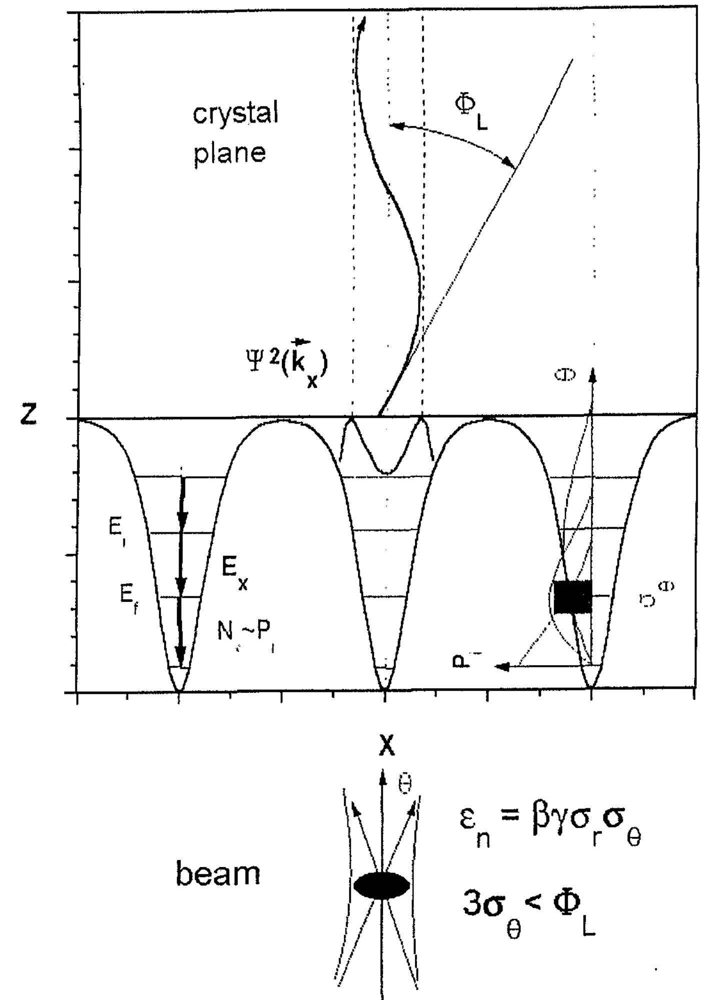

$\varepsilon_n = \beta\gamma\sigma_r\sigma_\theta$

$3\sigma_\theta < \Phi_L$

W. Wagner@fz-rossendorf.de
FZR Postfach 51 01 19 D - 01314 Dresden

Population probability of channeling states

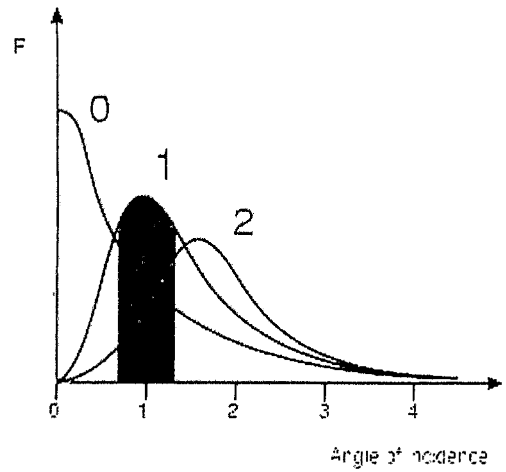

$\psi^2 (k_x)$: $\gamma \beta mc \theta = h (\pm k_x + jg) / 2\pi$ $j = 0,1,2...$

$g = 2\pi / d_p$

$k_x = g / 2$

d_p diamond (110) = 1.26 Å

Θ (90%) = 0.24 mrad

requirement to the beam divergence : **S**

$\sigma_\theta = 0.12$ mrad

emittance : **B**

20 MeV

$\sigma_r = 1$mm

$\varepsilon_t = 1.4 \pi$ mm mrad

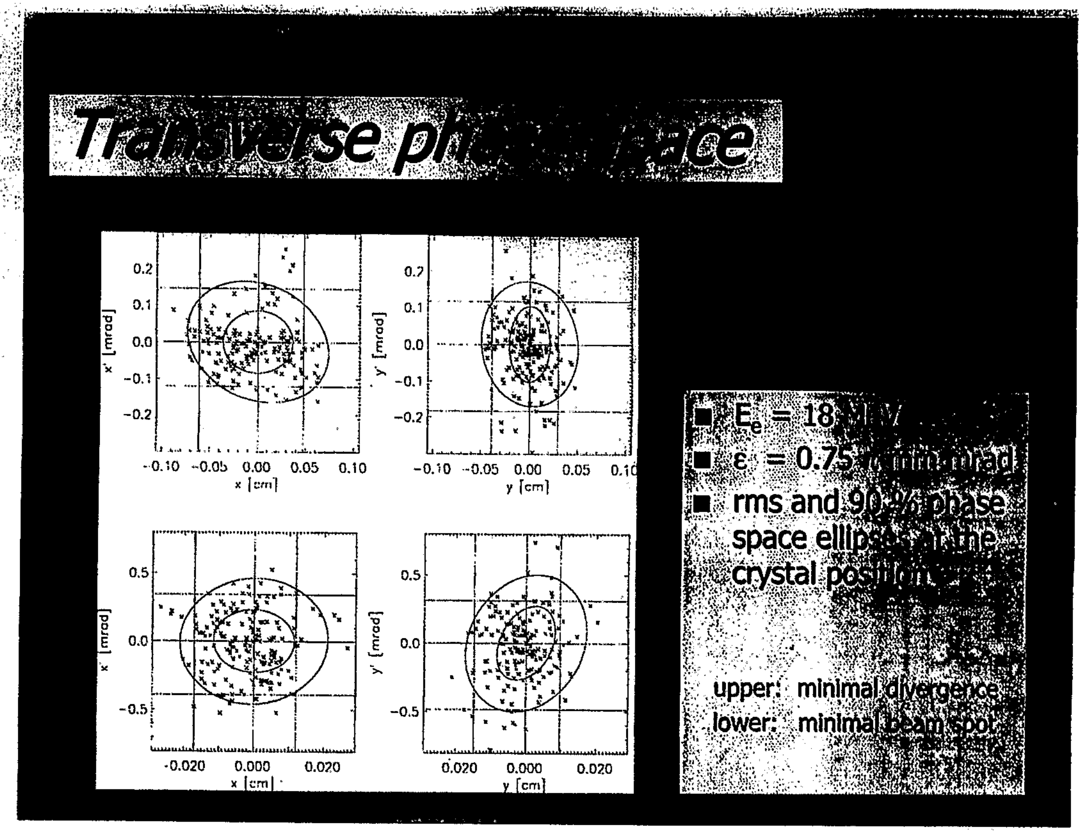

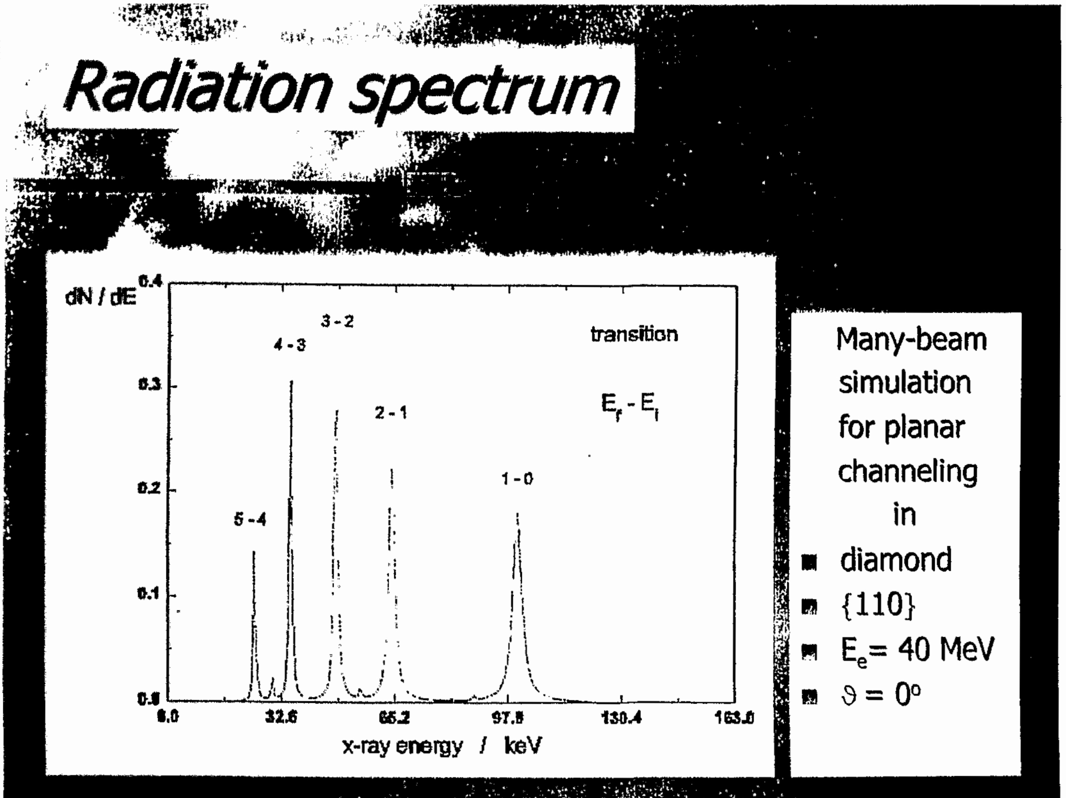

General expression for planar channeling

$$\frac{dI}{d\Omega d\omega} \equiv \frac{dE}{d\Omega d\omega dt} \equiv \hbar\omega \frac{dY}{d\Omega d\omega dt} \equiv \hbar\omega\beta c \frac{dY}{d\Omega d\omega dz}$$

$$= \frac{e^2}{2\pi m^2 c^3} \frac{p_T^2 \omega^2}{2\gamma^2 (1-\beta\cos\vartheta)} \times \delta\left(\omega - \frac{\omega_e}{1-\beta\cos\vartheta}\right)$$

$$\times \left[\left(\frac{\cos\vartheta - \beta}{1-\beta\cos\vartheta}\right)^2 \cos^2\varphi + \sin^2\varphi\right]$$

Scaling laws:

emission cone:	$\theta \sim 1/\gamma$
Doppler shift:	$\omega = \omega_0 / 1 + \gamma^2\theta^2$
photon frequency:	$\omega_0 = 2\gamma^2\omega_e$
forward frequency:	$\omega_0 \sim \gamma^{3/2}$
forward intensity:	$I_0 \sim \gamma^4$
forward yield:	$Y_0 \sim \gamma^{5/2}$
total intensity:	$I \sim \gamma^2$
total yield:	$Y \sim \gamma^{1/2}$
crystal thickness:	$Y \sim 1 - e^{-z/loc}$
	$Y \sim z^{1/2}$

Lorentz - transformed dipol pattern

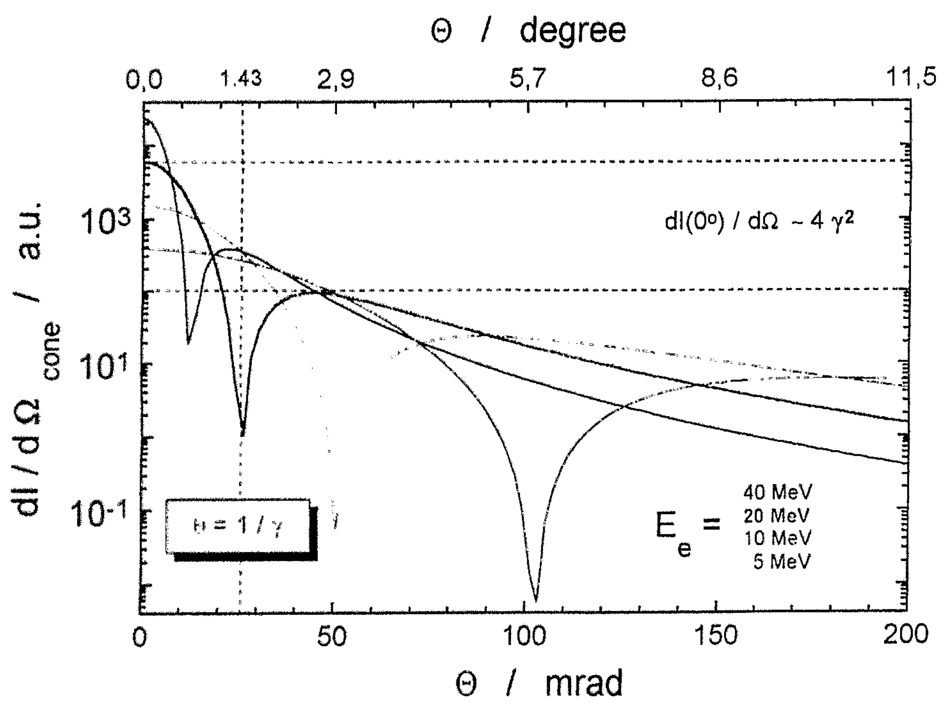

Photon frequency

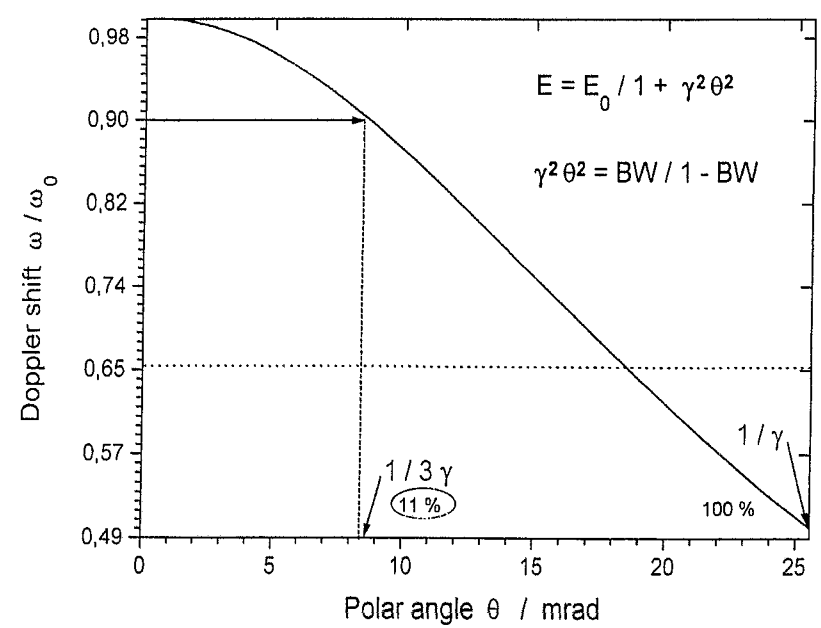

$\gamma = 3$

color $\hat{=}$ ω

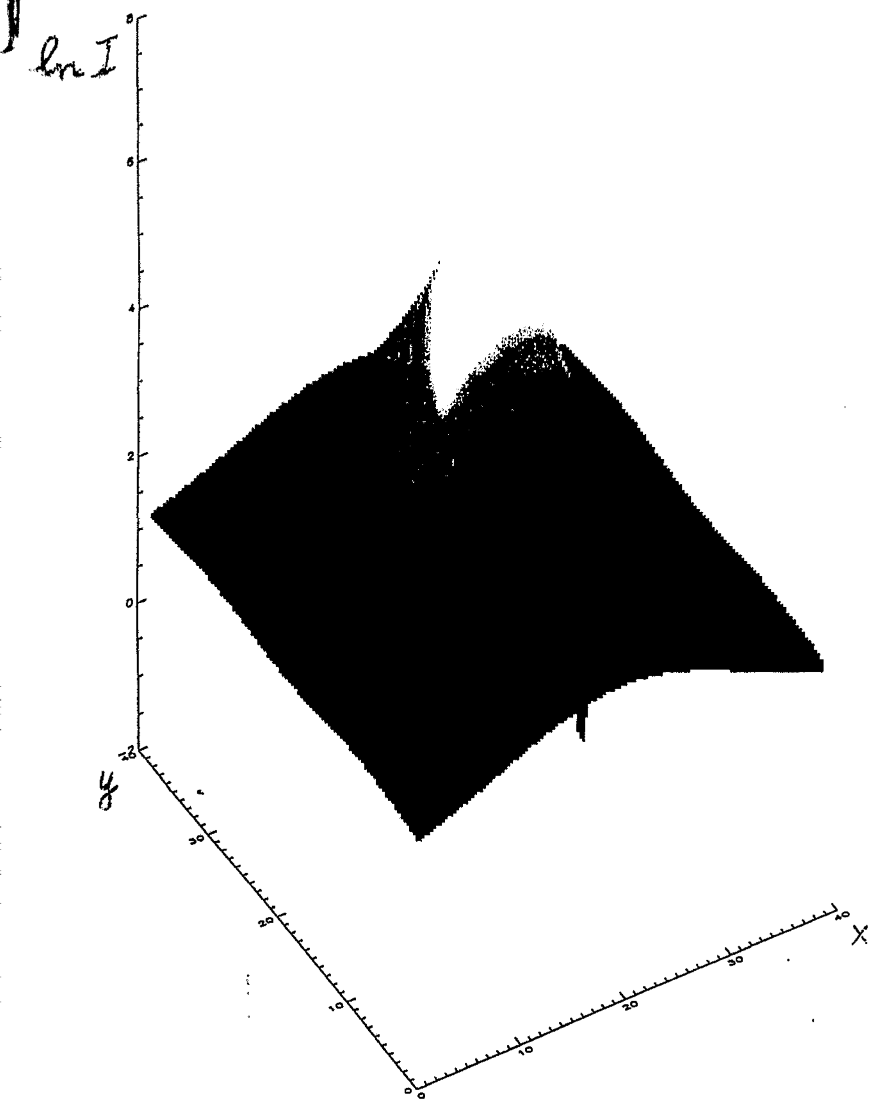

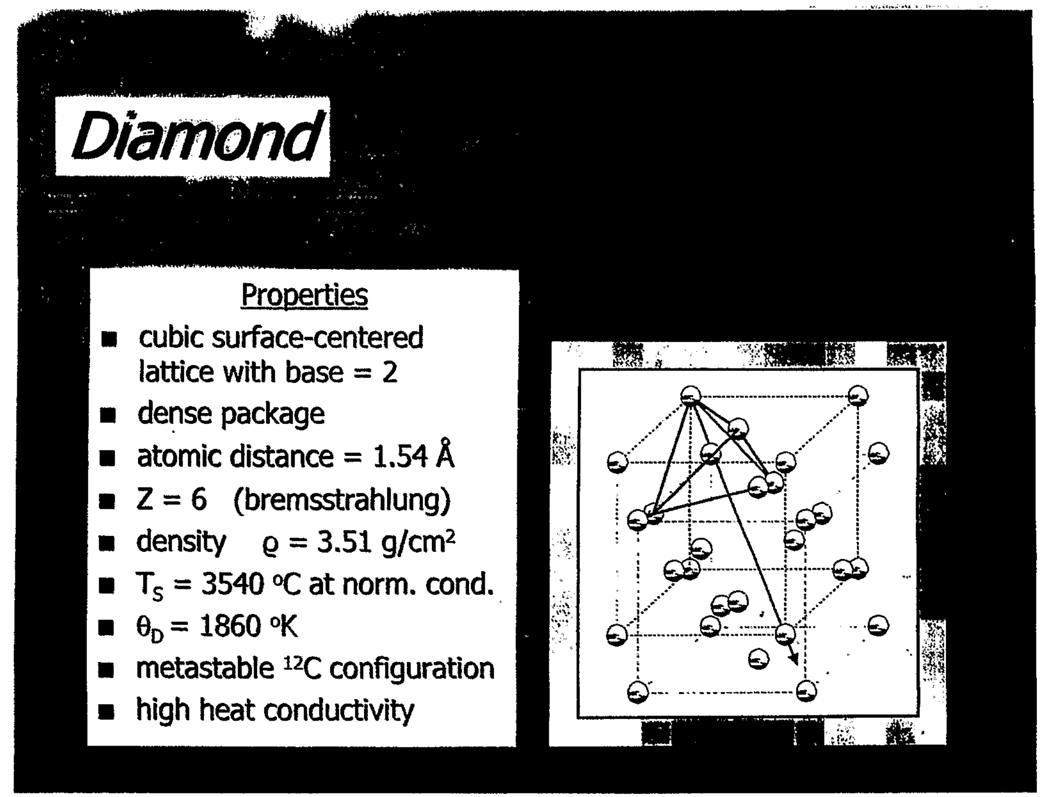

S-DALINAC data

Basic conditions

- E_e = 9 MeV ($\Delta E/E = 6 \cdot 10^{-3}$)
- i_e = 30 ÷ 60 μA
- ε_n = 3 π mm mrad
- diamond d = 55 μm
- planes {110}
- Ψ_{cr} = 2.6 mrad
- transition 1 - 0

Results

- $E_{1\text{-}0}$ = 7.9 keV
- $Y_{1\text{-}0}$ = 0.077 ph / sr e⁻
- $\Phi = 9.6 \cdot 10^{12}$ ph / sr · s
- $N_{1/3\gamma} = 1.1 \cdot 10^{10}$ ph / s

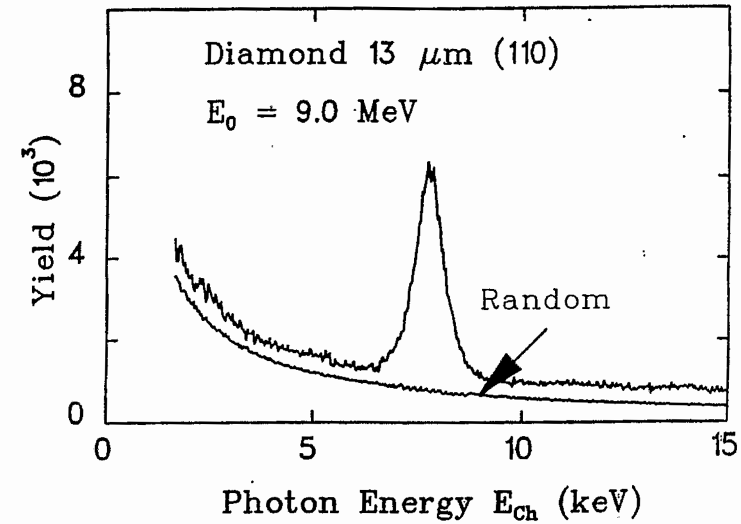

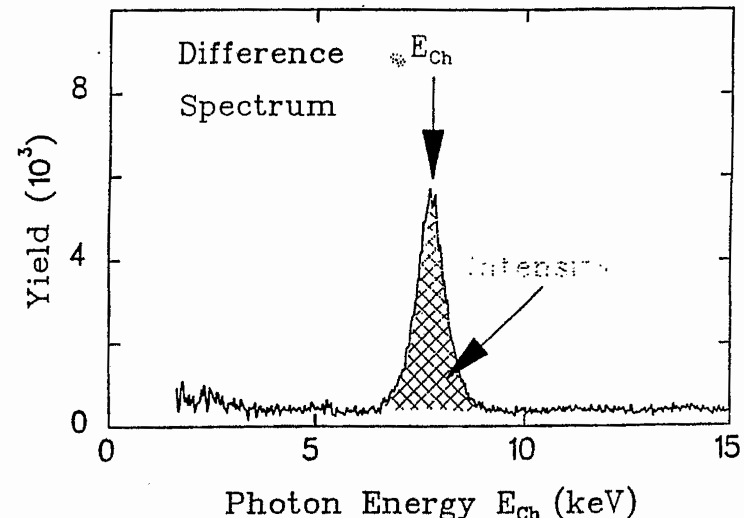

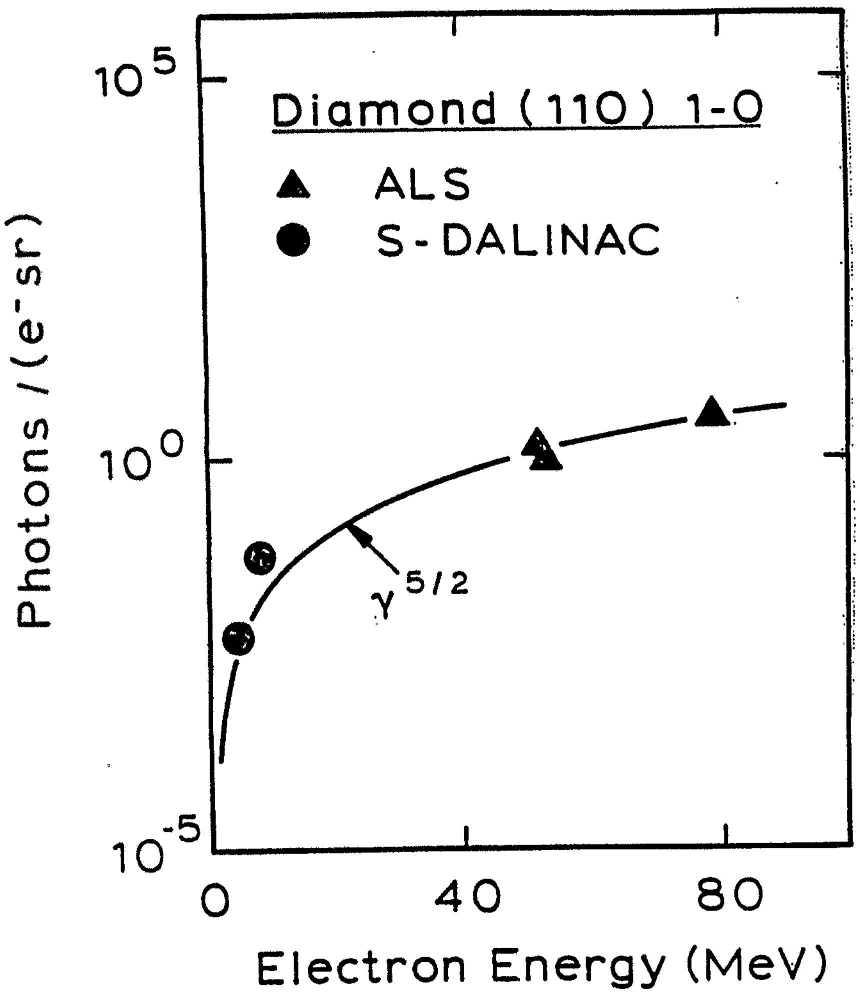

PRL-72, 2411

X-ray energy scaling

$$E_x = c\, E_e^{\,3/2}$$

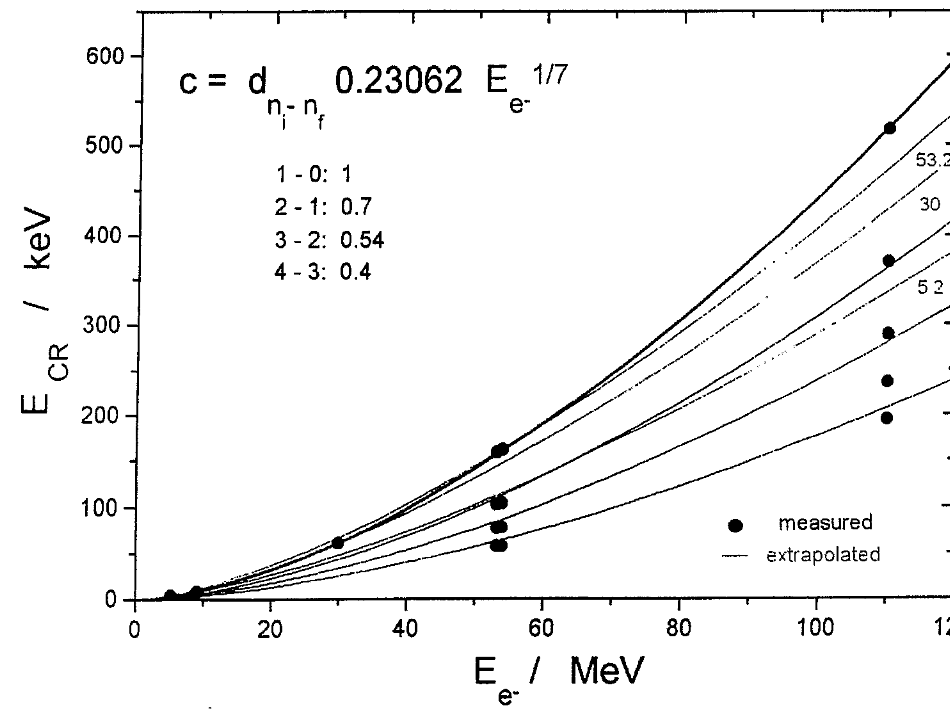

$$E_x = c'\, E_e^{\,3/2+1/7} = c'\, E_e^{\,23/14}$$

W. Wagner@fz-rossendorf.de

FZR
Postfach 51 01 19
D - 01314 Dresden

Occupation probability

De-channeling in diamond (1 1 0)

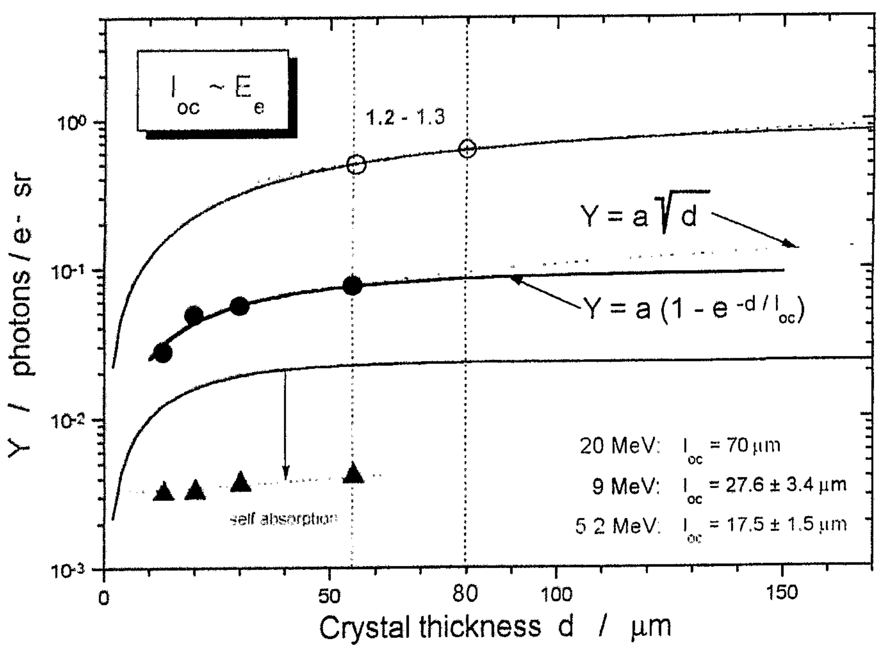

Amplifying factors

FZR

- larger beam current $\phi \sim i_e$
- higher electron energy $Y_e \sim \gamma^{5/2} \longrightarrow \gamma^{33/14}$
  $E_x \sim E_e^{3/2} \longrightarrow E_e^{23/14}$
- more narrow emission cone $\vartheta \sim 1/\gamma$
- less de-channeling $l_{oc} \sim E_e$
- larger crystal thickness $Y_e * 1.2$
- less self absorption $1/\mu(E_x) \sim E_e^{4.6}$

Planar channeling

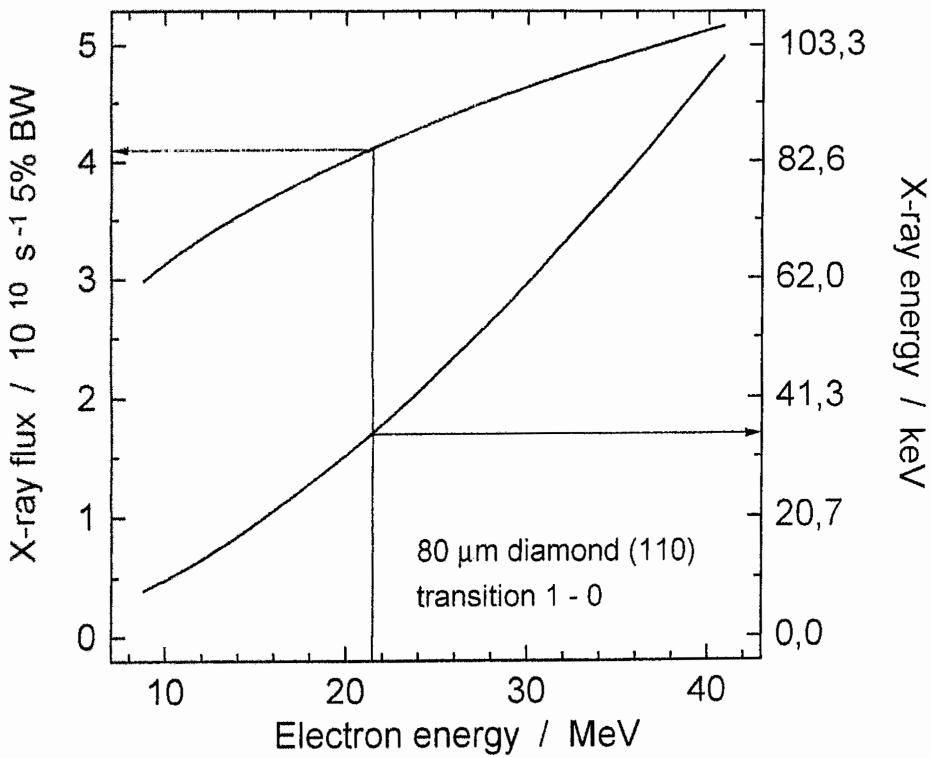

Planar channeling

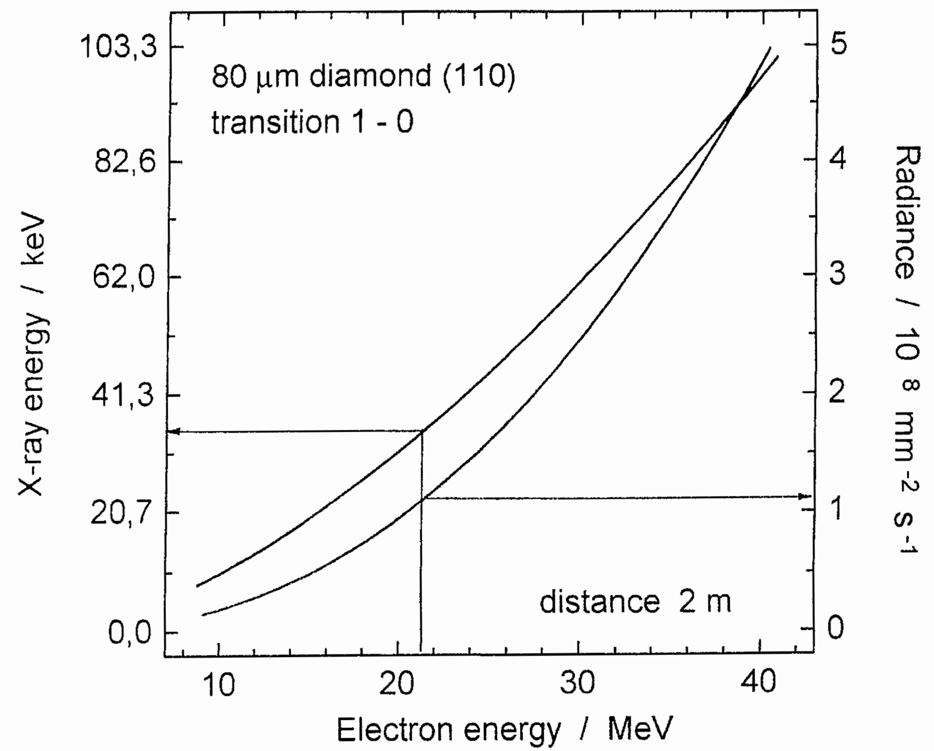

ELBE data *expected*

FZR

Basic conditions

- $E_e = 20$ MeV
- $\Delta E/E < 5 \cdot 10^{-3}$
- $i_e = 100\ \mu A$
- $\varepsilon_n \approx 1\ \pi$ mm mrad

- diamond $d = 80\ \mu m$
- planes {110}
- $\Psi_{cr} = 1.8$ mrad
- transition 1 - 0

CR data estimated

- $E_{1\text{-}0} = 29.36$ keV
- $Y_{1\text{-}0} = 0.61$ ph / sr e^-
- $d\Phi/d\Omega = 3.8 \cdot 10^{14}$ ph/sr s
- BW = 10 %

- $N_{1/3\gamma} = 8.2 \cdot 10^{10}$ ph/s

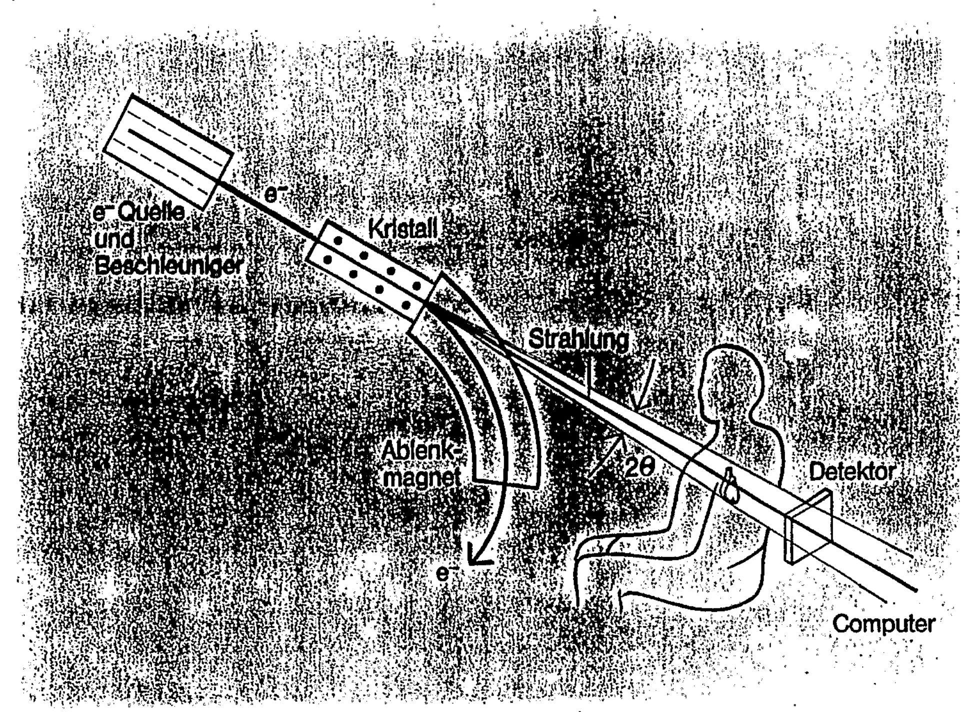

Angiographie mit Channelingstrahlung

Estimation with respect to DSA

Parameter	for $E_k(I)$	for $E_k(Gd)$
E_x / keV	33.17	50.24
Electron energy E_e / MeV	21.5	27.7
Yield Y / ph / e· sr	0.73	1.3
Flux density $d\phi / d\Omega$ / ph / sr s	4.55×10^{14}	8.2×10^{14}
$\theta_{5\%}$ / mrad	5.3	4.15
$\Delta\Omega_{5\%}$ / sr	8.9×10^{-5}	5.4×10^{-5}
Flux $\phi_{5\%}$ / ph / s	4.0×10^{10}	4.4×10^{10}
Distance d / m	2	2.5
Area A / mm ^{2} (D / mm)	355 (21.3)	338 (20.8)
Radiance / ph / mm ^{2} s	1.1×10^{8}	1.3×10^{8}
Fluence / ph / pixel (200 ms)	5.7×10^{7}	6.6×10^{6}
Required fluence / ph / pixel	1.8×10^{7}	6.0×10^{6}
Heart A = 3850 mm ^{2} at d / m	6.7	8.4
Fluence / ph / pixel (200 ms)	5.1×10^{6}	5.8×10^{5}
factors: current (2), thickness (2) monochromator (0.5)	(4)	(10)

W.Wagner@fz-rossendorf.de

FZR Postfach 51 01 19 D - 01314 Dresden

Comparison with DSA at NIKOS

(e$^+$ storage ring DORIS III at DESY Hamburg)

Parameter	for $E_k(I)$	
E_x / keV	33.17	
Electron energy E_e / GeV	4.5	
Heart at **NIKOS:** (simultaneous scanning at two energies)		
Radiance / ph / mm ^{2} s	2.7×10^{11}	
Fluence / ph / pixel	6.8×10^{7}	(3.8)
Required fluence / ph / pixel	1.8×10^{7}	
Heart at **ELBE:** (200 ms shot at one energy)		
Fluence / ph / pixel (200 ms)	5.1×10^{6}	(13)
factors: current 1 mA ???	10	

What agent concentration and what minimum irradiation area are acceptable for medics ???

What current can principally be operated ???

What image processing can provide ???

W.Wagner@fz-rossendorf.de

FZR Postfach 51 01 19 D - 01314 Dresden

Open problems

Energy loss in the crystal

$d = 80\ \mu m$

$i_e = 100\ \mu A$

- maximum heat conductivity

  $\lambda = 659\ W/m\ ^oK$

- high Debye temperature

  $\Theta_D = 1860\ ^oK$

- low heat radiation

- $\Delta E \approx 112$ keV per e^-

  $P_{100\mu A} \approx 11.2$ W

  $Q \approx 91\ W/mm^2$

- heat transport through crystal holder (cooling)
- crystal temperature 400 °C

  ⇒ maximum temperature ?

  ⇒ ultrahigh vacuum (10^{-7}mbar) ?

  ⇒ channel damage ?

  ⇒ crystal standing time ?

Bremsstrahlung

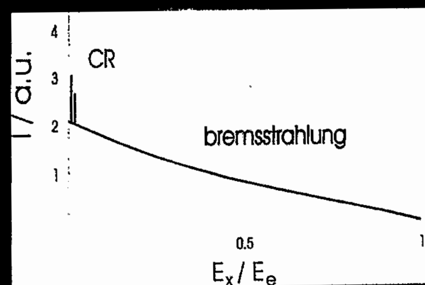

- $d^3N_B/d\Omega dE_x dz \sim \rho\, Z^2 \gamma^2 / E_x$
- $E_x \sim \gamma^{3/2}$
- $d^2N_{cr}/d\Omega dE_x \sim \gamma^{5/2}$
- $N_{cr}/N_B \sim \gamma^2$

Simulation of bremsstrahlung (W. Neubert)

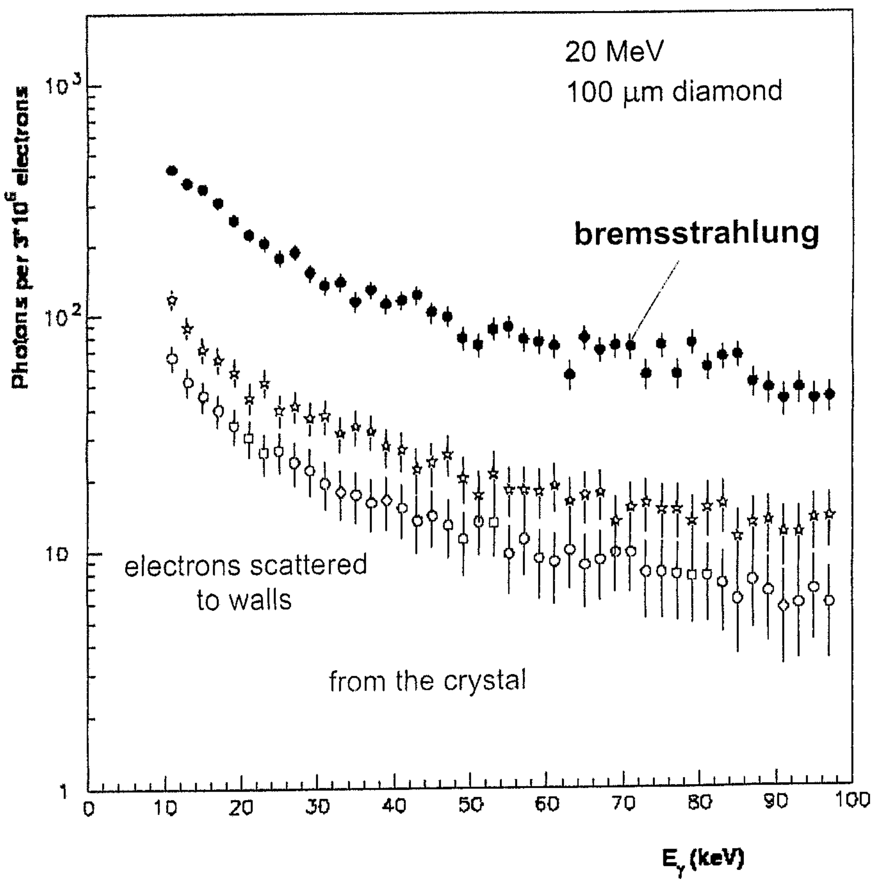

Quasi-monochromatic X-ray beams

Reduction of bremsstrahlung background

Bragg reflection :

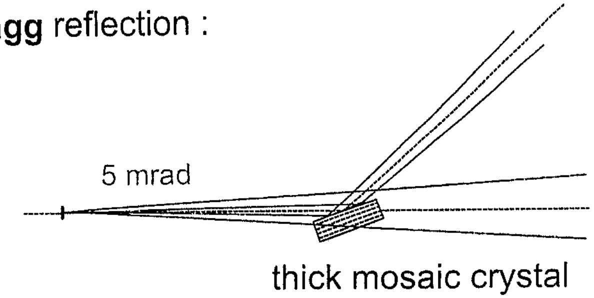

Intensity loss about 50 %

Dynamical **Laue** diffraction :

- temperature (T) gradient
- acoustic field

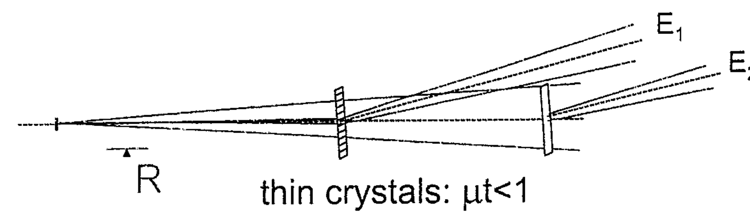

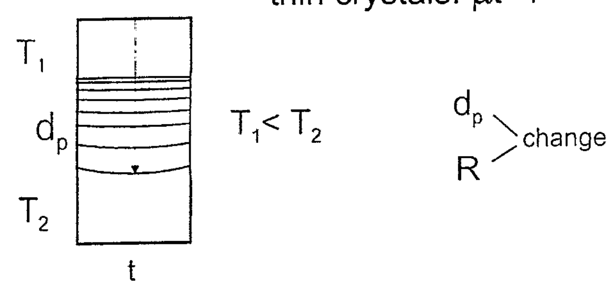

Theory predicts: Deflected intensity up to nearly 100 % !

Dynamical Laue diffraction

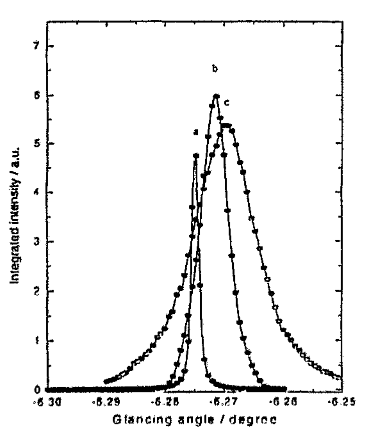

- E_x = 17 keV (ROBL ESRF)
  $\Delta E/E \approx 10^{-4}$
- quartz single crystal :
  $\mu t < 1$
- ultrasound :
  $\lambda = 2t$
- dynamical diffraction on acoustic superlattice of {10-11} planes
- increase of the integrated reflection power

Transmission

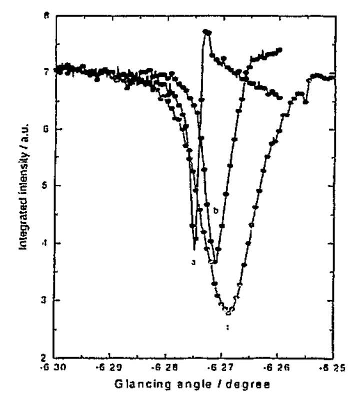

- E_x = 17 keV (ROBL ESRF)
  $\Delta E/E \approx 10^{-4}$
- quartz single crystal :
  $\mu t < 1$
- ultrasound :
  $\lambda = 2t$
- transmission near Θ_B
- decrease of transmission down to nearly total deflection

PXR at MAMI Mainz (A. Mkrtchyan)

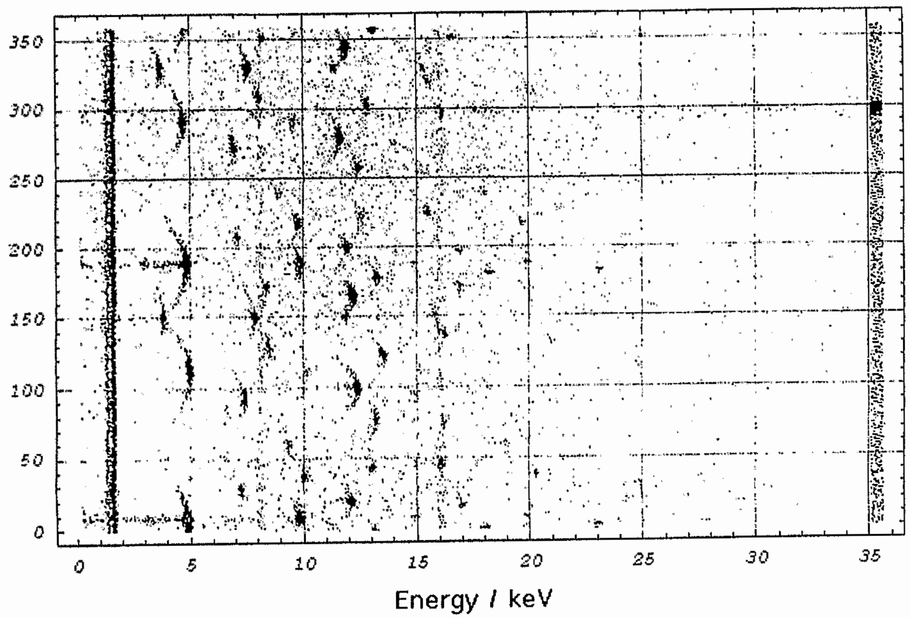

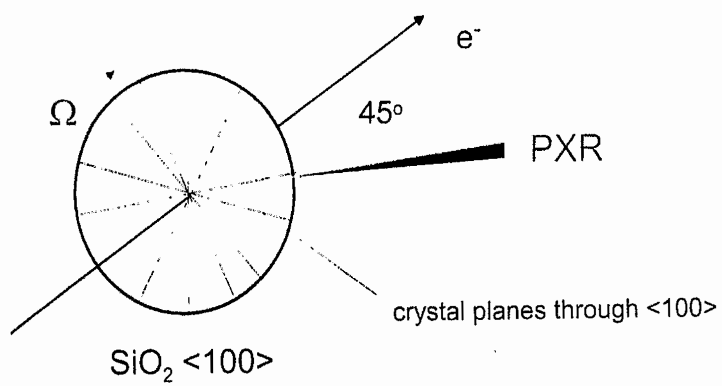

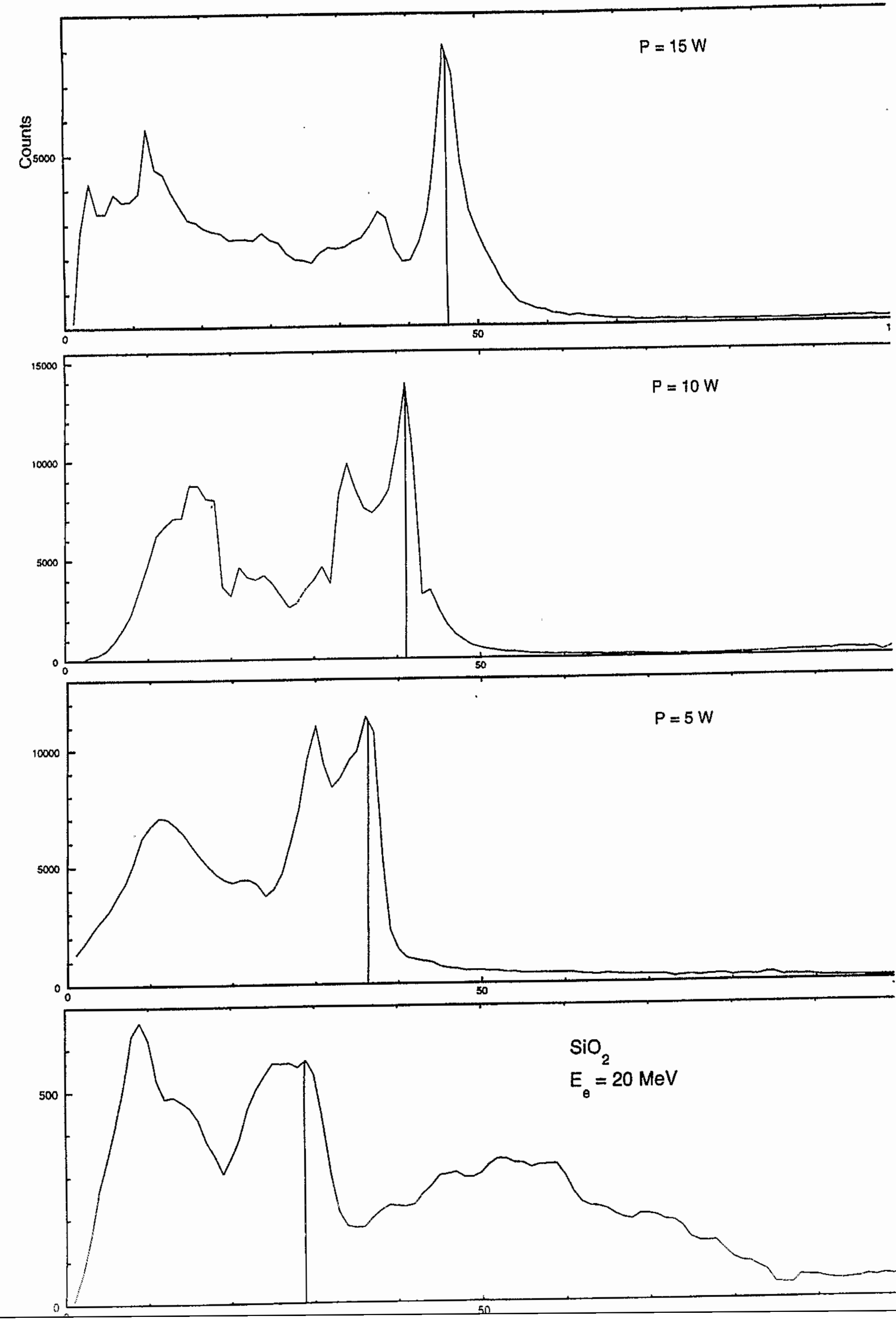

W. Wagner@fz-rossendorf.de

FZR
Postfach 51 01 19
D - 01314 Dresden

Summary

1. Intense tunable non-conventional X-ray sources can be obtained at the electron beam of ELBE using

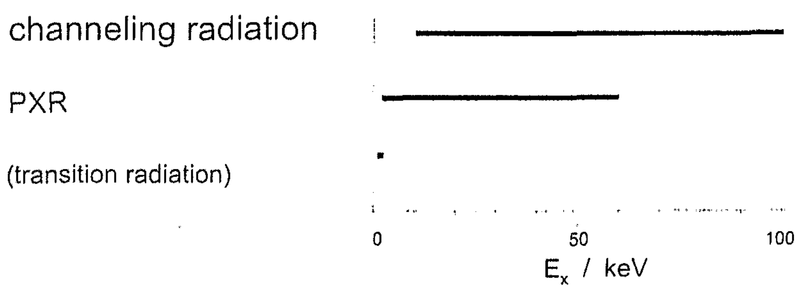

2. Bremsstrahlung background can be reduced by BRAGG reflection or dynamical Laue diffraction applying ultrasound.

3. Application of DSA would need maximum beam current (1 mA), but not continuously (makropulses), and image processing.

4. First application of CR: cell irradiation (J. Pawelke).

5. New method of structure analysis with PXR (A.H. Mkrtchyan).

6. Stimulation of CR by ultrasound (A.R. Mkrtchyan).

W.Wagner@fz-rossendorf.de

FZR
Postfach 51 01 19
D - 01314 Dresden

H. Backe:

Selected topics of X-ray research at MAMI

Selected Topics of X-Ray Research at MAMI

(H. Backe, Workshop on X rays from electron beams, February 24-26, 2000)

1. Introduction
2. Novel Interferometer with two Spatially Separated, Phase Correlated X-Ray Sources
3. Investigation of Parametric X Radiation
4. Transition Radiation as a Hard X-Ray Source
5. Conclusion

Mainz Microtron MAMI

E = 0.855 GeV
I = 100 μA c.w.
I_{peak} = 0.1 A
$\sigma_x = 7\,\pi$ nm rad (1σ)
$\sigma_y = 1\,\pi$ nm rad (1σ)

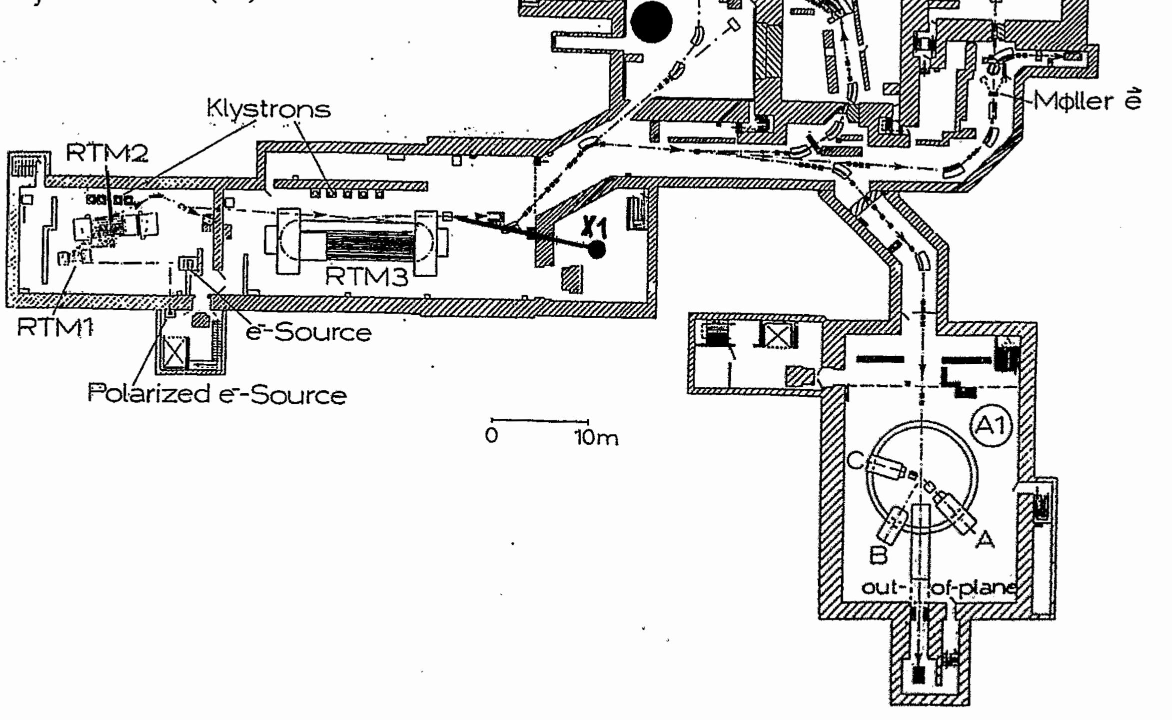

Processes

Channeling Radiation (CR)

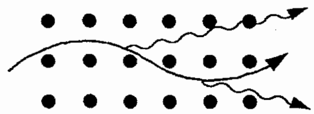

Parametric X-rays (PXR)

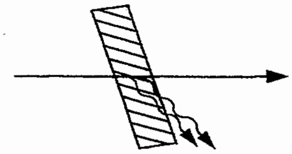

Transition Radiation (TR)

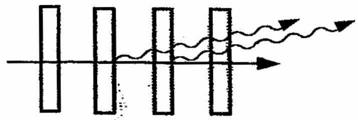

Undulator Radiation (UR)

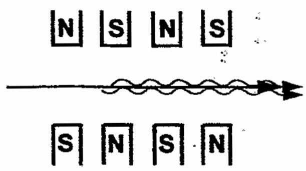

Smith-Purcell Radiation (SP)

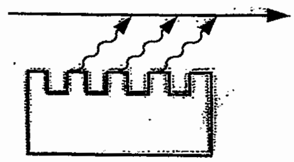

X-ray Radiation Research at MAMI

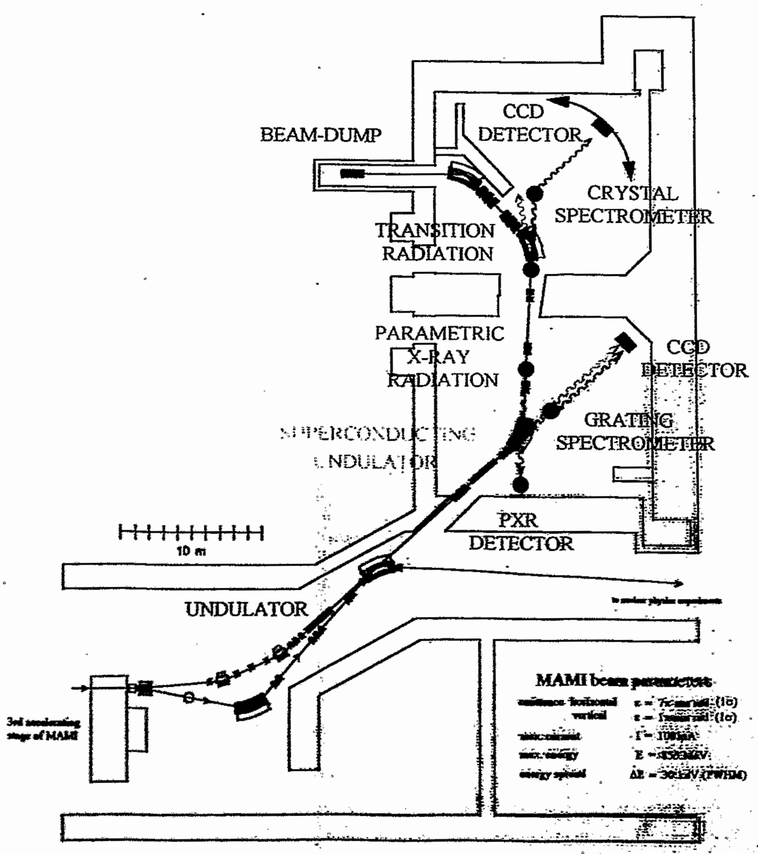

The Complex Index of Refraction

$$n(\omega)=1-\delta(\omega)-i\beta(\omega)$$

Dispersion — $\delta(\omega)$; Absorption — $\beta(\omega)$

$$A_m(x,t) = A_0 e^{i\left(\omega t - n(\omega)\frac{\omega}{c}x\right)}$$

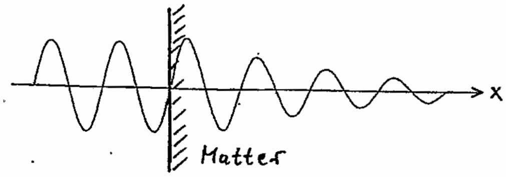

$$A_m(x,t) = \underbrace{e^{-\frac{\omega}{c}\beta(\omega)x}\, e^{i\frac{\omega}{c}\delta(\omega)x}}_{A_{m0}(x)} \cdot \underbrace{A_0 e^{i\left(\omega t-\frac{\omega}{c}x\right)}}_{\text{vacuum reference wave}}$$

Attenuation: $\left|A_{m0}(x)\right| / \left|A_0\right| = e^{-\frac{\omega}{c}\beta(\omega)x}$

Phase Shift: $\phi(x) = \phi_{0m}(x) - \phi_{vac}(x) = \frac{\omega}{c}\delta(\omega)x$

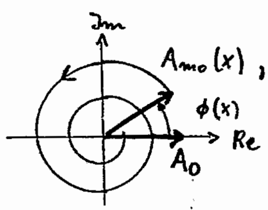

$\delta(\omega) > 0,\ n_r(\omega) = 1-\delta(\omega) < 1$

Motivation - Interferometer

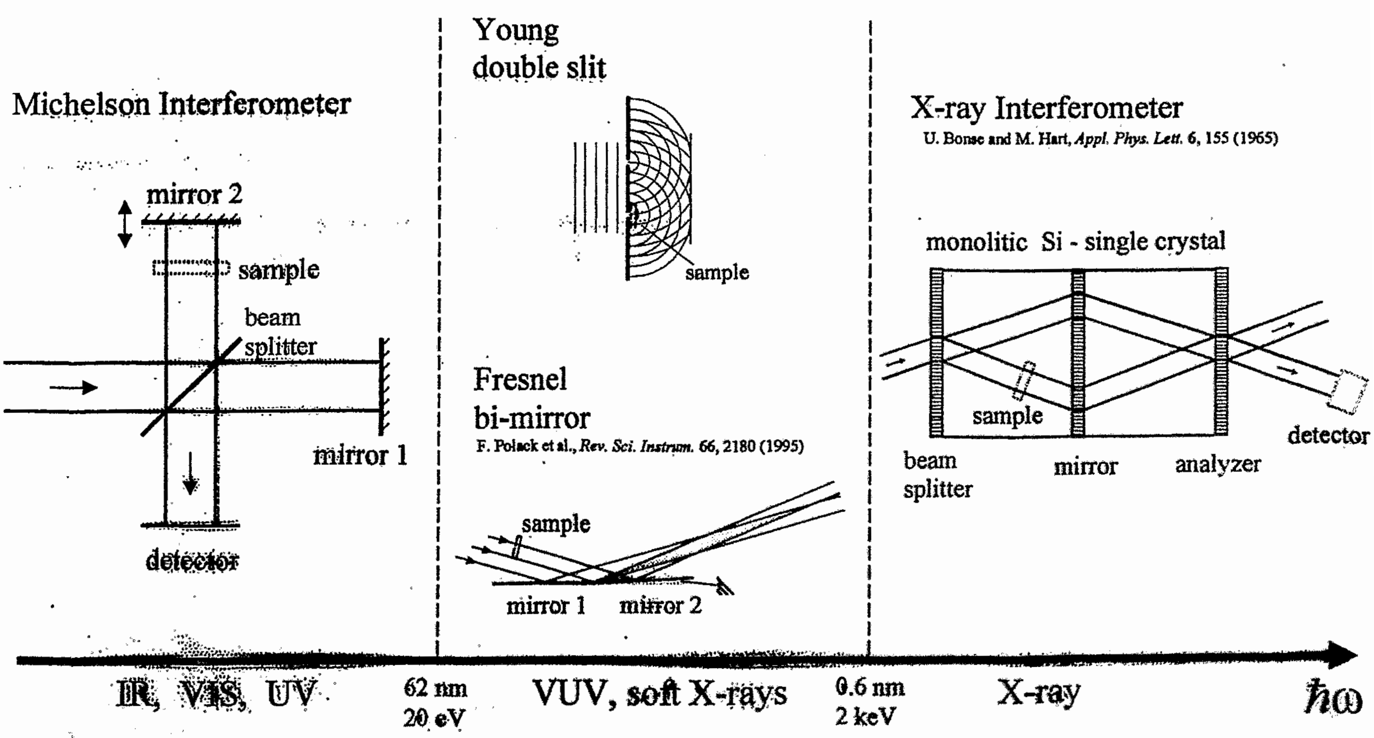

Novel Interferometer with two Spatially Separated, Phase Correlated X-Ray Sources

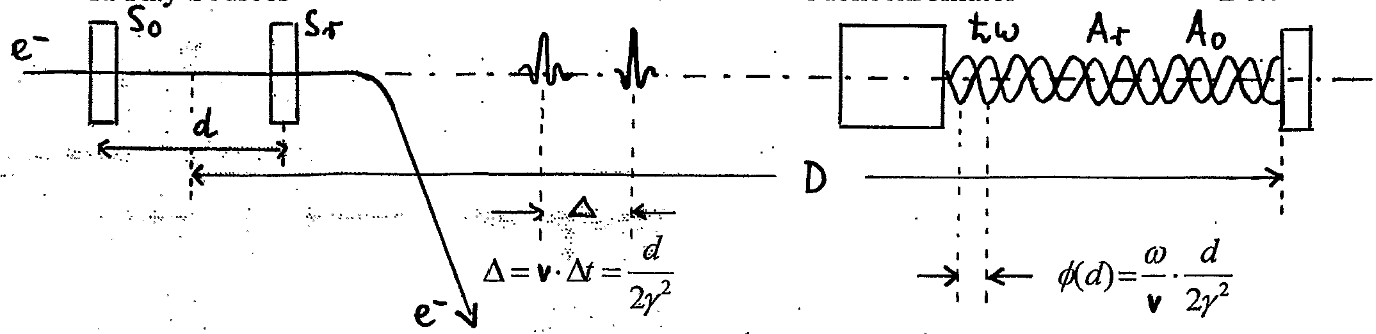

$$\Delta = v \cdot \Delta t = \frac{d}{2\gamma^2}$$

$$\phi(d) = \frac{\omega}{v} \cdot \frac{d}{2\gamma^2}$$

$$E = \gamma \cdot m_e c^2, \quad \gamma = \frac{1}{\sqrt{1-\beta^2}}, \quad \beta = \frac{v}{c}$$

Interference Oscillations

$$|A(d)|^2 = |A_r|^2 + |A_0|^2 + 2 \cdot |A_r| \cdot |A_0| \cos\phi(d)$$

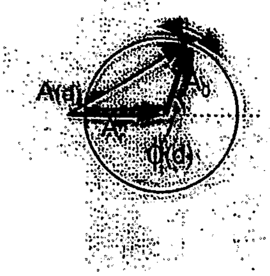

Coherence:

$$C = \frac{I_{max} - I_{min}}{I_{max} + I_{min}}$$

($C = 1$ ideally)

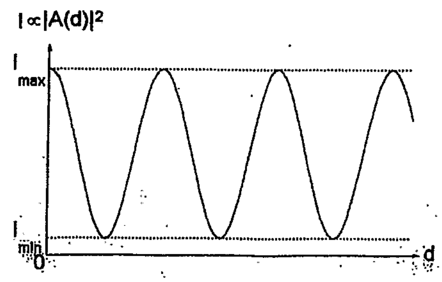

Soft X-Ray Interferometer
with Undulator Radiation

Basic Principle of the Interferometer

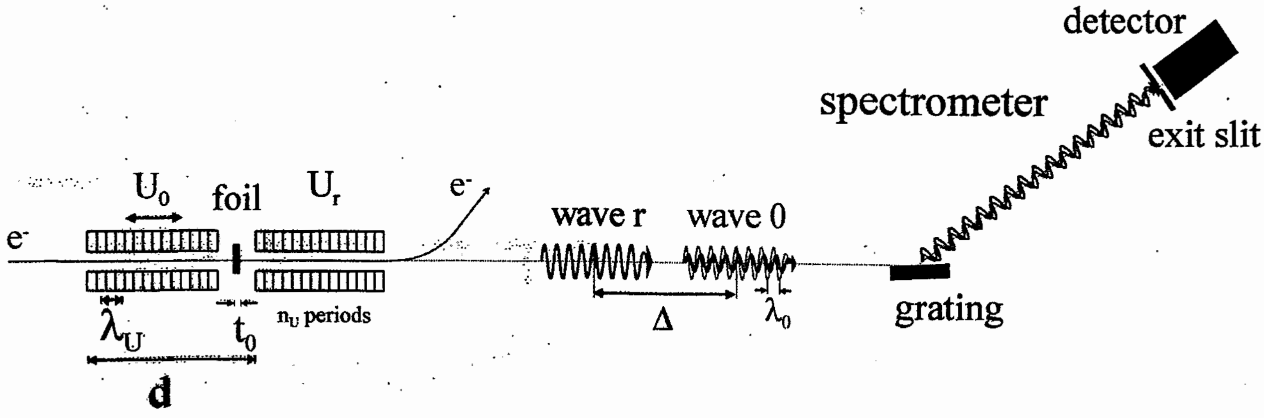

$$\Delta = \frac{d}{2\gamma^2}\left(1 + (\gamma\theta)^2\right) + \frac{K^2}{4\gamma^2} L_U \qquad \lambda_0 = \frac{\lambda_U}{2\gamma^2}\left(1 + \frac{K^2}{2} + (\gamma\theta)^2\right)$$

Intensity:

$$\boxed{I = |A_r|^2 + |A_0|^2 \exp\left[-2\frac{\omega}{c}\beta(\omega)t_0\right] + 2|A_r||A_0| \exp\left[-\frac{\omega}{c}\beta(\omega)t_0\right] \cos\left[\frac{\omega}{c}(\Delta+\delta(\omega)t_0)\right]}$$

Experimental Setup

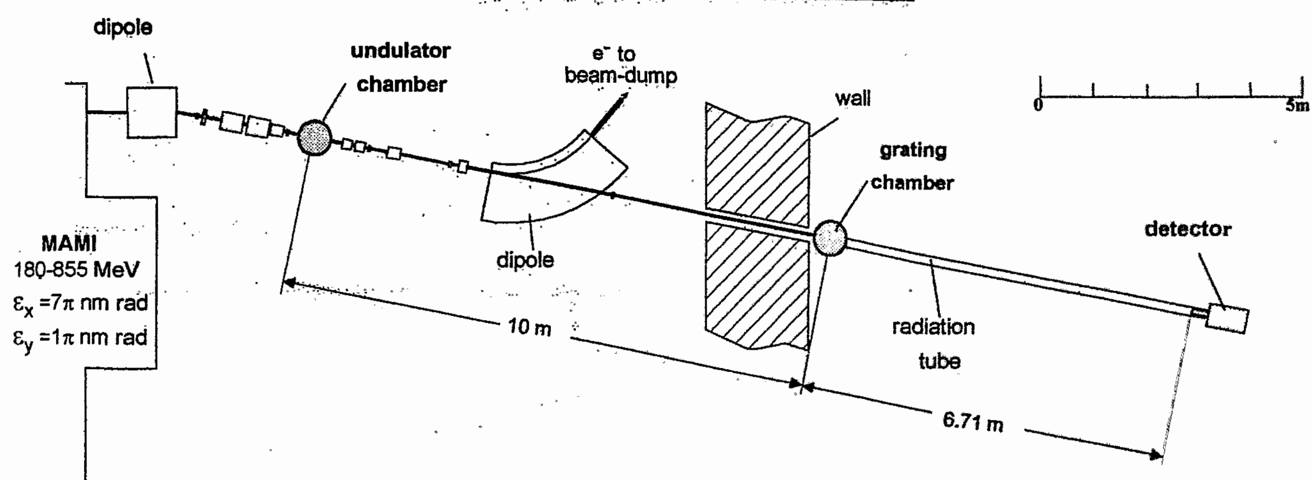

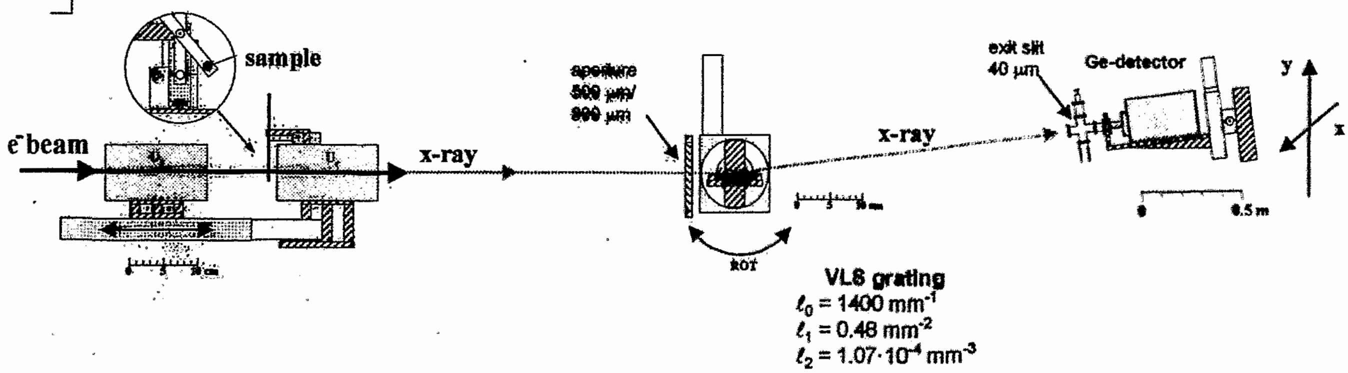

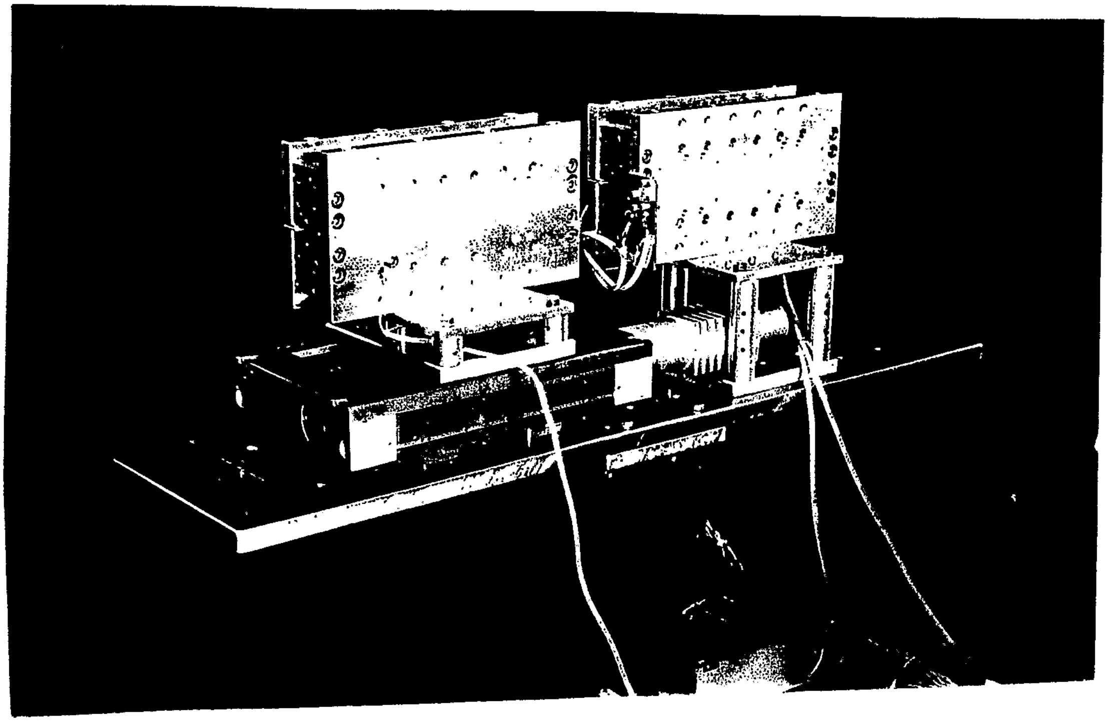

Oscillations

black: without foil
red: 65 $\mu g/cm^2$ C-foil

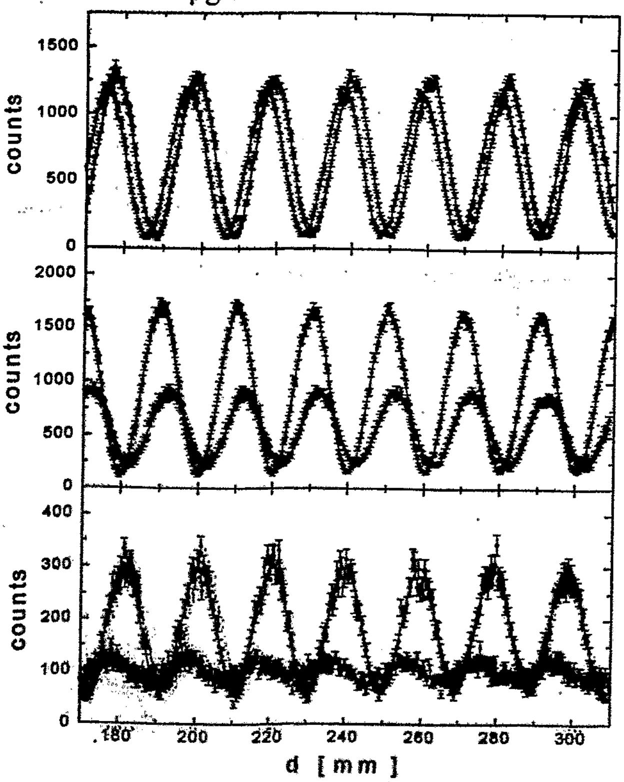

$\lambda_{osc} = 20.68$ mm
$\hbar\omega = 279.6$ eV

$\lambda_{osc} = 20.09$ mm
$\hbar\omega = 287.8$ eV

$\lambda_{osc} = 19.50$ mm
$\hbar\omega = 299.4$ eV

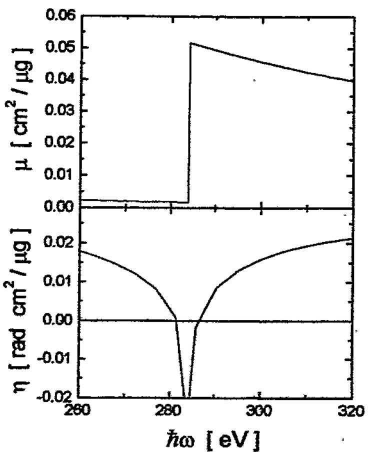

[]Henke et al, *Atomic Data and Nuclear Tables*, Vol.54, No.2 (1993)

Atomic Scattering Factors f_1, f_2
and the
Kramers-Kronig- Dispersion Relation

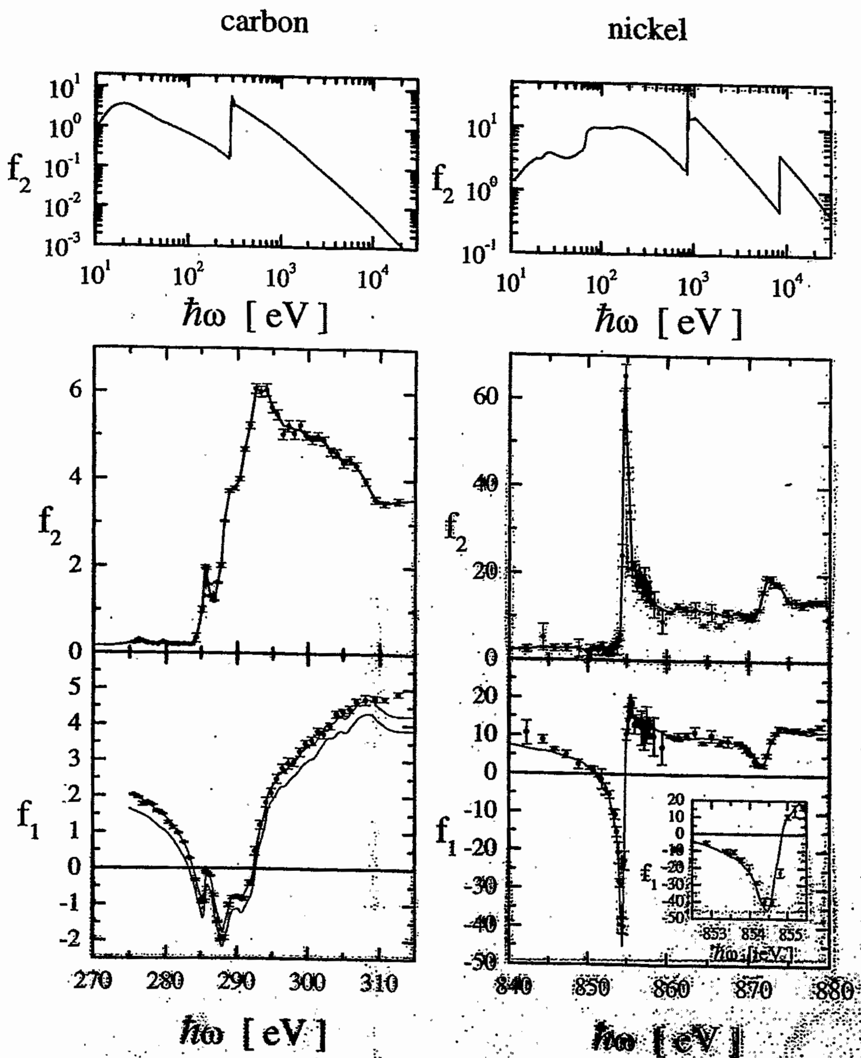

Development
of a Hard X-Ray Interferometer
with Transition Radiation

Transition Radiation

from single interface

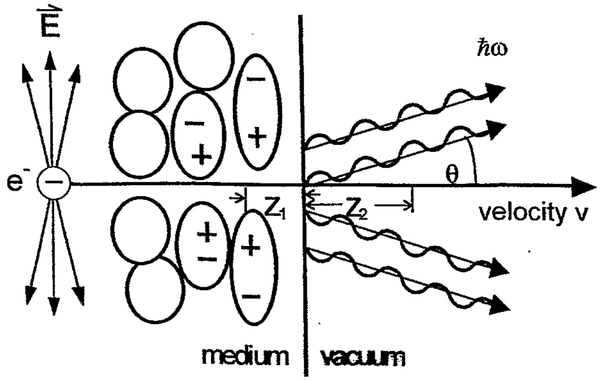

single interface intensity:

$$I_0 = \frac{d^2 N_0}{(d\hbar\omega/\hbar\omega)\, d\Omega} = \frac{\alpha\theta^2\omega^2}{16\,\pi^2 v^2}\,(Z_1 - Z_2)^2$$

formation length:

$$Z_i = \frac{4c}{\omega}\,(\gamma^{-2} + \theta^2 + \omega_p^2/\omega^2)^{-1}$$

plasma frequency $\omega_p^2 = 4\pi\, r_e\, c^2\, n_a Z$

atomic density n_a

classical electron radius $r_e = 2.818$ fm

Features of Transition Radiation
(single interface)

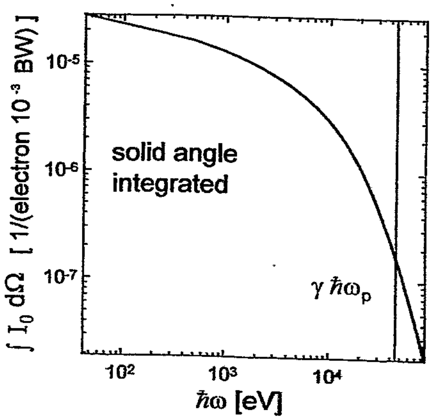

$\hbar\omega_p = 26.2$ eV (Be)

$\gamma = 1673$

$\gamma\,\hbar\omega_p = 44$ keV

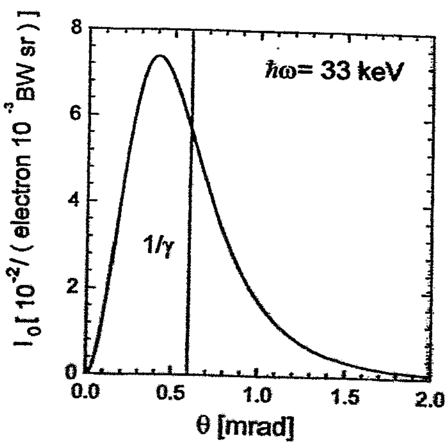

$\theta_{max} \approx 1/\gamma$

≈ 0.6 mrad

Transition Radiation

from single foil:

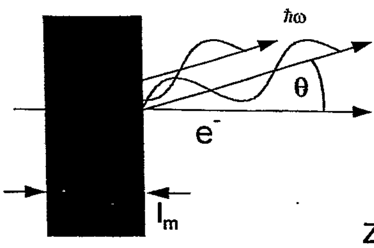

$$\frac{d^2 N_0}{(d\hbar\omega/\hbar\omega)\, d\Omega} = I_0 \cdot 4\sin^2\left(\frac{l_m}{Z_m}\right)$$

$$Z_m = \frac{4c}{\omega}\left(\gamma^{-2}+\theta^2+\omega_p^2/\omega^2\right)^{-1}$$

from two foils:

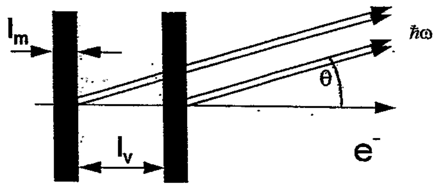

$$\frac{d^2 N_0}{(d\hbar\omega/\hbar\omega)\, d\Omega} = I_0 \cdot 4\sin^2\left(\frac{l_m}{Z_m}\right) \cdot 4\cos^2\left(\frac{l_m}{Z_m}+\frac{l_v}{Z_v}\right)$$

Transition Radiation Interferometry

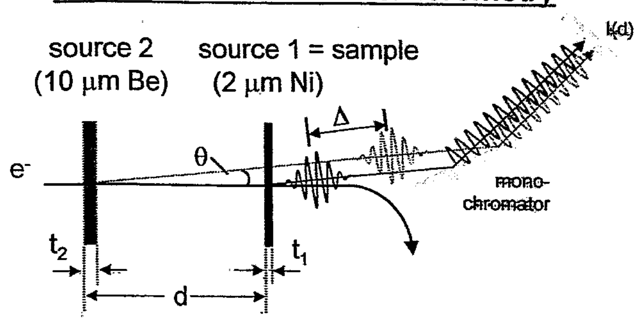

$$I(\theta,d) = |A_1|^2 + |A_2|^2 e^{-\sigma_1} + 2|A_1||A_2|\, e^{-\sigma_1/2} \times \cos\left\{\frac{\omega}{v}\Delta'(\theta,d) + \phi_1 + \arctan\left\{\frac{e^{-\sigma_1/2}\sin\phi_1}{1-e^{-\sigma_1/2}\cos\phi_1}\right\} - \arctan\left\{\frac{e^{-\sigma_2/2}\sin\phi_2}{1-e^{-\sigma_2/2}\cos\phi_2}\right\}\right\}$$

$\Delta'(\theta,d) = 1/2\,(\gamma^{-2}+\theta^2)(d - t_2) \quad \Rightarrow d = 0.01$ mm ..10 mm

$$A_i = \frac{\sqrt{\alpha}}{\pi}\,\theta\left\{\frac{1}{\gamma^{-2}+\theta^2+2\delta_i} - \frac{1}{\gamma^{-2}+\theta^2}\right\}\left(1+e^{-\sigma_i}-2\,e^{-\sigma_i/2}\cos\phi_i\right)$$

$$\phi_i = \frac{\omega t_i}{2v}\left(\gamma^{-2}+\theta^2+2\delta_i\right) \qquad \sigma_i = 2\,\frac{\omega}{c}\,\beta_i t_i$$

absolute measurement of foil distance d necessary

Experimental Set-up

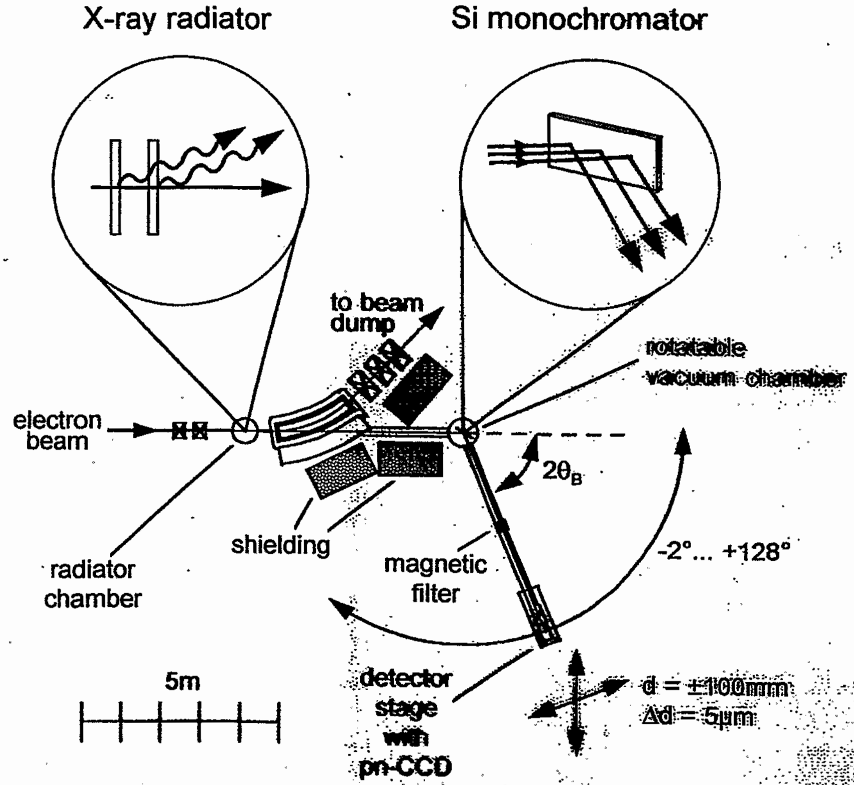

Complex Index of Refraction

$$n(\omega) = 1 - \delta(\omega) - i\beta(\omega)$$

dispersion ⇒ phase shift
absorption ⇒ attenuation

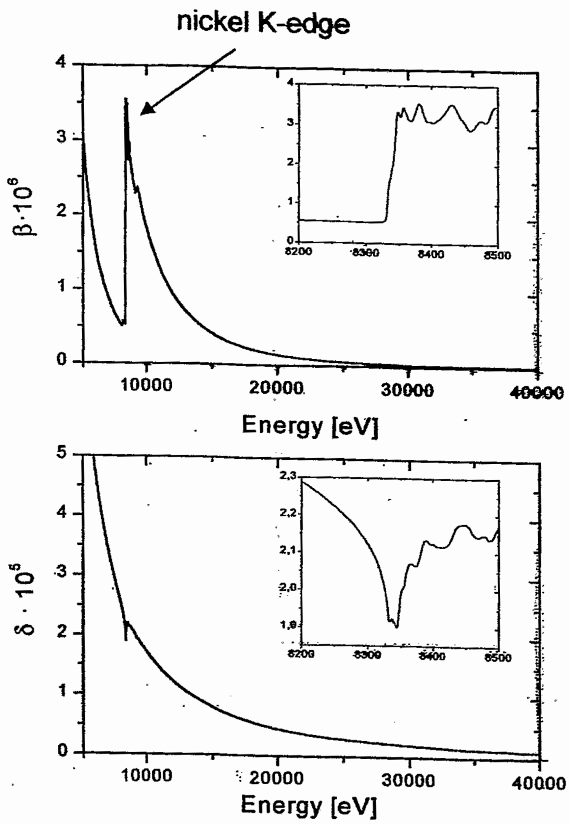

Energy Spectrum

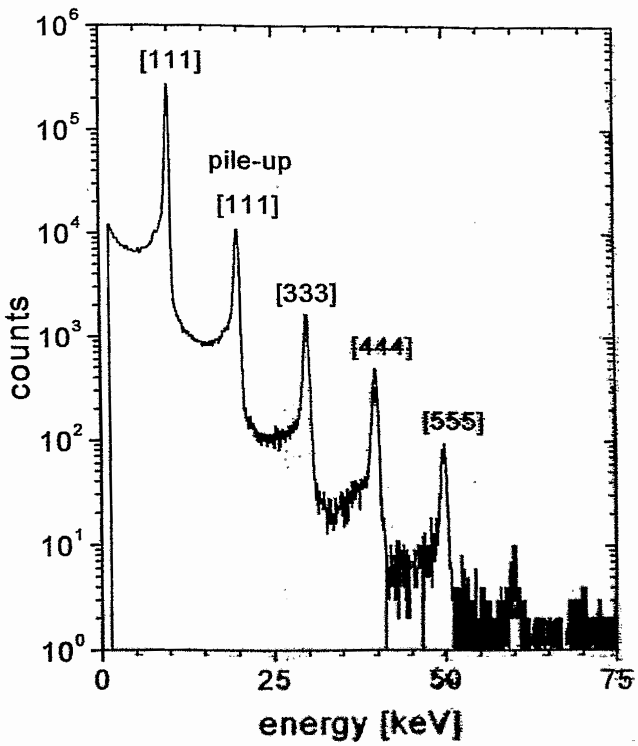

Fit of two dimensional TR Distribution

10 μm Be, 2 μm Ni, d =263 μm, $\hbar\omega$ = 9925 eV

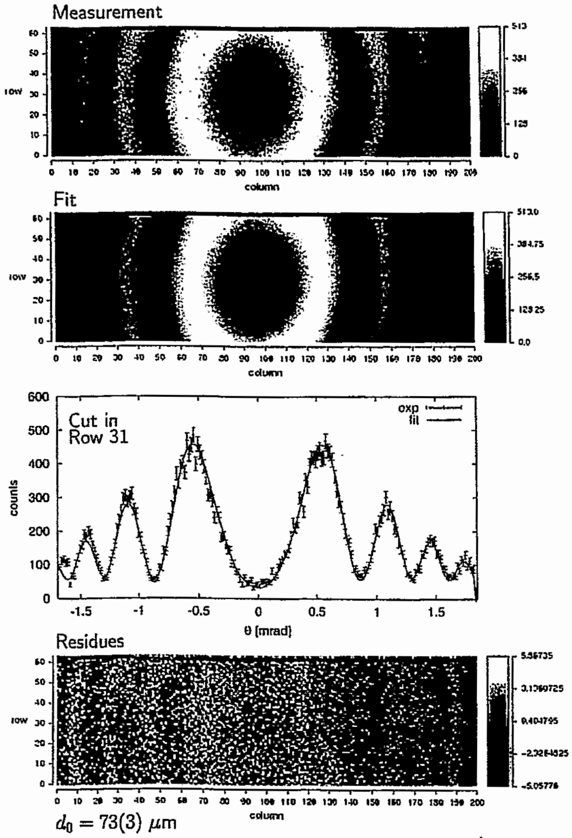

$d_0 = 73(3)$ μm

$\sigma_0 = 33(5)$ μrad [$\sigma_x = 250(12)$ μm, $\sigma_y = 138(4)$ μm]

Fit of two dimensional TR Distribution

10 μm Be, 2 μm Ni, d =668 μm, $\hbar\omega$ = 9925 eV

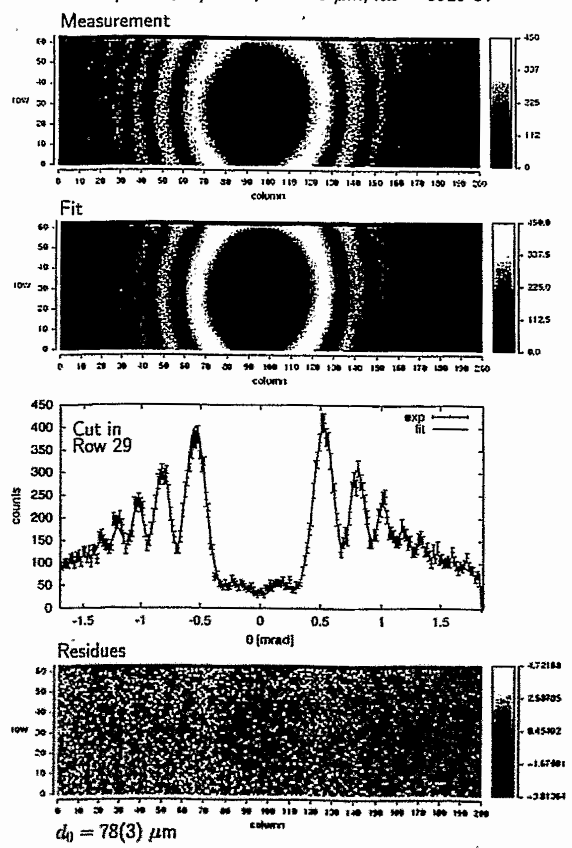

$d_0 = 78(3)$ μm

$\sigma = 25(5)$ μrad [$\sigma_x = 250(12)$ μm, $\sigma_y = 138(4)$ μm] fits of simulations at fixed θ and fixed $\hbar\omega$=9975 eV

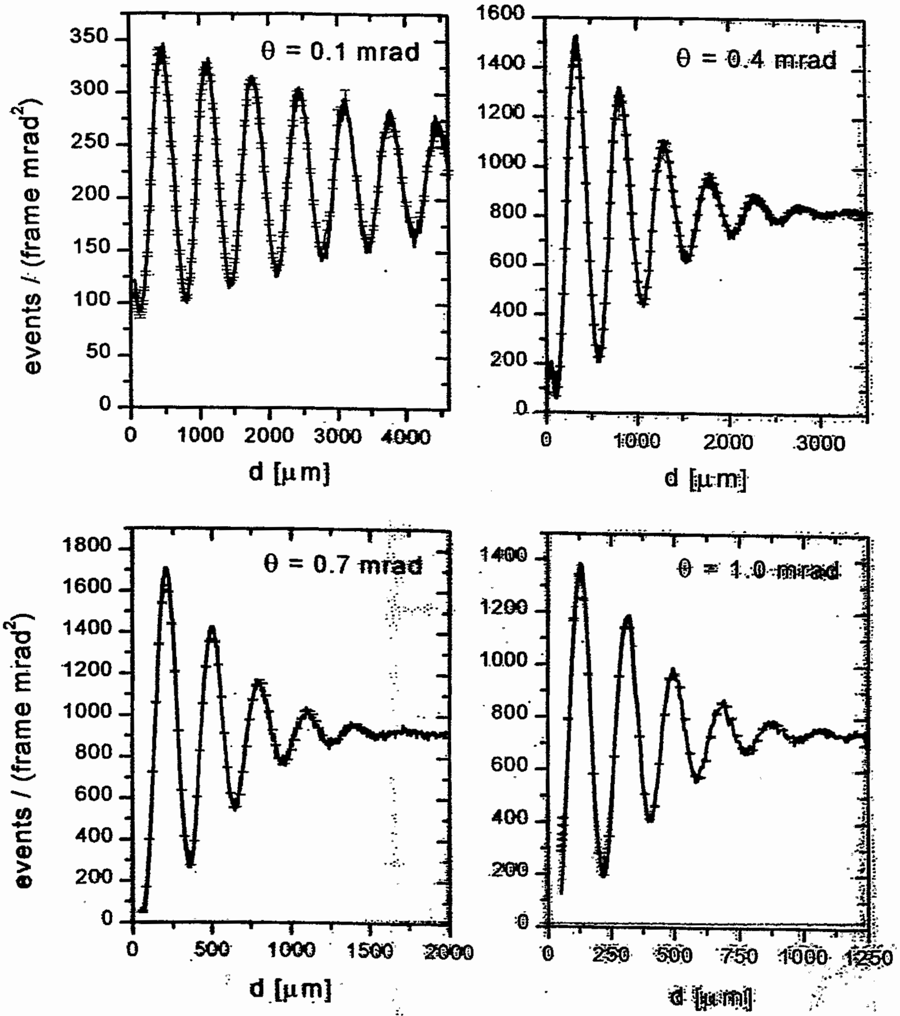

Preliminary Results

Dispersion δ of Nickel

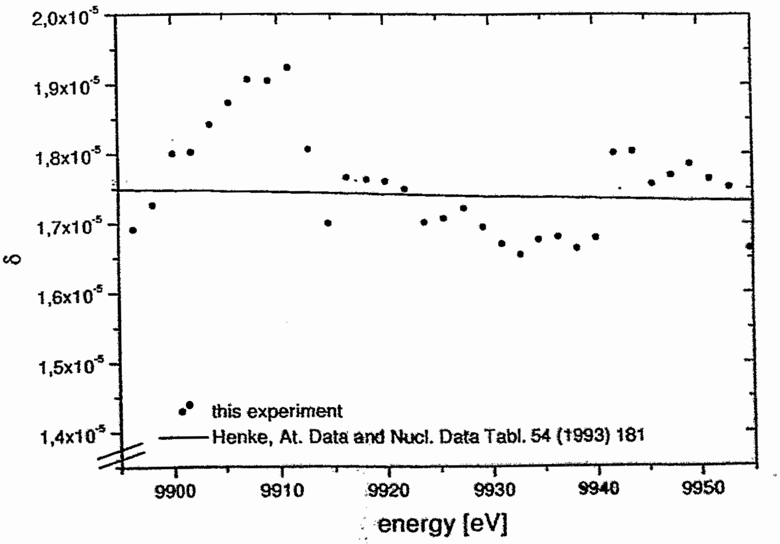

Parametric X-Ray Radiation

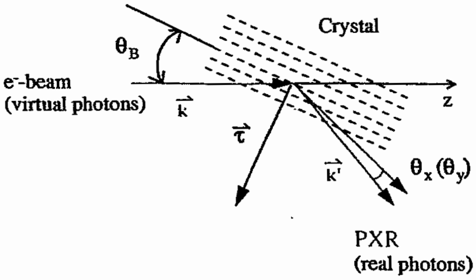

Bragg Condition

$\vec{k}'^2 = (\vec{k} + \vec{\tau})^2$

$n\lambda = 2\,d\,\sin\theta_B$

Feranchuk-Ivashin Model

$$\frac{d^2N}{d\theta_x d\theta_y} = \frac{\alpha}{\pi}$$ — coupling strength

$$\cdot |\chi_T|^2$$ — crystal structure factor

$$\cdot L_{eff}$$ — effective absorption length (self absorption)

$$\cdot \frac{\hbar\omega_B/\hbar c}{4\sin^2\theta_B}\,\frac{\theta_x^2\cos^2(2\theta_B)+\theta_y^2}{(\theta_x^2+\theta_y^2+\theta_{ph}^2)^2}$$ — angular distribution

$L_{eff} = \int e^{-f(z)/L_a} dz$ $\qquad \theta_{ph} = (1/\gamma^2 + |\chi_0|)^{1/2}$ $\quad , |\chi_0| \simeq \left(\frac{\omega_p}{\omega}\right)^2$

$f(z)$ - distance to crystal surface ; ω_p - plasma frequency

L_a - absorption length

Theoretical Angular Distribution

(I.D Feranchuk & A.V. Ivashin: J.Physique, **46** (1985)1981)

Si (111), $\theta_B = 22.5°$

$\theta_{ph} = (1/\gamma^2 + |\chi_0|)^{1/2}$ $\quad , |\chi_0| \simeq \left(\frac{\omega_p}{\omega}\right)^2, \hbar\omega_p = 31\text{eV}$

$\gamma = 1673$

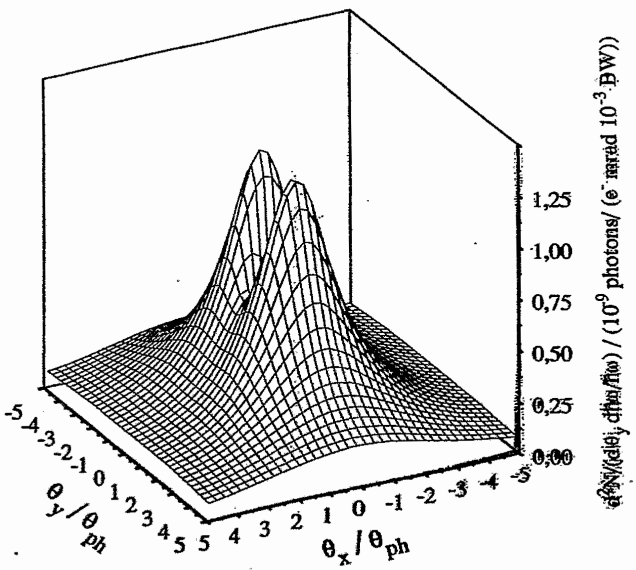

Investigation of the Production Mechanism of Parametric X-ray Radiation

K.-H. Brenzinger et al., Z. Phys. A 358 (1997) 107

Silicon (220) ; $\theta_B = 22.5°$; $\hbar\omega = 8420$ eV at maximum

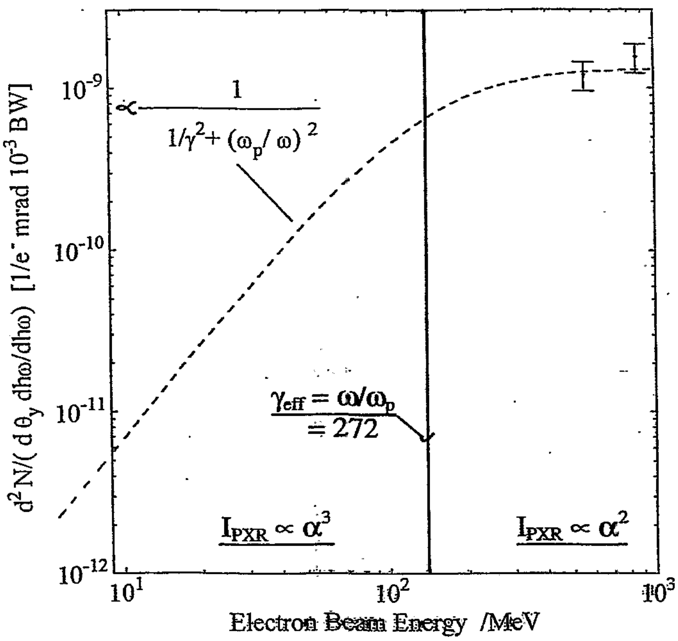

How Narrow is the Line Width of Parametric X-ray Radiation

K.-H. Brenzinger et al., Phys. Rev. Lett. 79 (1997) 2462

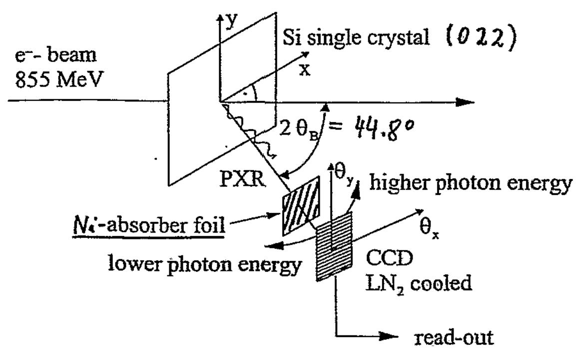

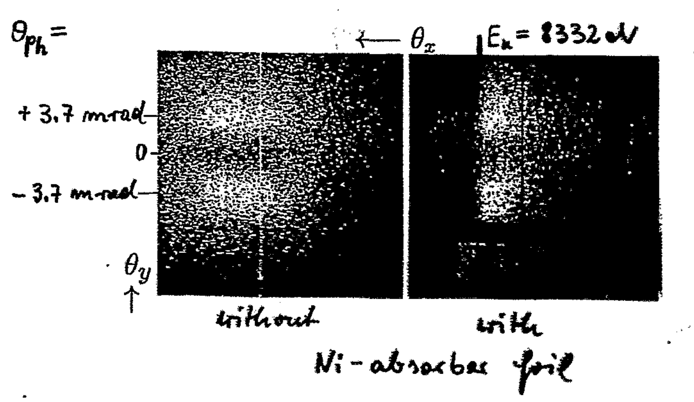

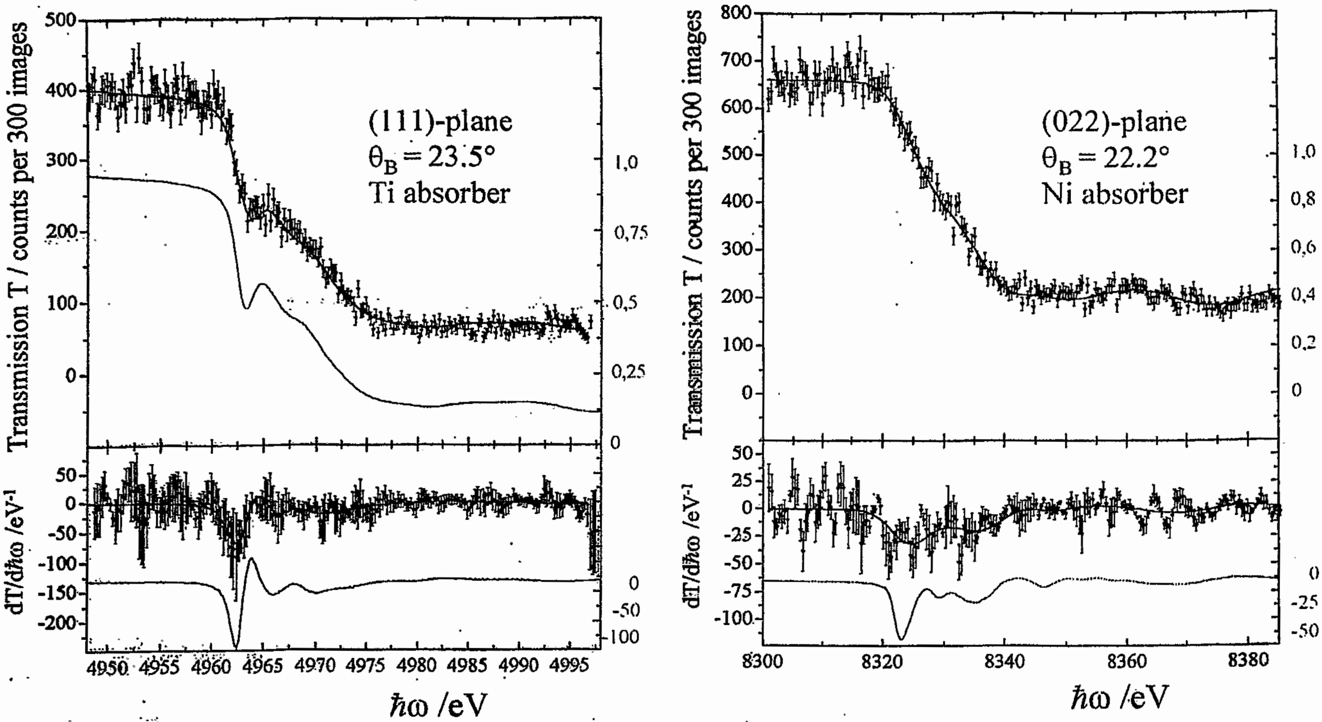

Fitfunction:

$$f_{fit}(E) = N\int \left[T_{\mu a}(E') \otimes g(E', \theta_x)\right] I_{PXR}(\theta_x, \theta_y)\, d\theta_y$$

$$\Delta E_{PXR} = \Delta E_{intr.} \otimes \Delta E_{geo}$$

$$\Delta E_{PXR,(111)} \leq 1.2 \text{ eV (95\%CL)}$$

$$\Delta E_{PXR,(022)} \leq 3.5 \text{ eV (95\%CL)}$$

Line Width of Backward PXR

for Diamond and Silicon at E = 855 MeV

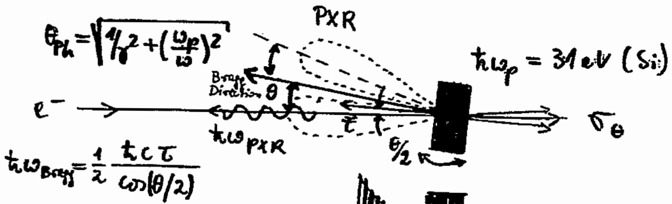

Natural Line Width

$\Gamma = \hbar / \tau$

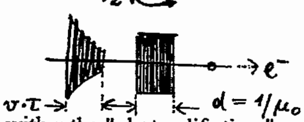

with τ the "photon life time"

Multiple Scattering (σ_θ space angular divergence)

$$\frac{\Delta\hbar\omega}{\hbar\omega}\Big|_{FWHM} = 0.6\sqrt{\ln 2}\cdot\sqrt{(\theta\cdot\sigma_\theta)^2 + \frac{1}{2}\sigma_\theta^4}\,,\quad \frac{\Delta\hbar\omega}{\hbar\omega}\Big|_{FWHM} \cong 0.5\cdot\sigma_\theta\frac{\omega_p}{\omega} \text{ at } \theta = \theta_{ph}$$

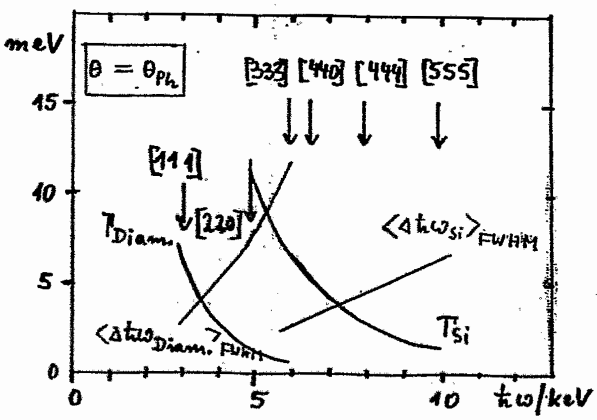

Backward PXR

Crystal: Silicon Single Crystal, Thickness 525 μm

Beam: 855 MeV, 10 nA

Energy Spectrum

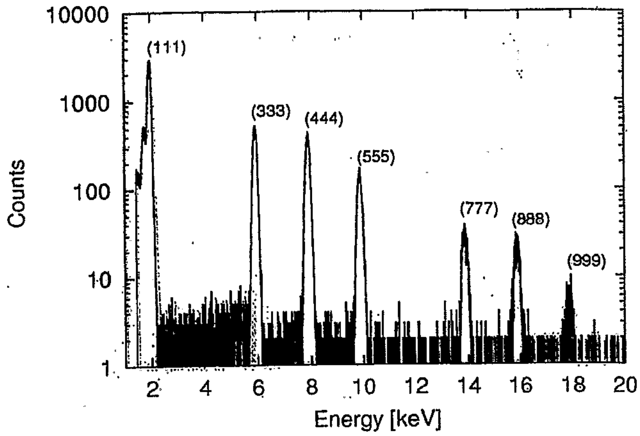

Angular Distribution

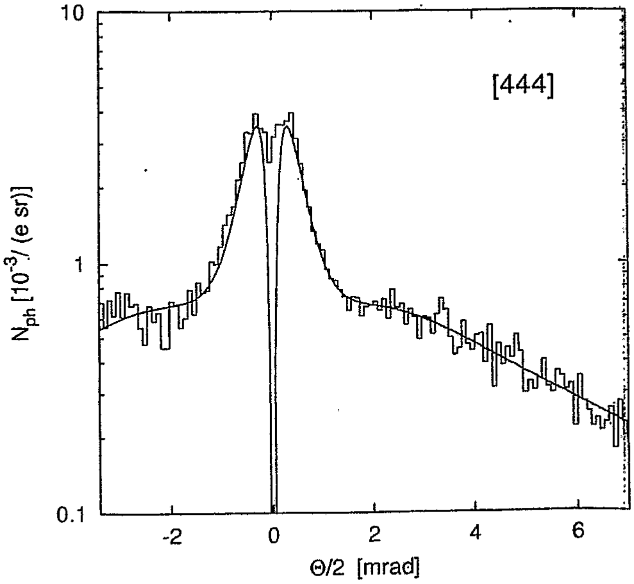

A. Catioha, Phys. Rev. **A 40** (1989), 4322

Diffracted Transition Radiation (DTR)

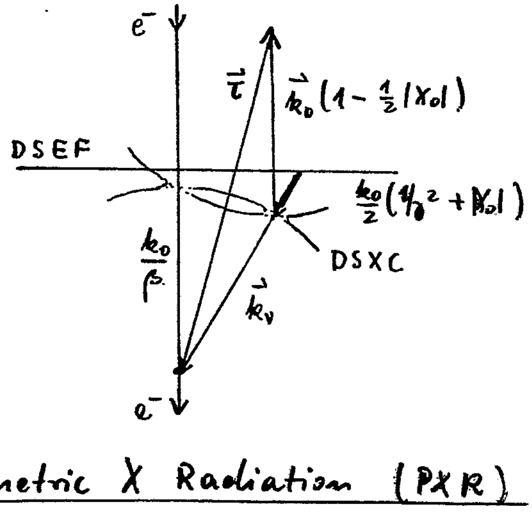

Parametric X Radiation (PXR)

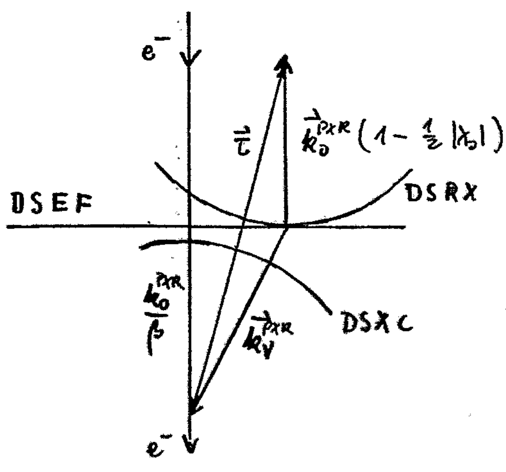

Radation Damage

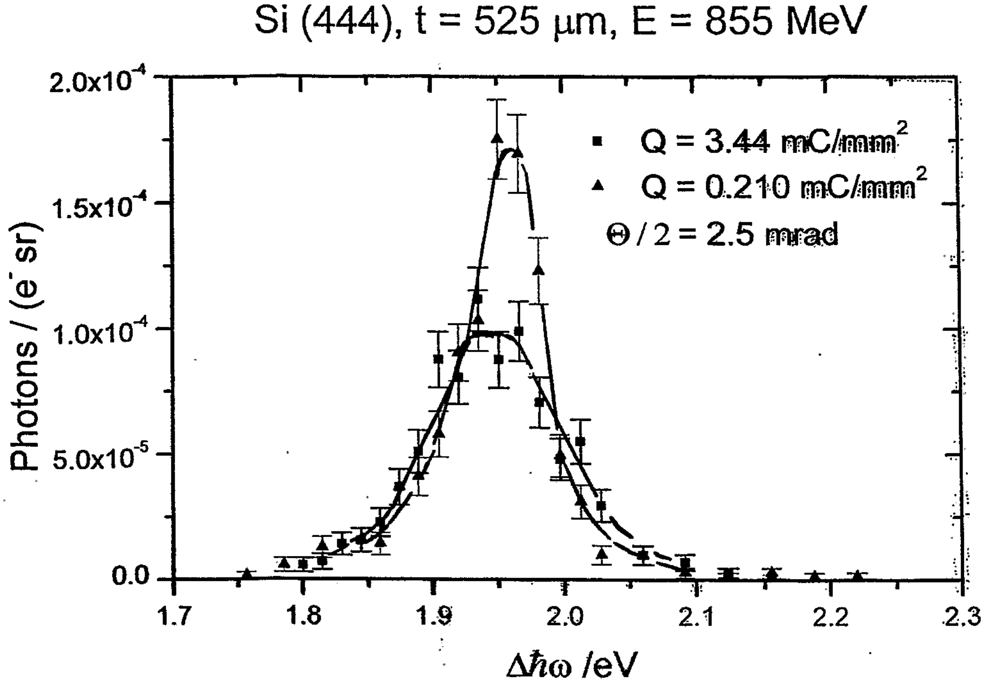

Principle of the Fast Tunable Monochromator for Digital Subtraction Imaging

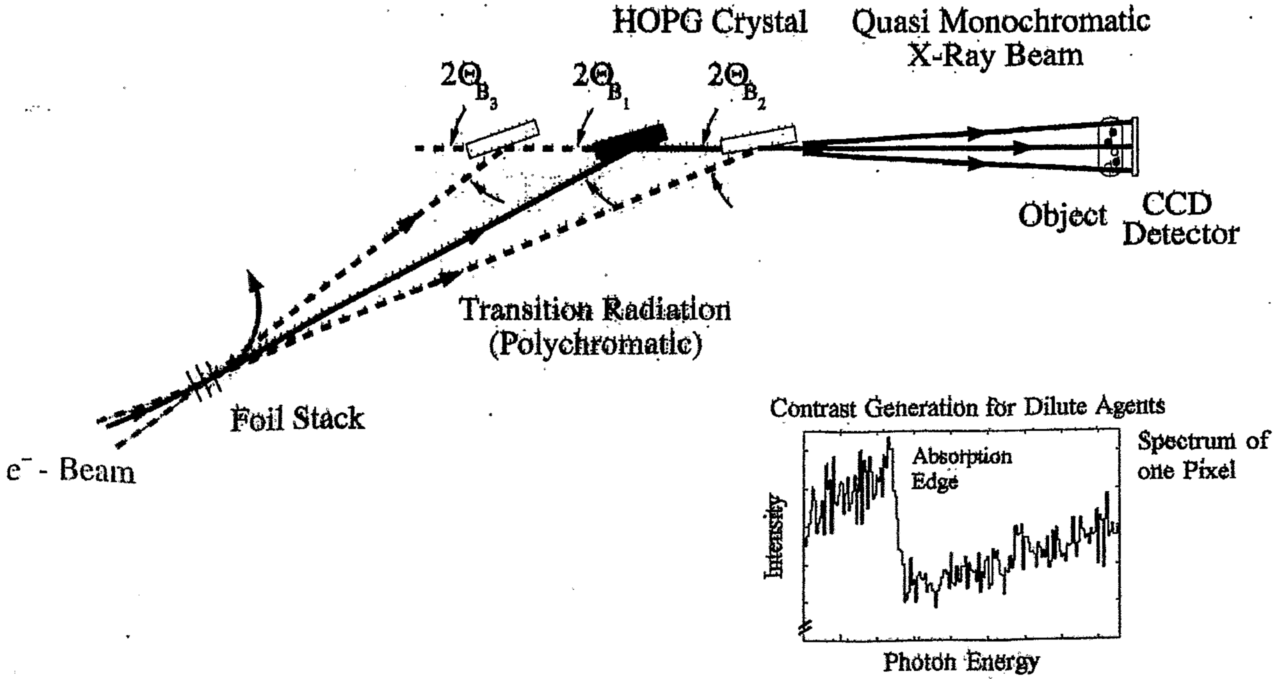

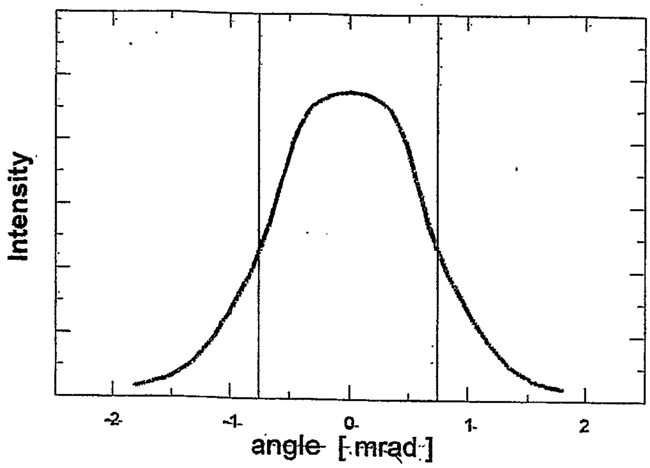

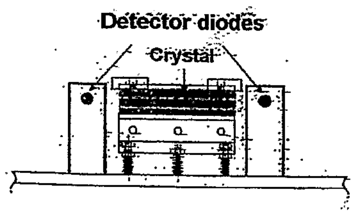

Experimental Set-up

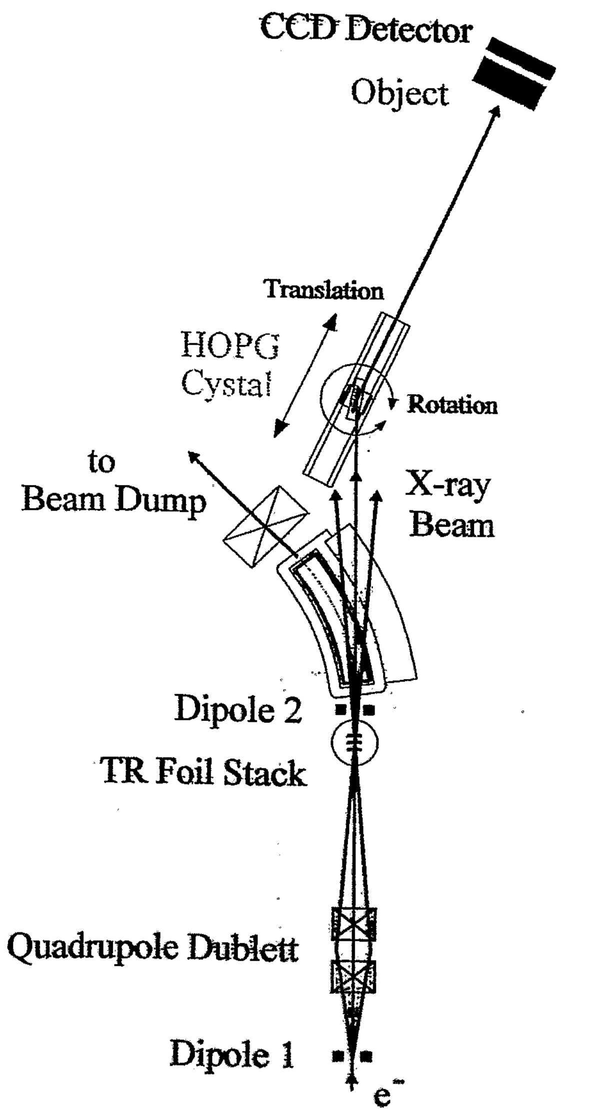

Contrast Generation

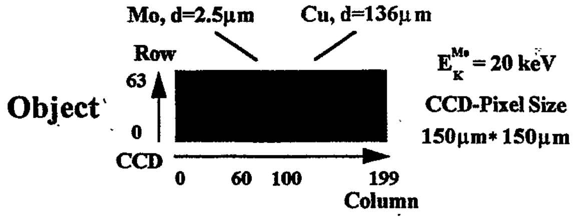

Column 69

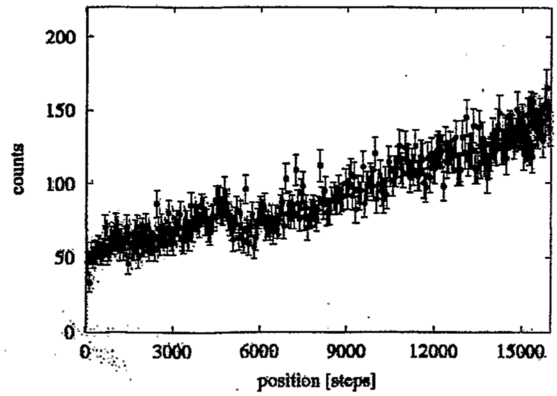

$d=(2.4 \pm 0.2)\mu m$

Column 111

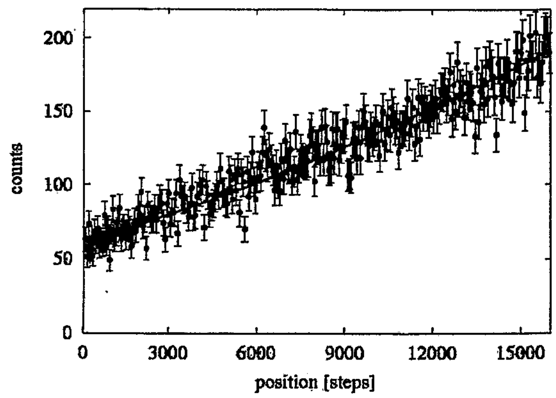

$d=(0.00 + 0.04)\mu m$

Contrast Generation

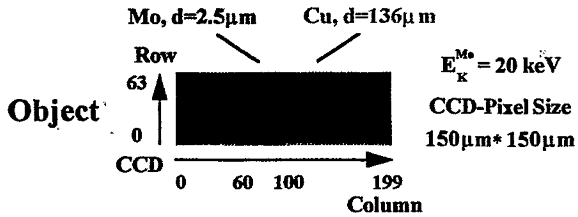

70

3 * 3 Pixel

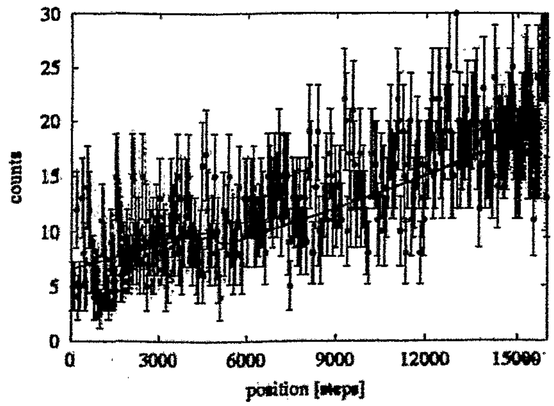

$d=(2.5 \pm 0.6)\mu m$

111

3 * 3 Pixel

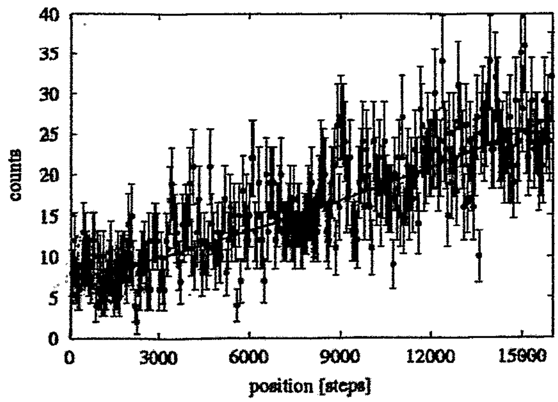

$d=(0.0 + 0.1)\mu m$

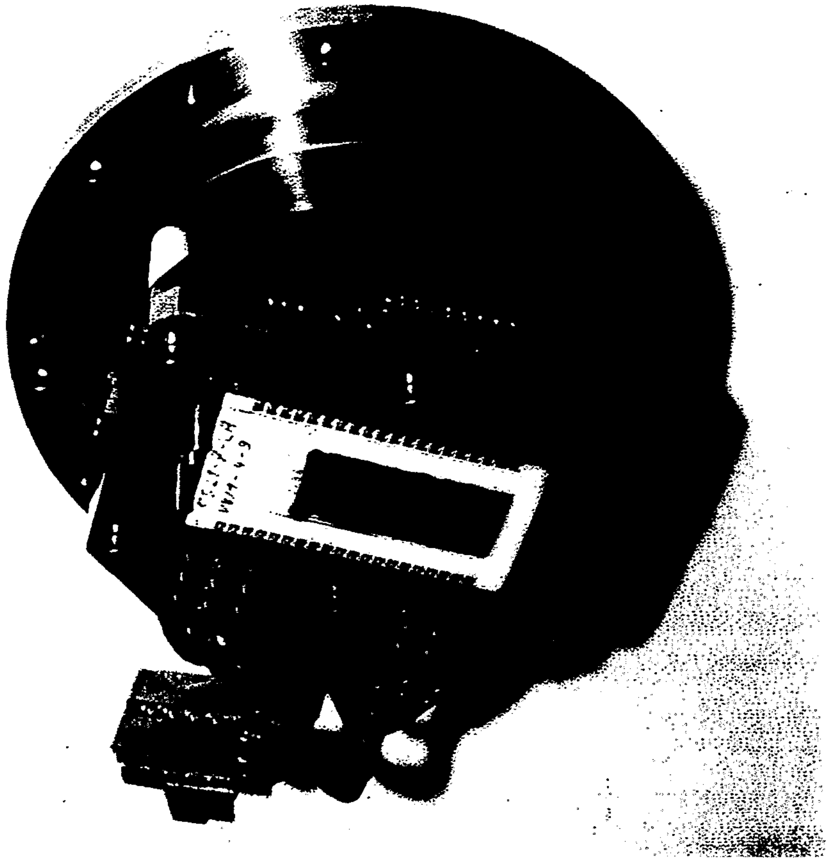

H. Backe, N. Clawiter, N. Elbai, H. Euteneuer, F. Hagenbuck,
H. Jacobs, K.-H. Kaiser, O. Kettig, G. Kube, W. Lauth,
H. Mannweiler, D. Schroff, Th. Walcher

X1-Collaboration, Institut für Kernphysik,
Johannes Gutenberg – Universität Mainz

Th. Kerschner, H. Koch, H. Matthäy, M. Schütrumpf,
A. Wilms, M. Zemter

Institut für Experimentalphysik, Lehrstuhl I,
Ruhr-Universität Bochum

L. Strüder
MPI-Halbleiterlabor München

P. Holl, J. Kemmer, R. Stötter, C.v. Zanthier

KETEK GmbH, Oberschleißheim

P. Rullhusen:

Radiation produced by relativistic electrons interacting with flat and modulated surfaces

Radiation produced by relativistic electrons interacting with flat and modulated surfaces

P.Rullhusen

Rossendorf, 24.2.2000

irm

Motivation:

Transition radiation:

advantage: intense ($P \propto i$)

but: continuous spectrum ($\omega_c = \gamma\omega_p$) for single foil

interference (stack of foils) ⇒ absorption losses

Smith-Purcell effect:

advantage: monochromatic $\frac{\Delta\lambda}{\lambda} = \frac{\sin\theta}{(\beta^{-1} - \cos\theta)}\Delta\theta$

but: intensity $\propto \exp(-z / h_{int})$, $h_{int} = \frac{1}{2}\beta\gamma\lambda\!\!\!^{-} \quad (\zeta = 0)$

irm

Transition Radiation:

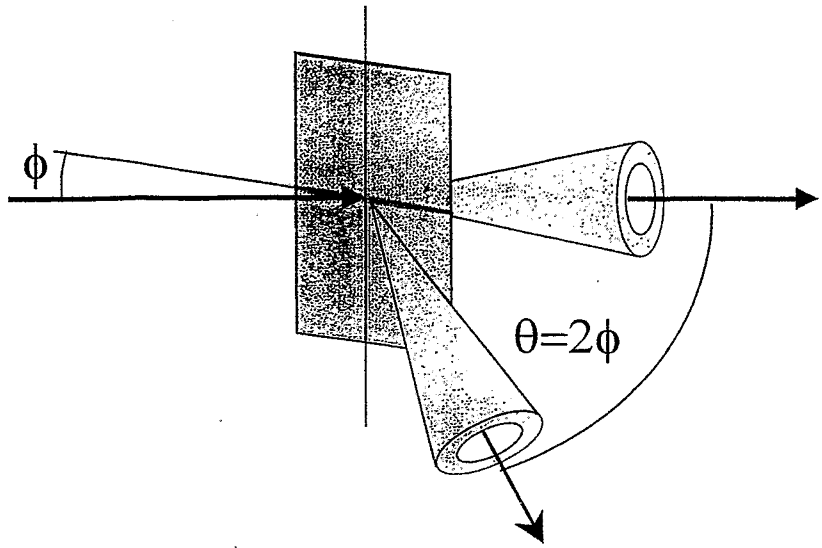

XTR: neglect reflections , $\varepsilon \approx 1 - (\omega_p/\omega)^2$

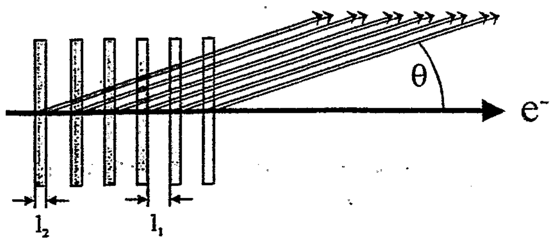

$$F = \frac{d^2W}{d\omega d\Omega} = F_1 F_2 F_3$$

formation length:

$$L_f = \frac{1}{\frac{\omega}{c}\left(\beta^{-1} - \sqrt{\varepsilon}\cos\theta\right)} \approx \gamma^2 ƛ \text{ for } \theta = \gamma^{-1} \ll 1, \omega \gg \omega_p$$

$$\approx \beta ƛ \text{ for } \theta \to \pi/2$$

single interface: $F_1 \propto \left|L_f - L_f^o\right|^2$

single foil: $F_2 = \left|1 - e^{il_2/L_f}\right|^2 \approx 4\sin^2(l_2/2L_f) \begin{cases} l_2 \ll L_f \Rightarrow F \ll F_1 \\ l_2 \gg L_f \Rightarrow F \approx 2F_1 \end{cases}$

N foils: $F_3 = \left|\frac{1 - C^N}{1 - C}\right|^2 \Rightarrow N \text{ for } l_1 \gg L_f^o$

Calculations of Transition Radiation:

1.) classical (e.g., Ter-Mikaelyan):

Fourier transf. (x,y,z,t) -> $(k_x,k_y,k_z,\omega) = (\alpha,\beta,\gamma,\omega)$
Maxwell eqs. + boundary conditions
$\Rightarrow$ Fresnel coefficients

2.) reciprocity theorem (e.g., Ginzburg-Frank, Pafomov, Wartski):
observer at large distances -> incident plane wave
$\Rightarrow$ use results from optics

Smith-Purcell

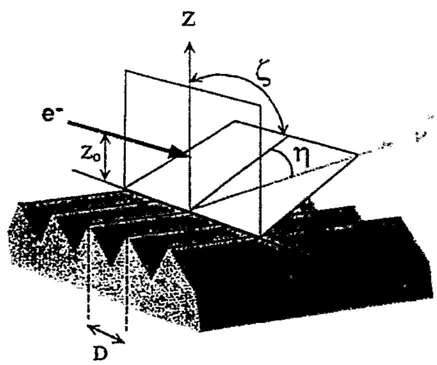

$$\left(\frac{dP}{d\Omega}\right)_n = \frac{e^2 D^2}{2\varepsilon_0 \, |n| \, \lambda^3} \cos^2\eta \cos^2\zeta \left|R_n(\eta,\zeta)\right|^2 \exp\left(-\frac{z_0}{h_{\rm int}}\right)$$

$$h_{\rm int} = \frac{\lambda}{4\pi\left(\beta^{-2} - 1 + \cos^2\eta \sin^2\zeta\right)^{1/2}} = \frac{1}{2}\beta\gamma ƛ \quad \textit{for } \zeta = 0$$

incident field: Fourier components

$$J(x, z; \beta, \omega) = q \exp(i\,\alpha_0 x)\,\delta(z - z_0)\,\mathbf{i}_x$$

$$E^i_y(x, z; \beta, \omega) = \frac{q}{2}(\mu_0/\varepsilon_0)^{1/2}\ (\beta/k_0)(\alpha_0/\gamma_0)\ \exp(\ i\alpha_0 x + i\gamma_0 |z - z_0|\ )$$

$$H^i_y(x, z; \beta, \omega) = -\frac{q}{2}\mathrm{sign}(z - z_0)\ \exp(\ i\alpha_0 x + i\gamma_0 |z - z_0|\ )$$

$$\alpha_0^2 + \beta^2 + \gamma_0^2 = k^2 \qquad \alpha_0 = \frac{\omega}{v} = \frac{c}{v}k > k \quad \Longrightarrow \quad \gamma_0 \text{ imaginary (evanescent wave)}$$

reflected field above grating:

radiation condition — γ_n real (propagative wave)

$$\alpha_n^2 + \beta^2 + \gamma_n^2 = k^2$$

$$\alpha_n = \alpha_0 + n\frac{2\pi}{D}$$

Helmholtz equations

$$\left(\partial_x^2 + \partial_z^2\right)\mathbf{E}_y + \left(k^2 - \beta^2\right)\mathbf{E}_y = \frac{\mu_0}{\varepsilon_0}\frac{\beta}{k}\partial_x \mathbf{J}_x$$

$$\left(\partial_x^2 + \partial_z^2\right)\mathbf{H}_y + \left(k^2 - \beta^2\right)\mathbf{H}_y = -\partial_z \mathbf{J}_x$$

boundary conditions

$$\mathbf{n} \times \mathbf{E} = 0 \qquad \mathbf{E} = \mathbf{E}^i + \mathbf{E}^r$$

$$\mathbf{n} \cdot \nabla H_y = 0 \qquad \mathbf{H} = \mathbf{H}^i + \mathbf{H}^r$$

irm

Solutions of the *grating problem*

Shallow sinusoidal gratings (h/D < 0.14) : Rayleigh method

$$\sum_{n=-\infty}^{\infty} E^r_{y,n}\, e^{i(xk_{x,n} + zk_{z,n})} = -E^i_y(x, z)$$

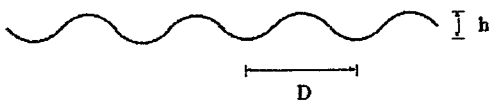

Integral method:

calculate $E^r_{y,n}(x,z), H^r_{y,n}(x,z)$ inside the grooves

from $E^r_{y,n}(x_p,z_p), H^r_{y,n}(x_p,z_p)$ on the grating surface

using Greens theorem -> system of coupled integral equations of 2nd kind :

$$\mathbf{n}\cdot\nabla E^i_y(r_p) = \frac{1}{2}\mathbf{n}\cdot\nabla E^r_y(r_p) - P\int_L (\mathbf{n}\cdot\nabla E^r_y)(\mathbf{n}\cdot\nabla G)\,ds$$

$$H^i_y(r_p) = \frac{1}{2}H^r_y(r_p) - P\int_L H^r_y(\mathbf{n}\cdot\nabla G)\,ds$$

irm

problem with inclined beam:

$$E_{y'}^{i}(x',y',z';\omega) = -i\frac{q}{2}\frac{c}{v}\left(\frac{\mu_0}{\varepsilon_0}\right)^{1/2}\int_{-\infty}^{\infty}\frac{d\beta}{2\pi}\;\frac{\beta}{(\beta^2+g^2)^{1/2}}\;\exp(\,iA\,)$$

$$H_{y}^{i}(x',y',z';\omega) = -\frac{q}{2}\;\mathrm{sgn}(z'\,)\int_{-\infty}^{\infty}\frac{d\beta}{2\pi}\;\exp(\;iA\;)$$

$A = \alpha_0 x' + \beta y' + \gamma_0|z'|$, $g^2 = \alpha_0^2 - k^2$, $\alpha_0 = kc/v$, $k = \omega/c = 2\pi/\lambda$, $\gamma_0 = i\,(\alpha_0^2 + \beta^2 - k^2)^{1/2}$

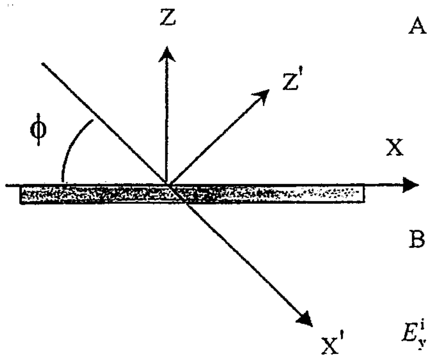

$$\frac{n\lambda}{D} = \frac{c}{v}\cos\phi - \sin\eta + \frac{\sigma}{k}\sin\phi$$

rotation $(x',y',z') \Rightarrow (x,y,z)$, $y=y'$

trick: Fourier transform in z

$B = \alpha_0 x' + \beta y' + s z' = (\,\alpha_0\cos\phi + \sigma\sin\phi\,)x + \beta y + (\,-\alpha_0\sin\phi + \sigma\cos\phi\,)z.$

$$E_{y}^{i}(\phi,x,y,z;\omega) = -iq\;\frac{c}{v}\left(\frac{\mu_0}{\varepsilon_0}\right)^{1/2}\int_{-\infty}^{\infty}\frac{d\beta}{2\pi}\int_{-\infty}^{\infty}\frac{d\sigma}{2\pi}\;\frac{\beta}{\sigma^2+\beta^2+g^2}\;\exp(\,iB\,)$$

$$H_{y}^{i}(\phi,x,y,z;\omega) = iq\int_{-\infty}^{\infty}\frac{d\beta}{2\pi}\int_{-\infty}^{\infty}\frac{d\sigma}{2\pi}\;\frac{\sigma}{\sigma^2+\beta^2+g^2}\;\exp(\;iB\;)$$

but: "plane waves" with $\alpha_0'^2 + \beta^2 + \sigma^2 > k^2$!?

grating diffraction

optics

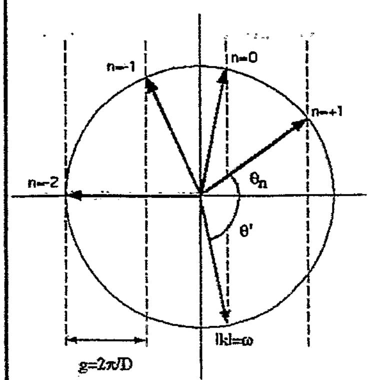

Smith-Purcell

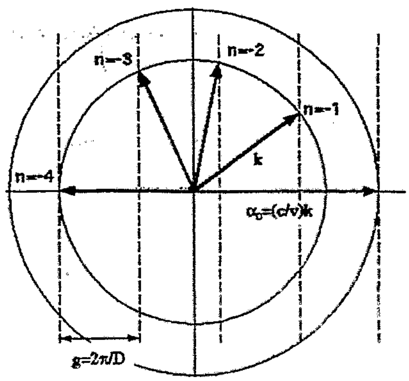

GTR

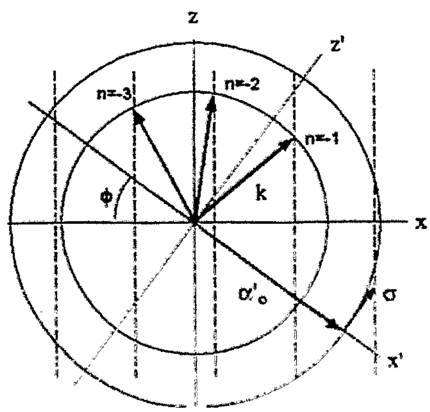

Grating diffraction

$$-n\lambda = D\,(\cos\Phi - \cos\theta)$$

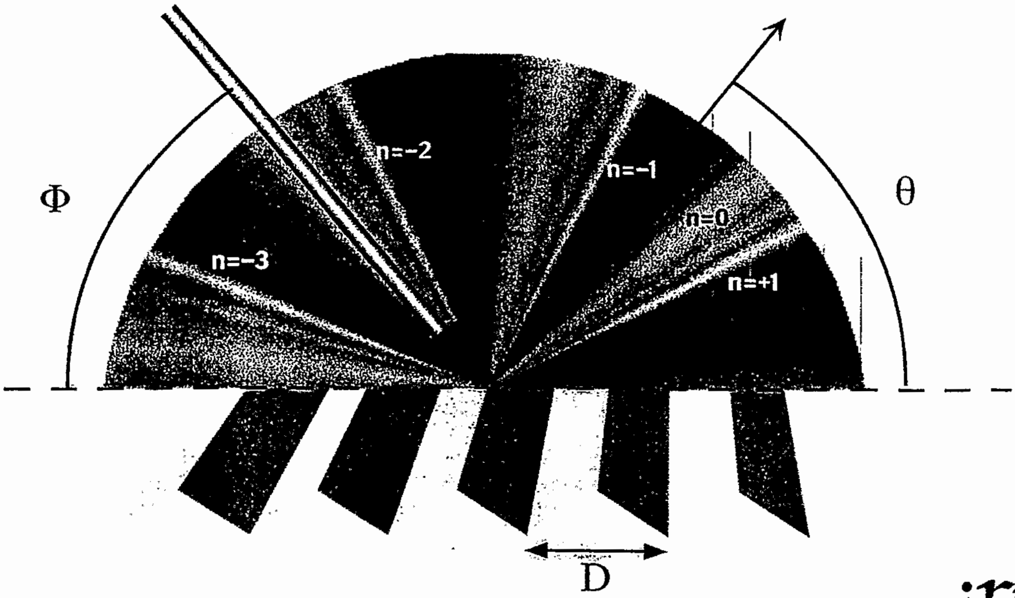

Smith-Purcell effect

$$-n\lambda = D\,(\beta^{-1} - \cos\theta)$$

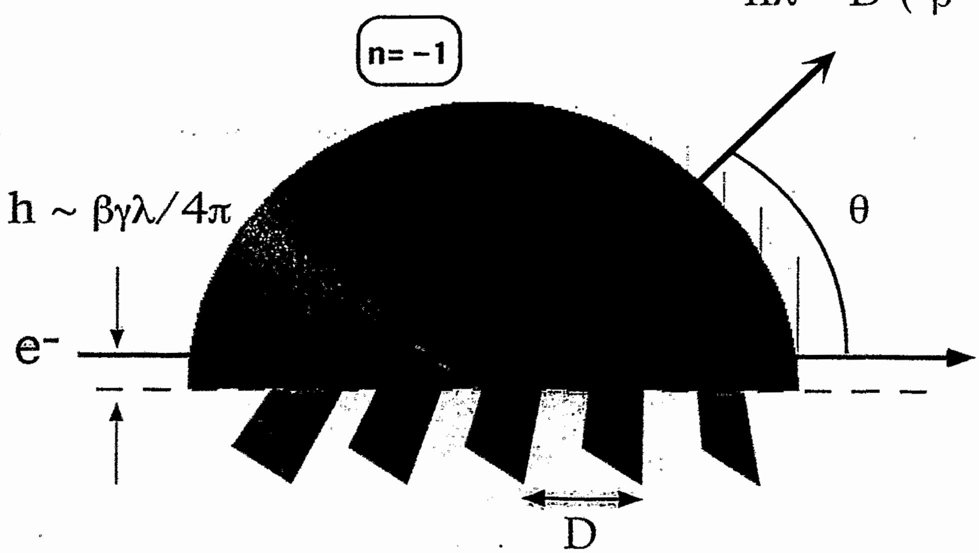

Grating Transition Radiation

$$-n\lambda = D\,(\,\beta^{-1}\cos\Phi - \cos\theta + \sigma\sin\Phi\,)\ ;\ \sigma \sim \gamma^{-1}$$

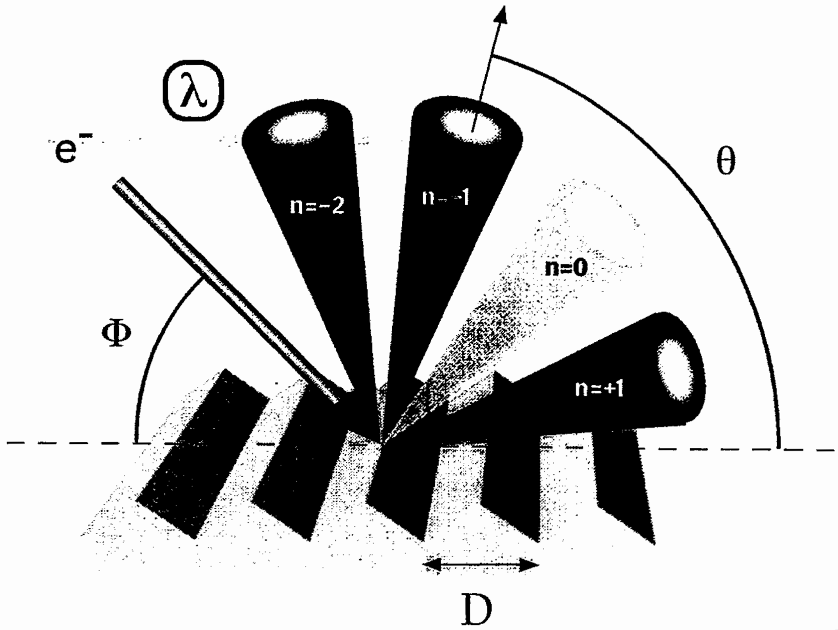

experimental setup:

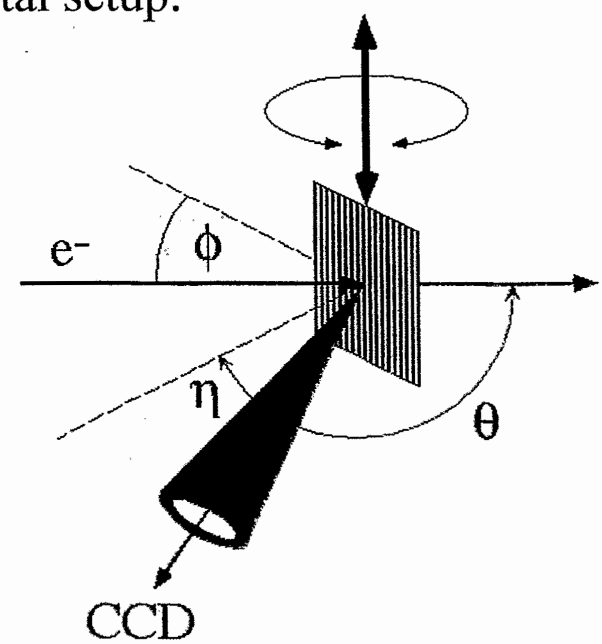

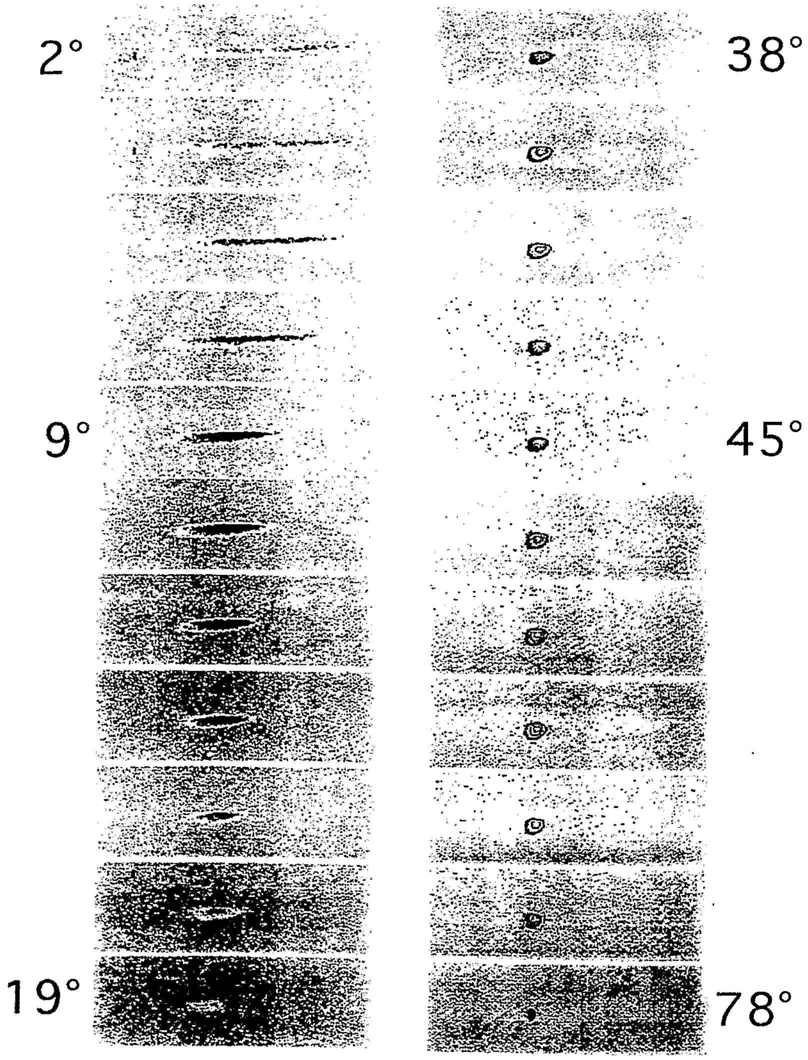
2°
9°
19°
38°
45°
78°

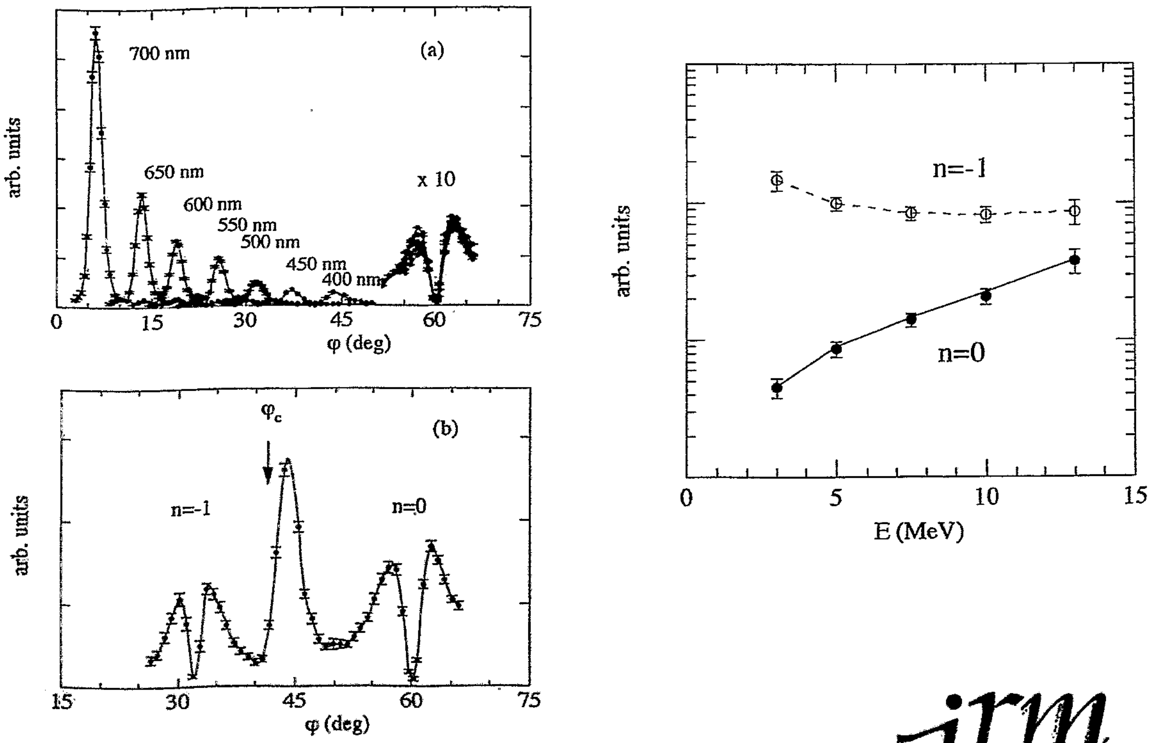
(a)
700 nm
650 nm
600 nm
550 nm
500 nm
450 nm
400 nm
x 10
arb. units
φ (deg)
(b)
φ_c
n=-1
n=0
arb. units
φ (deg)
n=-1
n=0
arb. units
E (MeV)

Wood-Rayleigh anomalies:

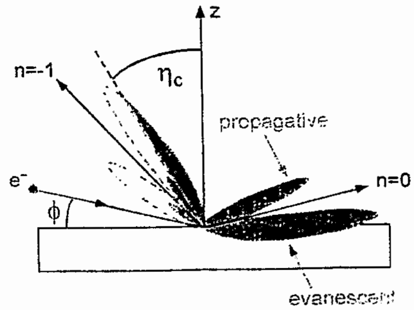

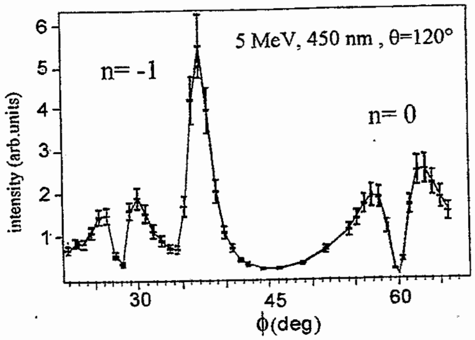

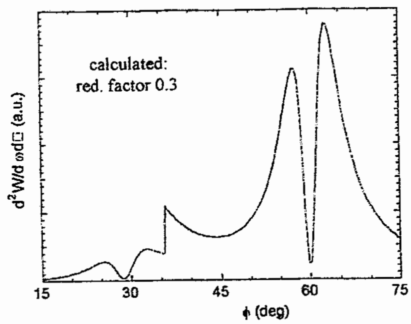

OTR , φ=30° , η-dependence

Al (perf.cond.) 5,10,50 MeV

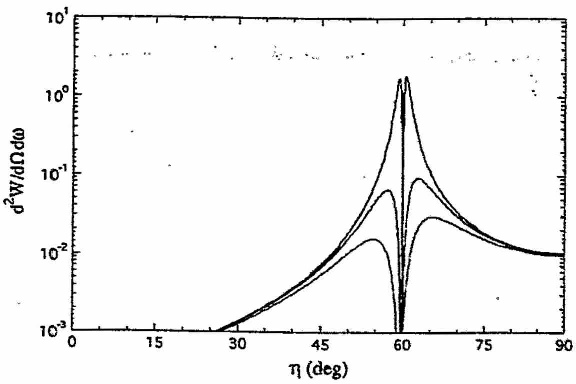

Al, 5 MeV
400 nm, 700 nm, perf.cond.

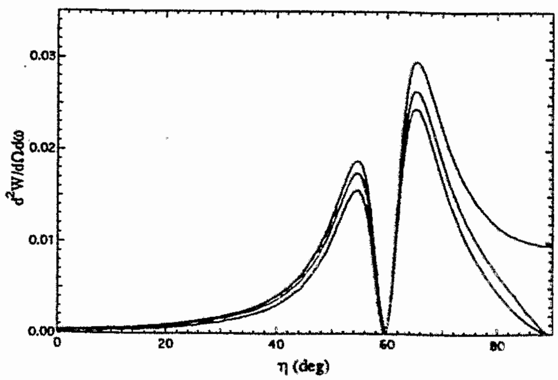

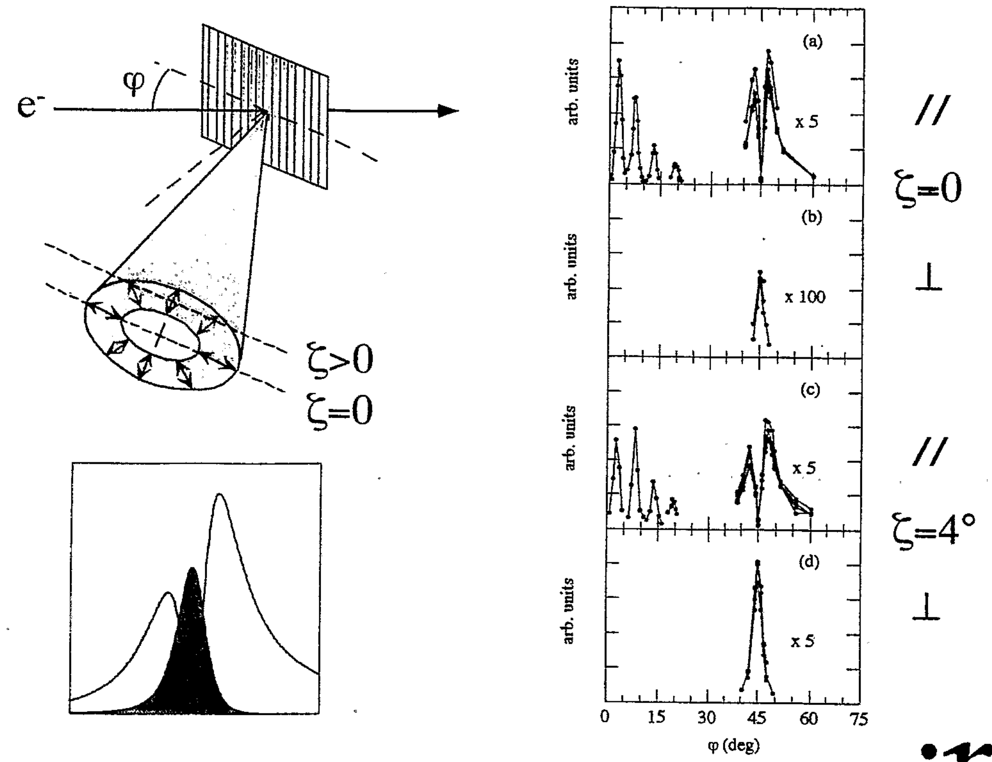

e⁻
φ
ζ>0
ζ=0
(a)
arb. units
x 5
//
ζ=0
(b)
arb. units
x 100
⊥
(c)
arb. units
x 5
//
ζ=4°
(d)
arb. units
x 5
⊥
0 15 30 45 60 75
φ (deg)

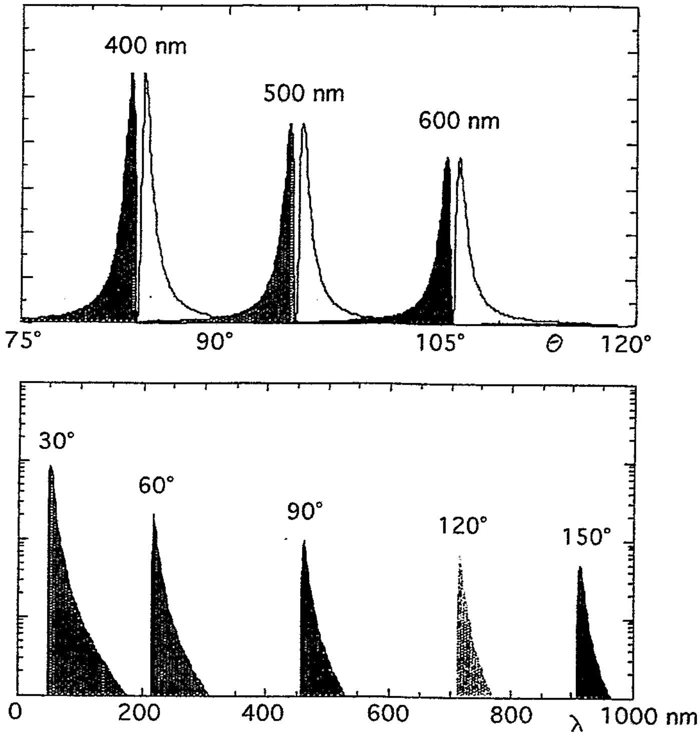

2000 lines/mm

5 MeV

$\varphi = 5°$

5 MeV , D=500 nm , θ=120°

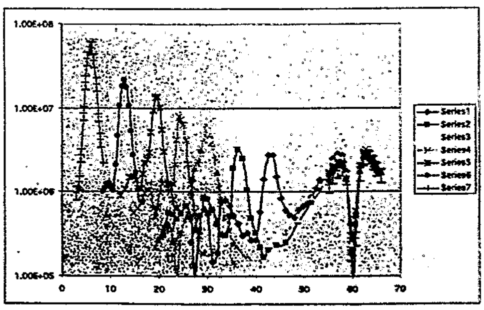

5 MeV , D=500 nm , θ=90°

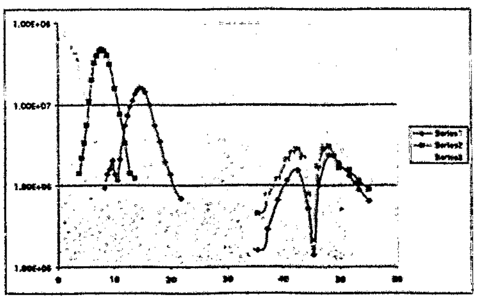

5 MeV , D=556 nm , θ=120°

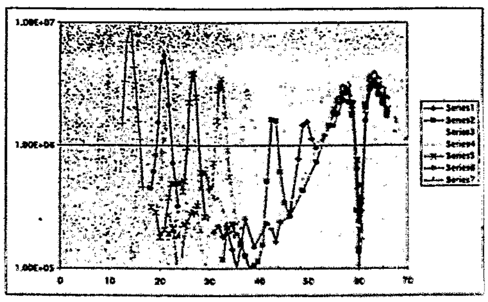

5 MeV , D=556 nm , θ=90°

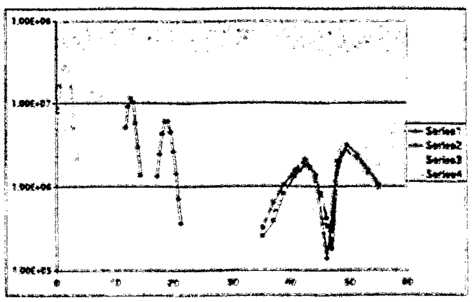

I. G. Grigorieva:

Highly oriented pyrolytic graphite for X-ray bending and focusing

Production

Pyrolysis of hydrocarbons with carbon deposition on heated substrate (t= 2100°C)

↓

Annealing under pressure at t>2800°C

↓

HIGHLY ORIENTED PYROLYTIC GRAPHITE (HOPG)

Structure

Block structure of commercially produced HOPG.
Acoustic microscope "Elzam", f=100 MHz
Scale 1000x800 microns, 125 microns under the surface
(in collaboration with V.M.Levin, Institute of Chemical Phisics of RAS)

Peculiarities of HOPG monochromators

1. High integral reflectivity

002 reflection	$R_i \approx 1\ 10^{-2}$ rad
004 reflection	$R_i \approx 1.5\ 10^{-3}$ rad

2. Wide mosaic spread

Standard crystals	1.0 (+/-0.2) degree
Best commercially available crystals	0.4 degree
Best crystals available in scientific research	0.3 degree

3. Carbon 99.99% with thermoconductivity 1400 Wm/K
Good thermo- and radiactive stability as the result

Short focus HOPG

4. Arbitrary shape
5. Large solid angle of detection (about90%)
6. Wide transmission band
7. Thickness variable with a step of 20 microns

K.V.Zolotarev
Budker Institute of Nuclear Physics,
630090 Novosibirsk, Russia

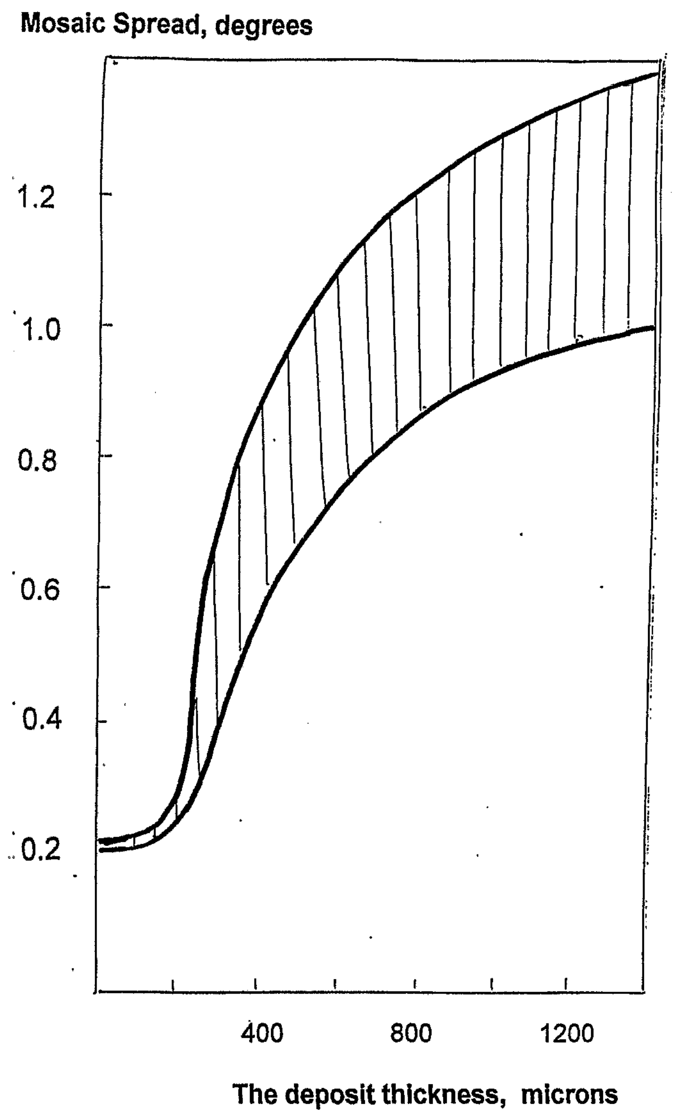

FIG.2. Mosaic spread of the HOPG crystal deposited on a flat mould as a function of thickness

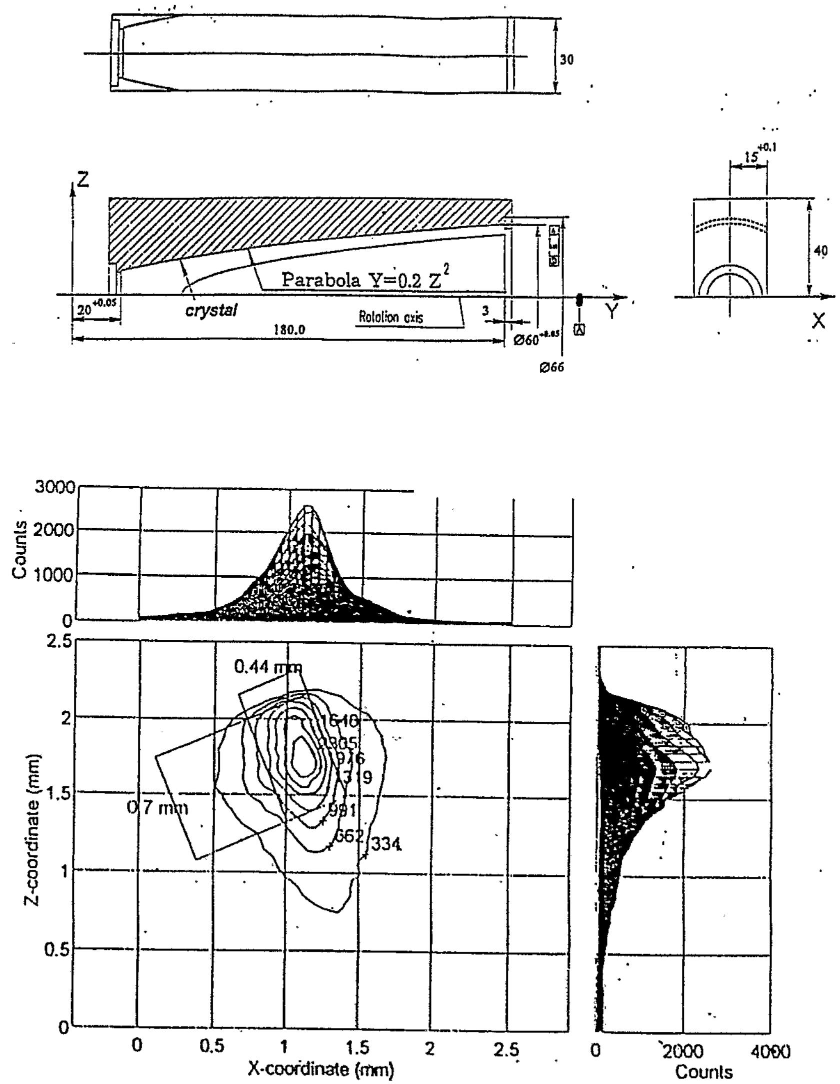

FIG.4. Parabolic HOPG crystal and the intensity distribution in the focal spot.

B.Beckhoff, B.Kanngiesser
Department of Physics,
P.O.330440,
D-28334 Bremen, Germany

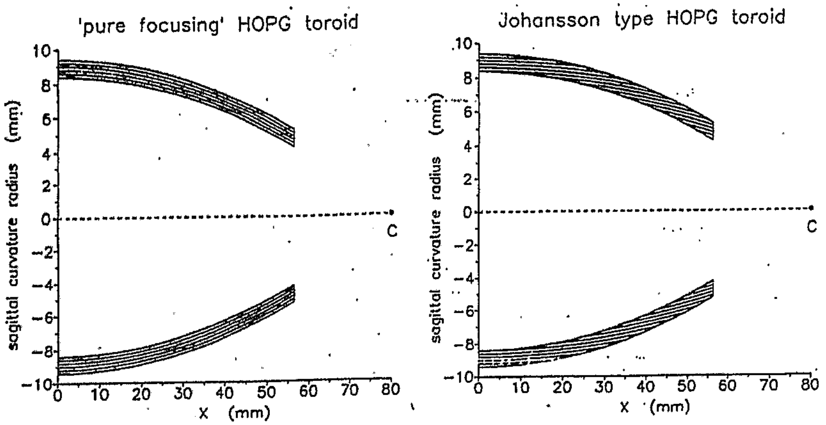

FIG.5A. Shape and schematical layer orientation of the 'pure focusing HOPG-' and the Johansson type toroid

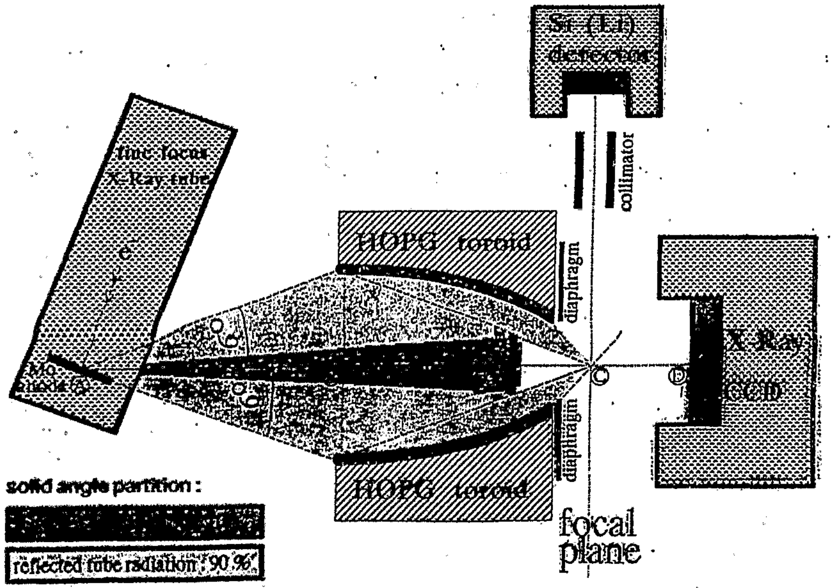

FIG.5B. Schematical sketch of experimental set-up for the measurements spatial intensity and energy distribution in focal spot.

B.Beckhoff, B.Kanngiesser
Physics Department,
University of Bremen
D-28334 Bremen, Germany

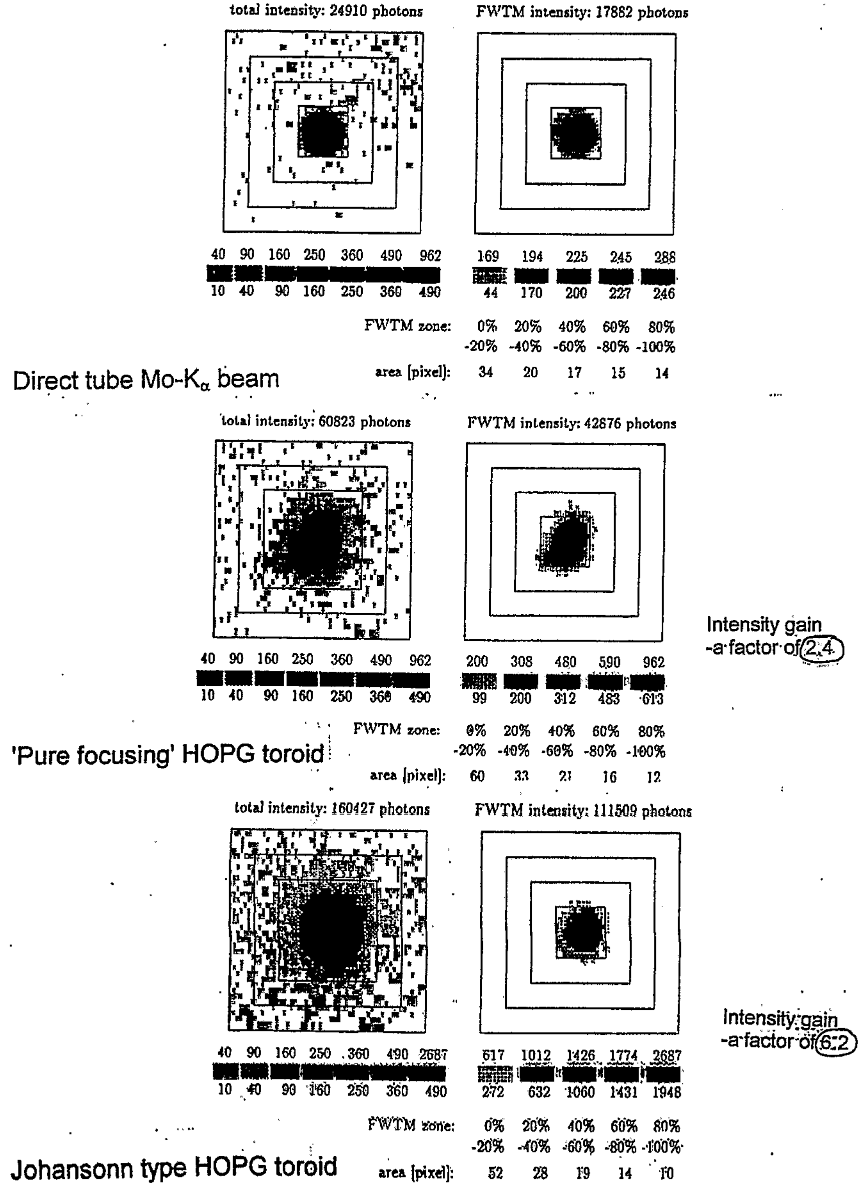

FIG. 6 Spatial intensity distribution in the focal spot in two different intensity scales.The four squares have side lengths of respectively 2mm, 4mm, 6mm and 8mm

B.Beckhoff, B.Kanngiesser,
Physics Department,
University of Bremen
D-28334 Bremen, Germany

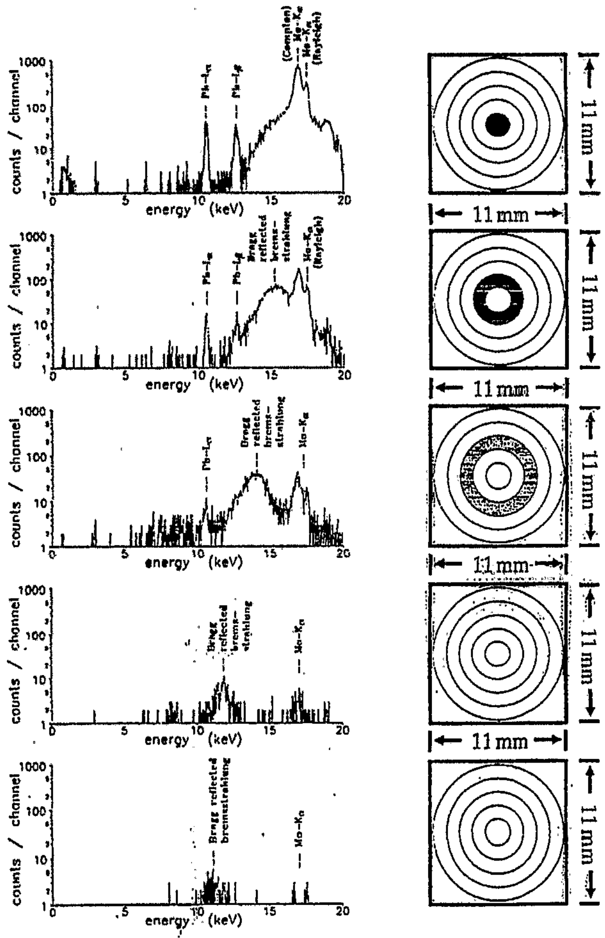

FIG. 7 Energy distribution of different spatial zones in the focal spot of the Johansson type HOPG toroid, obtained by a low Z scatterer.

J.Heckel

Spherical HOPG as a polarization target

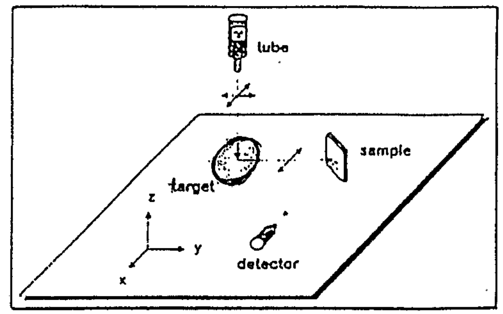

used in

SPECTRO XEPOS
- a benchtop X-ray fluorescence spectrometer

* Low powered X-ray tubes with a power of 50 W as the radiation source

* Simultaneous analysis of the elements Na- U.

* Detection limits of between 1 and 7 mg/g for the elements P,S,CL,Ca,Cu,Zn and Ba are achived within 300s in helium atmosphere.

Department of Physics,
P.O. 330440, D-28334 Bremen,
Germany

P. Chevallier,
LPAN, Université Pierre et Mar
Curie, Paris et LURE, Universit
Paris Sud, Orsay

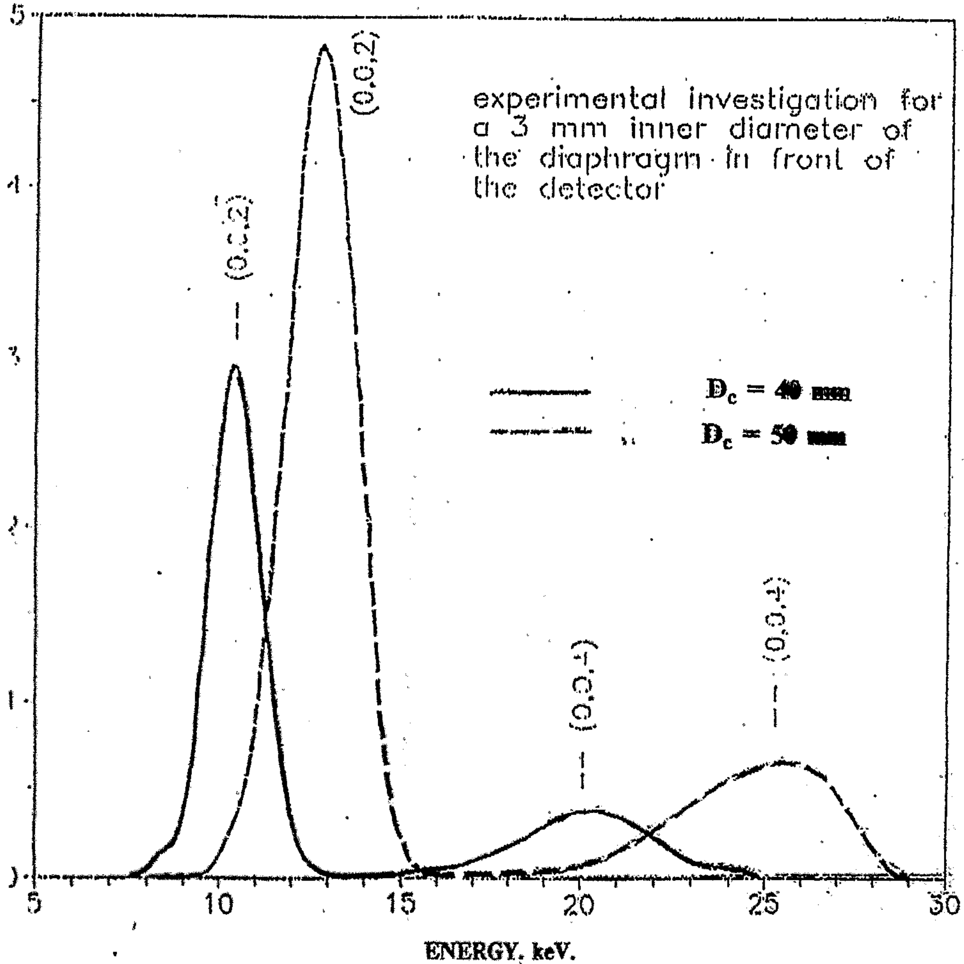

FIG.14. Energy band pass of a graphite cylinder for different sample-to-detector distance.

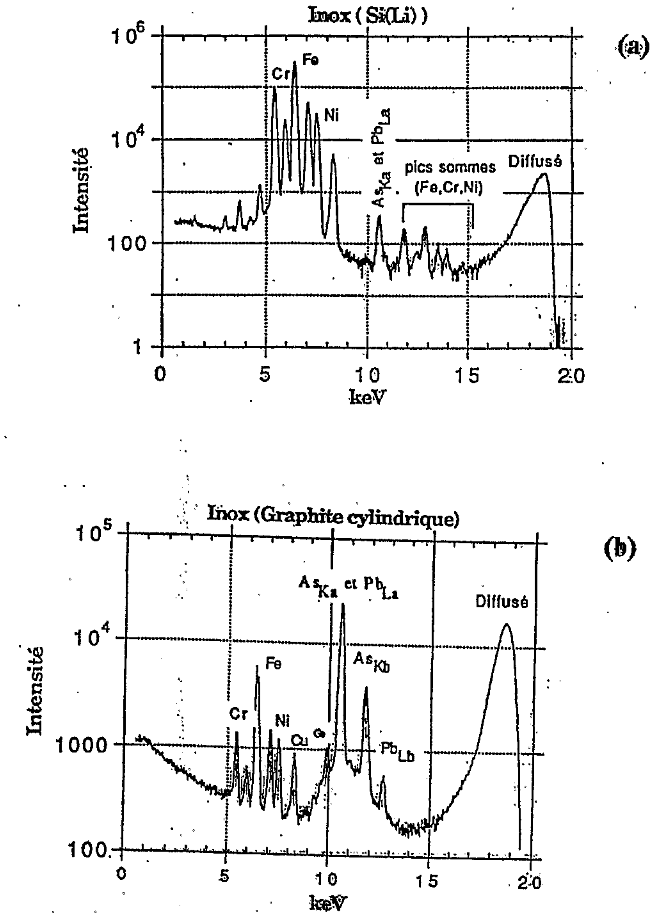

FIG.15. The spectra of stainless steel obtained without (a) and with the help of the dispersion filter . Filter made from a graphite cylinder of 16,2 mm of inner diameter

B.Beckhoff, B.Kanngiesser
Department of Physics,
P.O.330440, D-28334 Bremen, Germany

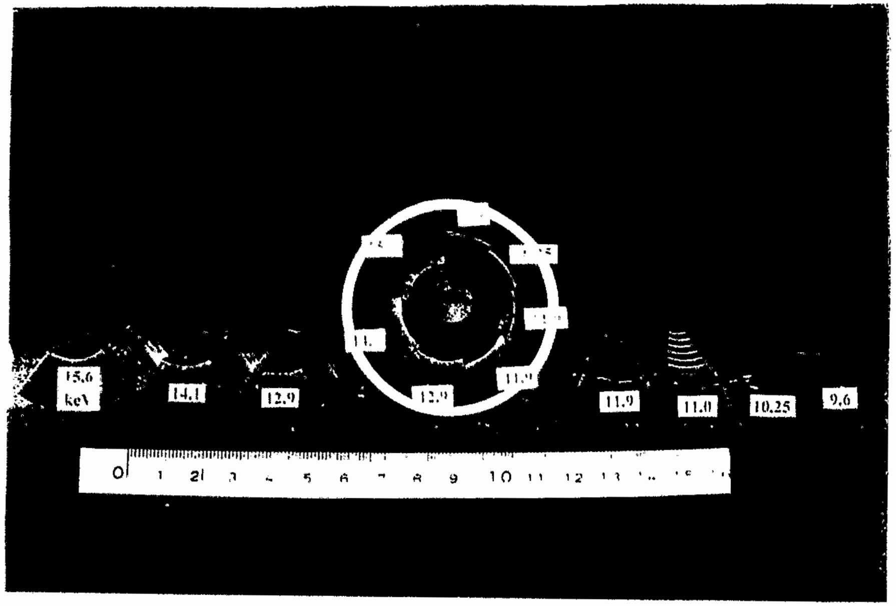

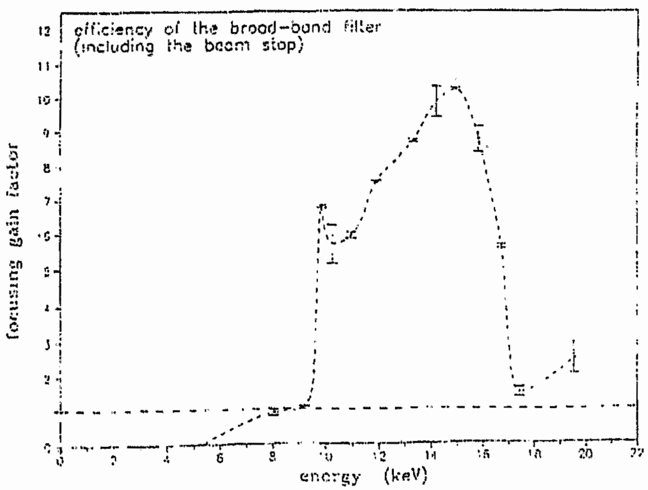

FIG. 9, The view of broad-band filter made from seven stepped toroidal segments and energy dependence of its focusing gain.

Yu.P. Kolmogorov
Institute of Geology SD RAS,
630090 Novosibirsk,
Russia

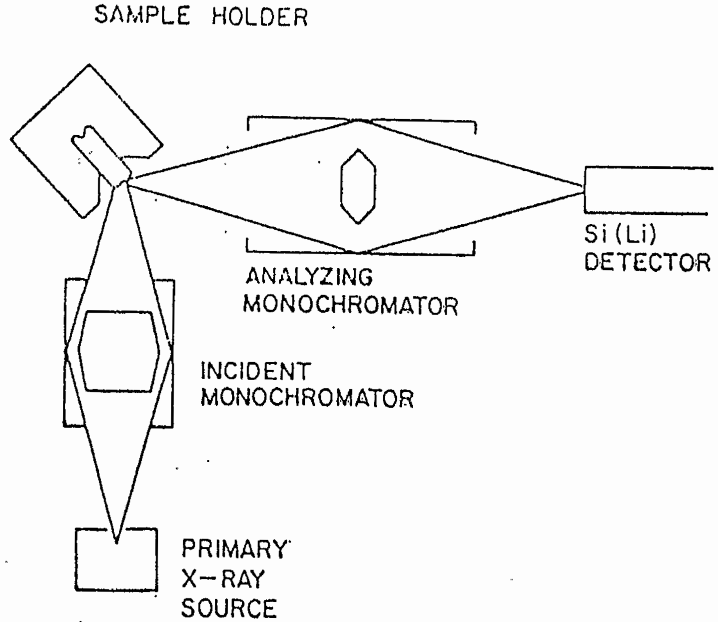

FIG. 11, The scheme included primary and secondary monochromatisation by two HOPG cylinder of 10mm inner diameter (45 kV, 30 mA Molybdenum and Silver anode X-ray tube).

Yu.P.Kolmogorov
Institute of Geology, 630090
Novosibirsk, Russia

Table3. The element content of ecological standards, analysed with the 'two cylinders' scheme.

The set-up includes:
45kV, 30 mA Molybdenum and Silver anode X-ray tube
25mm^2 165 eV resolution Si(Li) detector with analogue electronics
Multichannel amplitude analyser (IBM-286 + 300 MHz Wilkinson type ADC)
Graphite-optical device consists of primary monochromator and energy band filter from pyrolitic graphite.

A set of medico-biological standards has been examined. The results are represented in Table.3.

	IAET reference samples				NIES		SU reference samples		
	A11 Milk Powder	A13 Animal Blood	H-9 Mixed Human Diet	SOIL-7 Soil	VEP-8 Vehicle Exhaust Particulates	PS-2 Soil	Human Hair	CBMT-01 Grass Mixture	CBMT-02 Ash of Grass Mixture
K	17200	2500	8300	12100	1150	6800			
Ca	12900	286	2310	163	5300	8100			
Ti	48			3000		6400	70		122
V	0.1*			66	17	250			5
Cr	0.257*		0.15*	60	25.5	75	2		10
Mn	0.377*		11.8	631		770	0.5	108	1317
Fe	3.65	2400	33.5	25700		65300	50	200	2440
Ni	0.93	1	0.27	26	18.5	40	0.8		8
Cu	0.838	4.3	2.9	11	67	210	11	2.3	28
Zn	38.9	13	27.5	104	1040	343	150	34	415
Ga				10					
As	0.048*		0.088*	13.4	2.6	12	2.6	0.18	2.2
Se	0.034*	0.24	0.11	0.4	1.3		0.15		
Br	14	22	7.5	7	56	17	4.1	8	98
Rb	30.8	2.3	8	51	4.6	42	0.14	6.5	79
Sr	5.4		3	108	89	110	9.2	25	305
Y				21					5
Zr				185					
Nb				12					
Mo	1.3		0.24	2.5	6.4				
Ag					0.2				
Cd	0.526			1.3	1.1	0.82			
Sb				1.7	6	2			
Hg							0.06		
Pb	0.27	0.18	0.16	60	219	105	1.9	1.3	16

Elements with amount marked * were obtained in ash residuum.
The energy band filter from pyrolitic graphite was not used for elements with amount > 1 ppm.

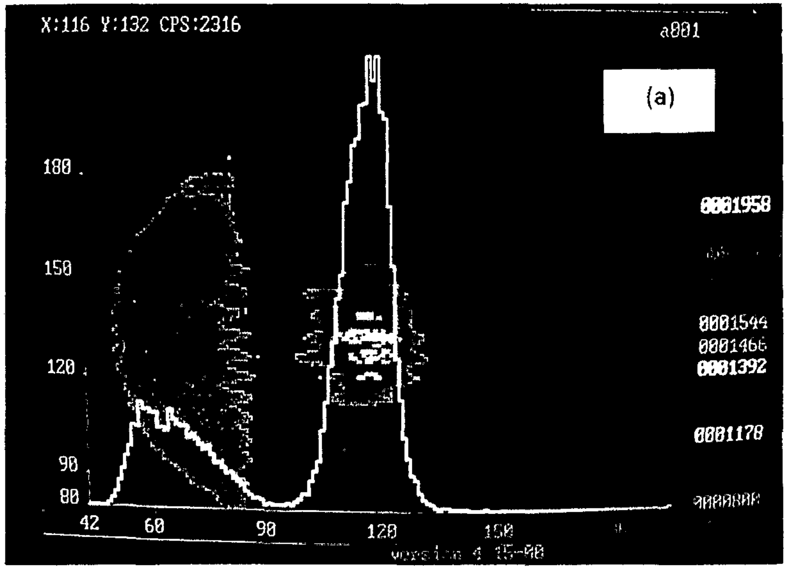

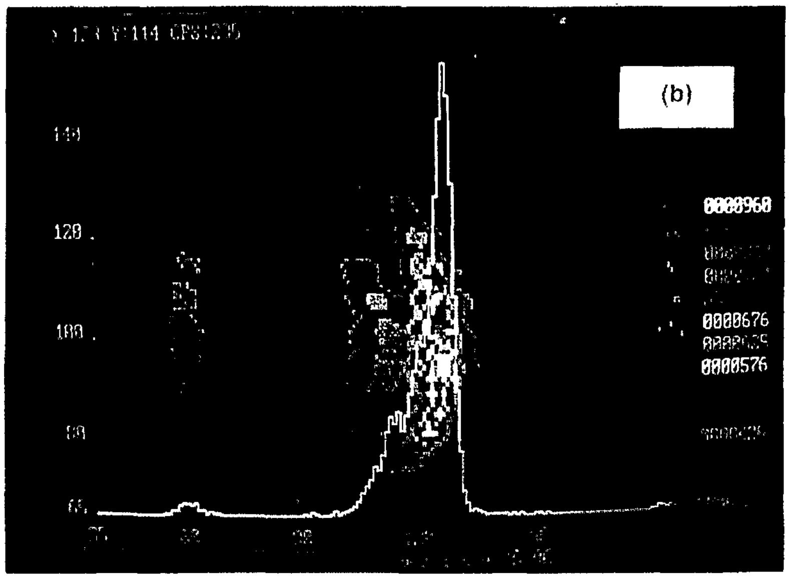

FIG. 7 Spectra of Fe samples on ellipsoidal HOPG as crystal-analyser (a)Screw of 4mm diameter energy resolution 123 eV (b) Nail of 2mm diameter energy resolution 70 eV

The 2-channel von Hamos spectrometer

Shevelko

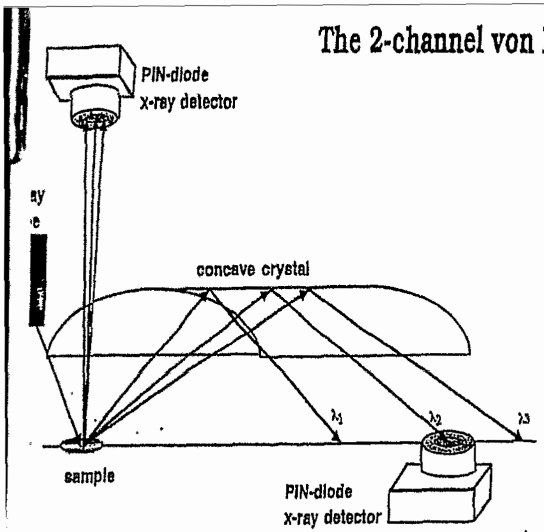

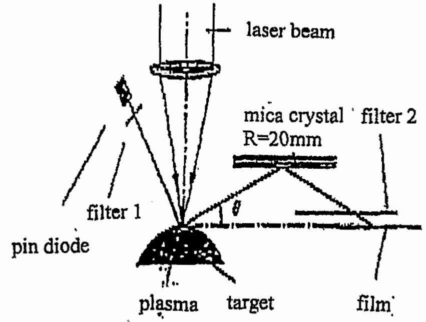

EXPERIMENT

X-ray source: Ti laser-produced plasmas (0.53 m/ 2.5 J/ 2 ns/ 10^{15} W/cm^2).
Hamos spectrograph, R=20 mm, orientation, detector – RAR 2492 photofilm.
Dispertion D=0.02324 A/mm
Spectra
Mica (III order of reflection)

Graphite (200 microns)

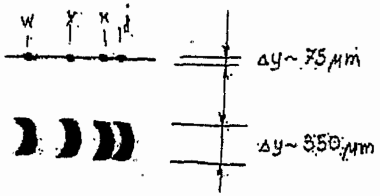

RESULTS

Maximum intensity:
I_{max}/I_{max} = Graphite/ Mica = 4 – 6
Integral intensity $I_{max}\,\Delta x\,\Delta y$:
Graphite/ Mica = 60
Integral reflectivity:
Graphite/ Mica = [120 – 300] 10^{-5} rad (Gilfrich – 120, good agreement)
Spectral resolution (observed):
Mica $\lambda/\Delta\lambda$ =1080
Graphite $\lambda/\Delta\lambda$=480 (line broadening)
$\lambda/\Delta\lambda$=764 (j and k satellites)
mosaic tg $\theta/\delta\theta$ = 50 for $\delta\theta$= 0.5°
Δy broadening → 0.24°

CONCLUSIONS

1. Maximum intensity – 4-6 times
2. Mosaic focusing (observed spectral resolution/ mosaic = 480 – 764/50= 10 – 15 times) !
3. Integral intensity – almost 2 orders (60 times), very perspective for fluorescence analysis!

D.M.Pease
Physics Department,
University of Connecticut
Storrs, Connecticut

Log Spiral HOPG Monochromator for Fluorescence XAFS

Fluorescence emitted from Cr50V50 Sample
Exitation due to tuning the incident beam energy just above the Cr edge

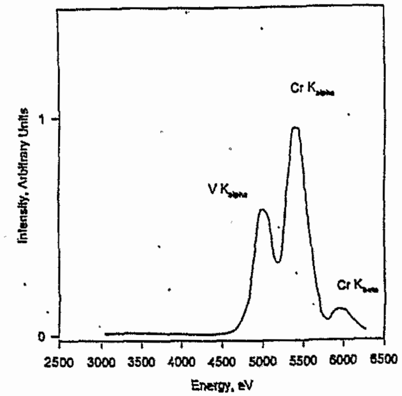

Direct fluorescence (detected by energy dispersive detector)

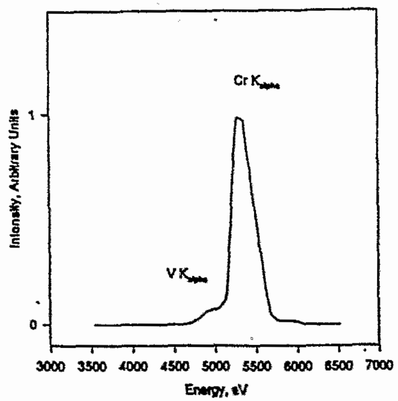

The spectrum is monochromatizated with the **log spiral**.
(energy dispersive detector detecs monochromatized fluorescence)

CONCLUSIONS

Short focus HOPG crystals is a **X-rays optic elements of a high intensity** based on unique brightness of the material and large solid angle of the accepted radiation.

They are an **efficient device at a reasonable price** for

- modification of the excitation beam
- filtration of characteristic radiation
- analysis of characteristic radiation in detection systems

It opens **the possibility to use** HOPG:

- in microprobing;
- in trace element XFA of objects with small mass or with heavy or radioactive matrix;
- in analysis of ultra thin films and coatings;
- in medical applications including irradiation of small pathological seat in human body without deterioration of the adjacent tissues.

The high efficiency of HOPG optics gives a chance to decrease the intensity and, hence, the radioactive hazard of the X-ray sources used for scientific and medical purposes.

A. R. Mkrtchyan:

Investigation of channeling radiation under the influence of acoustic waves

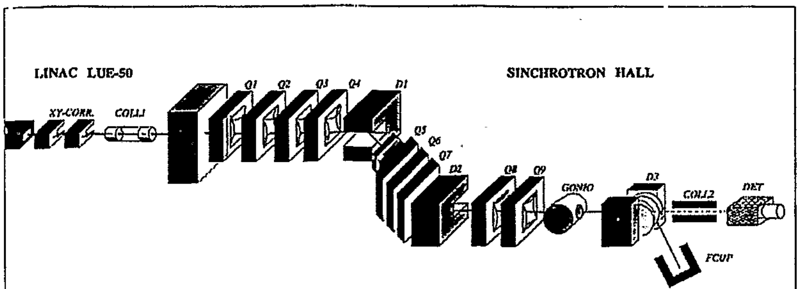

Schematic view of the setup

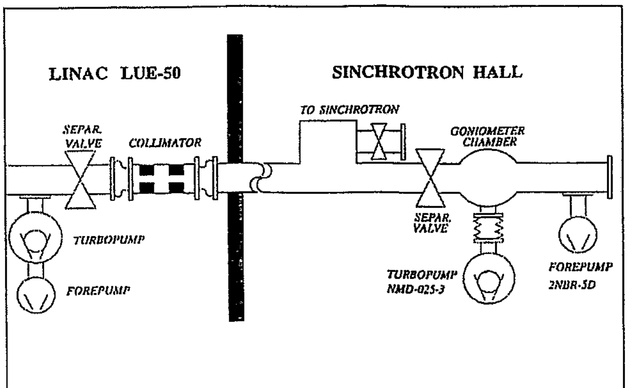

Scheme of the vacuum system

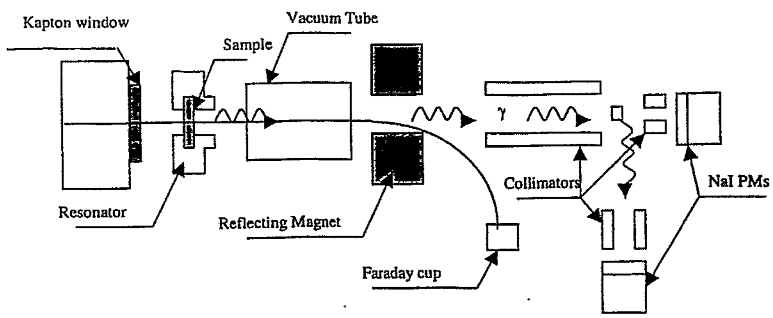

– 1 –

HF resonator.

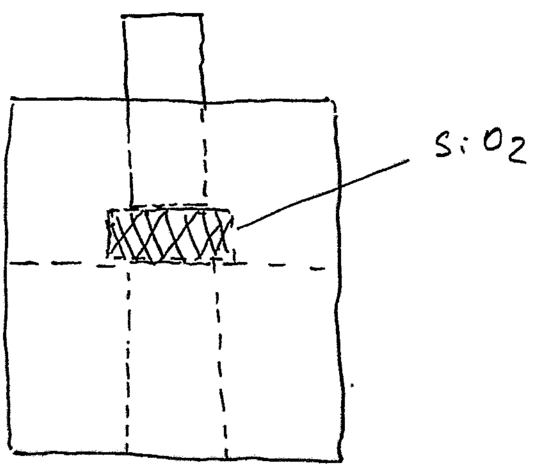

– 2 –

20MeV channeled electron radiation for X-cut single quartz crystall
under the influence of hypersonic waves (θ_g=2500,θ_v=5300,ω=10024KHz,P=10W,M= 5*10^5.)

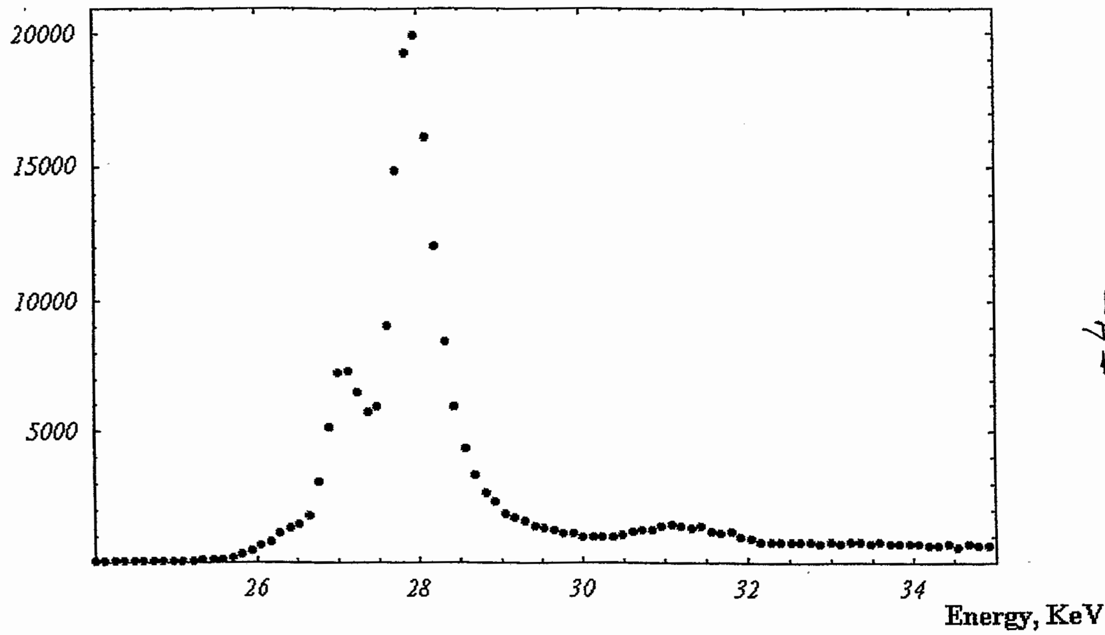

-4-

20MeV channeled electron radiation for X-cut single quartz crystall
under the influence of hypersonic waves (θ_g=2500,θ_v=5300,ω=0kHz,P= 0W,M=5*10^5)

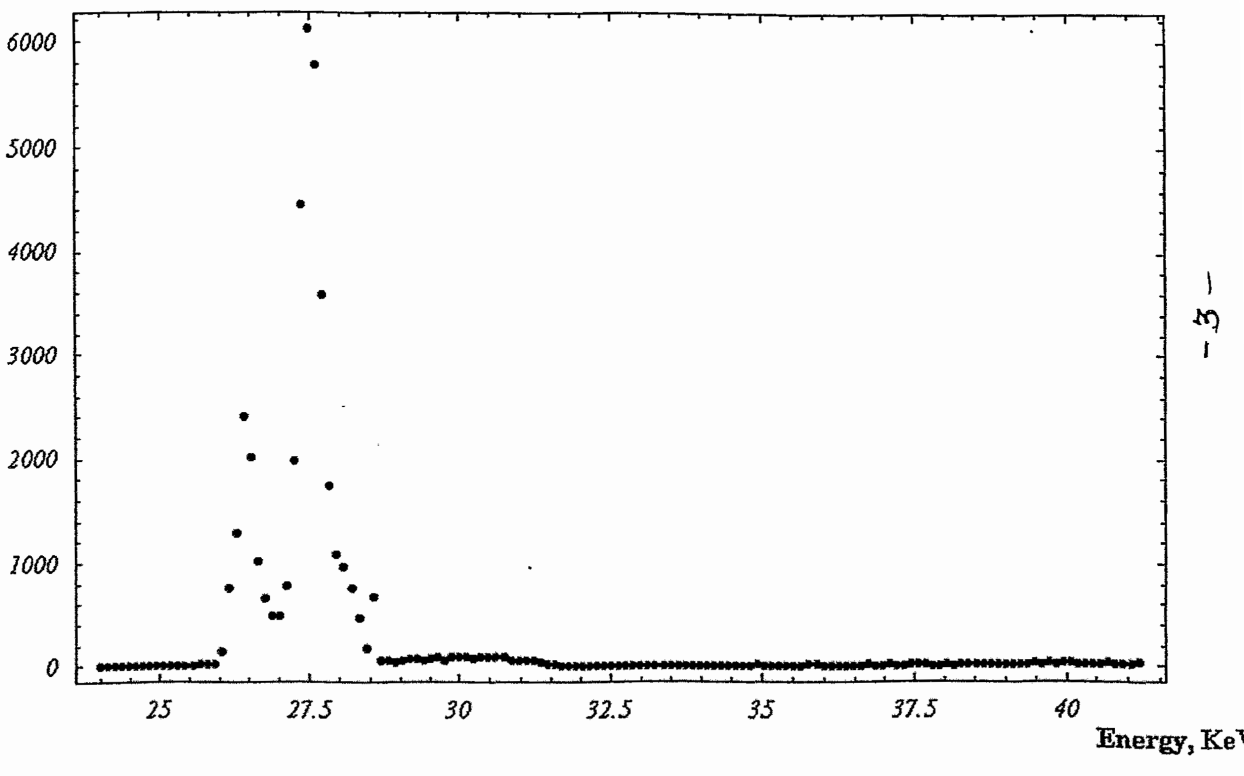

-3-

20MeV channeled electron radiation for X-cut single quartz crystall under the influence of hypersonic waves (θ_g=2400, θ_v=5300, ω=0KHz, P=0W, M=5*10^5)

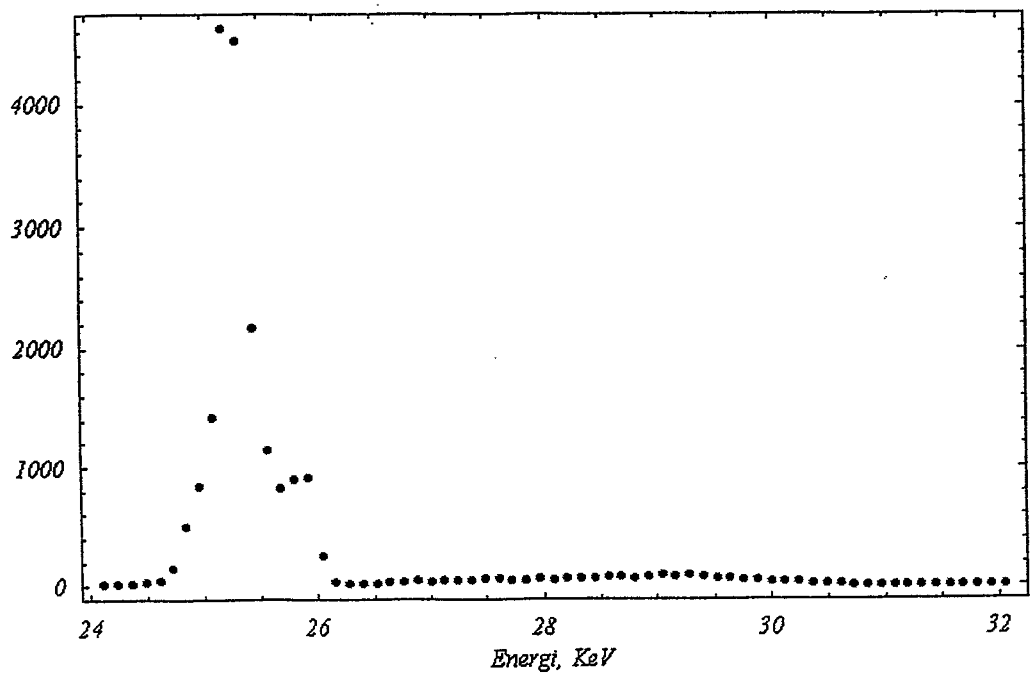

20MeV channeled electron radiation for X-cut single quartz crystall under the influence of hypersonic waves (θ_g=2500, θ_v=5300, ω=10024KHz, P=15W,, M= 5*10^5)

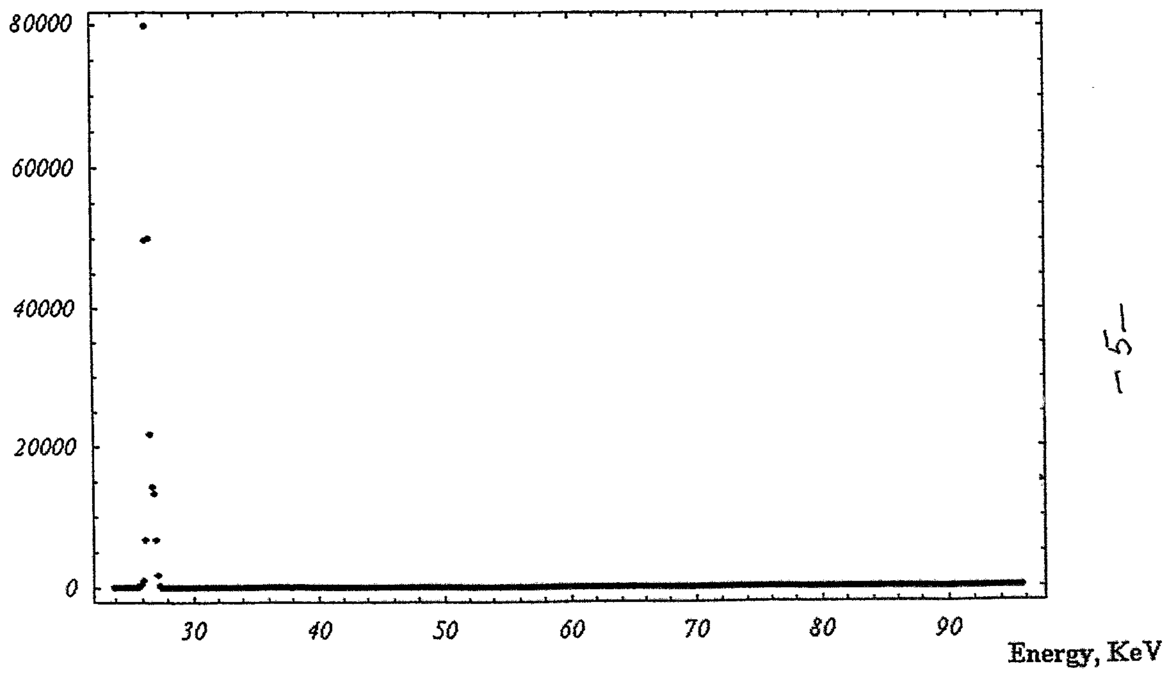

20MeV channeled electron radiation for X-cut single quartz crystall under the influence of hypersonic waves (θ_g=2400, θ_v=5300, ω=10024KHz, P=15W, M= $5*10^5$)

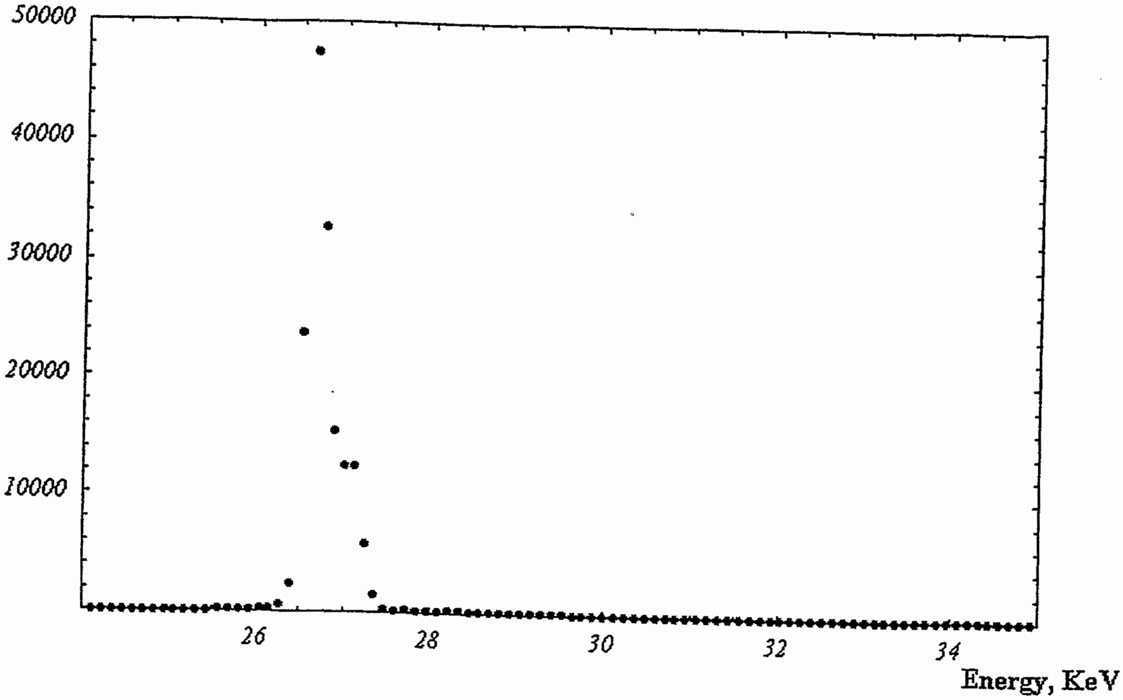

-8-

20MeV channeled electron radiation for X-cut single quartz crystall under the influence of hypersonic waves (θ_g=2400, θ_v=5300, ω=10024KHz, P=10W M=$5*10^5$)

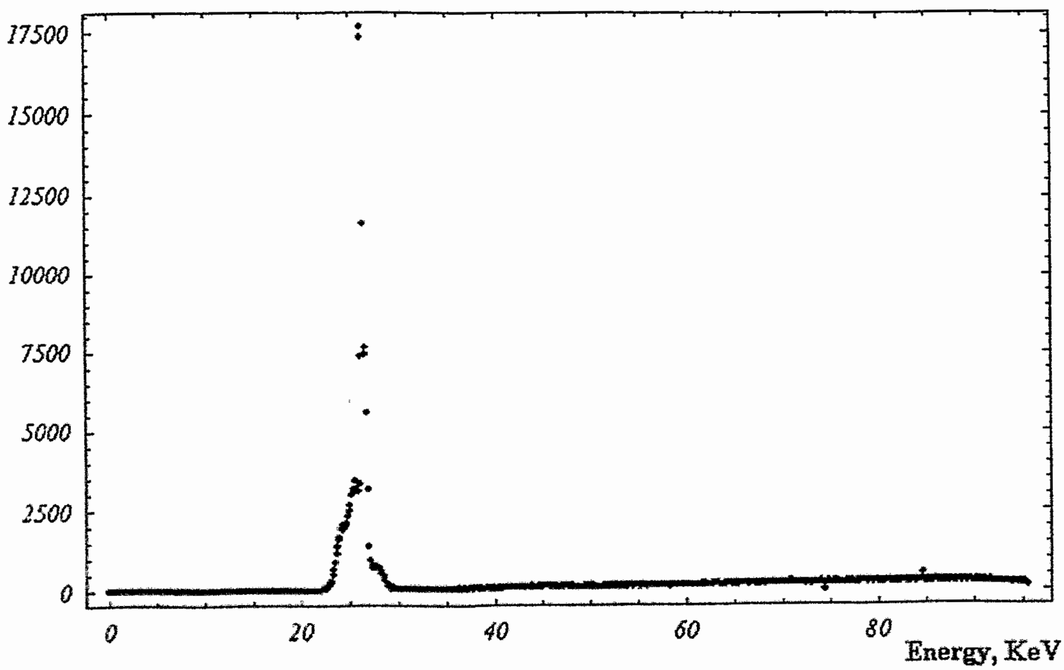

-7-

A. H. Mkrtchyan:

Investigation of PXR under the influence of acoustic waves

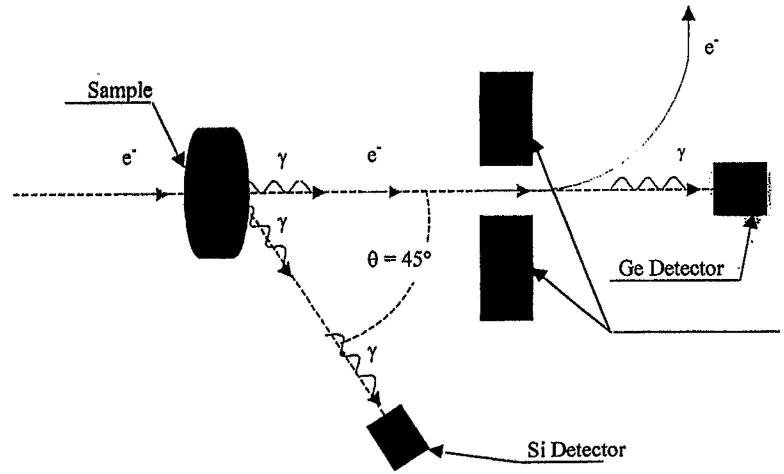

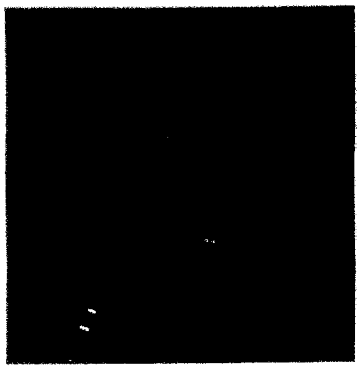

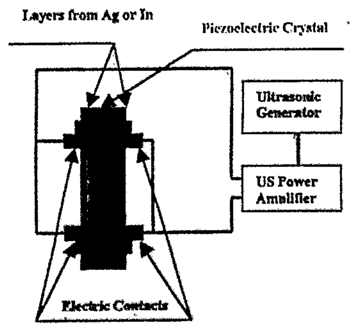

Orientation Scan For X-Cut SiO_2 Crystal, d=810m

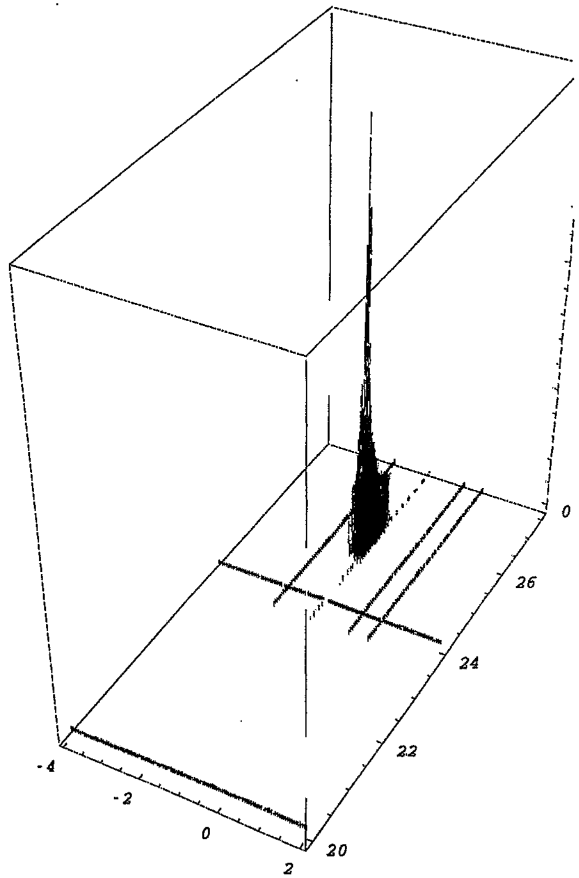

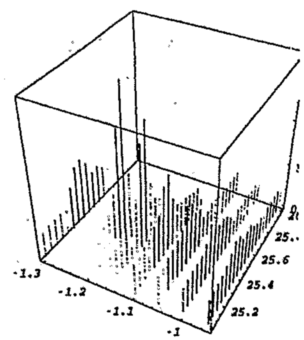

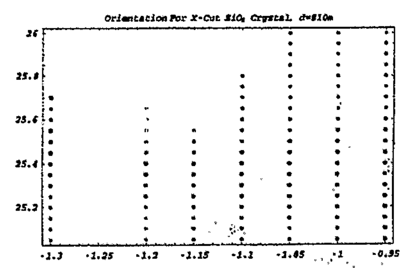

Energy DistributionFor X-Cut SiO_2 Crystal
d=0.795mm Working Planes Family 10$\bar{1}$1

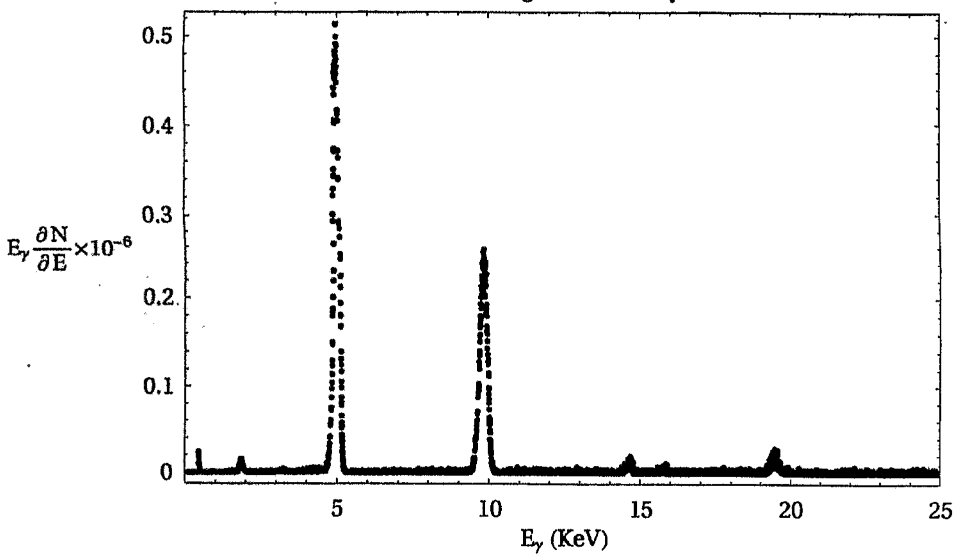

Energy DistributionFor X-Cut SiO_2 Crystal
d=0.795mm Working Planes Family 10$\bar{1}$2

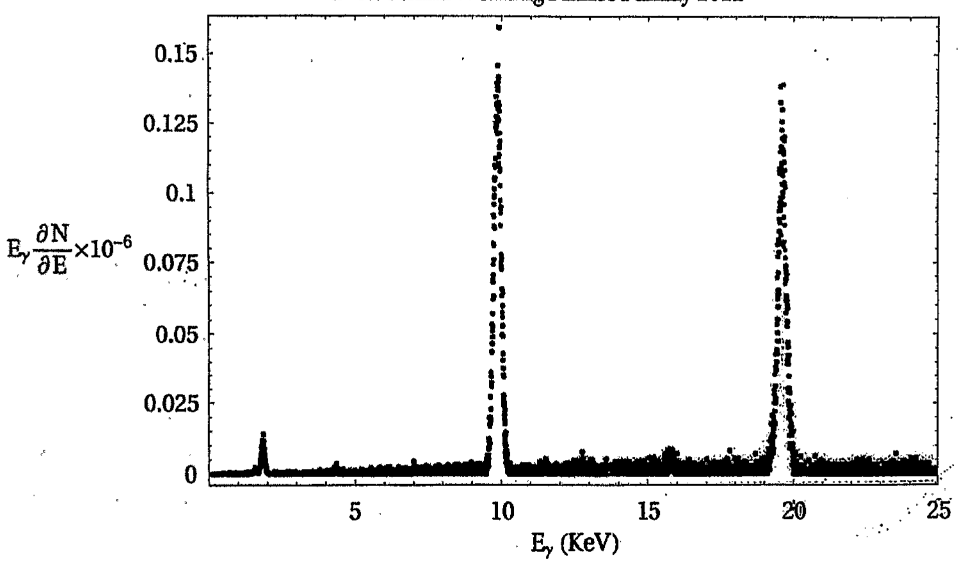

Rocking Curve For X-Cut SiO_2 Crystal,
d=0.795mm Working Plane 10$\bar{1}$1

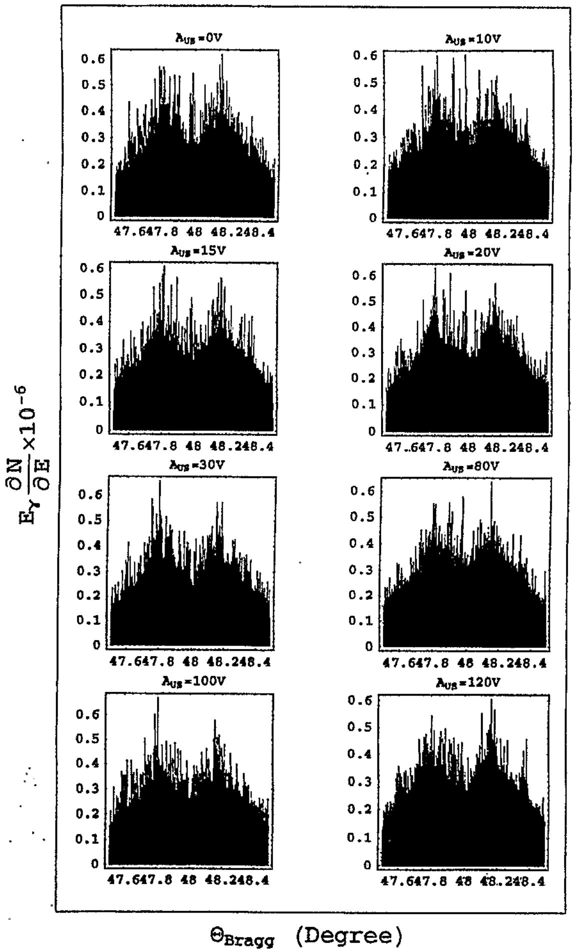

Rocking Curve For X-Cut SiO_2 Crystal,
d=0.795mm Working Plane $20\bar{2}2$

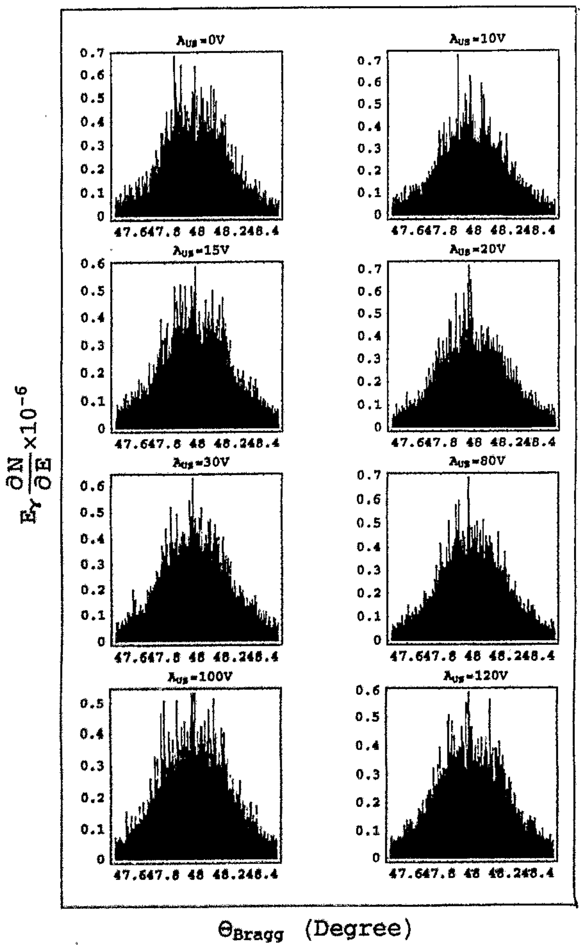

Rocking Curve For X-Cut SiO_2 Crystal,
d=0.795mm Working Plane $10\bar{1}1$

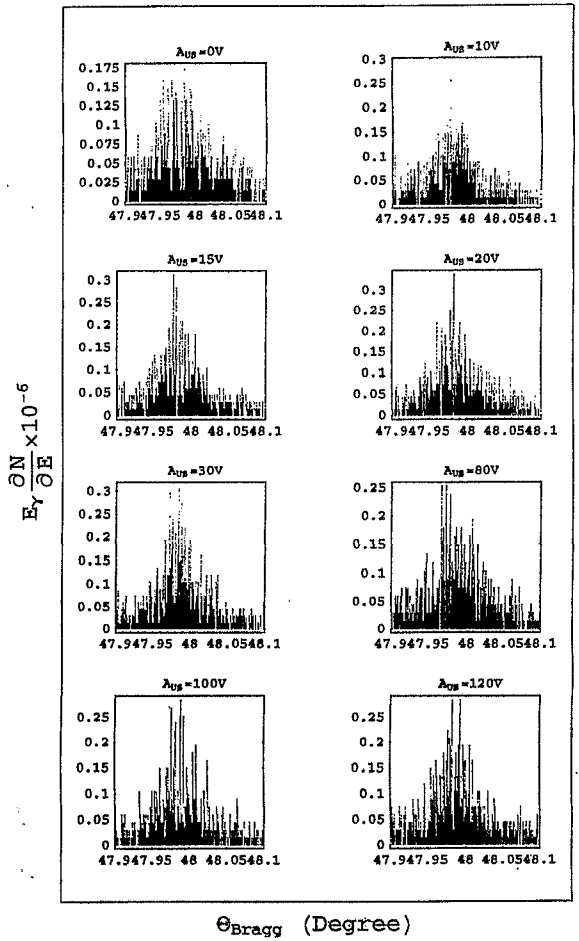

Rocking Curve For X-Cut SiO_2 Crystal,
d=0.795mm Working Plane $10\bar{1}2$

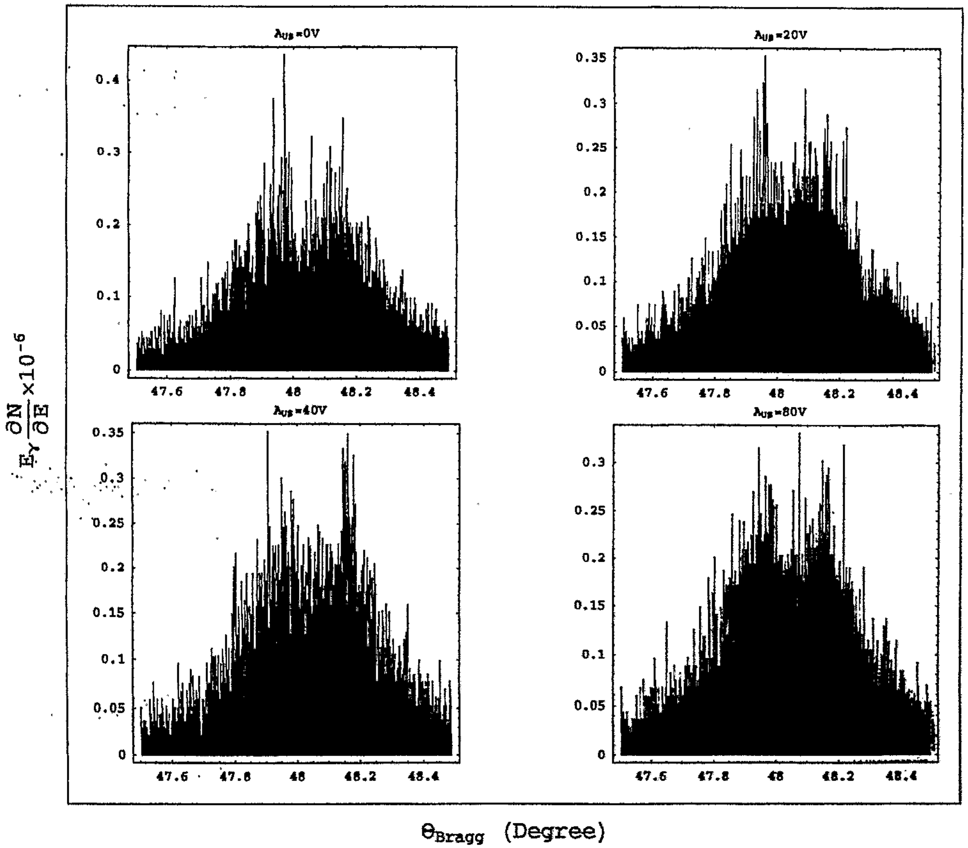

Rocking Curve For X-Cut SiO_2 Crystal,
d=0.795mm Working Plane $20\bar{2}4$

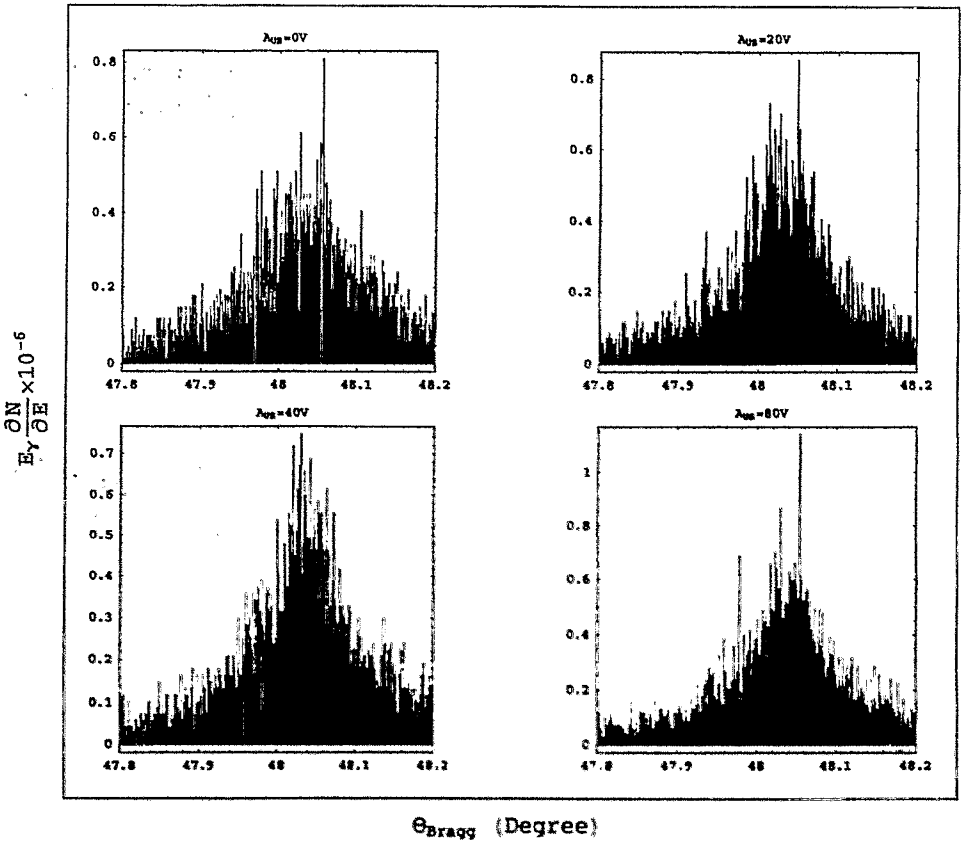

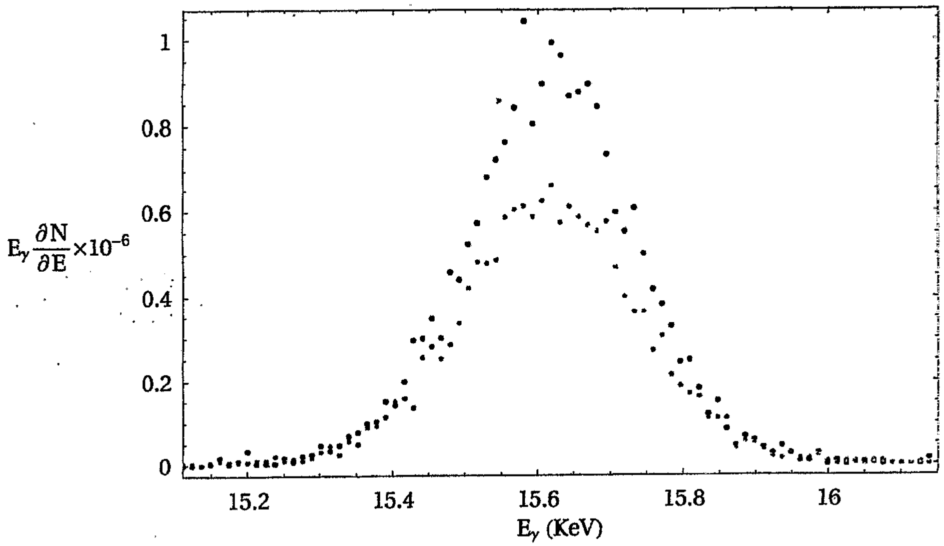

$E_\gamma \frac{\partial N}{\partial E} \times 10^{-6}$
E_γ (KeV)

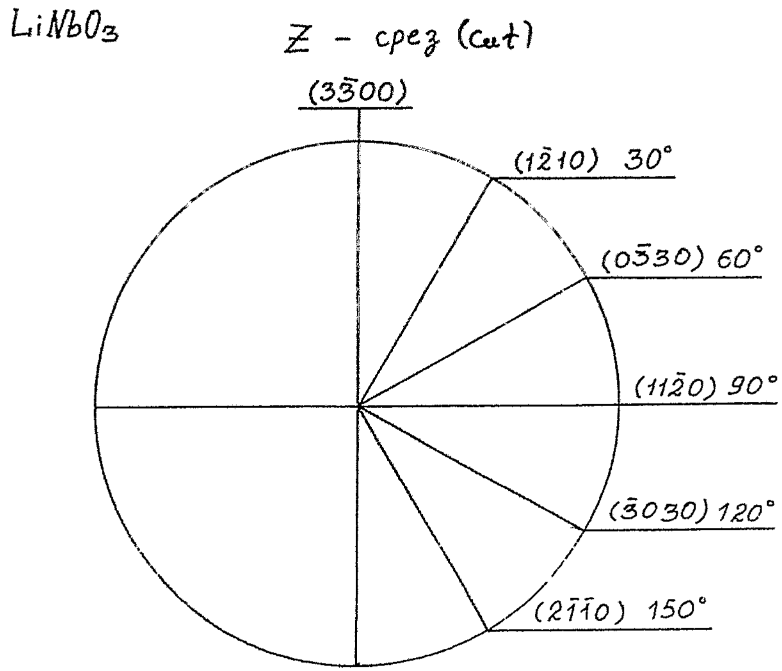

LiNbO3
Z - срез (cut)
(3$\bar{3}$00)
(1$\bar{2}$10) 30°
(0$\bar{3}$30) 60°
(11$\bar{2}$0) 90°
($\bar{3}$030) 120°
(2$\bar{1}\bar{1}$0) 150°

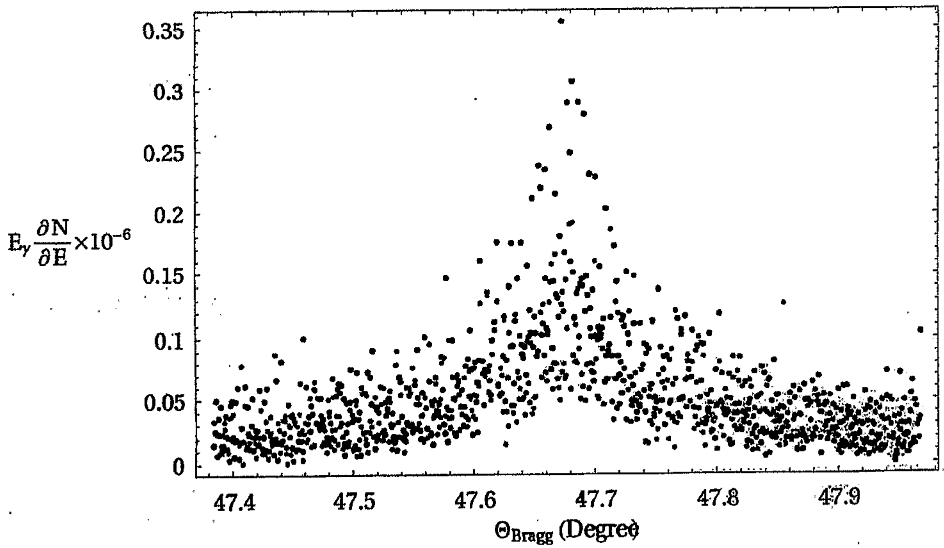

$E_\gamma \frac{\partial N}{\partial E} \times 10^{-6}$
Θ_{Bragg} (Degree)

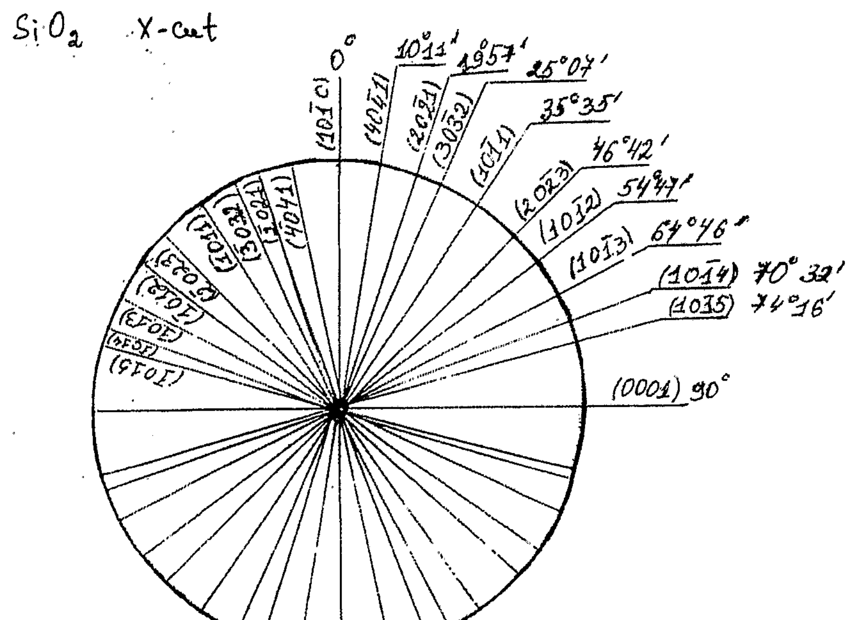

SiO2 X-cut
0°
10°11'
19°57'
25°07'
35°35'
46°42'
54°47'
64°46'
70°32'
74°16'
(0001) 90°

Alpikogramma For X-Cut SiO_2 Crystall, $d=290$m

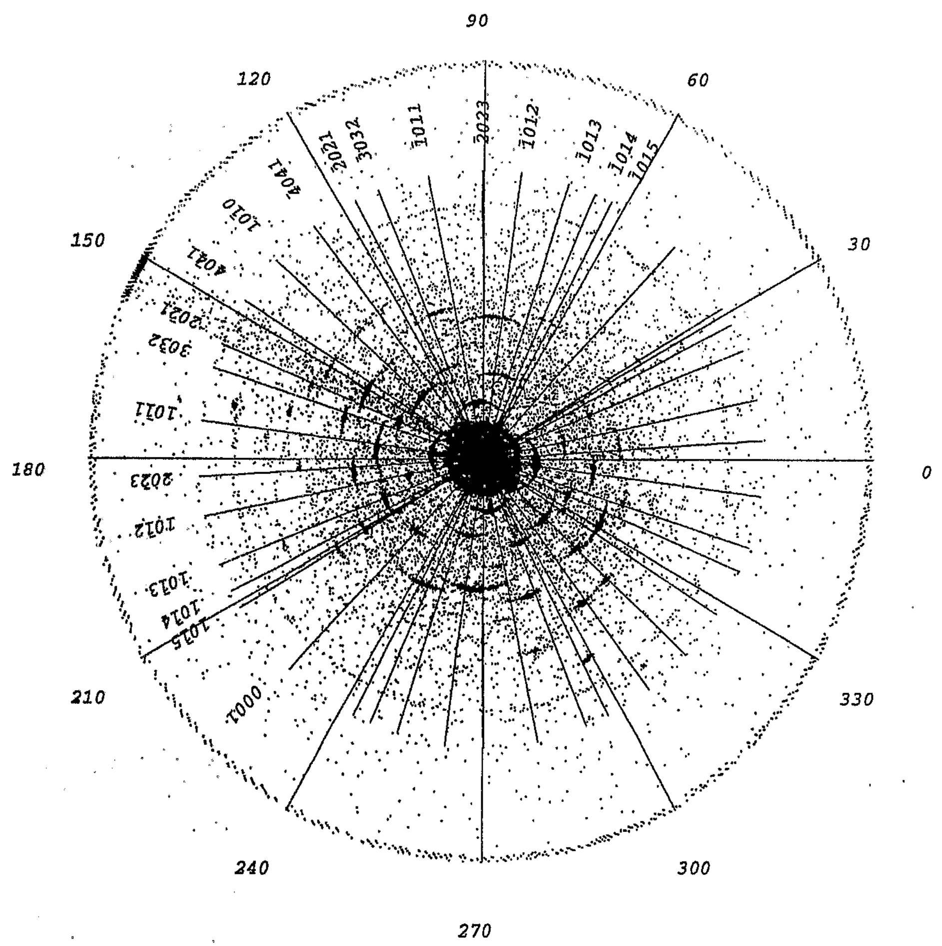

Alpikogramma for X-Cut SiO_2 $d=290$m

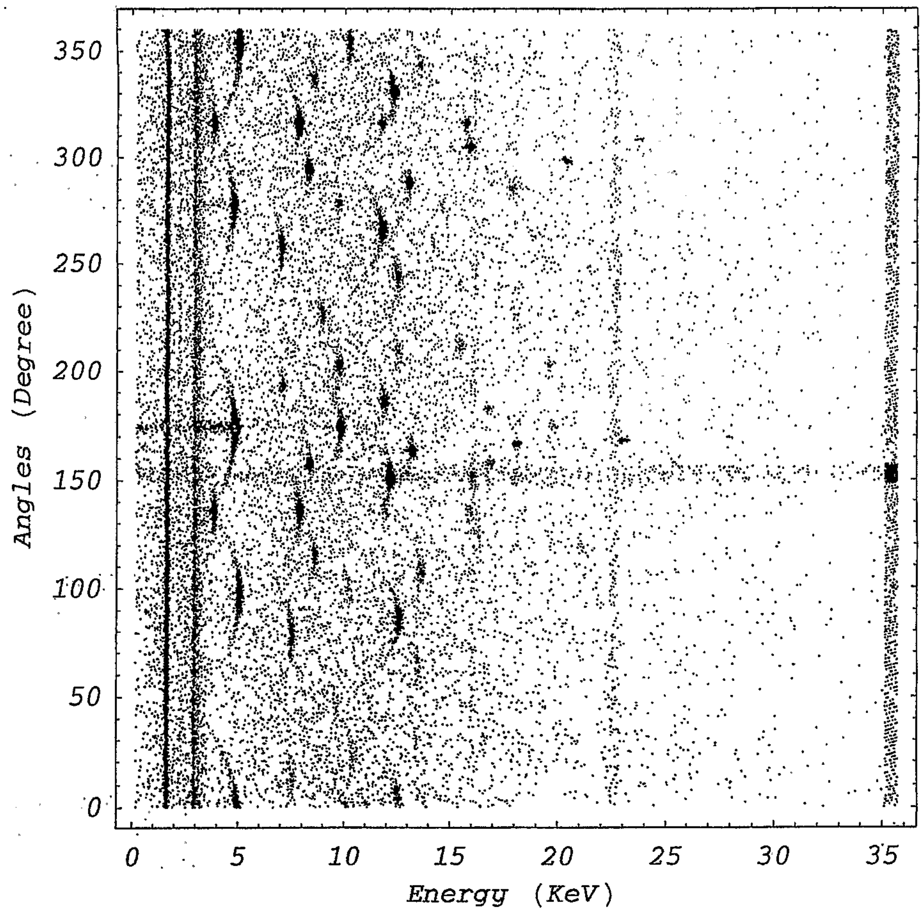

Alpikogramma For X-Cut SiO_2 Crystall, d=810m

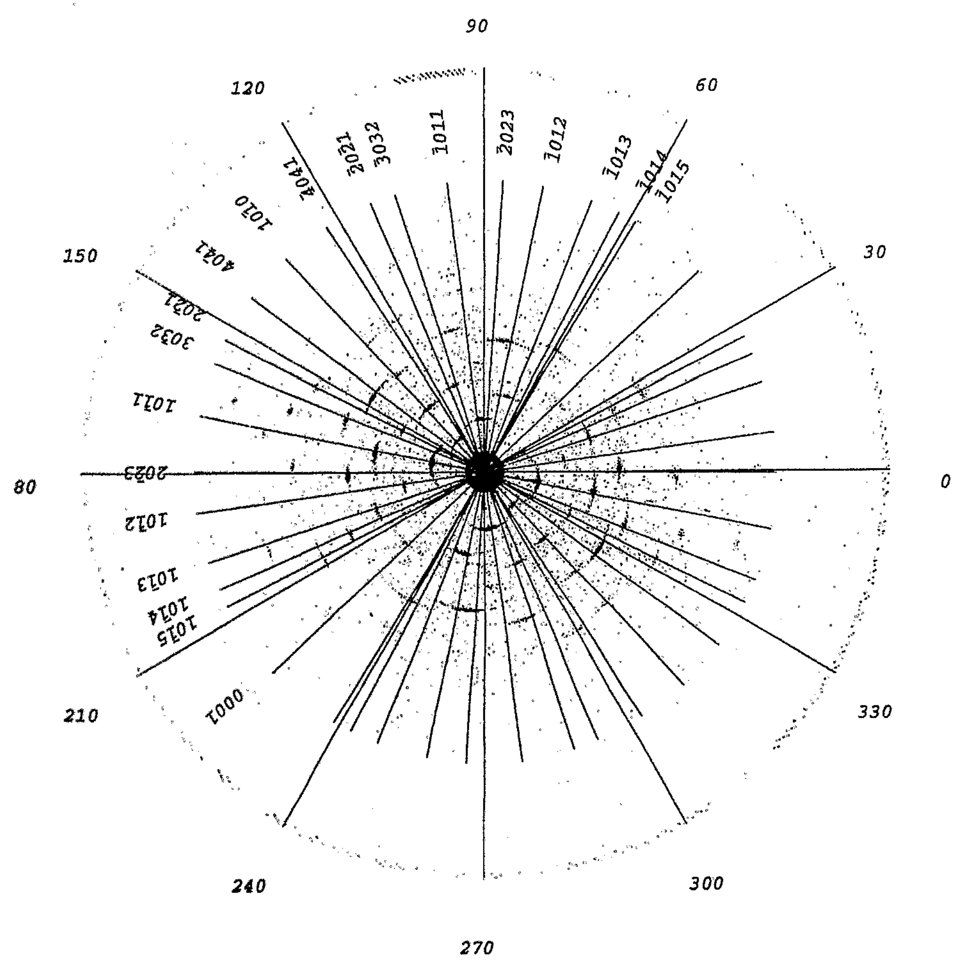

Alpikogramma For X-Cut SiO_2 Crystall, d=810m

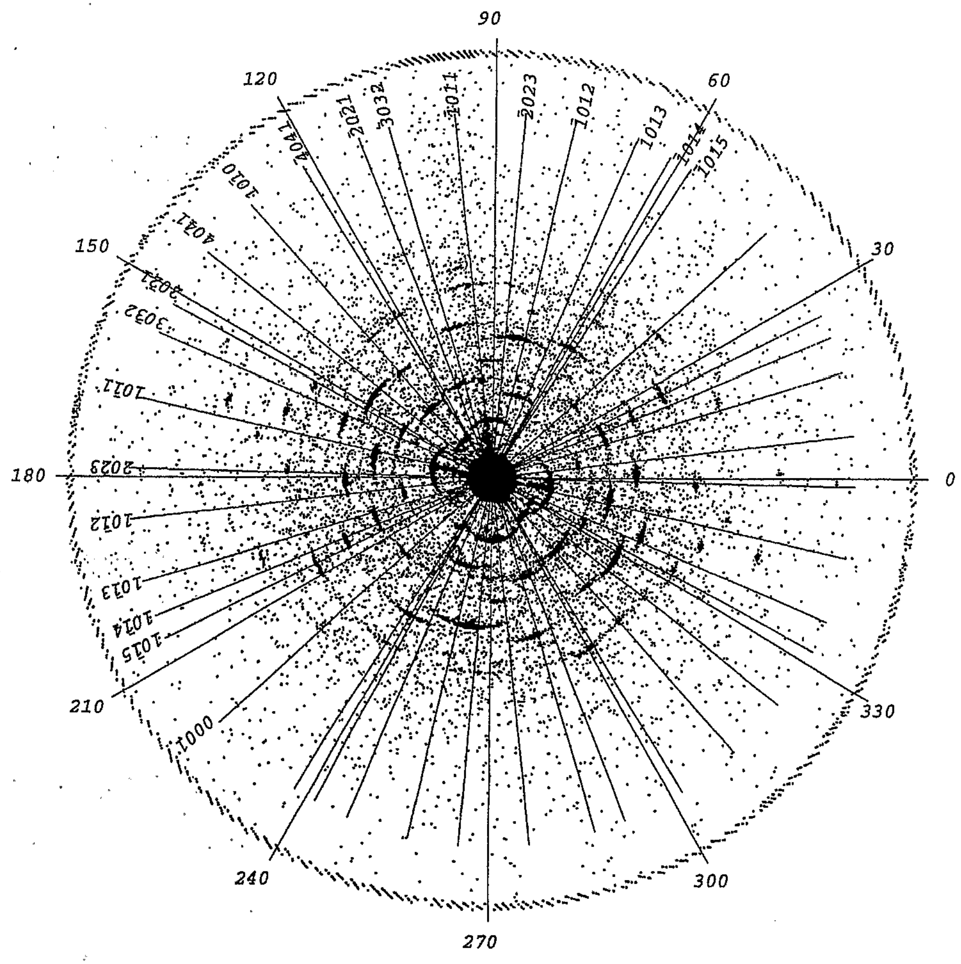

Alpikogramma for X-Cut SiO_2 d=810m

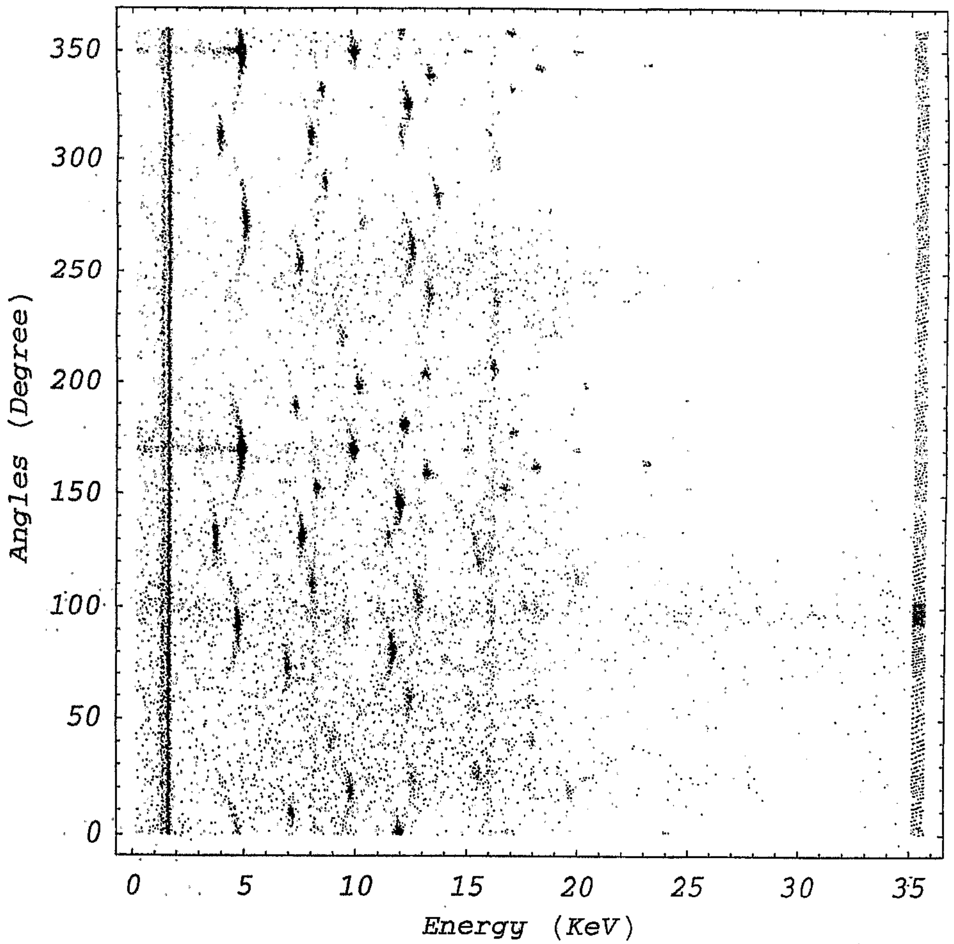

Alpikogramma For Z-Cut $LiNbO_3$ Crystall, d=650m

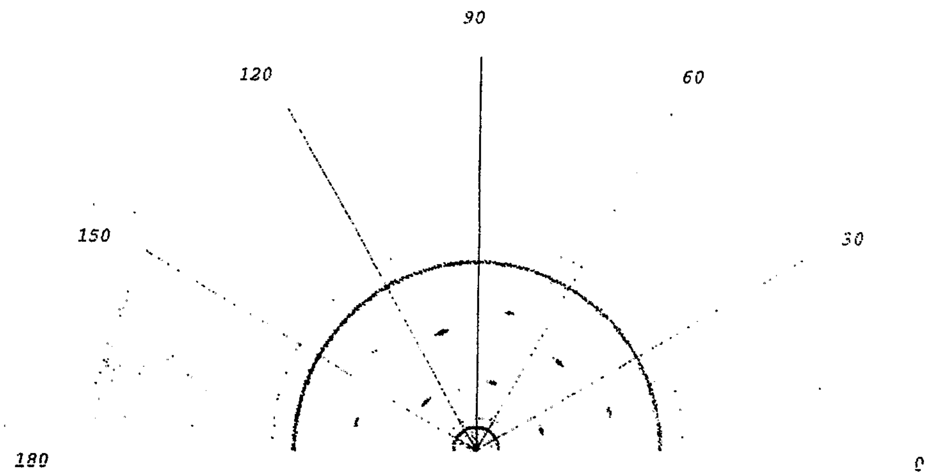

Alpikogramma For Z-Cut $LiNbO_3$ Crystall, d=650m

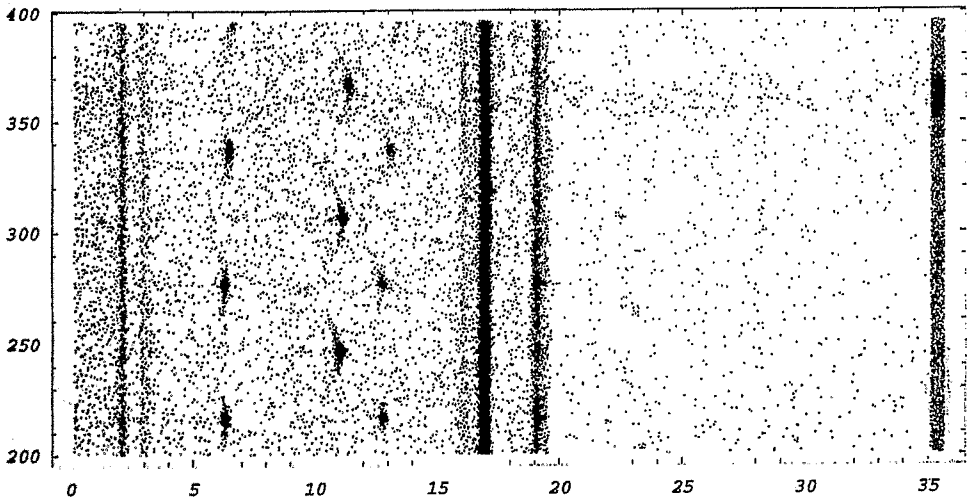

Rocking Curve For X-Cut SiO_2 Crystal,
d=0.810mm Working Plane $10\bar{1}2$

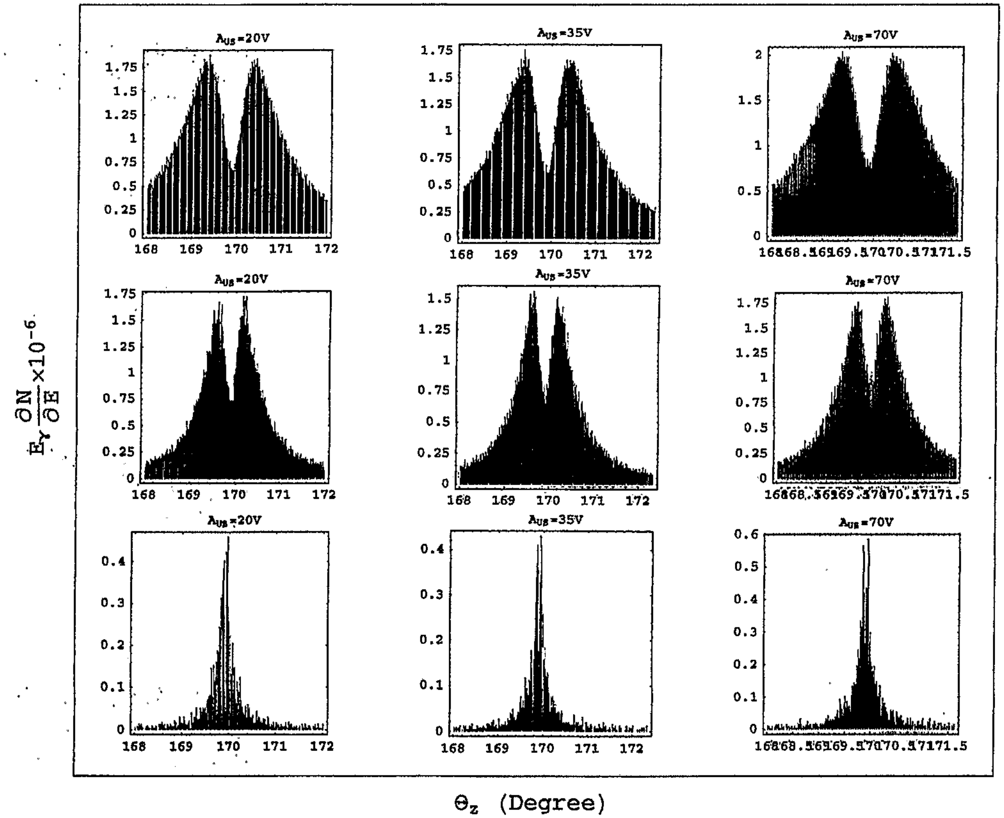

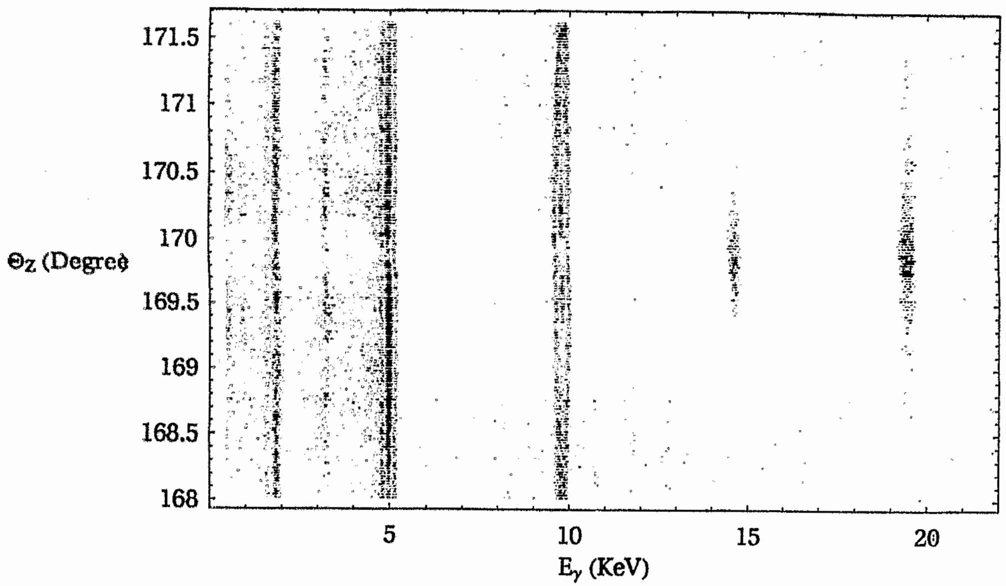

171.5
171
170.5
170
169.5
169
168.5
168
Θz (Degree)
5
10
15
20
Eγ (KeV)

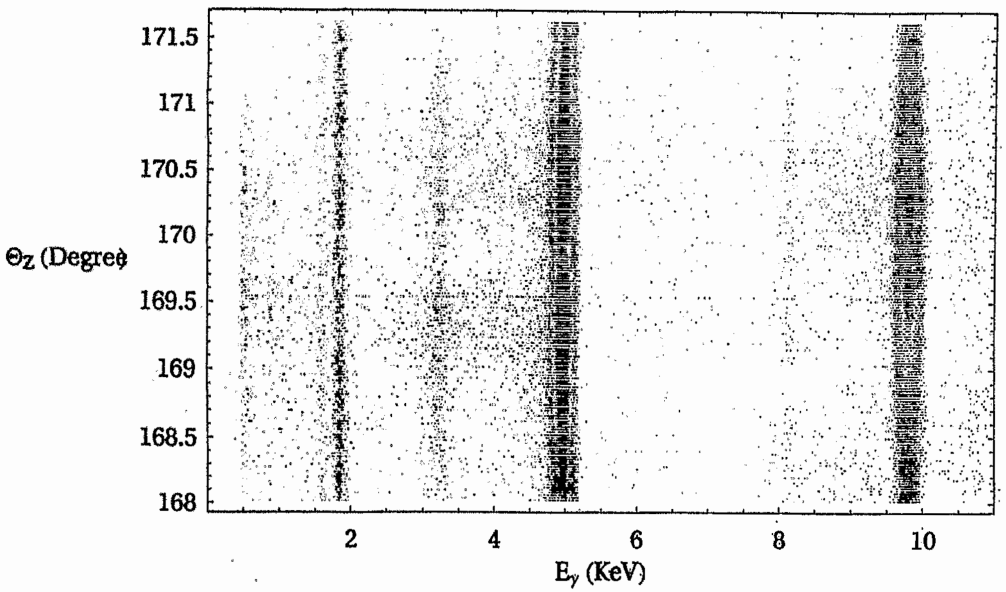

171.5
171
170.5
170
169.5
169
168.5
168
Θz (Degree)
2
4
6
8
10
Eγ (KeV)

H. W. Barz:

Compton backscattering of laser light off the ELBE electron beam

Compton backscattering of laser light off the ELBE electron beam

H.W. Barz

Institut für Kern- und Hadronenphysik
Forschungszentrum Rossendorf

1. Electrons in laser fields
2. Differential cross section and polarization
3. Effective cross sections, production rates

1. Electron in laser field

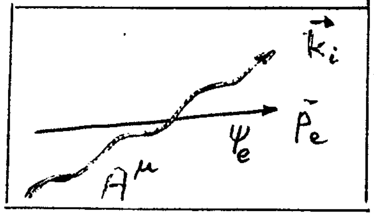

compton wave length : $\lambda\!\!\!^{-}_c = 0.4 \cdot 10^{-12}\ m$

classical e^- - radius : $r_0 = \alpha \lambda\!\!\!^{-} = 2.8 \cdot 10^{-15}\ m$

green laser : $\hbar\omega_i = 2.35\ eV$

Dirac - Equation:

$$[\,i\,\not\partial - e\not{A} - m\,]\,\psi_e = 0$$

plane wave solution:

$$\psi_E = \left(1 + \frac{e}{2}\frac{\not{k}\not{A}}{(kp)}\right) e^{-i\int^{kx} dx'\left[e\frac{pA}{pk} - \frac{e^2}{2}\frac{A^2}{kp}\right]} e^{ipx}\, u$$

D.M. Volkov 1935
Nikishov, Ritus 1964
Brown, Kibble 1964

Non-perturbative effects if $A > A_{crit} = \frac{m}{e}$

electric field strength $\frac{e\,\mathcal{E}_{crit}}{\omega/c} = m$

$\mathcal{E}_{crit} = 0.56 \cdot 10^{11}\ V/cm$

$j_{crit} = 10^{13}\ W/cm^2$

parameter

$$\eta = \frac{\epsilon}{\epsilon_{crit}} = 0 \ldots 0.3$$

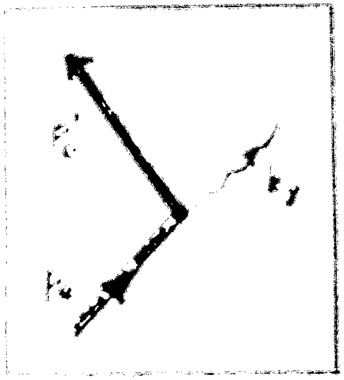

SLAC, 1997

$\eta \sim 1$ Cooperative effects.

$$s k_i + p_e \longrightarrow k_\gamma + p_e'$$

$$\sigma \sim \eta^{2(s-1)} \cdot r_0^2$$

$$\left\{ \begin{array}{l} e^- + 5 k_i \longrightarrow e^- + e^+ e^- \\ k_{Compton} + 4 k_i \longrightarrow e^+ e^- \end{array} \right.$$

$$(25\ \text{GeV}) + (4 \cdot 2.3\ \text{eV}) \longrightarrow 1\ \text{MeV}$$

2. Compton scattering

$T_{fi} =$ 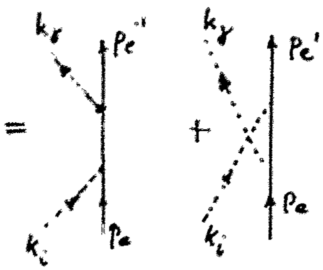

Feynman-diagrams

$$\boxed{k_i + p_e \rightarrow k_\gamma + p_e'}$$

$$\frac{1}{k_\gamma^2} \frac{d\sigma}{d\Omega_\gamma} = \frac{2}{s'} \sum_{ff'ii'} \varepsilon_{ff'}\, T_{fi}\, T^*_{f'i'}\, \rho_{ii'}$$

$$\sum_{fi} |T_{fi}|^2 = \frac{\alpha^2}{s'} \left[\frac{u'}{s'} + \frac{s'}{u'} + 2g + g^2 \right]$$

$s' = 2 p_e k_i$

$u' = 2 p_e k_\gamma \rightarrow (\Omega_\gamma)$

$g = 2m^2 \left(\frac{1}{s'} - \frac{1}{u'} \right)$

in lab - system : Klein - Nishina 1929

$$\frac{d\sigma}{d\Omega} = \frac{r_0^2}{2} \left(\frac{k_\gamma}{k_i} \right)^2 \left[\frac{k_\gamma}{k_i} + \frac{k_i}{k_\gamma} - (1 - P_t) \sin^2(\Theta) \right]$$

$$\sigma \rightarrow \left(\frac{8\pi}{3} r_0^2 \right) = 667\ \text{mb}$$

Thomson cross section

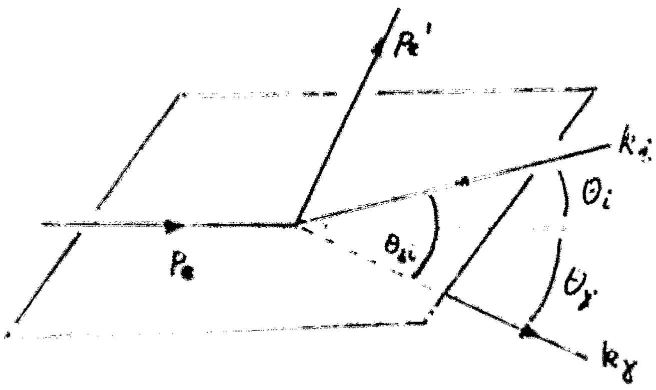

$$k_\gamma = k_i \frac{E_e + p_e \cos\theta_i}{E_e - p_e \cos\theta_\gamma + k_i(1 - \cos\theta_{\gamma i})}$$

$$k_\gamma \cong k_i \frac{4\gamma^2}{1 + \gamma^2\theta_\gamma^2 + \frac{4\gamma k_i}{m}}$$

$E_e = \gamma m \gg m$
$\theta_i = 0$
$\theta_\gamma \ll 1$

$\sigma d\Omega_\gamma \sim k_\gamma^2$

- Photons emitted in forward cone $\Delta\Theta \sim \frac{1}{\gamma}$
- $\left(\frac{d\sigma}{d\Omega}\right)_0$ ... $\frac{mb}{sr}$ γ^2
- two regimes $E_e \lessgtr \frac{m^2}{4k_i}$ ~ 30 GeV

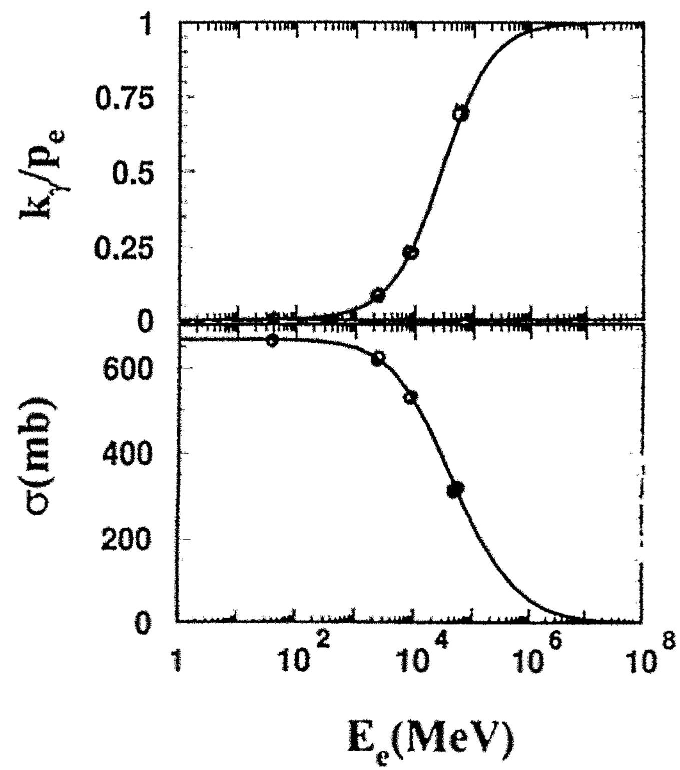

	E_e	E_γ
ELBE	40 MeV	60 keV
LEGS	2.6 GeV	220 MeV
SPRING8	8 GeV	1.8 GeV
SLAC	46 GeV	29 GeV

Scattering of unpolarized laser
off 40 MeV electrons

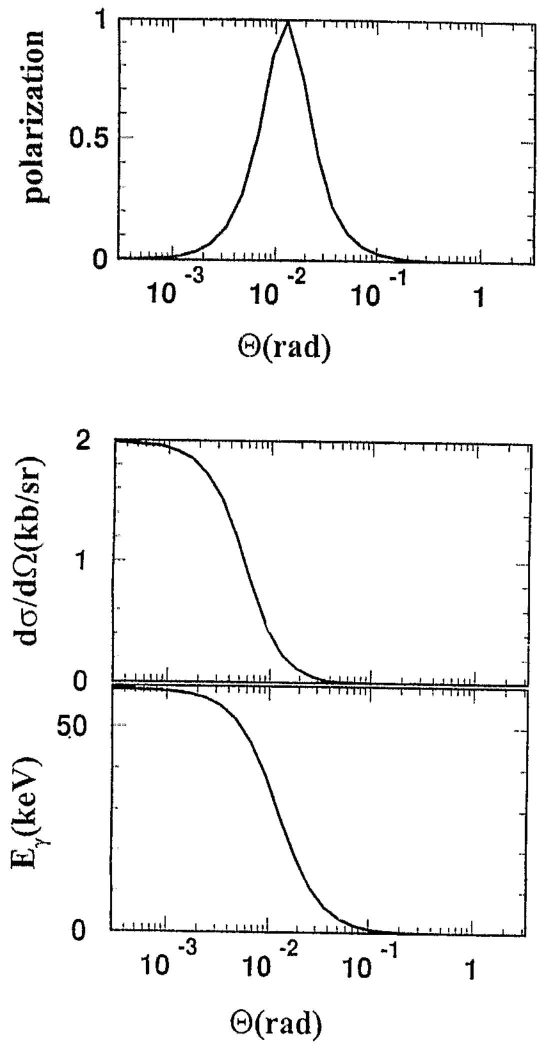

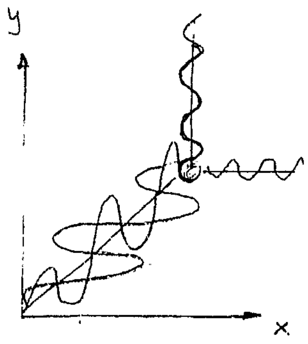

Polarization

$$\rho_{ii'} = \frac{1}{2}\left(1 + \vec{\xi}\,\vec{\sigma}\right) = \frac{1}{2}\begin{pmatrix} 1+\xi_3 & \xi_1 + i\xi_2 \\ \xi_1 - i\xi_2 & 1-\xi_3 \end{pmatrix}$$

$$= \begin{pmatrix} \uparrow\uparrow & \uparrow\downarrow \\ \downarrow\uparrow & \downarrow\downarrow \end{pmatrix}$$

$$P = |\xi|^2 < 1$$

convention : e^- beam direction

γ $\perp$ beam direction

ξ_2 : circular polarization:

Effects:

- electrons reflect polarized laser light
  $\Theta \ll 1$; $P_f = P_i$

- $E_e \gtrsim 30$ GeV

unpolarized e^- $\Longrightarrow$ ← circular polarized laser

→ 'linear' polarized e^-

compton polarimeter : $\sigma \sim 1 + \alpha(P)$

Scattering of linearly polarized (ϕ=90°) photons

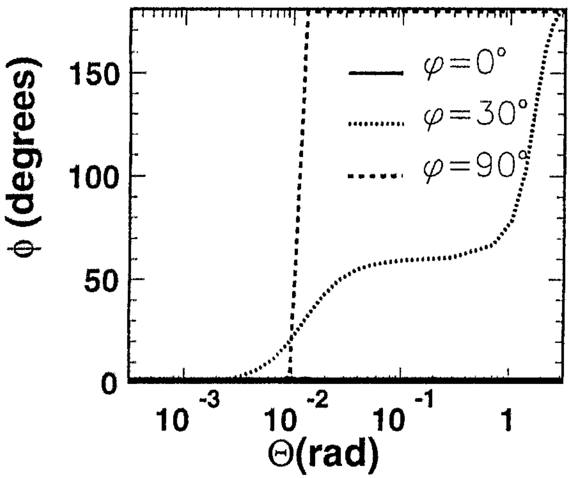

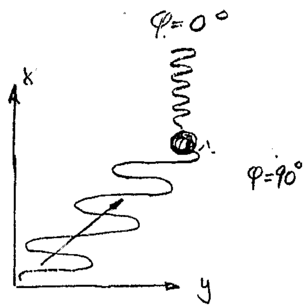

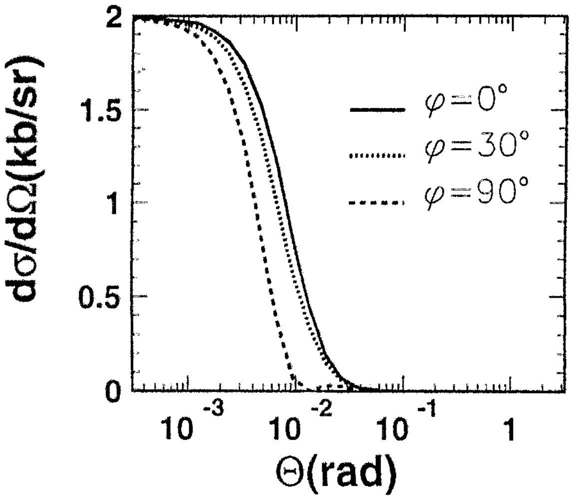

3. Production rates

Production rates $\frac{dN_\gamma}{dE_\gamma\, dt}$ depend on

- Luminosity L
- energy resolution ΔE_e
- angle spread $\Delta \Theta_e$

$$\boxed{\dot{N}_\gamma = L\,\sigma}$$

Luminosity

bunch - crossing

$$L = \int dV \left[(j_e j_i)^2 - j_e^2 j_i^2 \right]^{1/2} = \frac{1}{A} N_e \cdot N_i \cdot f$$

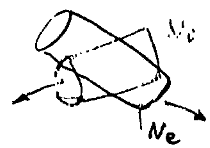

f: frequency

A: crossing area

$$\boxed{L = L_0 \frac{1}{\hbar\omega\,(2.35\,\mathrm{eV})} \frac{1}{A/\mathrm{mm}^2} \frac{1}{f/\mathrm{MHz}} \frac{I_e}{\mathrm{mA}} \frac{P_{laser}}{\mathrm{W}}}$$

$$L_0 = 10^{30} \frac{1}{\mathrm{cm}^2 \mathrm{s}} = \frac{10^3}{\mathrm{nb} \cdot \mathrm{s}}$$

Effective Cross section

$$\boxed{\frac{d^2\sigma}{dE_\gamma d\Omega_\gamma} \sim \int dp_e\, e^{\frac{-(p_e-p_0)^2}{2\Delta E_e^2}} \int d\Omega_e\, e^{\frac{-\Theta_e^2}{2\Delta\Theta_e^2}} \times \frac{d\sigma}{d\Omega_\gamma} \cdot \delta\left(E_\gamma - k_\gamma(p_e,\Omega_e,\Omega_\gamma)\right)}$$

ELBE: $\Delta E_e = 25$ keV $\quad \Delta\Theta_e = 0.07$ mrad

$A = \pi\ mm^2$; $\quad \sigma_{eff} = 15 mb$; $E_\gamma = 60$ keV $\quad \underline{\dot{N}_\gamma = 10^3/s}$

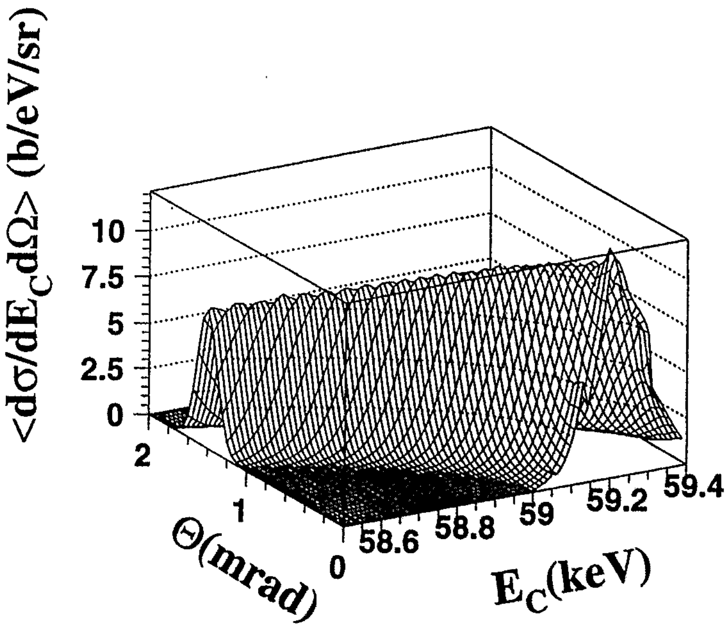

For comparison: Vanderbilt, Nashville

- macro pulse $\quad 25$ Hz, $\quad \tau = 2.5\,\mu s$
- micro pulses

$$\left.\begin{aligned} f &= 2\cdot 10^9\ s^{-1} \\ A &= \pi\,(0.15mm)^2 \\ N_e &= 4\cdot 10^8 \\ N_i &= 2\cdot 10^{13}\ (IR,\ \hbar\omega = 0.5eV) \end{aligned}\right\} \begin{aligned} L &= 4\cdot 10^{34}/cm^2 s \\ \dot{N}_\gamma &= 10^9/s \end{aligned}$$

$$\left(\dot{N}_\gamma\right)_{macro} = 10^5/s \quad \left(exp:\ 4\cdot 10^4\, s^{-1}\right)$$

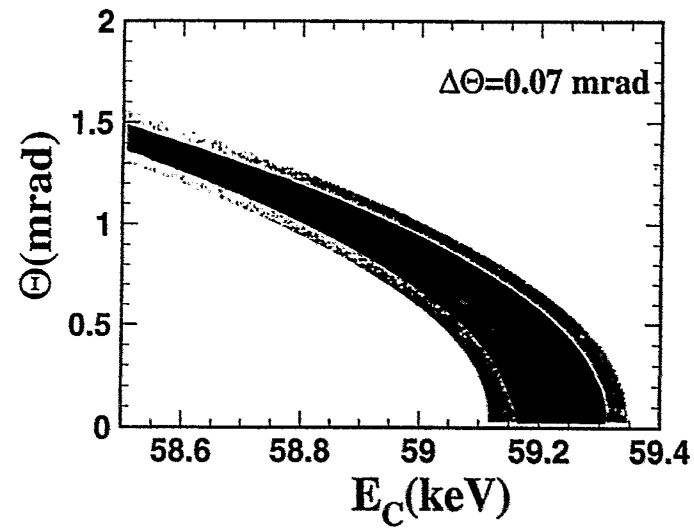

higher intensity

- narrow focus $A = \pi (0.1\,mm)^2$

  $\rightsquigarrow$ $\Delta\Theta_e = 0.7$ mrad

  $\dot{N}_\gamma = 10^5/s$

- internal IR laser field in the optical resonator

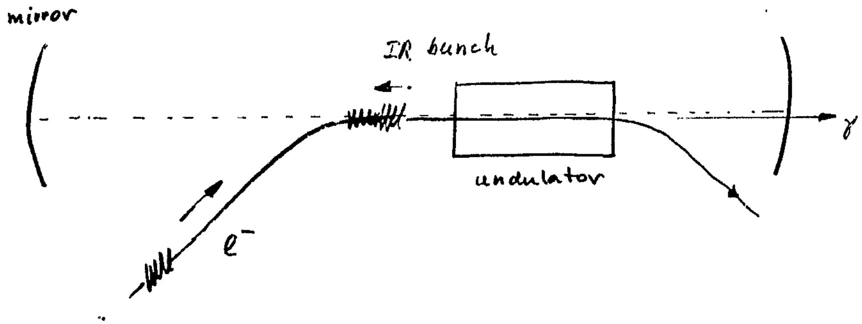

$\bar{P} = 10^4$ W

$E_i = 0.2$ eV ($5\mu m$); $E_\gamma = 6$ keV

$\dot{N}_\gamma = 10^8/s$

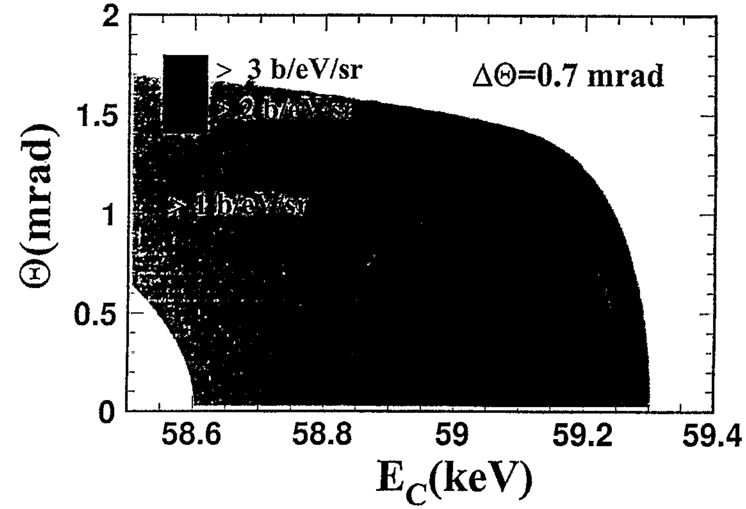

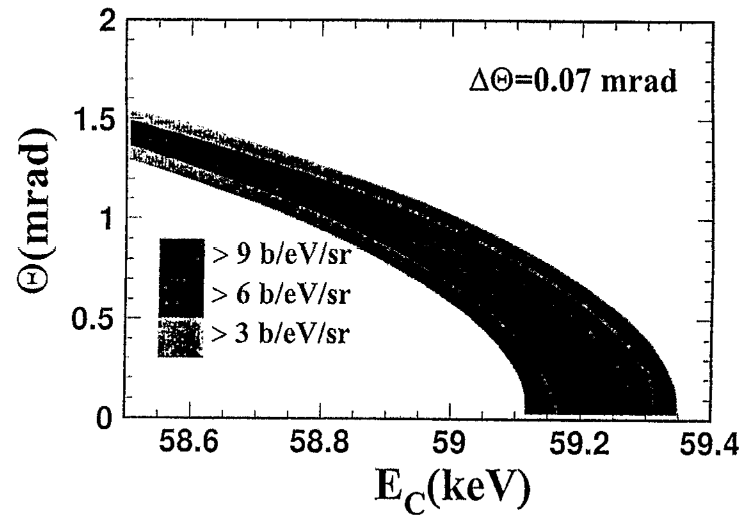

Summary

Expected rates:		$\Delta E_\gamma / E_\gamma$	
usual	$\sim 10^{3}\ s^{-1}$	0.5 %	(beam)
strong focused	$\sim 10^{5}\ s^{-1}$	1.5 %	
interne FEL	$\sim 10^{8}\ s^{-1}$	$\sim$	

M. A. Piestrup:

Compound refractive lenses for novel X-ray sources

Compound Refractive Lenses for Novel X-ray Sources

Melvin A. Piestrup, H. Raul Beguiristain,
Charles K. Gary, Richard H. Pantell*,
J. Theodore Cremer, Roman Tatchyn* *

Adelphi Technology, Inc.
2181 Park Blvd.
Palo Alto, California, 94306

*Stanford University
** Stanford Synchrotron Radiation Laboratory

Adelphi Technology, Inc.

D Publications and Patents

- Toshihisa Tomie, US Patent #5,594,773 "X-ray Lens" (Jan. 14, 1997) filed Jan. 1994.
- A. Snigivrev, V. Kohn, I. Snigireva and B. Lengeler, "A compound refractive lens for focusing high-energy X-rays, Nature 384, 49 (1996).
- J. T. Cremer, M. A. Piestrup, H. R. Beguiristain, C. K. Gary, R. H. Pantell, R. Tatchyn "Refractive X-ray Lenses using Low Density Plastics," Rev. of Scientific Instruments 70, (Sept. 1999)

Adelphi Technology, Inc.

Focusing: Papers and Patents

- M. A. Piestrup, R. H. Pantell, J. T. Cremer and H. R. Beguiristain, "Refractive X-ray Lenses," US Patent submission (filed May 1999).
- B. Lengeler, C. G. Schroer, M. Richwin, J. Tòmmeler, M. Drakopolulos, A. Snigirev and I. Snigireva, "Appl. Phys. Lett. 74, 3924 (1999).
- H. R. Beguiristain, M. A. Piestrup, R. H. Pantell, C. K. Gary and J. T. Cremer "Development of compound refractive lenses for x-rays," Conference proceedings, 11th US National Synchrotron Radiation Instrumentation Conference (Oct. 1999).
- M. A. Piestrup H. R. Beguiristain, R. H. Pantell, C. K. Gary, J. T. Cremer and R. Tatchyn, "Compound Refractive Lenses for Novel X-ray Sources," Conference proceedings, RREPS(99) submitted to Nucl. Instrum. Methods A. (1999)

Holes Work as Lenses!!

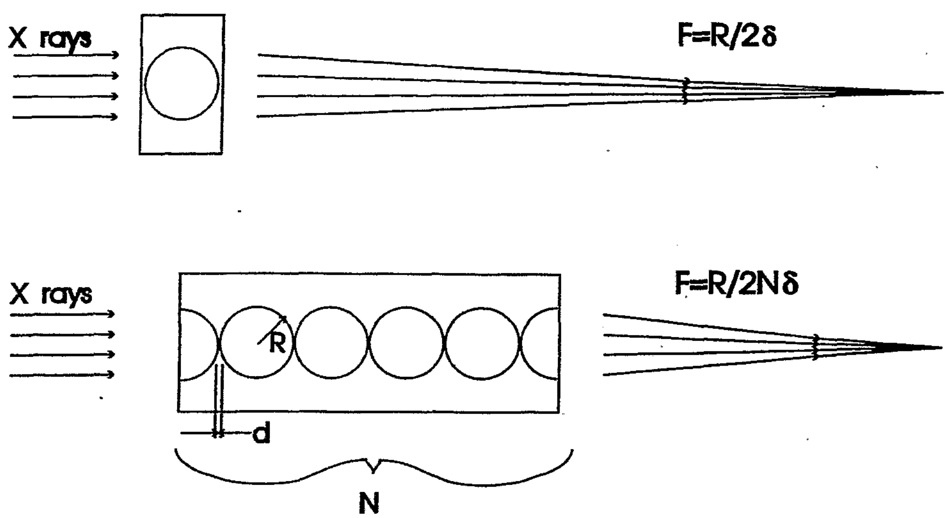

Example CRL capable of 1-D focusing

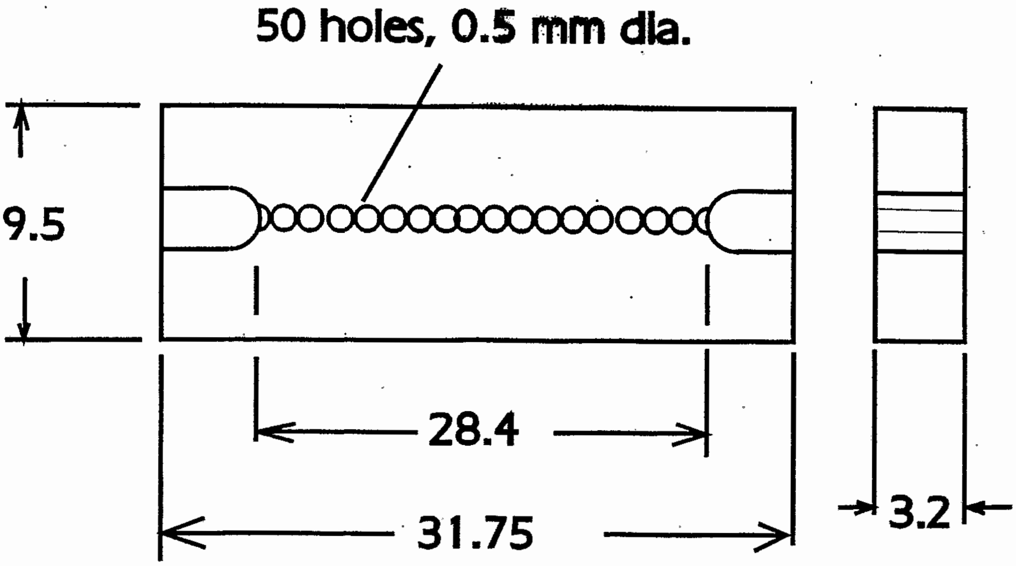

Adelphi Technology, Inc.

Two lenses

Pedrotti "Introduction to Optics" 1987 p. 60

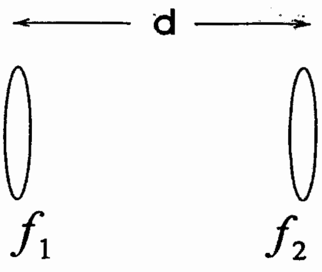

$$\frac{1}{f_{ev}} = \frac{1}{f_1} + \frac{1}{f_2} - \frac{d}{f_1 f_2} \approx \frac{1}{f_1} + \frac{1}{f_2}$$

$$d \to 0$$

$$f_1 = f_2$$

$$f_{ev} = \frac{f}{2}$$ for N lenses $\rightarrow f_{ev} = \frac{f}{N}$

Adelphi Technology, Inc.

fraction at x-ray photon energies

$$n = 1 - \delta + i\beta$$

δ is between 10^{-5} and 10^{-7}

n is less than 1

$$f = \frac{R}{2\delta}$$ single lens, if R= 0.3 mm, d = 3×10^{-6}, then f = 50 meters

$$f = \frac{R}{2N\delta}$$ N lenses, if N = 100 then f = 50 cm!

Adelphi Technology, Inc.

Holes Work as Lenses!!

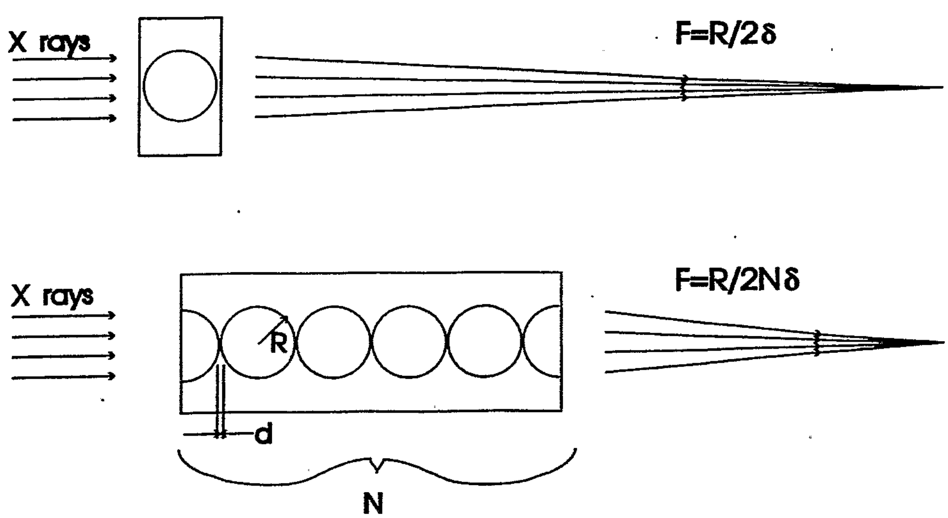

Adelphi Technology, Inc.

Apertures of Lenses

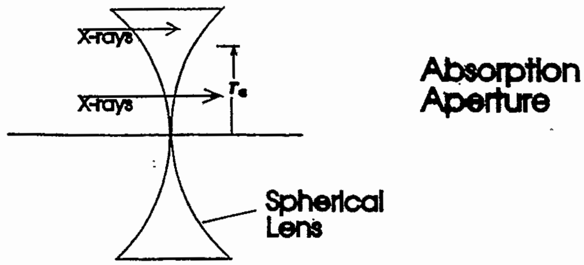

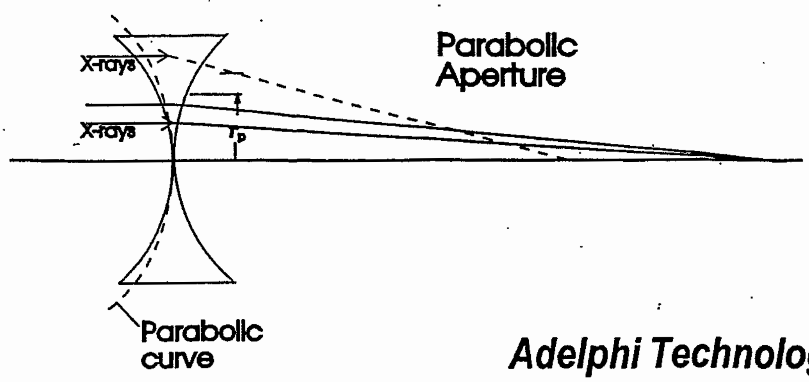

Adelphi Technology, Inc.

B. Aperture

1. Physical aperture = 2R

2. Spherical aberration aperture, A_s

This occurs for a circular lens and not a parabolic lens. The aperture is defined as twice the radius at which there is π phase shift error due to the non-parabolic curvature.

$$\frac{A_s}{2} = \left[4R^2\lambda\, r_i\right]^{.25}$$

where r_i = distance between lens and image

3. Absorption aperture, A_a

$A_a / 2$ = radius at which the power through the lens is reduced by the factor Exp[-2]

$$A_a = 4\sqrt{\frac{f\delta}{\mu}}$$

Absorption Aperture for Selected Materials

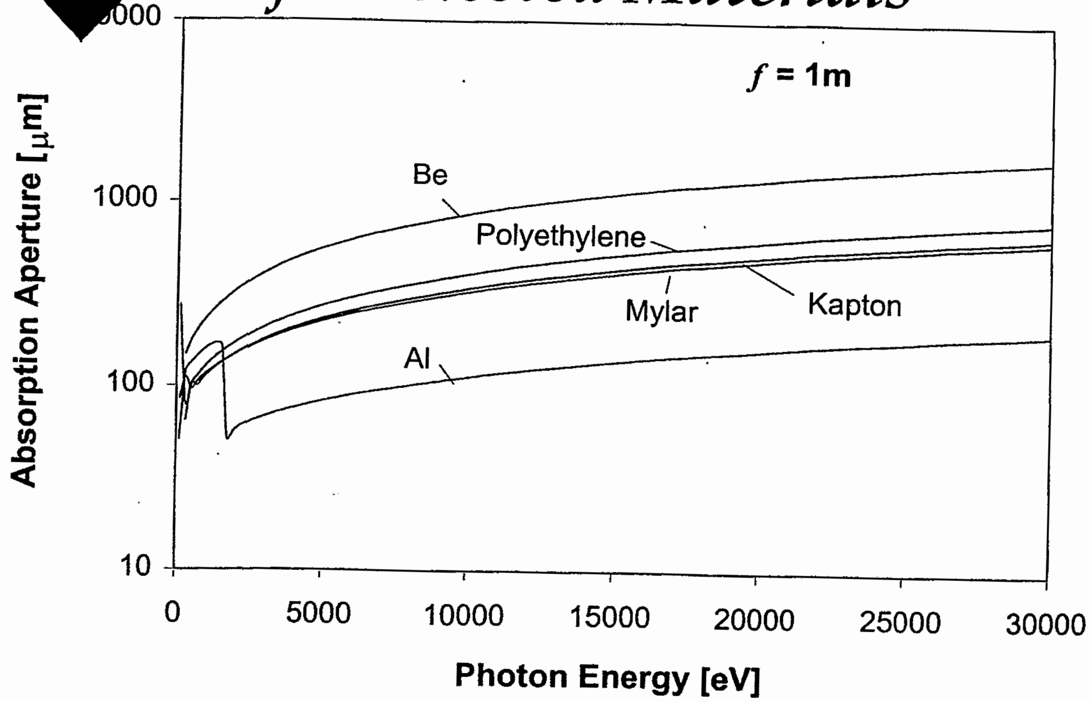

Adelphi Technology, Inc.

ABSORPTION APERTURE vs WAVELENGTH

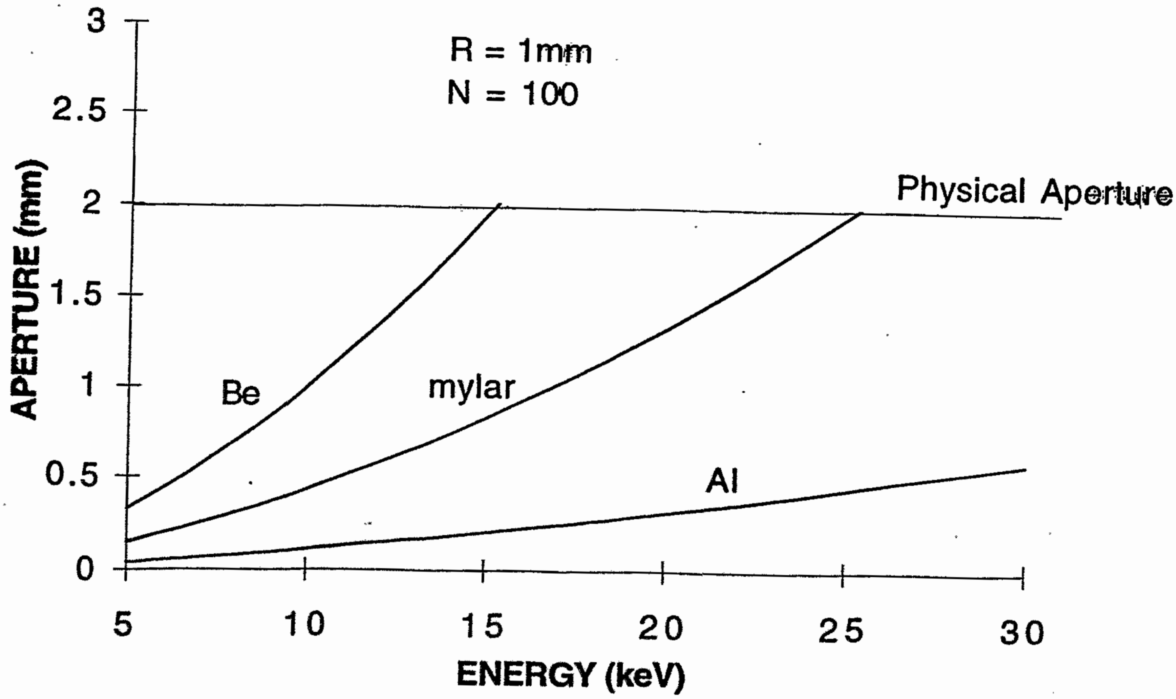

[redacted]al Length

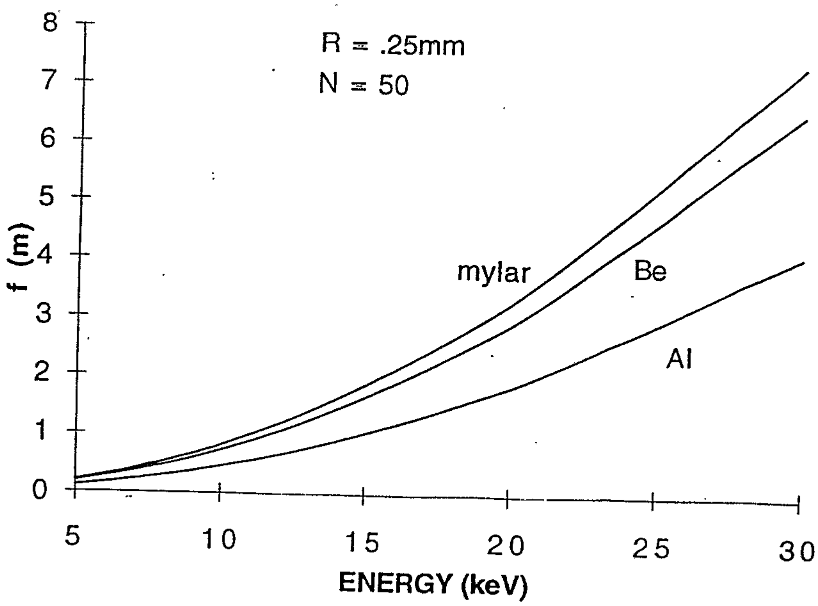

Adelphi Technology, Inc.

[redacted]ain: *the ratio of the on-axis intensity [redacted]with and without the lens in place*

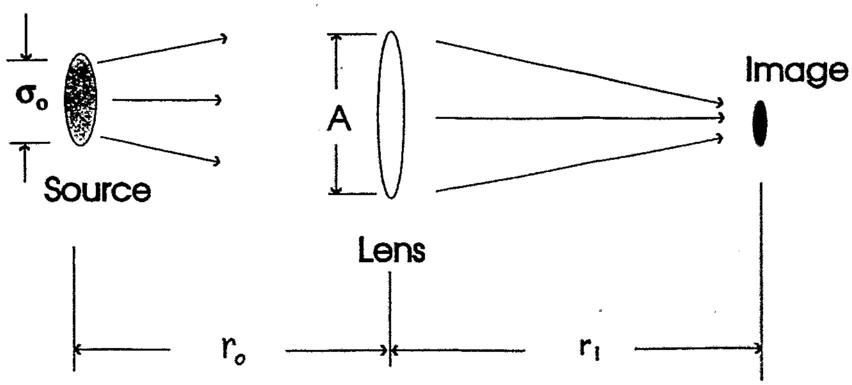

$$G = T\left(\frac{A}{\sigma_o}\right)M$$

T = transmission through lens
M = Magnification = r_o/f

Adelphi Technology, Inc.

C. Gain

Gain = ratio of the on-axis intensity with and without the lens in place

$$\text{1-d Gain for an incoherent source} = \frac{Ar_0}{\sigma_0 f}$$

where r_0 = distance from source to lens

σ_0 = source size

For a symmetrical source, 2-d Gain = $[\text{1-d Gain}]^2$

Including base absorption:

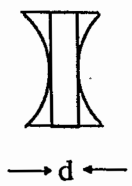

Gain (with base) = Exp($-\mu$Nd) X Gain (without base)

Typical parameters: σ_0 =.4mm, r_0 =17m, f =1m, d = .01mm, N =100

With Be at 8keV: μ =.17mm^{-1}, A_a = .71mm

This gives: 1-d Gain = 25   2-d Gain = 760

NORMALIZED GAIN vs WAVELENGTH

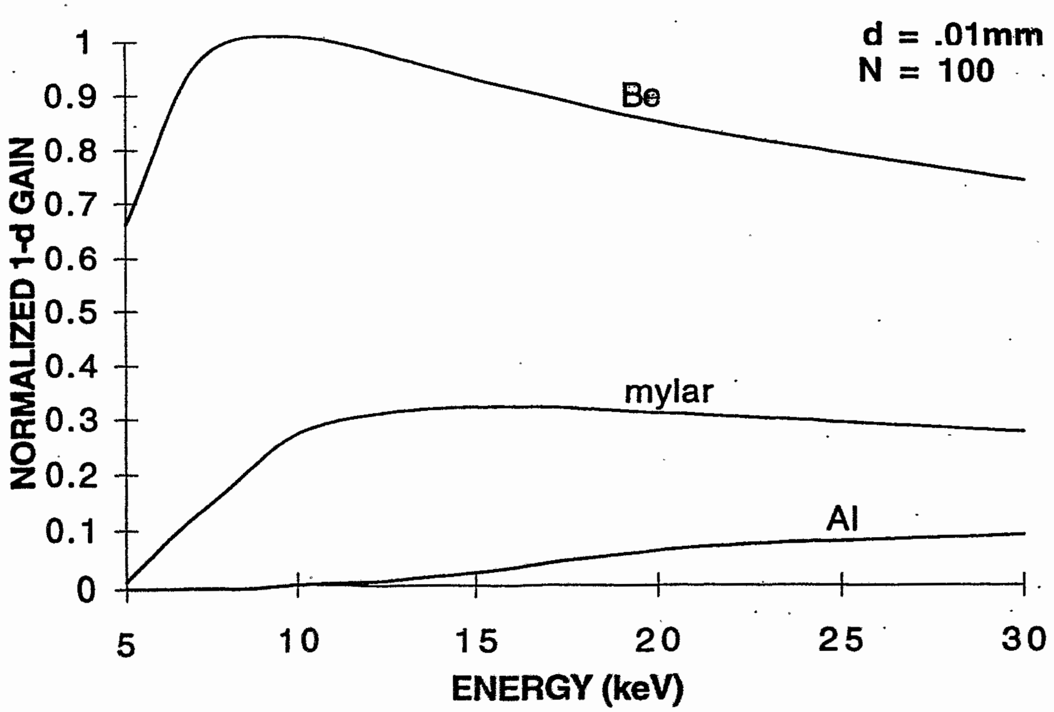

VI. Testing the lens

Source: synchrotron radiation (SSRL)

distance from source to lens = 16.8m

source size = .44 X 1.7mm

2.4 to 30 keV energy tuning

5 X 10^{-4} energy resolution

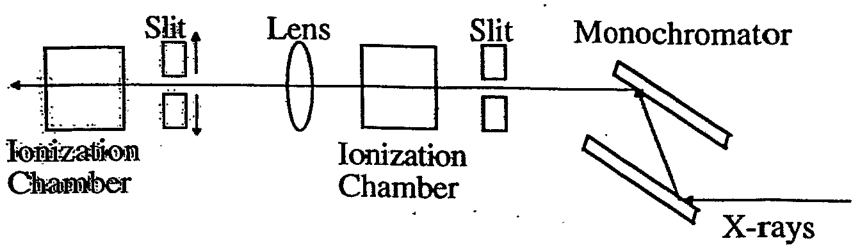

The intensity profile of the radiation is measured by the translatable slit on the left.

1-D Focusing of 19.5-keV X-rays

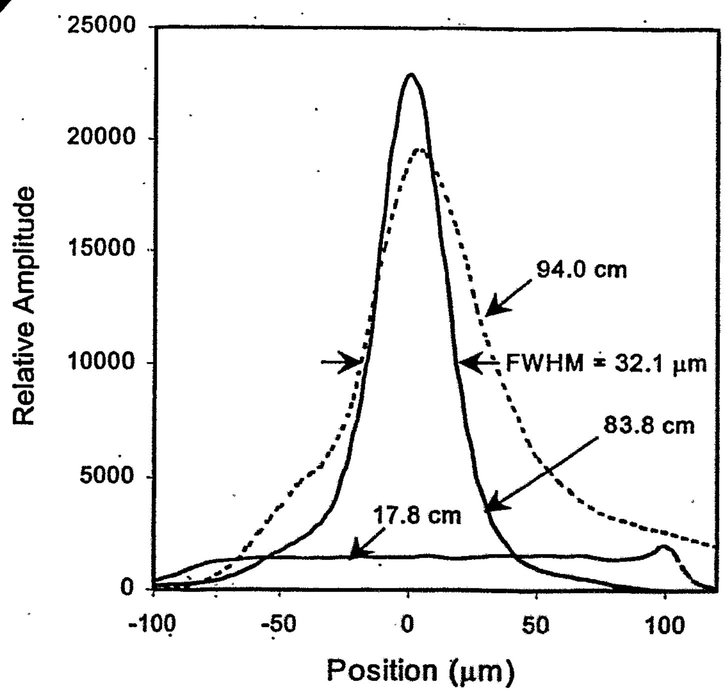

Source Size = 0.45 mm

1-D Lens Parameters

Lens Number Designation	1.2	3.1
Material	Acrylic (Lucite)	polyethylene
Chemical Formula	$C_5H_8O_2$	CH_2
ρ, Density (gm/cm^3)	1.2	0.96
δ	2.87×10^{-6}	4.34×10^{-7}
μ(1/m)	498	18
N, Numbers of holes	50	200
R, Hole Radius (μm)	250	160
f, Calculated Focal Length (cm)	87.1	93
Δ, Min. Wall thickness (μm)	50	75
S_d, Vertical Source size[6] (μm)	445	445
Source-to-lens distance (m)	16.8	16.8
Photon Energy (keV)	9.0	19.5
F_d, Calculated Focal Line Width (μm)	24.3	26.0
Measured Focal Line Width (μm)	70 (Fig. 3)	32.1 (Fig. 4)
I_d, Calculated Image Distance (cm)	92	98
Measured Image Distance (cm)	68.6	84
G, Calculated Gain	1.5	3
Calc. Ave. Transmission through Lens	24%	75%
R_p, Calc. parabolic radius, (μm)	75	50
R_a, Calc. absorption radius, (μm)	142	298

Adelphi Technology, Inc.

Focal Length as a Function of Photon Energy

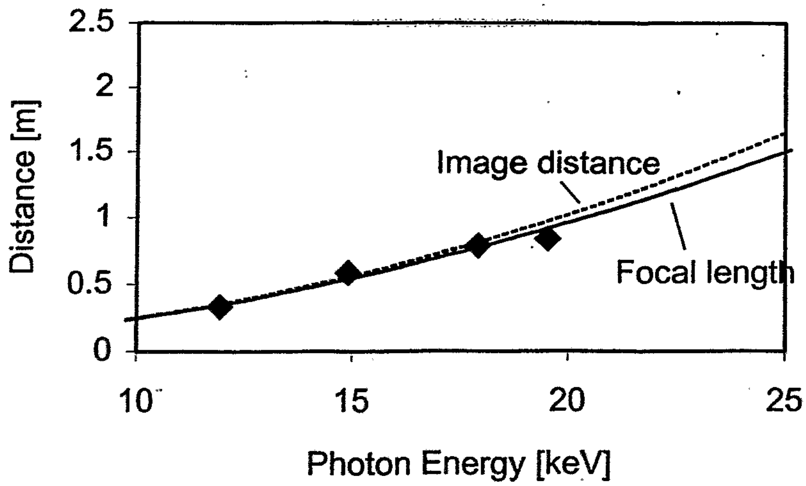

Adelphi Technology, Inc.

Measure Image Distance and Image Spot Size for Lens

Photon Energy (keV)	Calculated Focal length [m]	Calculated Image Distance[m]	Measured Image Distance[m]	Measured Image Line Width [μm]	Source Width from Image line width [μm]
12	0.35	0.35	0.33	21	1070
15	0.55	0.56	0.58	25	720
18	0.79	0.82	0.79	30	640
19.5	0.92	0.97	0.84	32	644

Adelphi Technology, Inc.

Multilenses

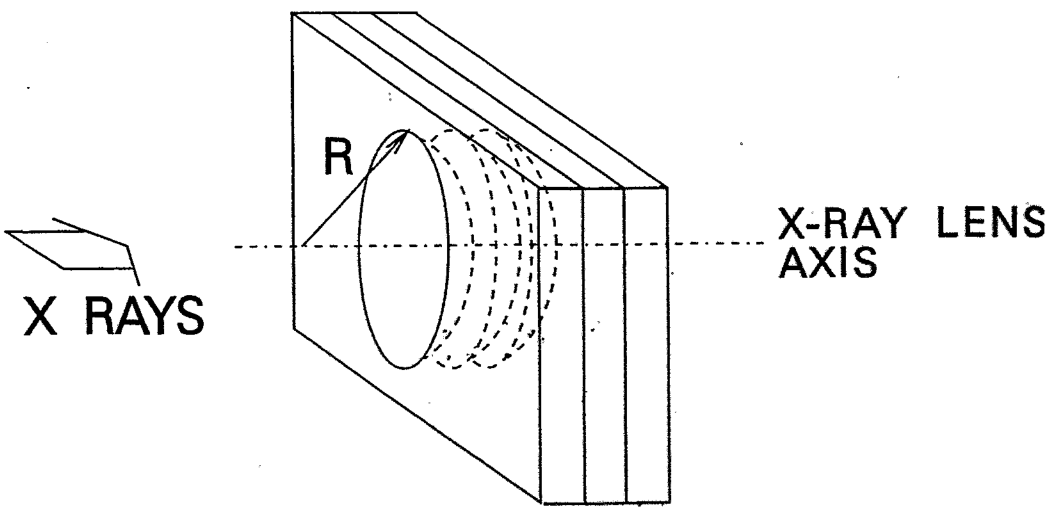

Adelphi Technology, Inc.

Unit Lens

- 0.4 mm diameter
- Absorption aperture 180 μm
- 23 μm thick
- 5 μm minimum

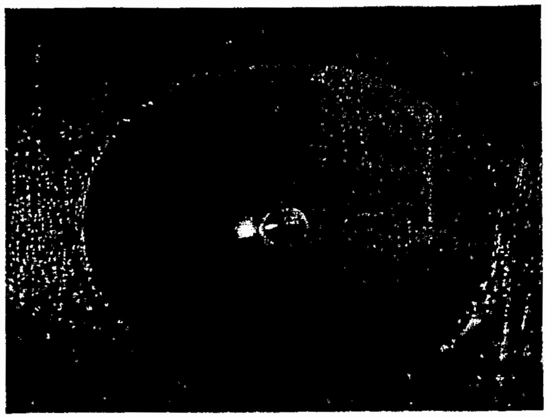

Adelphi Technology, Inc.

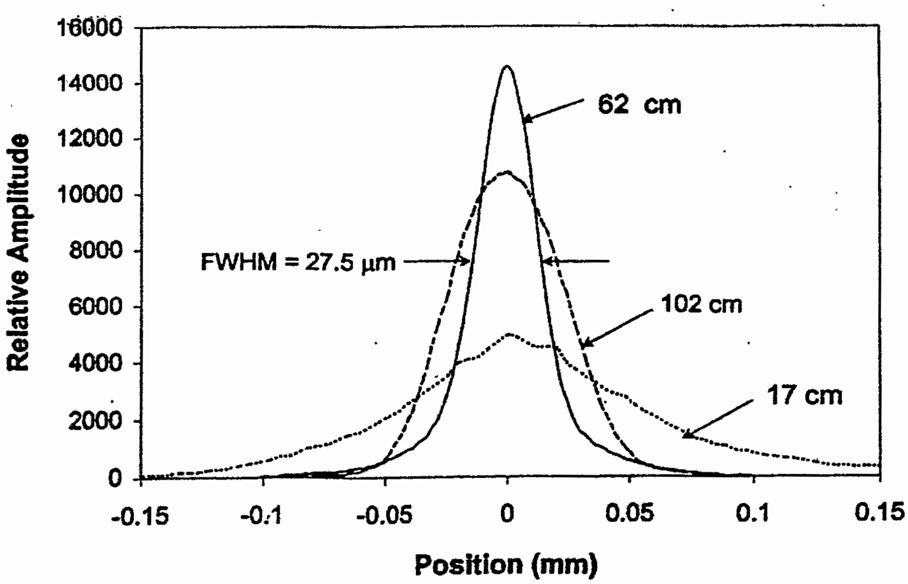

Waist as a Function of Distance

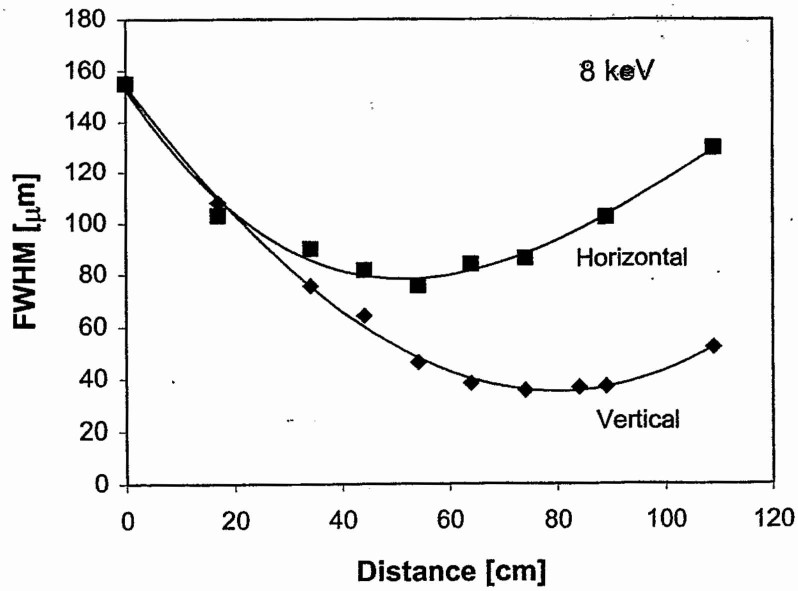

Source Size:
Vertical: 0.45 mm
Horiz.: 1.7 mm

Adelphi Technology, Inc.

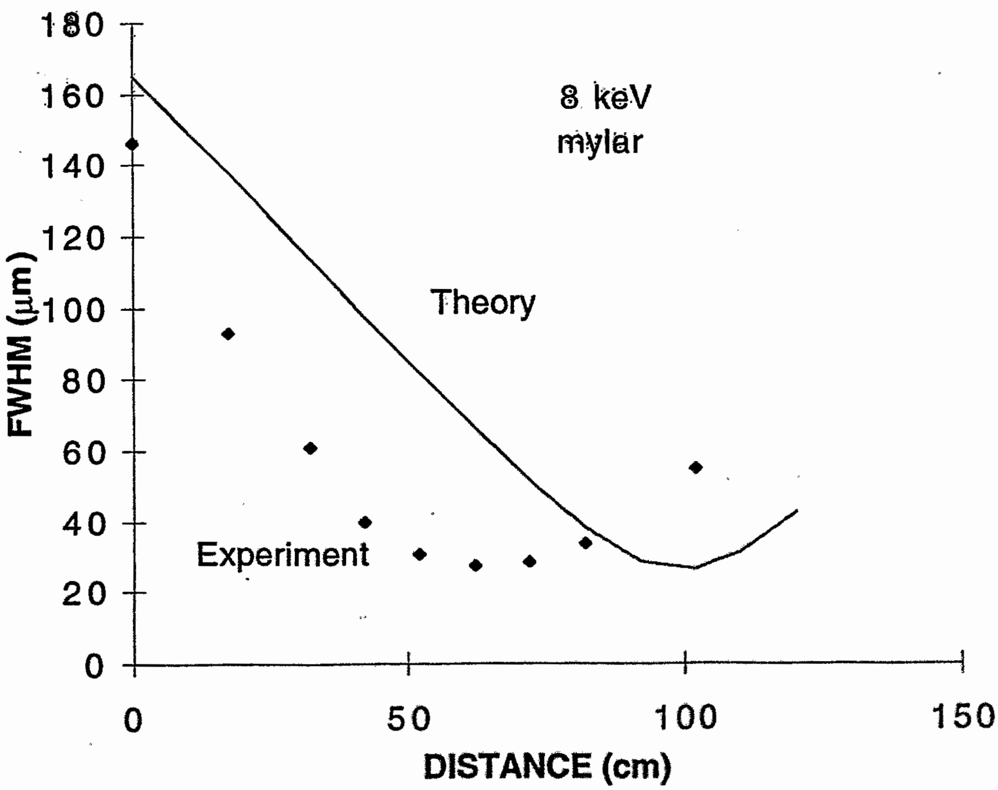

Waist as a function of distance (Vertical)

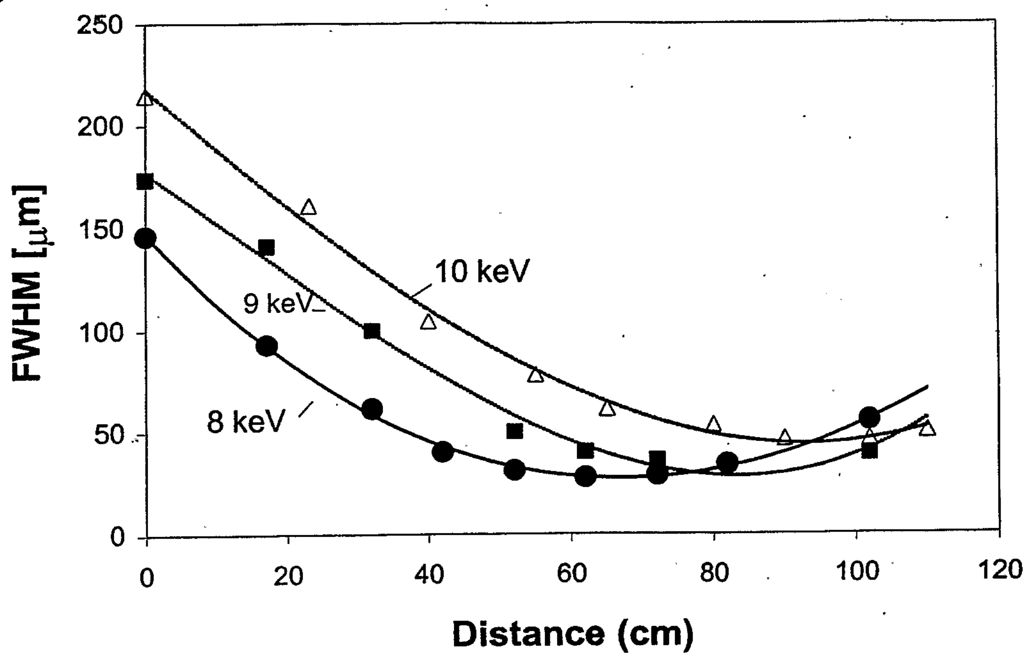

Transmission through the 2-D Lens

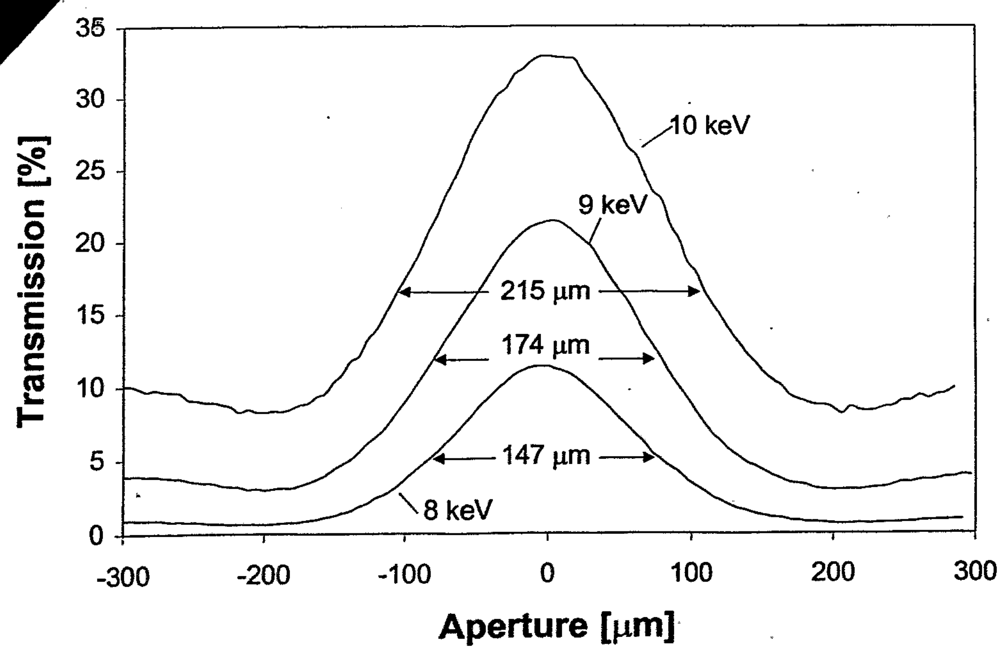

Adelphi Technology, Inc.

2-d Gain for mylar lens

	8 keV	10 keV
Calculated	5.6	13.1
Measured	1.5	2.0

Waist as a function of distance (Vertical)

Parabolic
N= 380
Kapton
R= 1.5mm

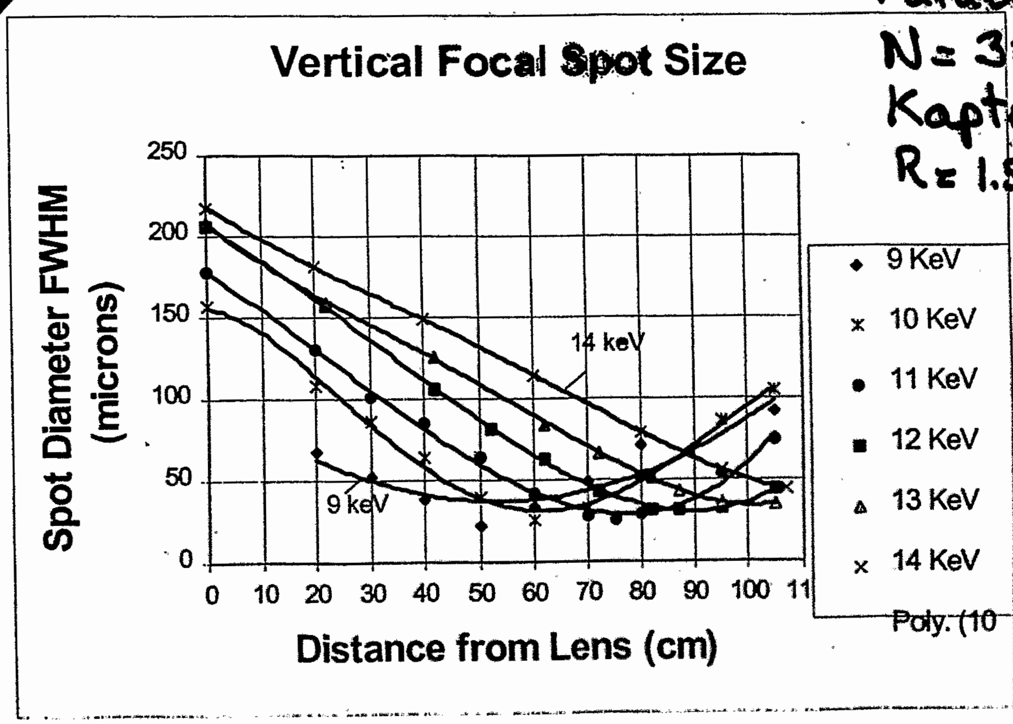

What Adelphi CRLs can give you!

- Focal lengths below 1 meter
  - 20 cm has been done with 1-D
  - 60 cm has been done with 2-D
- Good transmission and gain at moderate photon energies!
- Expected apertures of 1 mm or larger!

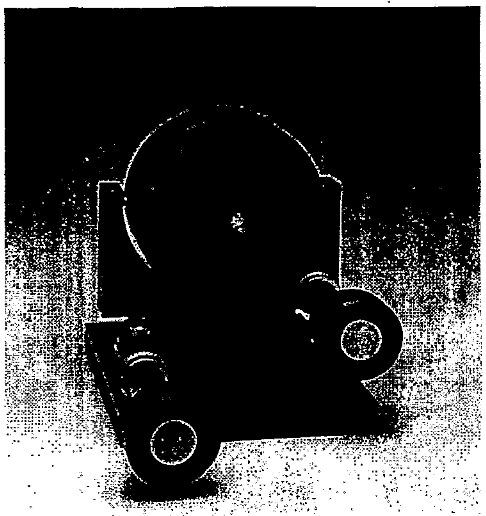

Adelphi Technology, Inc.

X-ray Lenses with Novel Sources (PXR, TR, CR, Combinations)

- Only done experimental work with synchrotron radiation
- Should work well with novel sources
  - Source size can be small (size of electron beam)
  - Sources are collimated like synchrotron radiators
  - Near Field of TR source looks Guassian

Adelphi Technology, Inc.

Cost ≃ \$2000 - \$4000

6 KeV to 16 KeV 2-D. lenses.

Benefits!

- "In-line Optic"
- Works at Hard X-rays
- Works with Novel X-ray Sources
- Inexpensive
- Imaging Possible (Unlike Capillary Optic)

D Compound Refractive Lens

- Number of lenses 200
- R = 1.6 mm
- Mechanical Aperture = 0.4 mm
- Absorption Aperture = 0.31 mm at 8 keV
- Minimum Thickness = 5 microns
- Focal Length = 97 cm

Adelphi Technology, Inc.

H. Genz:

Channeling radiation as a probe in the solidstate plasma accelerator regime

Channeling Radiation
as a probe in the solid state plasma accelerator regime

Harald Genz
Institut für Kernphysik
Technische Universität Darmstadt

- **Motivation**
- **Channeling**
- **Experiment and first result**

Rossendorf, February 24 - 26 2000; Workshop on X-rays from electron beams

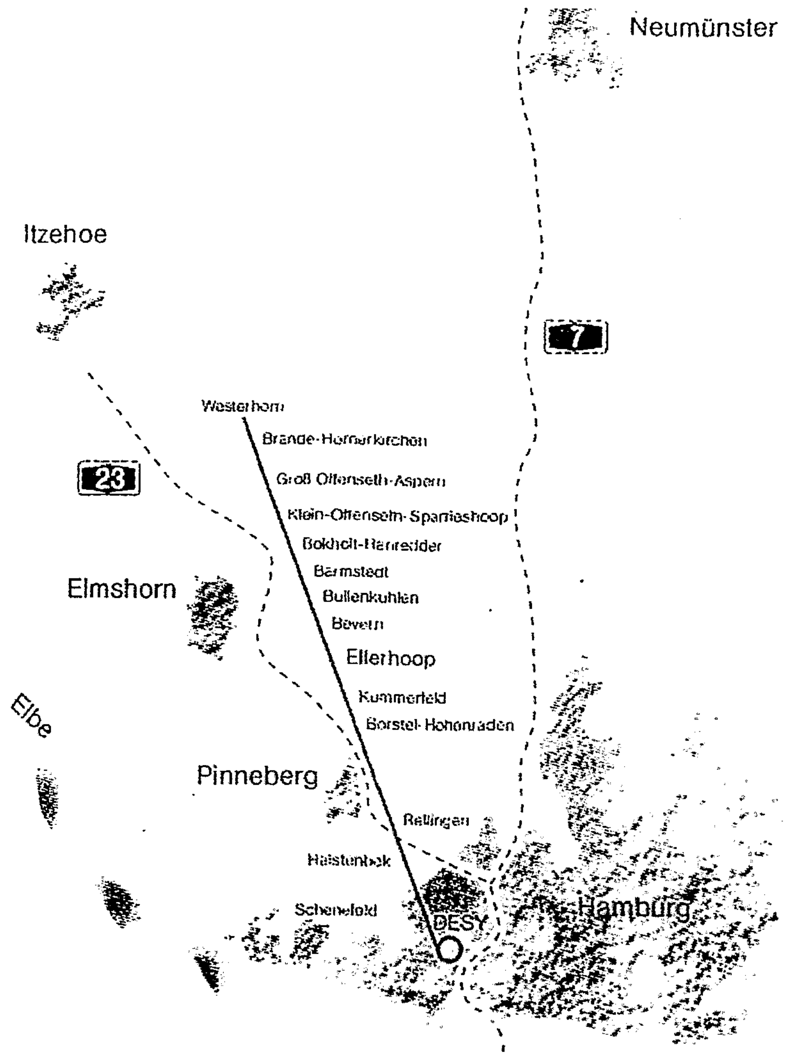

Progress in Energy

High energy physics: 12 orders of magnitude

- **Limit of electromagnetic acceleration:** **35 MeV/m**
- **Large dimensions** **TESLA**

R. Hofstadter (1968):

"To anyone who has carried out experiments with a large modern accelerator there always comes a moment when he wishes that a powerful spatial compression of his equipment could take place. If only the very large and massive pieces could fit in a small room"

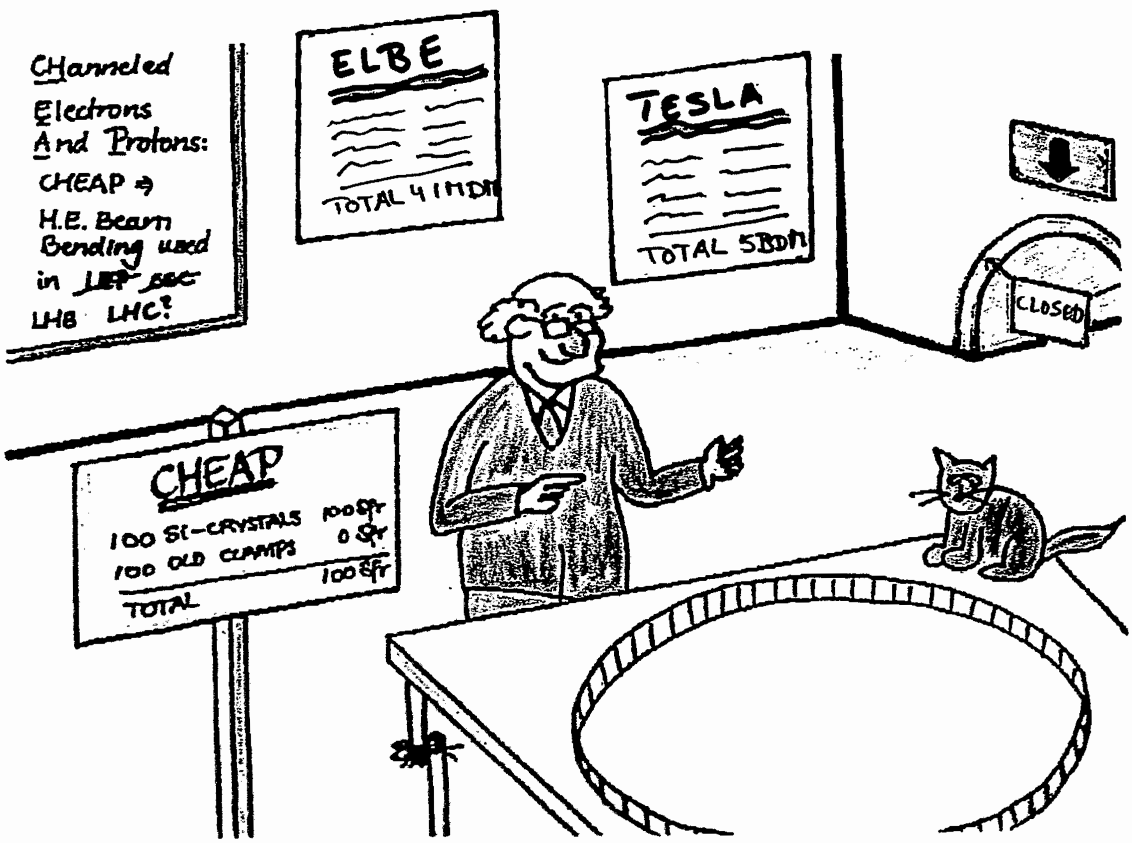

Importance of plasma acceleration

- Considerably larger gradients in plasma

$$eE_{max} = 0{,}97\ (n_0)^{1/2}\ \text{eV/cm}$$

Gaseous plasma:	1 GeV/cm
Solid state plasma:	100 GeV/cm

Gaseous plasma

- Acceleration of electrons
- Laser induced plasma wave

`95: proof of principle
`99: short distances
moderate acceleration

Solid state plasma acceleration

Chen, Noble:

- **Make use of plasma in solid state**
- **Plasma electron beam induced**
- **Channeling to guide the particles through the crystal**
- **Channeling process as cooler**

<u>Types of accelerators</u>

laser wakefield

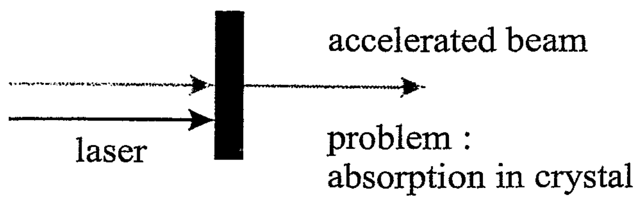

side injected laser

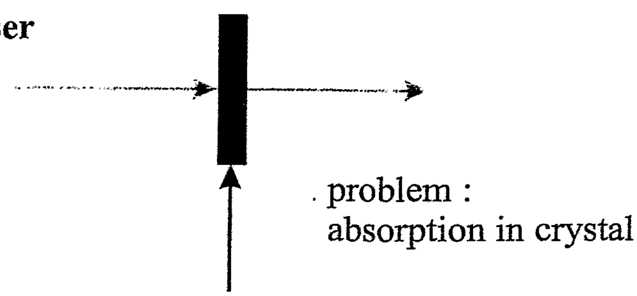

particle wake field

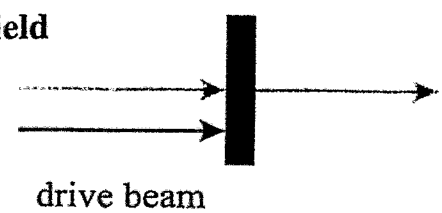

Open questions:

- Can the electron couple to the field?
- Do the crystals stand the field?

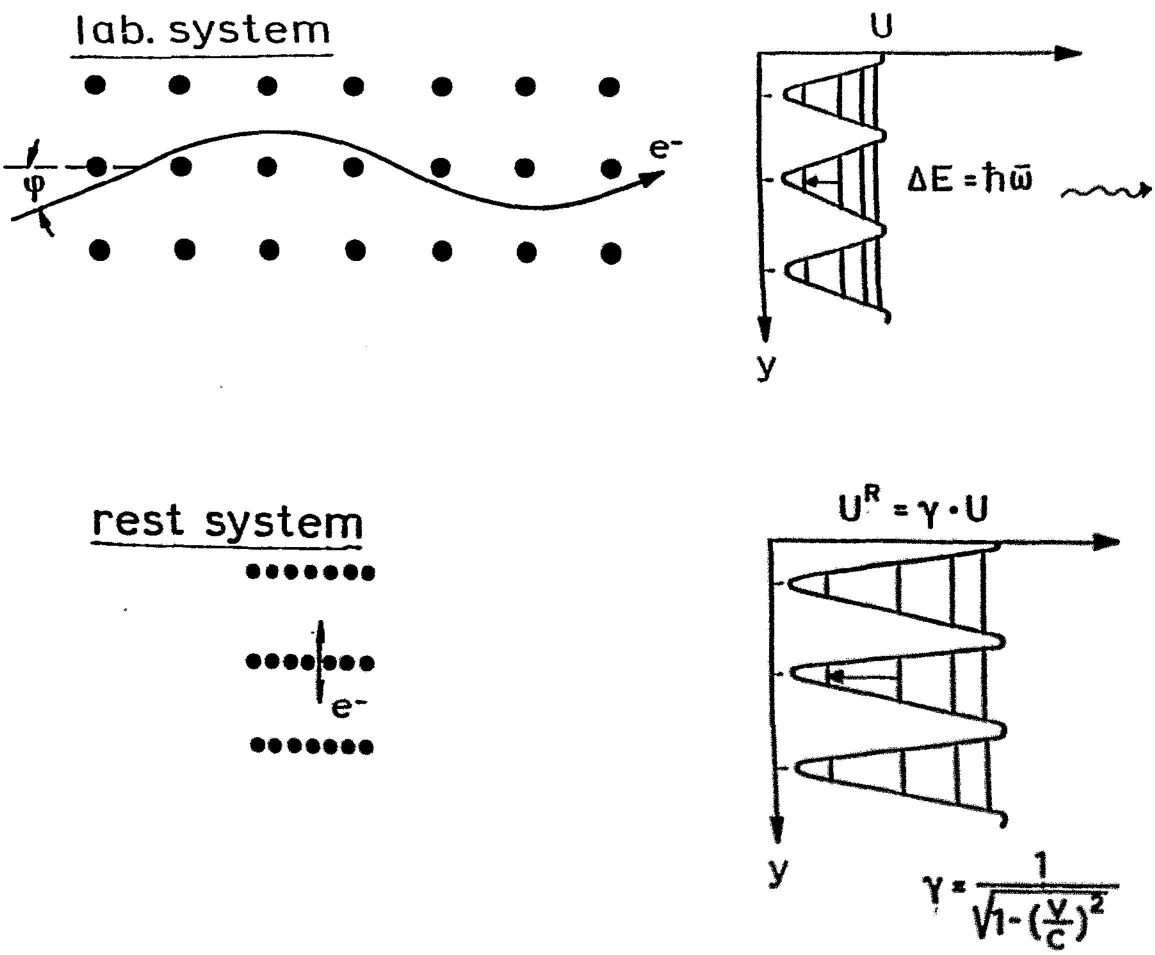

rest system

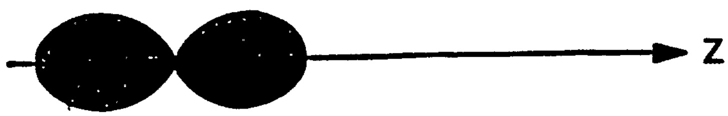

$$\hbar\omega^R = \gamma\hbar\bar{\omega}$$

lab. system

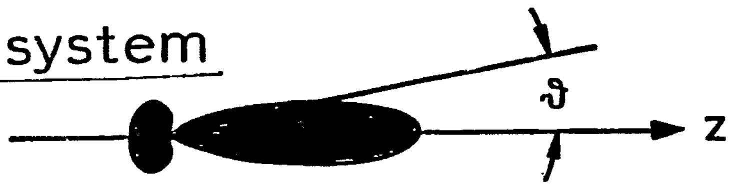

$$E_{Ch} = \hbar\omega = 2\gamma^2\hbar\bar{\omega}$$

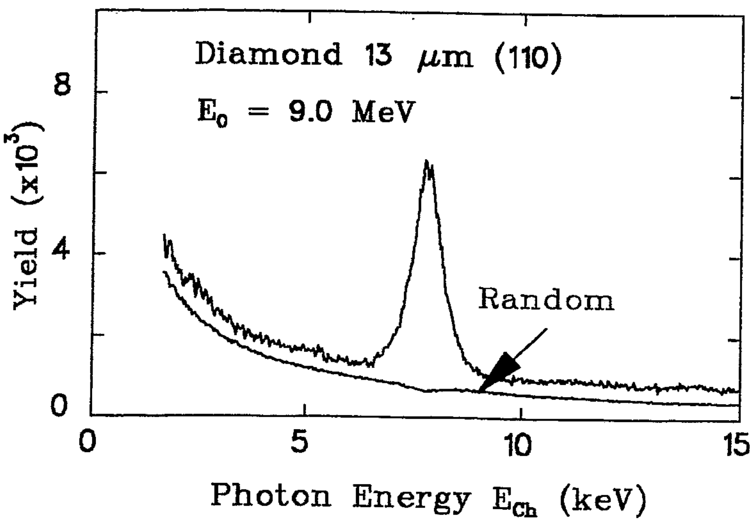

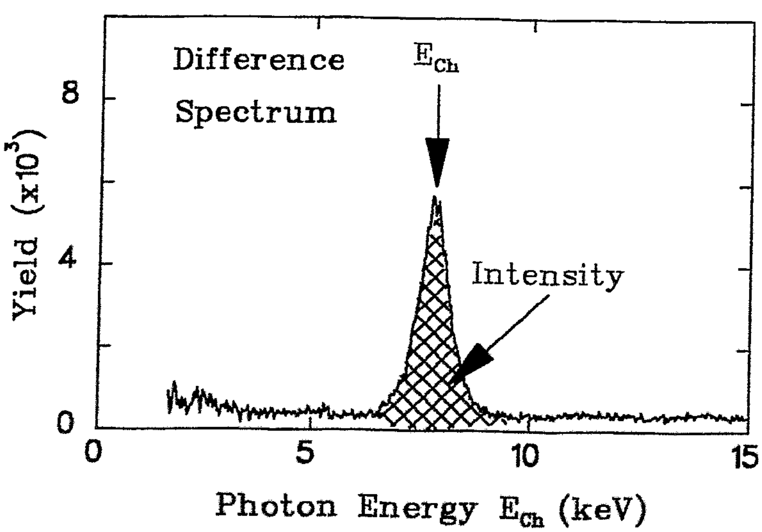

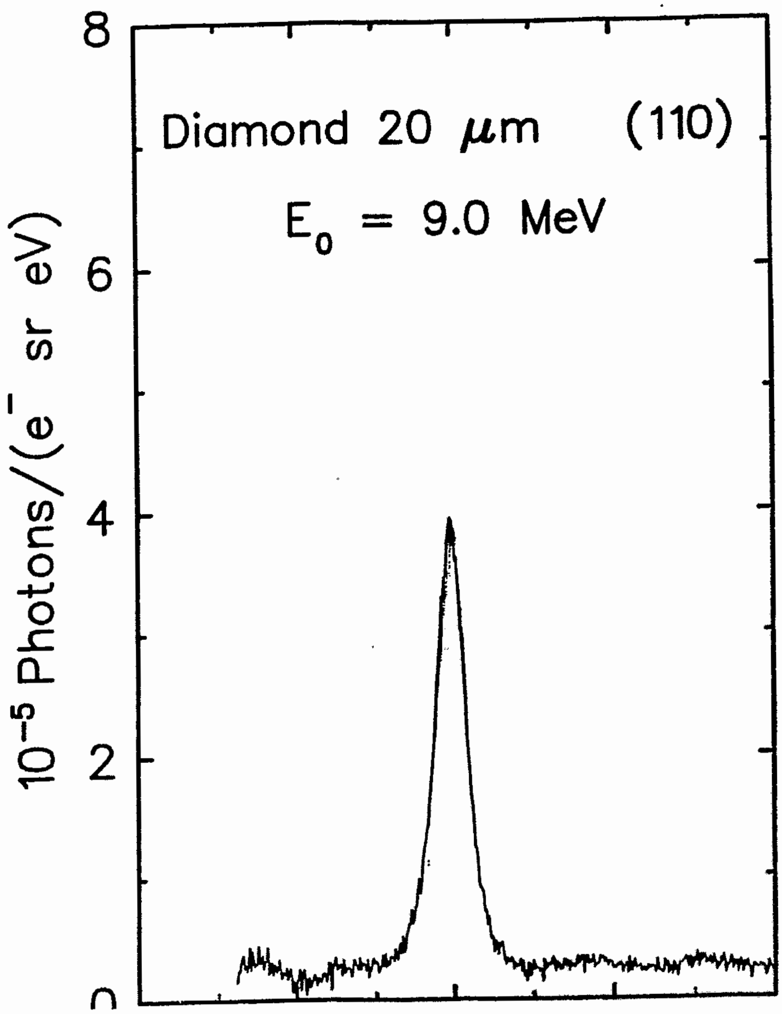

Photon counting

- 10 nC/puls x 500 pulses/macrobunch x 1/500 μs = 10 mA average
- **photon flux** 3.1 10^9 photons/s sr
- **peak photon flux** 4.3 10^{20} photons/sr (in 10 ps)
- **photon energy** 15 - 25 keV

photon flux 10^5 higher than at S-DALINAC

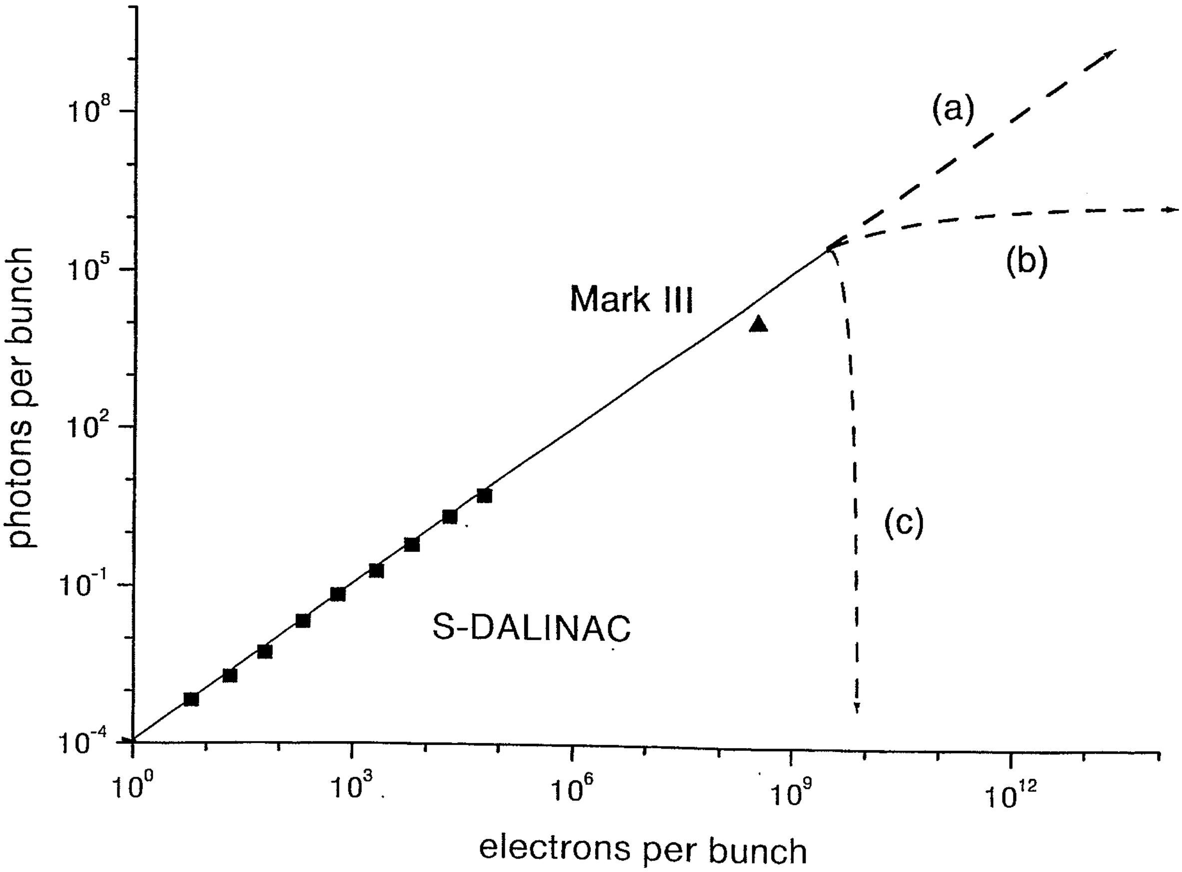

photons per bunch
electrons per bunch
10^8
10^5
10^2
10^-1
10^-4
10^0
10^3
10^6
10^9
10^12
Mark III
S-DALINAC
(a)
(b)
(c)

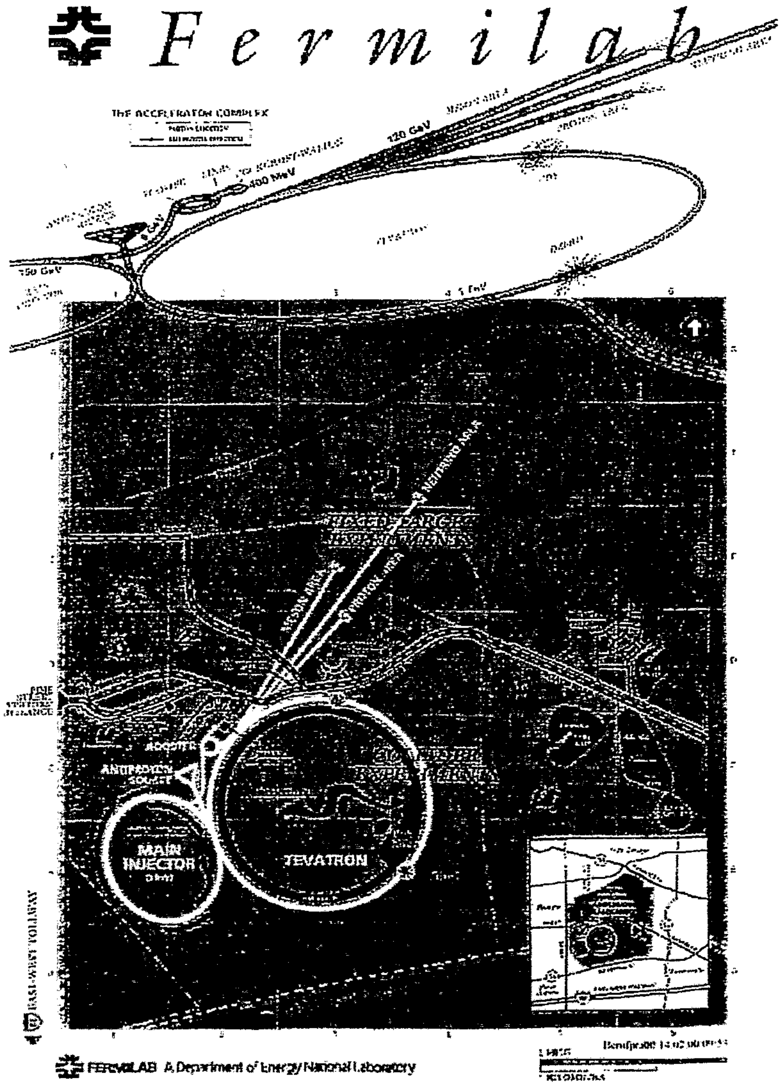

Fermilab
120 GeV
400 MeV
BOOSTER
ANTIPROTON SOURCE
MAIN INJECTOR
TEVATRON
FERMILAB A Department of Energy National Laboratory

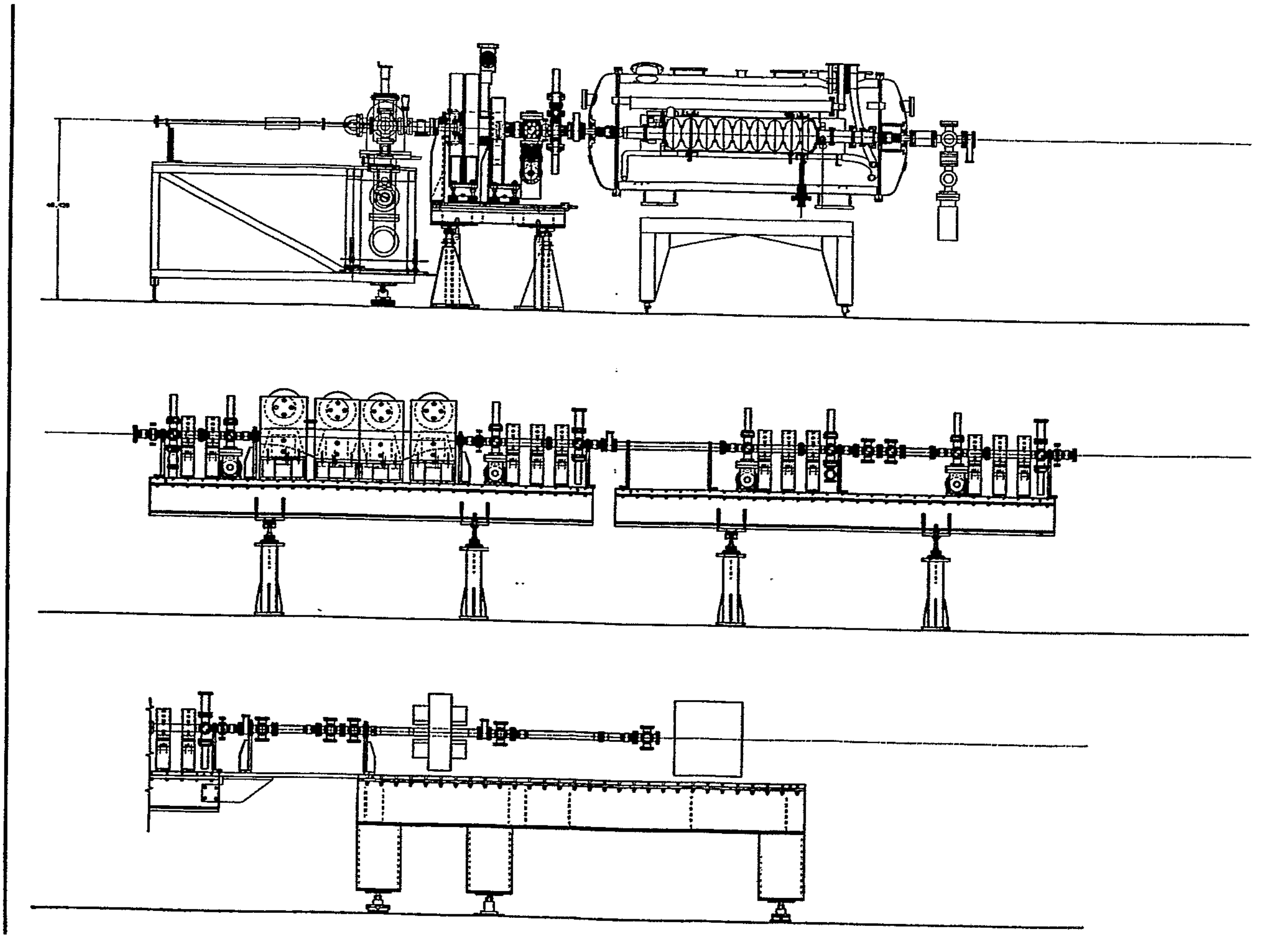

Block Diagram of Laser System

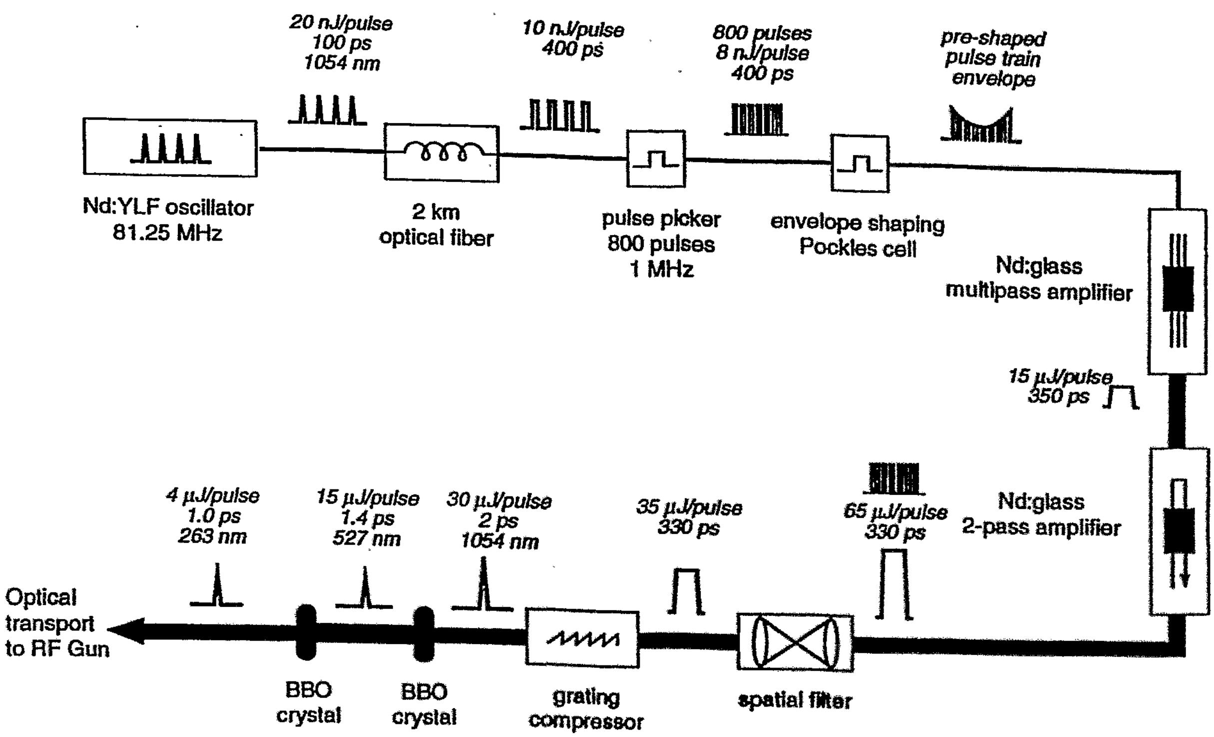

A0 photo injector

Injector: **1.625-cell rf Gun;1.3 GHz, electric field up to 50 MV/m**

Cs_2Te photo cathode

Superconducting 9-cell Nb structure, 1.3 GHz, 11 MeV/m

Magnetic chicane
four dipole magnets pulse compression by a factor 2-3

Laser: **Nd:YLF; 4th harmonic**
263 nm, 1 - 20 ps FWHM, 10 μJ pulse, 1 μs at 1 Hz

S-DALINAC

Strahleigenschaften

- *normalized transverse RMS emittance* :

$$\varepsilon_{n,y} = \beta\gamma\,(<y^2><(y')^2> - <yy'>^2)^{1/2} = \underline{5{,}5 \pm 0{,}8\ \text{mm mrad}}$$

- *bunch length* :

$$\underline{\sigma_t = 7{,}1 \pm 0{,}2\ \text{ps}}$$

- *charge* :

$$\underline{q = 1\ \text{nC} - 18\ \text{nC}}$$

- *charge density* :

$$\rho_{bunch} = \underline{3 \times 10^{15}\ \text{electrons / cc}} \quad (1\ \text{nC})$$

Darmstadt-Fermilab experiment

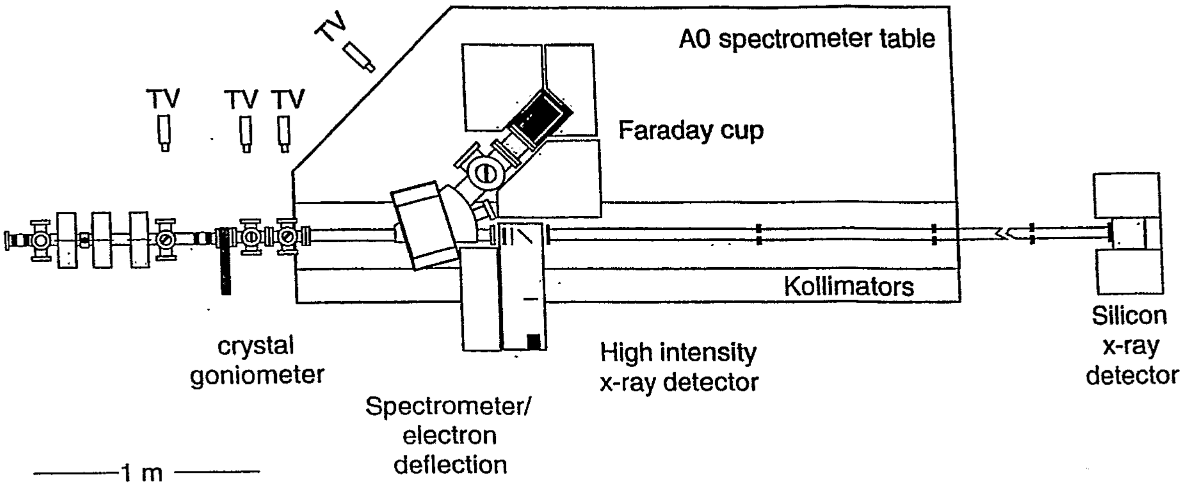

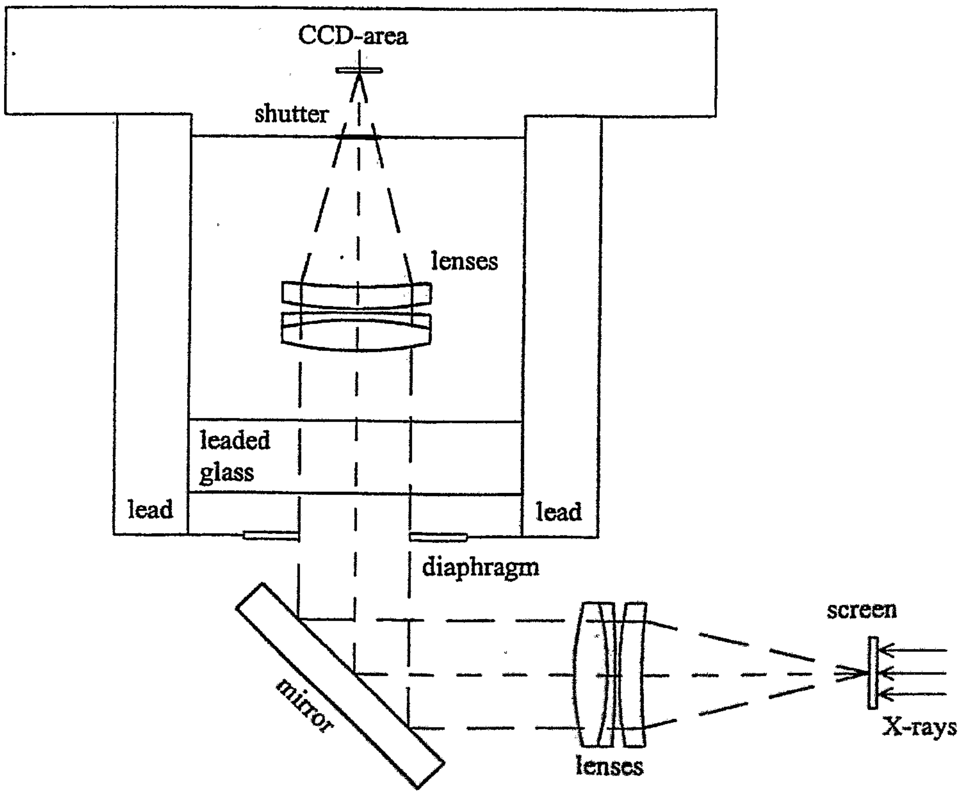

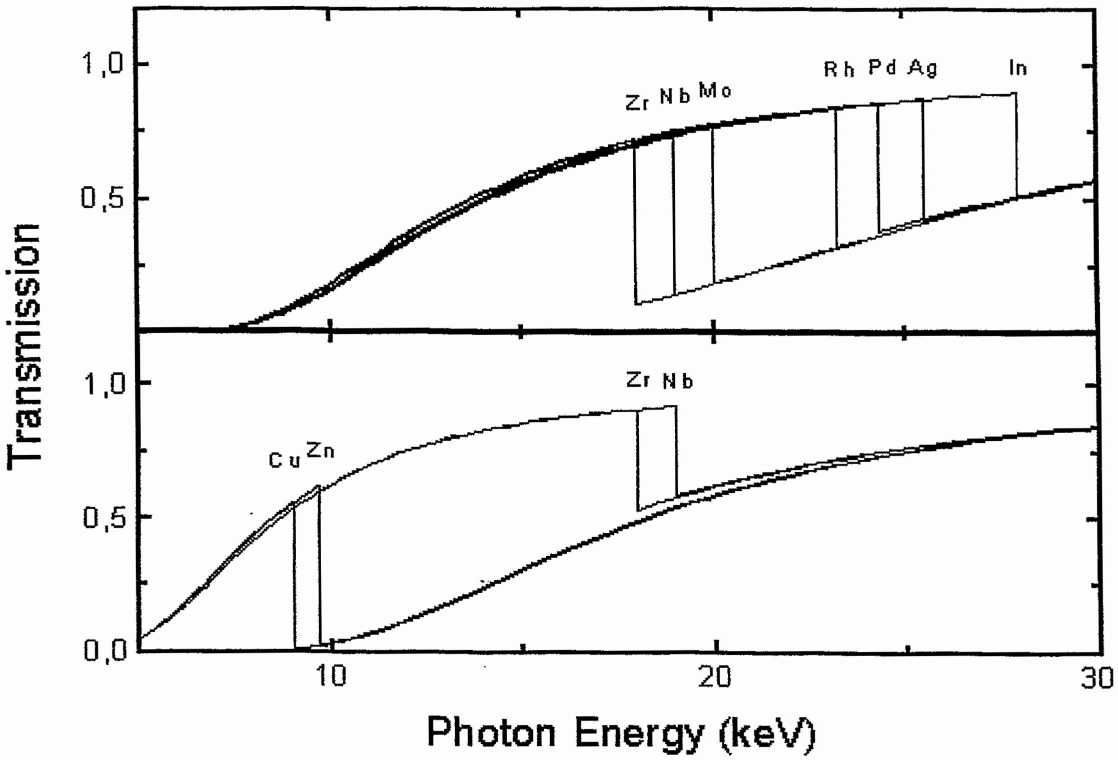

Transmission
1,0
0,5
0,0
Zr Nb Mo
Rh Pd Ag
In
Zr Nb
Cu Zn
10
20
30
Photon Energy (keV)

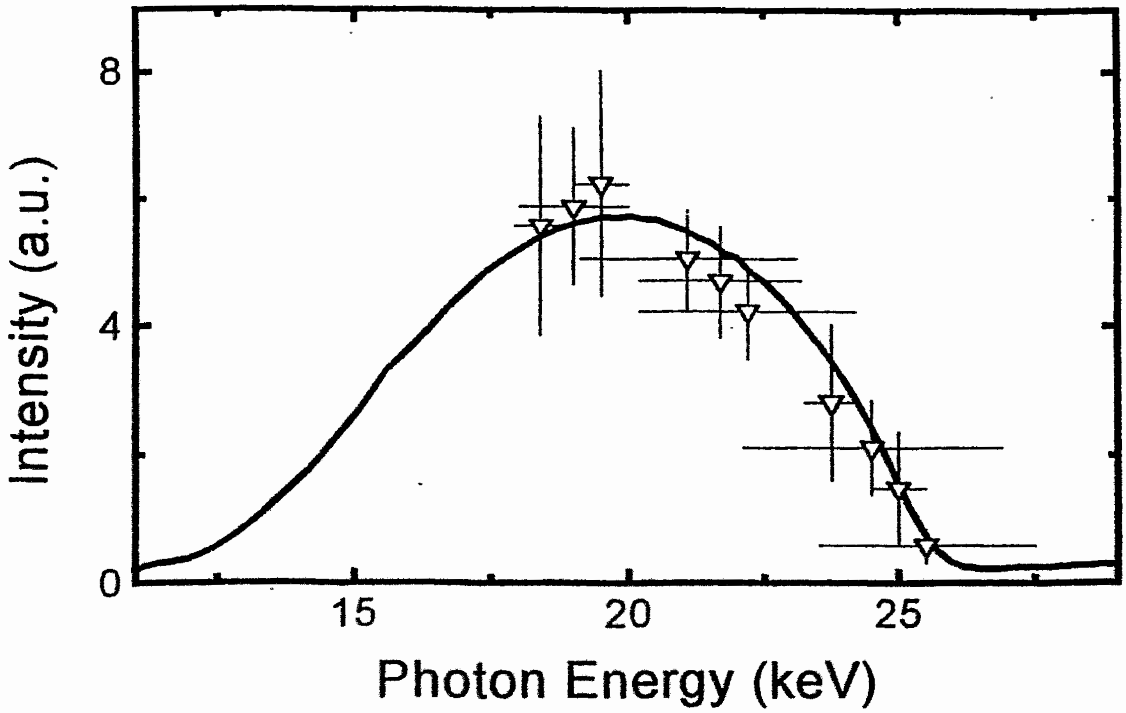

Intensity (a.u.)
8
4
0
15
20
25
Photon Energy (keV)

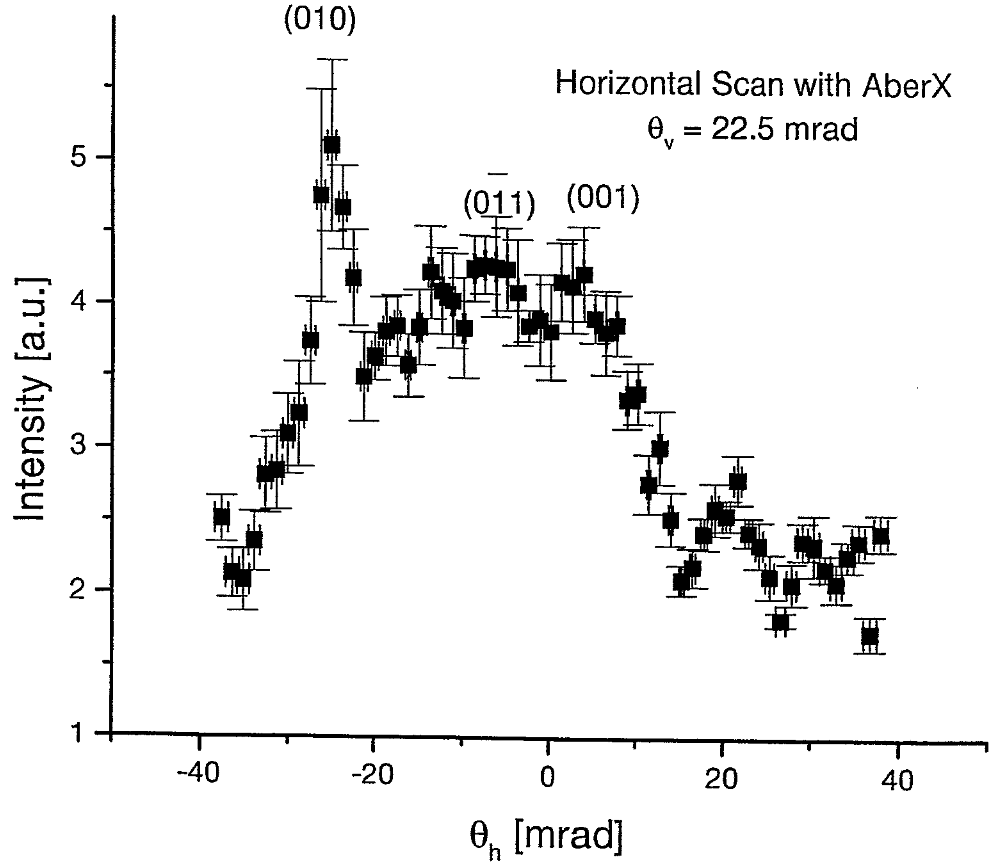
(010)
Horizontal Scan with AberX
θ_v = 22.5 mrad
$(0\bar{1}1)$
(001)
Intensity [a.u.]
θ_h [mrad]

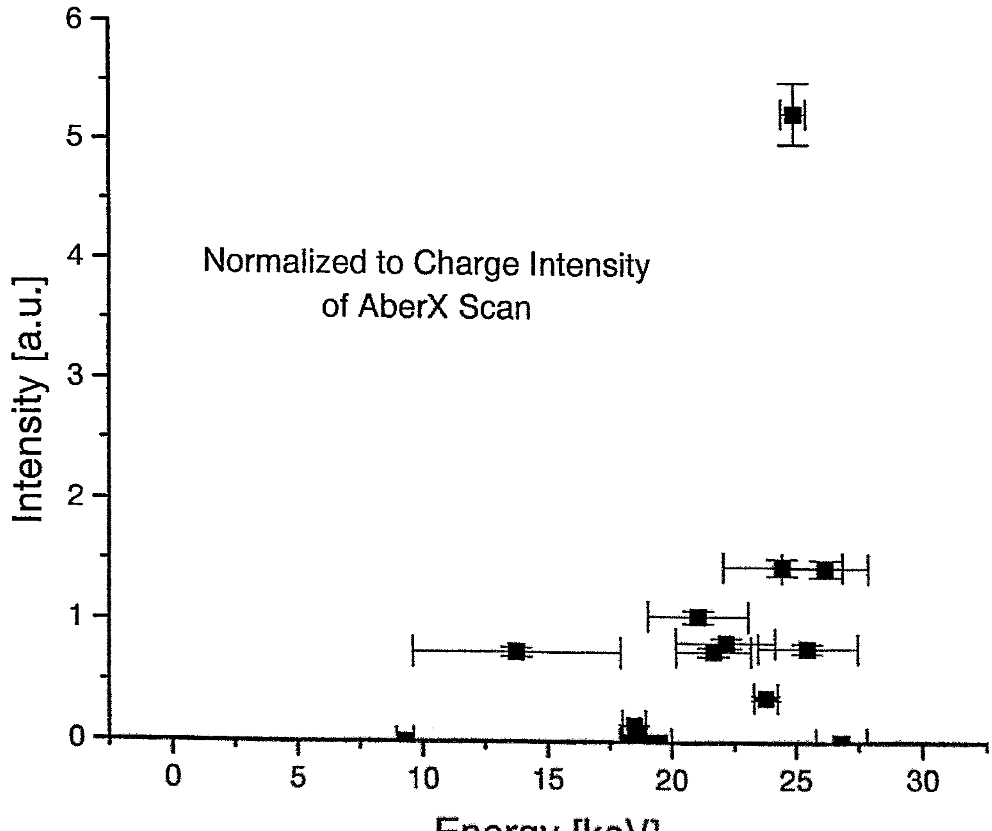
Normalized to Charge Intensity
of AberX Scan
Intensity [a.u.]
Energy [keV]

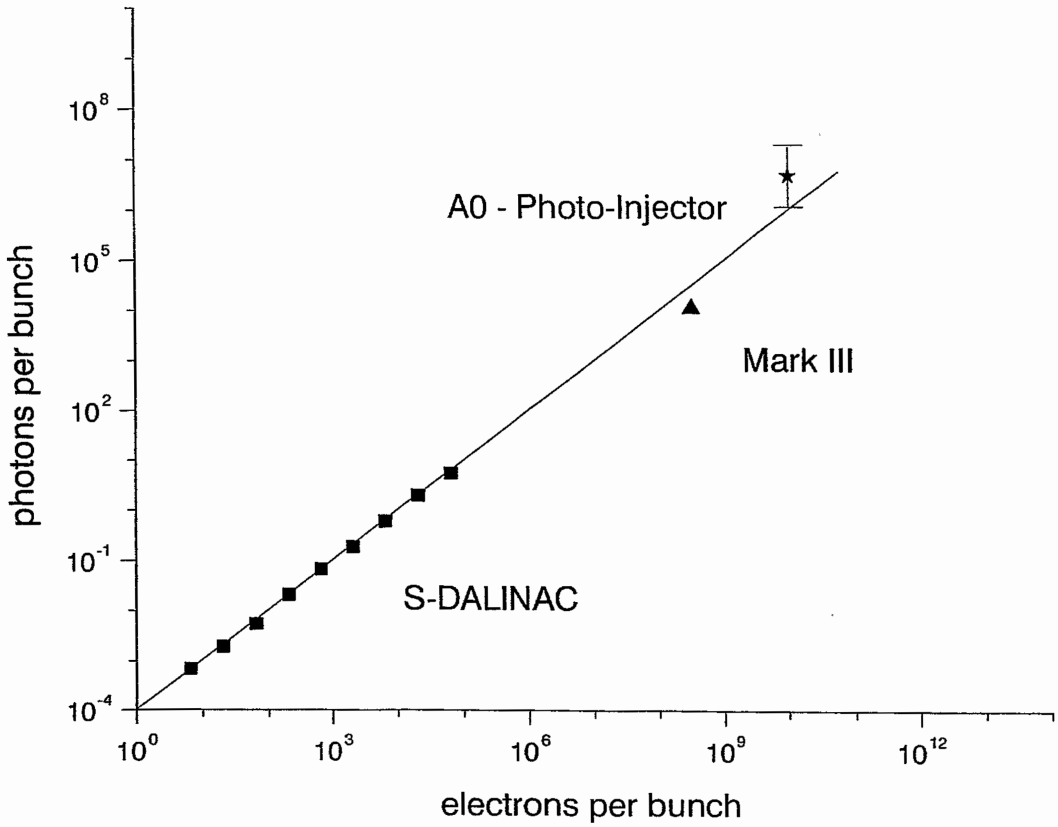

A channeling radiation experiment

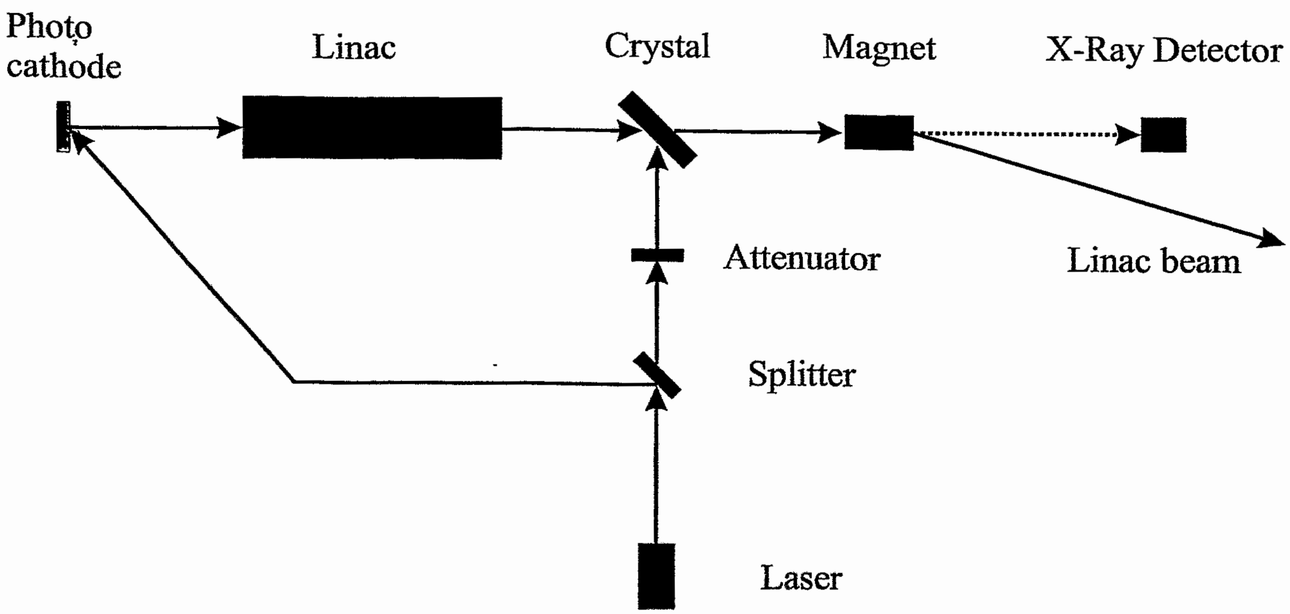

The Darmstadt-Fermilab-A0-team

Fermilab
R.A. Carrigan, Jr., J.-P. Carneiro, P.L. Colestock, H.T. Edwards, W.H. Hartung and K.P. Koepke

Rochester
M. J. Fitch

UCLA
N. Barov

Darmstadt
J. Freudenberger, S. Fritzler, H.G., A. Richter and A. Zilges

Johannesburg
J.P.F. Sellschop

Biomedical Applications of Quasi-Monochromatic X-Rays

D. Frankenberg:

Relative biological effectiveness of X-rays for mammography

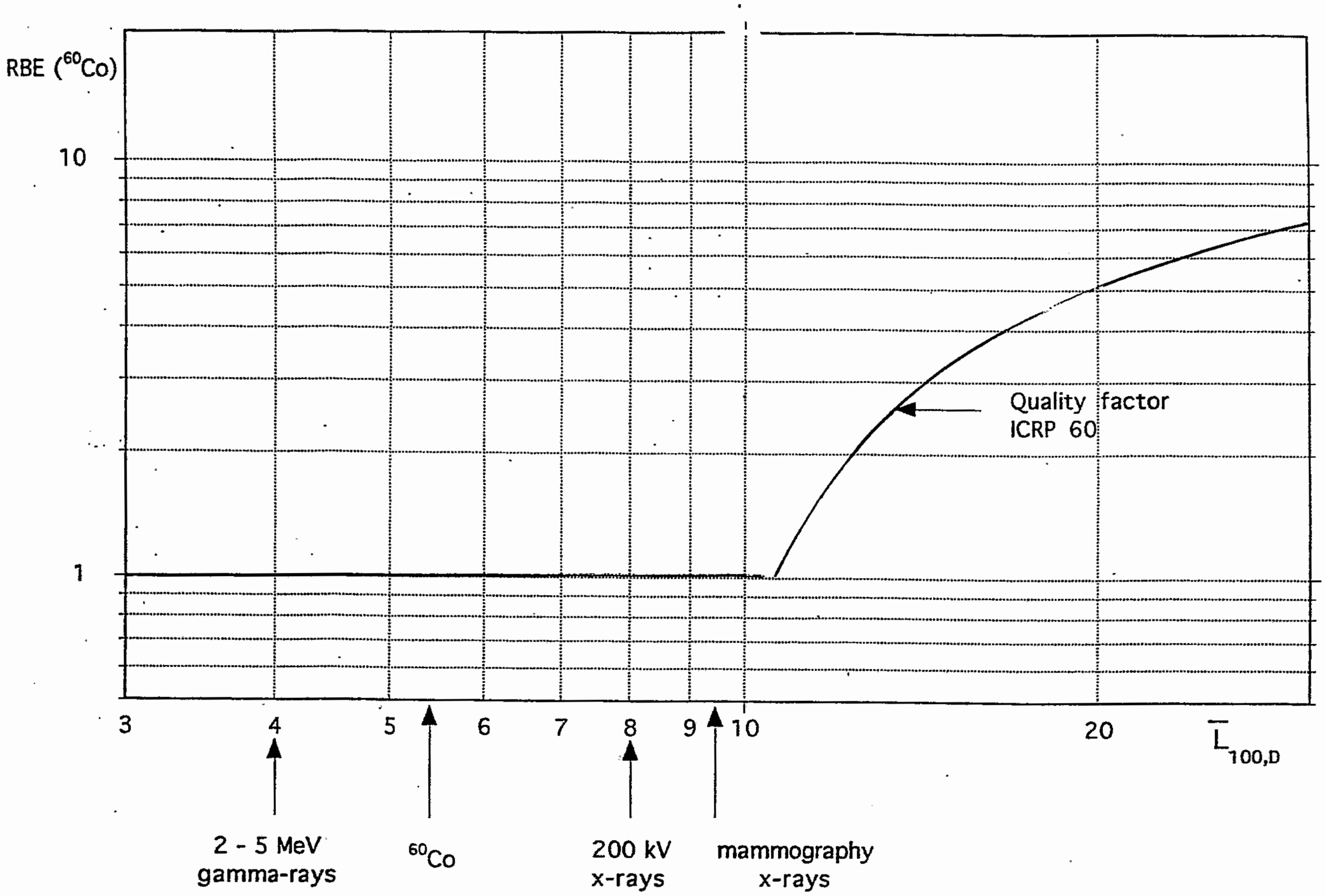
RBE (^{60}Co)
10
1
3
4
5
6
7
8
9
10
20
$\bar{L}_{100,D}$
Quality factor
ICRP 60
2 - 5 MeV
gamma-rays
^{60}Co
200 kV
x-rays
mammography
x-rays

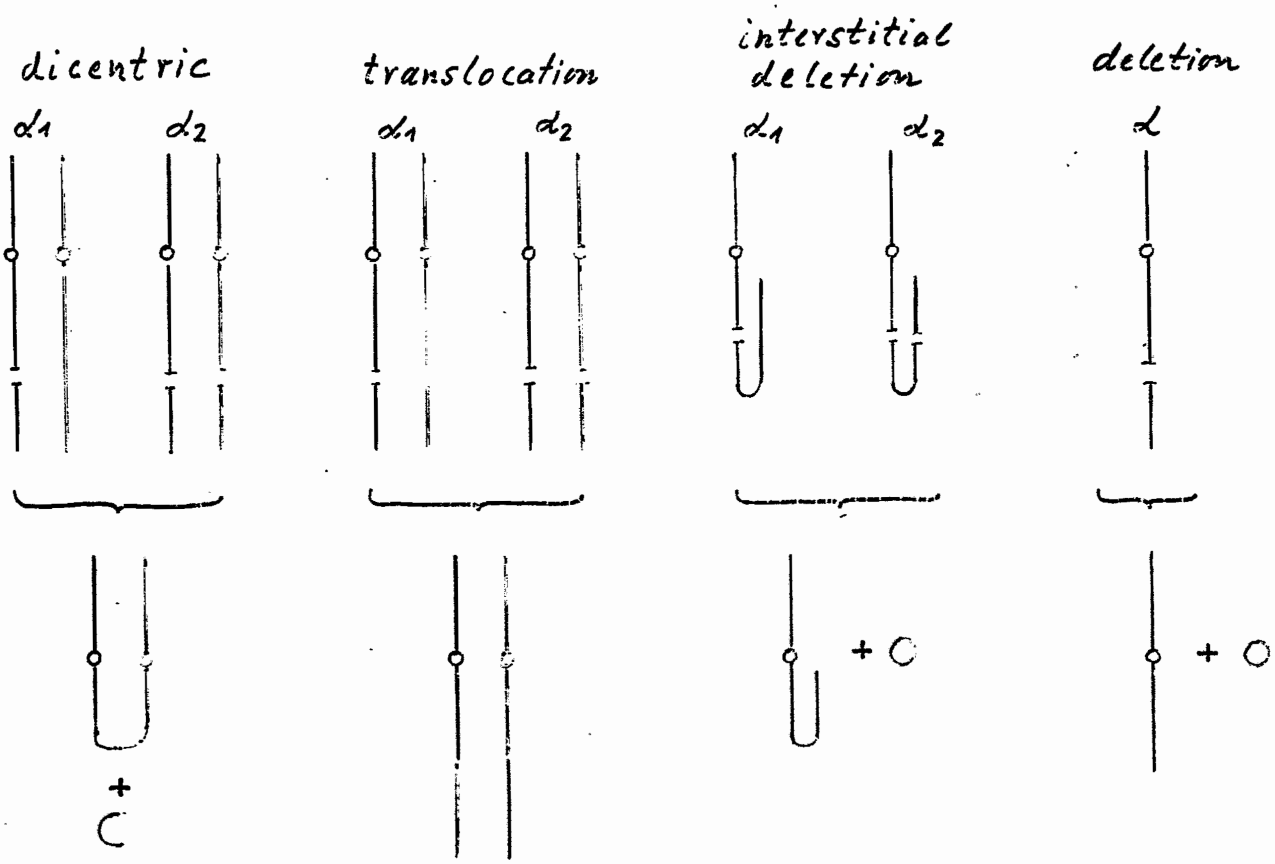
dicentric
α_1
α_2
translocation
α_1
α_2
interstitial
deletion
α_1
α_2
deletion
α

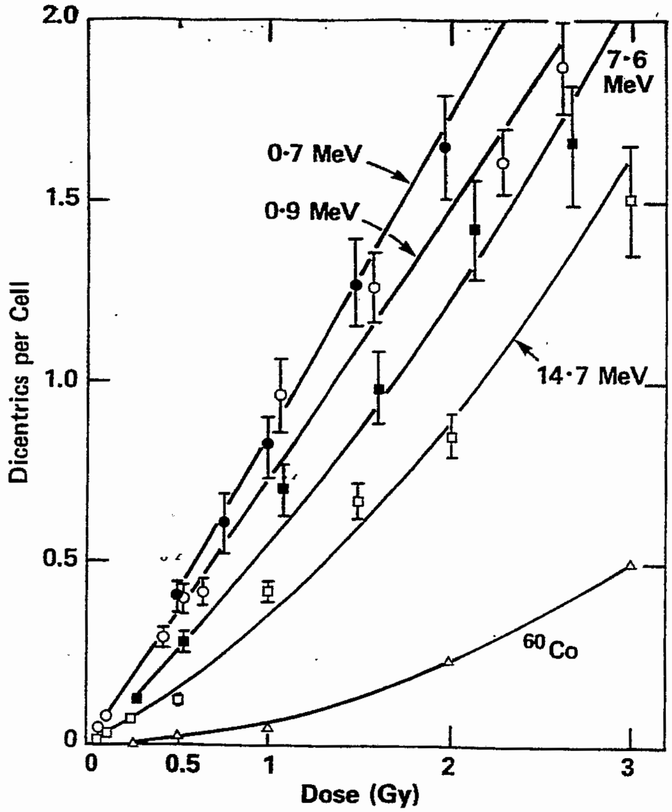

Fig. 2.7 Comparisons of dicentrics induced in human lymphocytes exposed to ^{60}Co gamma radiation versus neutrons of four different energies (neutron spectra are mean energies for 0.7, 0.9 MeV). (Adapted from Lloyd *et al.*, 1976.)

$$Y = \alpha \cdot D + \beta D^2$$

Yield of exchange aberrations:

$$y = \alpha \times D + \beta \times D^2$$

Values of α for ^{60}Co gamma rays (reference)

(12 values in the literature)

$\bar{\alpha} = (2.26 \pm 1.6)10^{-2}Gy^{-1}$

Range: $(0.33 - 5.5)10^{-2}Gy^{-1}$

Values of α for x-rays (180 - 250 kVp)

(16 values in the literature)

$\bar{\alpha} = (5.07 \pm 1.93)10^{-2}Gy^{-1}$

Range: $(2.38 - 9.50)10^{-2}Gy^{-1}$

$RBE_{60Co} = 2.26 \pm 2.5$

TABLE 2.8—*Low Dose RBE*$_M$ for x rays versus gamma rays for dicentrics in human lymphocytes[a]

Radiation	Dose Range (Gy) (Rate)	$\alpha \pm$ S.E. ($\times 10^{-2}$ Gy^{-1})	Limiting RBE (α_x/α_γ)	Reference
220 kVp X rays	0.5–4 (0.5 Gy min^{-1})	4.04 ± 0.3	3.8	Bauchinger (1984)
^{60}Co γ rays	0.5–4 (0.5 Gy min^{-1})	1.07 ± 0.41		
250 kVp X rays	0.05–2 (1.0 Gy min^{-1})	4.37 ± 0.99	1.5	Fabry *et al.* (1985)
^{60}Co γ rays	0.05–2 (acute)	2.97 ± 0.80		
250 kVp X rays	0.05–6 (1.0 Gy min^{-1})	3.64 ± 0.53	2.6	Lloyd (1986a)
^{60}Co γ rays	0.05–6 (0.5 Gy min^{-1})	1.42 ± 0.44		
220 kVp X rays	0.25–3.75 (0.5 Gy min^{-1})	4.34 ± 0.81	2.8	Littlefield *et al.* (1989)
^{60}Co γ rays	0.25–4 (0.5 Gy min^{-1})	1.57 ± 0.66		

[a]Data from scoring first division metaphases.

$\overline{RBE} = 2.7 \pm 0.9$

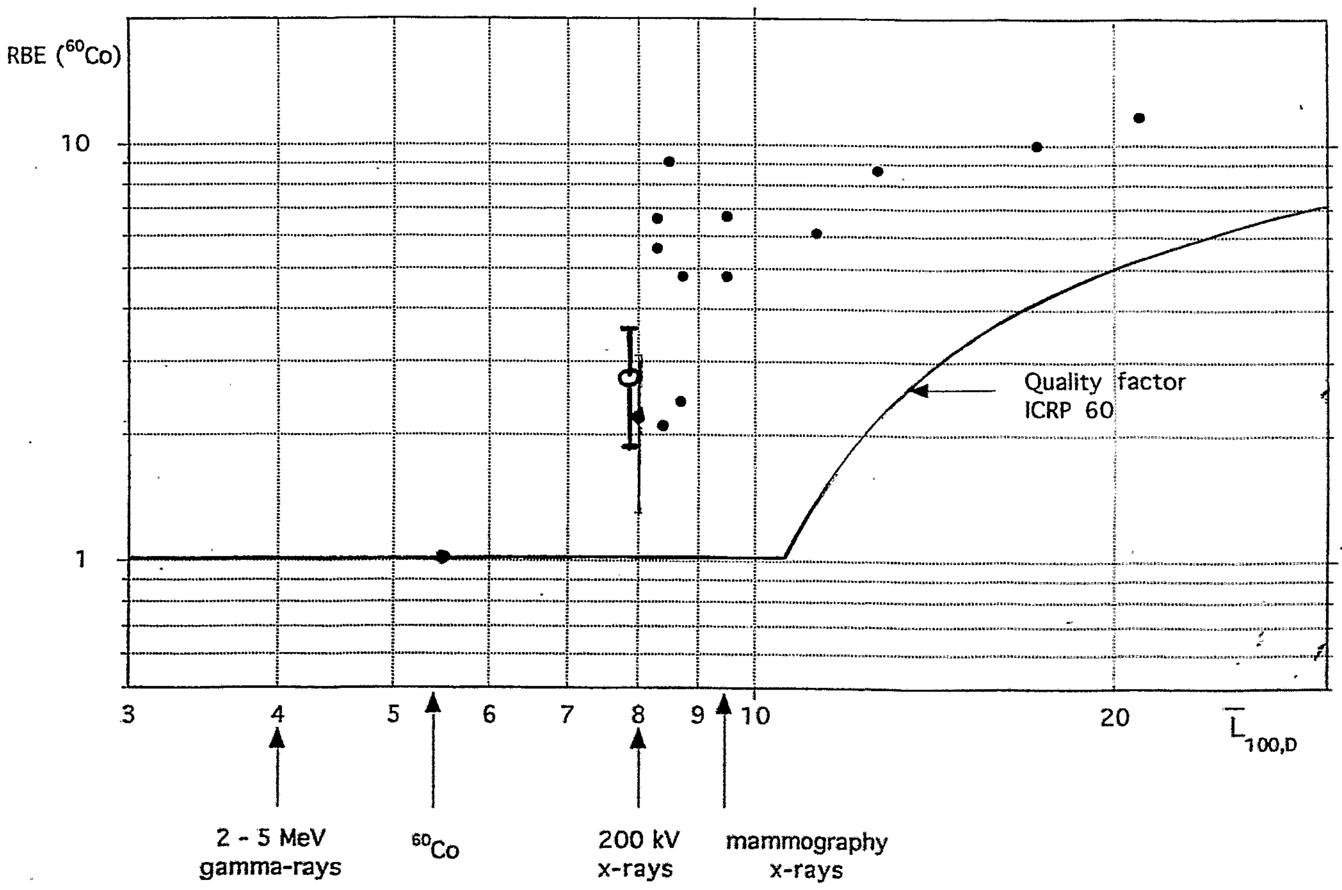

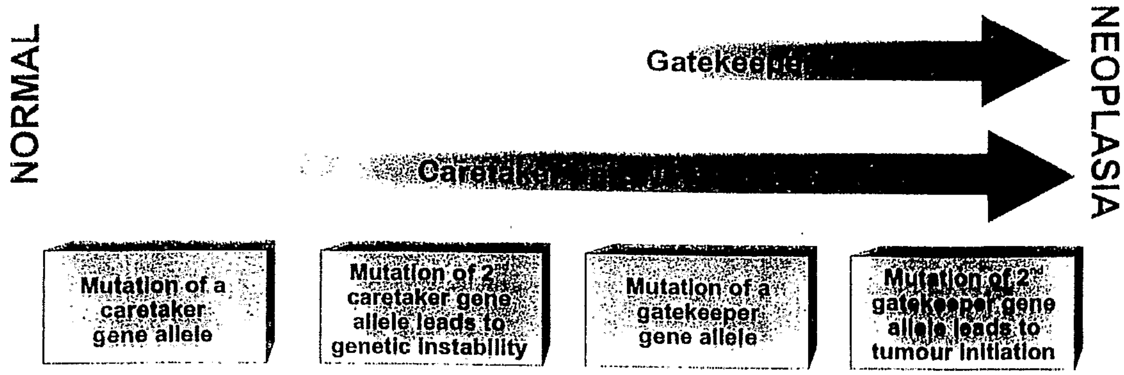

KINZLER u. VOGELSTEIN

<u>Cell systems available to investigate radiation -induced neoplastic transformation</u>

SHE	(embryonic Syrian hamster cells)
BALB/3T3	(embryonic mouse cells)
C3H10T1/2	(embryonic mouse cells)
CGL1	(hybrid HeLa x human skin fibroblast)

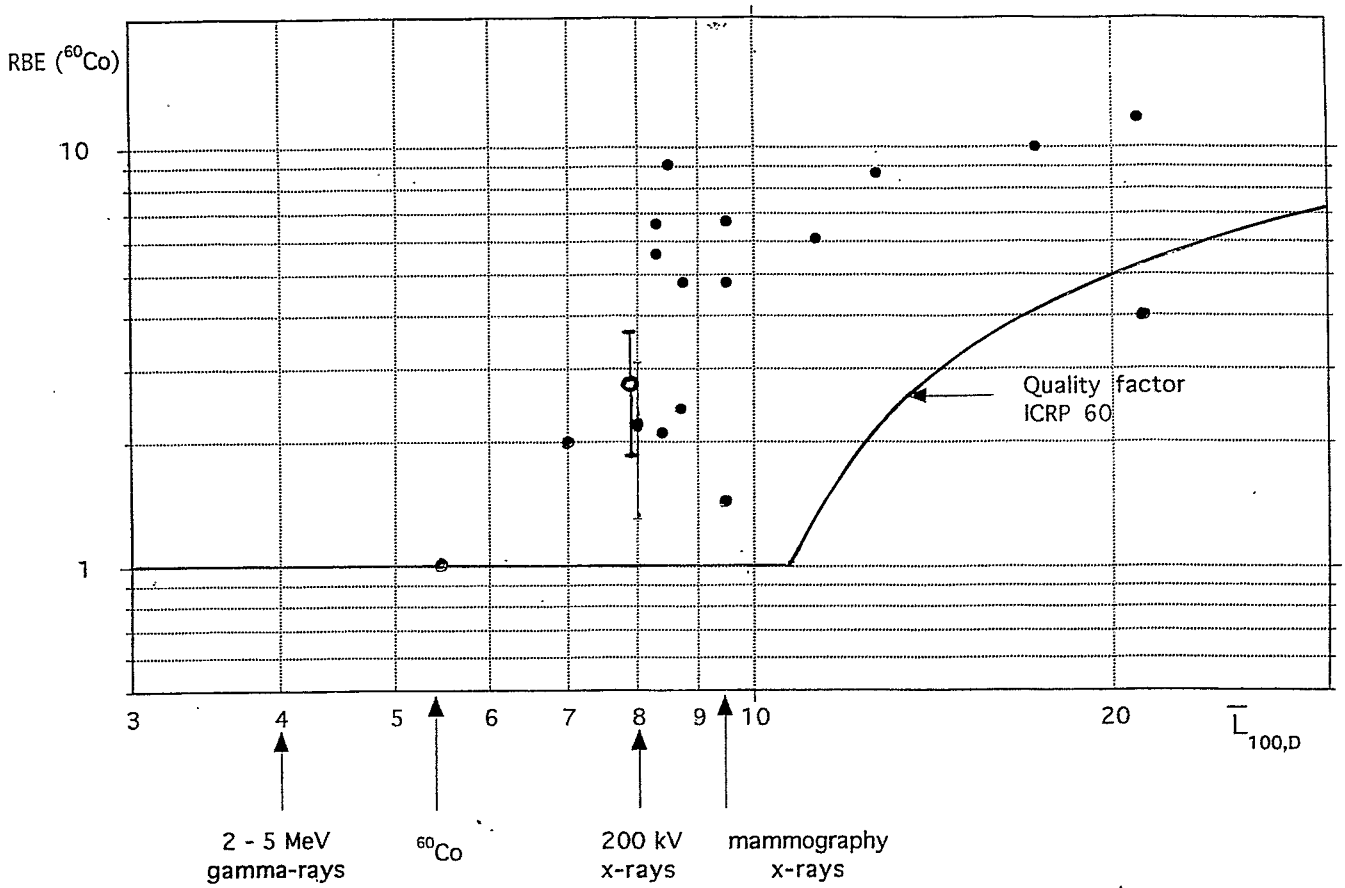

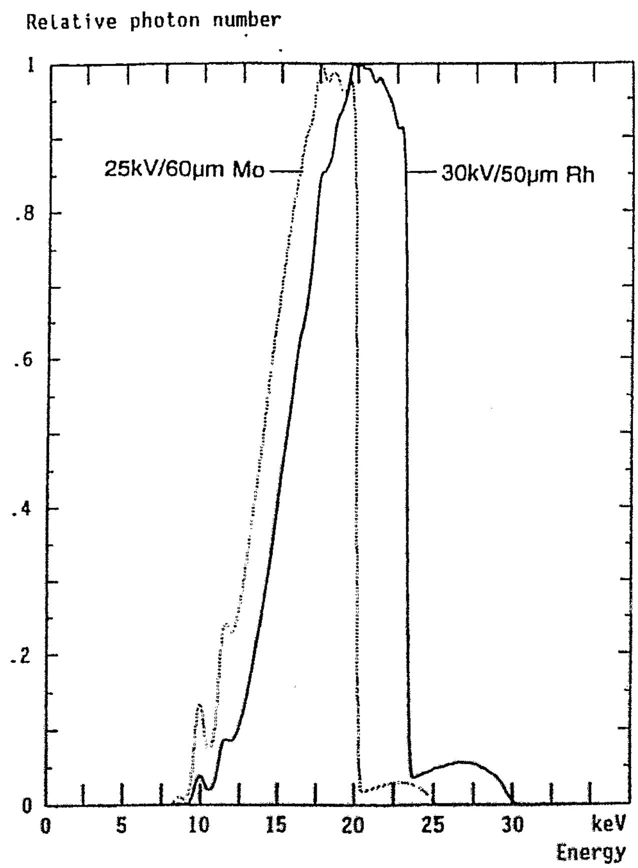

Figure 3. Molybdenum-filtered and rhodium-filtered x-ray spectra produced with a tungsten anode at 25 kV and 30 kV, respectively.

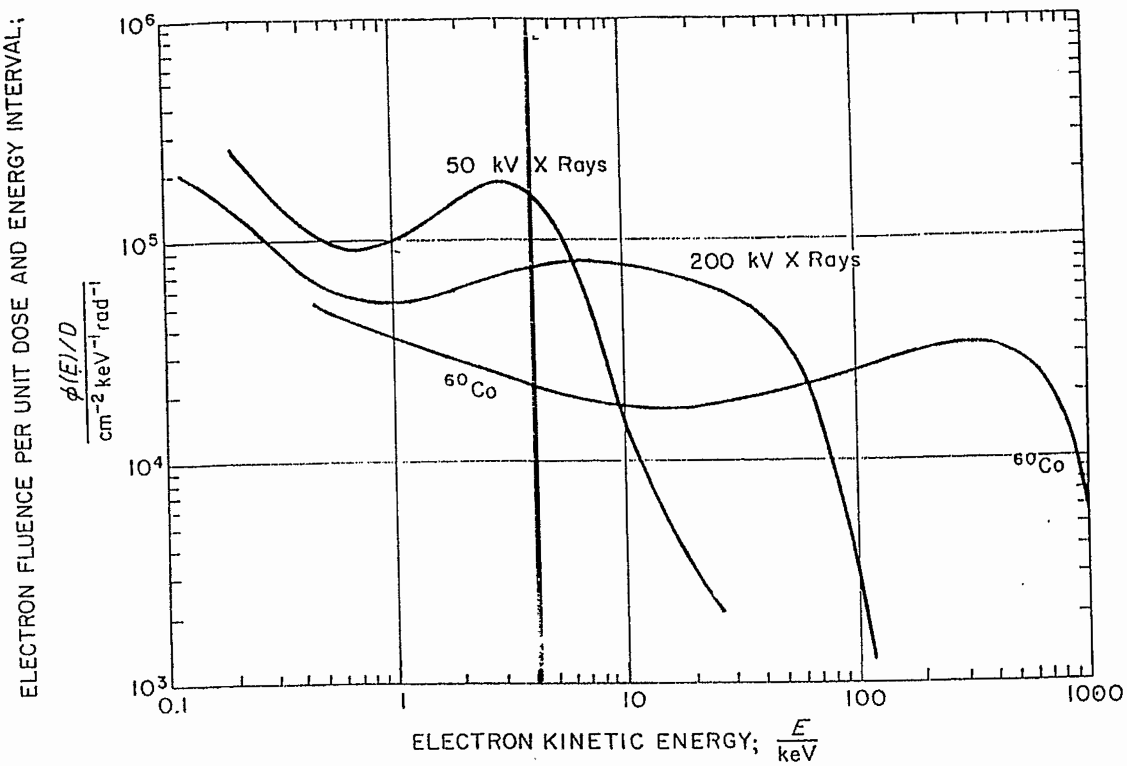

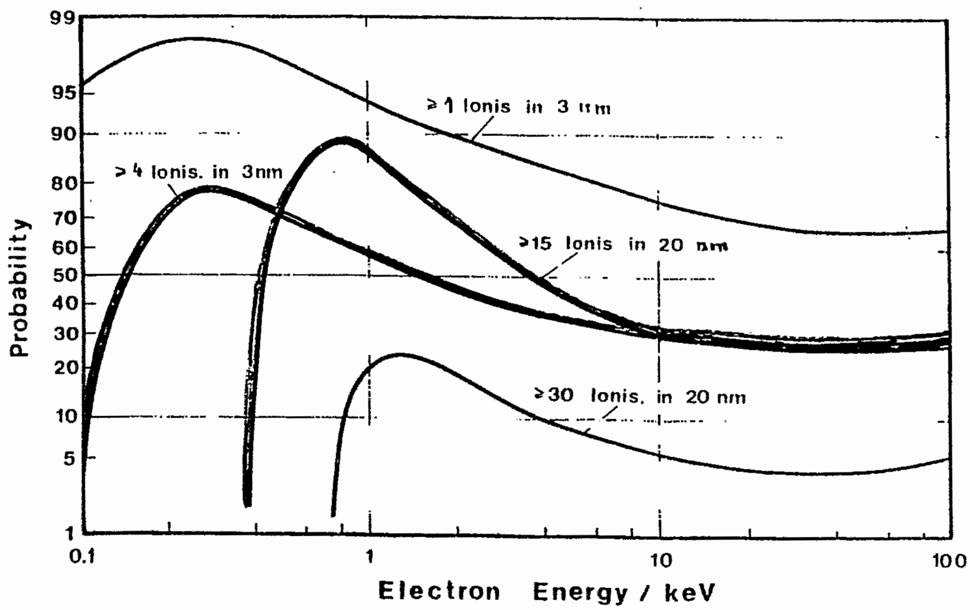

Fig.11 Probability to find a certain number of ionizations within a certain distance in e$^-$-tracks

PARETZKE et al. 1981

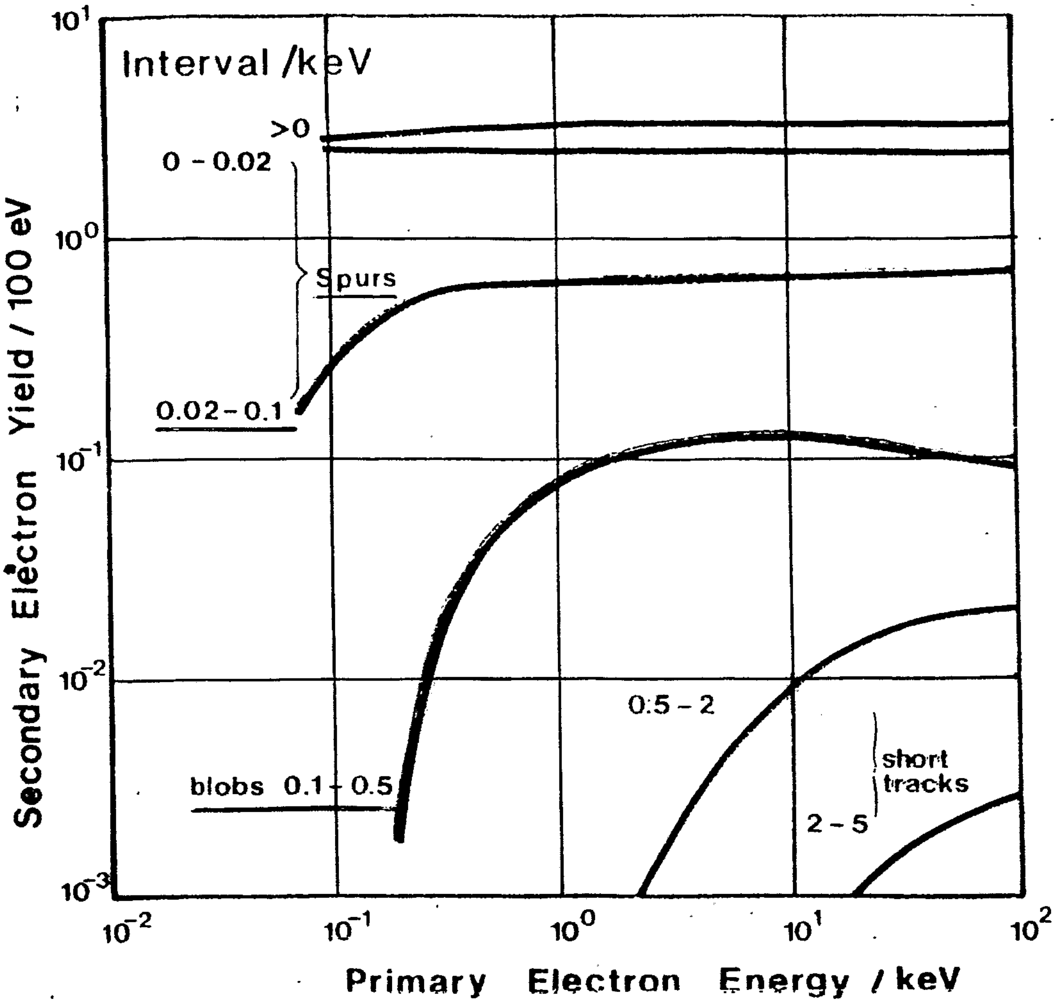
Interval /keV
>0
0 - 0.02
Spurs
0.02 - 0.1
blobs 0.1 - 0.5
0.5 - 2
short tracks
2 - 5
Secondary Electron Yield / 100 eV
Primary Electron Energy / keV

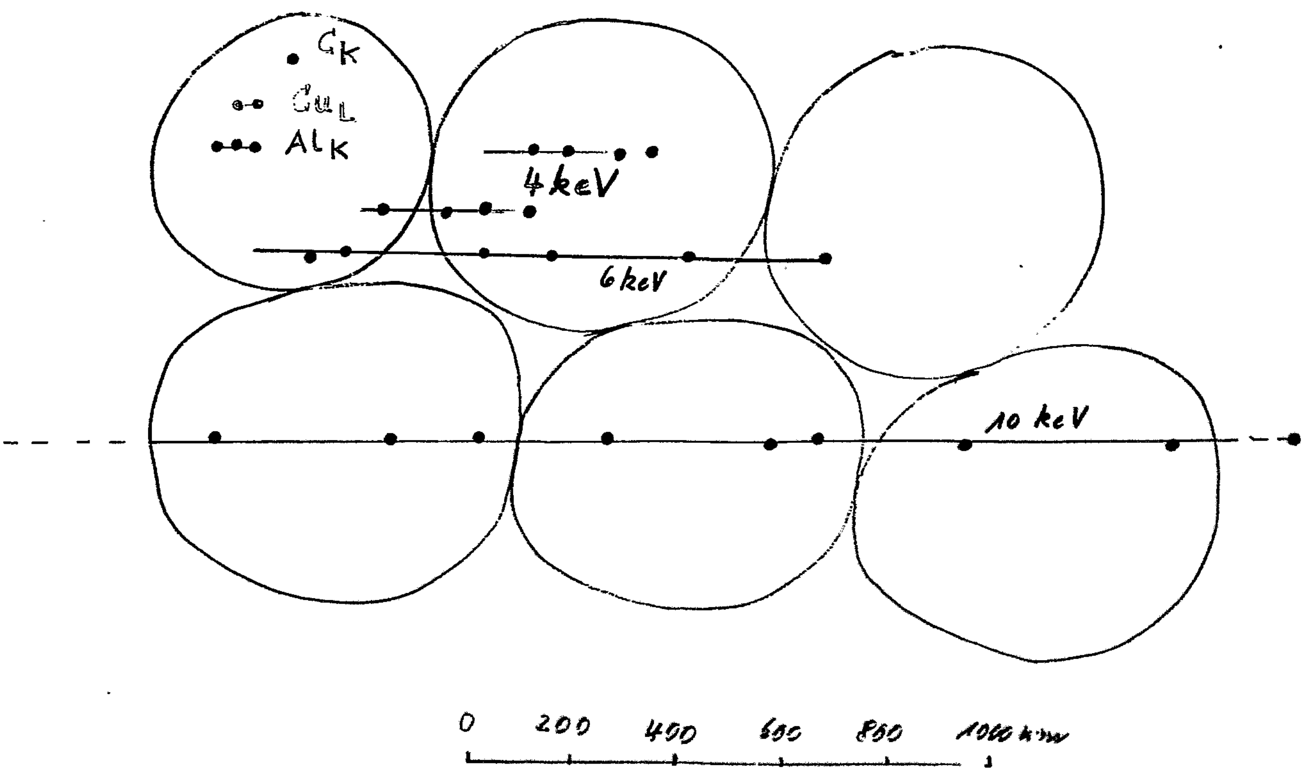
C_K
Cu_L
Al_K
4 keV
6 keV
10 keV
0 200 400 600 800 1000 nm

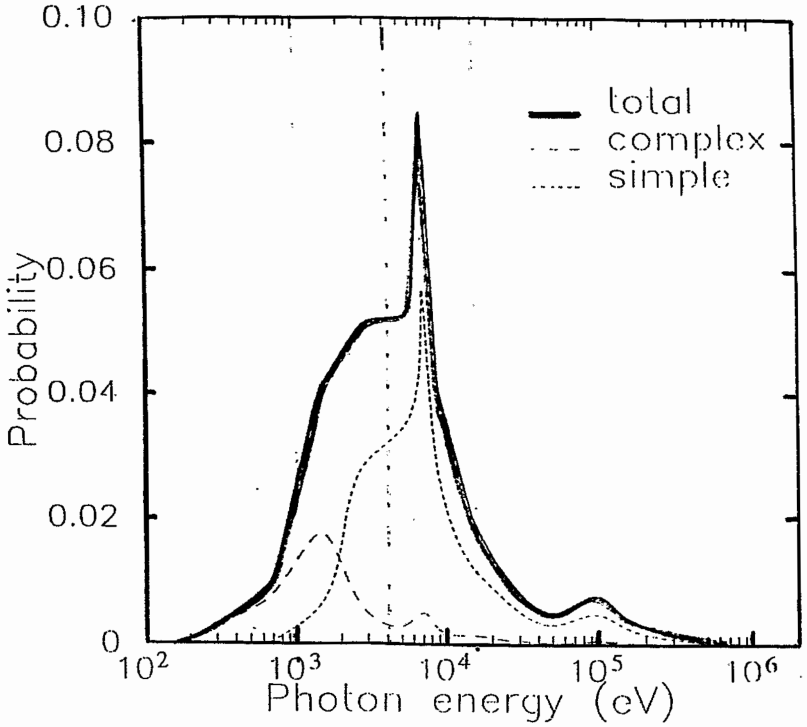

Probability of a photon to induce two dsb in a volume with a 600 um Cord length

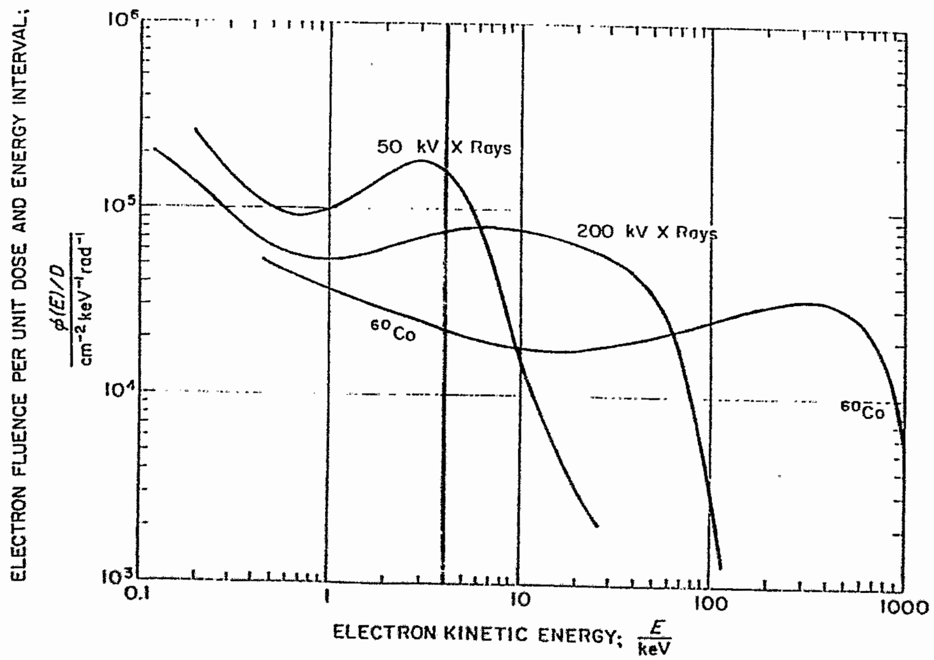

Genomic frequencies of radiation-induced translocations in G_0-lymphocytes using FISH

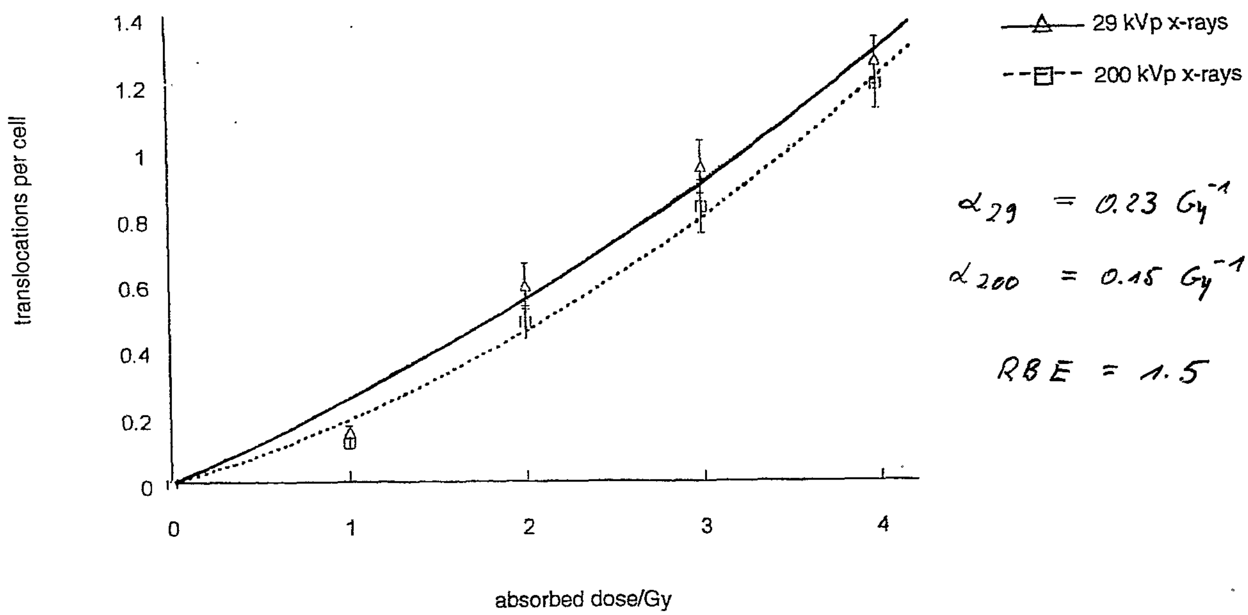

$\alpha_{29} = 0.23\ Gy^{-1}$

$\alpha_{200} = 0.15\ Gy^{-1}$

$RBE = 1.5$

The most important characteristics of the CGL system

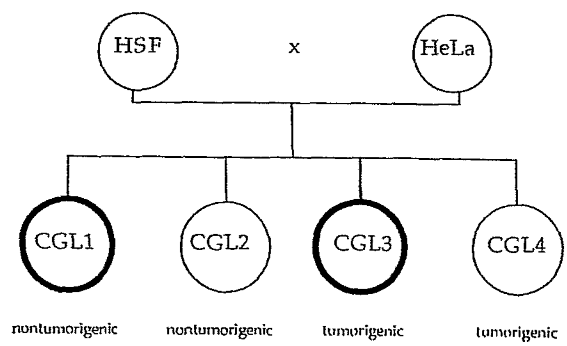

- Very stable cell lines with 90 - 100 chromosomes.
- On chromsomes 11 and 14 are loci of tumor suppressor genes.
- Tumorigenicity is induced when one chromos. or one tumor suppressor gene of each of the fibroblast chromosomes 11 and 14 is lost.
- Tumorigenicity is associated with the expression of the intestinal alkaline phosphatase (IAP). (IAP is expressed by the HeLa cells.) Thus, neoplastically transformed cells (or clones) can be identified by the expression of IAP.
- Expression of IAP can be detected simply and rapidly by a substrate of IAP, i. e. "Western Blue (WB)". This compound is cleaved by IAP leading to a blue insoluble precipitate.

References

Stanbridge et al., Somatic Cell Genet. 7, 699-712, 1981

Redpath et al., Radiat. Res. 110, 468-472, 1987

Mendonca et al., Radiat. Res. 131, 345-350, 1992 und Radiat. Res. 149, 246-255, 1998

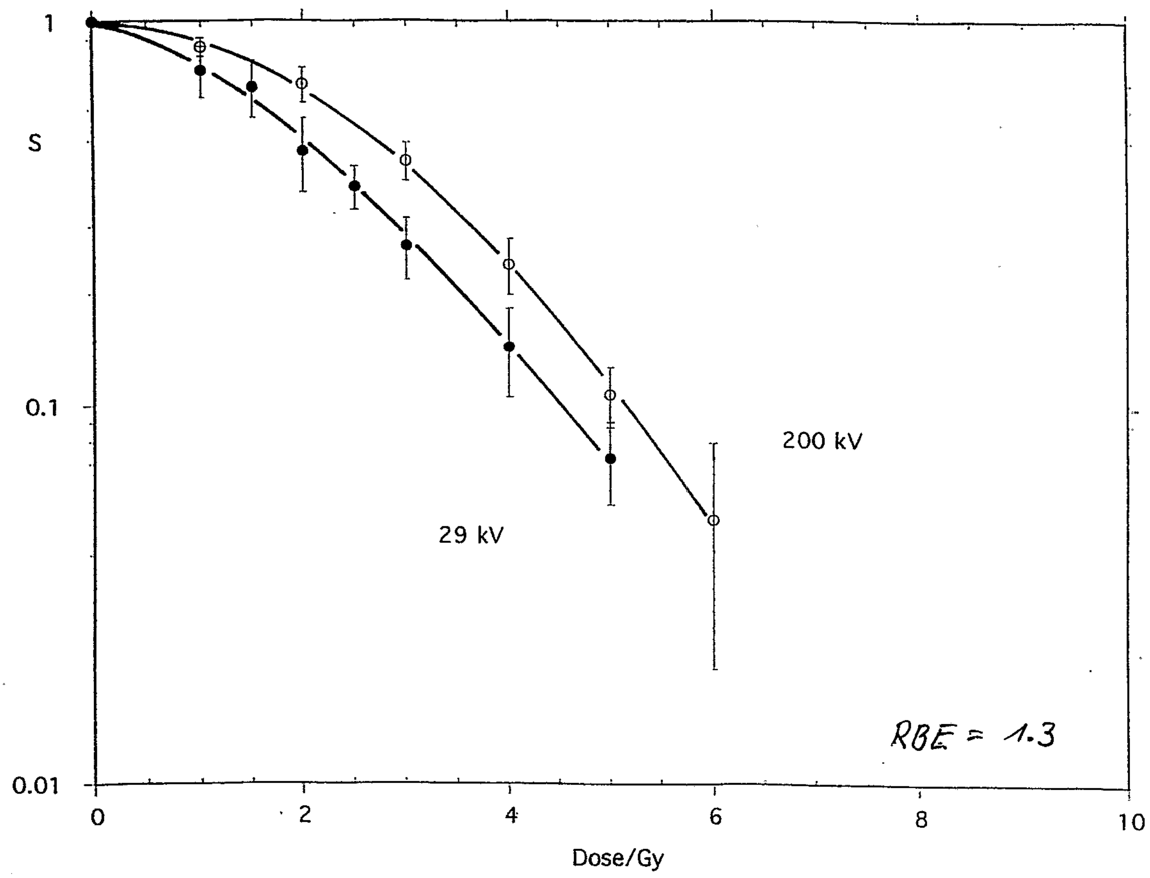

1
S
0.1
0.01
0
2
4
6
8
10
Dose/Gy
200 kV
29 kV
RBE = 1.3

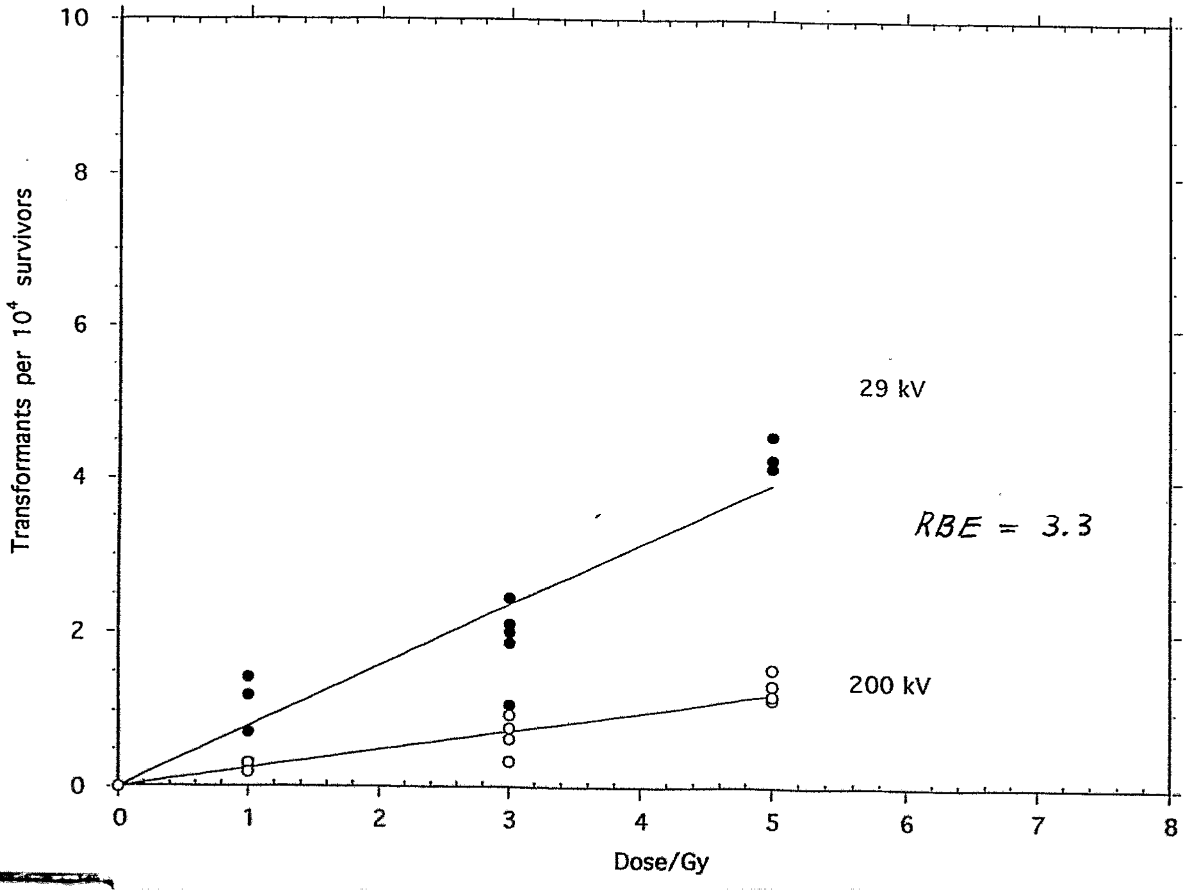

10
8
6
4
2
0
Transformants per 10^4 survivors
0
1
2
3
4
5
6
7
8
Dose/Gy
29 kV
200 kV
RBE = 3.3

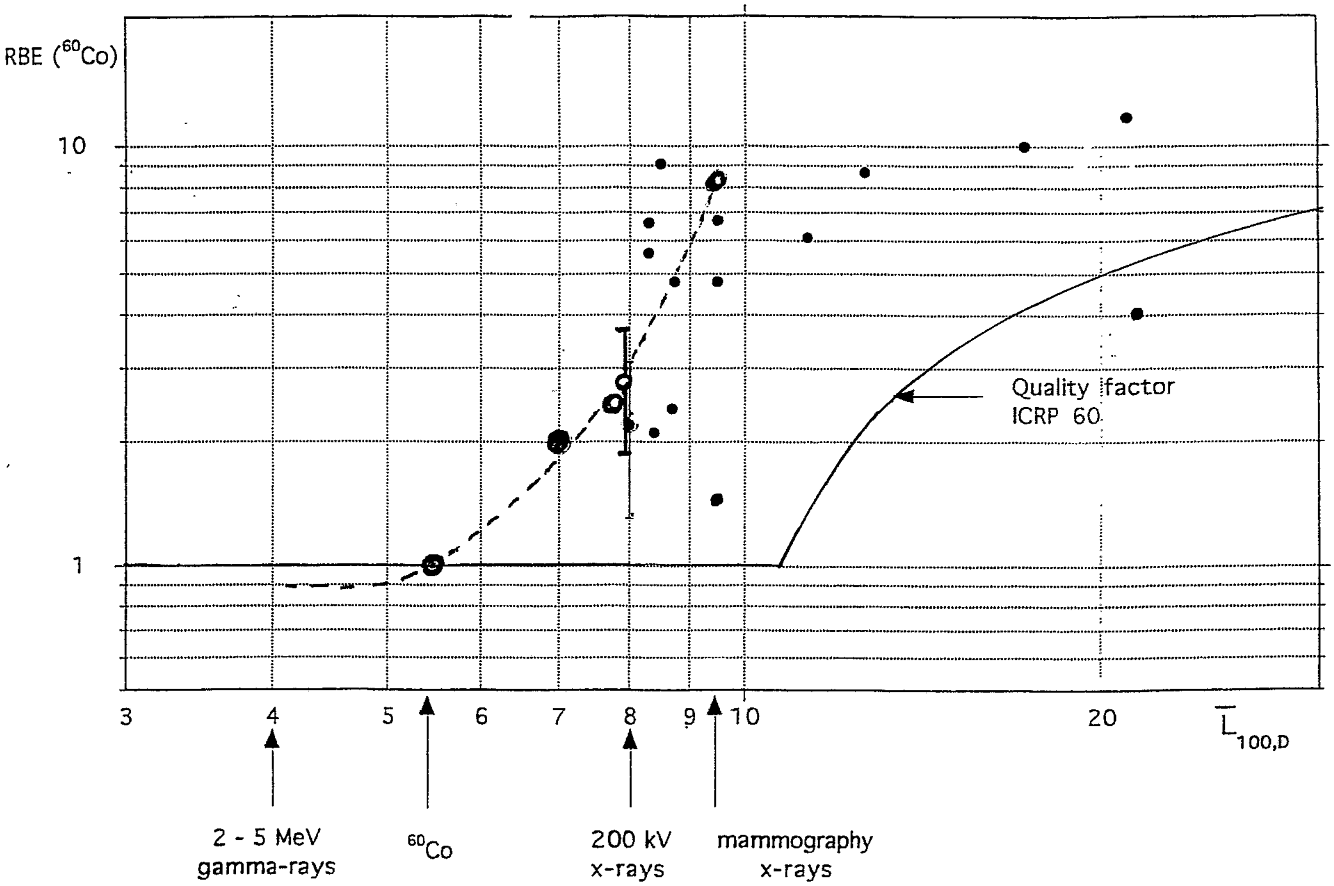

Summary

- Current radiation risk estimates are based on the efficiency of 2 - 5 MeV gamma rays.
- It is assumed that the efficiency of gamma- and x-rays as well as electrons with LETs up to 11 keV/µm are all equally effective.
- Data in the literature suggest that this assumption is not valid.
- Therefore, there is a need to determine the LET-dependence of the RBE up to 11 keV/µm (2 - 5 MeV gamma-rays up to mammography x-rays, i. e. 29 kVp x-rays) for the relevant end points.
- Using a human hybrid cell line the RBE of mammography x-rays relative to 200 kVp x-rays for neoplastic cell transformation amounts to 3.3.
- Considering the RBE of 300 kVp x-rays relative to ^{60}Co gamma-rays an RBE of at least 7 can be expected for mammography x-rays relative to ^{60}Co gamma-rays.
- This means an underestimation of mammography x-rays by a factor of at least 7.

Project
"Mammography x-rays"

P. Virsik-Peuckert

K. Konstantin

K. Kelnhofer

K. Bär

M. Frankenberg-Schwager

D. Frankenberg

D. Harder:

Chromosome aberrations by soft and ultrasoft X-rays: Microdosimetric and radiobiological aspects

Proposed mechanisms of radiation-induced chromosome exchange:

<u>β component</u>

Pairwise interaction between double-strand breaks of DNA via NHEJ (non-homologous end joining)

<u>α component</u>

a) Deletion of DNA segments + single strand invasion

b) Denaturation of nucleosome by thermal spike + single strand invasion.

Proposed experiments:

1) Acoustic pulse by 10 ps electron bunch

2) Ultrasoft X-rays: Search for DNA segments

3) Tunable ultrasoft X-rays: energy requirement

4) BrdUrd experiments

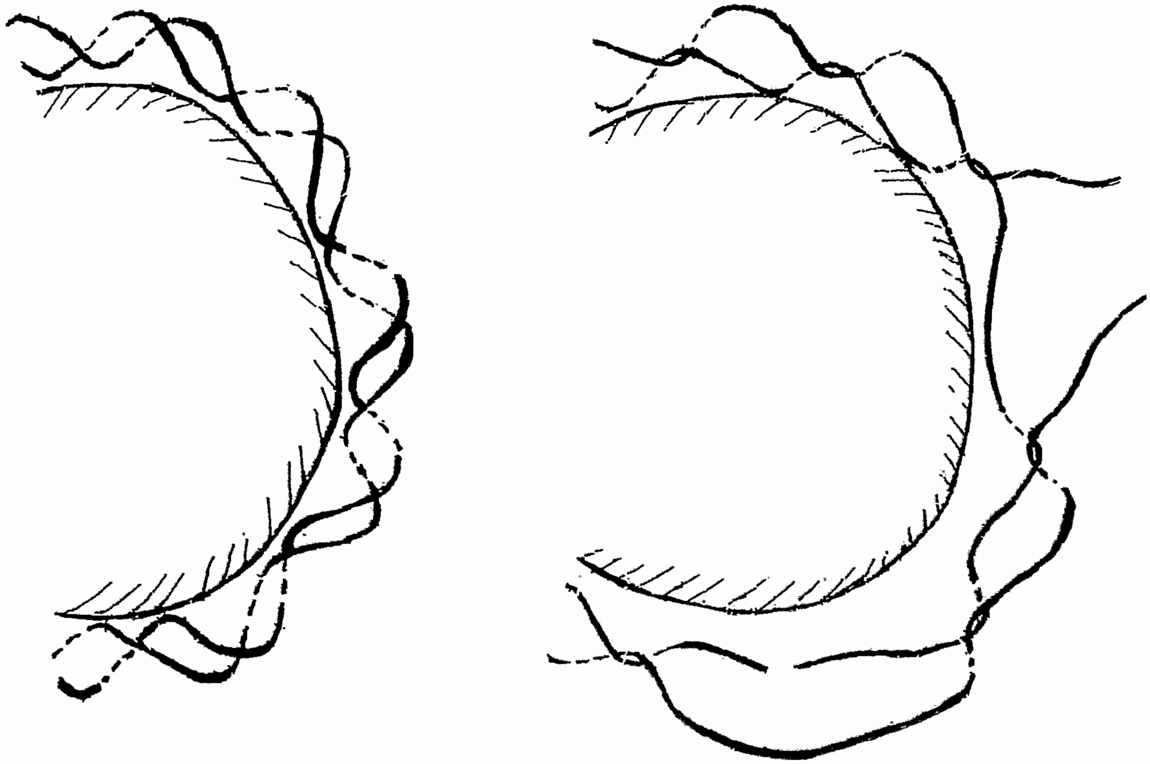

Proposed thermal dissociation of hydrogen and Van der Waals bonds in nucleosomal DNA

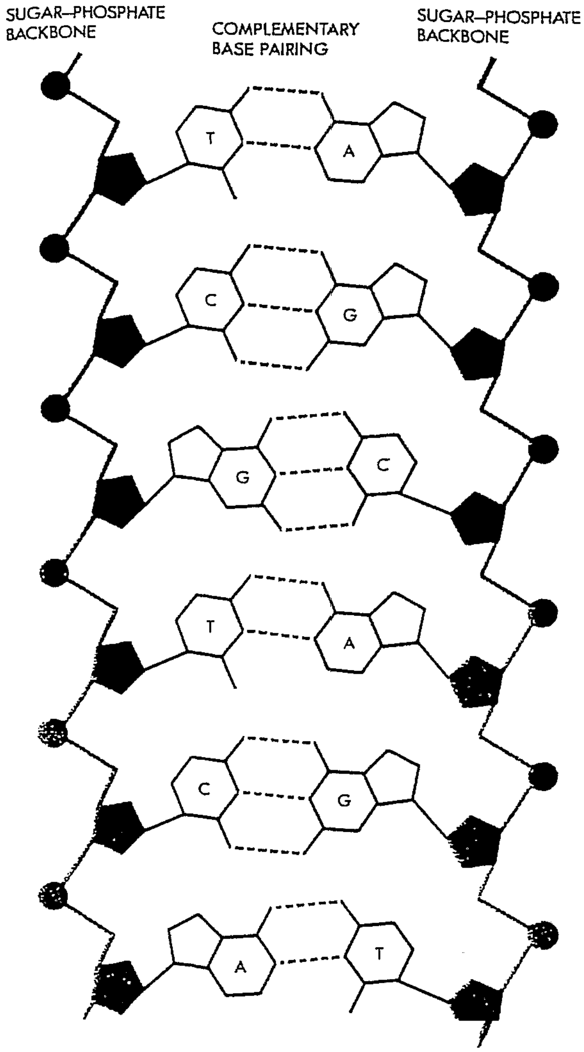

Time resolved properties of acoustic pulses generated in water and in soft tissue by pulsed proton beam irradiation—A possibility of doses distribution monitoring in proton radiation therapy

Junichiro Tada and Yoshinori Hayakawa
Institute of Basic Medical Sciences, University of Tsukuba, Tsukuba, Ibaraki 305, Japan

Katsuhisa Hosono
Proton Medical Research Center, University of Tsukuba, Tsukuba, Ibaraki 305, Japan

Tetsuo Inada
Institute of Basic Medical Sciences, University of Tsukuba, Tsukuba, Ibaraki, 305, Japan

1100 Med. Phys. 18 (6), Nov/Dec 1991

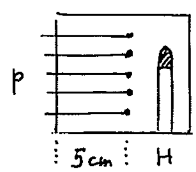

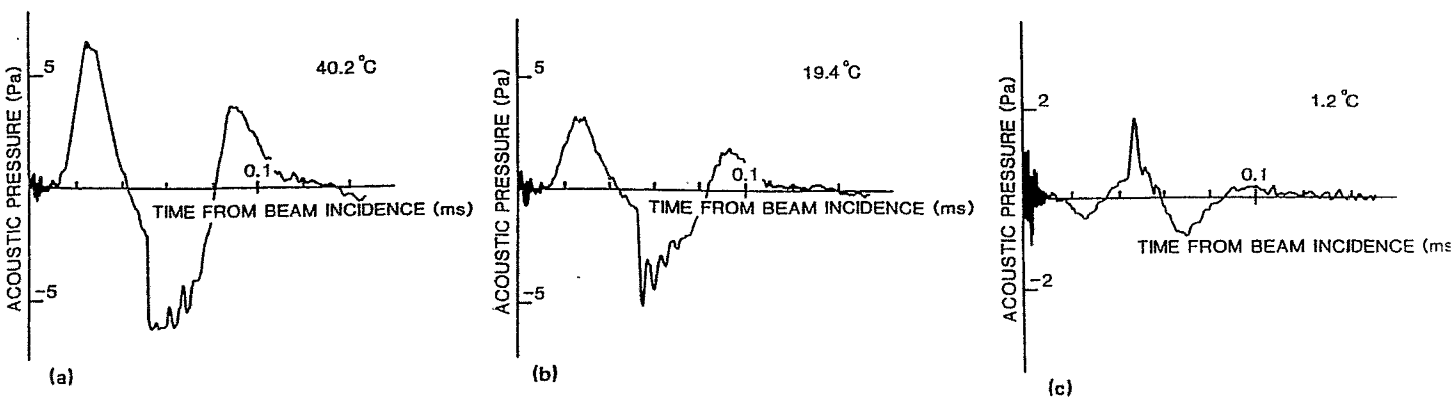

Acoustic pulses generated in water by pulsed proton beam irradiation at three different temperatures.

Pulse duration: 50 ns; proton energy: 100 MeV; absorbed dose (Bragg peak): 5 cGy/pulse.

Pressure wave generated by the passage of a heavy charged particle in water

Y. Y. Sun and Ravinder Nath
Department of Therapeutic Radiology, Yale University School of Medicine, 333 Cedar Street, New Haven, Connecticut 06510

633 Med. Phys. 20 (3), May/Jun 1993

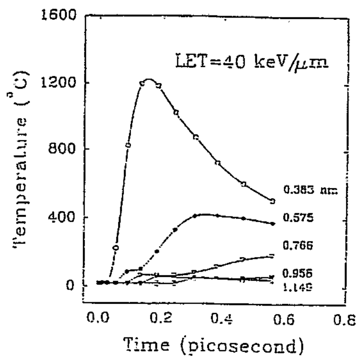

Temporal evolution of temperature distribution around the track of a charged particle with LET=40 keV/μm, traversing through water at 20°C.

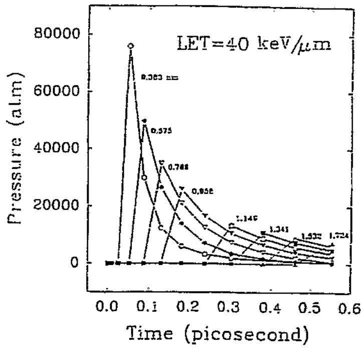

Temporal evolution of pressure distribution around the track of a charged particle with LET=40 keV/μm, traversing through water at 20°C.

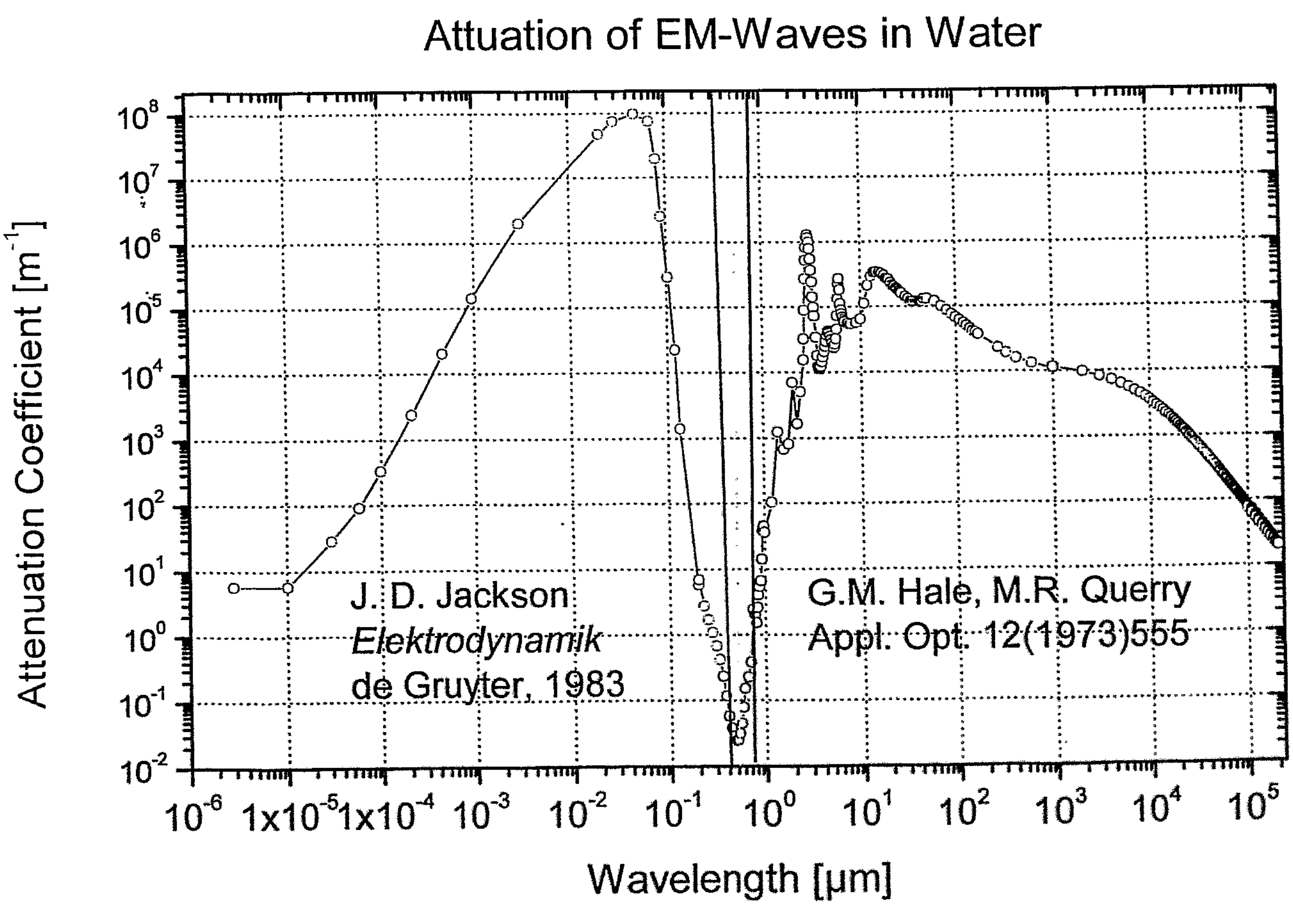

4.67 Gy of 5 MeV electrons at various irradiation temperatures

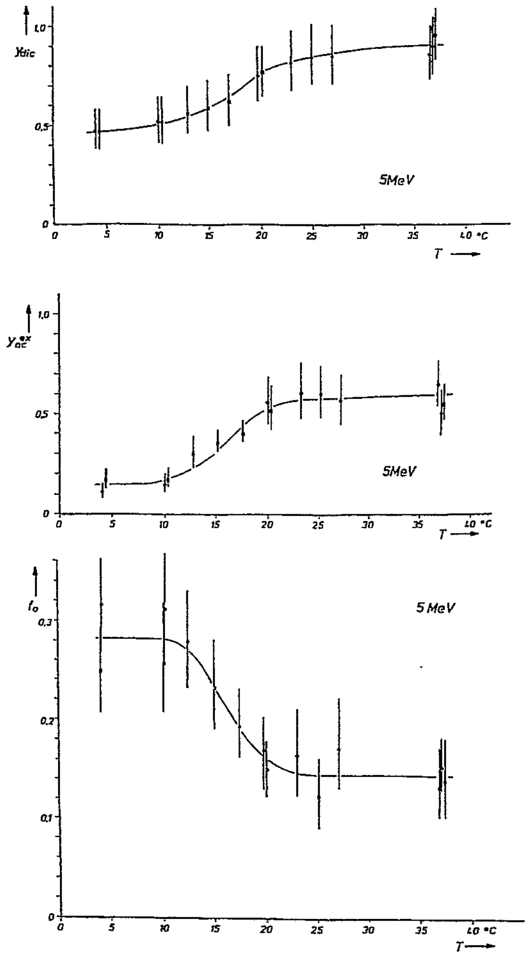

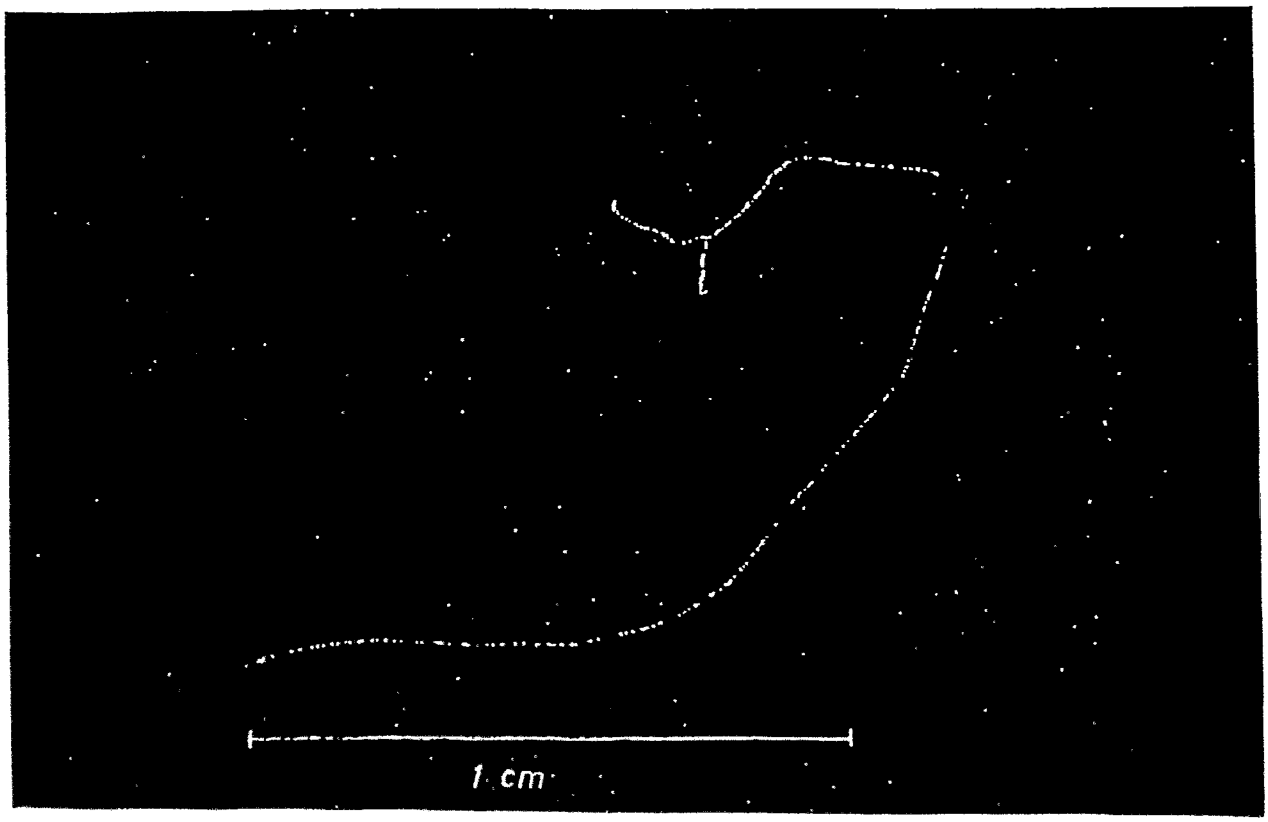

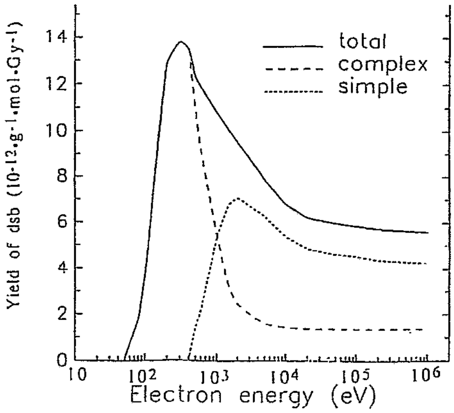

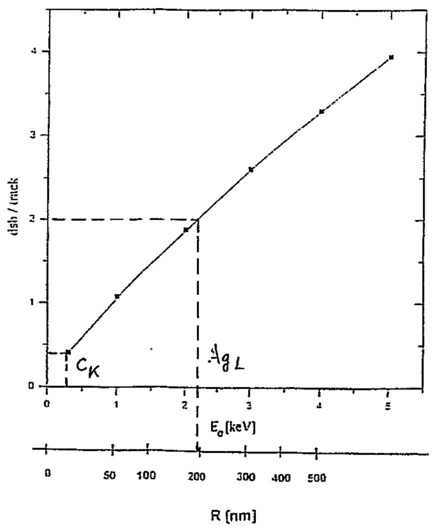

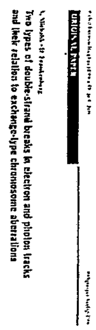

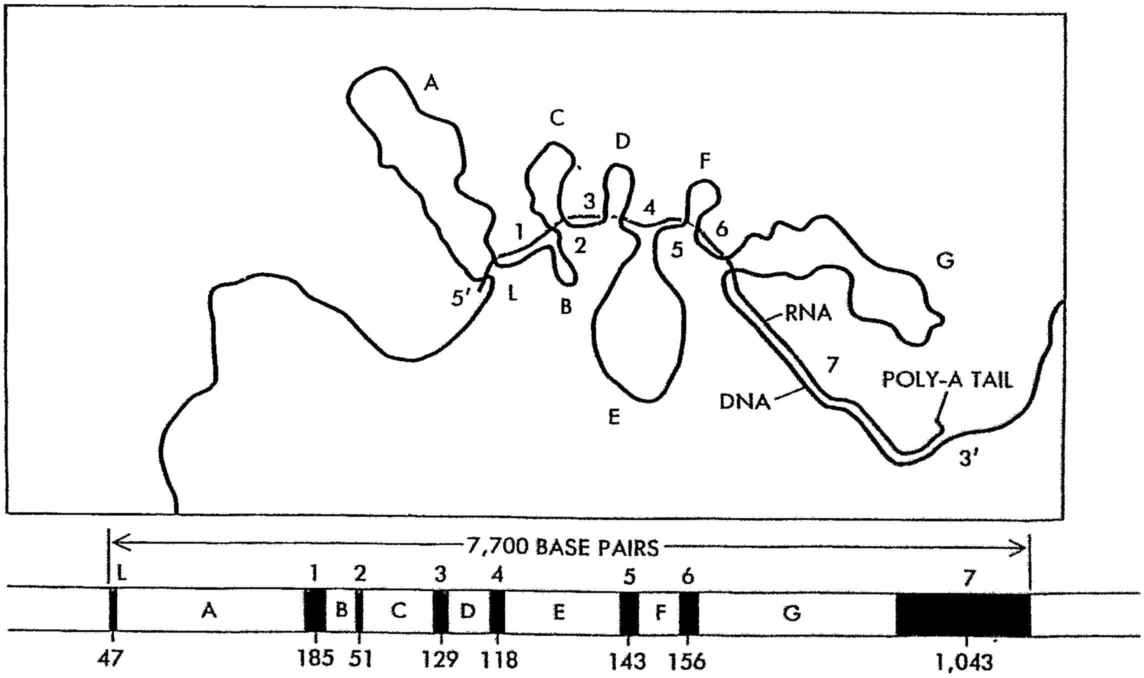

SINGLE-STRANDED DNA CONTAINING THE GENE FOR THE PROTEIN OVALBUMIN WAS ALLOWED TO HYBRIDIZE WITH OVALBUMIN MESSENGER RNA. THE EIGHT EXONS (L, 1-7) OF THE GENE ANNEAL TO THE COMPLEMENTARY REGIONS OF RNA, AND THE SEVEN INTRONS (A-G) LOOP OUT FROM THE HYBRID. THE 5' AND 3' ENDS OF THE MESSENGER ARE INDICATED, AS IS THE POLY-A TAIL.

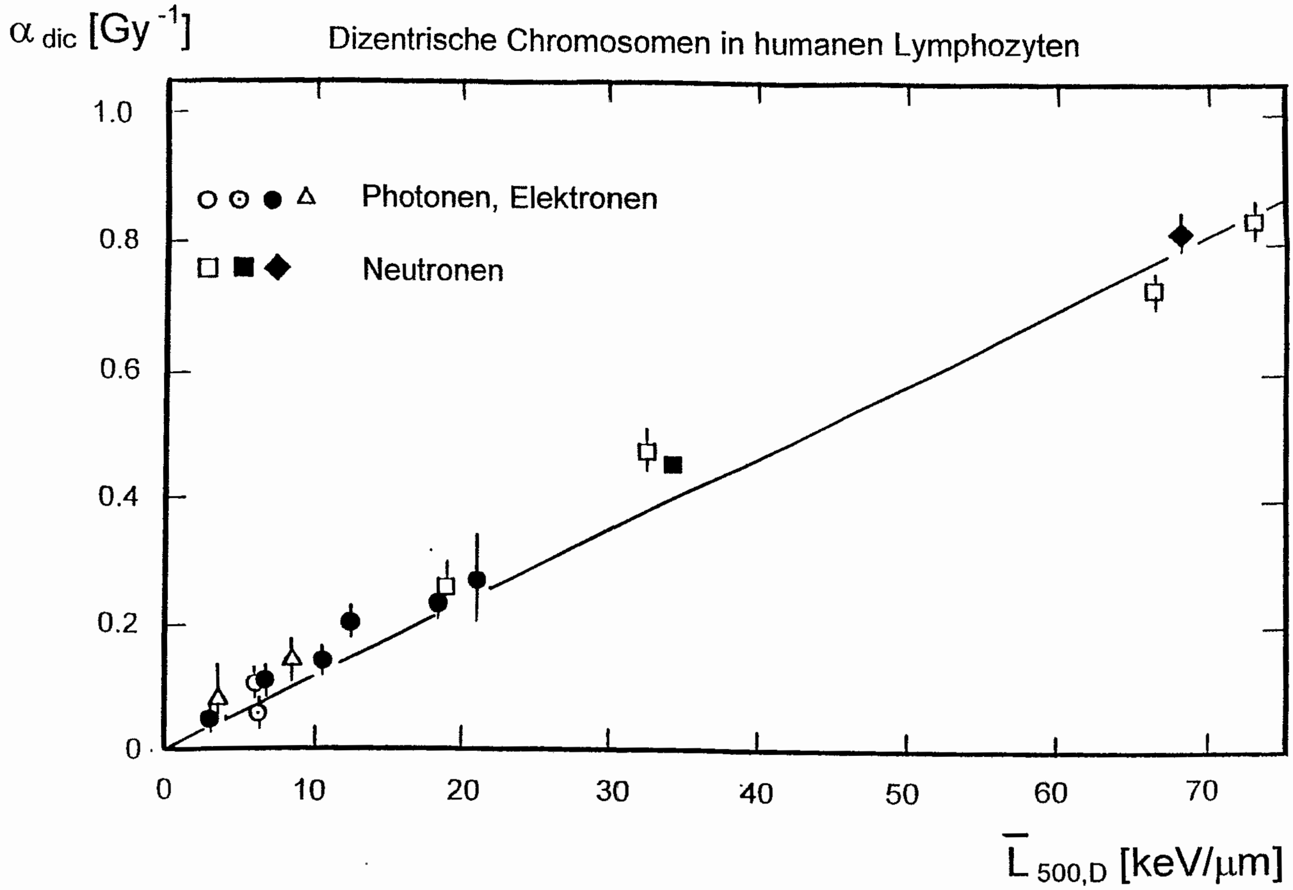

α_{dic} [Gy^{-1}]
Dizentrische Chromosomen in humanen Lymphozyten
1.0
0.8
0.6
0.4
0.2
0
Photonen, Elektronen
Neutronen
0
10
20
30
40
50
60
70
$\bar{L}_{500,D}$ [keV/µm]

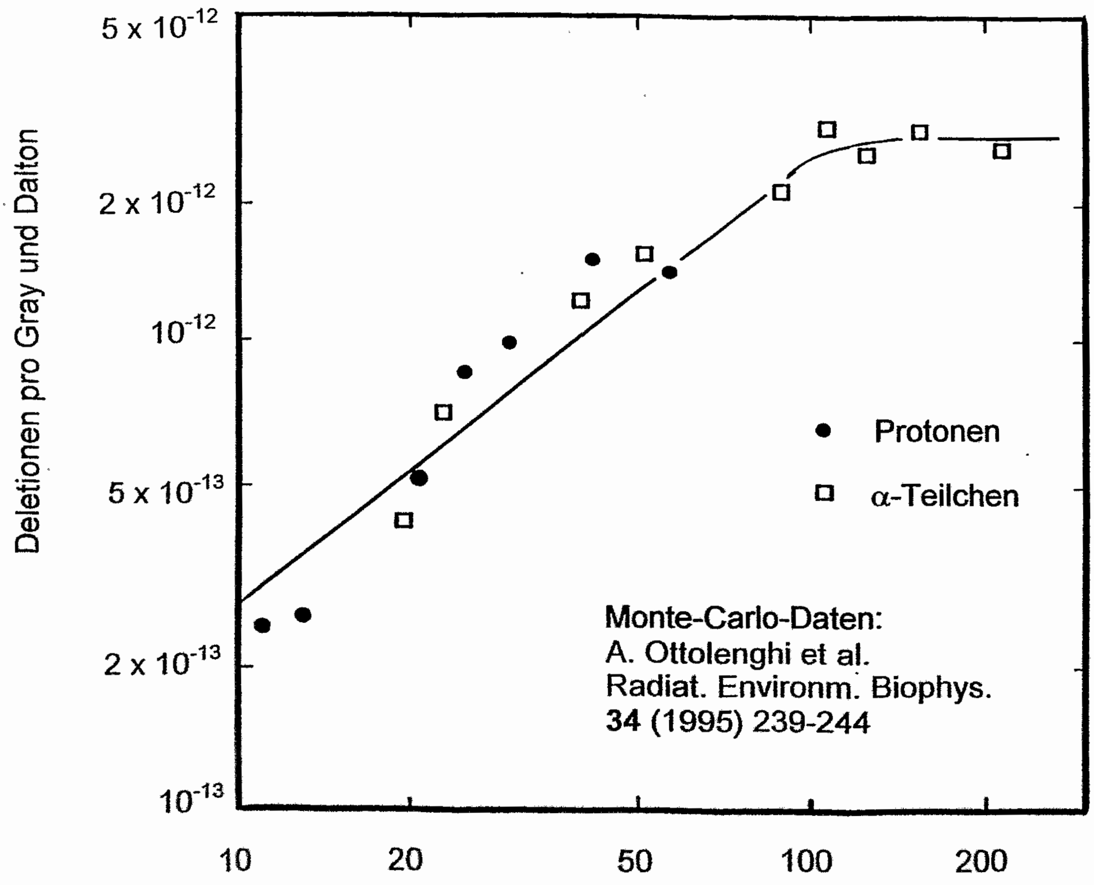

Deletionen pro Gray und Dalton
5 x 10^{-12}
2 x 10^{-12}
10^{-12}
5 x 10^{-13}
2 x 10^{-13}
10^{-13}
Protonen
α-Teilchen
Monte-Carlo-Daten:
A. Ottolenghi et al.
Radiat. Environm. Biophys.
34 (1995) 239-244
10
20
50
100
200

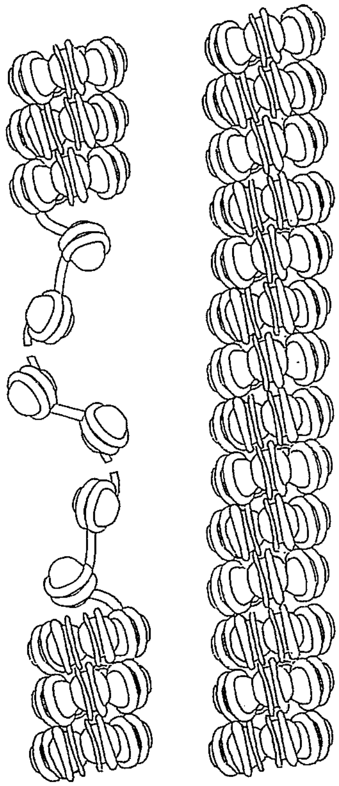

Suggested lesion-nonlesion interaction mechanism:
DNA loops or free ends, originating from clustered damage, determine the range of interaction.

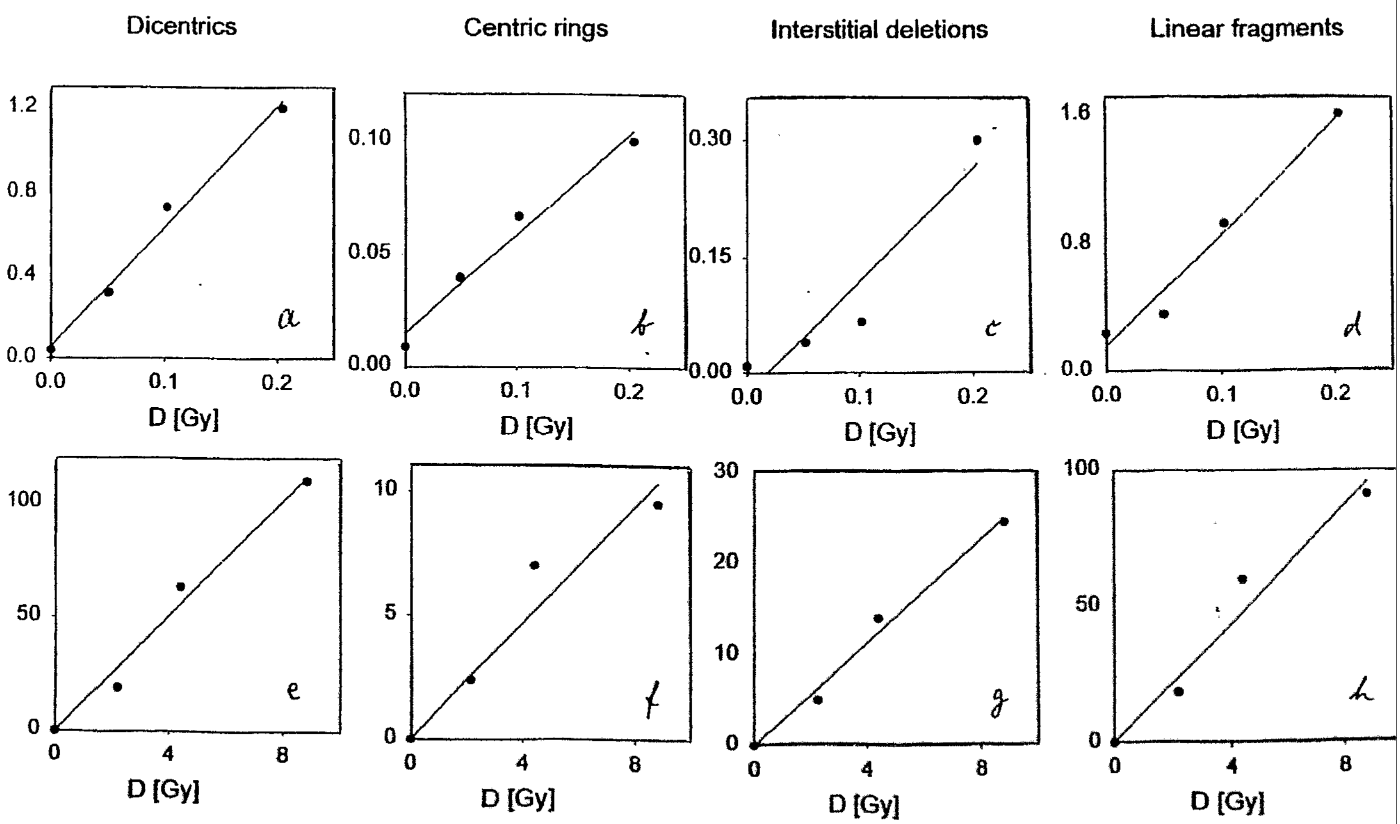

Chromosome aberration yields in 100 cells without (a-d) and with gold foil (e-h)

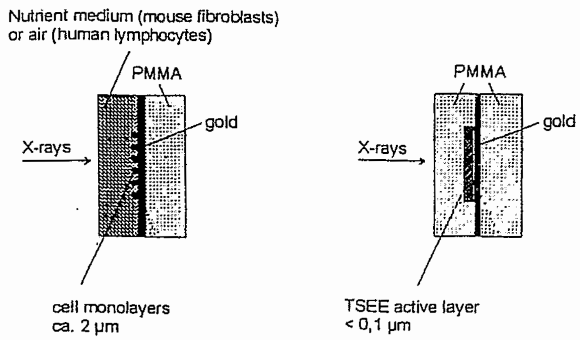

Schematic representation of the interface geometry
for irradiation with x-rays.

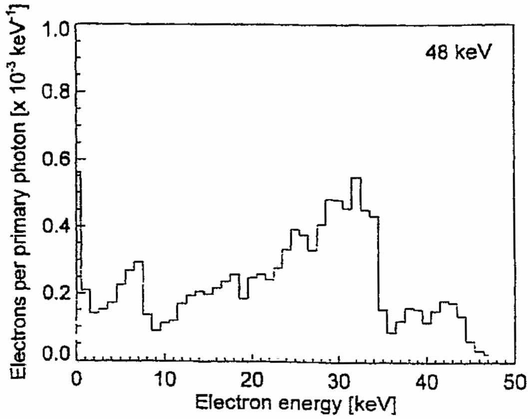

Electron spectrum at the gold surface: Photo- and Auger electrons

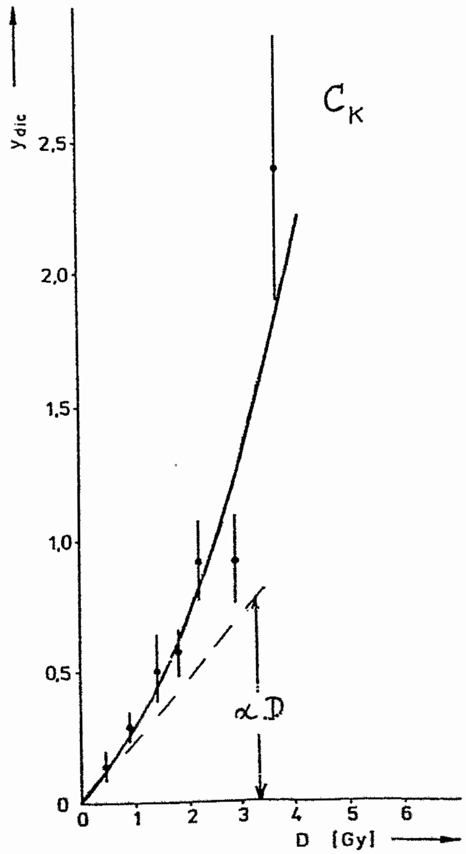

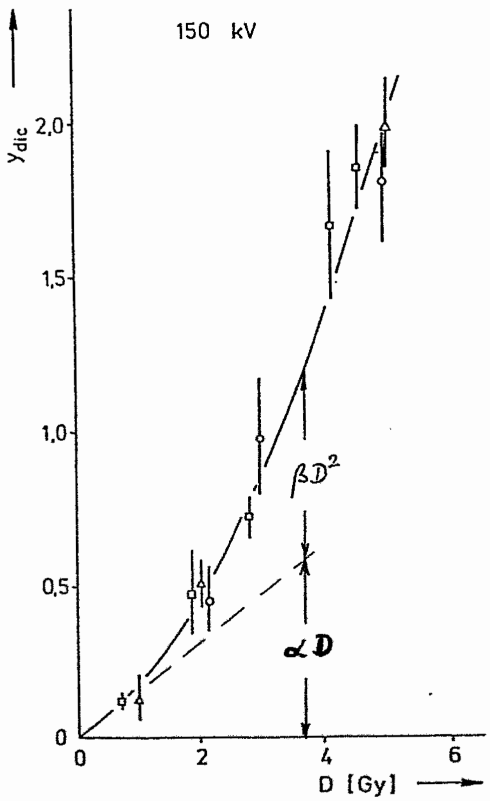

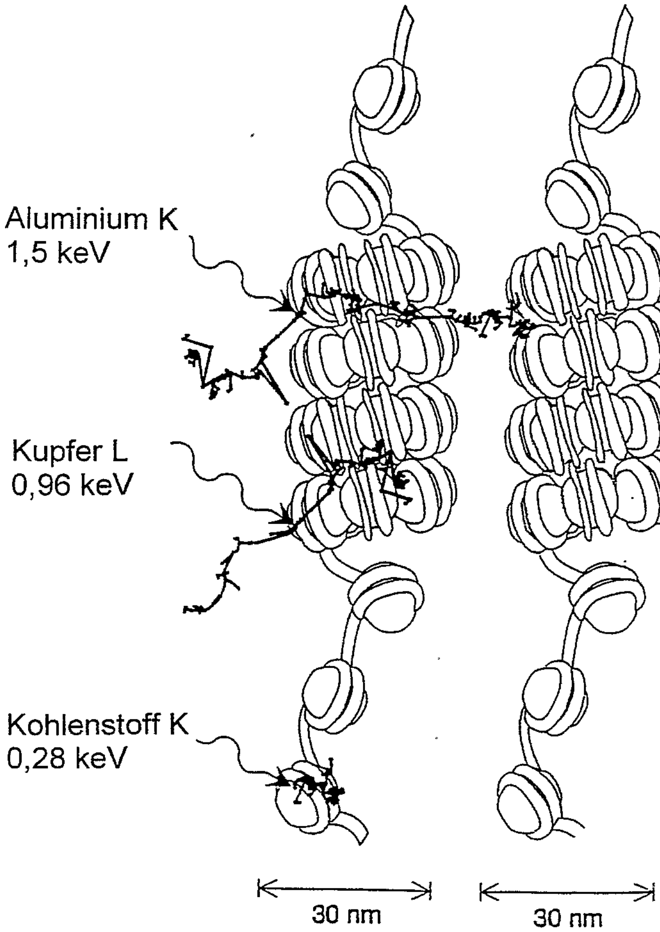

Chromatinfaser und Elektronenreichweite:
Doppeltreffer bei niedriger Energie unmöglich

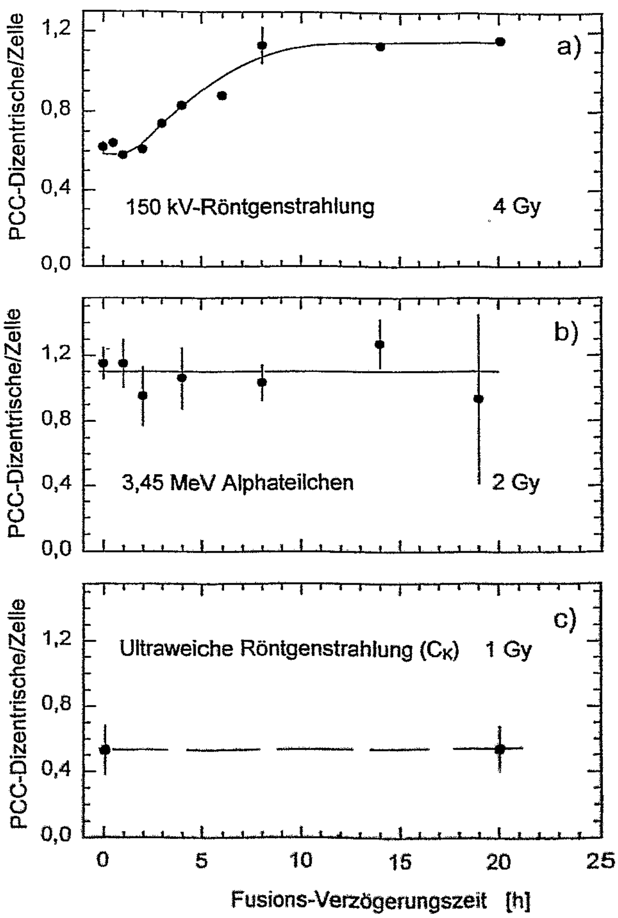

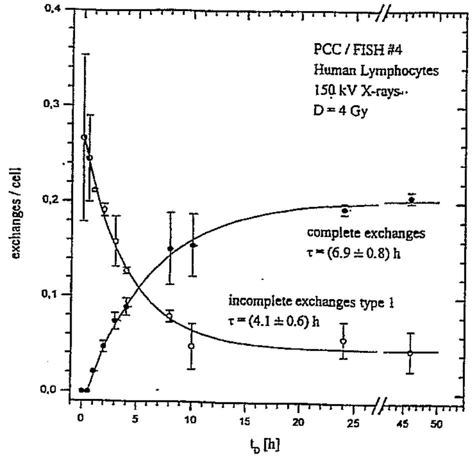

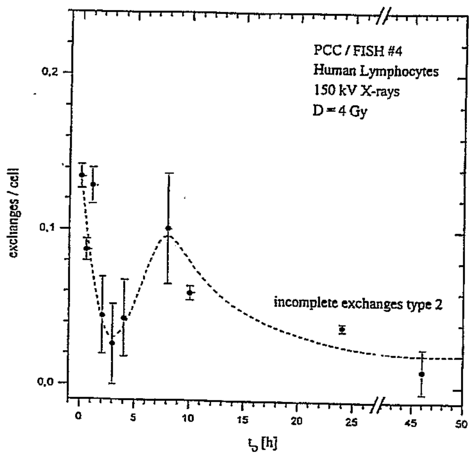

PCC / C-banding

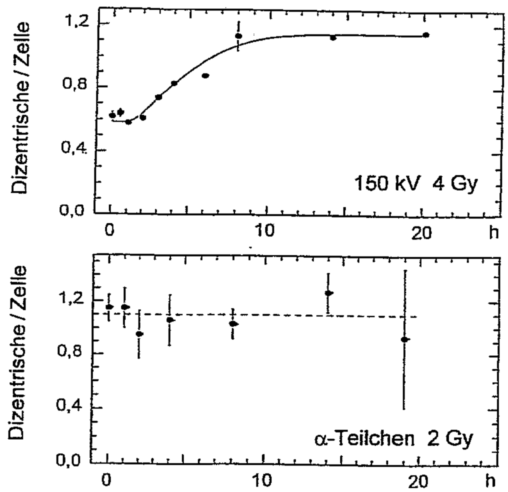

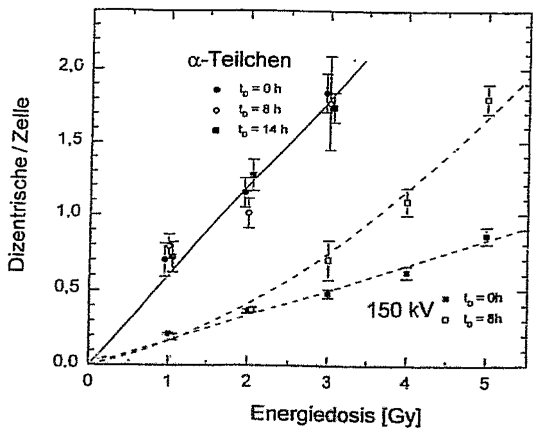

Mutation Research, 149 (1985) 67–72
Elsevier

MTR 03983

Direct analysis of radiation-induced chromosome fragments and rings in unstimulated human peripheral blood lymphocytes by means of the premature chromosome condensation technique

Gabriel E. Pantelias[1,2] and H. David Maillie [1]

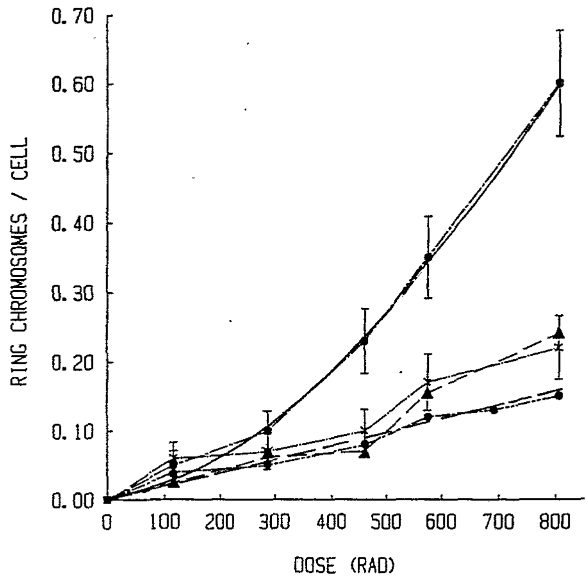

Fig. 2. Yield of ring chromosomes per cell in human peripheral blood lymphocytes exposed in vitro to varying X-ray doses up to 805 rad. Rings were analyzed immediately after exposure (●) or 1 h (×), 2 h (▲), or 24 h (●) after exposure. Bars indicate standard deviations calculated from 2–3 independent Expts.

Direct analysis of radiation-induced chromosome fragments and rings in unstimulated human peripheral blood lymphocytes by means of the premature chromosome condensation technique

Gabriel E. Pantelias[1,2] and H. David Maillie [1]
[1] *Department of Radiation Biology and Biophysics, University of Rochester, School of Medicine and Dentistry, Rochester, NY 14642, and* [2] *Laboratory of Radiobiology and Environmental Health, University of California, San Francisco, CA 94143 (U.S.A.)*

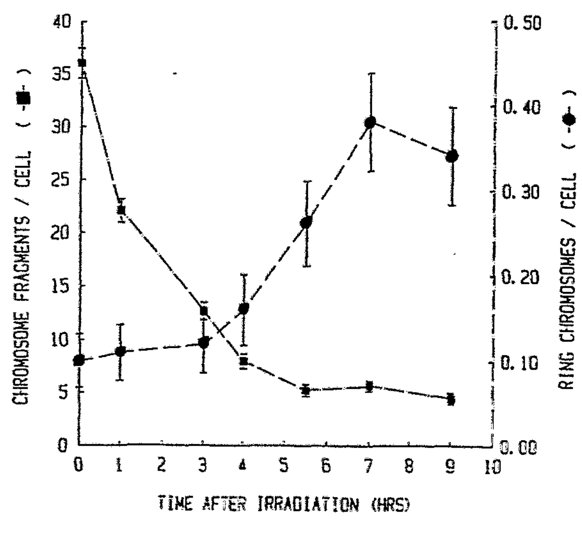

Fig. 3. Yield of chromosome fragments (■) and ring chromosomes (●) per cell in human peripheral blood lymphocytes exposed in vitro to 645 rad of X-rays and analyzed at various times after exposure.

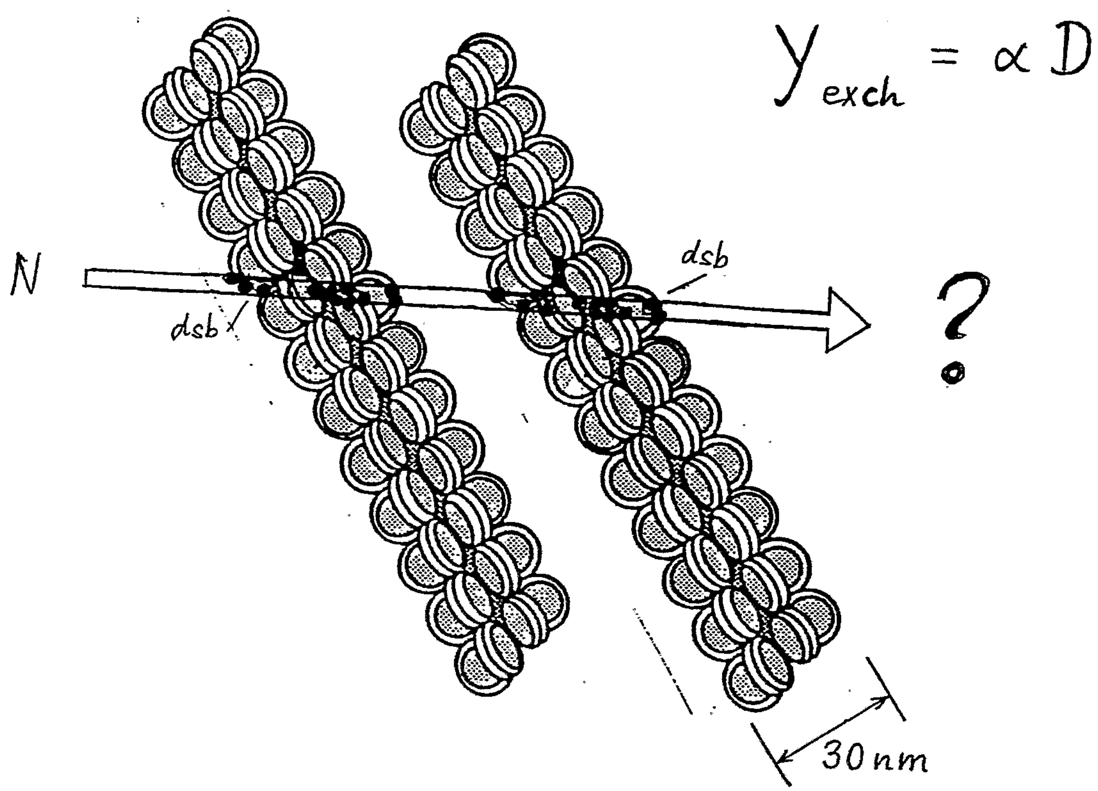
$y_{exch} = \alpha D$
N
dsb
dsb
?
30 nm

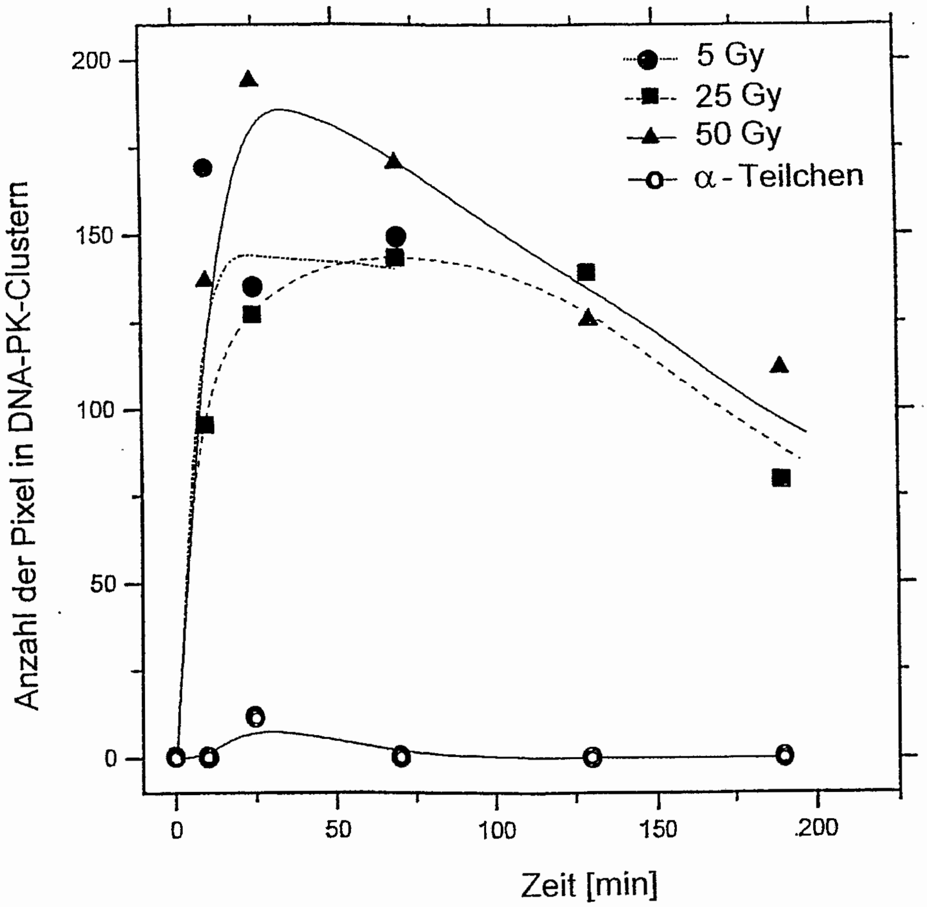

Kis 70/80
50 Gy

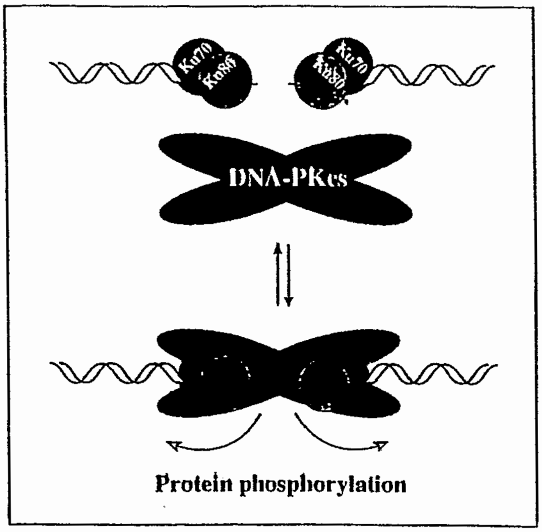

Binding of Ku heterodimer to dsb ends, recruitment and activity of DNA-PK$_{CS}$

C. Featherstone and S. P. Jackson,

Mut. Res. 434 (1999) 3 - 15

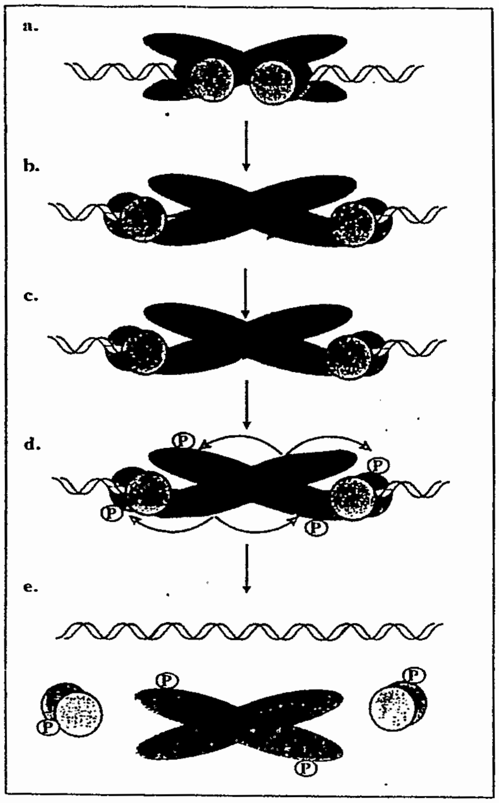

Model for nonhomologous end joining (NHEJ) by annealing broken strands at sites of microhomology

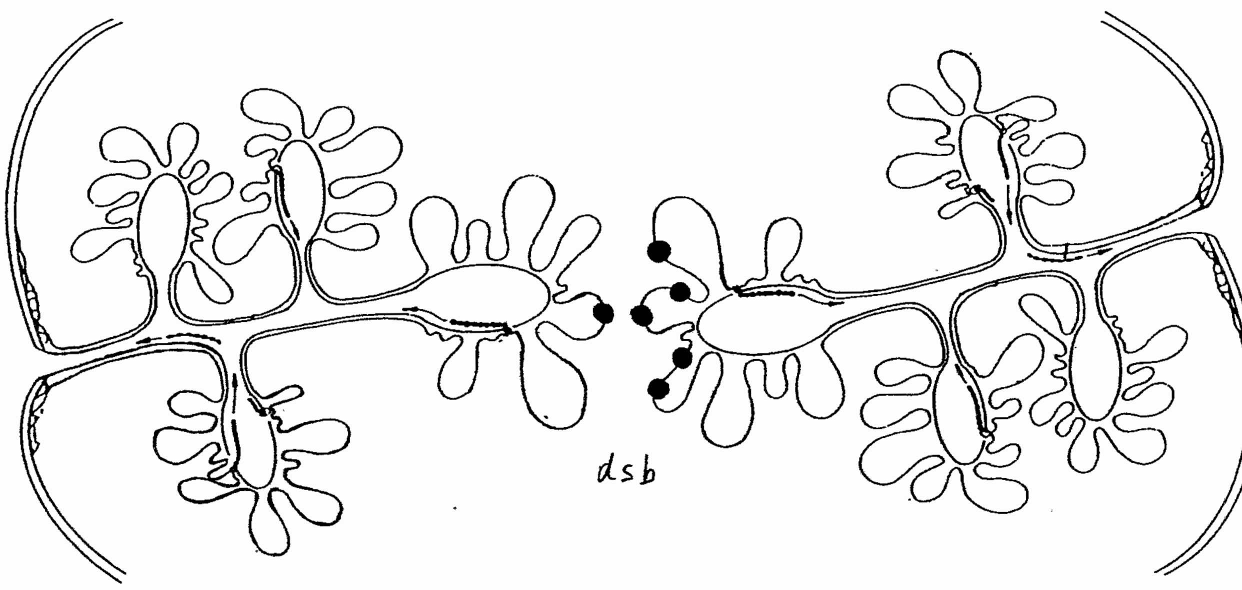

Topologie der paarweisen Läsions-Interaktion

zwischen Chromosomen-Domänen

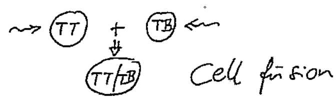

M. N. Cornforth, On the nature of interactions leading to radiation-induced chromosomal exchange. *Int. J. Radiat. Biol.* 56, 635 - 643 (1989)

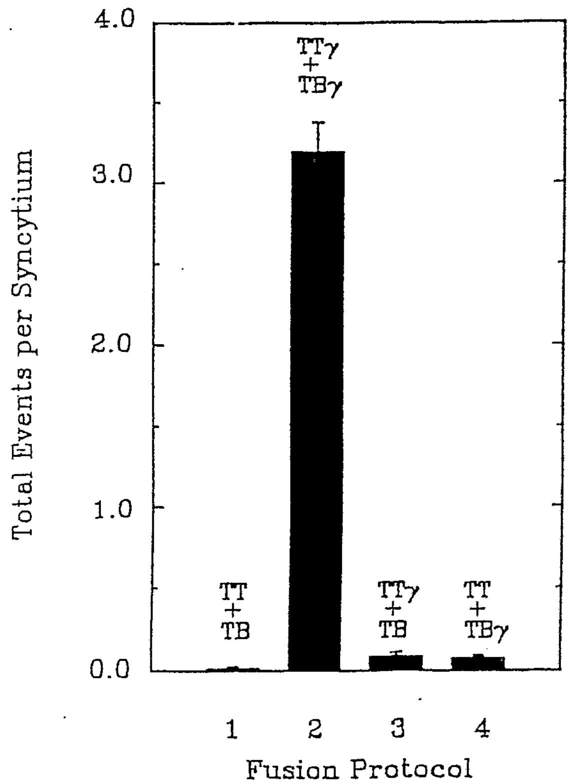

FIG. 3. Total frequency of intergenomic exchange events resulting from the four different fusion protocols described in the legend to Fig. 1. Total events include symmetrical exchanges (reciprocal translocations) as well as asymmetrical exchanges (dicentrics).

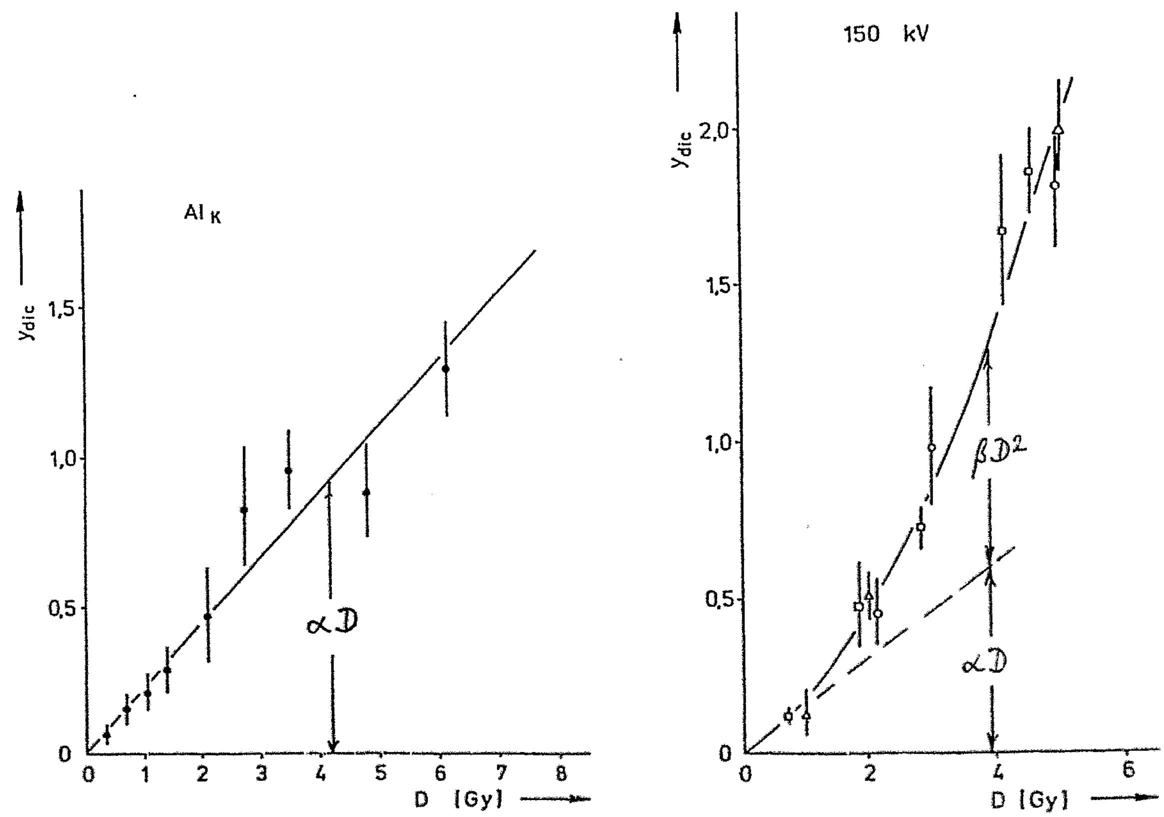

$$Y_{exch} = \beta D^2$$

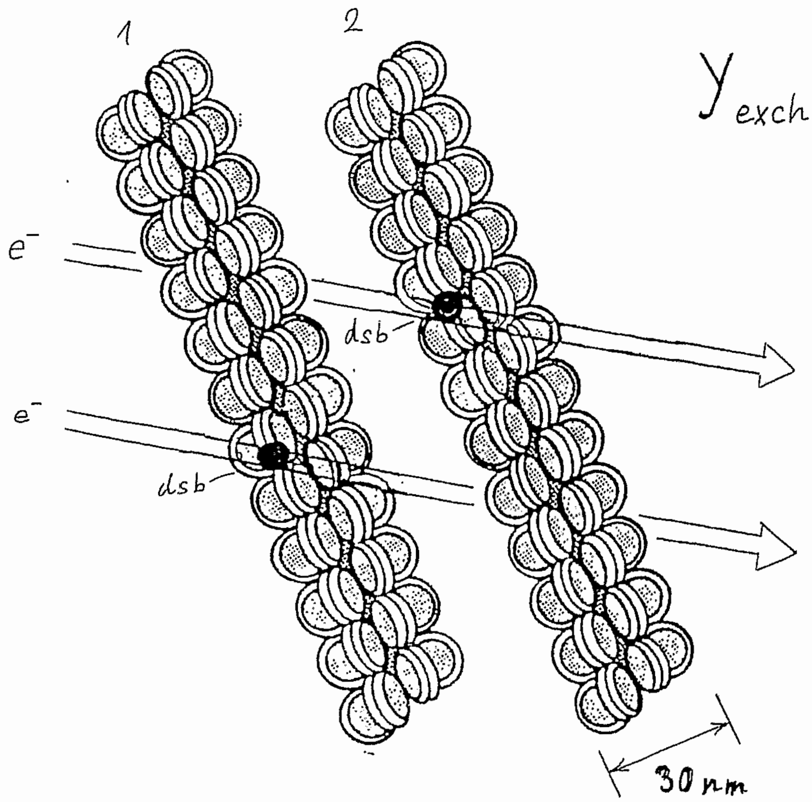

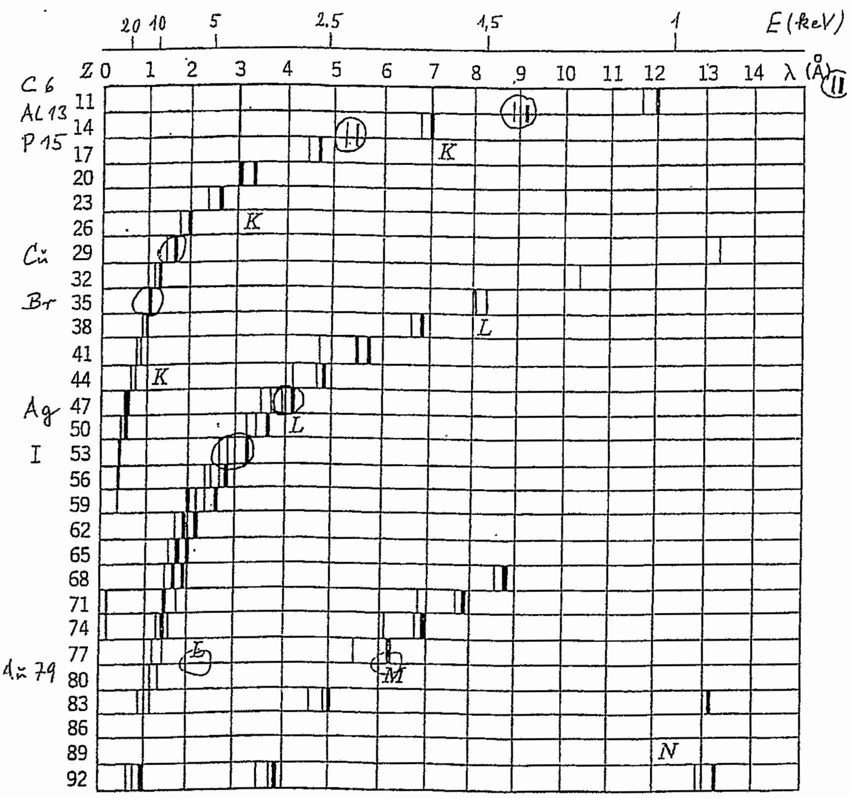

Characteristic K, L ... line spectra of the elements of atomic number Z as a function of wavelength λ.

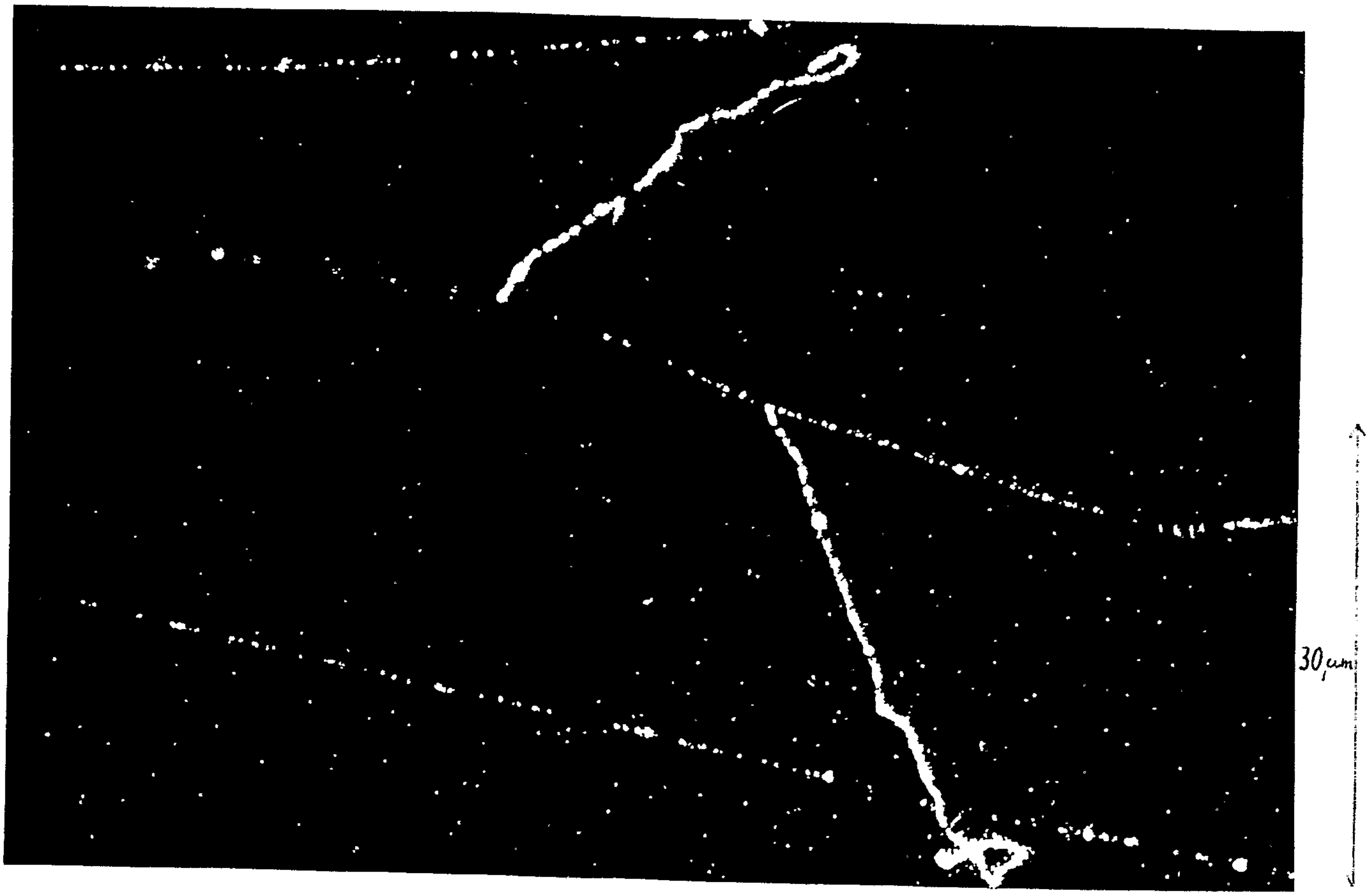

Linear energy transfer $L_\Delta = \left(\frac{dE}{dx}\right)_\Delta$

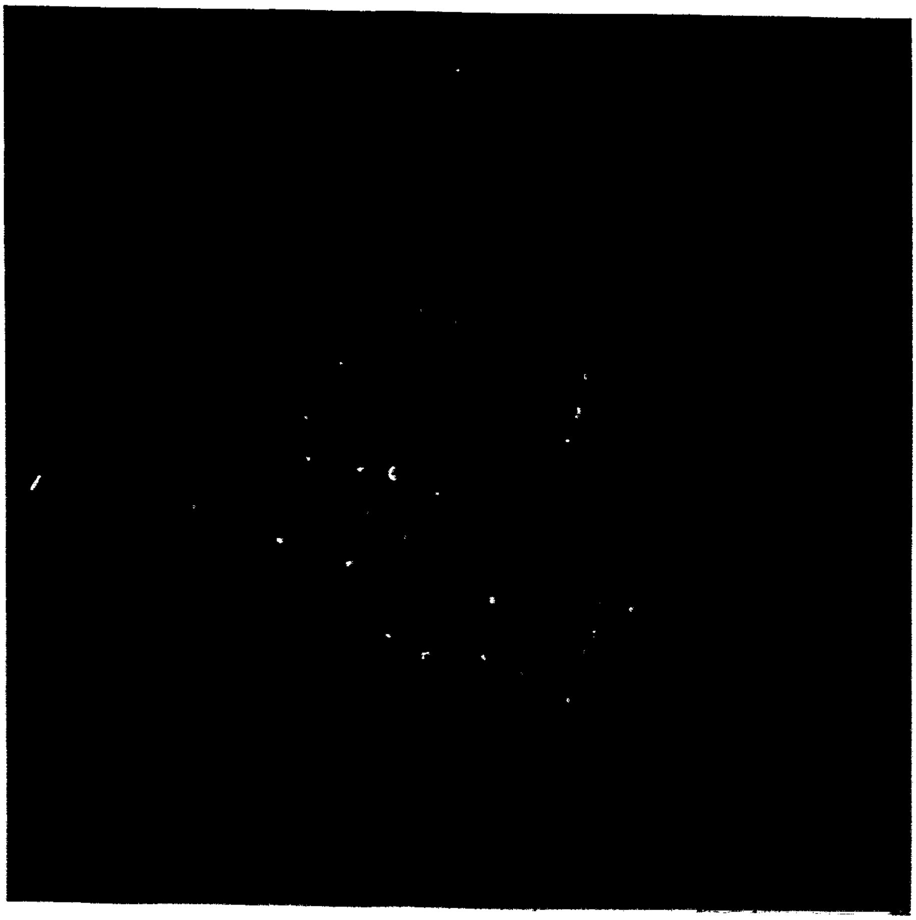

Consistent chromosomal changes in leukemias and lymphomas (examples)

Neoplasm	chromosome aberration
Acute lymphocytic leukemia	t(9;22)(q13;q32) t(4;11)(q21;q23)
Chronic lymphocytic leukemia	t(11;14)(q13;32) Trisomy 12
Chronic myeloid leukemia	t(9;22)(q34;q11)

Cline, M.J.: The molecular basis of leukemia, New Engl. J. Med. **330** (1994)328-336
Luzzatto, L., and Pandolfi, P.P.:Leukemia, a genetic disorder of hemopoetic cells Brit. Med. J. **307** (1993)579-580
Mitelman,F., Heim,S.: Quantitative acute leukemia cytogenetics. Genes, Chromosomes and Cancer **5** (1992)57-66

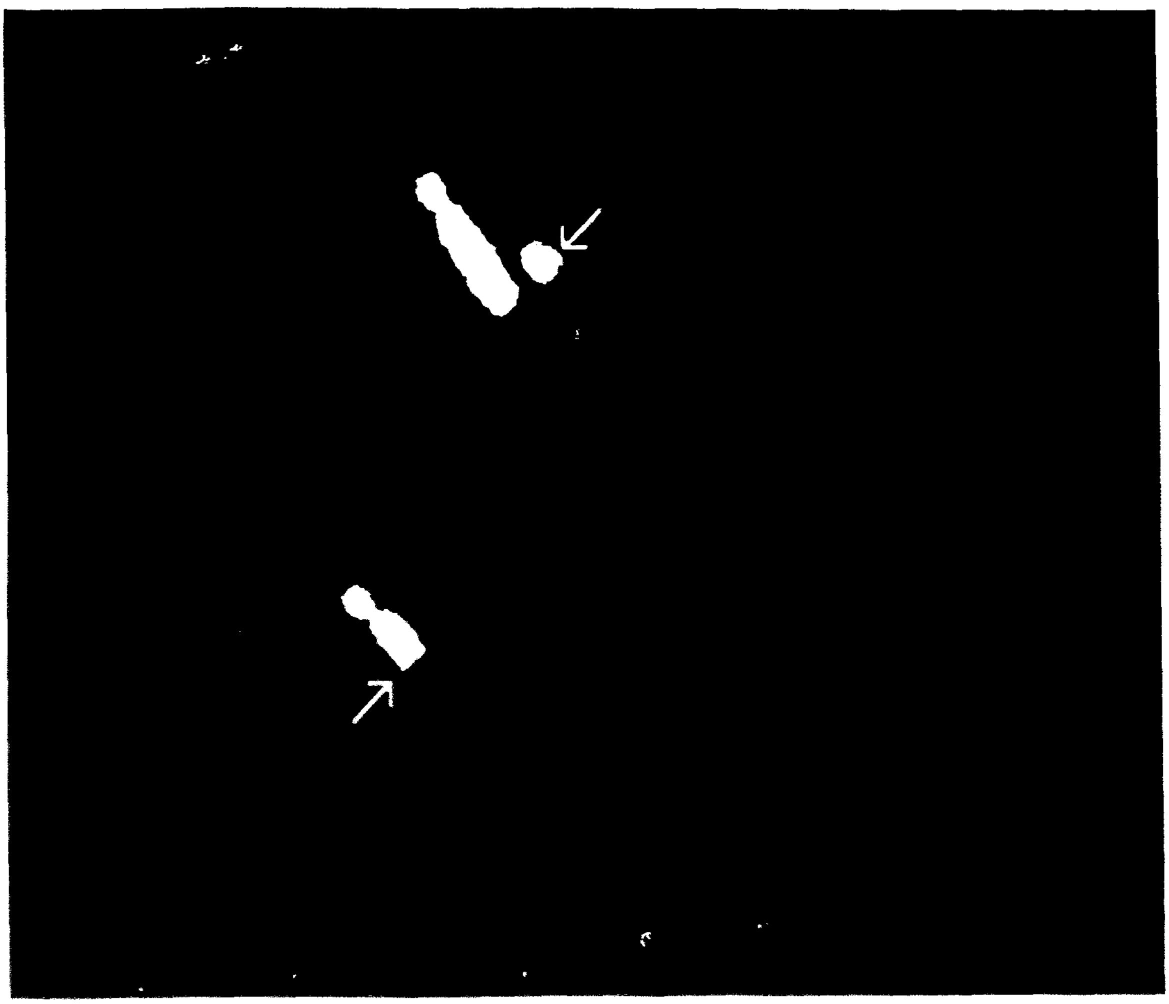

M. Hill:

Radiobiological investigations with monochromatic soft X-rays

Radiobiological investigations with 'monochromatic' soft X-rays

Mark A. Hill

MRC, Radiation & Genome Stability Unit,
Harwell, Oxfordshire, OX11 0RD, U.K.

Overview

- Biological effects of radiation
- Why use ultrasoft X-rays?
- Practicalities of irradiating biological samples
- A few examples of biological experiments
  - Mammalian cell survival
  - Induction and repair of DNA double-strand breaks
  - Chromosome aberrations
  - Plasmid DNA studies - radiation chemistry
- Summary

Biological effects of radiation

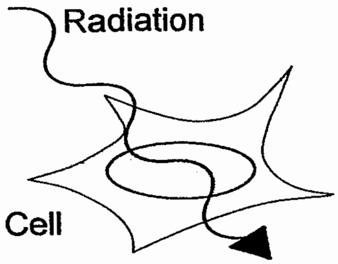

Molecular -	damage to macromolecules such as DNA, RNA, enzymes...
Cellular -	chromosome aberrations apoptosis reproductive cell death gene mutations transformation genomic instability
Organism -	death (high dose) cancer (low dose)
Population -	Genetic modification

Radiation induced DNA strand breaks

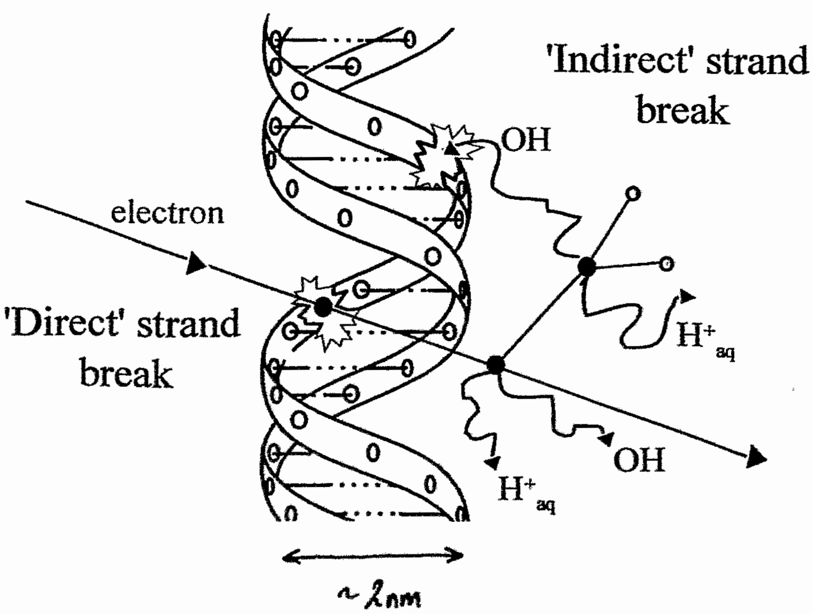

A small clustered damage (simple DSB) resulting from a local cluster of ionisations within a single track

Radical diffusion distances in cells are very small (<4nm)

Damage to DNA

Simple damage

Base damage

Single strand break (SSB)

Double strand breaks (DSB)

Complex damage

Complex SSB

Complex DSB

Very complex DSB

Relevance of ultrasoft X-rays

Why use ultrasoft X-rays?

- Provide a unique tool for investigating energy and spatial requirements of radiation damage
  - produce isolated tracks of electrons
  - small, well defined energies
  - very short tracks - comparable to critical structures of the cell, such as DNA, nucleosomes and chromatin fibre

Energies available at the MRC:

X-ray	energy (keV)	dominant electron energy (keV)		combined csda range (nm)	attenuation length in tissue (μm^{-1})
		photo-	auger-		
C_K	0.28	0.25	-	7	0.56
Cu_L	0.96	0.42	0.52	38	0.47
Al_K	1.49	0.96	0.52	68	0.14
Ti_K	4.55	4.02	0.52	500	0.007

Sample ultrasoft X ray tracks

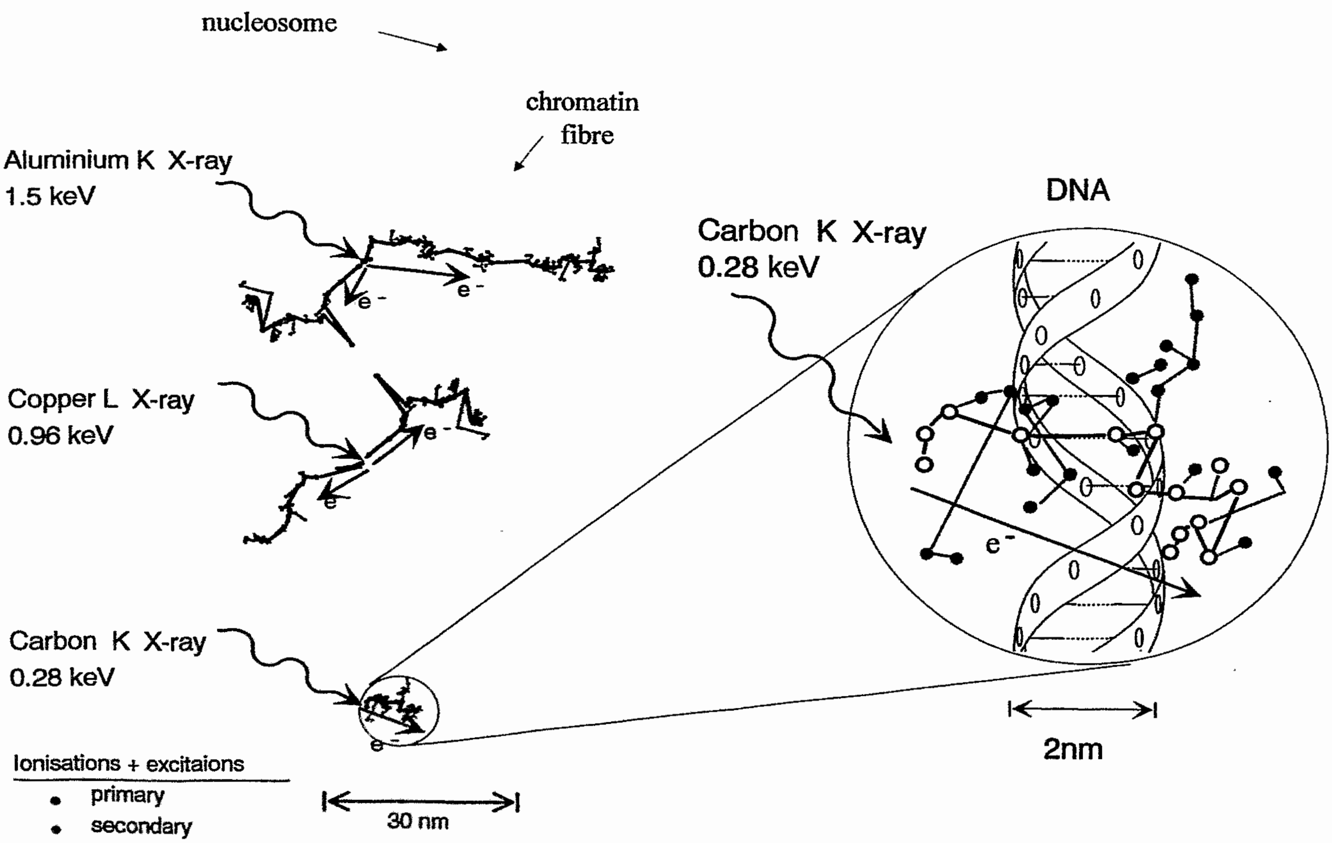

Schematic of radiation tracks in chromatin fibre

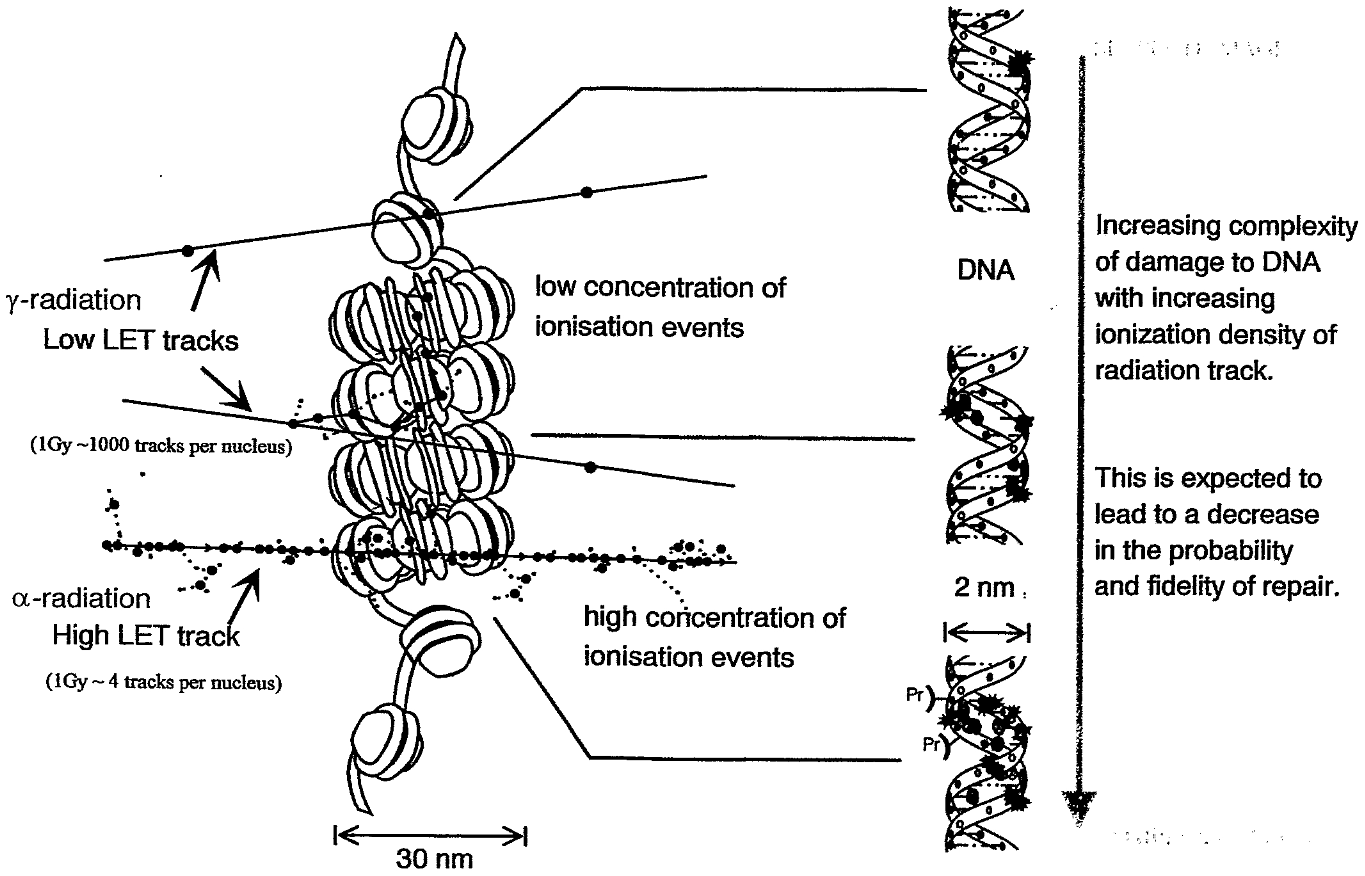

Relevance of ultrasoft X-rays

- These low energy electrons are similar to the numerous secondary electrons produced by most irradiations

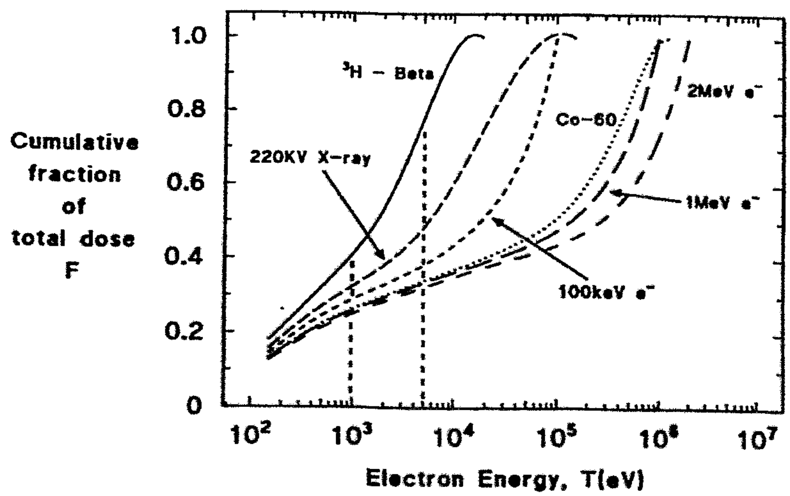

(~30% of absorbed dose produced by low energy electrons 0.1-5keV for ^{60}Co γ-rays)

Nikjoo and Goodhead (1991) *Phys. Med. Biol.*, 36, 229

Irradiation of biological samples with ultrasoft X-rays

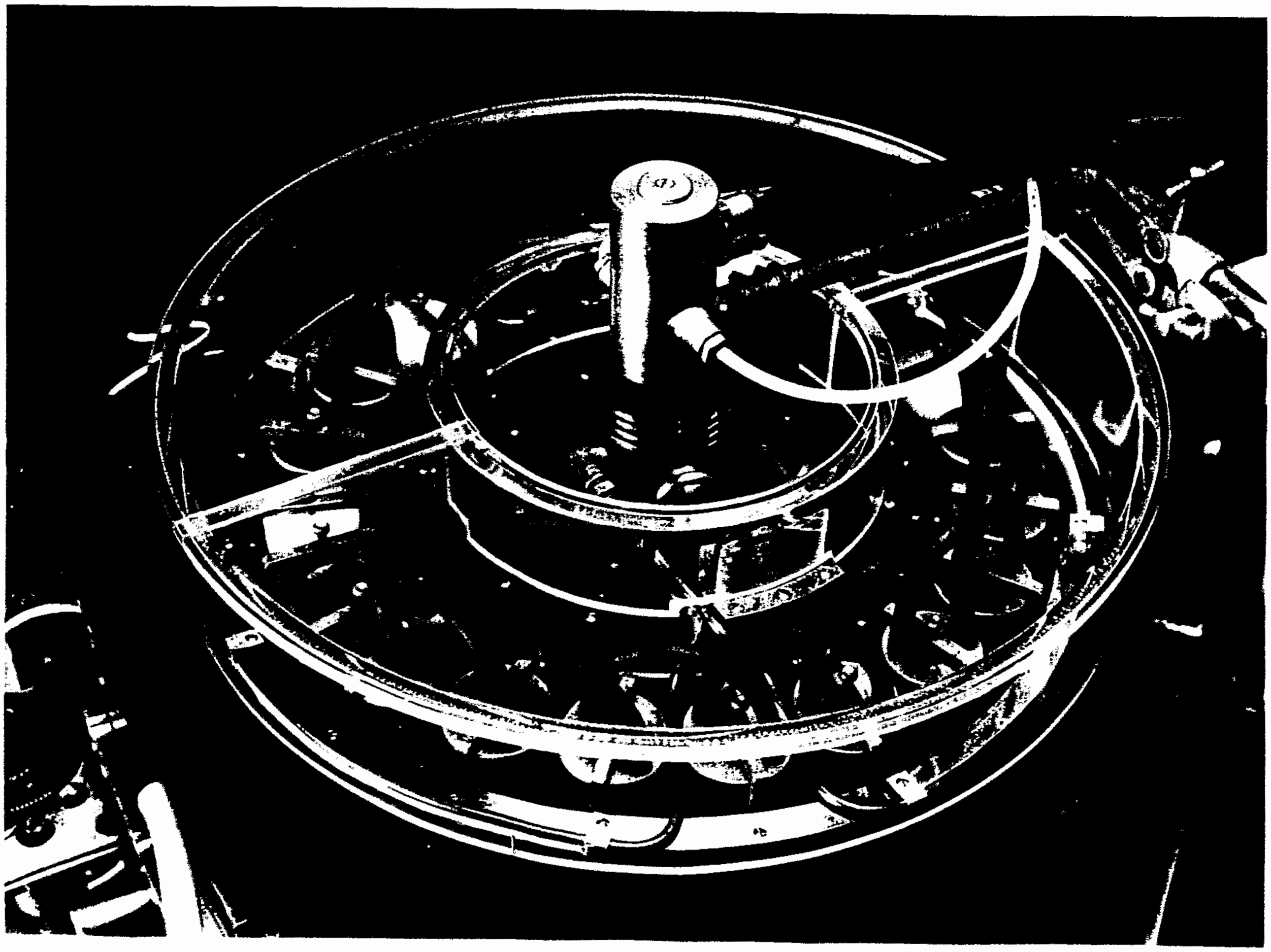

MRC ultrasoft irradiation rig

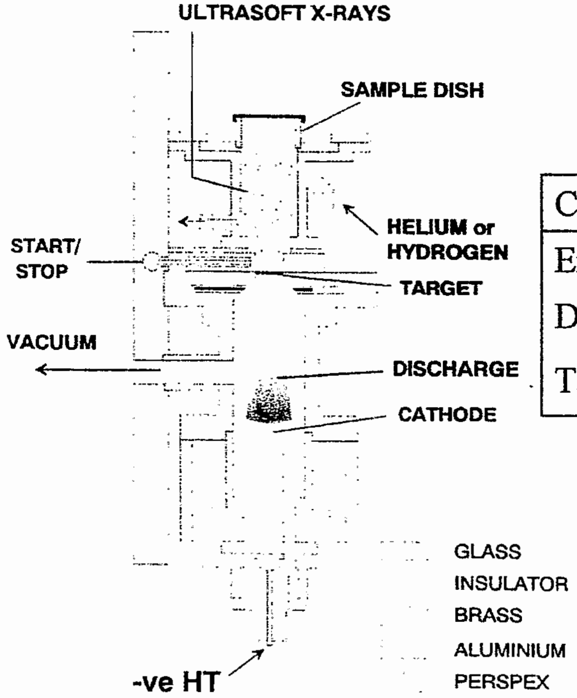

Characteristic X-ray	C_K	Cu_L	Al_K	Ti_K
Energy (keV)	0.28	0.96	1.49	4.55
Dose rate (Gy/min)	2	1	50	5
Target lifetime	50min	12 hr	years	5 hrs

(Brem < 1%)

MRC Low Dose Rate Irradiation Rig

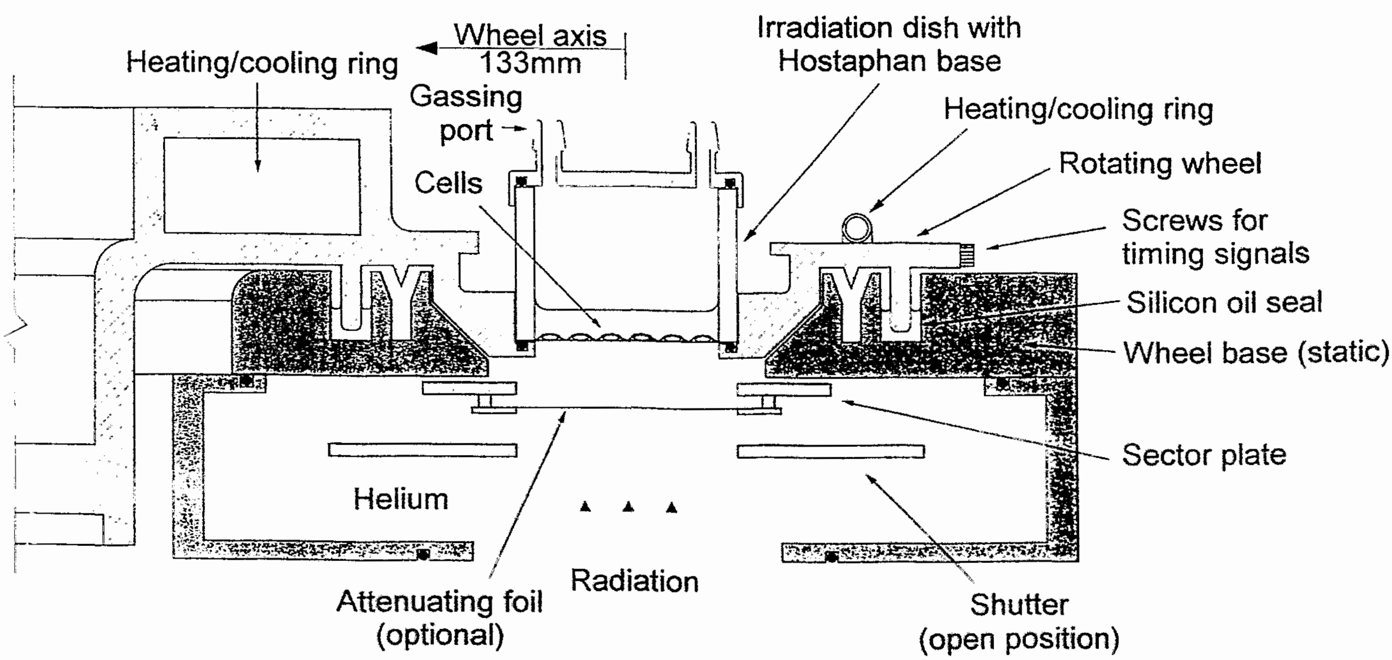

Biological sample irradiation

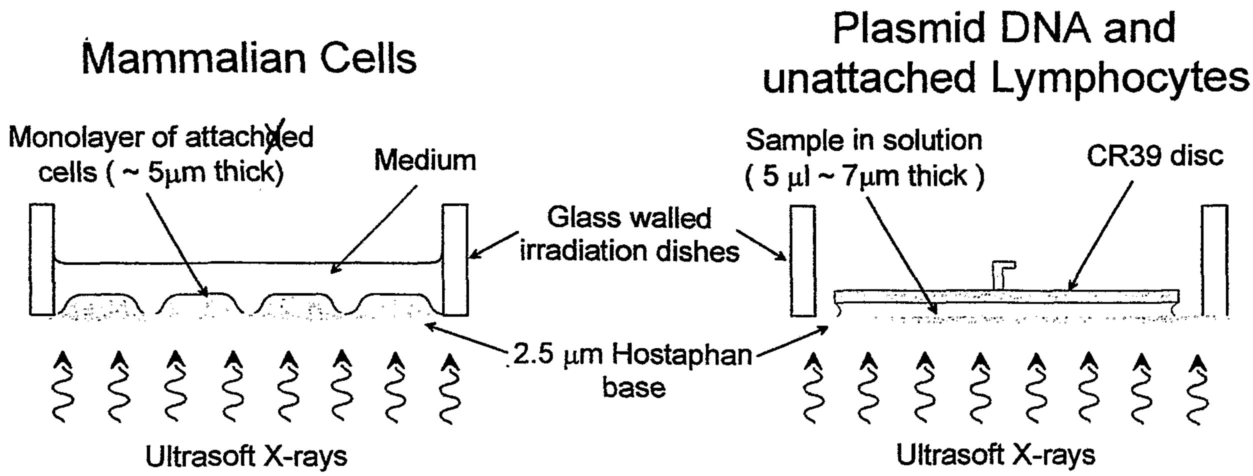

X-ray attenuation and Cell Morphology

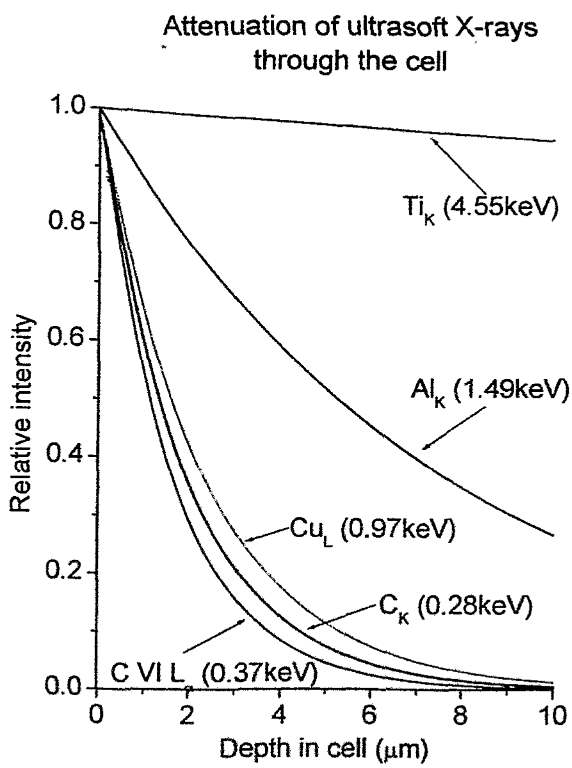

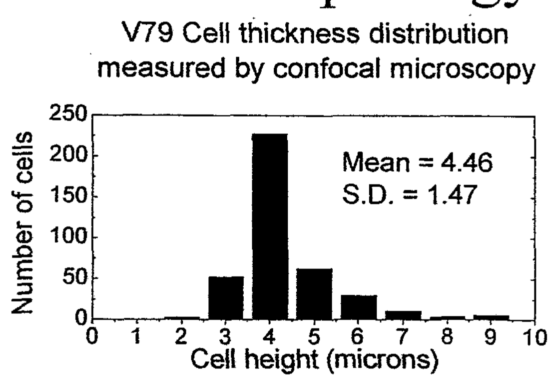

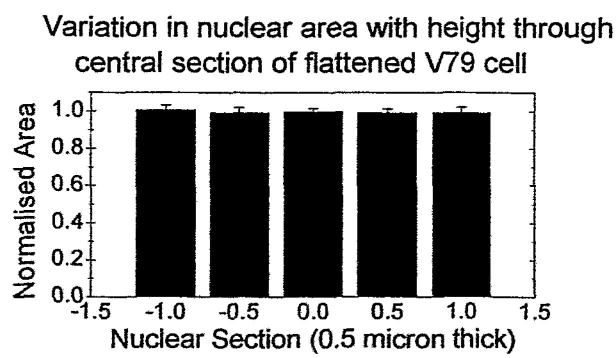

Hill *et al.* (1998) *Phys. Med. Biol.*, **43**, 351.

Importance of cell morphology

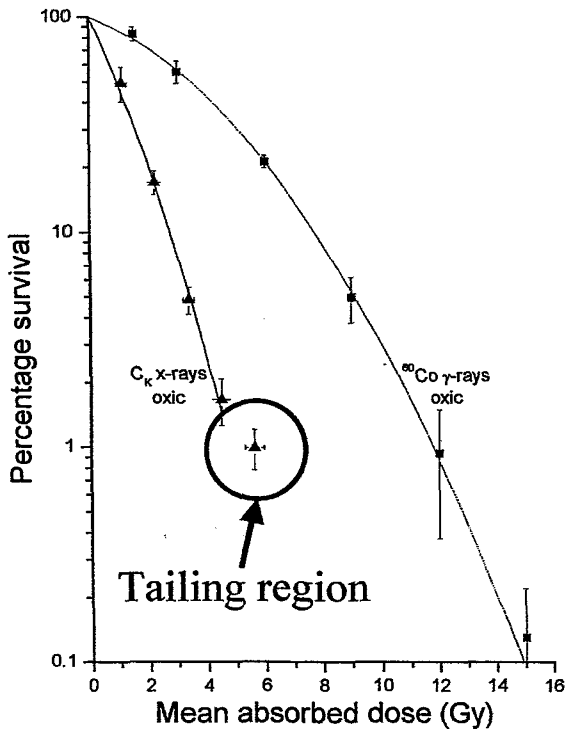

Tailing is a well know phenomenon for low-penetration radiations

Tight control of the cell growth conditions is essential to minimise the effect of the tail.

Specifically,optimising growth ~~conditions~~ conditions to reproducibly obtain:

• a good cell monolayer

• well attached and well flattened cells

Examples of radiobiological experiments

Biological effectiveness of ultrasoft X-rays

Induction of DSB (V79 cells)

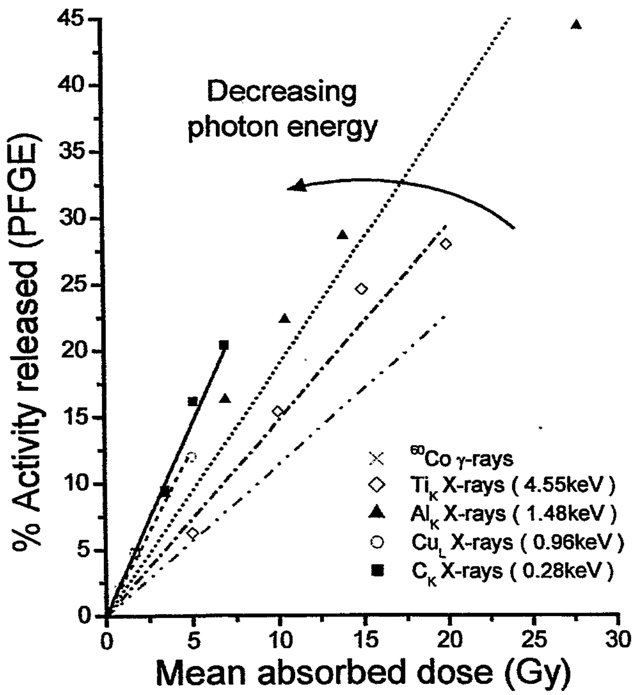

Inactivation of V79 cells

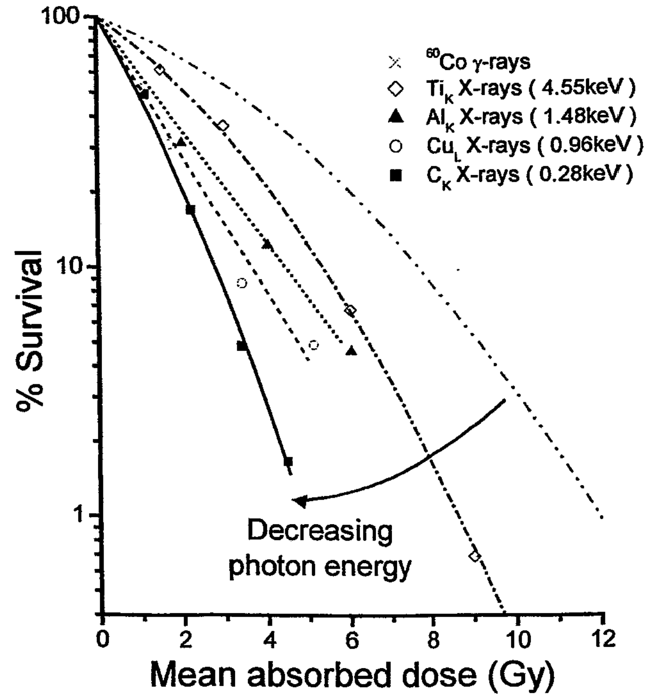

DeLara, Hill, O'Neill

Repair of DNA DSB by the cell

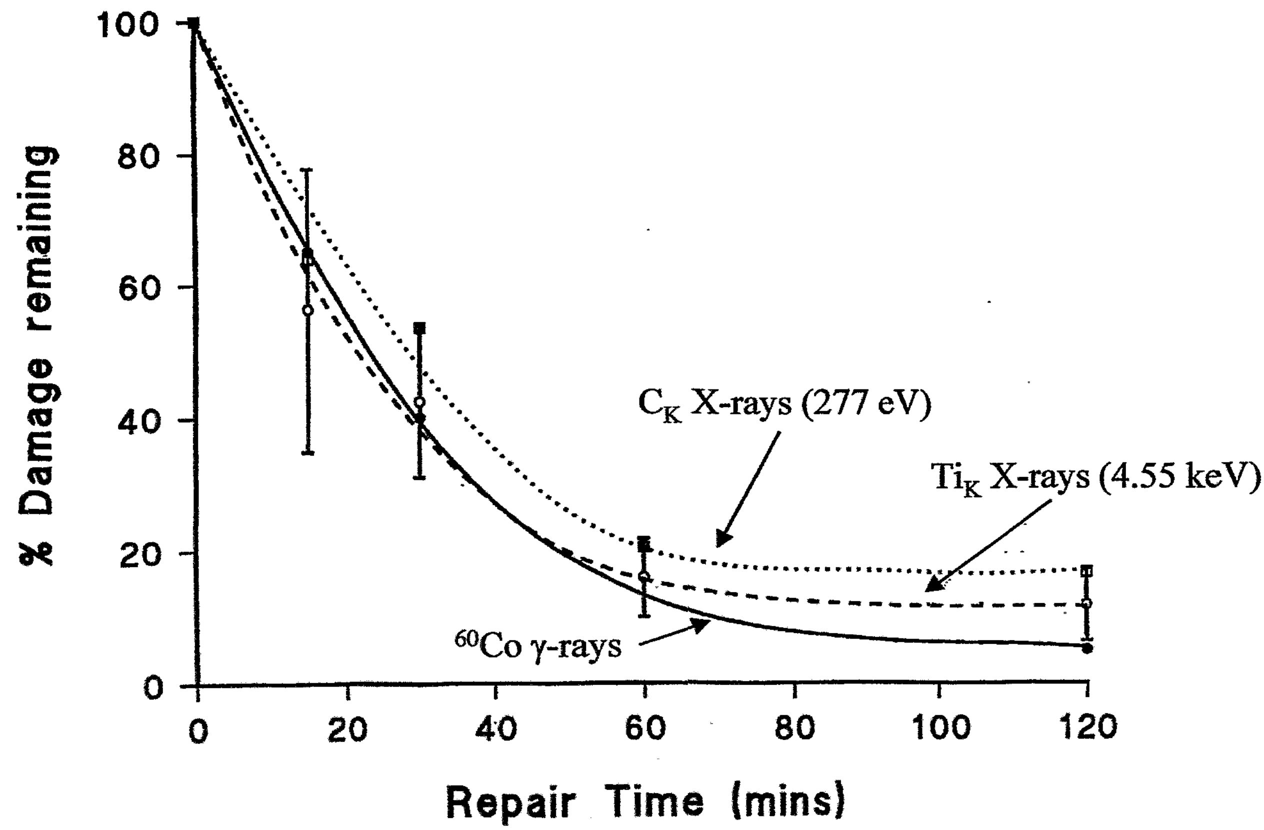

What is the critical feature of γ-rays leading to biologically significant DNA damage?

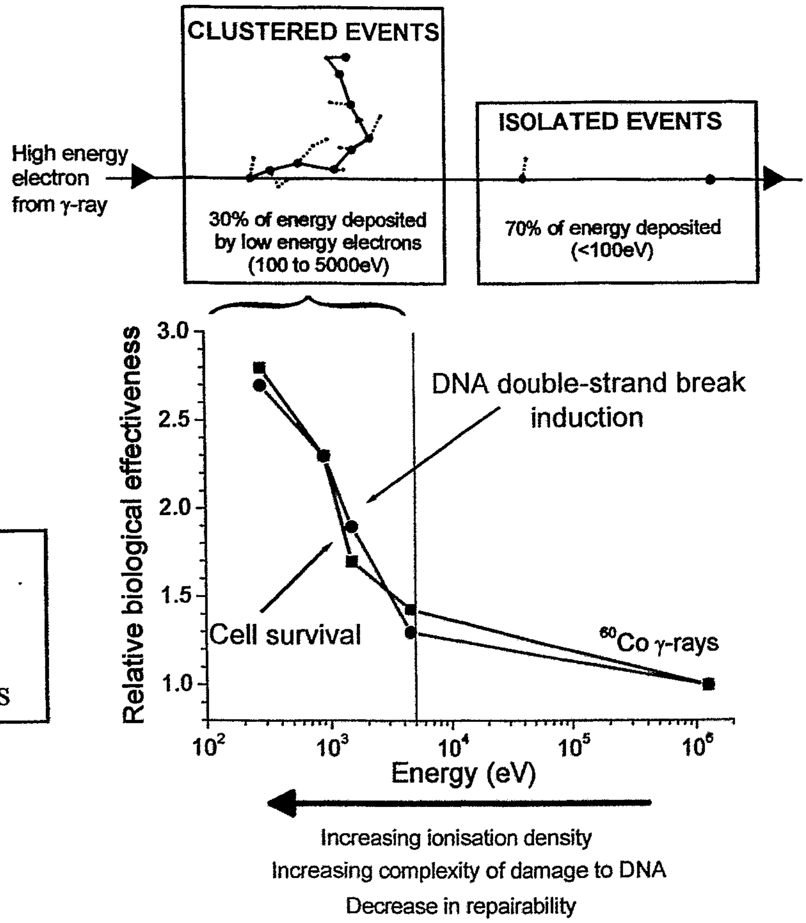

Low energy, secondary electrons are the critical component of low LET radiations tracks rather than the more numerous isolated events

Chromosome aberrations viewed using FISH

Simple exchanges

- With apparently 2 breaks in 2 chromosomes

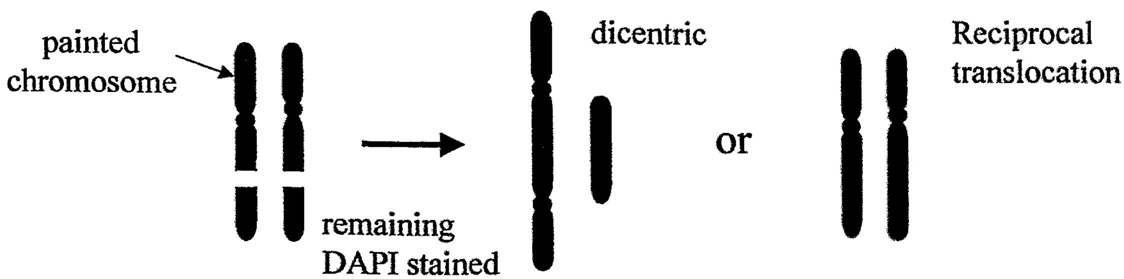

Visible complex exchanges

- Involving 3 or more breaks in 2 or more chromosomes

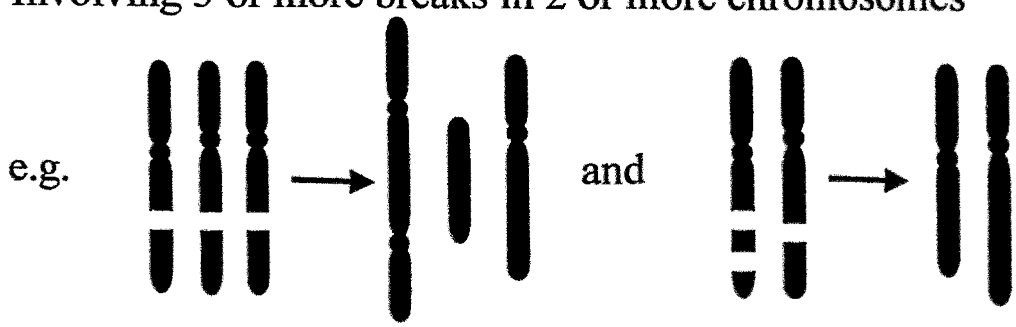

Aberrations induced in chromosome 1

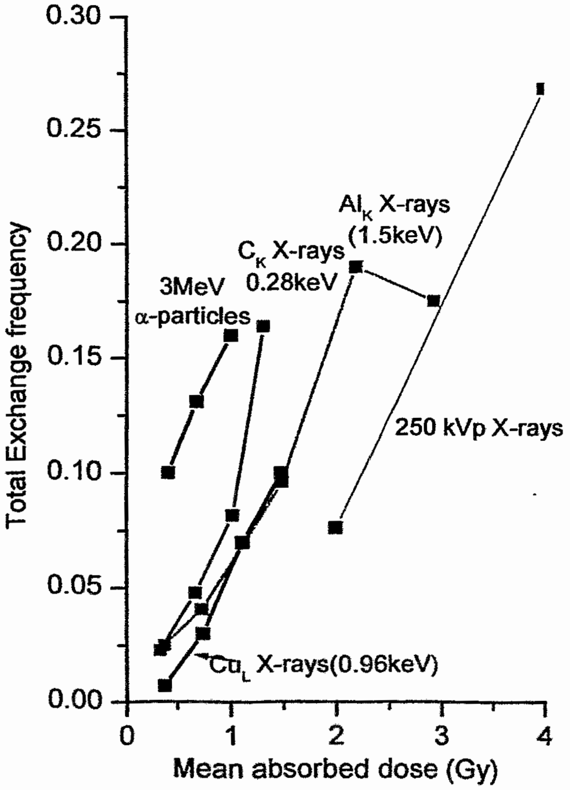

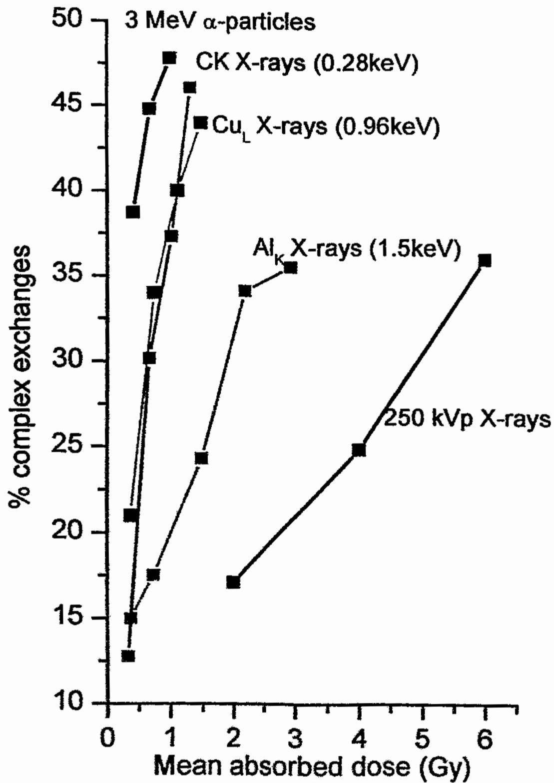

Griffin, Hill, Simpson, Savage

Can single electrons produce biologically relevant damage ?

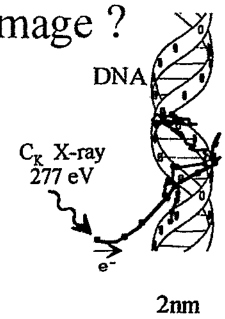

- Carbon K ultrasoft X-rays produce a single electron with a range <7nm
- Probability of producing 2 double-strand breaks in 2 seperate chromosome is practically zero

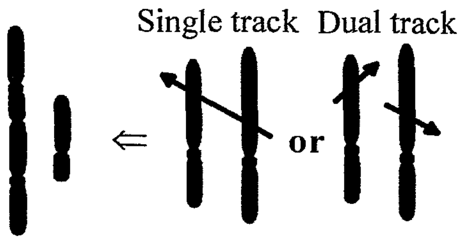

For short electron tracks expect:

Yield $= \cancel{\alpha D}^{0} + \beta D^2$

however, experimental results show:

Yield $\sim \alpha D$

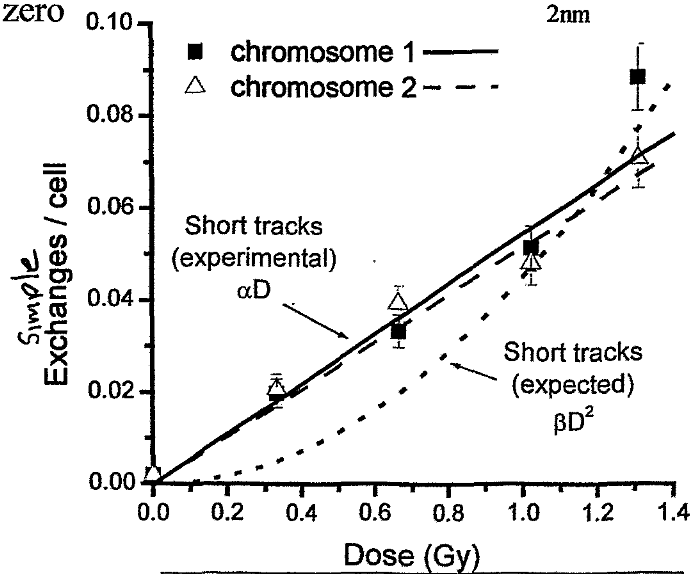

Griffin *et al.* (1998), *Int. J. Radiat. Biol.*, **73**, 591

Carbon K aberration data

- Provides further support for the hypothesis that damaged DNA may be able to interact with undamaged DNA
- Data suggest that a simple chromosome exchange can be induced by the passage of a single electron track.
- Suggests that even for the lowest dose of low-LET radiation there is a finite probability of producing DNA rearrangement.

Radiation induced DNA strand breaks

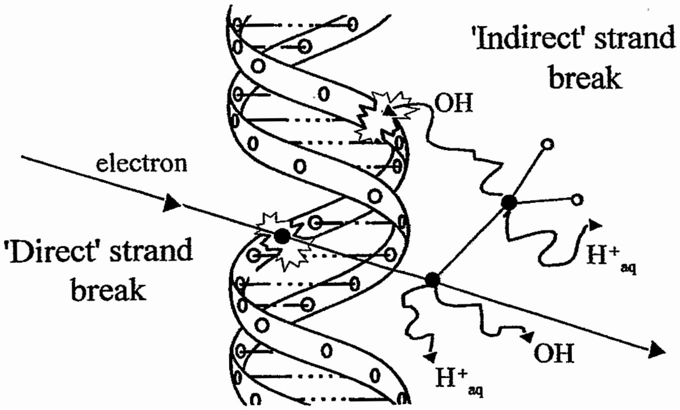

Low scavenging capacities

DNA strand breakage dominated by reaction with the numerous OH radicals produced in the surrounding water and able to diffuse to the DNA.

High scavenging capacities

Diffusion distance of OH radicals very small (<4nm in cells) significantly reducing OH induced strand breaks to a level similar to that produced directly by radiation in DNA.

Plasmid DNA studies

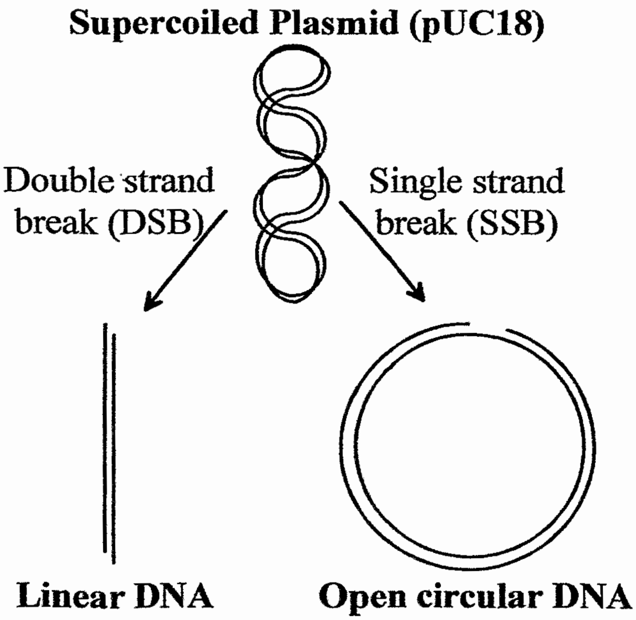

• Relative proportions can be determined by gel electrophoresis

• Scavenging capacity determined by concentration of Tris.

Low scavenging capacity

- Probe of yield of OH radicals escaping radiation track.

High scavenging capacity

- Model system for DNA damage in cell

A typical 1 keV electron track

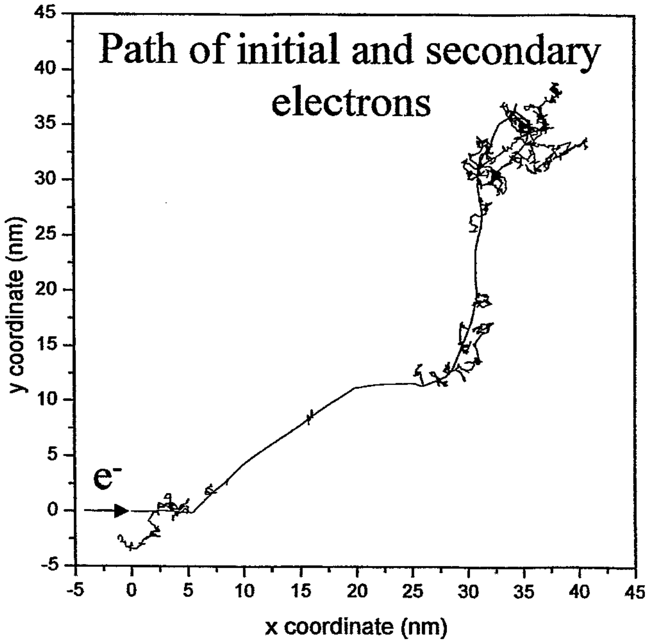

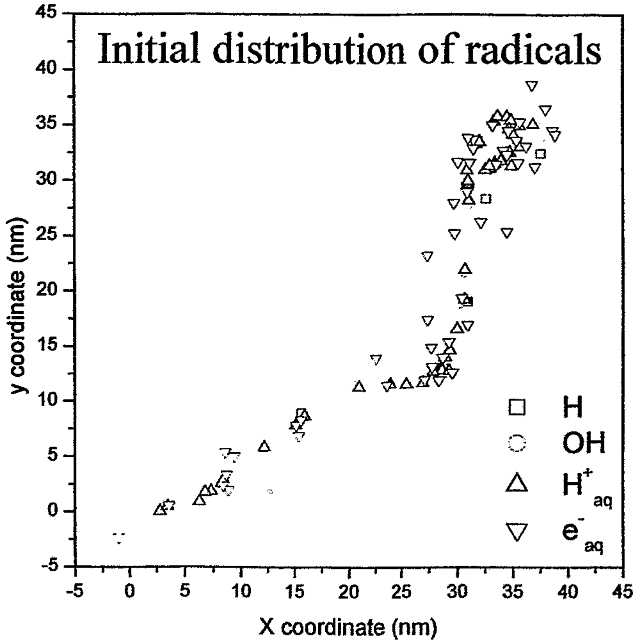

Hill and Smith (1994) *Radiat. Phys. Chem.*, **43**, 265.

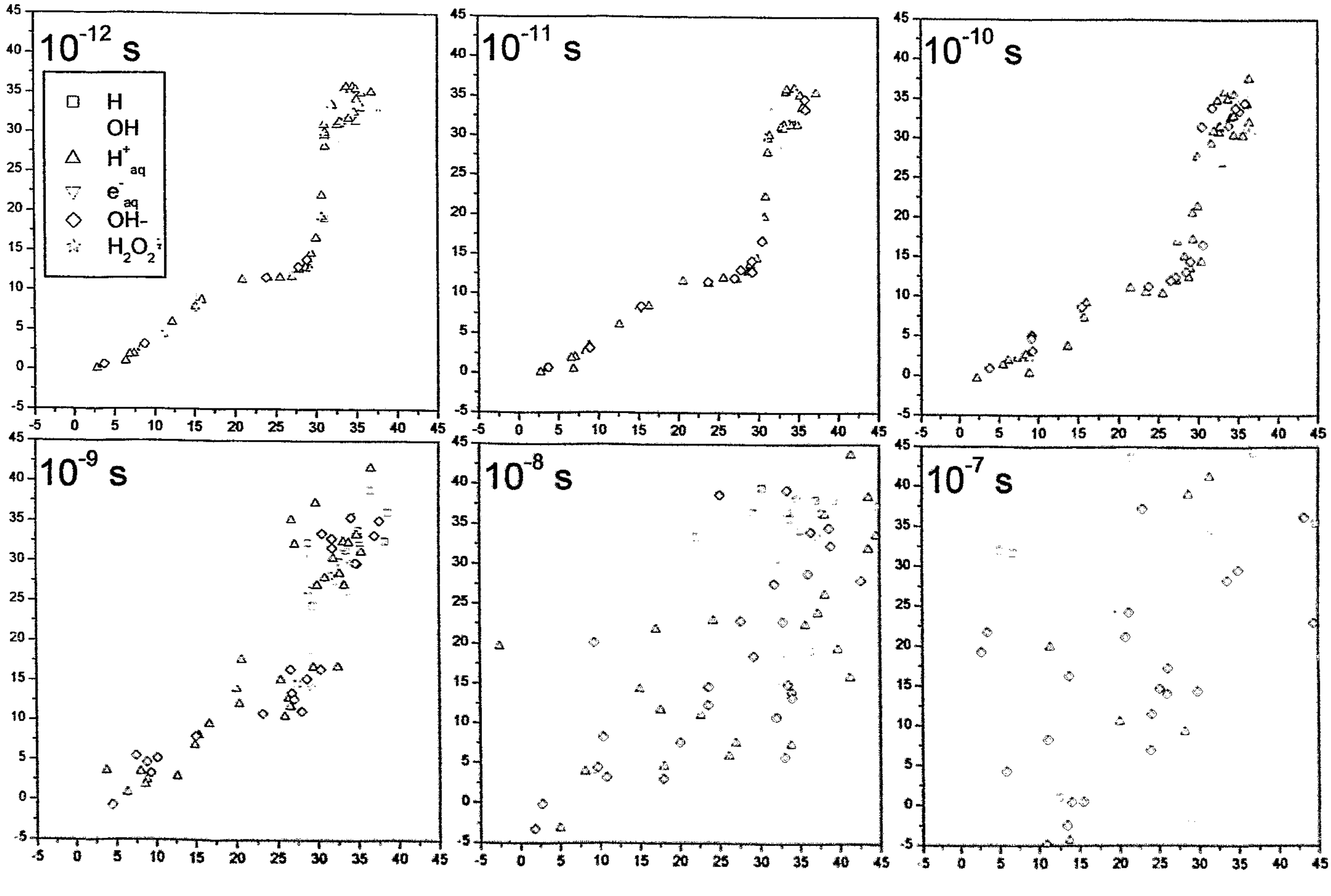

Dose dependence for loss of supercoiled plasmid DNA (pUC18)

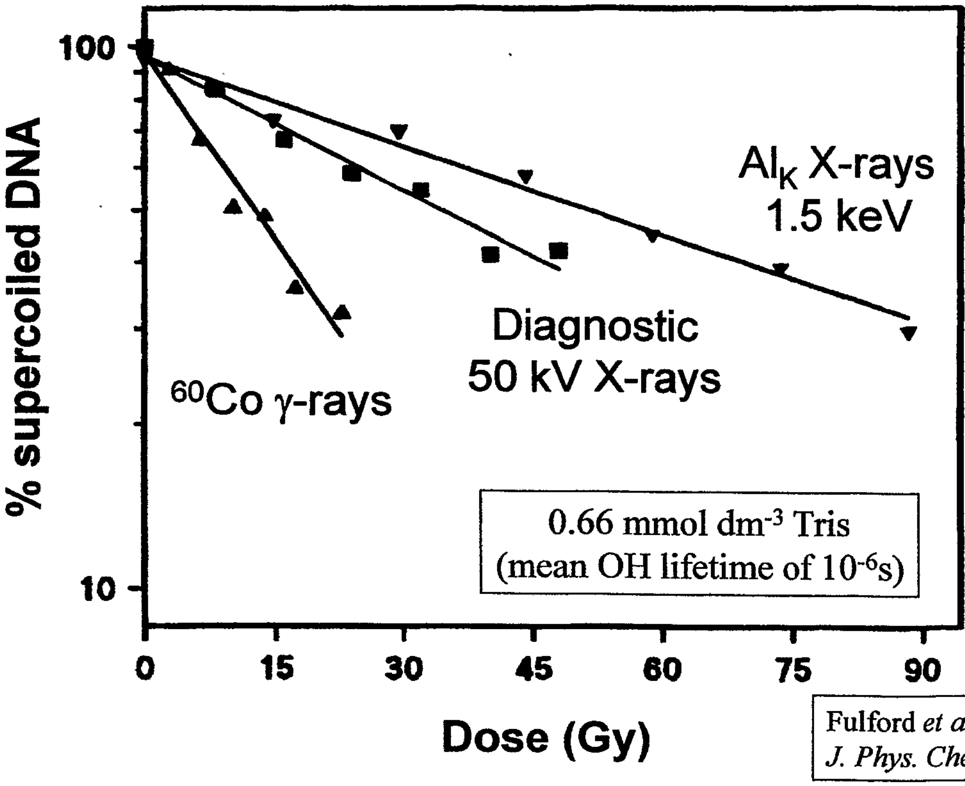

Fulford *et al.* (1999)
J. Phys. Chem. A **103,** 11345

Yield of OH radicals escaping radiation tracks vs photon energy

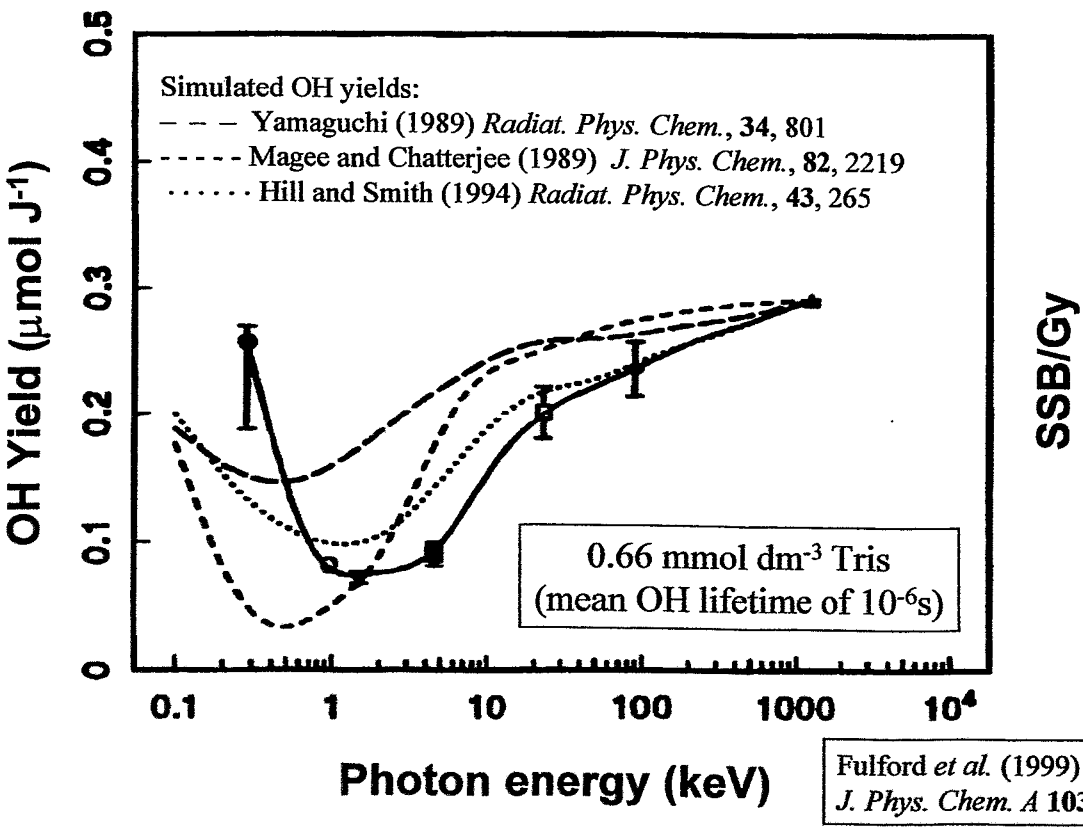

Fulford *et al.* (1999)
J. Phys. Chem. A **103,** 11345

Ultrasoft X-ray Summary

- Ultrasoft X-rays can be used to investigate the energy and spatial requirements of radiation damage.

- Low energy electrons are similar to the numerous secondary electrons produced by most radiation.

- Due to the significant attenuation through the cell: It is essential to have a tight control on the growth conditions to reproducibly obtain:
  - a good cell monolayer.
  - well attached and well flattened cells.

Experimental Summary

- Ultrasoft X-rays are generally more effective at producing biological damage than γ-rays for a given dose, due to the increasing clustering of ionisations on the nanometer scale.

- Low energy, secondary electrons (100eV - 5000eV) are believed to be the critical component of low LET radiation tracks rather than the more numerous isolated events.

- C_K X-ray aberration data provides further support for the hypothesis that damaged DNA may be able to interact with undamaged DNA.

- Ultrasoft X-ray experiments can provide invaluable bench mark data for theoretical simulations. For example:
  - DSB yield with photon energy
  - OH yield with photon energy

Acknowledgements

MRC Radiation and Genome Stability Unit

Biophsics group
Dudley Goodhead
David Stevens
Hooshang Nikjoo

DNA damage group
Peter O'Neill
Cathy deLara
Stan Botchway

Cytogenetics
Carol Griffin
Paul Simpson
John Savage

Microscopy
Stuart Townsend

B. D. Michael:

A focused soft X-ray microbeam for investigating the radiation responses of individual cells

A FOCUSED SOFT X-RAY MICROBEAM FOR INVESTIGATING THE RADIATION RESPONSES OF INDIVIDUAL CELLS

G Schettino[1], M Folkard[1], AG Michette[2], KM Prise[1], B Vojnovic[1] and BD Michael[1]

[1]Gray Laboratory Cancer Research Trust,
Mount Vernon Hospital, Northwood, Middlesex, U.K.

[2]Department of Physics, King's College London, U.K.

Work supported by:

- Cancer Research Campaign, U.K.
- Biotechnology and Biological Sciences Research Council, U.K.
- European Union
- U.S. Department of Energy

Two main experimental approaches to radiation biology of cells

Conventional or "broad-field"

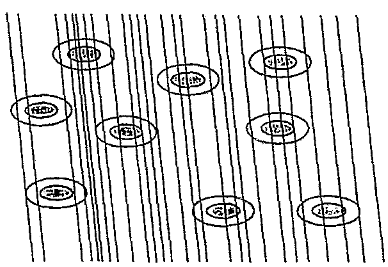

- In general, cells are randomly traversed by radiation tracks
- Results are generally scored as an average throughout the exposed population

Microbeam

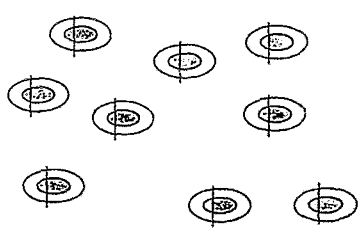

- Cells are targeted individually with counted tracks under automated control
- Results are generally scored in individual cells, or their progeny

Early work on ionising radiation microbeams with cells

Zirkle and co-workers in the 1950's

New generation of radiobiology microbeams developed since ~1990

a) **Charged-particle microbeams**

- Texas A&M University (formerly at Battelle Pacific Northwest Labs.)
- Columbia University, New York
- Gray Laboratory, U.K.
- Others under development in Japan, U.S.A. and Europe

JAERI, Takasaki, Japan

b) **X-ray/electron microbeams**

- Gray Laboratory, U.K.
- Others under development in Japan and U.S.A.

Uncertainties in extrapolation of radiation risk

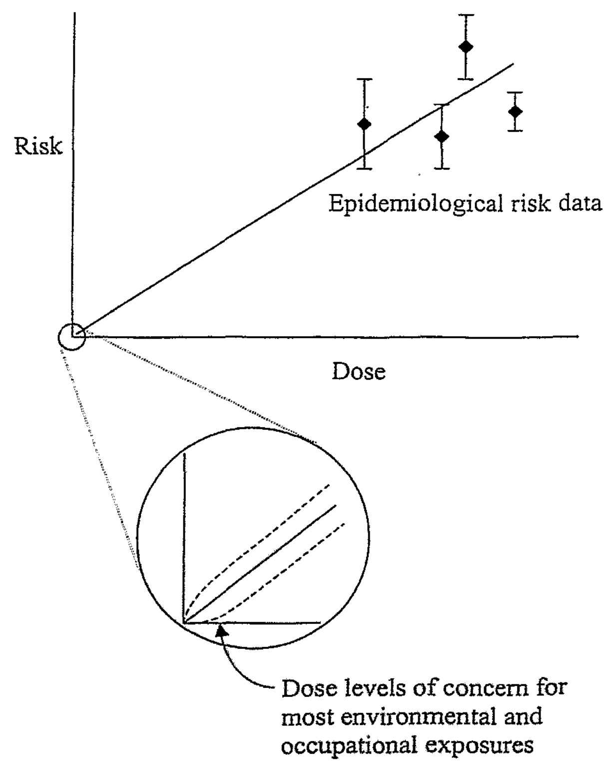

Applications of microbeams in radiation biology

Spatial resolution

- To resolve the targets and pathways involved in cellular effects of radiation

Dose resolution

- To determine cellular radiation effects down to the ultimate low-dose limit - traversal by a single track

Overall objective

Information to develop improved models of radiation effects

- for radiotherapy
- for estimation of radiation risks

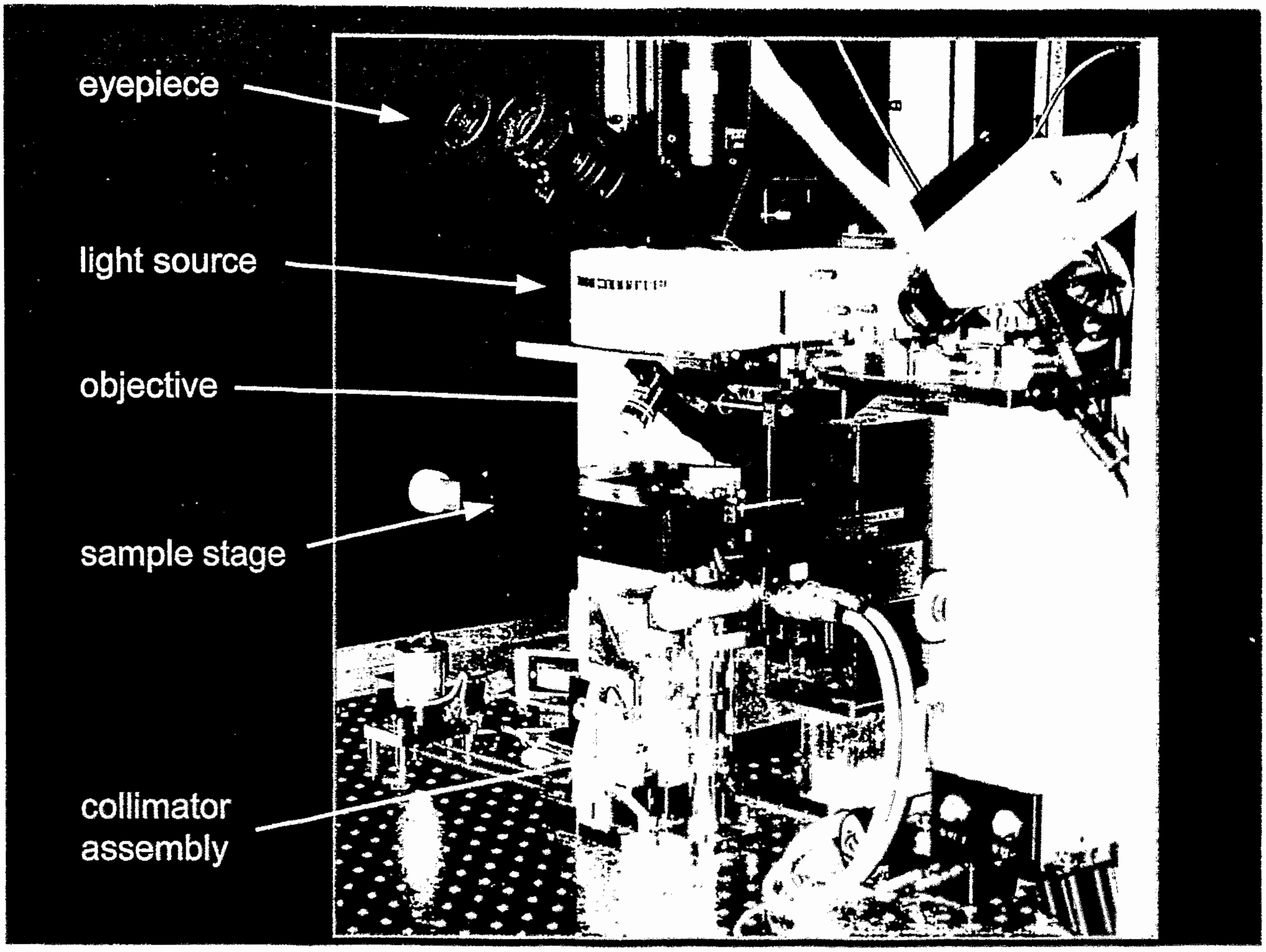

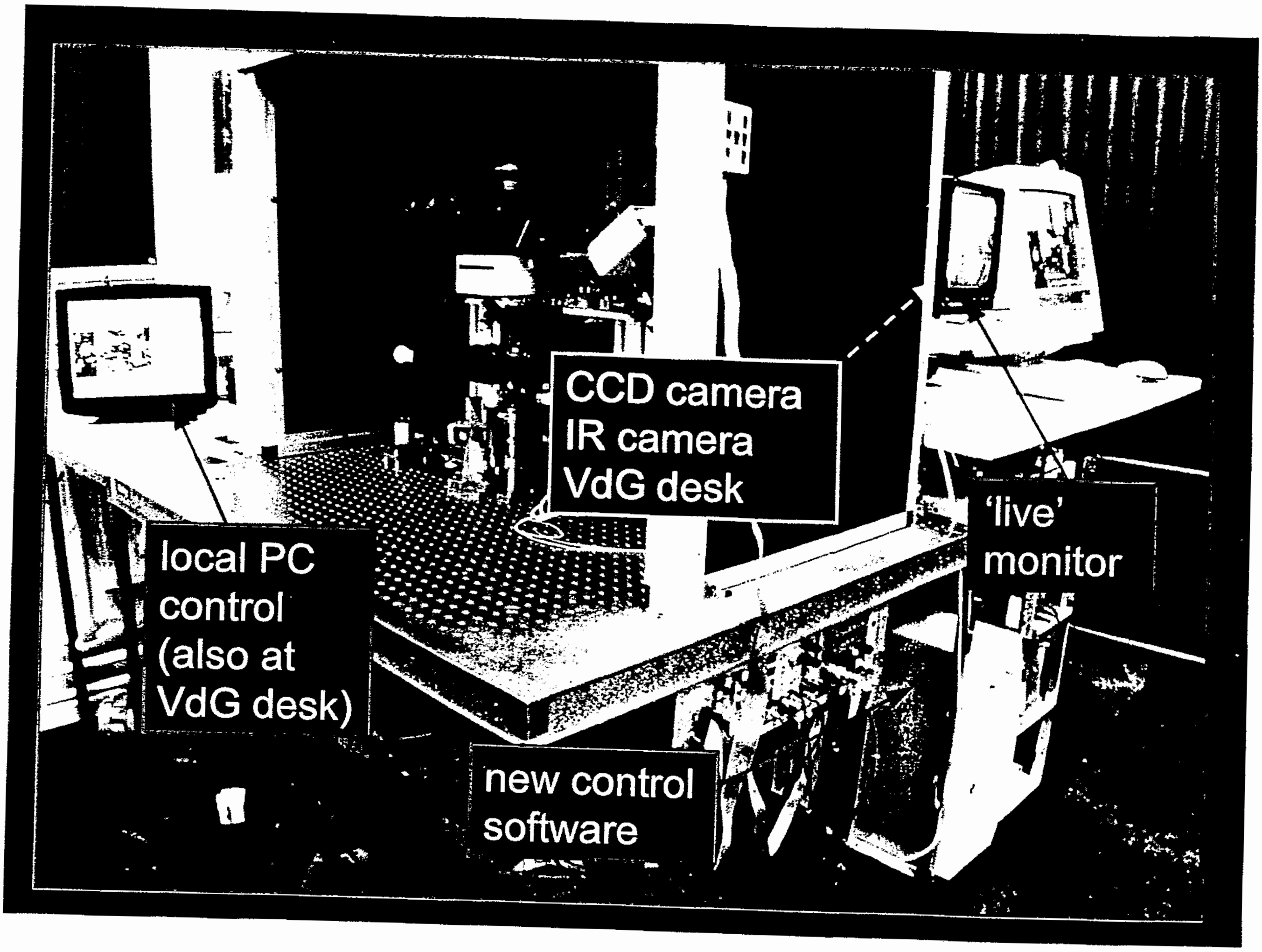
CCD camera
IR camera
VdG desk
'live'
monitor
local PC
control
(also at
VdG desk)
new control
software

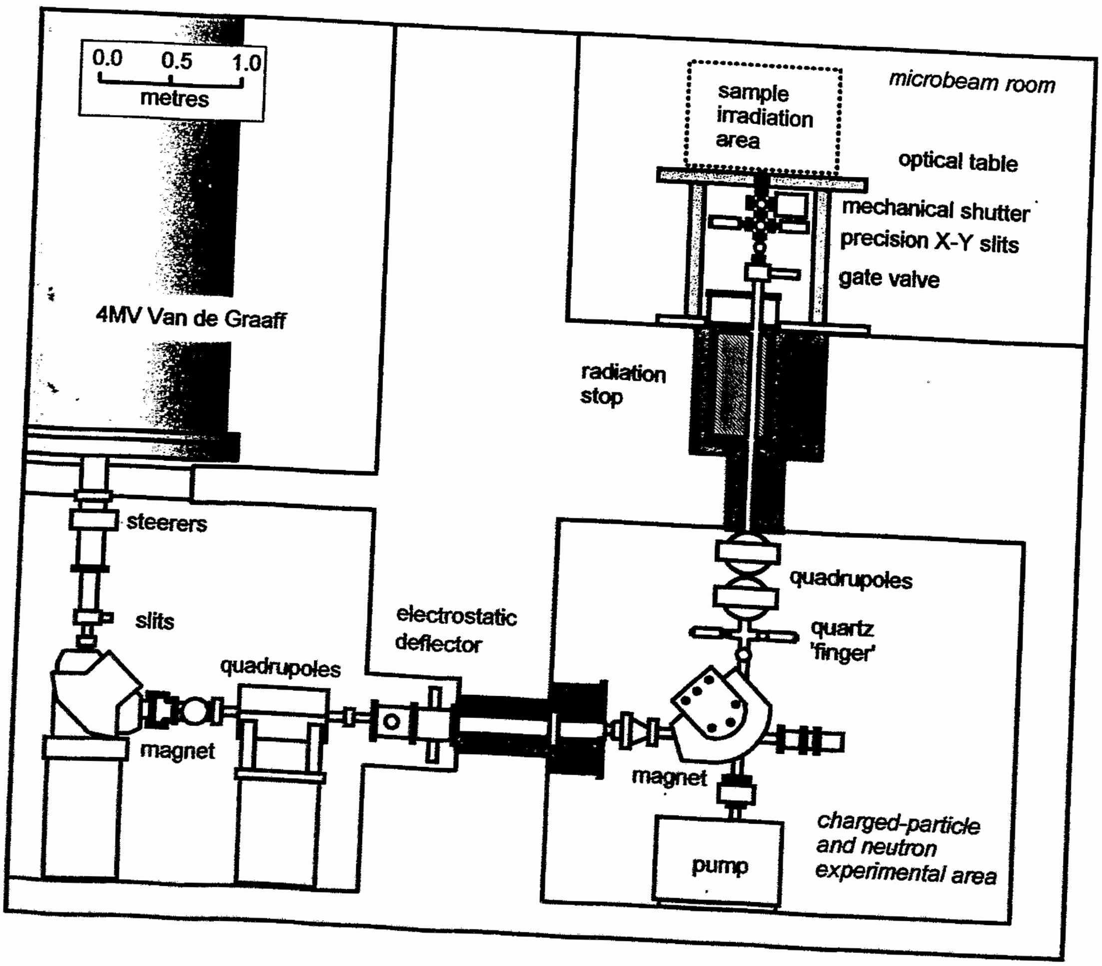
0.0
0.5
1.0
metres
4MV Van de Graaff
microbeam room
sample
irradiation
area
optical table
mechanical shutter
precision X-Y slits
gate valve
radiation
stop
steerers
slits
quadrupoles
magnet
electrostatic
deflector
quadrupoles
quartz
'finger'
magnet
pump
charged-particle
and neutron
experimental area

Particles Available

Particle	Energy at cell surface (MeV)	LET at cell surface (keV/µm)
Protons	< 4.0	> 10
Helium-3	< 5.6	> 65
Helium-4	< 4.0	> 100

Microbeam irradiation

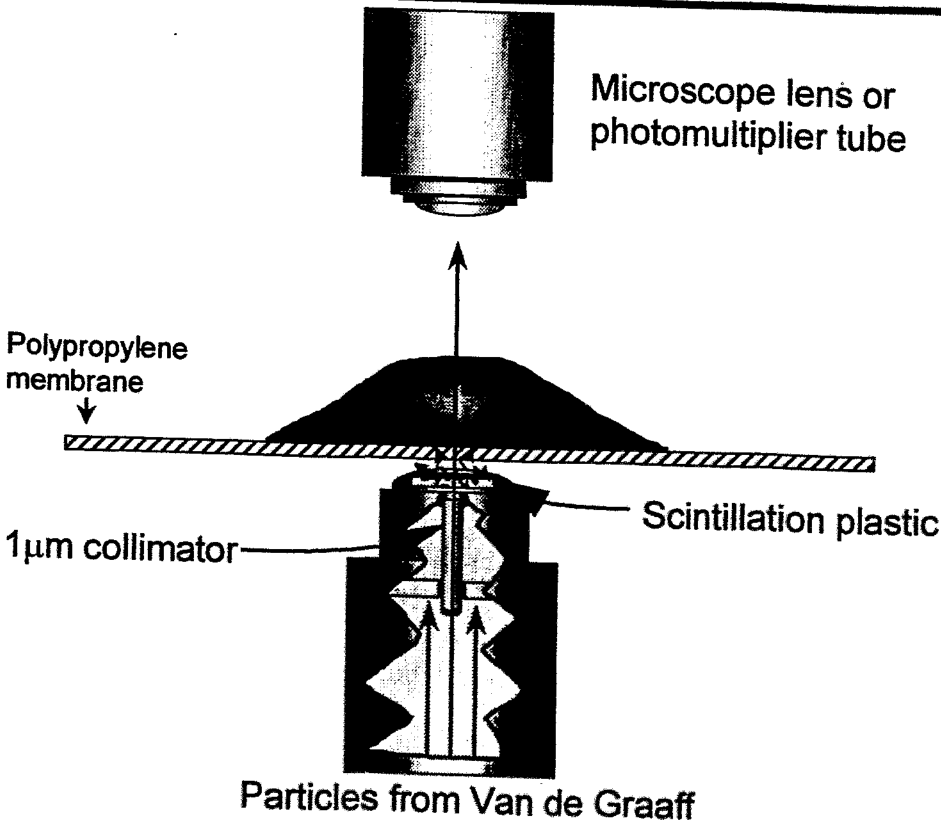

$^{3}He^{++}$ ions

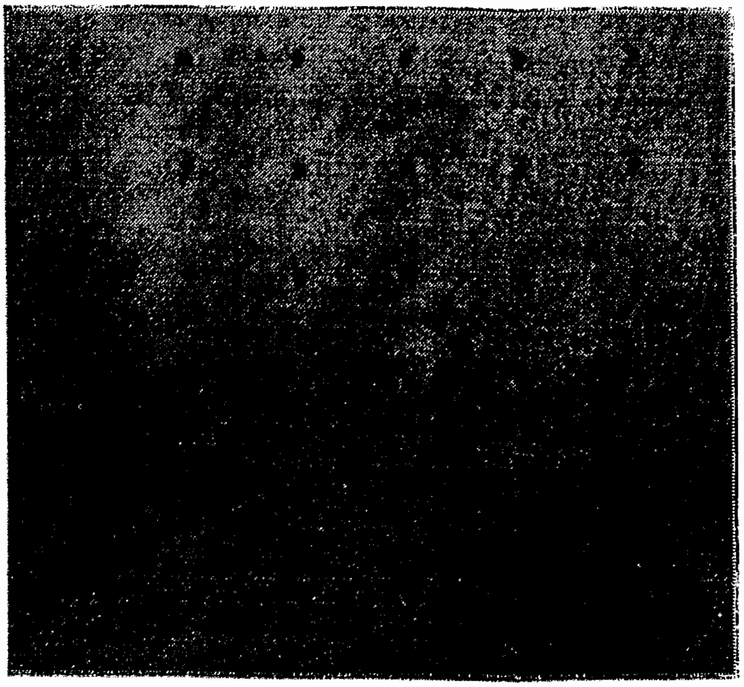

- $1\mu m$ collimator
- 10 ions per cluster

100μm

Target every cell nucleus within a population -1

- V79 cells
- 3.2 MeV protons
- Micronuclei scored 24 hours later
- One proton deposits 0.02 Gy/nucleus

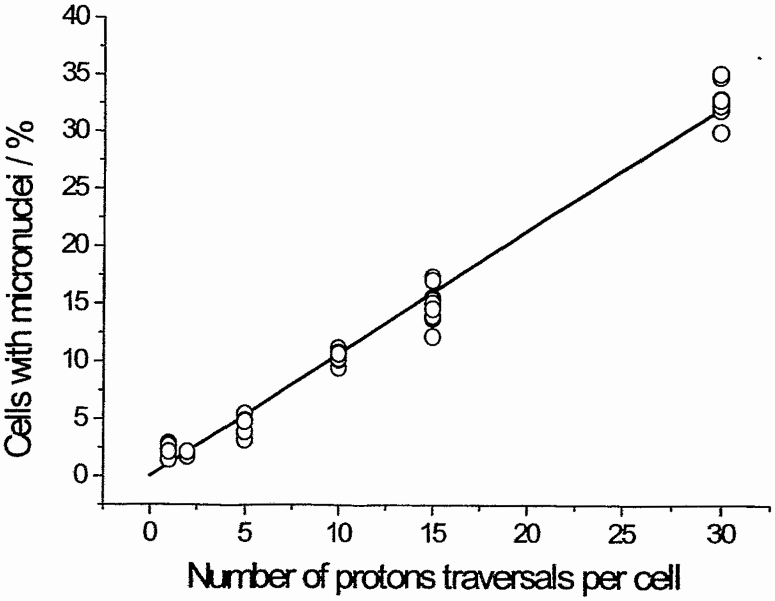

Prise *et al.*, 1999

Marples et al., Int. J. Radiat. Biol., 71, 721, 1997

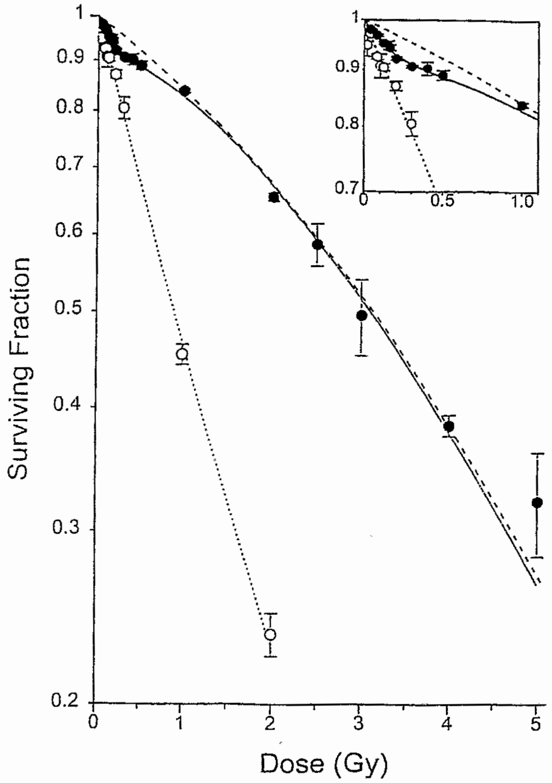

Figure 1. Survival of V79 cells irradiated with 250 kVp X-rays (solid) or neutrons (open). Symbols represent mean ± SEM. Survival was measured using the DMIPS survival assay, see text. The lines represent the fit of the Induced Repair model to the X-ray data (solid line), the LQ fit to the X-ray data (dashed line) and exponential fit to the neutron data (dotted line).

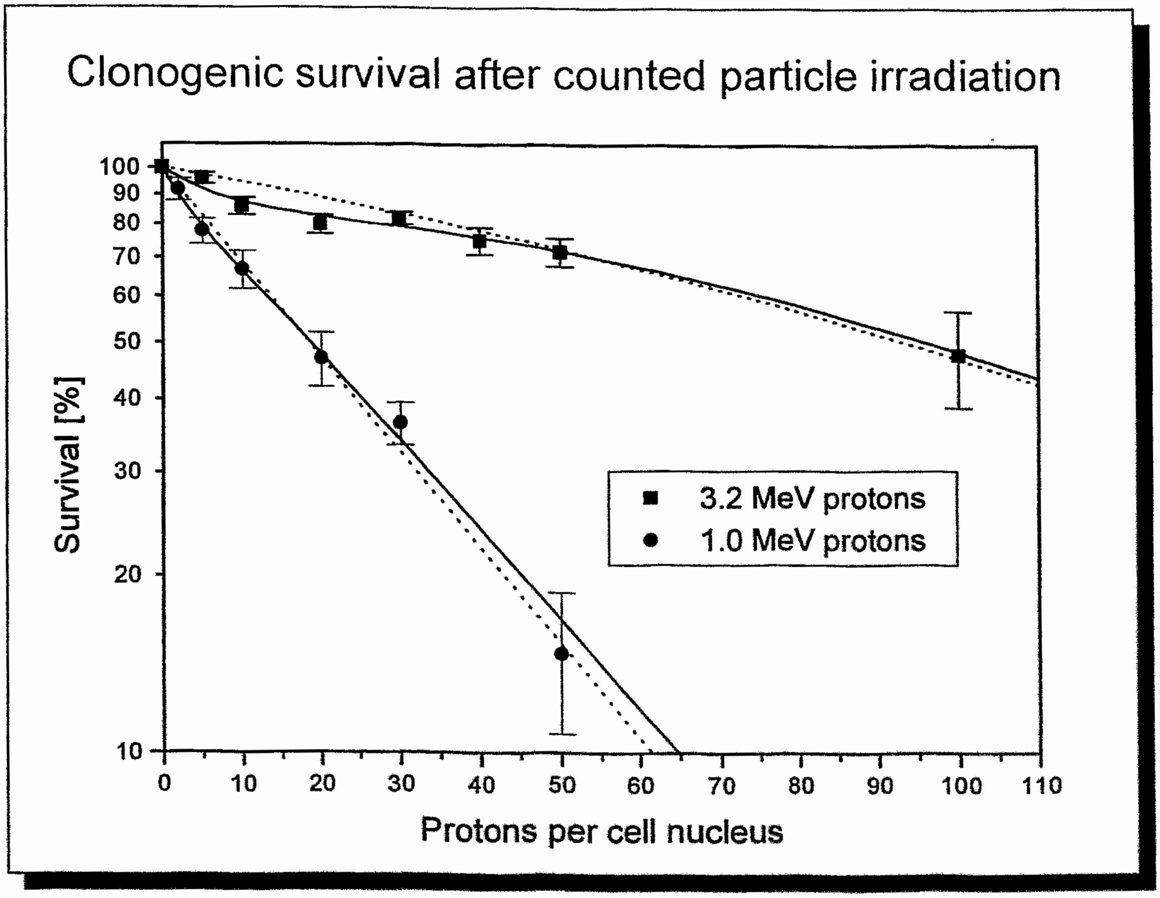

Evidence for bystander effects

- Increased levels of SCE in CHO cells irradiated with low doses of α-particles
  - *Nagasawa and Little, ~~1994~~.* 1992
- Increased p53 expression in lung epithelial cells exposed to low doses of α-particles
  - *Hickman et al., 1994*
- Extracellular factors involved in SCE following α-particle exposure
  - *Lehnert and Goodwin, 1997*
- Medium from irradiated cells reduces the survival of unirradiated cells
  - *Mothersill and Seymour, 1997*
- Target for chromosomal damage larger than the nucleus
  - *Manti et al., 1997*
- Bystander effects and genomic instability
  - *Lorimore et al., 1998*
- Bystander effects and cell-cell communication
  - *Azzam et al., 1998*
- Bystander effect after single cell irradiated
  - *Prise et al., 1998*

Using microbeams to study the role of extranuclear targets and bystander effects

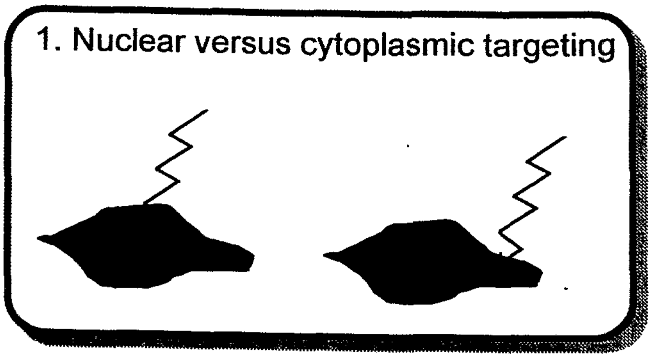

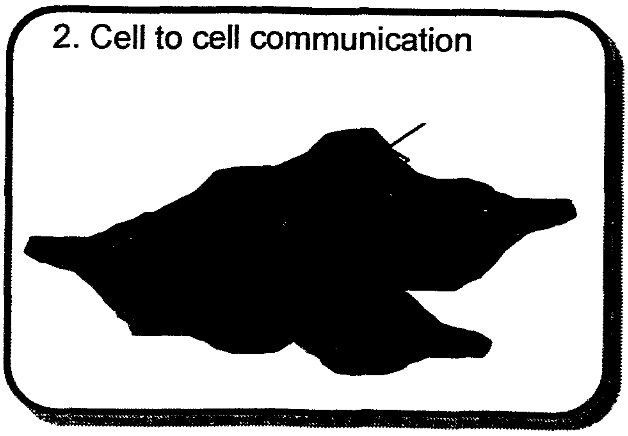

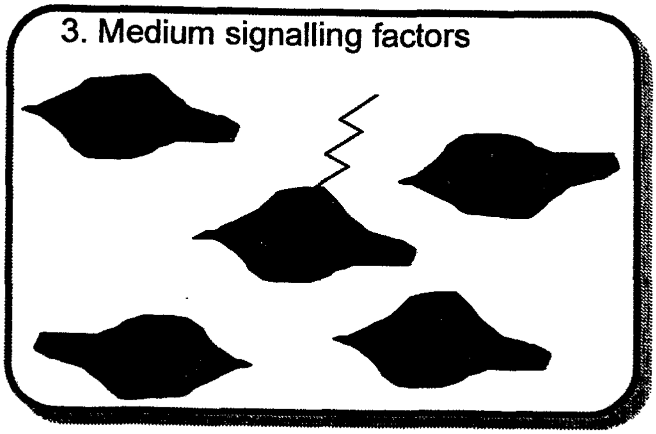

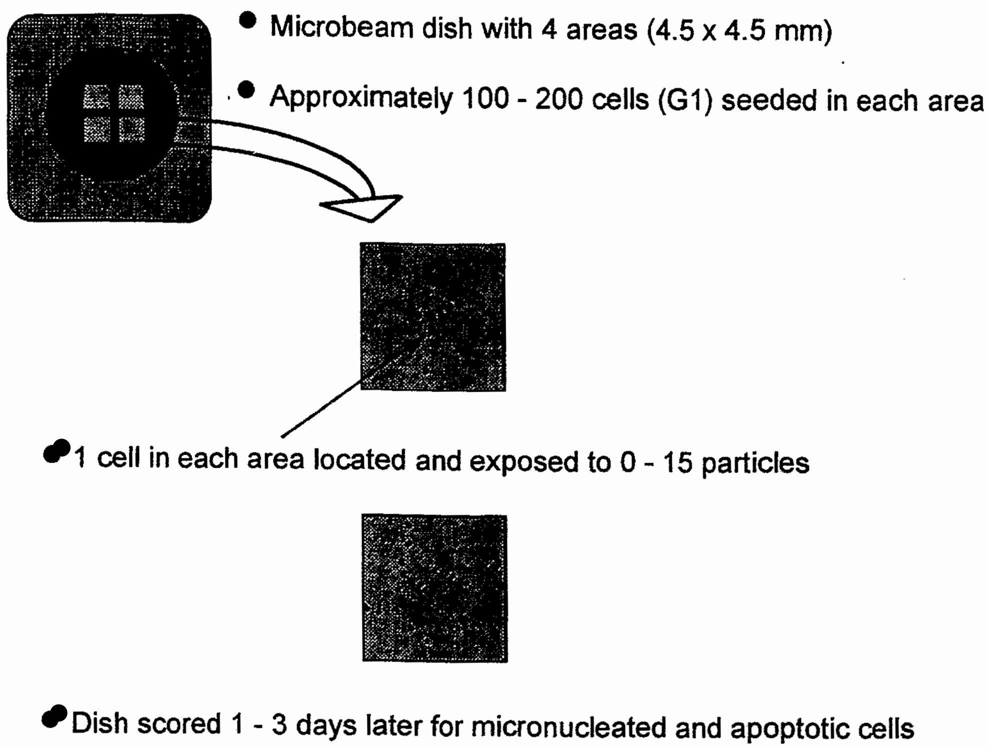
Microbeam dish with 4 areas (4.5 x 4.5 mm)
Approximately 100 - 200 cells (G1) seeded in each area
1 cell in each area located and exposed to 0 - 15 particles
Dish scored 1 - 3 days later for micronucleated and apoptotic cells

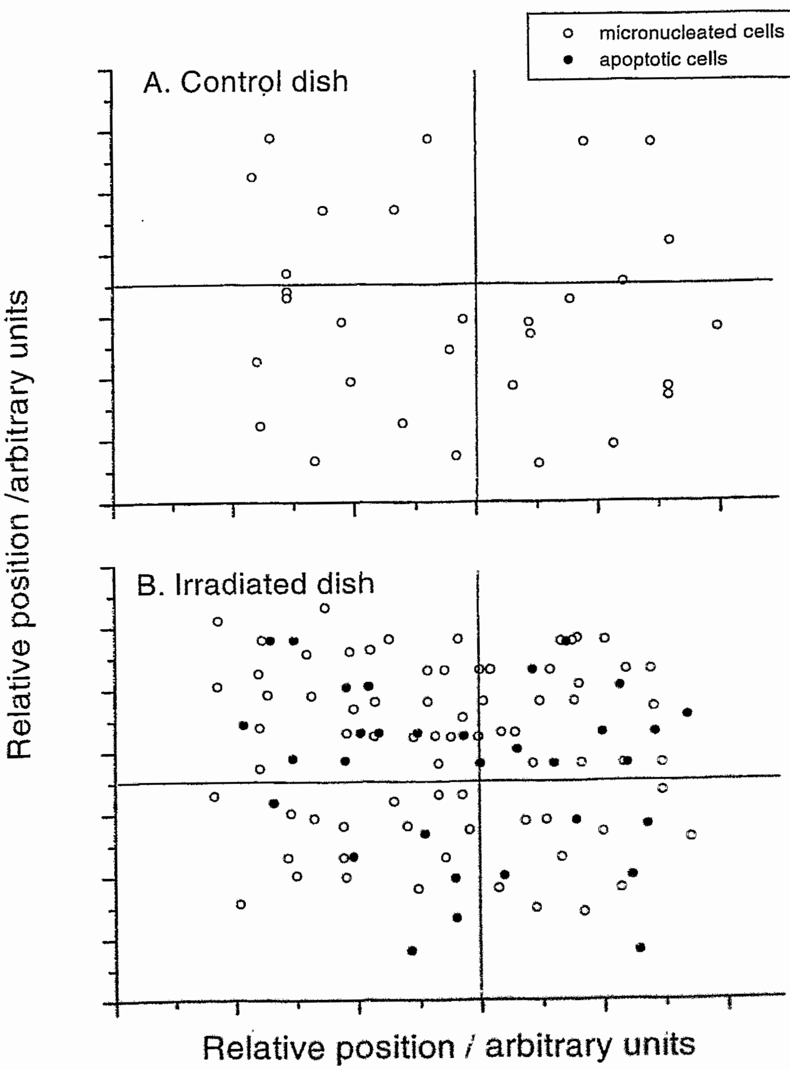
micronucleated cells
apoptotic cells
A. Control dish
B. Irradiated dish
Relative position /arbitrary units
Relative position / arbitrary units

1 cell per dish targeted

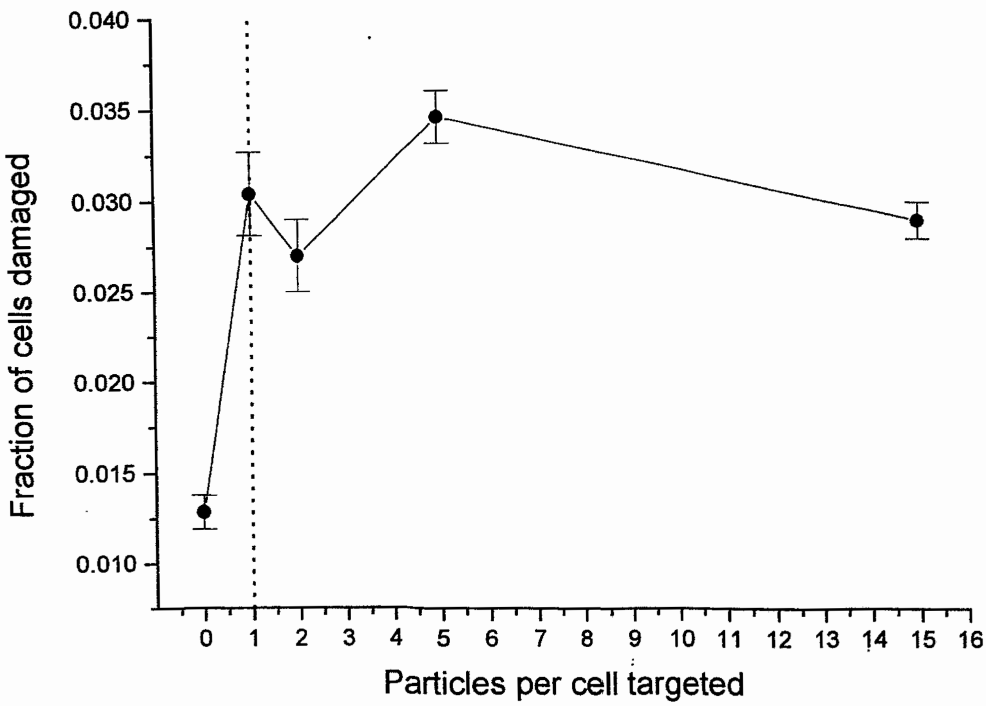

Gray Laboratory Focused Soft X-ray facility

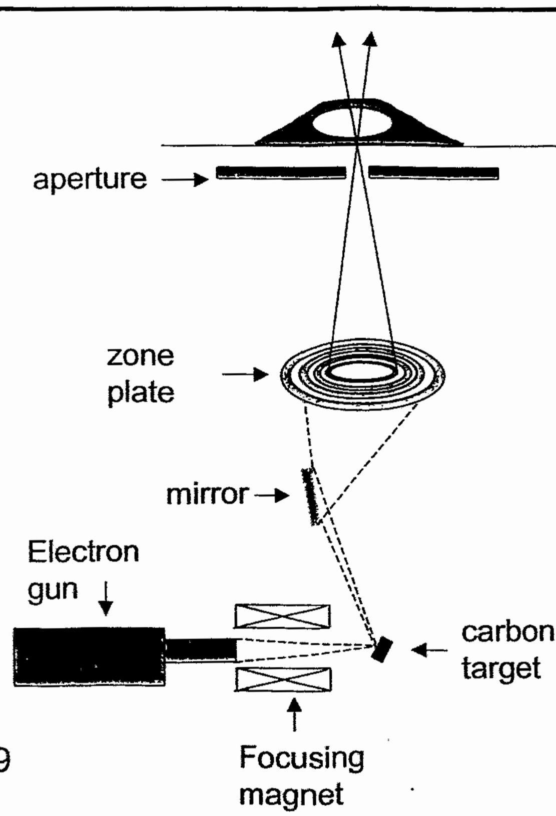

Folkard and Schettino, 1999

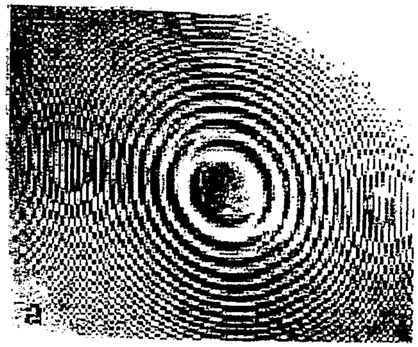

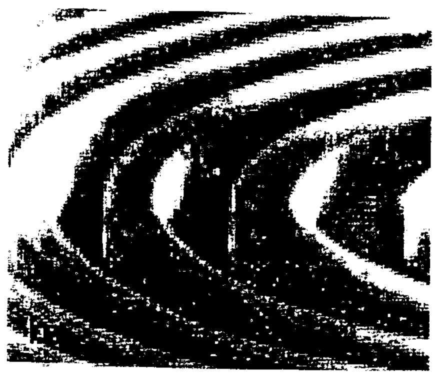

Microprobe Source

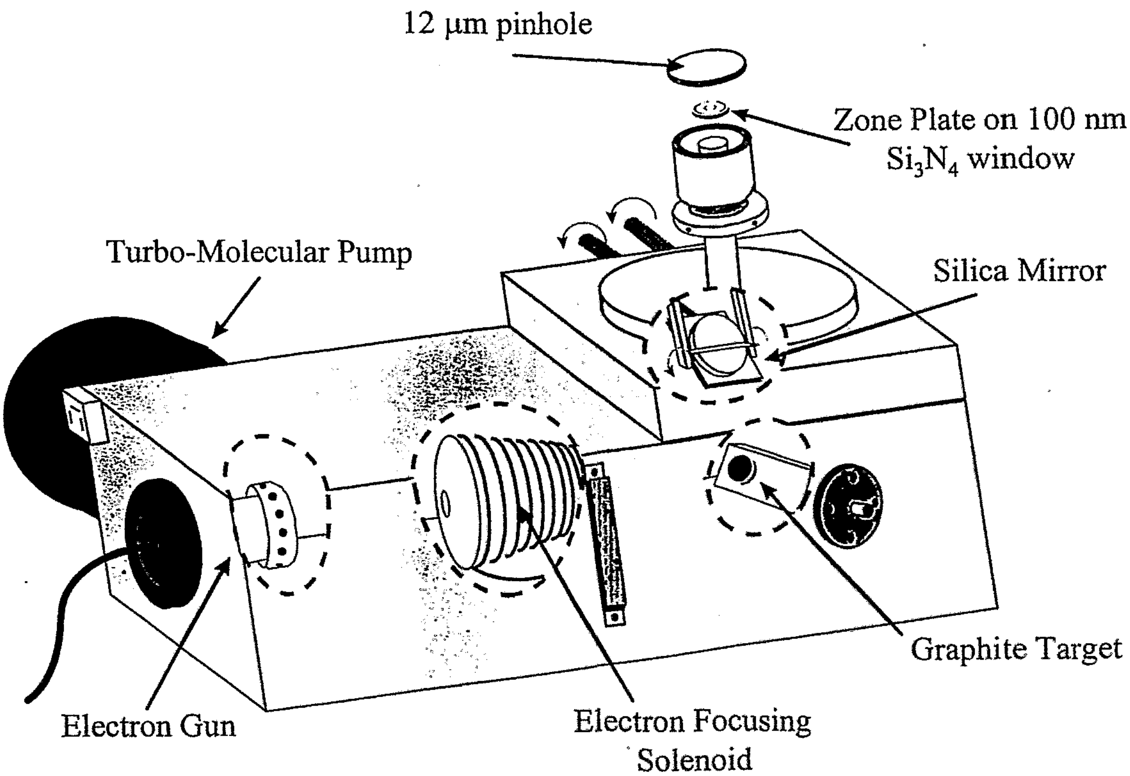

Schematic of the Gray Laboratory Microfocus X-ray source

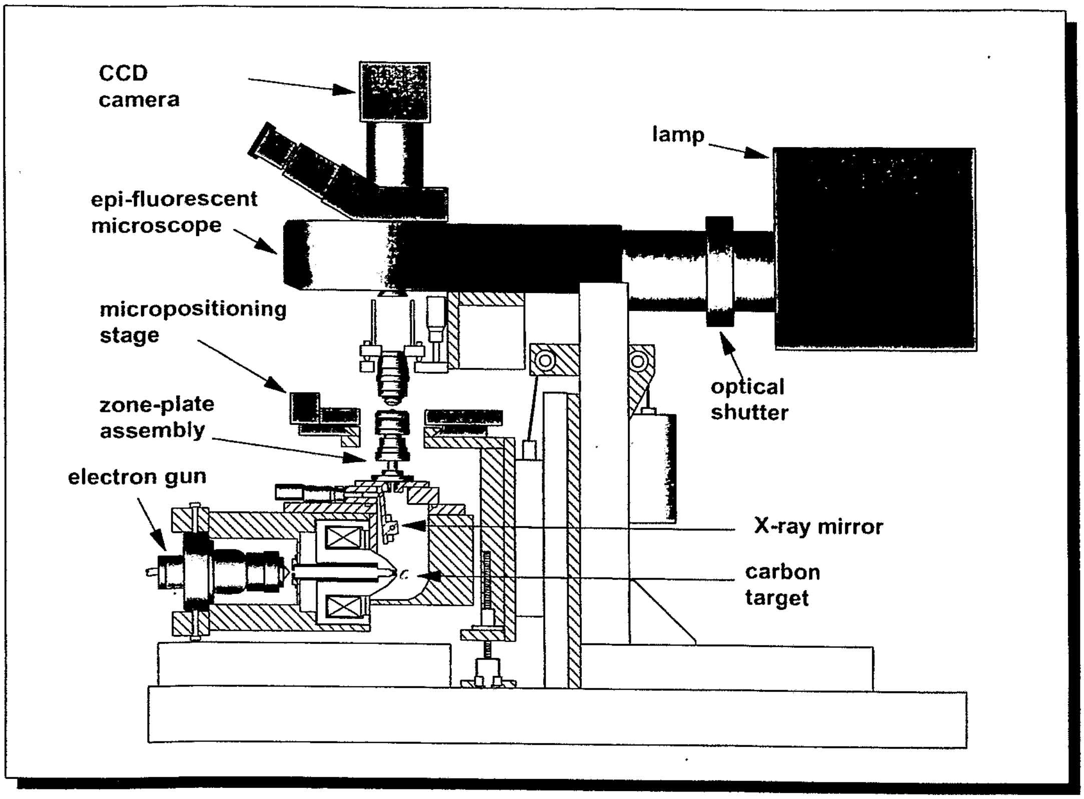

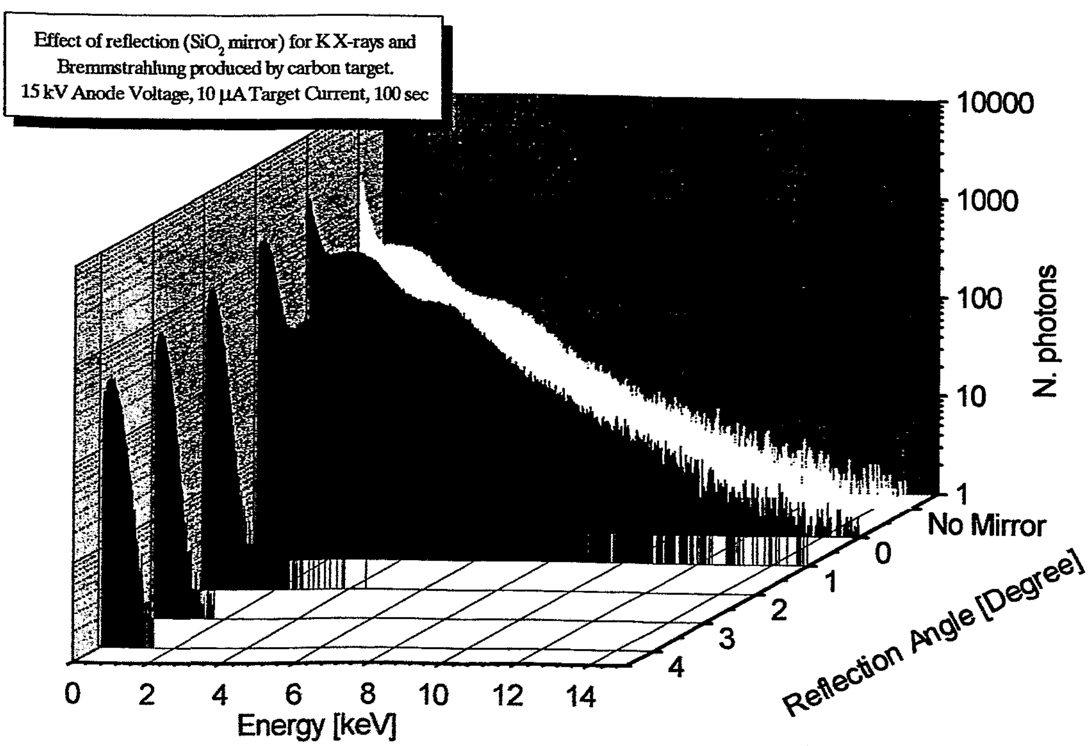

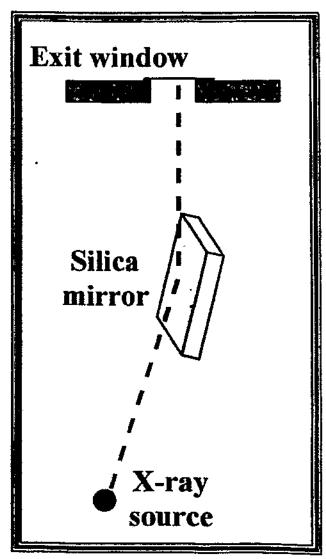

Beam Characteristics

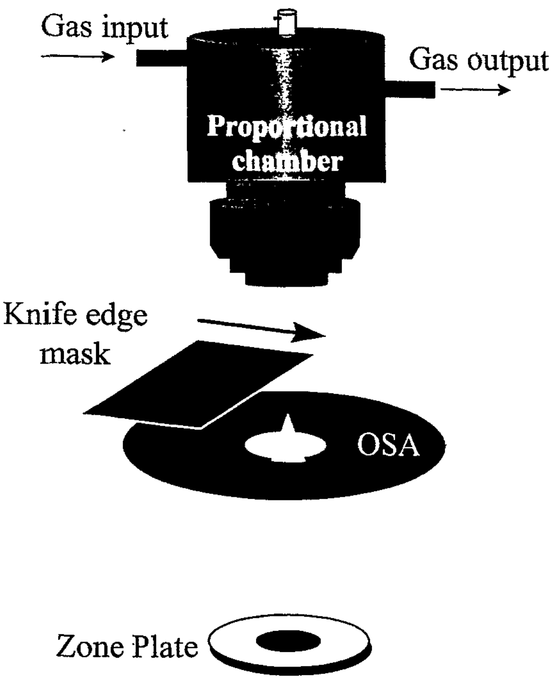

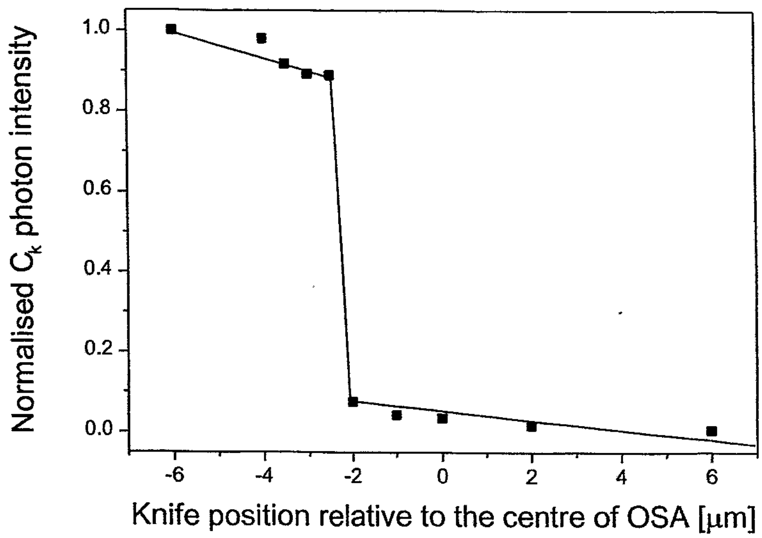

Beam radius < 250 nm

Dose rate ~ 1500 C_K photons / sec

Ultrasoft X-ray Microprobe

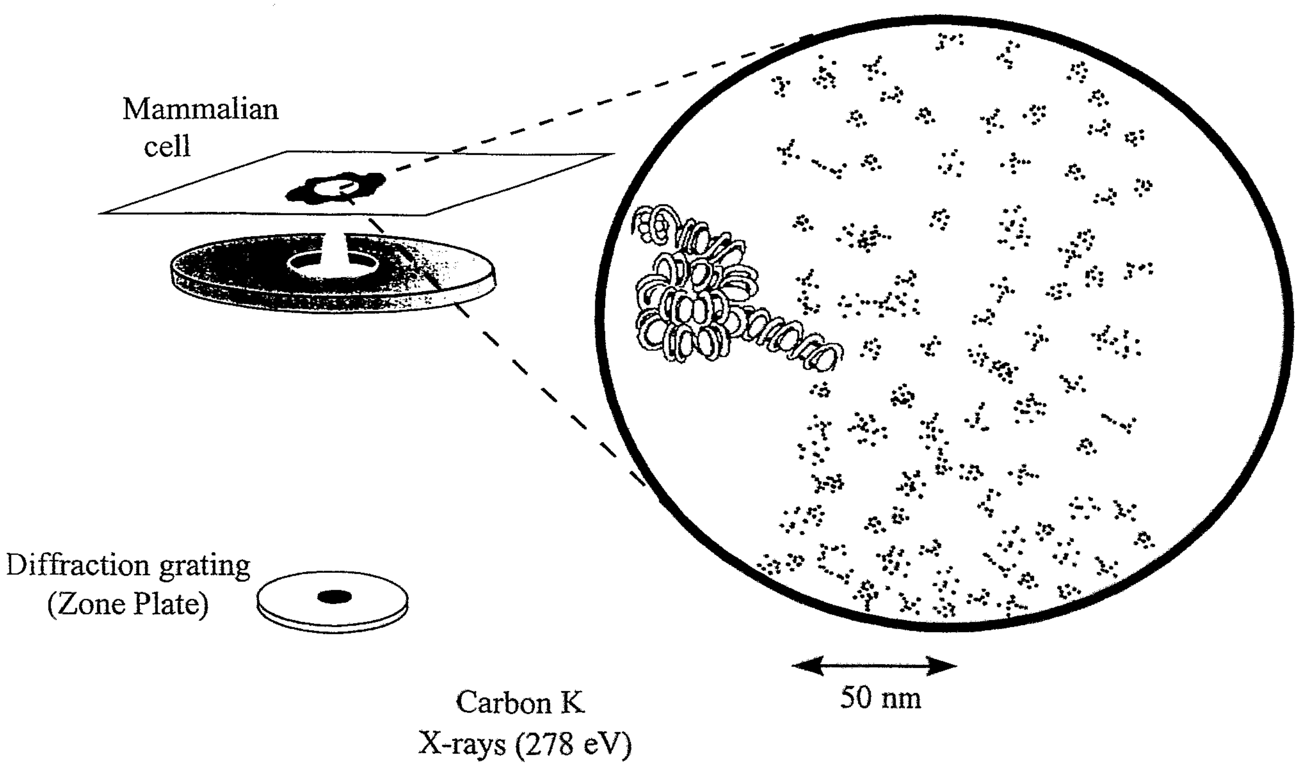

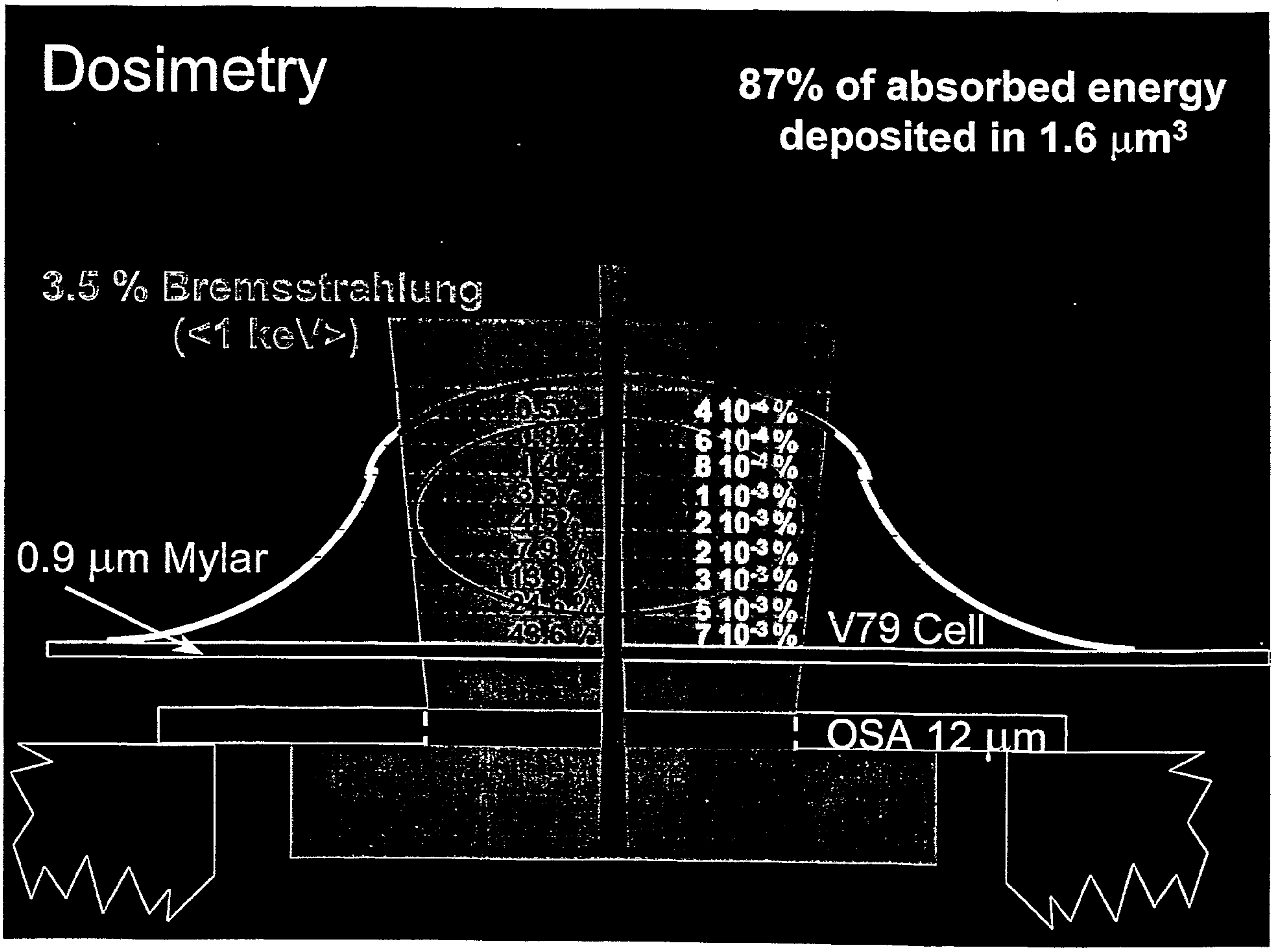

Dosimetry
87% of absorbed energy
deposited in 1.6 μm³
3.5 % Bremsstrahlung
(<1 keV>)
3.5 %
4.5 %
7.9 %
13.9 %
43.6 %
4 10⁻⁴ %
6 10⁻⁴ %
8 10⁻⁴ %
1 10⁻³ %
2 10⁻³ %
2 10⁻³ %
3 10⁻³ %
5 10⁻³ %
7 10⁻³ %
0.9 μm Mylar
V79 Cell
OSA 12 μm

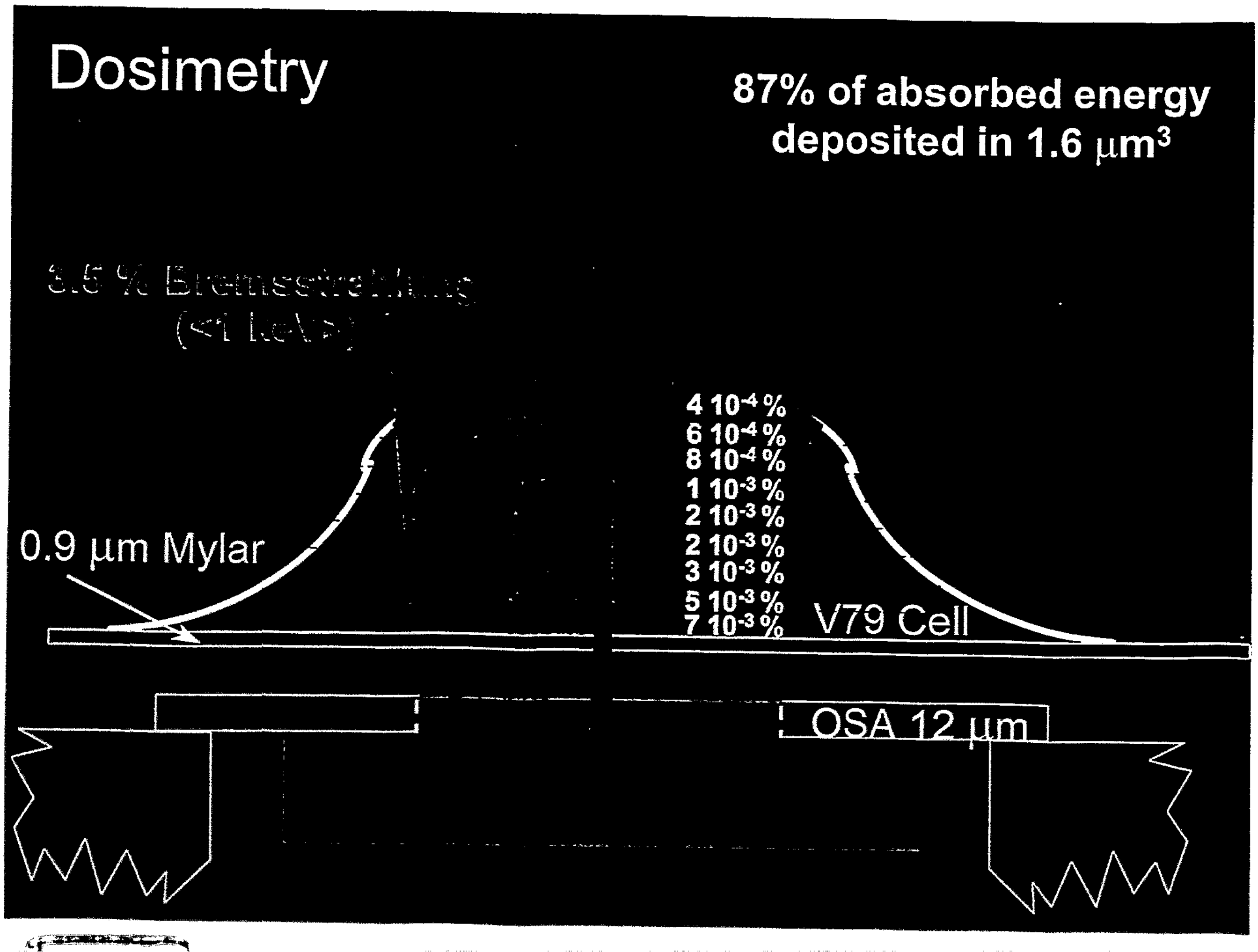

Dosimetry
87% of absorbed energy
deposited in 1.6 μm³
3.5 % Bremsstrahlung
(<1 keV>)
4 10⁻⁴ %
6 10⁻⁴ %
8 10⁻⁴ %
1 10⁻³ %
2 10⁻³ %
2 10⁻³ %
3 10⁻³ %
5 10⁻³ %
7 10⁻³ %
0.9 μm Mylar
V79 Cell
OSA 12 μm

Survival Assay : C_k X-rays

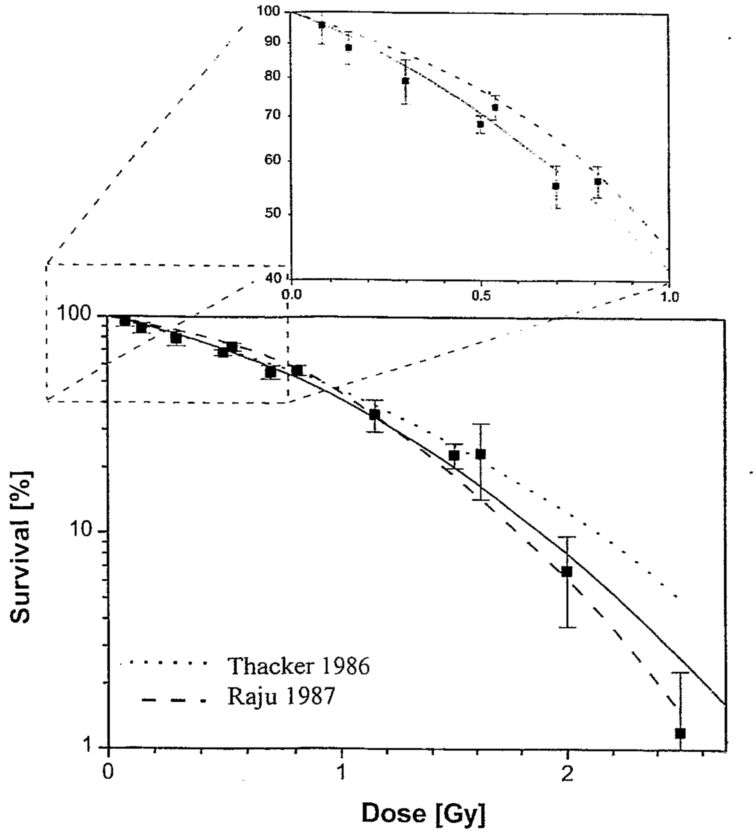

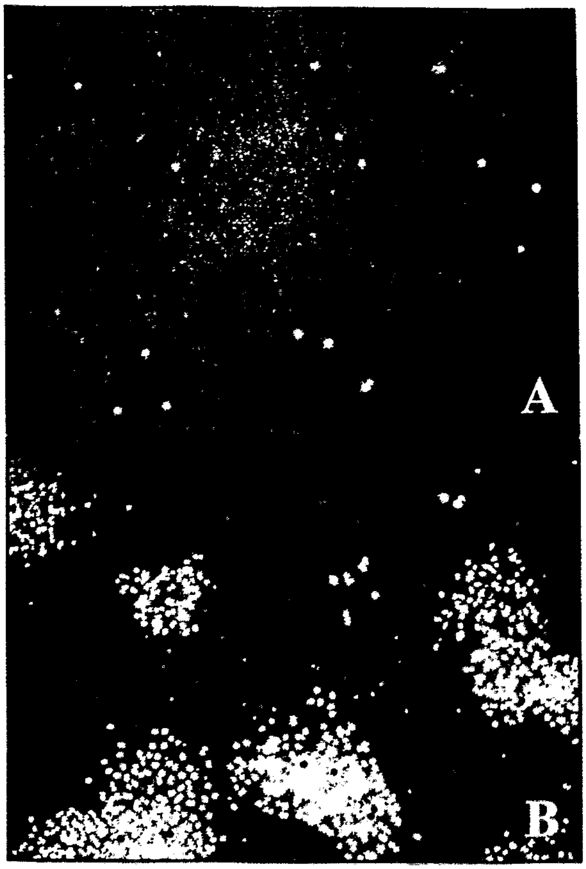

Radiation-induced bystander effects

Targeted
α-particles

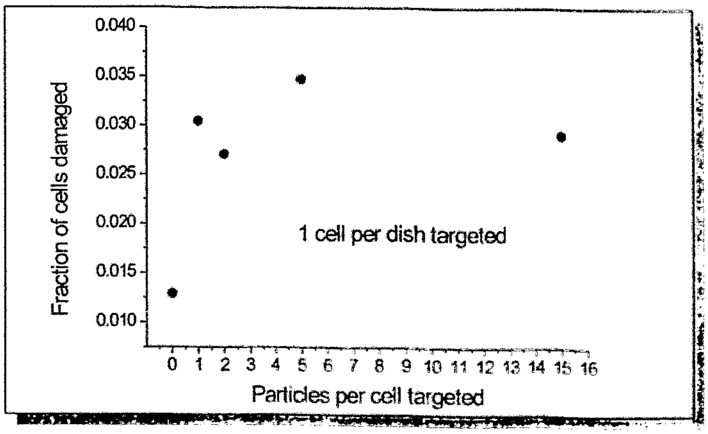

Focused
soft X-rays

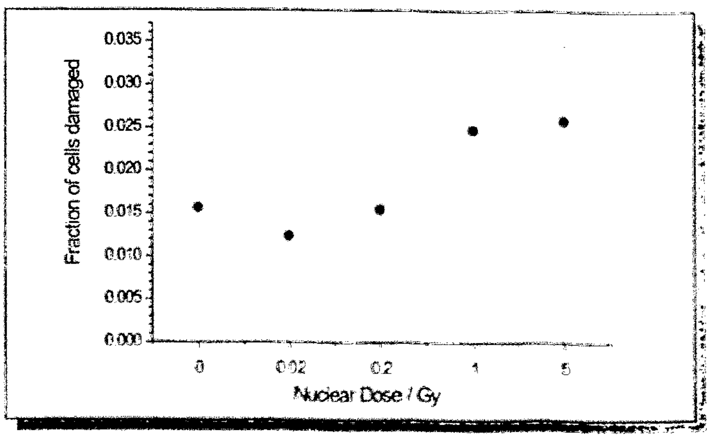

Summary

1) The modern generation of microbeams provides an important tool to investigate new aspects of how cells respond to radiation:
   a) Identification of targets and pathways
   b) Determination of extreme low-dose responses

2) At present, the development of light-ion microbeams is more advanced than that of X-ray, electron and heavy-ion microbeams

3) Data obtained so far demonstrate the power of microbeam methods to study:
   a) Radiation bystander effects
   b) Effects related to the distribution of energy deposition within the cell
   c) Low-dose adaptive responses
   d) Single-track effects

W. Mondelaers:

Application of X-rays for biomedical purposes

APPLICATION of X-RAYS
for BIOMEDICAL PURPOSES

at the

GENT UNIVERSITY

15 MeV LINEAR ELECTRON
ACCELERATOR FACILITY

W.Mondelaers

Workshop on X-rays from electron beams
with special emphasis on
possible developments at ELBE

Overview

- Accelerator facility

- High-power white photon beams
  - high-dose radiotherapy
  - medical standard dosimetry
  - human grafts and implants
  - novel biomaterials

- Tunable monochromatic photon beams
  - biomedical applications

15 MeV 2% duty factor
LINEAR ELECTRON ACCELERATOR
FACILITY

- intense electron beams

  up to 2 mA

- high beam power density

  up to 140 kW/cm²

- good energy resolution

  $\Delta E/E < 1\%$ (50 - 80%)

- high pulse repetition frequency

  up to 5000 Hz

- intense X-ray beams

  polarised and unpolarised

ACCELERATOR

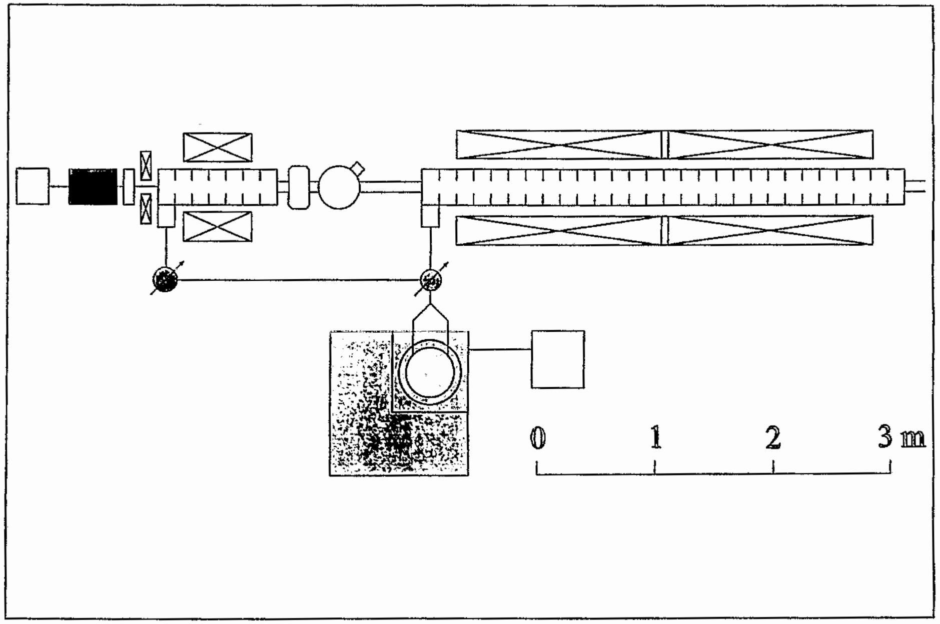

BEAM TRANSPORT SYSTEM

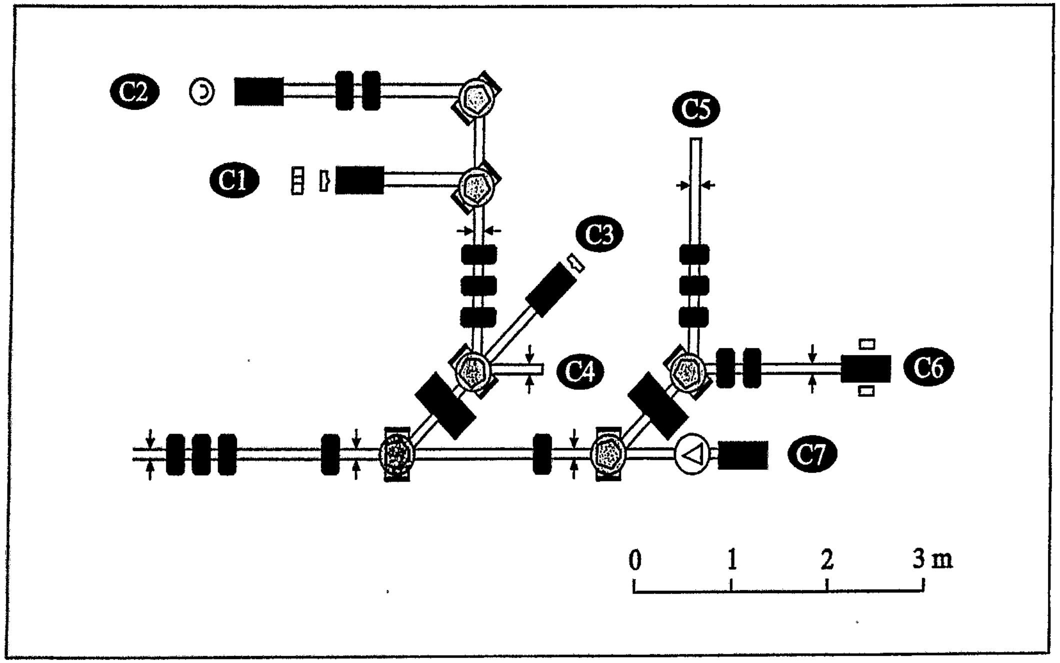

- radiation physics
- biomaterials research ⇐
- polymer chemistry
- atomic and solid-state physics
- medicine ⇐
- food technology
- space research
- agriculture
- high-dose dosimetry

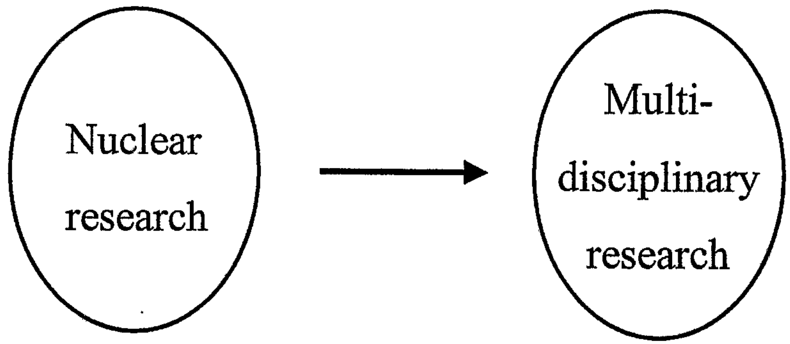

Biomedical applications of intense broad photon fields

- High-dose radiotherapy
  - extracorporeal bone tumours therapy
- Medical dosimetry
  - primary standard dosimetry
  - *in vivo* dosimetry
- Irradiation of implants
  - human grafts
  - artificial implants
  - graft-versus-host disease
- Synthesis of biomaterials
  - hydrogels
  - surface modification

Intraoperative extracorporeal irradiation in primary bone tumours therapy

Radical ablative surgery

⇒ limb saving techniques
- endoprosthesis
- allograft
- bridging techniques

Disadvantages:
- loosening or breakage
- well-fitting allograft
- immunological rejection
- bone bank

⇓

extracorporeal irradiation
of endograft

One operative session:

- excission of bone
- extracorporeal irradiation 300 Gy
- reimplantation

↪ slow revitalisation of matrix

- neovascularization
- resorption of graft bone
- depsoition of new host bone

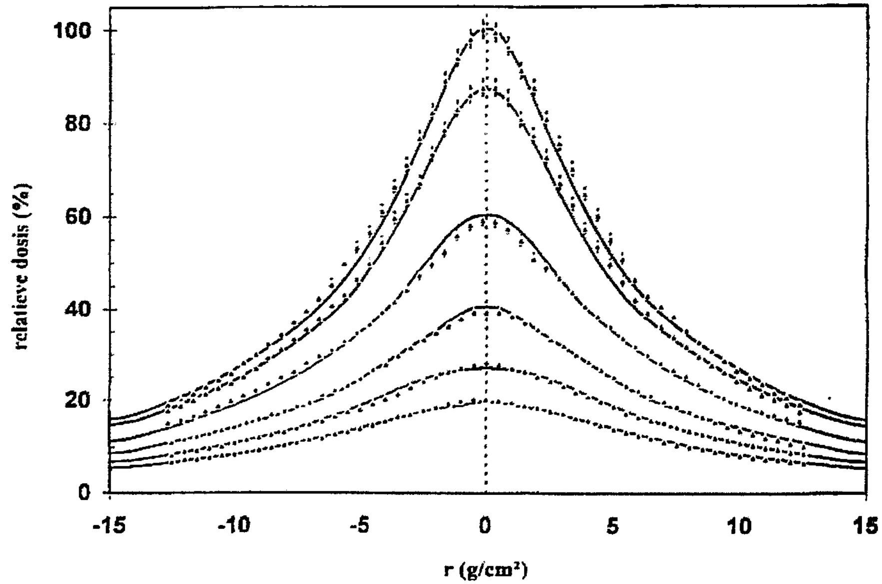

Homogeneous photon irradiation field

- homogeneity ± 2%
- diameter 20 cm
- dose rate 3 Gy/s

?? Conventional radiotherapy machines ??

- Dynamic electron beam scanning
- Static photon beam flattening

Classical solution: high-Z target and filter

⇒ systematic theoretical and experimental study

Monte Carlo: EPCOT

EGS4, BEAM, DOSXYZ

3D dose mapping

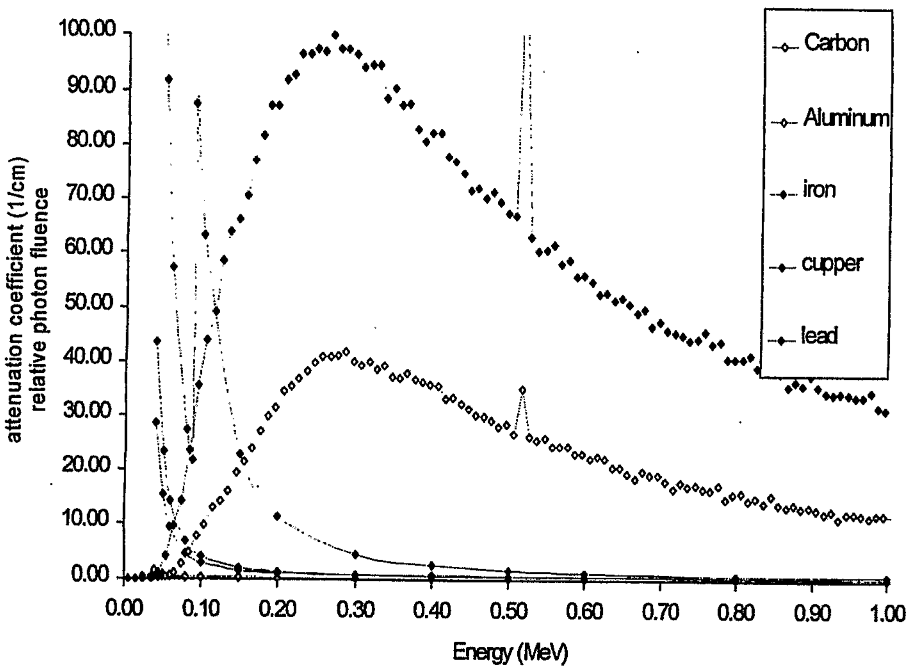
attenuation coefficient (1/cm)
relative photon fluence
100.00
90.00
80.00
70.00
60.00
50.00
40.00
30.00
20.00
10.00
0.00
0.00
0.10
0.20
0.30
0.40
0.50
0.60
0.70
0.80
0.90
1.00
Energy (MeV)
Carbon
Aluminum
iron
cupper
lead

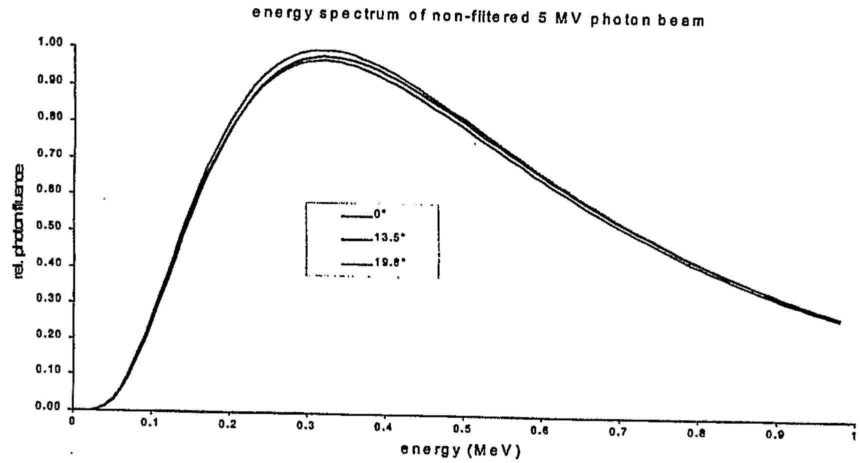
energy spectrum of non-filtered 5 MV photon beam
rel. photon fluence
energy (MeV)
0°
13.5°
19.8°

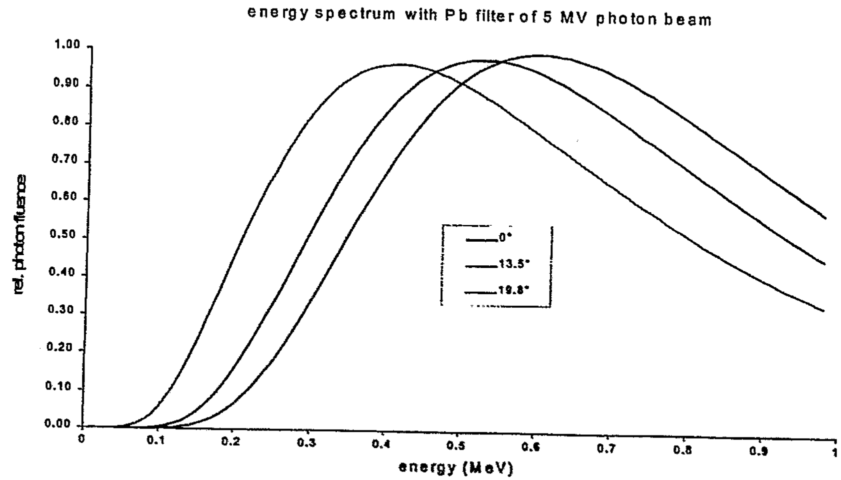
energy spectrum with Pb filter of 5 MV photon beam
rel. photon fluence
energy (MeV)
0°
13.5°
19.8°

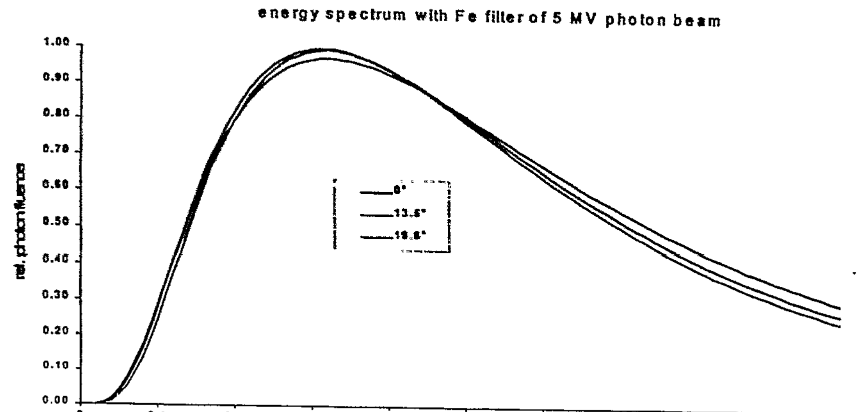
energy spectrum with Fe filter of 5 MV photon beam
rel. photon fluence
0°
13.5°
19.8°

energy (MeV)

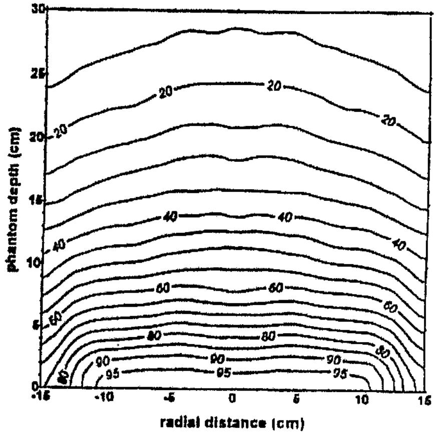

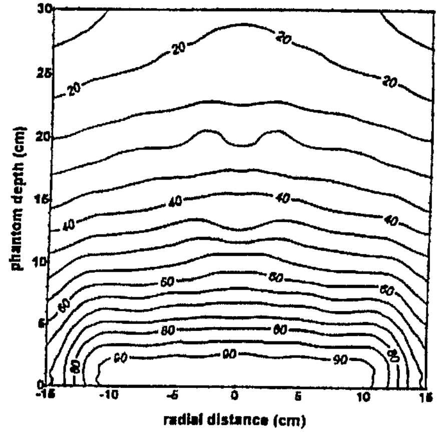

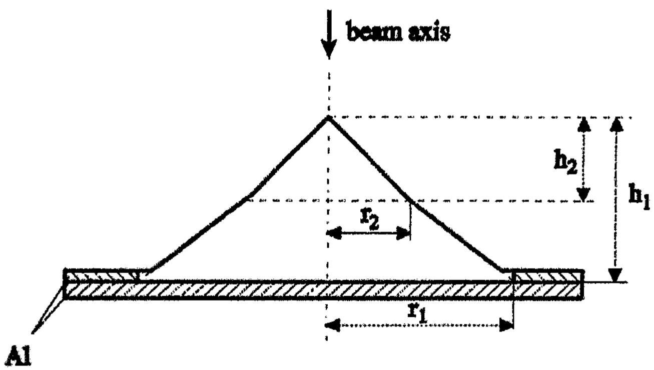

$\varnothing$ = 30 cm
35 kGy / h

$\varnothing$ = 10 cm
150 kGy / h

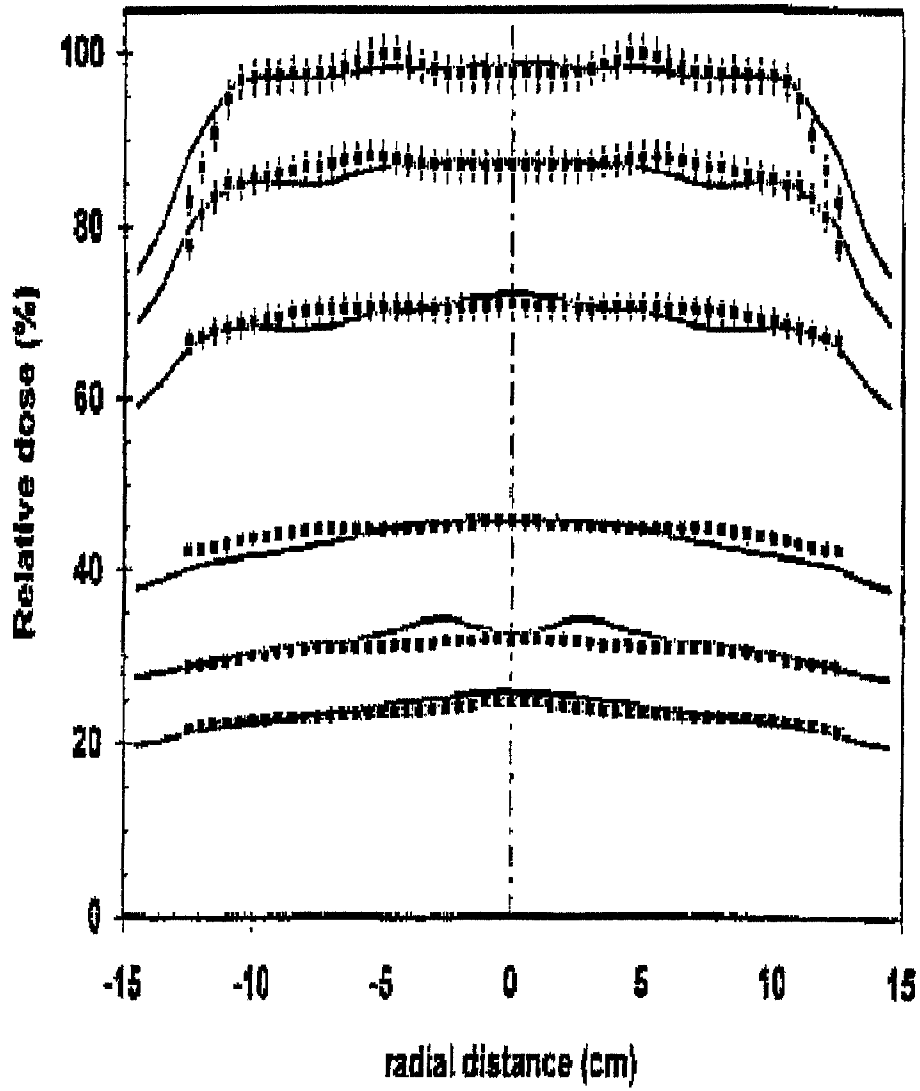

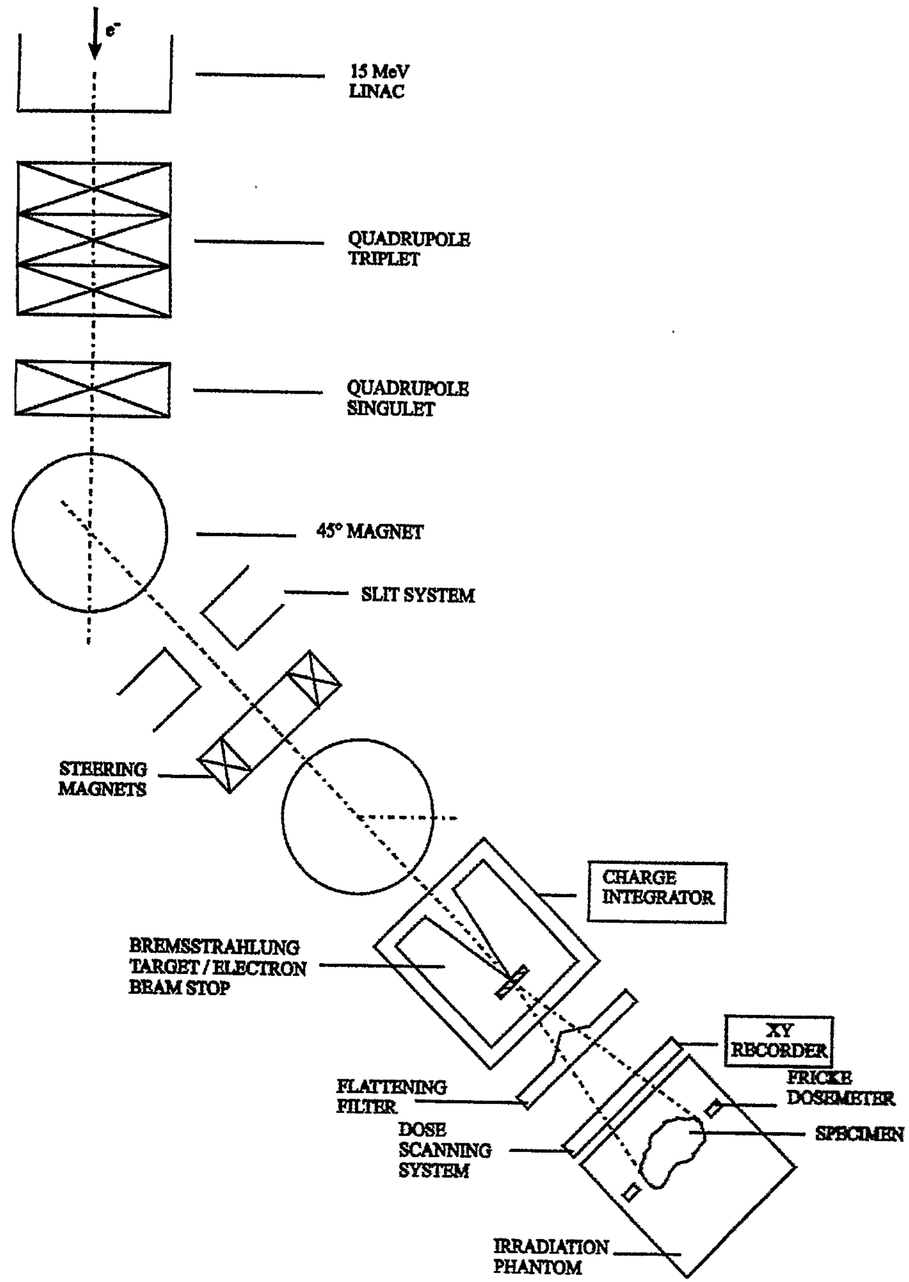

Conformal and intensity-modulated radiotherapy

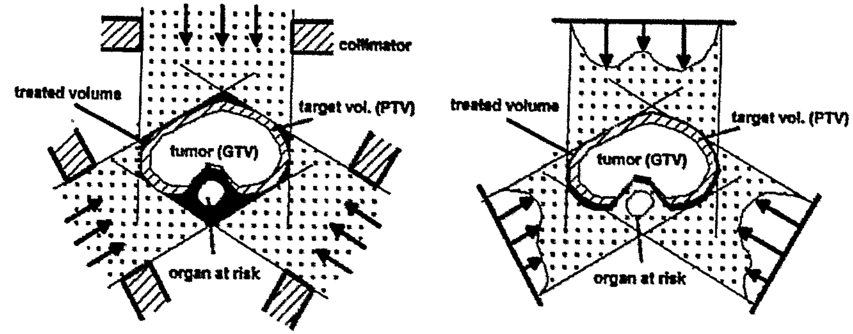

Comparison of conventional and intensity-modulated radiotherapy.

1. mechanical scanning with multileaf collimator
2. scanning of photon beam

Karolinska Institute (Söderstrom 1999): superficial and deep-seated tumours
6 - 15 MeV

Intraoperative extracorporeal irradiation in primary bone tumours therapy

~ 100 patients treated

proximal and distal femur	46 %
pelvic rim	22 %
proximal tibia	11 %
humerus	8 %
fibula	5 %
radius, ulna, scapula	

⇓

78 % 10 years actuarial survival rate

↔ 60 - 80 % other techniques

Heidelberg, Tubingen, Osaka

Bremsstrahlung configuartion for intensity-modulated therapy

theoretical and experimental of
broad beams
↓
narrow beams

- FWHM 30 - 40 mm at 1 m
- energy range 6 - 15 mV
- high electron photon conversion yield

- full stopping low-Z target
- full stopping sandwich target
- optimised mono- or multilayer target

+ purging magnet

Primary standard dosimetry

Belgian Primary Standard Laboratory

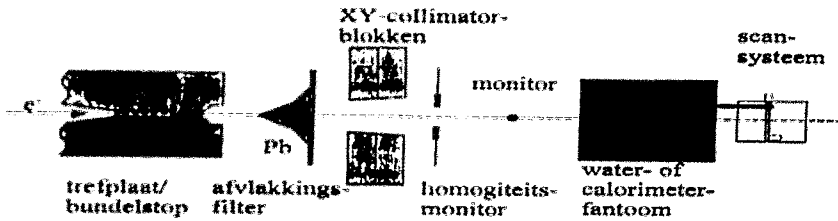

ionisation chambers ↔ primary standard

Water calorimetry
< 0.1% level

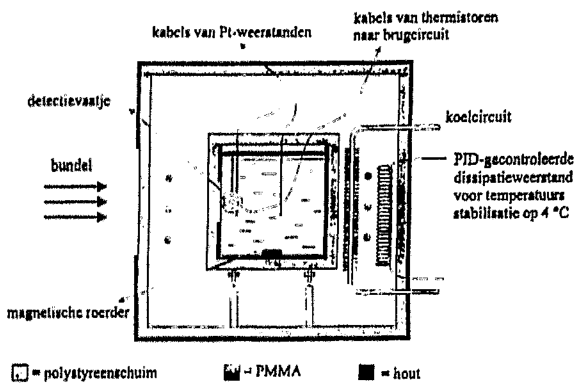

- correction factors
- heat chemical defect

Primary standard dosimetry

- Calibration standard

- Beam quality specifiers:
  - spectral characteristics of X-ray field
  - depth-dose distributions

%dd(10) = % depth dose at 10 cm

↔ TPR^{20}_{10} = dose at 20 cm / dose at 10 cm

- Beam quality dependence factor k_q:
  - ionization chamber → dose in water

calibration factor N_{DwQ}

0.2% uncertainty

$$k_q = \frac{[illegible]}{N_{DwQ(0)}}$$

- Chemical heat defect by radiation-induced species:
  - dose dependence
  - oxygen content
  - hydrogen saturation

Radiation treatment of human grafts and artificial implants

- sclerae of the human eye

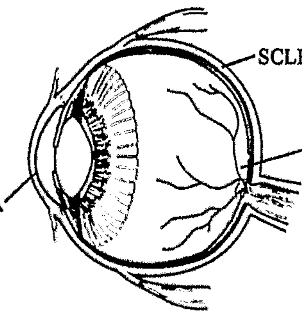

prosthesis → imflammation, rejection

⇒ 'packed' in human sclerae
- less reactions
- synchronous movement

lyophylization → sterilization 25 kGy → tissue bank

- bone fragments: maxillo-facial reconstruction
- human implants: cardiological stents, polymeric implants, hydrogels for burn wounds
- blood: lymphocytes 40 Gy, graft-versus-host disease

Radiation treatment of biomaterials

- RADIATION-INDUCED POLYMERISATION:
  for synthesis of new biomaterials:
  - biodegradable polymers
  - hydrogels for burn wound treatment
  - porous polymeric hydrogels for advanced drug delivery systems
    → constant release
    → signal-responsive
- RADIATION-INDUCED SURFACE GRAFTING:
  to improve biocompatibility
  to immobilise bioactive agents
    → heparine filter
    → fixation of HD cell cultures on PE
- RADIATION-INDUCED STERILISATION:
  biodegradability
  mechanical properties
  swelling and permeability of hydrogels

- Signal-responsive hydrogels

macromolecular networks swollen in water

PVME
60 kGy at 100 kGy/h
temperature controlled

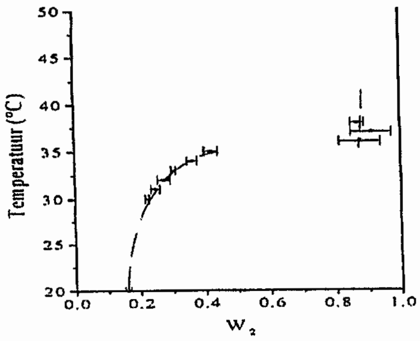

→ discontinuous swelling behaviour

- Grafting of biofunctional groups on PVC beads

Hemodyalisis of uremic patients: blood + artificial surfaces
→ coagulation

↓

heparine absorbing filter

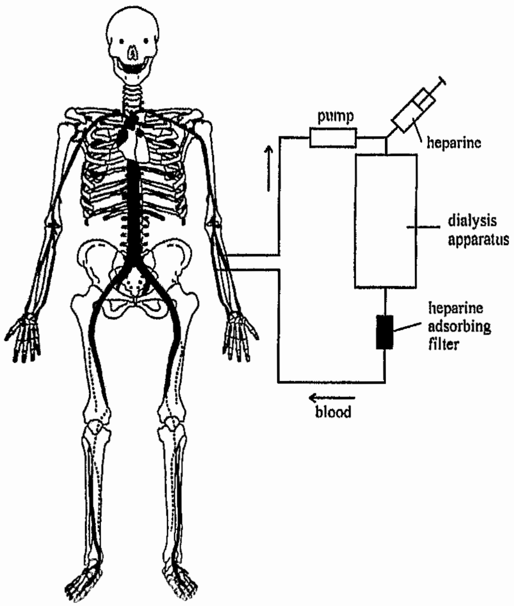

- X-ray induced grafting of HEMA on PVC beads (2-hydroxyethyl methacrylate)

- hydroxyl groups couple chemically with functional polyamidoamines
→ heparine absorber

Other research applications

- TREATMENT of FOOD PRODUCTS and PACKAGING MATERIALS
  - chemical, physical, sensorial, microbial and nutritional characteristics
  - identification and dose assesment
  - interaction food - packaging materials
- HIGH-DOSE DOSIMETRY
  - EPR spectra of alanine and other systems
- RADIATION-INDUCED PLANT MUTATION
- DETECTOR CALIBRATION (SOHO project)
- RADIATION DAMAGE STUDIES
- e^- IRRADIATION-INDUCED DEFECTS in Si
- BIODEGRADABILITY OF PLASTICS
- STERILISATION OF WOOD AND SOIL PRODUCTS

Tunable monochromatic X-ray source

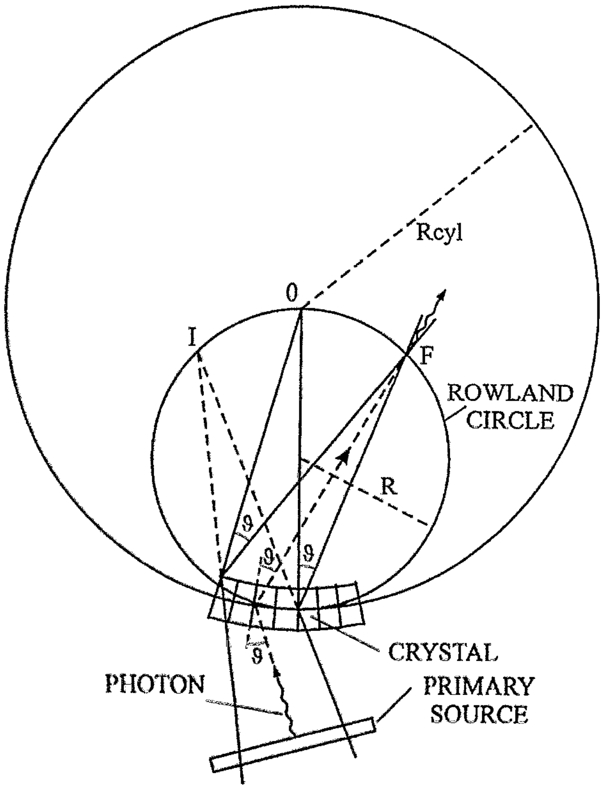

$$n\lambda = 2d\sin\theta$$

$$\Delta E = \frac{2d}{nhc}\frac{d_R}{R}$$

Tunable monochromatic X-ray source

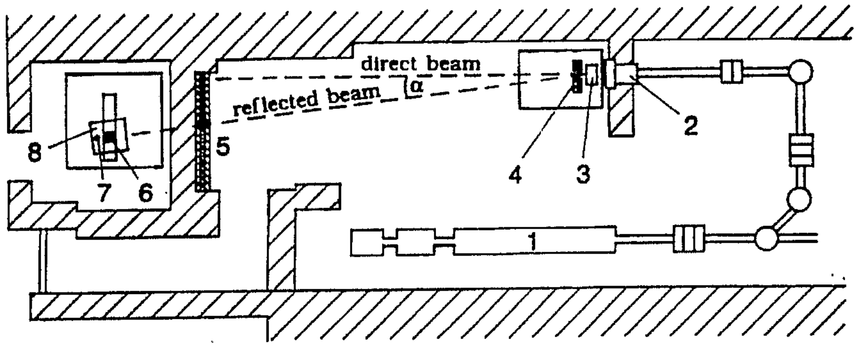

low-Z bremsstrahlungradiator BEAM

- max. X-ray production at required energy
- max. peak-to-background
- thermal constraints

↓

C-target of variable thickness + cleaning magnet

Range	60 - 700 keV
FWHM	< 0,1%
P/B	400/1
Intensity	10^5 ph/sec-cm² ↓
ESRF HE	10^8 ph/sec-cm²

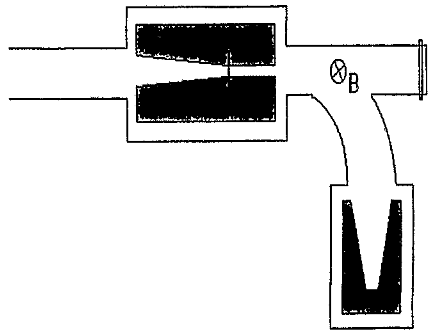

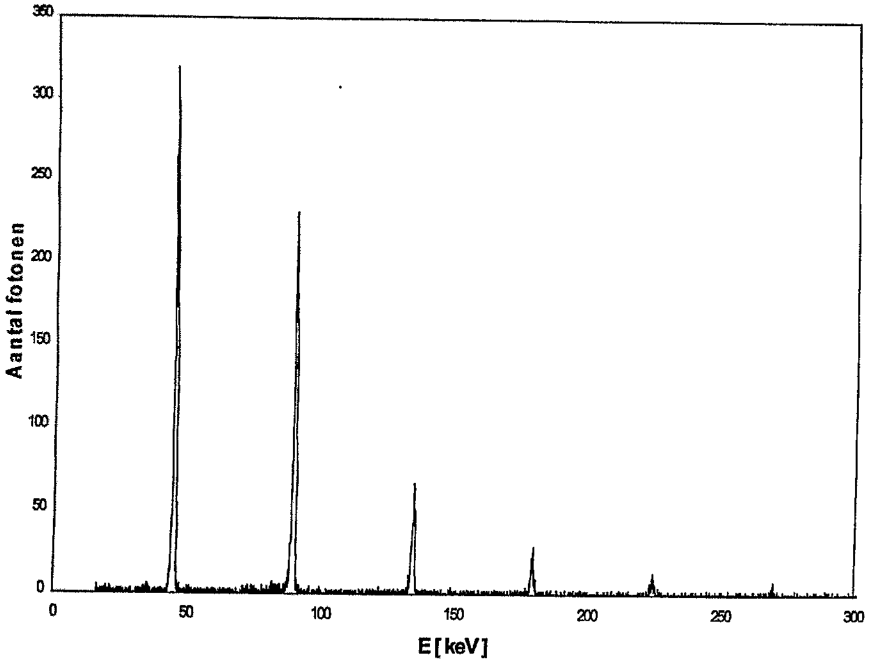
Aantal fotonen
E [keV]

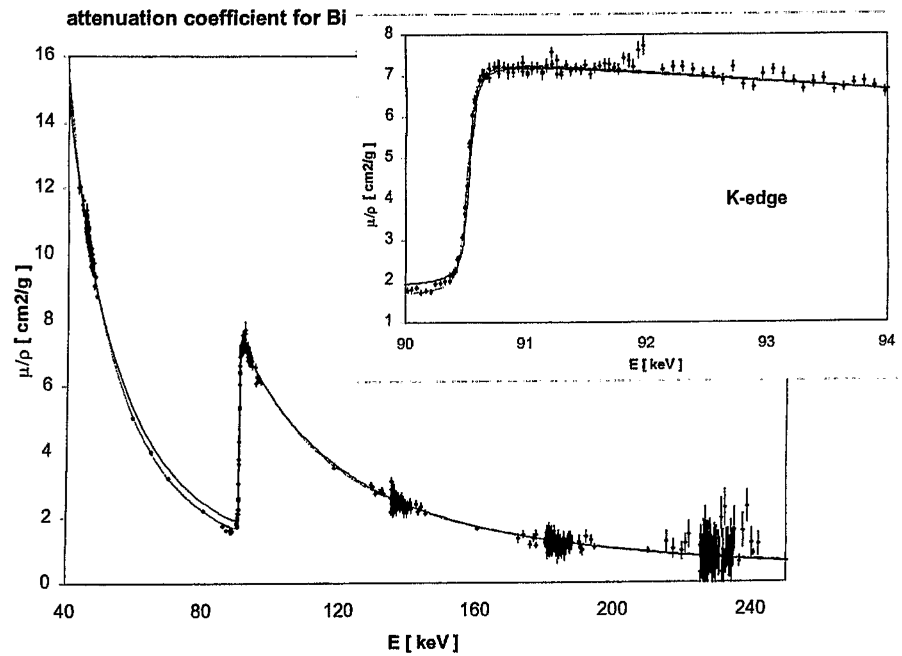
attenuation coefficient for Bi
μ/ρ [cm2/g]
E [keV]
K-edge

K. Kobayashi:

Radiation biology at the KEK Photon Factory

Workshop on X-rays from electron beams (Feb. 24-26, 2000)

Radiobiology at the KEK Photon Factory

Katsumi Kobayashi
Photon Factory
National Accelerator Research Organization
Japan

University of Tokyo
Takashi ITO
Atsushi ITO

Rikkyo University
Kotaro HIEDA
Yoshihiko HAYAKAWA
Akira AZAMI
Taisuke HIRONO
Mikio SAITO
Hiroyuki YAMADA

Tokai University
Hiroshi MAEZAWA
Yoshiya FURUSAWA

National Cancer Research Institute
Nobuo MUNAKATA

International Christian University
Kaoru TAKAKURA
Ritsuko WATANABE

Yokohama City University
Masami WATANABE
Masao SUZUKI

Japan Atomic Energy Research Institute
Akinari YOKOYA

National Institute of Radiological Sciences
Takeshi YAMADA

Photon Factory
Noriko USAMI
Katsumi KOBAYASHI

Radiobiology at the KEK Photon Factory

1. Introduction
   Rationale to use synchrotron radiation for radiobiology

2. Facility and apparatuses
   Beam line, irradiaition apparatus and supporting facilities for biology

3. Some of the results
   3a. Energetics of strand break induction in DNA using dry plasmid

   3b. Molecular fragmentation dependent upon the photoabsorption site

   3c. Energy dependence of chemical reactions in aqueous systems
   Fricke solution, strand breaks in plasmid DNA in solution

   3d. Research on cell lethality and mutagenesis

<u>Radiobiological processes</u>

Ionization/excitation — Photoabsorption, Energy deposition

↓

Thermalization (deactivation) — Spatial distribution

↓

Radicals (water)

↓

Biomolecule radicals

↓

Stable molecular changes (damage)

↓

Repair

↓

Biological effects

Action of ^{60}Co - γ rays

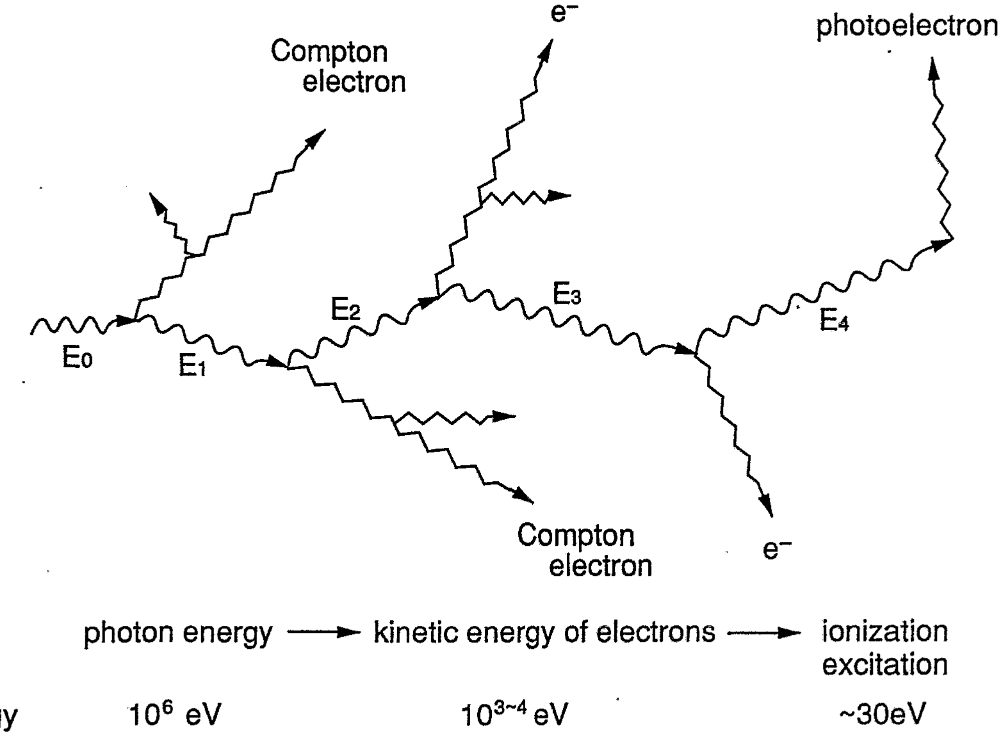

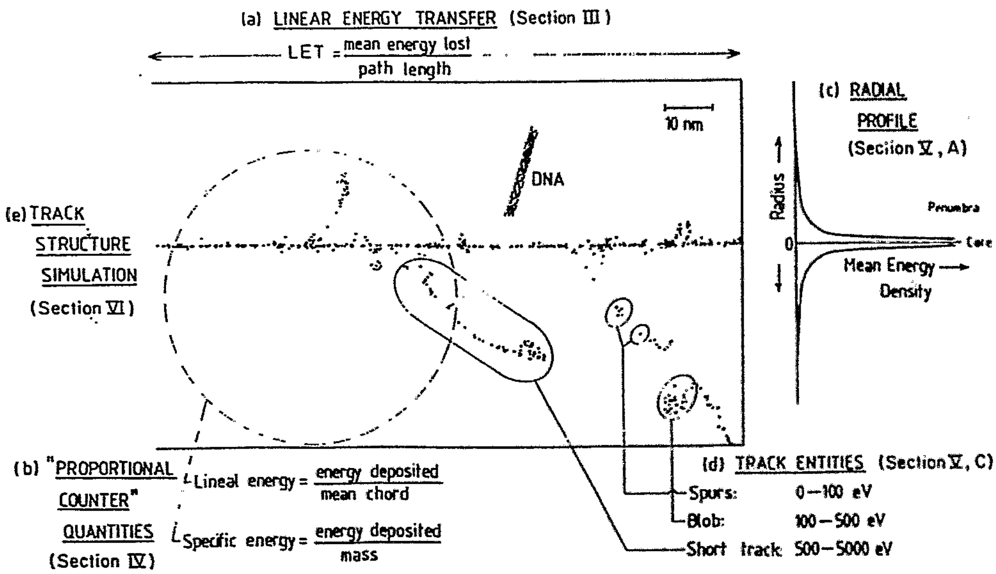

Fig. 4. Alternative microscopic descriptions of radiation quality. The diagram shows the individual atomic interactions along a random 120-nm-long segment of the path of an 8-MeV α particle and various microdosimetric descriptions which can be applied to it. Delta rays with ranges as great as ~0.4 μm are possible from such an α particle. Shown for comparison is a DNA double helix (diameter 2 nm) on the same scale.

Energy deposition by high energy particles

Amount of energy per deposition event has wide variety.

Energy deposition by monochromatic photons

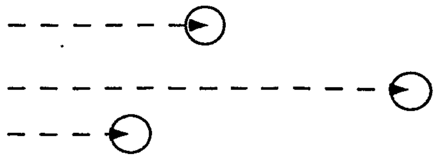

Vacuum UV photons
No photoelectrons

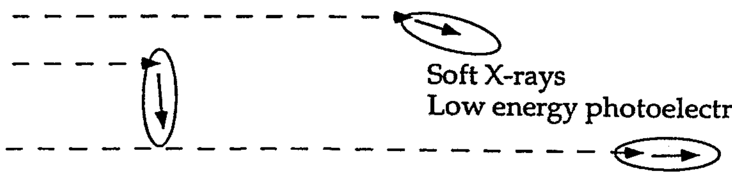

Auger effects after inner shell photoabsorption.
Several Auger electrons from the atom

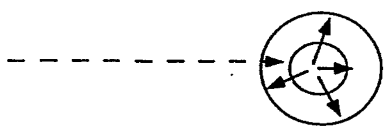

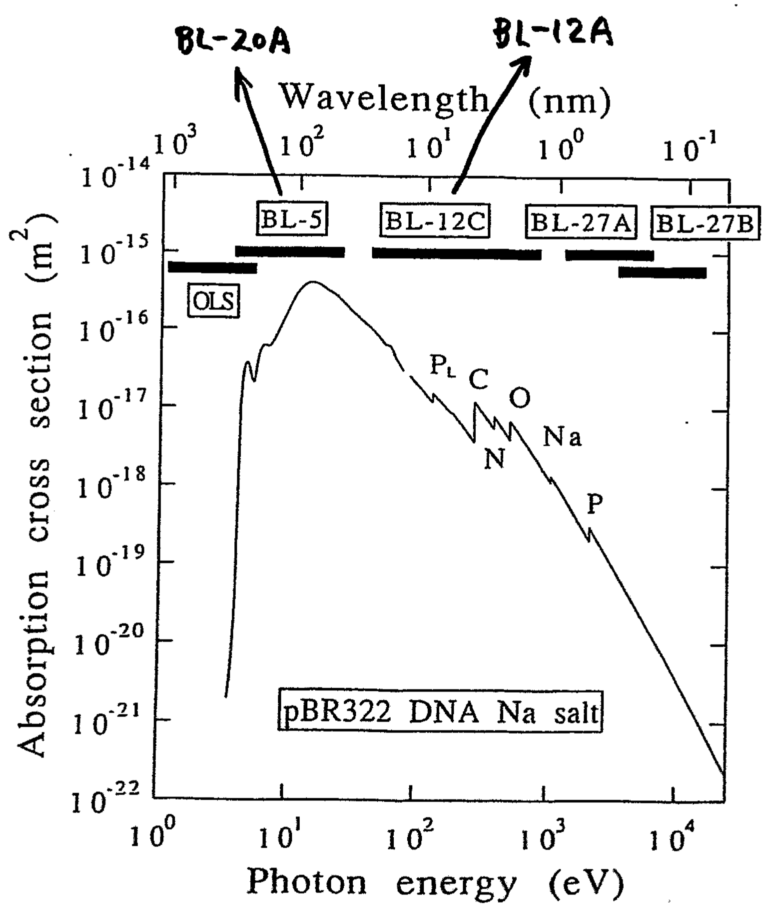

Characteristics of synchrotron radiation (SR)

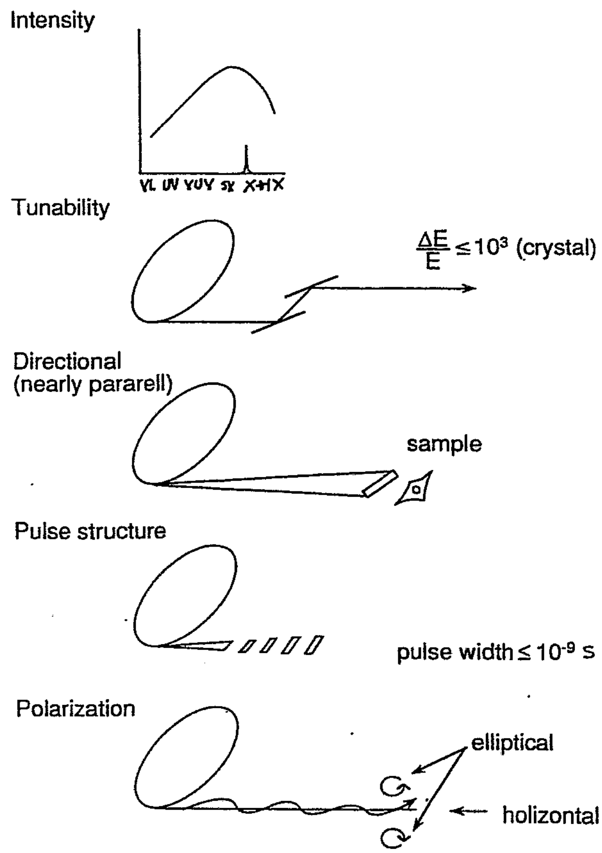

放射光実験施設配置図
Plan View of the Photon Factory

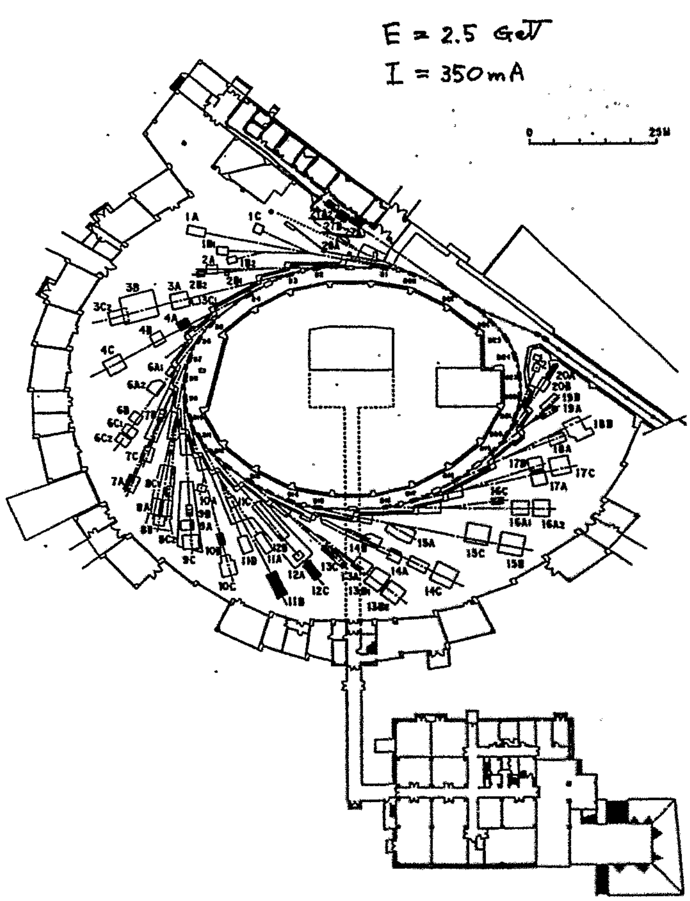

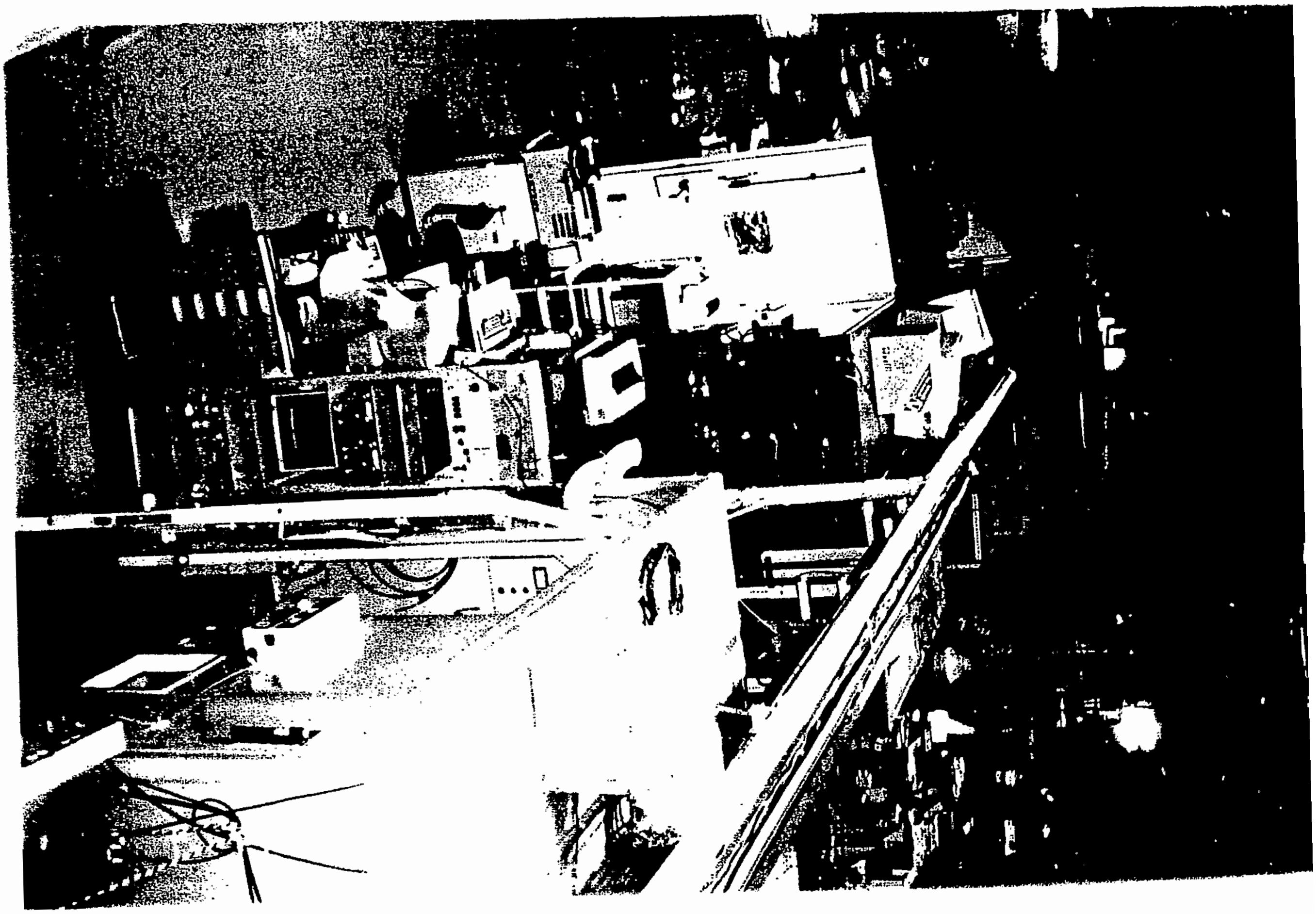

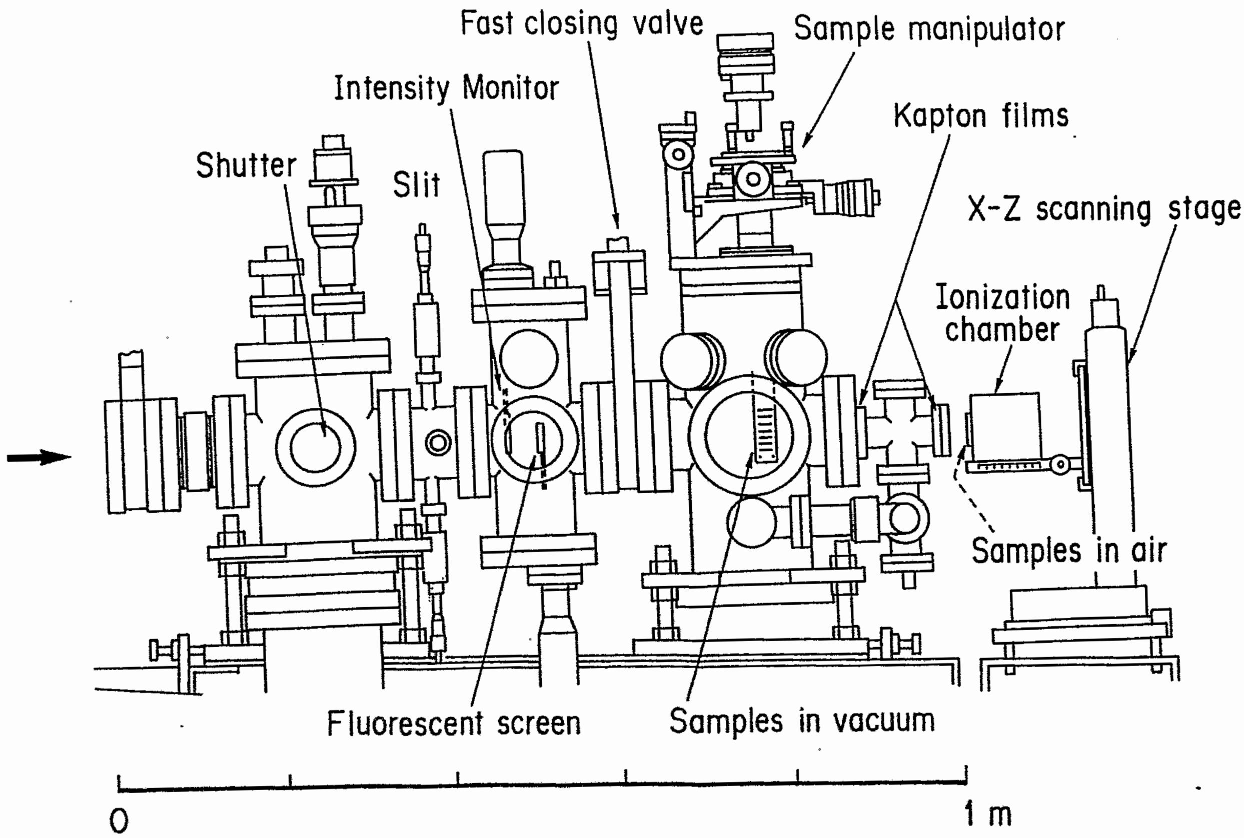
Fast closing valve
Sample manipulator
Intensity Monitor
Kapton films
Shutter
Slit
X-Z scanning stage
Ionization chamber
Samples in air
Fluorescent screen
Samples in vacuum
0
1 m

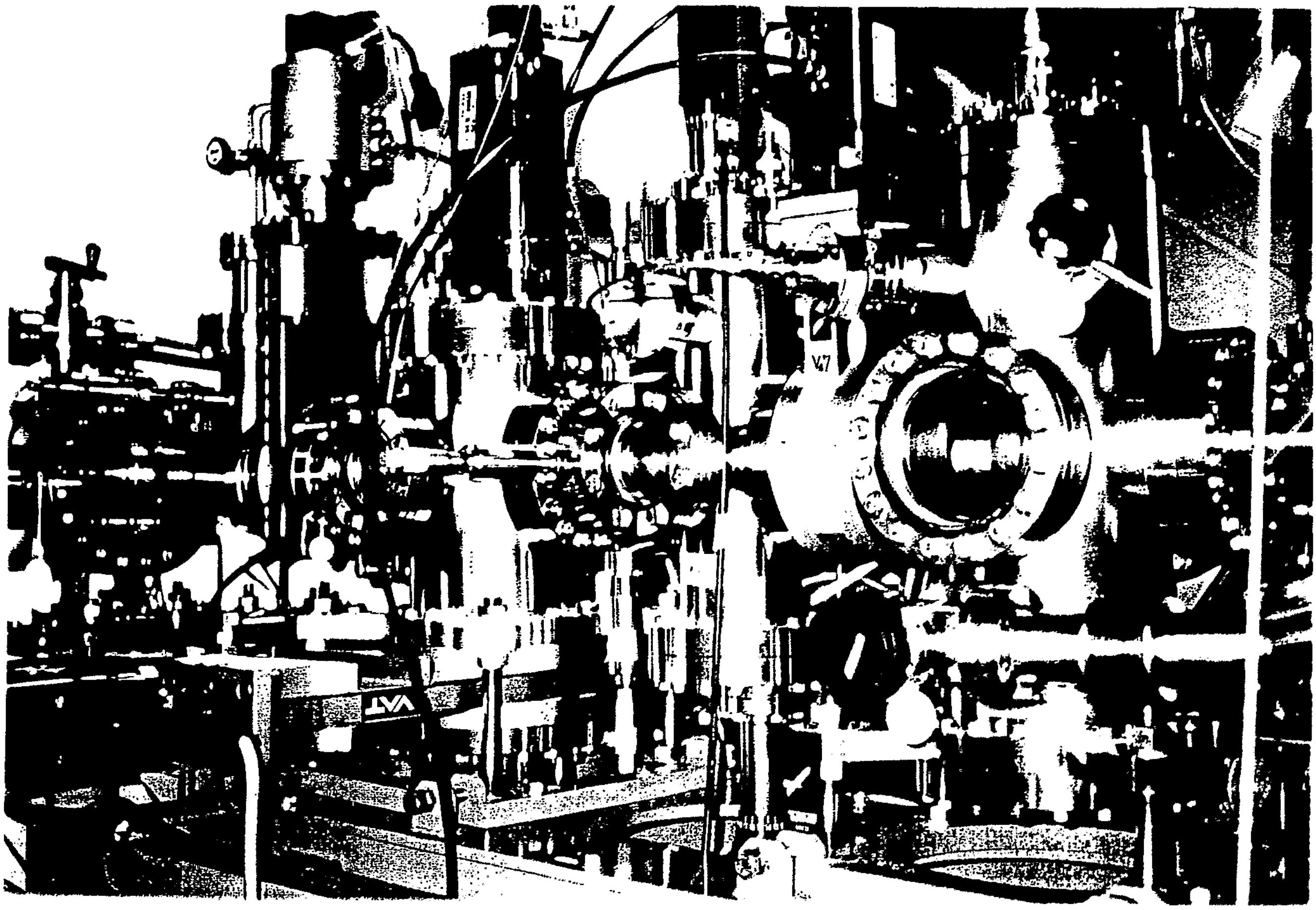

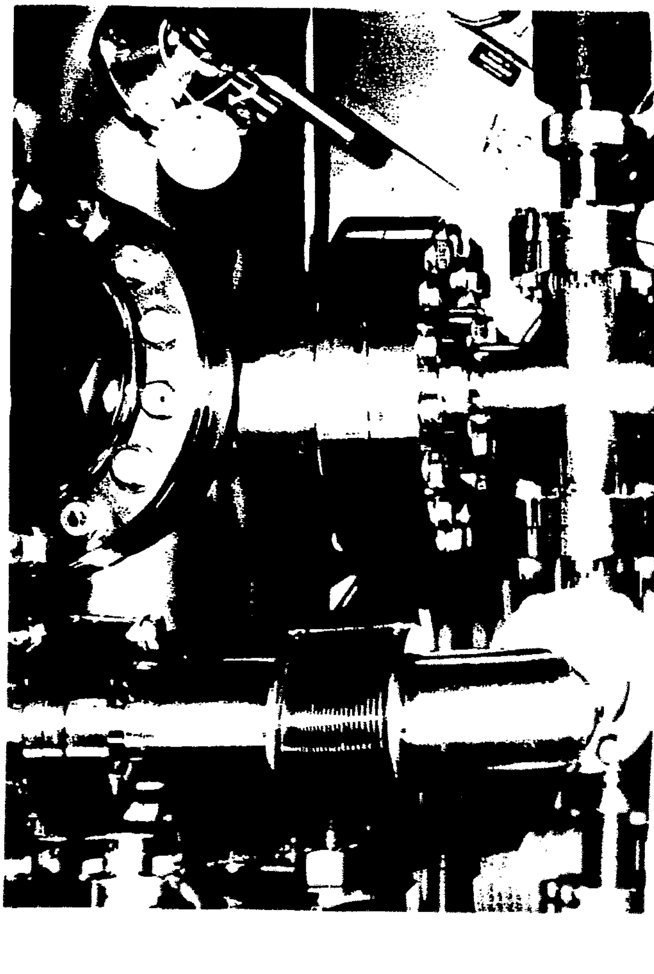

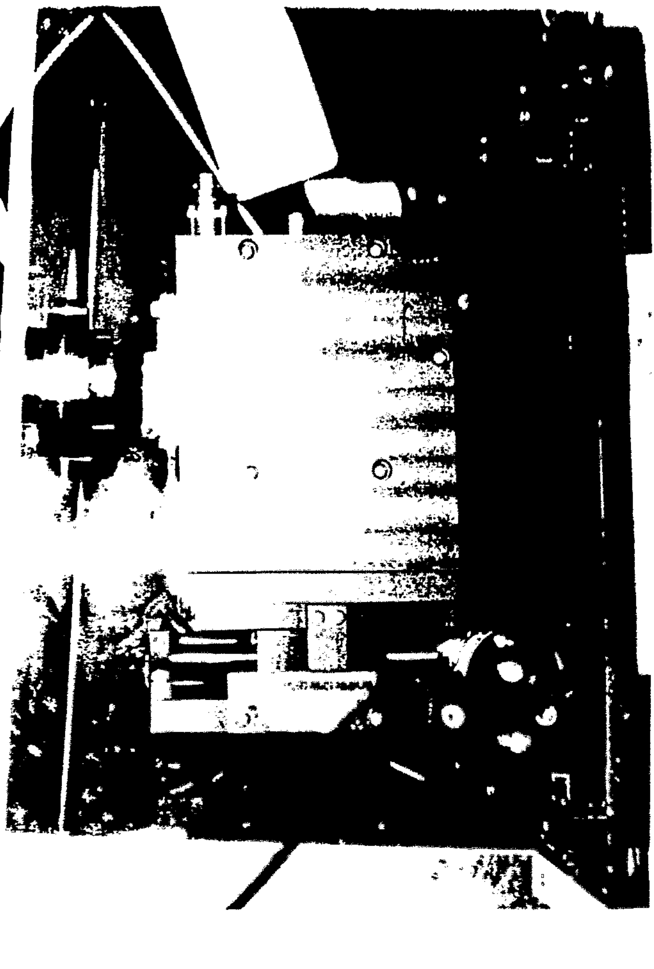

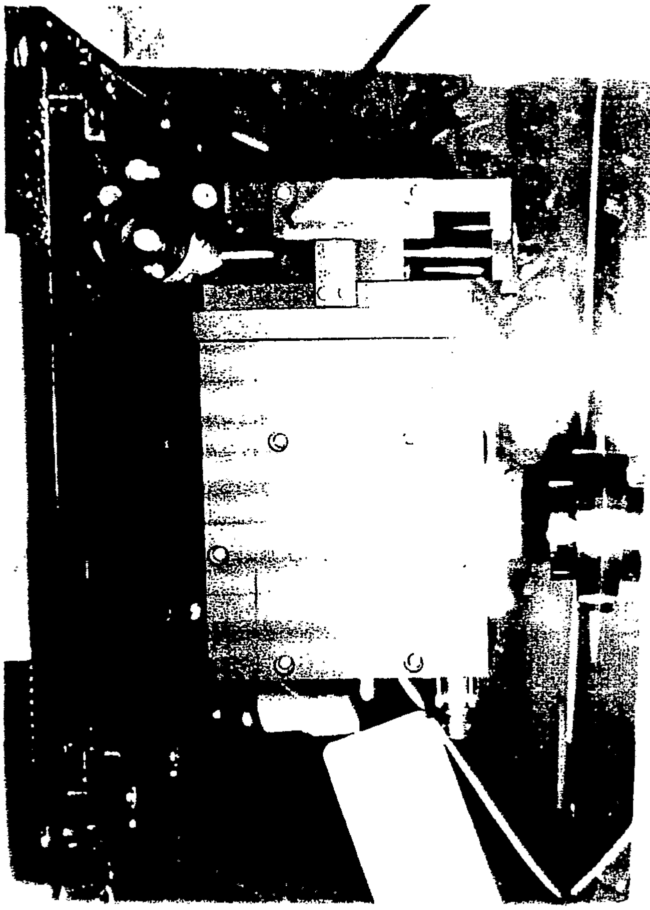

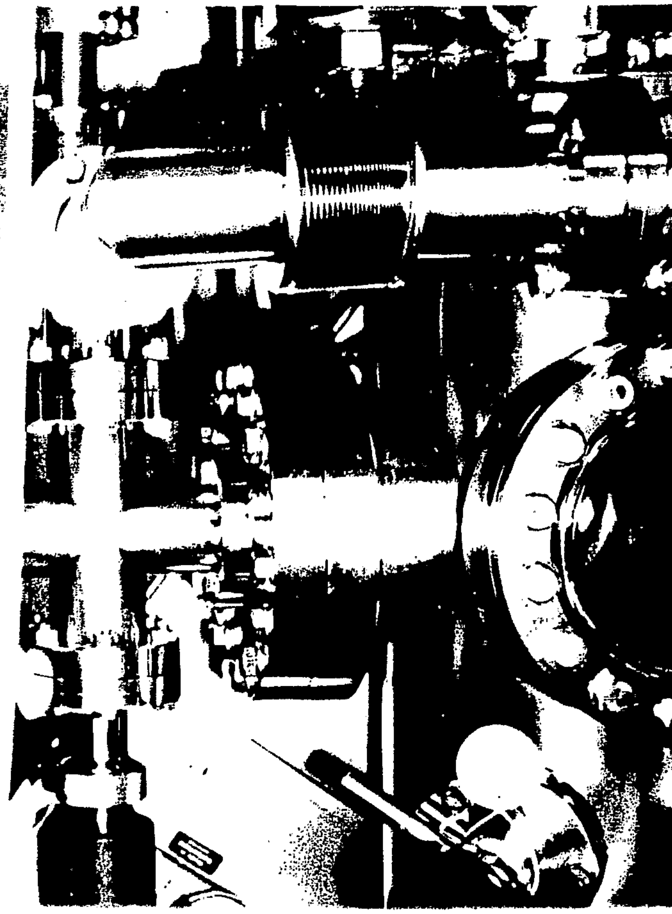

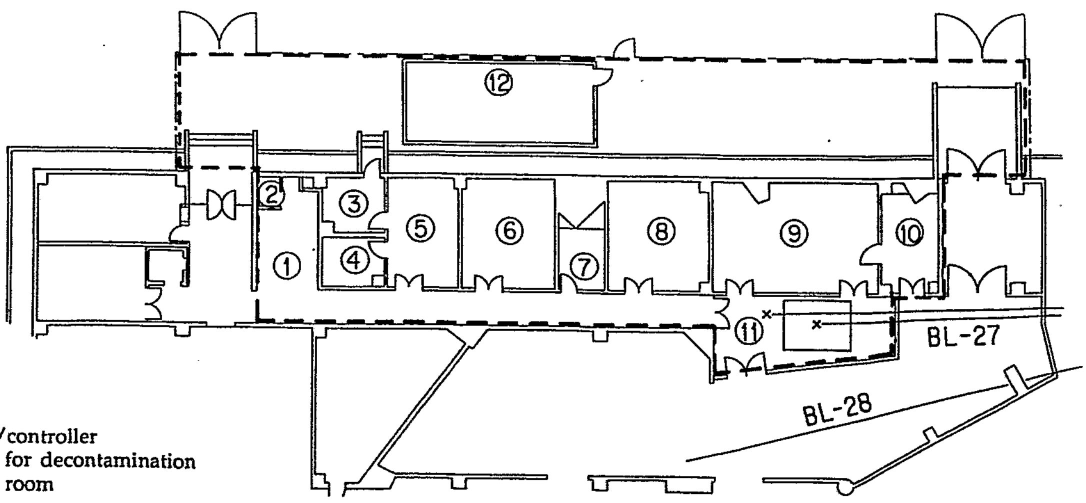

1. Gate monitor/controller
2. Shower room for decontamination
3. Waste storage room
4. Image process room
   Fluorescence microscopy, Cooled CCD camera, Image data analyzer (Mac quadra 950)
5. Radioisotope handling room
   Autoclaves(2)
6. Mammalian cell laboratory
   CO_2 incubators(3), Clean benches(3), Microscopes(2), Coulter counter, Low-temp centrifuge, Shakers(2), Refrigerator
7. Storage room for radioisotopes
8. Micro-organism laboratory
   Incubators(4), Shakers(3), Microscope, Centrifuge, Balances(2), Refrigerators(2)
9. Biochemistry laboratory
   Ultracentrifuge, HPLC system, Electrophoresis apparatuses(4), Ice-maker, Deep freezer, Drying sterilizer, Spectrophotometer
10. Radioisotope measurement room
    Liquid scintillation counter, Gas flow counter
11. Experimental station for irradiation
12. Sewer tanks

plasmid DNA

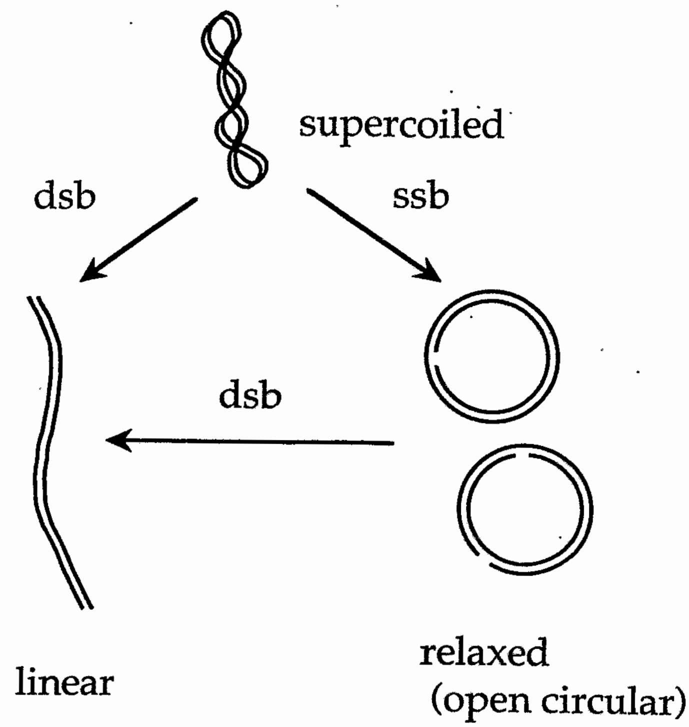

$$f_{sc}(D) = e^{-(b_{ssb} + b_{dsb})D}$$

$$f_{lin}(D) = b_{dsb}\, D\, e^{-b_{dsb}D}$$

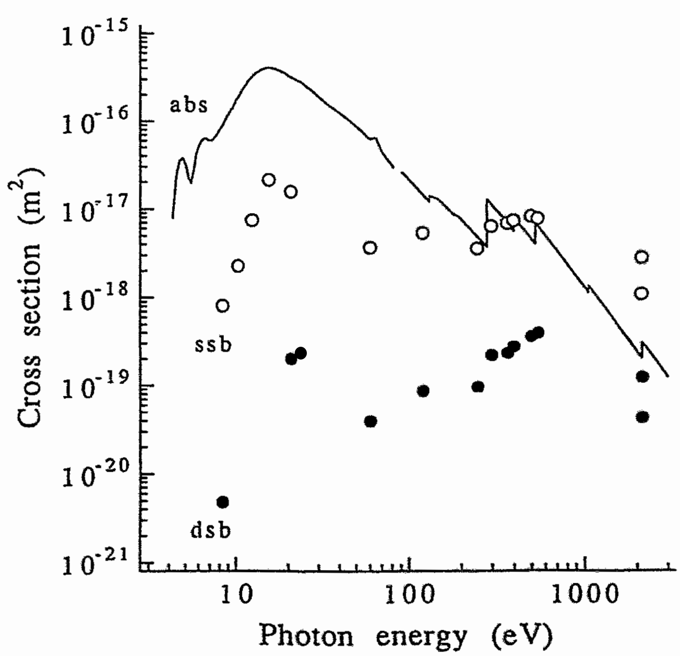

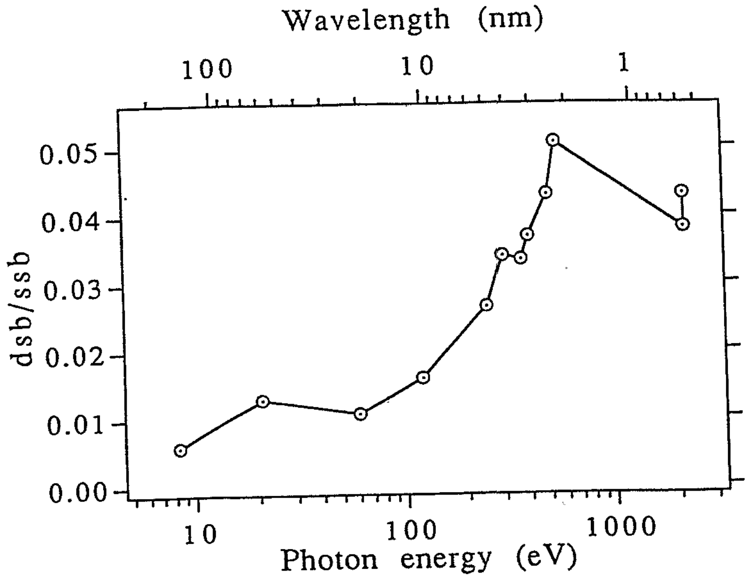

Molecules tested

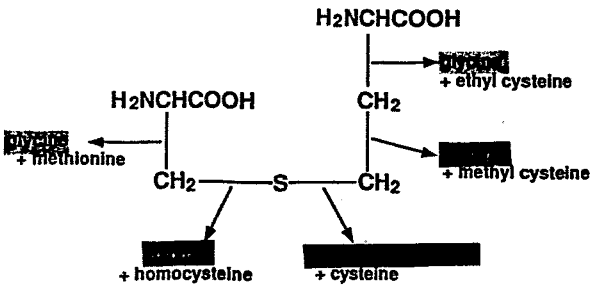

Cystathionine

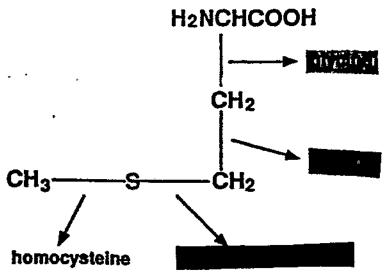

Methionine

Absorption spectrum of cystathionine
around K-shell absorption edge of sulfur

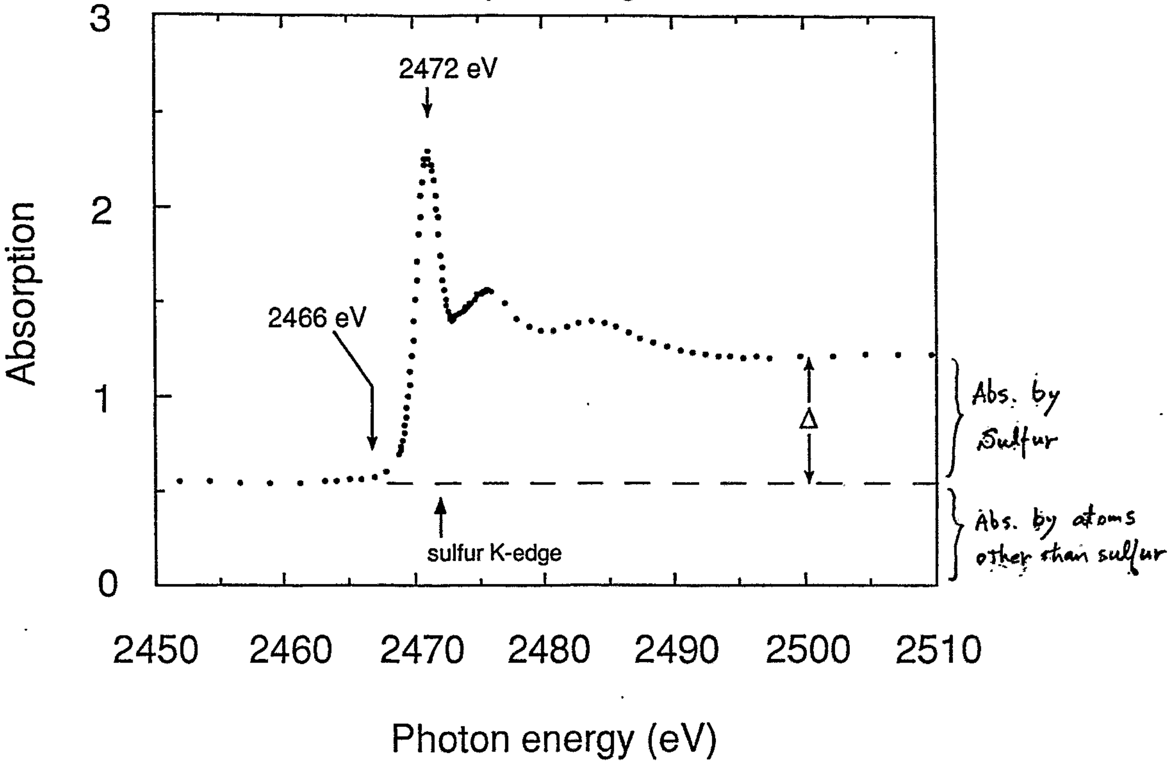

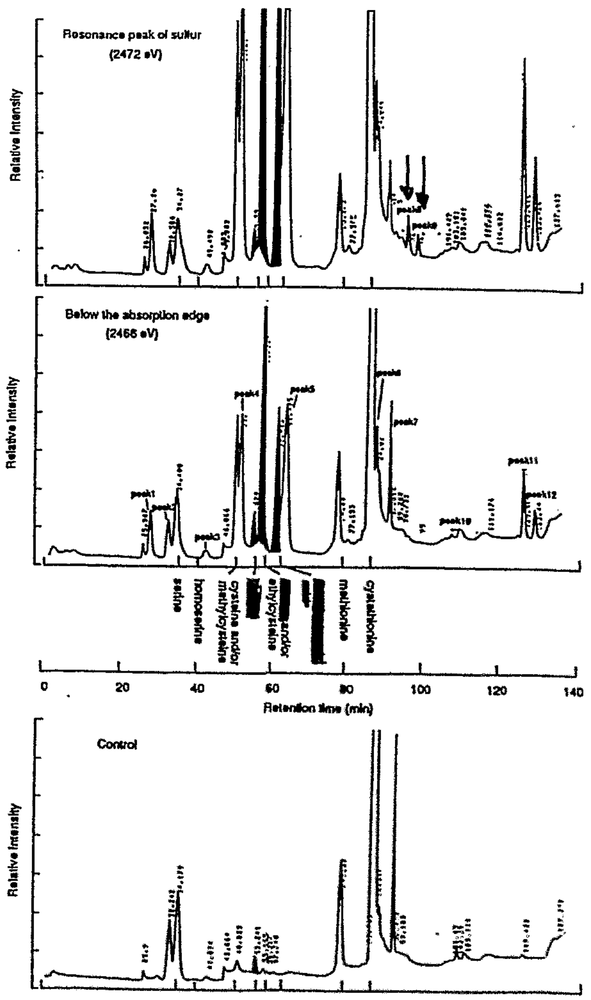

Production efficiencies (pmol/MR) of a-aminobutyric acid and glycine from cystathionine and methionine irradiated at the X-ray energies of 2472 eV and 2466 eV. Efficiencies for alanine was calculated by assuming the peak of alanine and/or ethylcysteine contains alanine only.

Product	Cystathionine		Methionine	
	2472 eV	2466 eV	2472 eV	2466 eV
α-Aminobutyric acid	38	13	41	11
Glycine	1.2	1.0	1.9	0.77
Alanine	75	28	n.d.	n.d.

n.d. : not detected

photoelectron

X-ray photon

H_2O

Photoelectric effect

$$E_{el} = E_{h\nu} - I$$

Oxygen K-shell $I \sim 0.5\,keV$

LET along the electron tracks of different energies

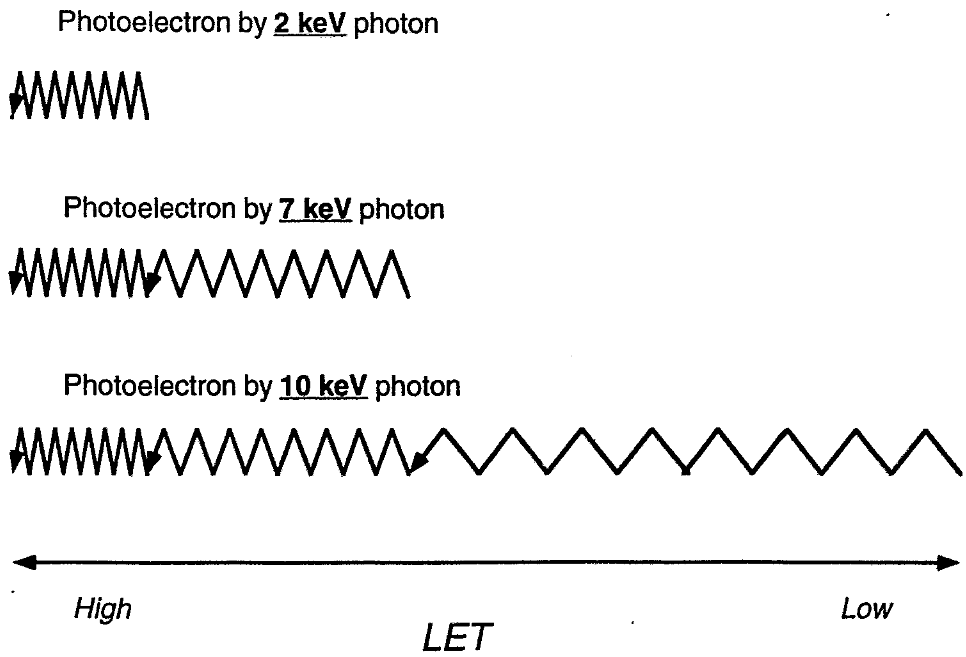

Fricke Dosimeter

1 mM Fe^{2+}
0.8 N H_2SO_4
pH 0.4

$$G(Fe^{3+}) = g(OH) + 3g(e^-_{aq}) + 3g(H) + 2g(H_2O_2)$$

Oxidation yield of Fe^{2+} to Fe^{3+}: (γ-ray)
15.6 ions per absorbed energy of 100 eV

Increase of Fe^{3+} :
Detected with absorption at 304 nm

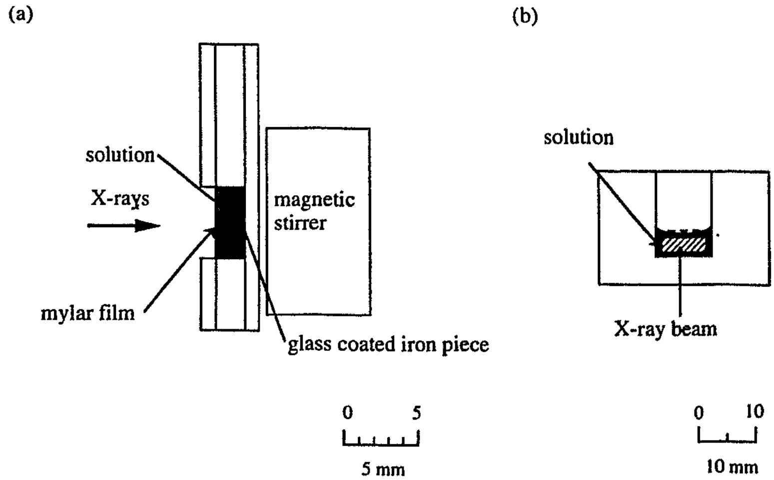
(a)
solution
X-rays
magnetic
stirrer
mylar film
glass coated iron piece
0
5
5 mm
(b)
solution
X-ray beam
0
10
10 mm

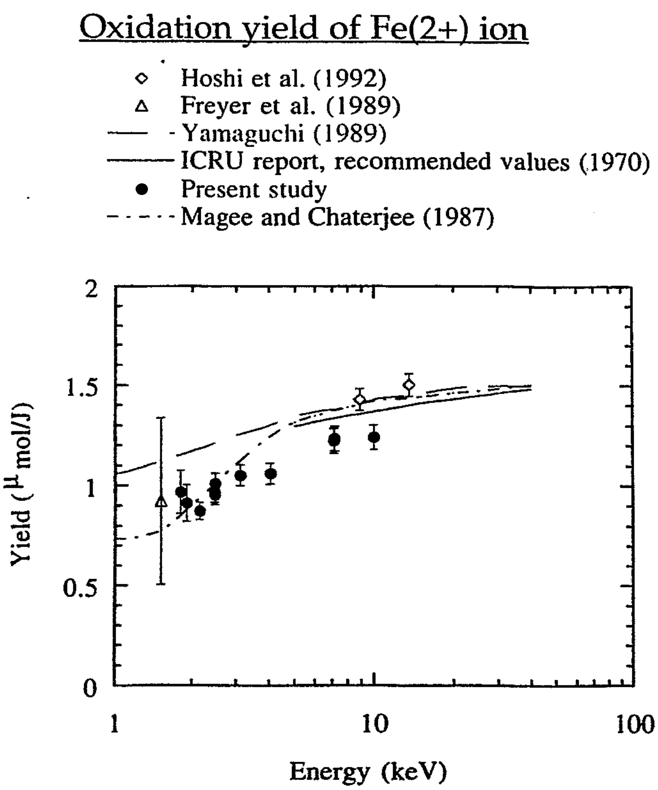
Oxidation yield of Fe(2+) ion
Hoshi et al. (1992)
Freyer et al. (1989)
Yamaguchi (1989)
ICRU report, recommended values (1970)
Present study
Magee and Chaterjee (1987)
Yield (μ mol/J)
Energy (keV)
0
0.5
1
1.5
2
1
10
100

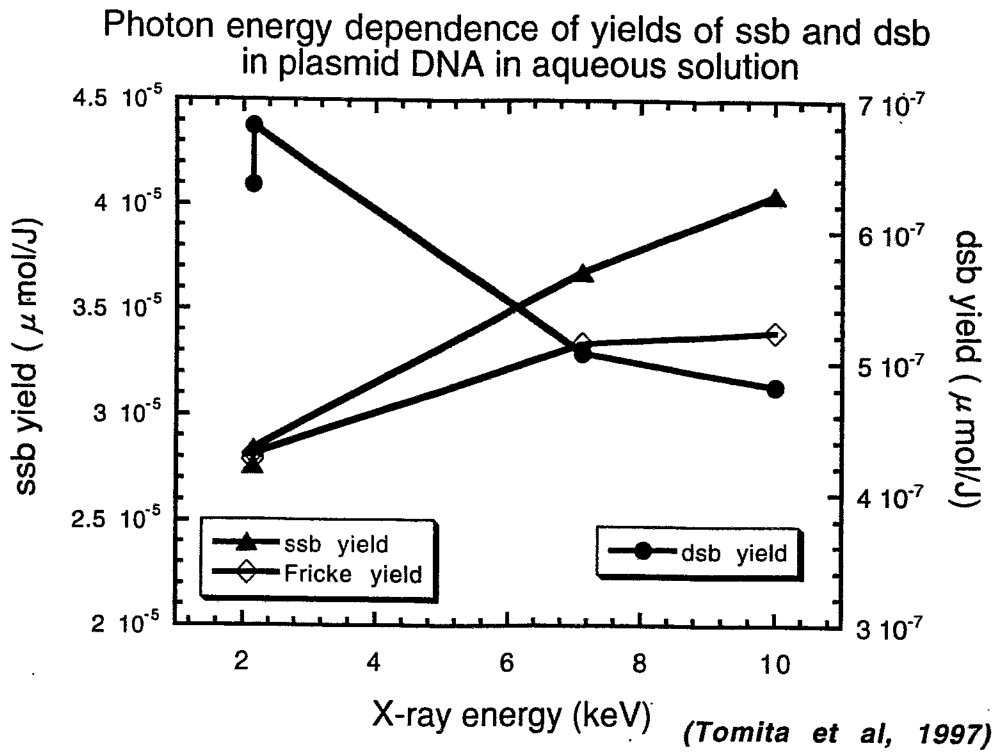

(Tomita et al, 1997)

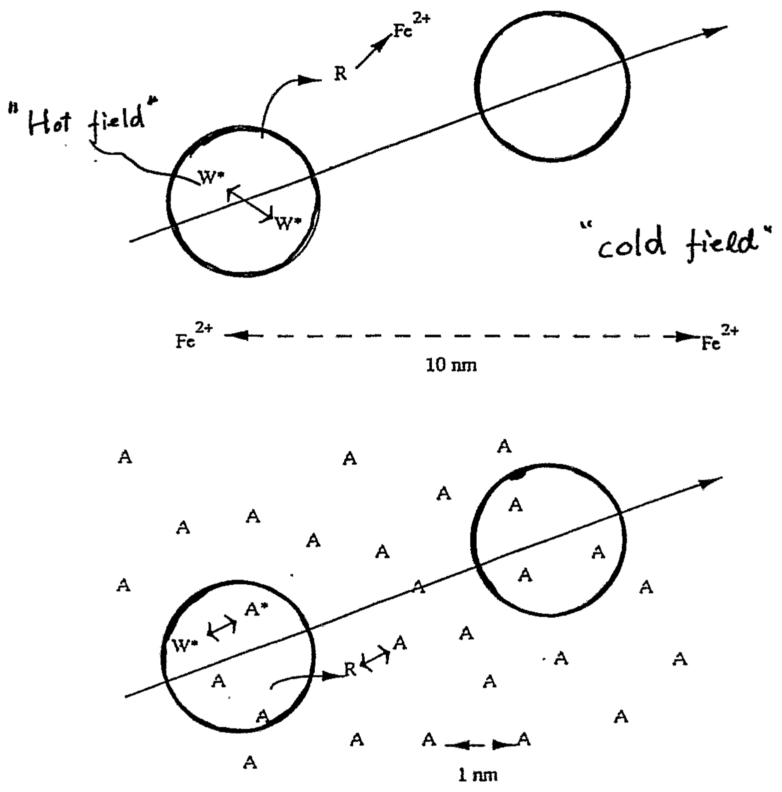

"Hot field" and "Cold field".
"Hot field" is produced transiently along the trajectory of charged particles. In highly concentrated solution, solute molecules exist in "Hot field", and can participate into the reactions between radicals.
W* or R : water radicals, Fe^{2+}: ferrous ion in Fricke solution, A: ATP molecule

LET along the electron tracks of different energies

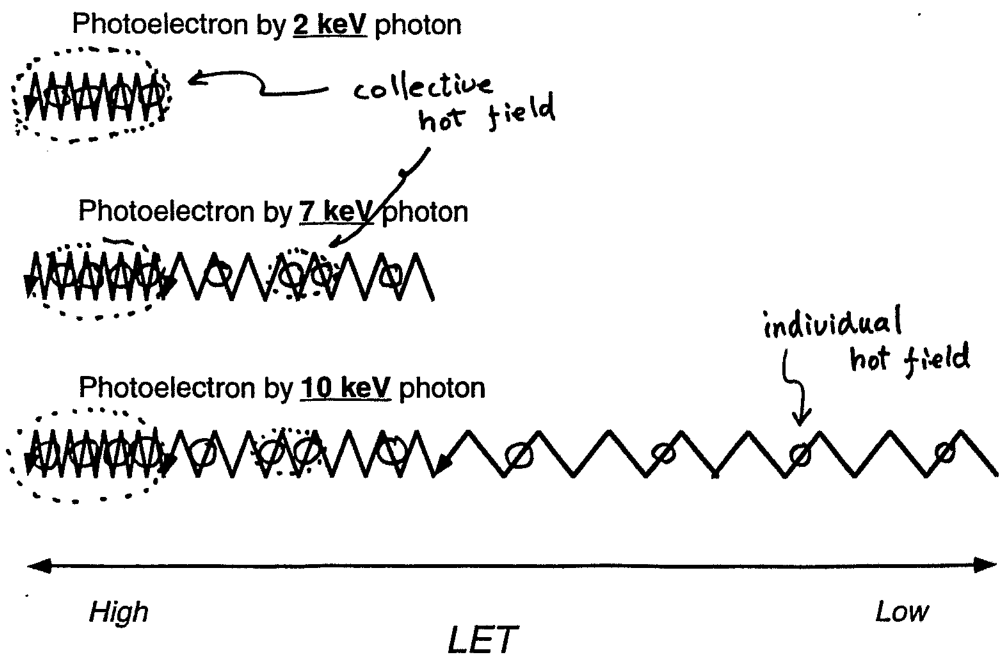

Absorption spectrum of DNA film around the K-shell absorption edge of Phosphorus. (Kobayashi et al., 1991)

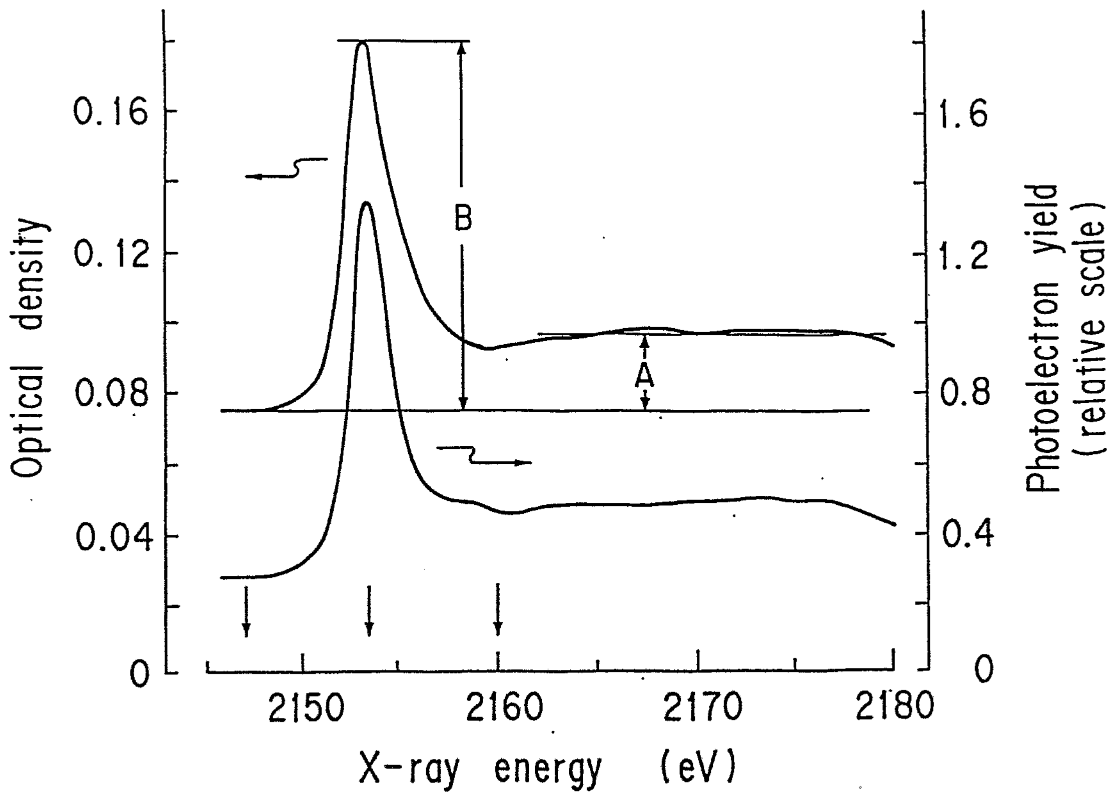

Biological effects of phosphorus photoabsorption on yeast cells.

a) Lethal effect

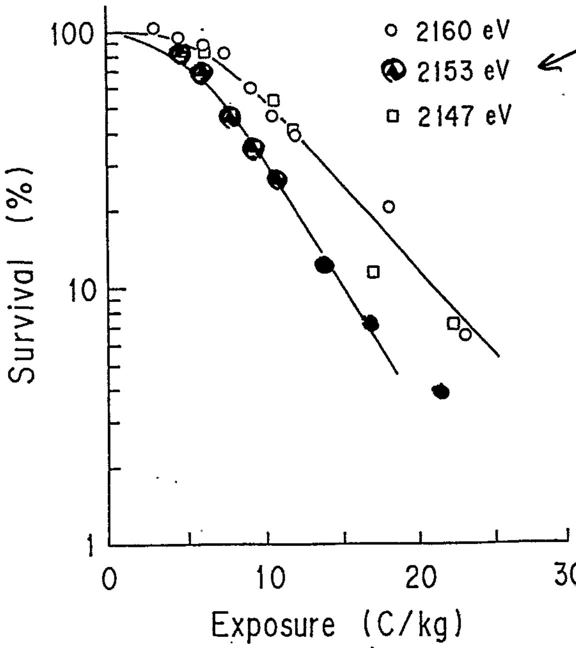

b) Induction of genetic changes

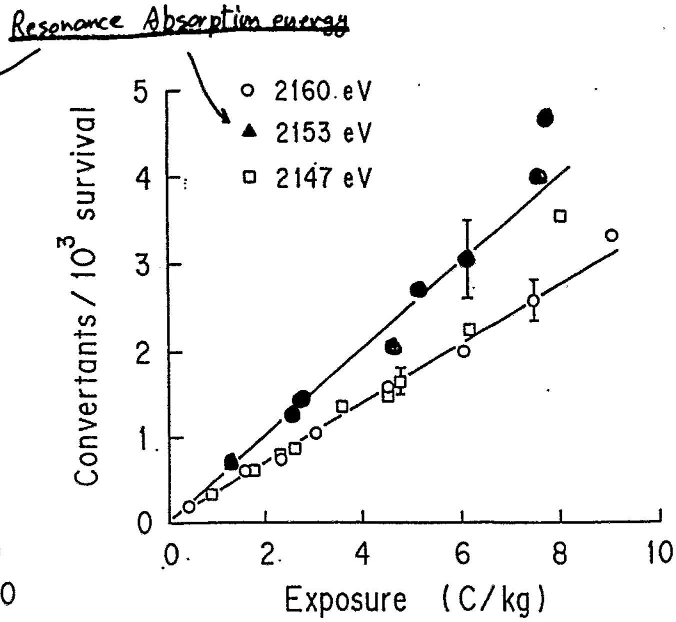

(Kobayashi et al., 1991)

Induction of excess fragments of chromosome by monochromatic soft X-rays around K-shell absorption edge of phosphorus.
-Lesions irreparable by post-irradiation incubation-

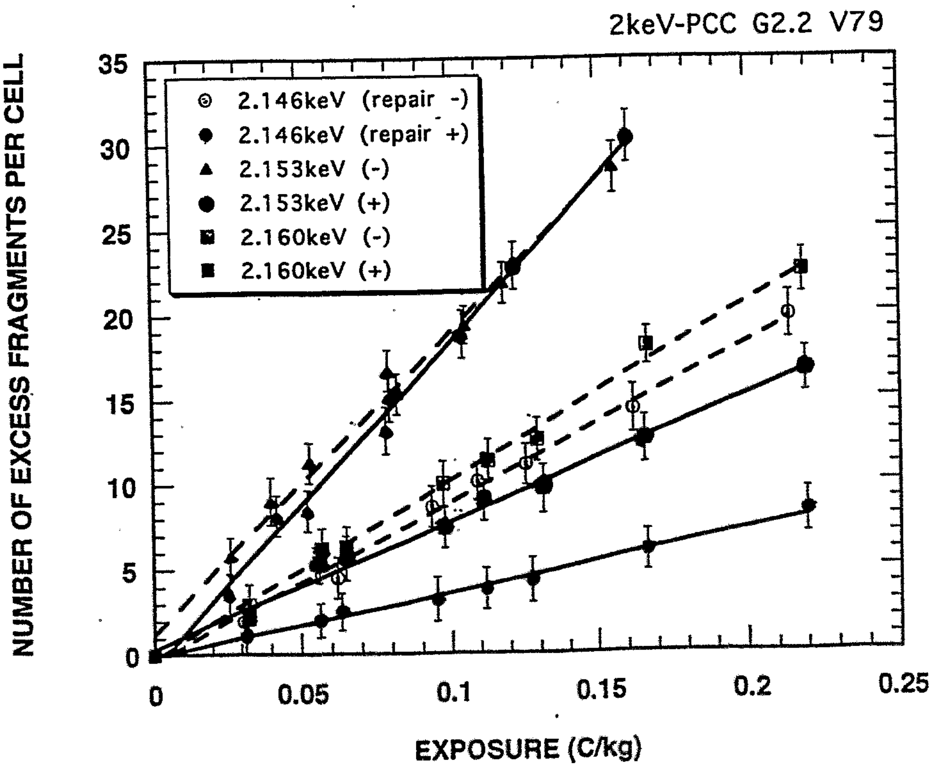

W. Thomlinson:

Synchrotron medical imaging: From amplitude to phase

ESRF

Synchrotron Medical Imaging: From Amplitude to Phase

W. Thomlinson
ESRF
Grenoble, France

ESRF

SYNCHROTRON BRILLIANCE AND ESRF FLUX

Brilliance of the X-ray beams
(photons / s / mm² / mrad² / 0.1% BW)

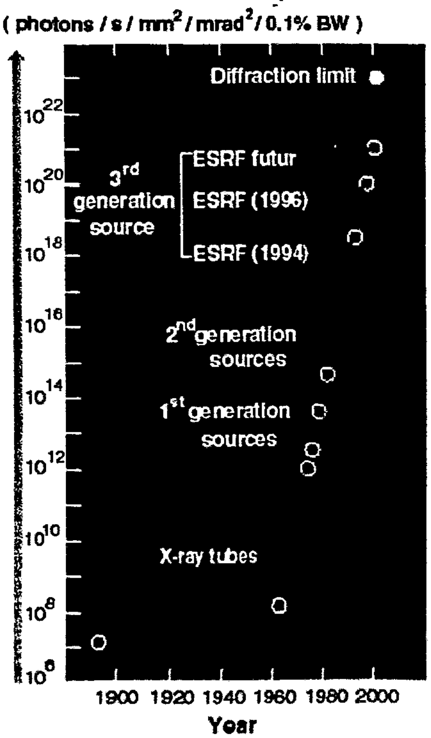

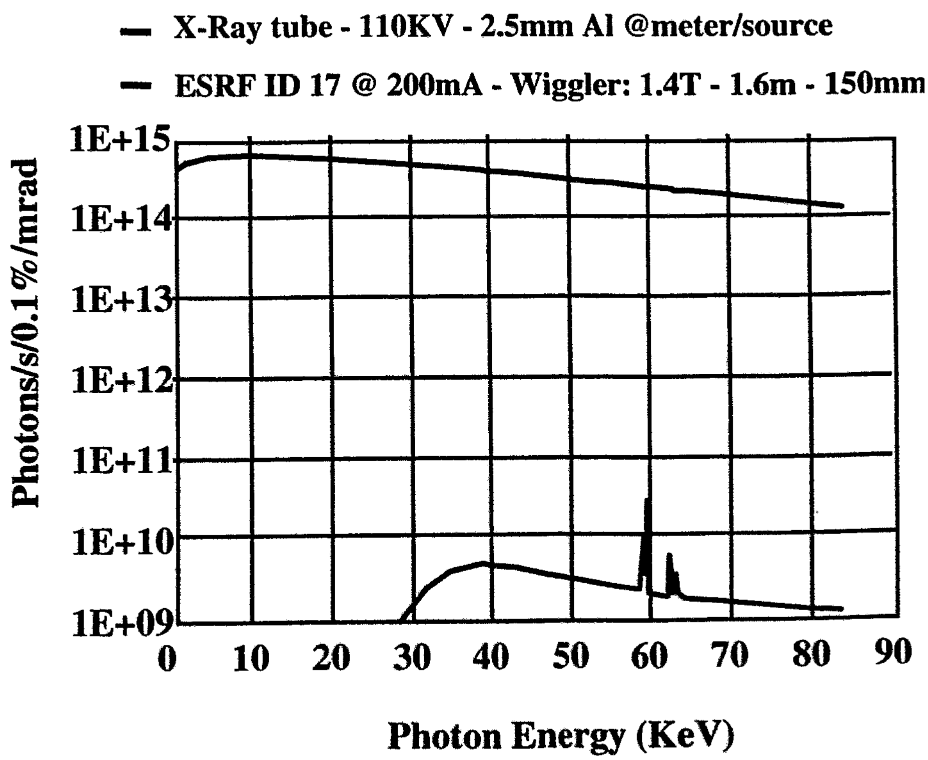

ESRF

DUAL-ENERGY K-EDGE SUBTRACTION

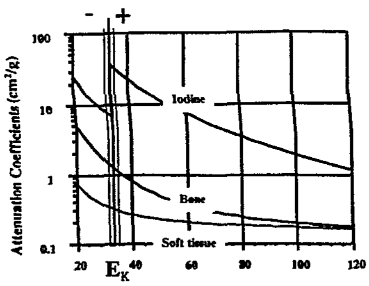

TWO EQUATIONS - TWO UNKNOWNS

$$I_\pm = I_0\left[e^{-\left(\frac{\mu}{\rho}\right)_I^\pm(\rho t)_I} * e^{-\left(\frac{\mu}{\rho}\right)_T^\pm(\rho t)_T}\right]$$

$$-\ln\left(\frac{I_\pm}{I_0}\right) = \left(\frac{\mu}{\rho}\right)_I^\pm(\rho t)_I + \left(\frac{\mu}{\rho}\right)_T^\pm(\rho t)_T$$

Solution:

$$(\rho t)_I = \frac{\ln\left(\frac{I}{I_0}\right)^+ - \ln\left(\frac{I}{I_0}\right)^-}{\left(\frac{\mu}{\rho}\right)_I^+ - \left(\frac{\mu}{\rho}\right)_I^-}$$

With a similar equation for the soft tissue.

ESRF

AMPLITUDE AND PHASE

Complex Index of Refraction n in a medium:

$$\boxed{n = 1 - \delta + i\beta}$$

Plane wave: $e^{inkz} = e^{i(1-\delta)kz} \times e^{-\beta kz}$

$$k = \frac{2\pi}{\lambda}$$

Phase shift related to δ: $(1-\delta)$

Absorption related to β: $\mu = \frac{4\pi}{\lambda}\beta$

Energy Dependences:

$$\beta(E) = (hc/4\pi E)\mu(E) \sim O(E^{-4})$$

$$\delta = (r_0 h^2 c^2/2\pi E^2)N_0 f_R \sim O(E^{-2})$$

$$\boxed{\delta \approx 1.3x10^{-6}\rho\lambda^2 \sim 10^{-6}}$$

Refraction Angles:

$$\boxed{\alpha = \int_0^{t(y,z)} \frac{1}{n(x,y,z)}\frac{\partial n(x,y,z)}{\partial z}dx \sim \mu radians}$$

ESRF

PHASE/AMPLITUDE RATIO FOR LIGHT ELEMENTS

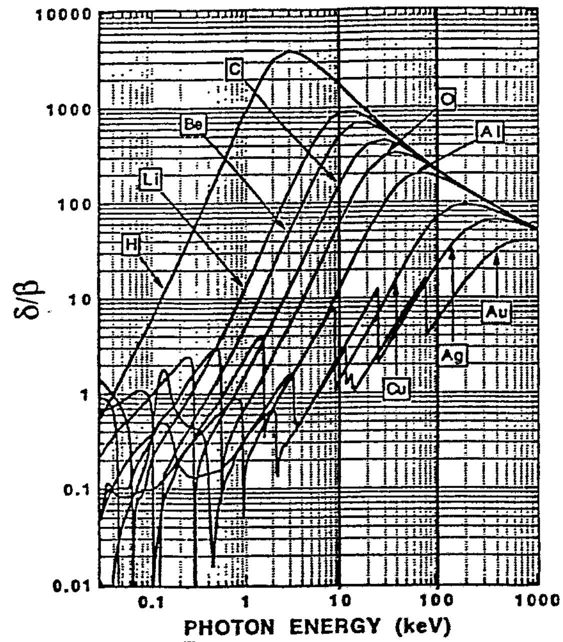

ESRF

"BIOMAN"
SR MEDICAL RESEARCH

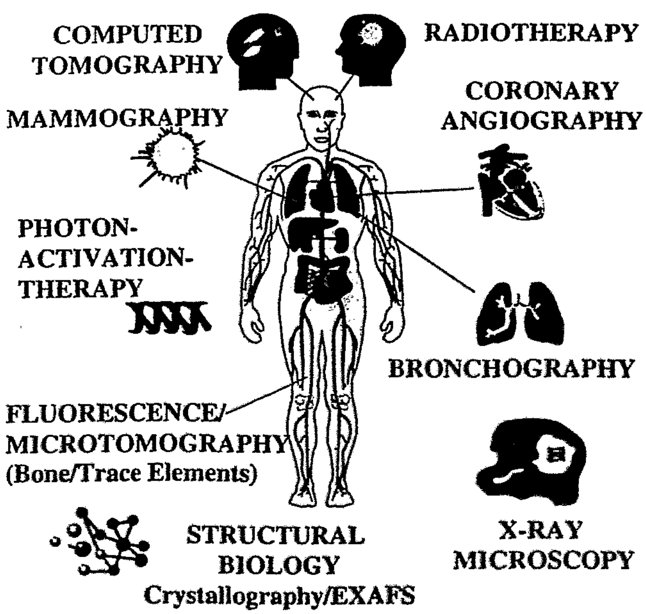

ESRF

Basic Configuration for Computed Tomography

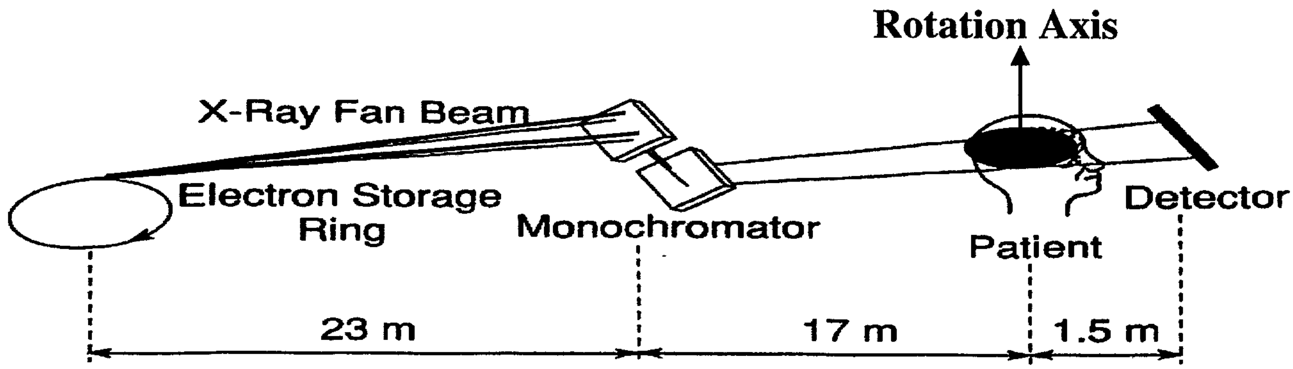

ESRF

Iodine and Gadolinium K-Absorption Edges

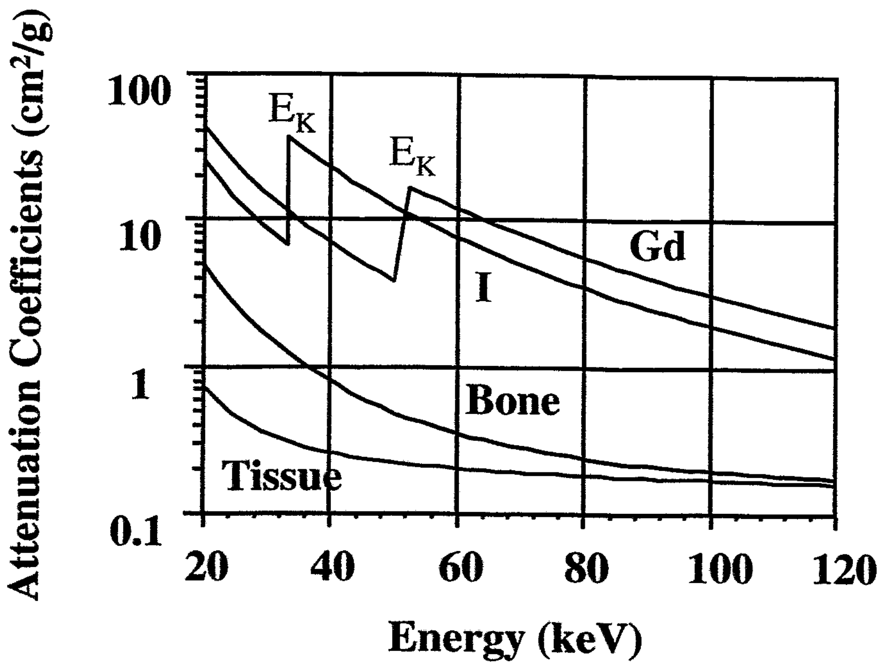

ESRF

CHU

Above

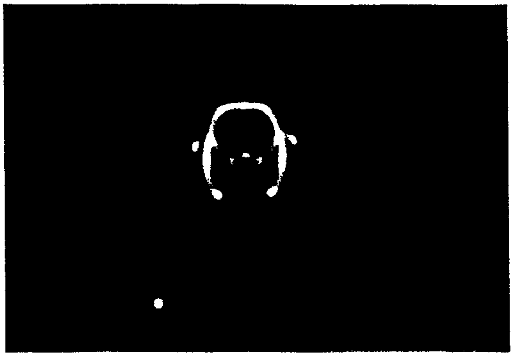

Below

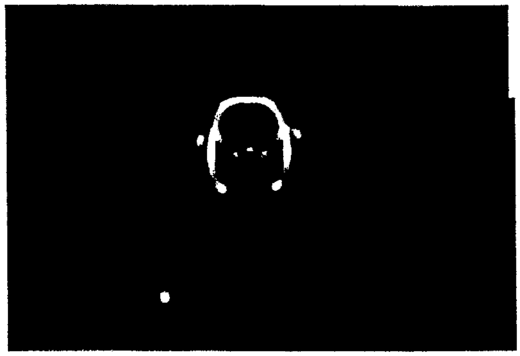

Subtraction

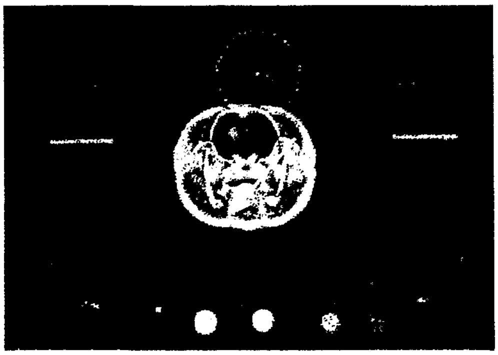

ESRF

SRCT images obtained on rats bearing glioma

CHU

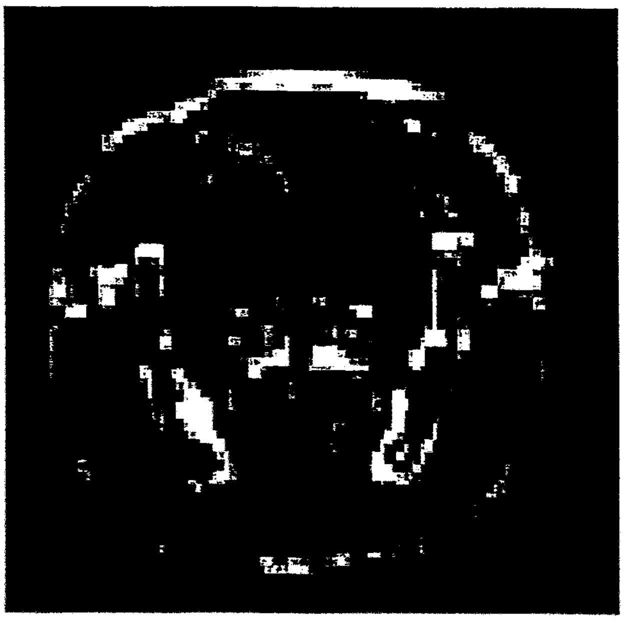

Iodine

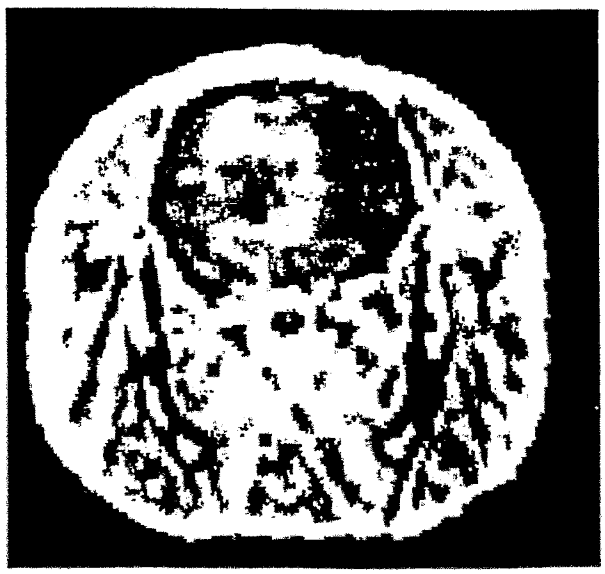

Gadolinium

SRCT images after gadolinium injection

Kinetic study on a rat brain bearing a glioma

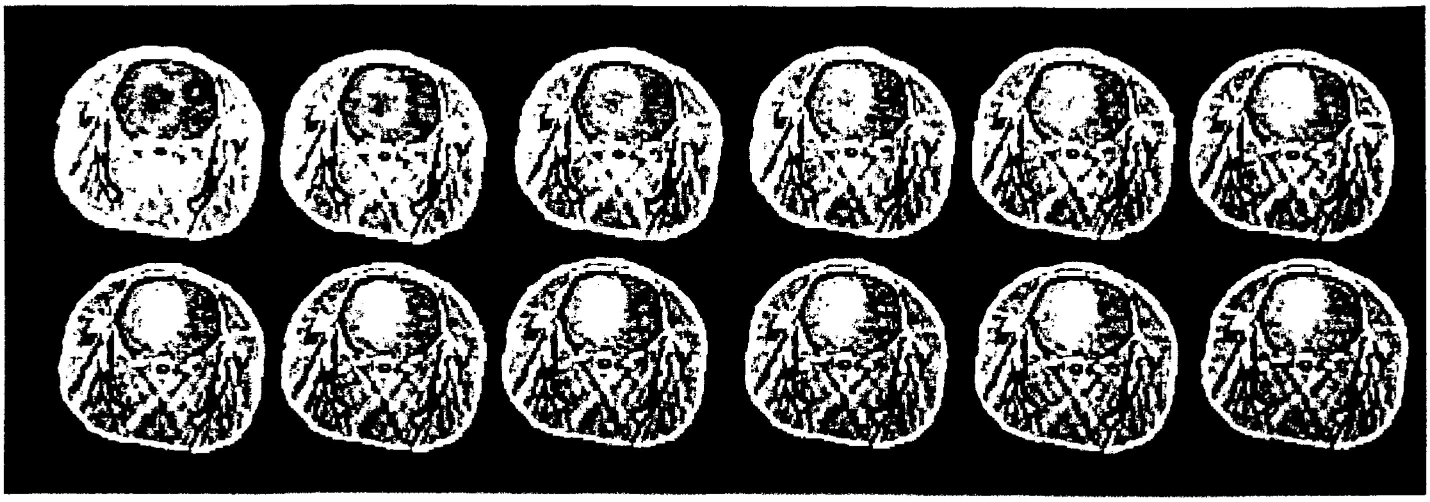

Iodine SRCT images

mg/cm³ (SD/mean %)

periphery	1.35 (15%)
center	0.6 (30%)
contralateral	0.17 (36%)

iodine *@ 4 ml/kg (X4)*

@ 23.3 mgI/ml

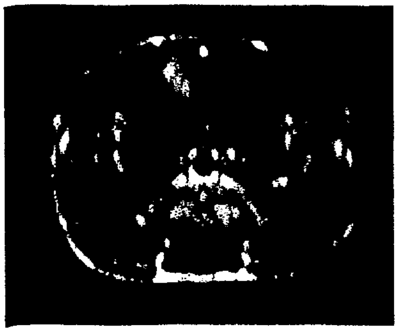

MRI

SRCT

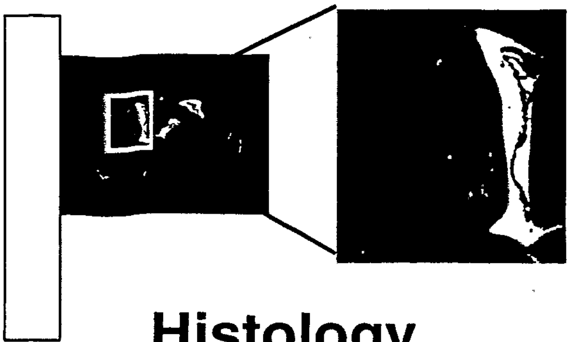

Histology

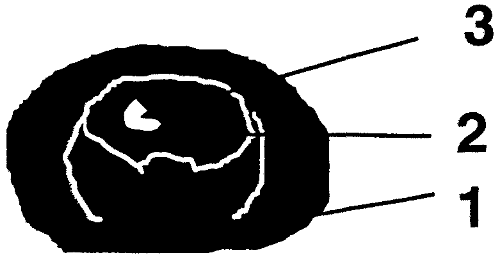

1. Skull, 2. Brain
3. Tumor contrast enhancement

THE LUNGS

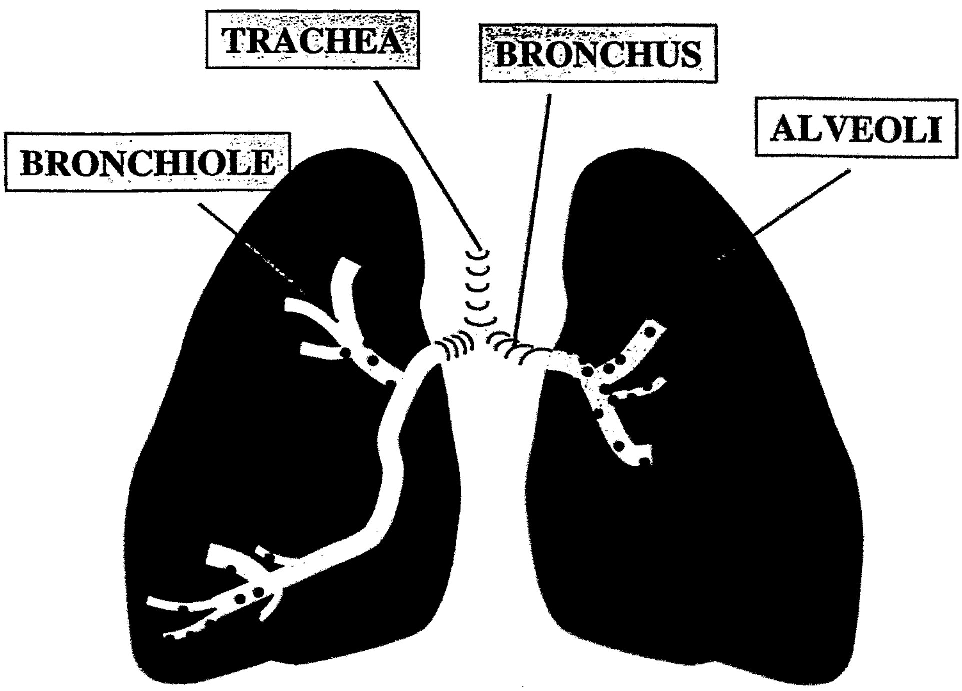

ESRF

Mass Attenuation Coefficient of Xe

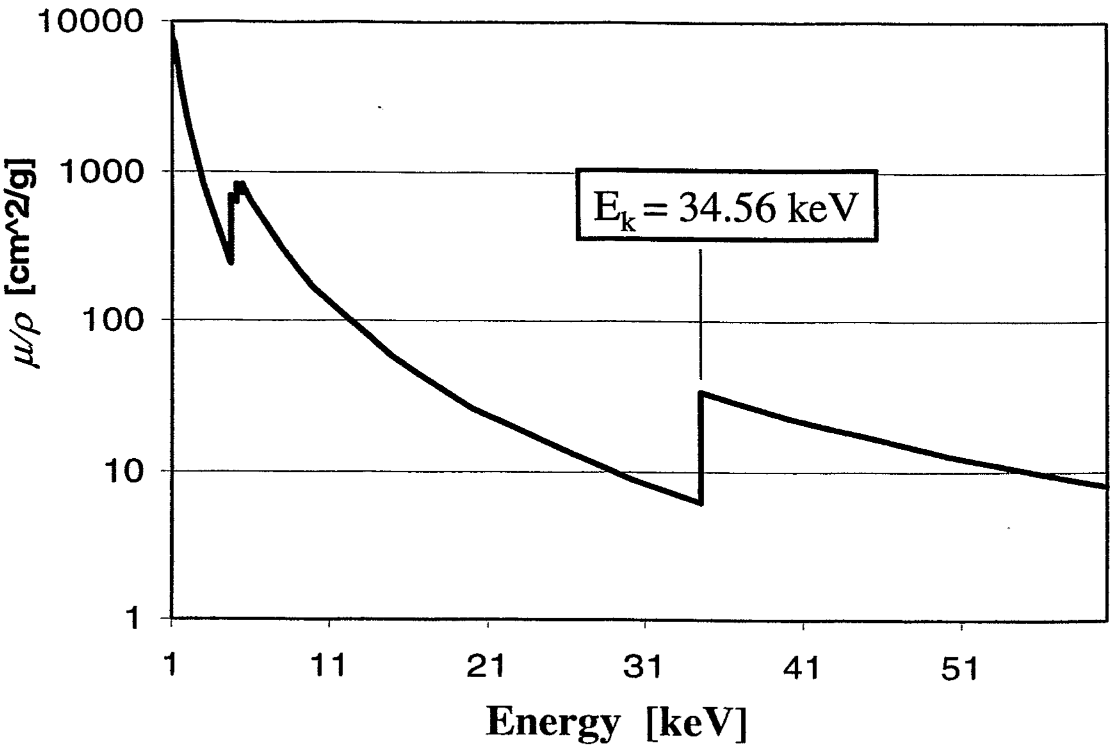

ESRF

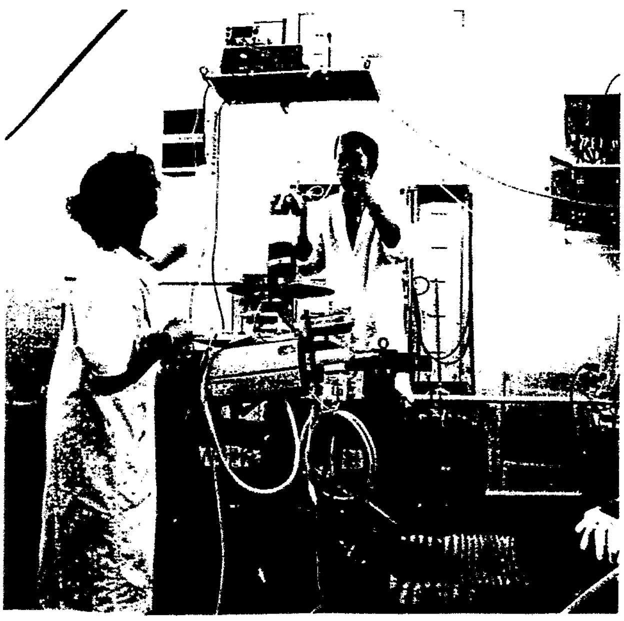

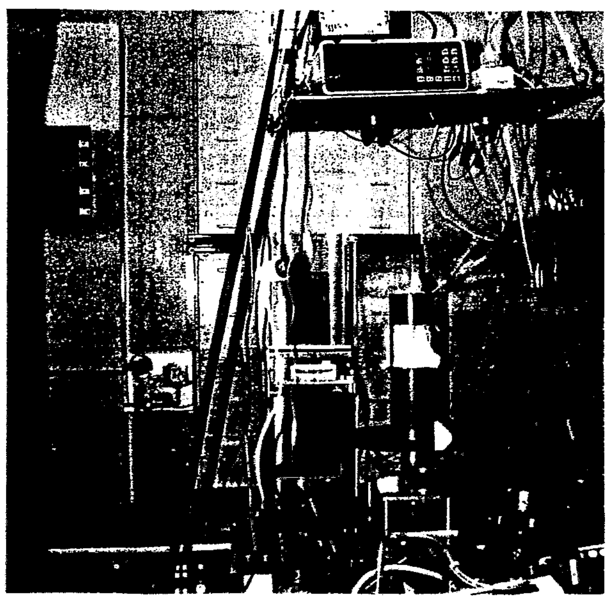

ESRF

Phantom120_scan4
image "tissue"

ESRF

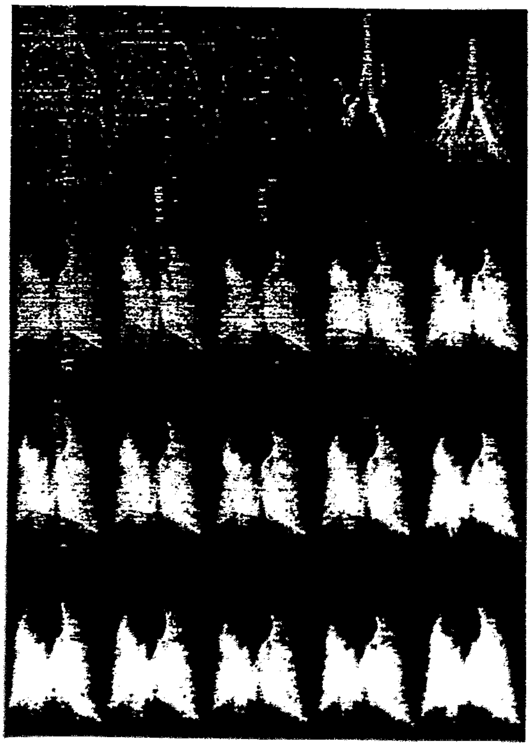

ESRF

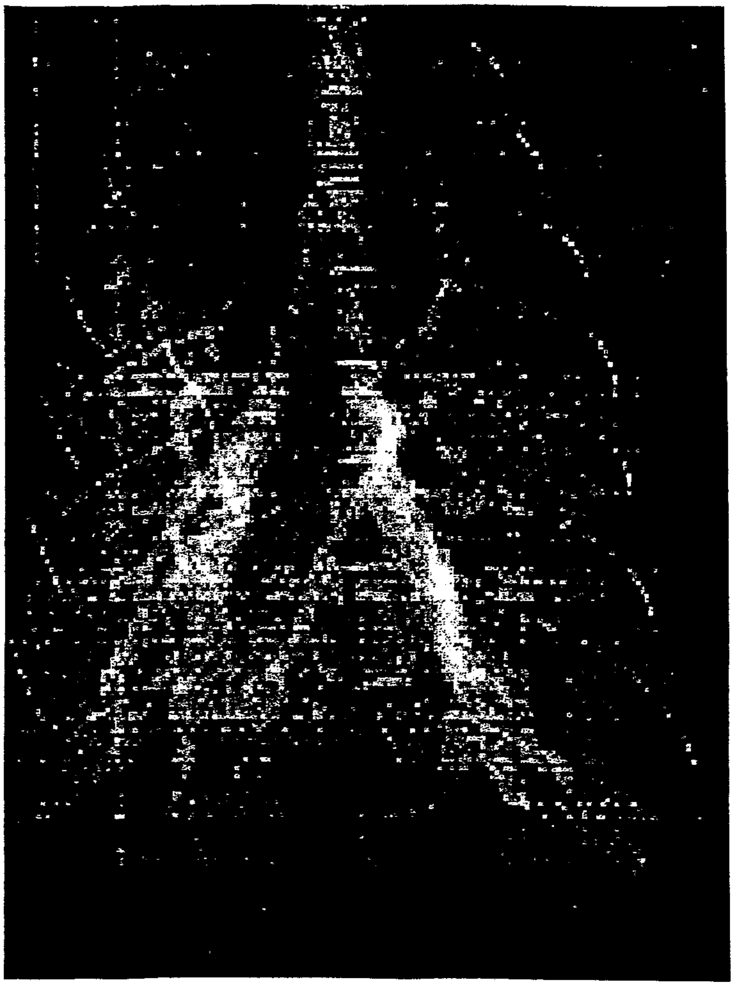

ESRF

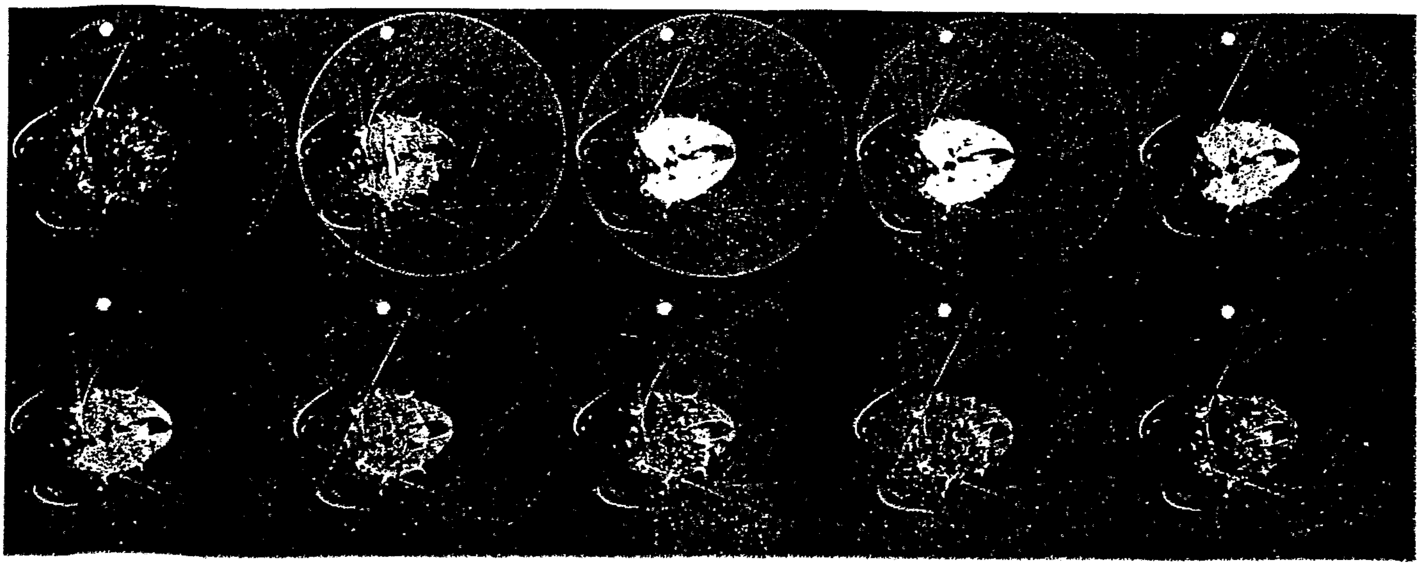

PHASE CONTRAST

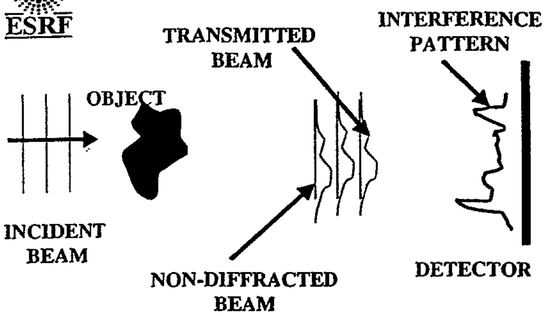

PHASE CONTRAST MICROSCOPE - Schmahl *et al*
HOLOGRAPHIC MICROSCOPE - Howells *et al*
FOURIER HOLOGRAPHY - McMulty *et al*
INTERFEROMETER - Bonse & Hart
PHASE CONTRAST IMAGING -Ando *et al*; Momose

PHASE CONTRAST MICROTOMOGRAPHY
- Spanne *et al*

MULTICRYSTAL:
"SCHLIEREN" - Goetz *et al*
"REFRACTION" - Shilstein & Podurets
"DISPERSION" - Ingal & Beliaevskaya
"PHASE CONTRAST" - Wilkins *et al*

"DIFFRACTION ENHANCED IMAGING"
- Chapman *et al*

PHASE CONTRAST IMAGING

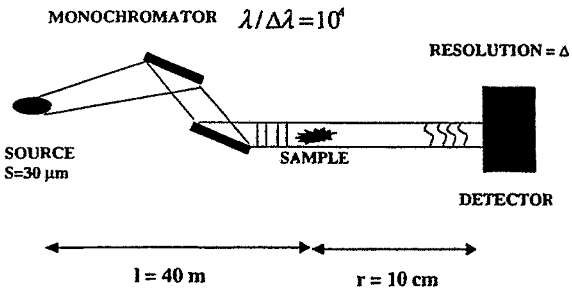

Intensity Distribution: $I = \left|1 + P_r * (1 - A)\right|^2$

A = absorption function

$$P_r(x, y) = \frac{1}{\sqrt{i\lambda r}} \exp\left(i\pi \frac{x^2 + y^2}{\lambda r}\right)$$

If $r << \Delta^2 / \lambda$ ➡ **Contrast = Absorption**

If $\sqrt{\lambda r} \sim \Delta$ ➡ **Contrast = Edge Enhanced**

Optimal Distance
for Spatial Frequency f is: $r_{opt} \approx \frac{1}{2} \lambda f^2 \sim r$

Coronary Artery

Phase Contrast
Computed
Tomography

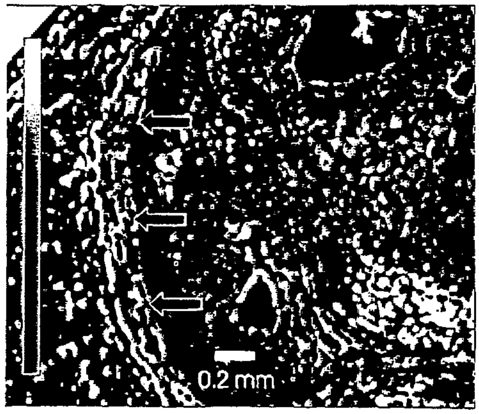

Conventional
Absorption
Computed
Tomography

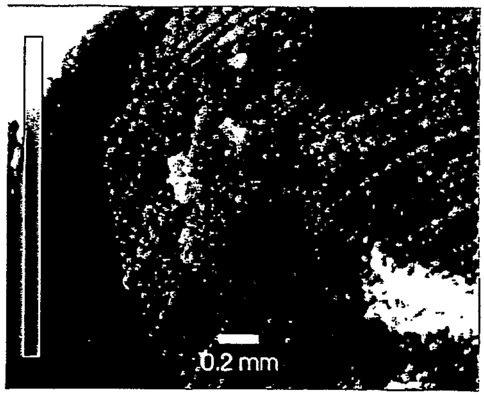

P. Spanne et al

ESRF

X-RAY SCHLIEREN IMAGING

Schlieren
Refraction
Dispersion
Phase-contrast
Diffraction Enhanced Imaging

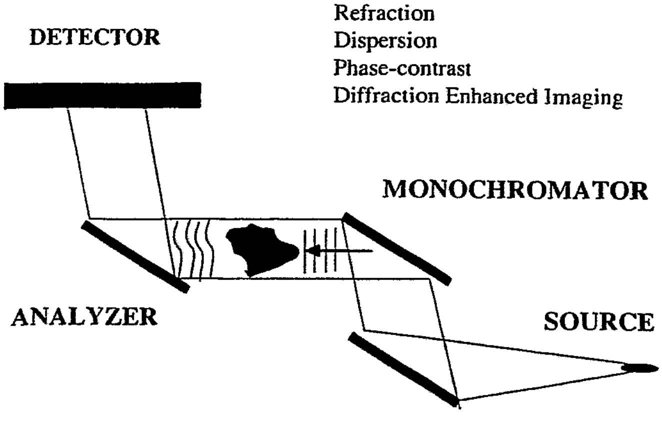

SINGLE RAY:

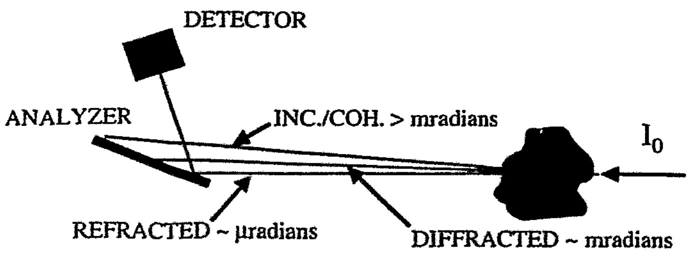

DUAL-ANGLE DIGITAL SUBTRACTION

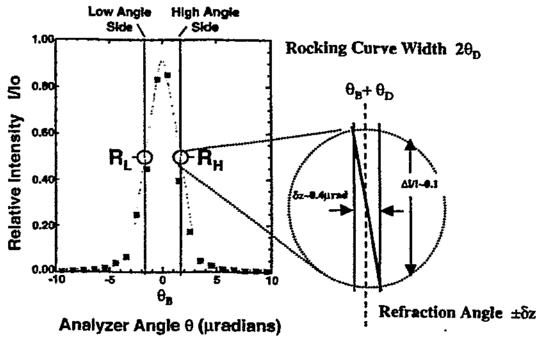

$$I_B^{\pm} = I_R R\left(\theta_B \pm \tfrac{\theta_D}{2} + \delta z\right)$$
$$\approx I_R\left[R\left(\theta_B + \tfrac{\theta_D}{2}\right) + \tfrac{dR}{d\theta}\left(\theta_B + \tfrac{\theta_D}{2}\right)_{\pm} \delta z\right]$$

2 equations - 2 unknown: I_R and δz

Absorption: $\boxed{I_R = \frac{I_B^+ + I_B^-}{2R}}$

Refraction Angle: $\boxed{\delta z = \frac{R}{\left(\frac{dR}{d\theta}\right)}\left(\frac{I_B^+ - I_B^-}{I_B^+ + I_B^-}\right)}$

Synchrotron Radiography and DEI

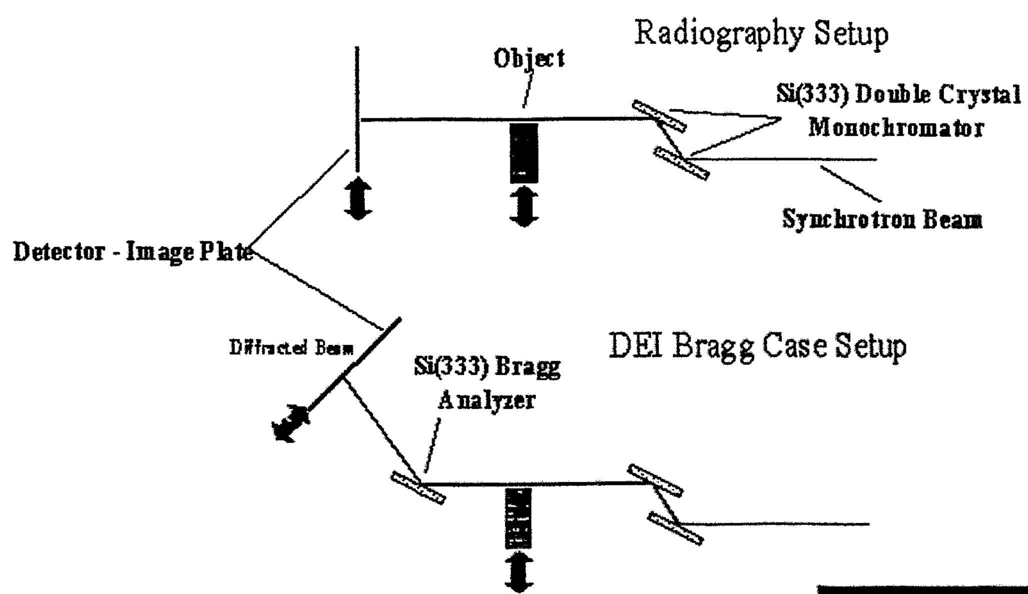

ESRF

Discovery of DEI

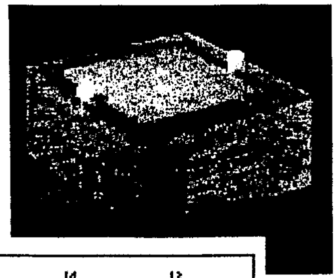

- **Mammography Quality Assurance Object**
  - American College of Radiology Mammography Phantom
  - This phantom contains objects which simulate features presented by lesions in breast tissue (masses, fibrils and specks). Images are scored according to the number of targets detected in a category (i.e. masses, fibrils and specks).
  - Manufactured by Gammex RMI: Model 156.
  - Sketch at right shows objects imbedded in phantom
  - Phantom is approximately 3 in x 3 in x 2 in

Region Materials
1. 1.56 mm nylon fiber
2. 1.12 mm nylon fiber
3. 0.89 mm nylon fiber
4. 0.75 mm nylon fiber
5. 0.54 mm nylon fiber
6. 0.40 mm nylon fiber
7. 0.54 mm simulated micro-calcification
8. 0.40 mm simulated micro-calcification
9. 0.32 mm simulated micro-calcification
10. 0.24 mm simulated micro-calcification
11. 0.16 mm simulated micro-calcification
12. 2.00 mm tumor-like mass
13. 1.00 mm tumor-like mass
14. 0.75 mm tumor-like mass
15. 0.50 mm tumor-like mass
16. 0.25 mm tumor-like mass

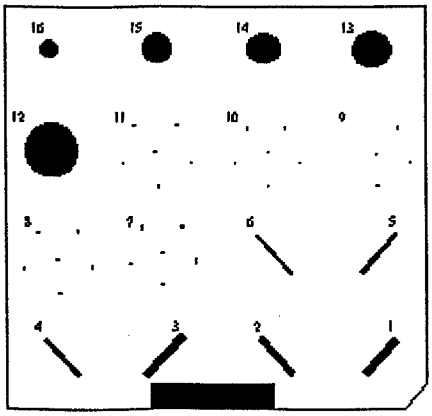

DEI Group

ESRF

Comparison - Conventional and DEI

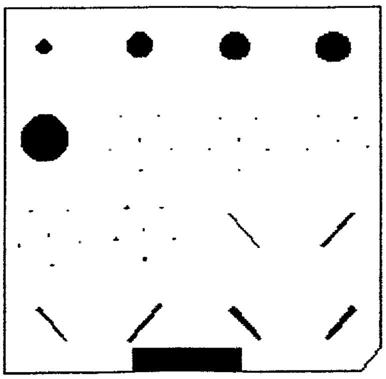

Map

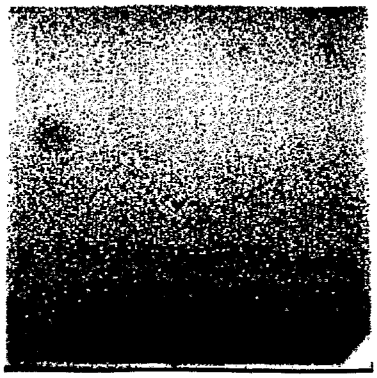

Conventional

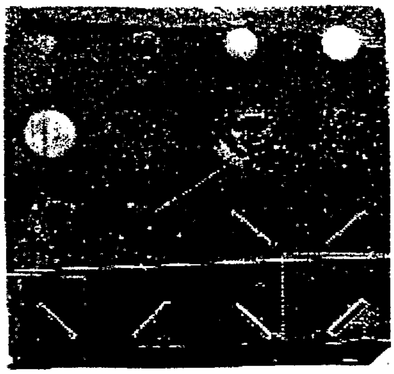

DEI

DEI Group

ESRF

Physics of DEI

NSLS X27C June 1996

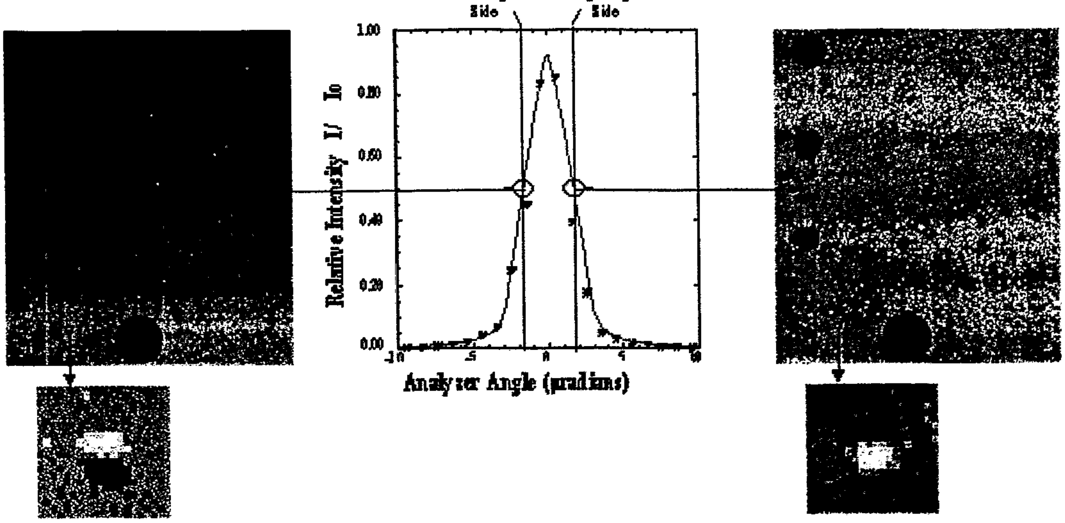

DEI Group

ESRF

Refraction - Absorption Analysis

Low Angle Image

High Angle Image

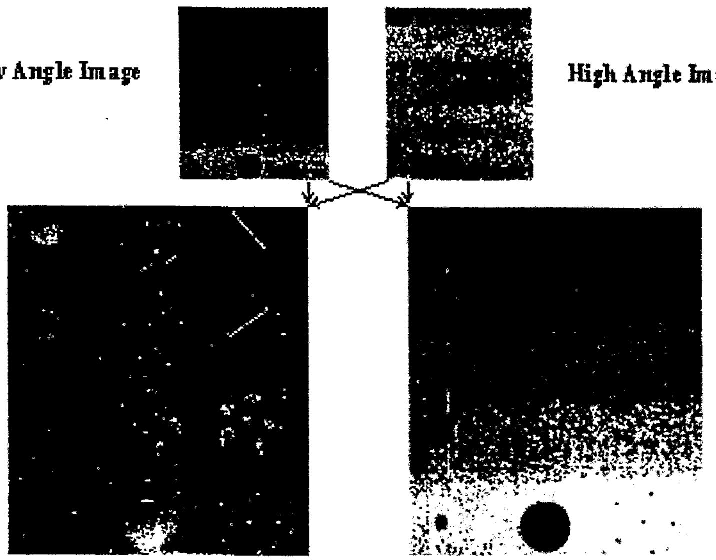

Refraction Image

Absorption Image

DEI Group

ESRF

Where did excess contrast come from?

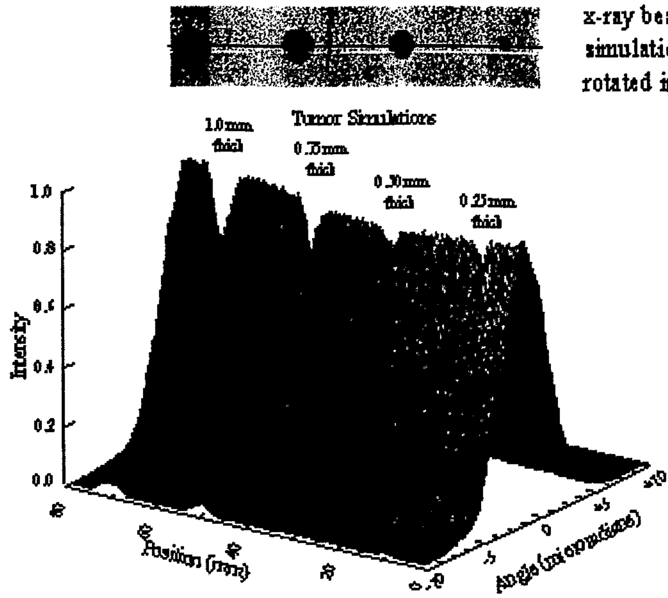

x-ray beam fixed on on tumor simulations - then analyzer is rotated in angle

DEI Group

Human Breast Tissue DEI Image

DEI Group
NSLS Feb. 1998

Radiograph | Apparent Absorption

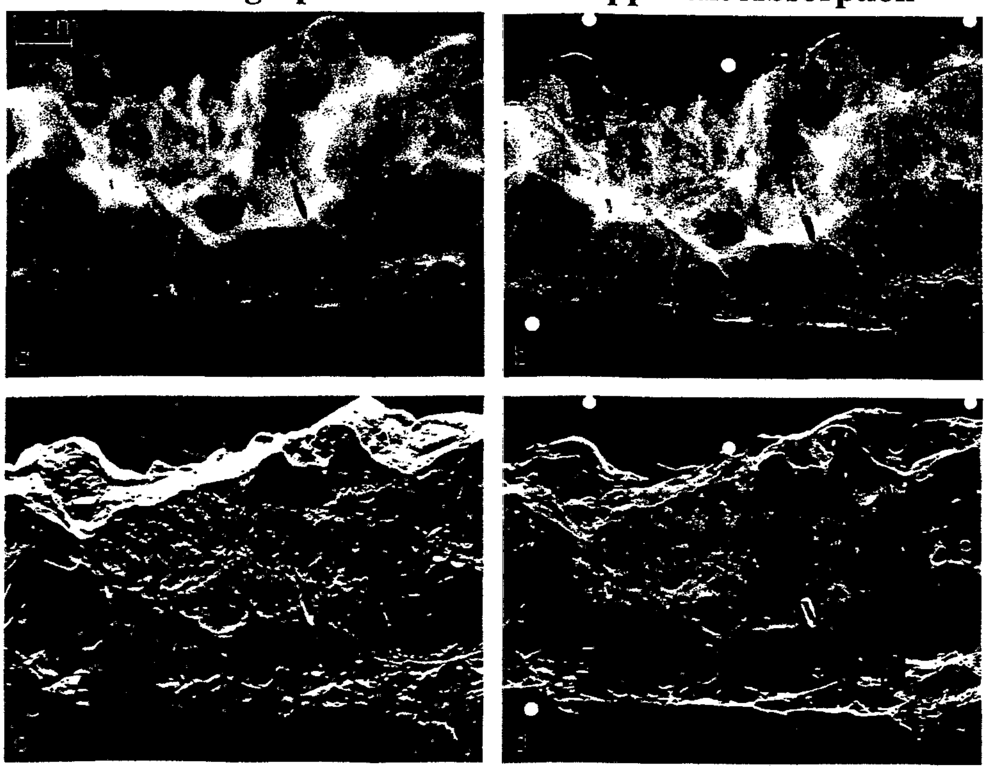

Refraction | At Peak of Rocking Curve

30keV DEI Mouse Images

- Normal Absorption at 30keV
- With DEI, the lungs of the mouse are the most "absorbing" objects present in the images!!

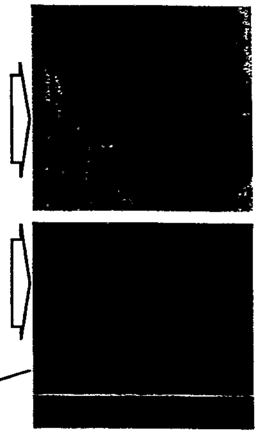

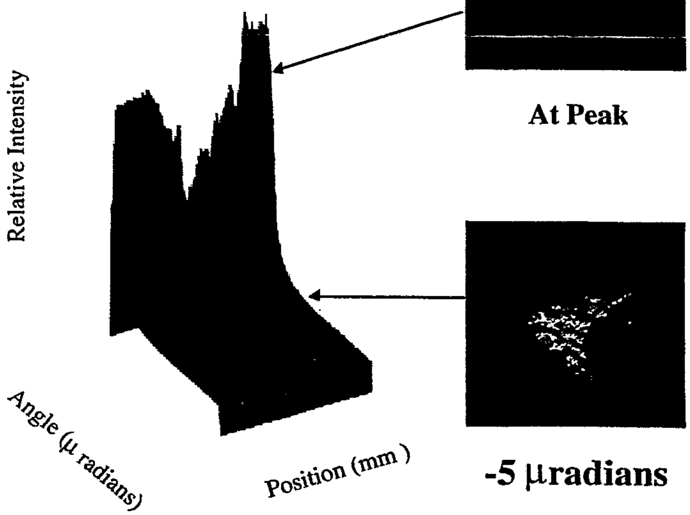

ESRF

DEI Sources of Contrast

- DEI
  - Normal Absorption
  - Refraction
  - Extinction -or- Scatter Rejection
- Compare with Radiography...
  - Normal Absorption

ESRF

ESRF

SCIENTISTS: S. Fiedler, G. Le Duc, C. Nemoz, P. Spanne,
A. Snigirev, W. Thomlinson
POST-DOCS: A. Bravin, I. Troprès
ENGINEERING: M. Renier, E. Brauer-Krisch
TECHNICIAN: T. Brochard
COMPUTING: G. Berruyer
SAFETY: P. Berkvens
STUDENT: C. Johannessen

CHU GRENOBLE

MEDICAL PERSONNEL: B. Bertand, F. Estève, J.F. Le Bas
SCIENTISTS: S. Bayat, A.M. Charvet, H. Elleaume, F. Grimbert
STUDENTS: S. Corde, J.F. Adam
MANIPULATORS: S. Michelland, E. Pierrard

UNIVERSITY OF HELSINKI

MEDICAL PERSONNEL: A. Sovijärvi, CG. Standertskjöld-Nordenstam,
S. Savolainen
SCIENTIST: P. Suortti
STUDENTS: J. Keyriläinen, Liisa Porra

DIFFRACTION ENHANCED IMAGING GROUP

MEDICAL PERSONNEL: E. Pisano
SCIENTISTS: D. Chapman, E. Johnston, D. Sayers, Z. Zhong

S. Fiedler:

Current status of the coronary angiography project at the ESRF

Current status of the coronary angiography project at the ESRF

by Stefan Fiedler ESRF

Collaborators

ESRF

SCIENTISTS: W. Thomlinson, S. Fiedler, G. Le Duc, C. Nemoz
POST-DOCS: A. Bravin, I. Troprès
ENGINEERING: M. Renier, E. Brauer-Krisch
TECHNICIAN: T. Brochard
COMPUTING: G. Berruyer
SAFETY: P. Berkvens

University Grenoble / CHU Grenoble

MEDICAL PERSONNEL: B. Bertand, F. Estève, J.F. Le Bas
SCIENTISTS: A.M. Charvet, H. Elleaume
MANIPULATORS: S. Michelland, E. Pierrard

University Helsinki

P. Suortti

Outline

- Medical Motivation
- K-edge subtraction angiography
- instrumentation and procedures
- comparison of contrast agents (I versus Gd)
- first human patient at the ESRF
- conclusions & perspectives

History of Synchrotron coronary angiography patient programs

- Stanford / SSRL (Rubenstein et al.; '86)
- Brookhaven / NSLS(Thomlinson et al.; '90)
- Hamburg / Hasylab (Dix et al.; '90)
- Tsukuba / Photon Factory (Ando et al.; '96)

Cardiovascular diseases

ESRF

Epidemiology (industrialized countries)

Cardiovascular diseases is 1st cause of adult mortality.
30% of all deaths.
300.000 deaths/year (USA).
In half of the cases the first sign of the disease is death !

Infarct

Stenosis of the coronary arteries.
Ischemia of the heart muscle.
Death.

Coronary Angiography

ESRF

aim:

imaging of coronary arteries down to 1mm diameter to detect narrowing of the aterial lumen due to atherosclerosis

difficulty:

small and moving structure

conventional method:

intra-arterial (femoral artery) catherterization

injection of iodine contrast agent to obtain image with filtered radiation from X-ray tube

wide spread method (e.g. 300 000 examinations per year in France)

Coronary Angiography Techniques

Conventional method

- advantages ⊕
  - excellent image quality
  - 'cinematographic' imaging ⇒ combination with angioplasty
- disadvantages ⊖
  - invasive i.e.
  - ≈ 1.5% complications (≈0.5% serious)
    - ≈0.1% mortality, ≈0.3% myocardial infarctus, ≈0.1% cerebral vascular accident!
  - allergic reaction to contrast agent

minimal invasive techniques:

- MRI
- Fast CT
- Dichromography with SR

ESRF

ANGIOGRAPHY VIEW OF A TYPICAL HUMAN

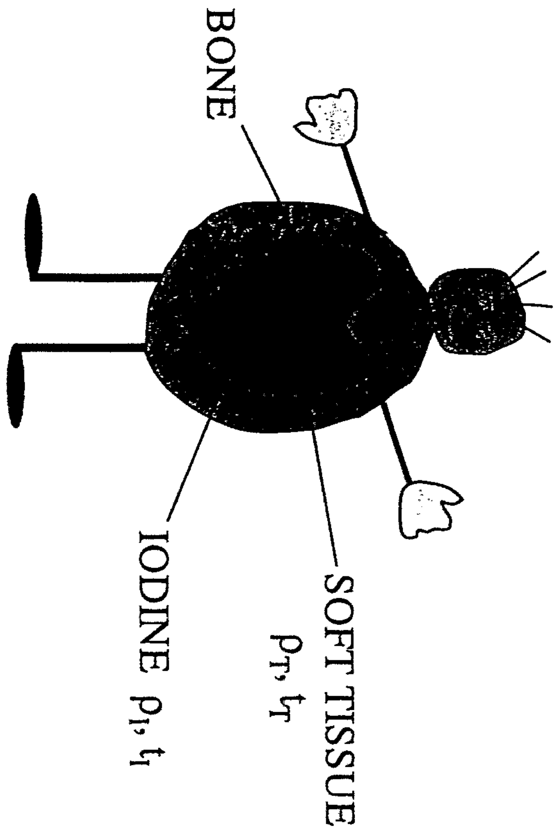

Assume: ρ_T, t_T Includes Bone

K-edge Digital Subtraction Angiography

principle :

- **intravenous injection of contrast agent (I,Gd)**
- **simultaneous recording of two images with two energies above and below the K-edge of the contrast agent**
- **subtraction of the images (suppression of tissue and bone contrast)**

requirement for radiation source :

- **two monochromatic beams wide enough to cover human heart**
- **intense enough to image arteries with a contrast agent diluted (by factor of ~40) faster than one heartbeat i.e. ~10Gy/s**

→ synchrotron

The aim is not to replace conventional angiography but to provide minimal invasive diagnostic tool particularly for follow up examinations after angioplasty (danger of re-stenosis: 30%).

ESRF MEDICAL RESEARCH FACILITY

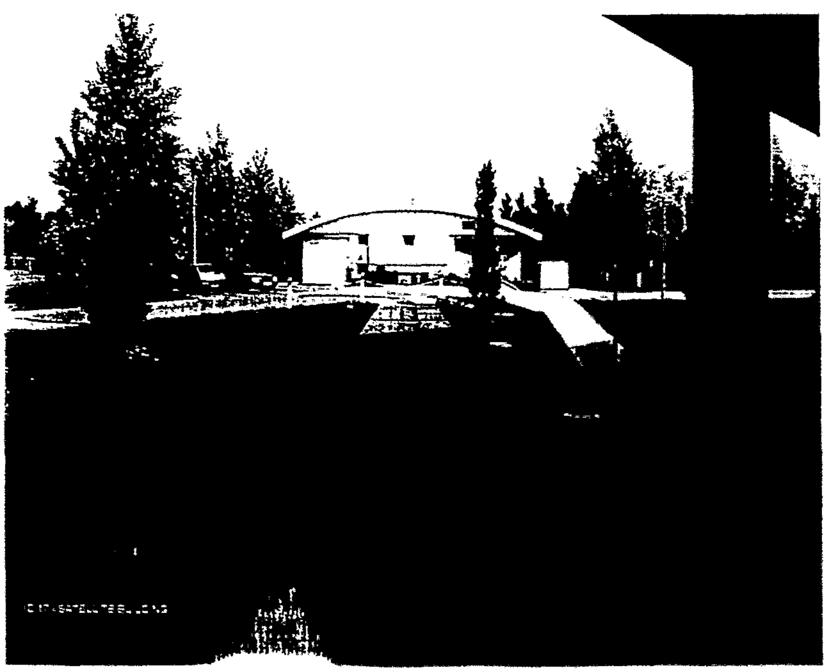

Angiography Setup

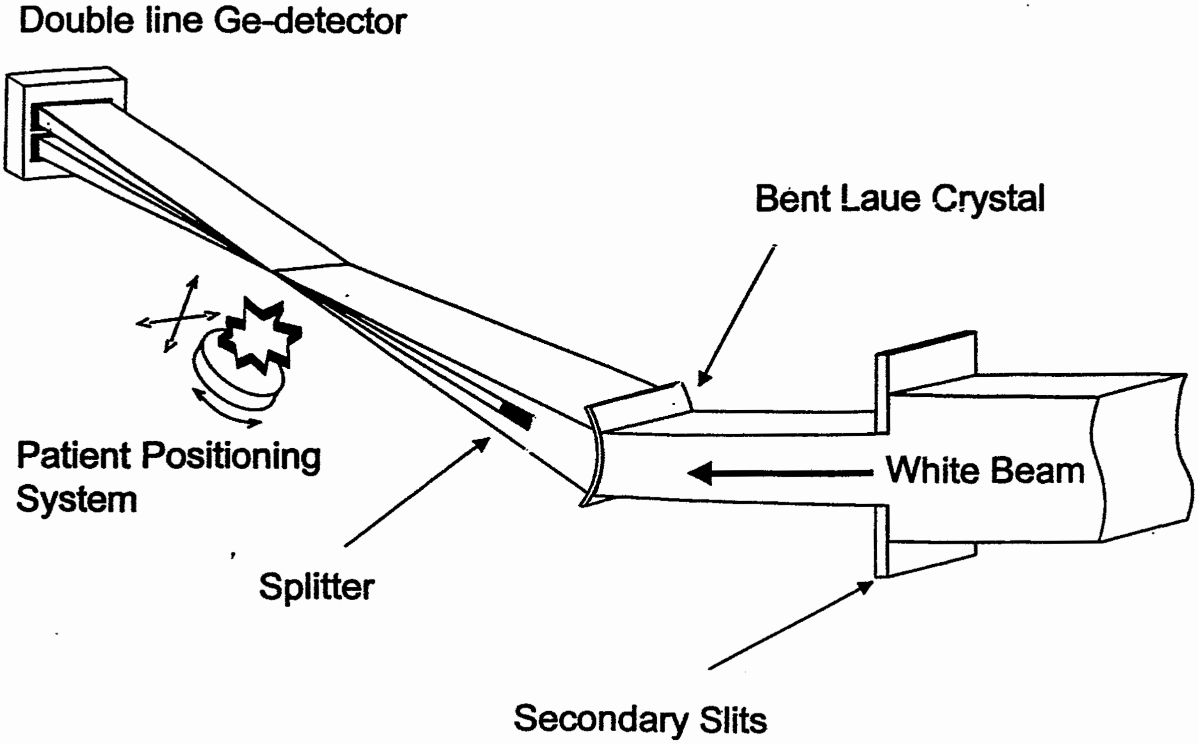

Angiography Monochromator

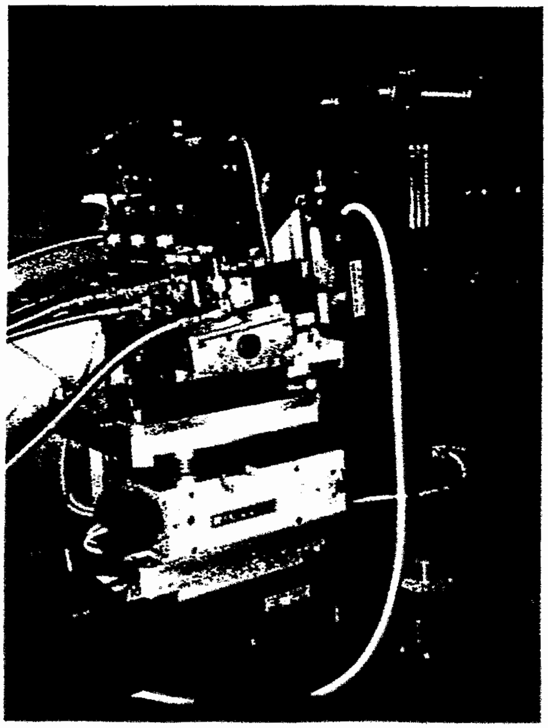

Bent Laue monochromator

- Asymmetrically ct Si(111) crystal
- water cooled (gravity flow); in He atmosphere
- Energy range:17 – 51 keV
- Focal spot: 0.75 * 150 mm^2
- Focal distance: 7m (bending radius 12m)
- Energy bandwidth: 450eV
- flux (angiography conditions) : 2.5 * 10^{12} ph/s
- Harmonic content (60mm gap for 33keV) : 0.3%

Patient Positioning System / Imaging huch

ESRF

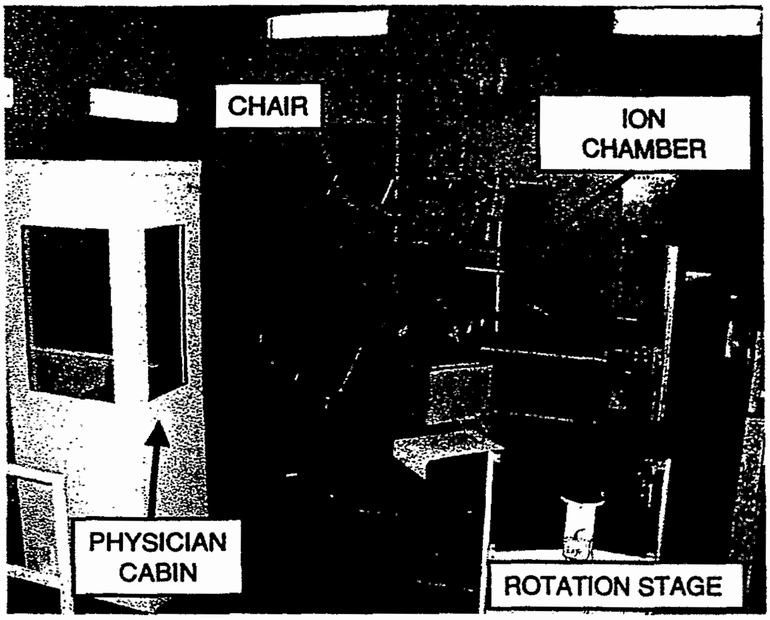

Design for angiography & CT

(6 degrees of freedom)

Z-axis:

- pneumatically assisted DC motor
- max. speed: 500mm/s
- max. acceleration: 1m/s^2
- 600 mm stroke
- Moving mass: 2.6T

Detector System

ESRF

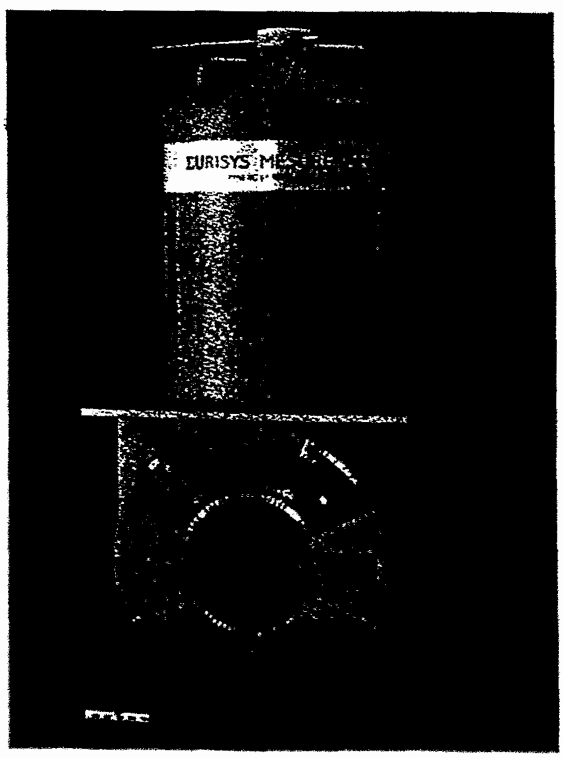

Germanium Detector

- Monolithic P-type Ge crystal
- Thickness: 2mm
- LN cooled
- Two lines with 432 pixels
- Spatial resolution: 350μm
- Active zone: 20 * 150 mm^2
- Leakage current < 5pA/pixel

Electronics

- Charge integration mode (1ms – 100ms)
- Dynamic range: 16bit (8 gain settings corresponding to 1.5pA – 16μA)
- 1 integrator and 1 ADC / pixel

PAtientSafetySystem

ESRF

Simplified PASS diagram (if condition is ok, the contact is closed)

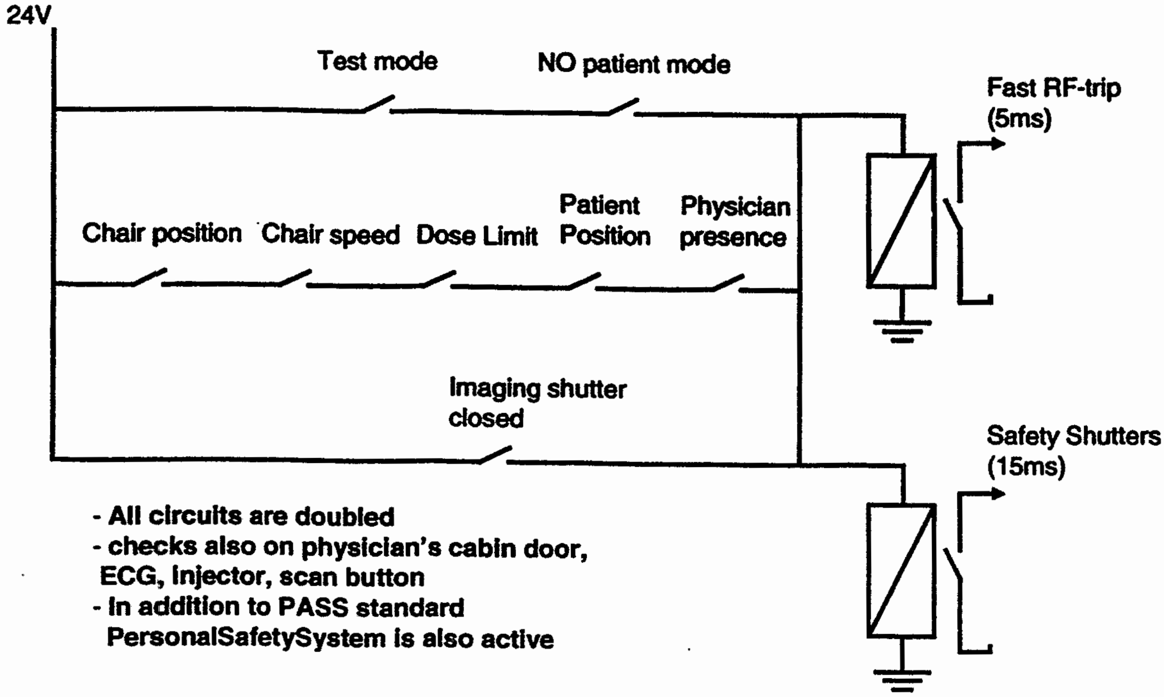

- All circuits are doubled
- checks also on physician's cabin door, ECG, injector, scan button
- In addition to PASS standard PersonalSafetySystem is also active

Dosimetry

ESRF

- Doserate used for patient studies : approx.10Gy/s

(depending on wiggler gap, ring current , slit settings, filters)

- Dose per scan: 5 – 35mGy

(depending on chair speed and dose rate)

- Dose for entire examen: 200mGy

(comparable to conventional angiography)

- Dose is monitored during scan and inhibits exposure when exceeded

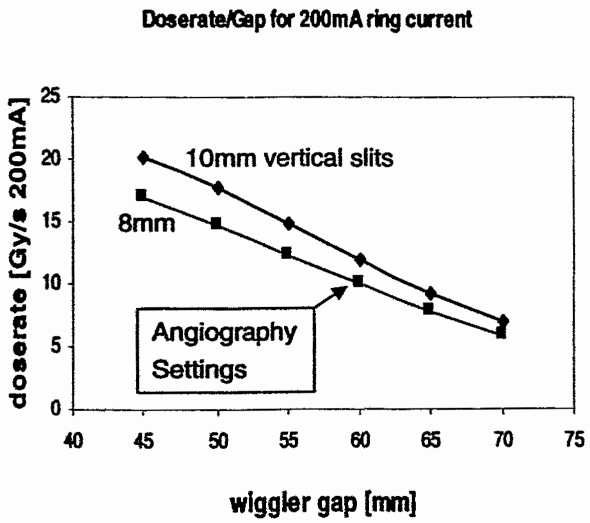

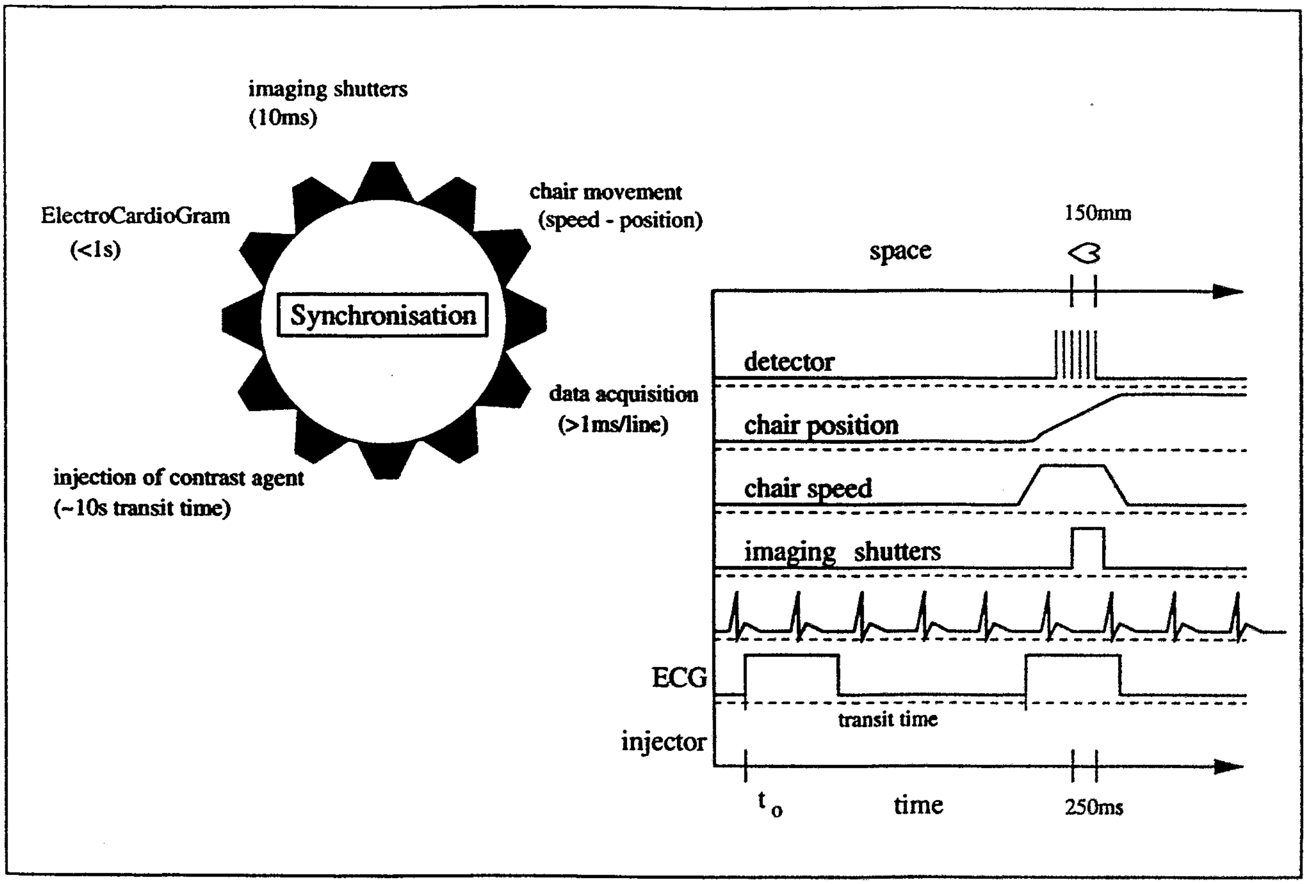
imaging shutters
(10ms)
ElectroCardioGram
(<1s)
Synchronisation
chair movement
(speed - position)
data acquisition
(>1ms/line)
injection of contrast agent
(~10s transit time)
150mm
space
detector
chair position
chair speed
imaging shutters
ECG
transit time
injector
t o
time
250ms

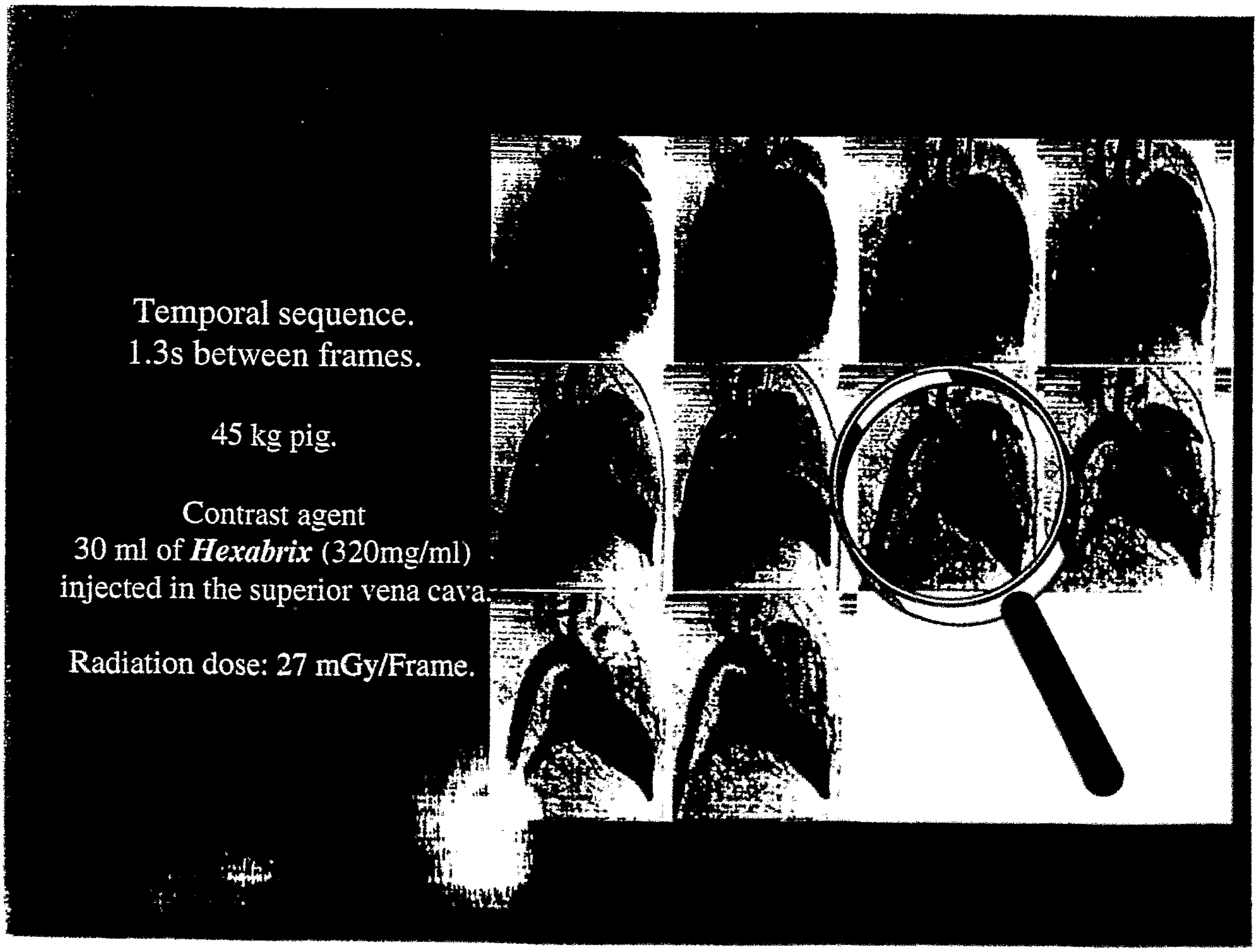
Temporal sequence.
1.3s between frames.
45 kg pig.
Contrast agent
30 ml of *Hexabrix* (320mg/ml)
injected in the superior vena cava.
Radiation dose: 27 mGy/Frame.

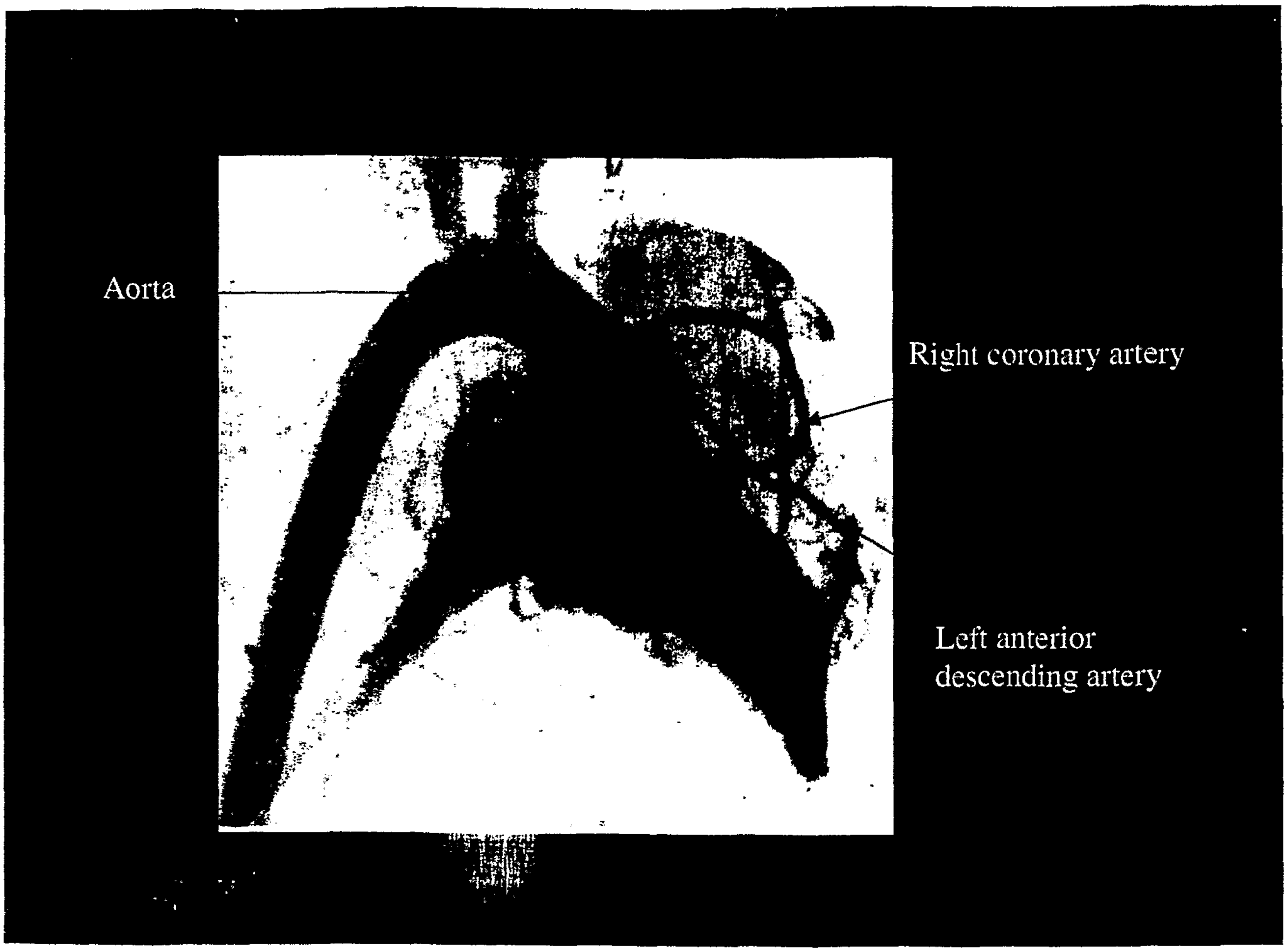

physical properties of Iodine and Gadolinium

- for in vivo studies radiation dose is main limitation

→

large tissue attenuation at 33.17keV

→

choice of higher Z material as contrast agent

e.g. Gadolinium (50.2keV)

problem: available concentrations

Contrast medium	Iodine	Gadolinium
Atomic number	53	64
Atomic weight	126.9	157.25
Density [g/cm3]	4.92	7.88
Energy K-edge [keV]	33.169	50.239
$\frac{\mu}{\rho}[cm^2/g]$ contrast agent (E < Ek)	6.55	3.8
$\frac{\mu}{\rho}[cm^2/g]$ contrast agent (E > Ek)	35.93	18.53
$\frac{\Delta\mu}{\rho}[cm^2/g]$ contrast agent	29.38	14.73
$\frac{\mu_{att}}{\rho}[cm^2/g]$ tissue	0.330	0.232
$\frac{\mu_{abs}}{\rho}[cm^2/g]$ tissue	0.116	0.041
$\frac{\mu_{att}}{\rho}[cm^2/g]$ bone	0.630	0.230

Comparison of contrast agents

Equivalent contrast for different concentration:

Iodine Hexabrix 2*mmol/kg*
Atomic number : 53
K-edge: 33.17 *keV*
Attenuation (20*cm*) : 500

$$\frac{\Delta \mu}{\rho} = 29 cm^2 / g$$

Coronary concentration : 10 *mg/cm*^{3}

Gadolinium Gadobutrol 0.5*mmol/kg*
Atomic number : 64
K-edge : 50.2 *keV*
Attenuation (20*cm*) : 80

$$\frac{\Delta \mu}{\rho} = 14 cm^2 / g$$

Coronary concentration : 3 *mg/cm*^{3}

Detail SNR

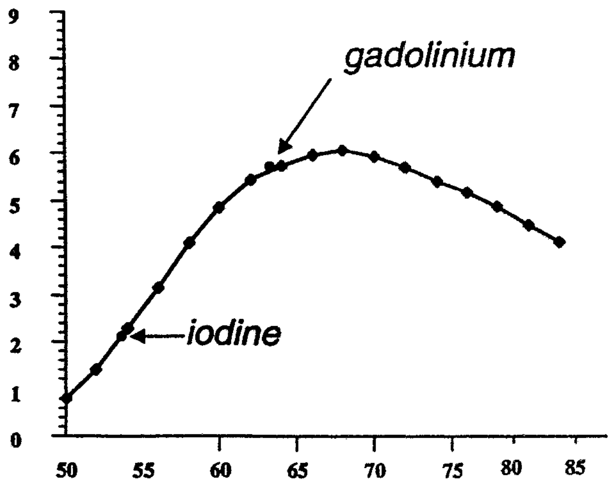

Atomic number of contrast agent (Z)
Conditions of comparison
X-ray dose: 50 mGy
19cm Tissue - 1cm Bone
Same concentration of contrast agents

Temporal sequence
1.3 s between two frames.

Pig 70 kg

Contrast agent
Gadobutrol (84 ml @ 157 mg/ml)
Injected in the superior vena cava

Radiation dose
23.6 mGy/Frame

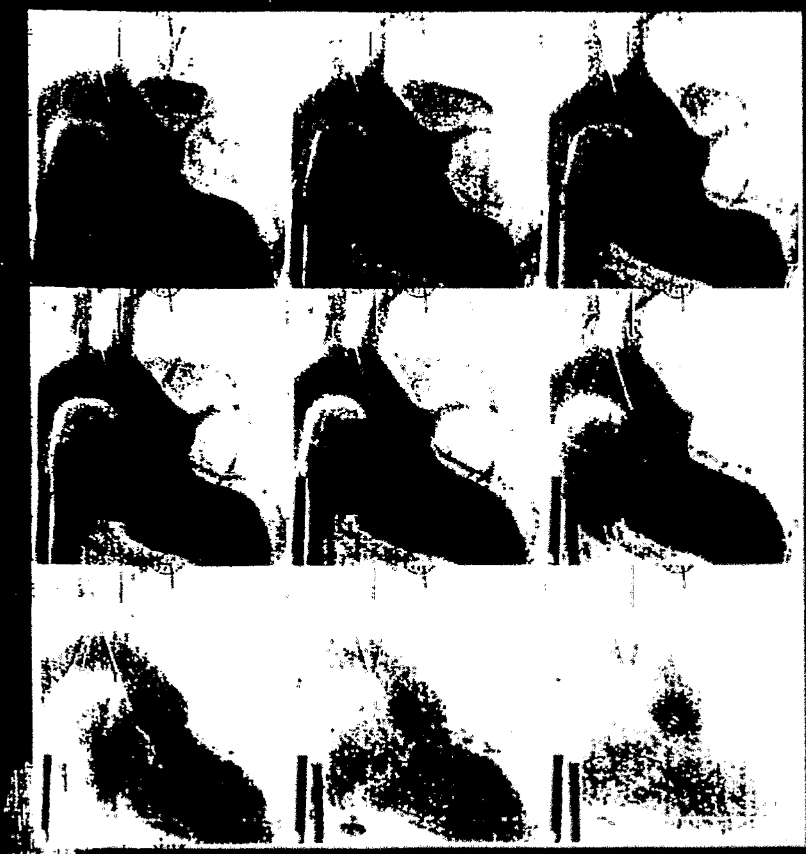

Gadolinium

Cochon de 70 kg

Séquence temporelle
(1.3 sec entre 2 images)

Agent de contraste : Gadobutrol
(84 ml @ 157 mg/ml)

Injecté en veine cave supérieure

Dose de rayonnement **X**
24 mGy/Image

H. Elleaume INSERM 2000

Angiography Protocol

ESRF

STEP 1: **Conventional angiogram followed by angioplasty**

STEP 2: **Follow-up medical examination 3 - 4 months later**

If new angiogram is required :

STEP 3: **ESRF Transvenous Angiography within 1 week (target vessel: RCA)**

STEP 4: **Conventional angiogram within 1 day**

ESRF

LAO 40^0 IODINE CONTRAST AGENT
ESRF JAN. 26, 2000

CHU

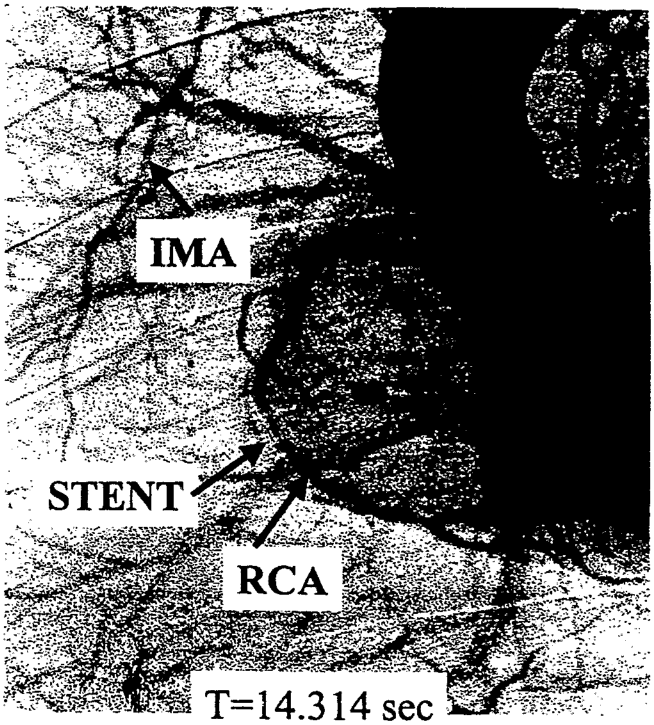

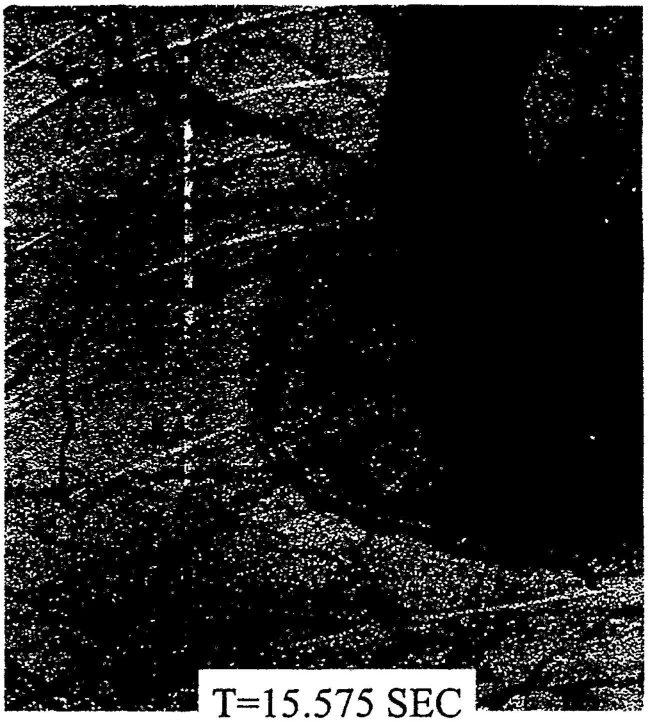

ESRF

FIRST HUMAN ANGIOGRAM
ESRF – JAN. 26, 2000
LAO 40^0 PROJECTION

CHU

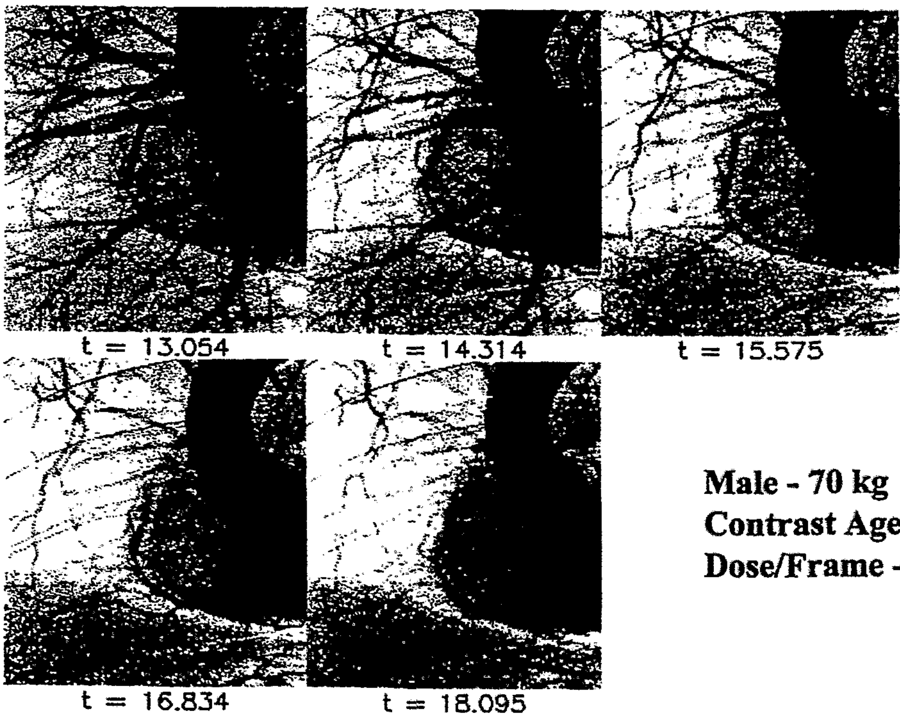

Male - 70 kg
Contrast Agent - Iodine
Dose/Frame - 32 mGy

ESRF

LAO 30^0 IODINE CONTRAST AGENT
ESRF JAN. 27, 2000

CHU

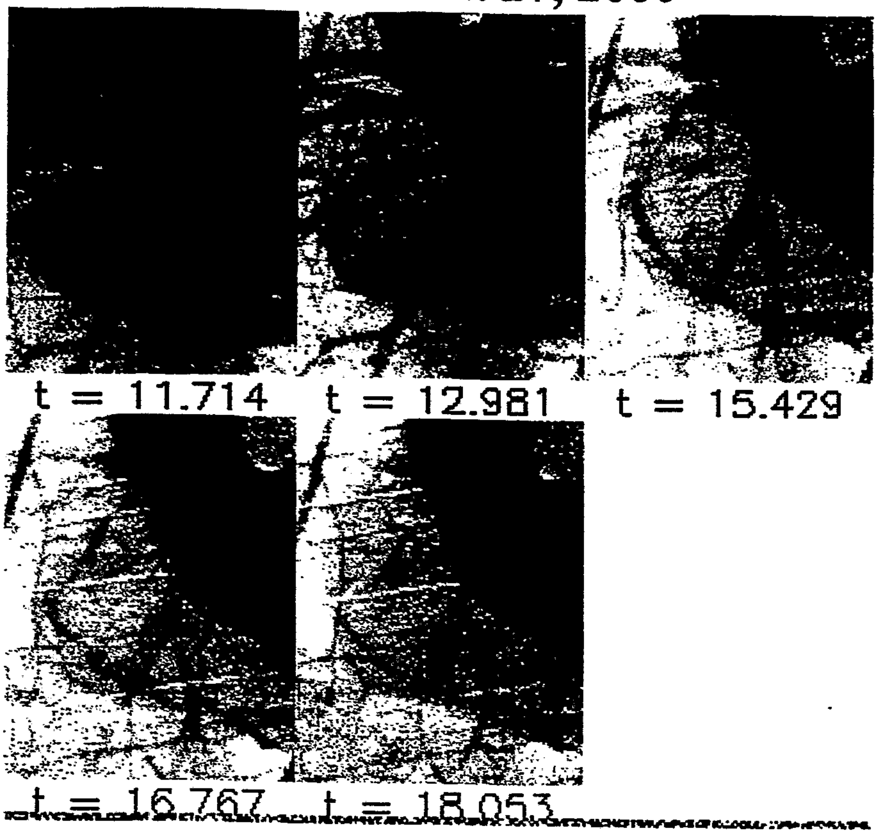

ESRF

LAO 30^0 IODINE CONTRAST AGENT
ESRF JAN. 27, 2000

CHU

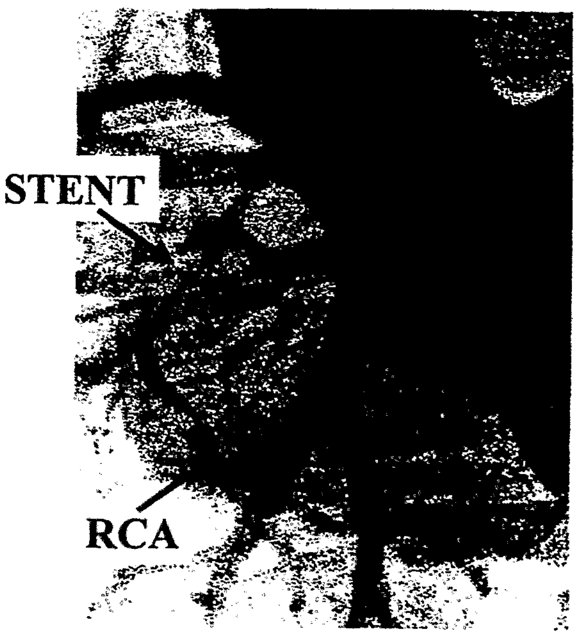

T=12.981 sec

T= 15.429 sec

Experimental challenges

ESRF

Source & X-ray Optics:

- presence of higher harmonic energies (0.5% at 60mm wiggler gap) in monochromatic radiation reduces image contrast
- strong heat-load on crystal optics deforms horizontal beam profile
- filters & windows can produce phase contrast

Procedures and others

- superposition of arteries due to non-stereoscopic projection complicates diagnosis
- exact determination of transit times of contrast agent to coronary arteries needed to achieve optimum contrast
- synchronization of chair movement with ECG at high cardiac frequency in series of scans difficult (one scan within every heartbeat is desirable)

Summary

ESRF

- **Beamline for in-vivo k-edge subtraction technique commissoned**
- **Intravenous coronary angiography on pigs**
- **Comparison of I and Gd contrast agents - higher concentrations of Gd needed**
- **First human patients examined**
- **Images of clinical relevance obtained (diagnosis confirmed by conventional angiograms)**

In future :

- **Extension of Medical protocol to other target vessels**
- **Improvement of optics (harmonics, heat-load)**
- **Faster Imaging**
- **Stereoscopic imaging?**

D. Hermsdorf:

Biological experiments with low energetic charged particles

Biological Experiments with Low Energetic Charged Particles

B. Dörschel, D. Hermsdorf und H. Kühne

Dresden University of Technology,
Institute for radiation Protection Physics
D- 01062 Dresden

Contents

Motivation

- a lot of experiments with high energetic charged particles stimulated by research projects in astronautics and heavy ion therapy (GSI and HMI)
- rare experiments with low energetic charged particles (E< 10 MeV) with partially contradictory results
- further need for scientific research in:
  - ⇒ biological effect of Radon and Radon daughters (α-particles with E_α < 7.7 MeV) (environmental exposition of human population)
  - ⇒ biological effect of neutrons (charged secondary particles, mainly recoil-protons with $E_p < E_n$) (safeguards and personal dosimetry)
  - ⇒ test of models for description of the biological effect of ionising radiation in dependence on
    - → type of particle,
    - → LET,
    - → distribution structure of the deposited energy and others

State of Art

Demands for accelerator technique

- beam line with extraction (irradiation in air)
- acceleration of different particles (low and medium masses)
- acceleration in the energy range of interest (E< 10 MeV)
- operability of the accelerator in the nA current regime
- homogeneous radiation field in the order of 10 cm^2

Facilities with extracted particle beam in Germany:

Institution	Type of Accelerator	Particles and Energy/MeV	External beam	Remarks
HMI	Cyclotron	p ~ 70	horizontal	essentially for therapy
LMU (Garching)	Tandem	p/d/α 24/24/36	vertical upwards	Test phase
PTB	Cyclotron van de Graff	p/α 20/28	vertixal down	under construction
FZR	Cyclotron	p/d/α 13/14/28	horizontal	put out of operation 12/1999
FZR/TUD	Tandem	p/d/α/C/O 9/9/14/24/32	horizontal	project for 2000

First Experiments

Cyclotron U-120 at Rossendorf Research Centre

Particles and nominal energies (at the exit window):

⇒ protons 7 and 13 MeV
⇒ deuterons 14 MeV
⇒ α-particles 28 MeV

Particle flux reduction :

⇒ scattering foil and beam collimation
⇒ Rutherford scattering

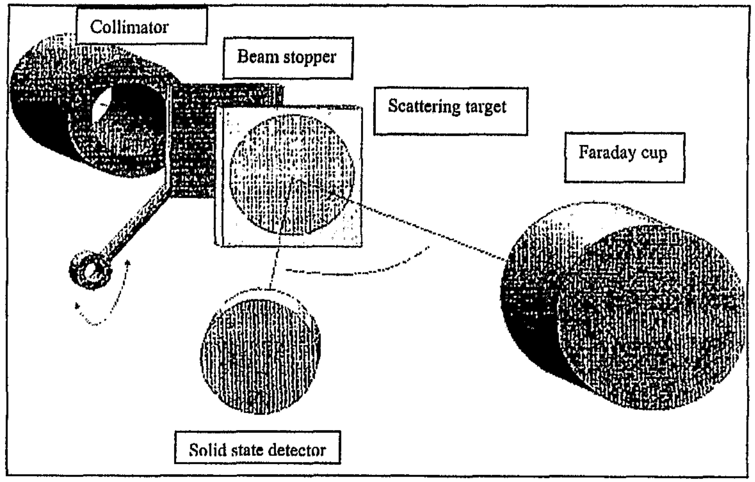

Ranges of particle flux:

⇒ direct beam up to 10^8 cm^{-2} s^{-1}
⇒ scattered beam < 100 cm^{-2} s^{-1}

Homogeneous radiation field

Beam softening by sctering targets and air distance

Example: 8.2 MeV protons

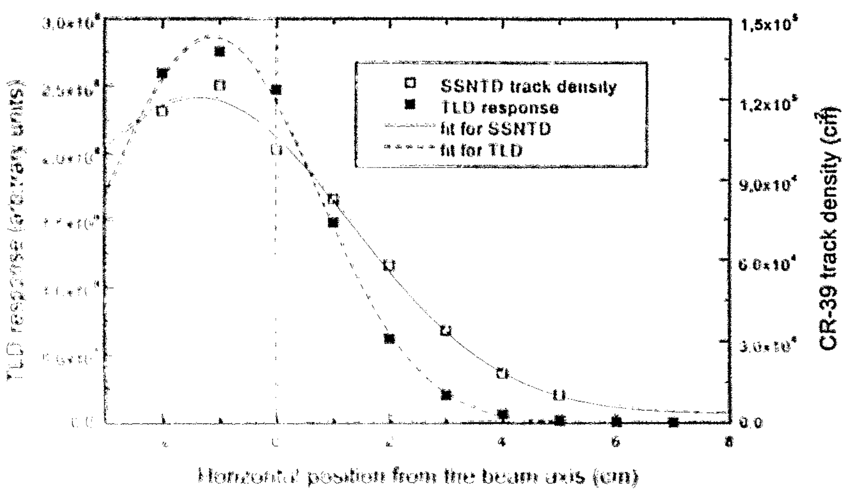

Homogeneity of ± 10% in a distance of ± 1 cm from the beam axis

Determination of the Dose

Example: 8.2 MeV protons

- Thickness of the cell layer : $d \approx 5 - 10\ \mu m$
- Energy loss within the layer: $\Delta E \approx 30 - 60$ keV

⇒ LET roughly constant in the layer
LET = 5,5keV/µm

⇒ **Dose D can be approximated by:**

$$D = \varphi \frac{1}{\rho} LET\, t$$

with

φ :	particle flux density
ρ :	density of the cell
LET:	linear energy transfer
t :	irradiation time

⇒ **Important:**
in the case of a stronger energy loss within the cell layer the dependence of LET on the penetration depth in the layer has to be taken into account by using the spectral flux density resulting in a twofold integration procedure

Biological Test Experiments

Cell culture: R1 fish liver cells (Institute for Zoology, TUD)

Particles: 8.2 MeV protons

Range of Doses: 1 to 100 Gy

Biological end point: cell survival

Method of Analysis: MTT-Test

(measurement of the enzymatic activity of the culture)

⇒ Advantage: simple photometry
⇒ Disadvantage: detection of survived but non fertile cells
(background enhancement at higher Doses)

Method of Evaluation: $S = \exp(-\alpha D - \beta D^2)$
Determination of
⇒ initial slope α
⇒ curvature β (shoulder)

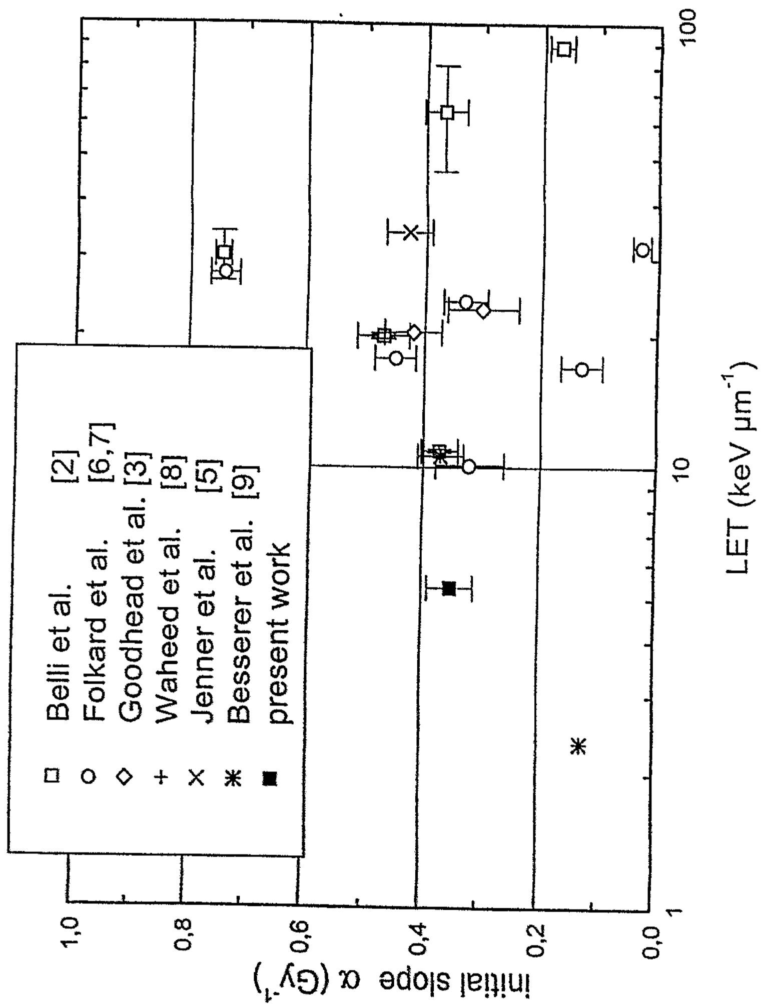

Future Activities

- **beam extraction and set-up of a new irradiation facility at the Tandem of the Rosendorf research Centre**

- **improvement of the experimental conditions**

⇒ Homogeneity of the radiation field
⇒ Management of the biological samples
⇒ other cell cultures (conventional cell types)

- **Experiments with cells seeded and cultivated on radiation sensitive detectors**

⇒ solid state nuclear track detectors (SSNTD, CR-39)
⇒ best properties for simultaneous
  ⇒ particle identification
  ⇒ localisation of hitted cells by image analysing system
  ⇒ energy loss measurement
  ⇒ cell layer thickness determination

⇒ **position resolved dosimetry (Micro-Dosimetry)**

DFG-Project

„Correlation of physical parameters with the cellulare effect of soft photons and low energetic charged particles“

Participants:

⇒ **Institute for Zoology (Prof. Gutzeit)**
⇒ **Clinic for Radiation Therapy (Dr. Dörr)**
⇒ **Institute for Radiation Protection Physics**

- **Biological experiments**

⇒ cell survival studies (improved analysis)
⇒ DNA- damage studies (Comet assay)
⇒ cytogenetic studies (FISH)
⇒ specific cell cycle studies (ELISA)
⇒ stress response studies (hsp70 expression)
⇒ genetic expressions (cDNA arras)

- **Theoretical activities**

⇒ Description of the biological effect in dependence on the energy deposited by δ-electrons in the vicinity of the track of a charged particle within a cell

⇒ Comparison with experimental results obtained by irradiations with soft photons from the

ELBE source

A. Panteleeva:

Cell survival studies after X-ray irradiation

Cell Survival Studies after X-ray Irradiation

A.Panteleeva, W. Enghardt, U. Lehnert, J. Pawelke, H. Prade

Forschungszentrum Rossendorf e.V., Dresden

W. Dörr, B. Dörschel

TU Dresden

Workshop on X-rays from electron beams

February 24 - 26, 2000

Introduction

The **ELBE** Radiation Source
for radiobiological studies

- Superconducting electron accelerator, producing an Electron beam of high quality (high Brilliance and low Emittance)
- In comparison to the synchrotron facilities, ELBE radiation source is cheaper
- in comparison to the sources of characteristic X-rays, ELBE produces X-rays of tuneable energy

•

Measurement of RBE of X-rays in the
energy range 10-50 keV
is the first research project

•

First stage of the project
(performed at the Medical Science Dept. of
TU Dresden)

- Acquiring experience with cell culture, and determination of growth conditions of the particular cell line
- Obtaining a reference cell-survival curve at a conventional X-ray source
- Determination of the special requirements to soft X-ray irradiation

Determination of cell culture conditions

Cell line: NIH/3T3 mouse embryo
- *wide - spread use for various studies*
- *well-established cell line*
- *contact-inhibited*

Growth conditions :
- *37^0 incubator*
- *humidified atmosphere with 5% CO_2*

Tested NIH/3T3 sources:
- *ATCC collection*
- *DKFZ collection*

Tested media: Medium1:

Dulbecco's MEM
- *10 % Fetal Calf Serum*
- *20mM HEPES buffer*
- *100U /100µg /ml penicillin / streptomycin*
- *1mM Sodium pyruvate*
- *1% (v/v) non-essential aminoacids*

Medium2:

Dulbecco's MEM
- *10 % Fetal Calf Serum*
- *20mM HEPES buffer*
- *100U /100µg /ml penicillin / streptomycin*

Irradiation with a conventional X-ray source:

- *Cells are seeded in 25 cm^2 polystyrene culture flasks, allowed to reach confluence*
- *Irradiated as monolayer*
- *X-ray generator, operated at 200 kV / 20 mA, yielding a dose rate of 1.2 Gy/min*

Survival assay:

- *Cells are trypsinized immediately after irradiaiton*
- *Appropriate numbers of cells for each dose are seeded in 5mm Petri dishes*
- *Cultures are fixed and stained after 10-11 days*
- *Colonies with more than 50 cells are scored as survivors*

Plating efficiency of NIH/3T3 cells from DKFZ source in different media

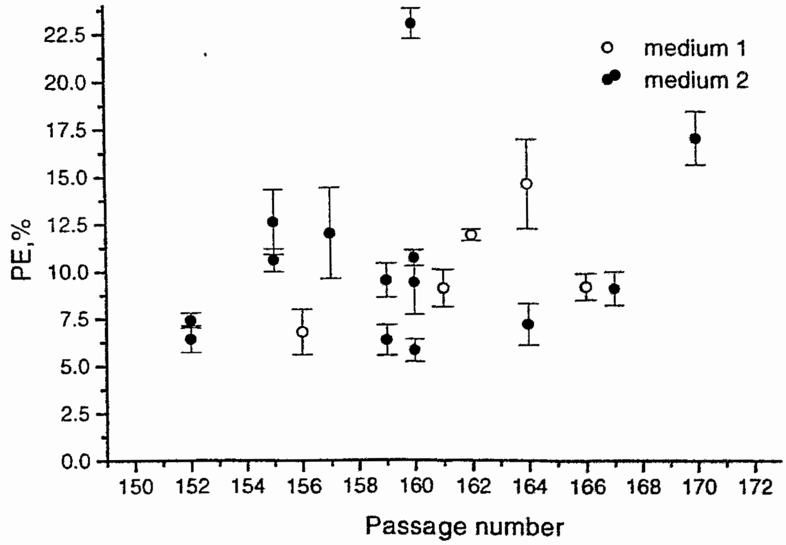

Mean values for PE, %:

DKFZ source, *medium 1*	10.5 ± 0.6	ATCC source, *medium 1*	12.2 ± 1.1
DKFZ source, *medium 2*	10.5 ± 0.6	ATCC source, *medium 2*	11.7 ± 0.7

Survival of NIH/3T3 cells (DKFZ source)

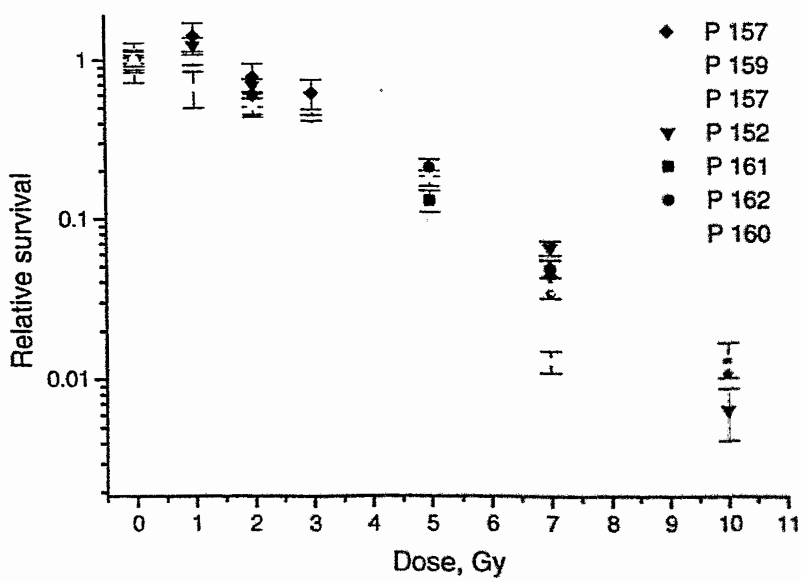

- *Irradiation with conventional X-ray tube*
- *Different passages investigated*

Survival of NIH/3T3 cells (ATCC source)

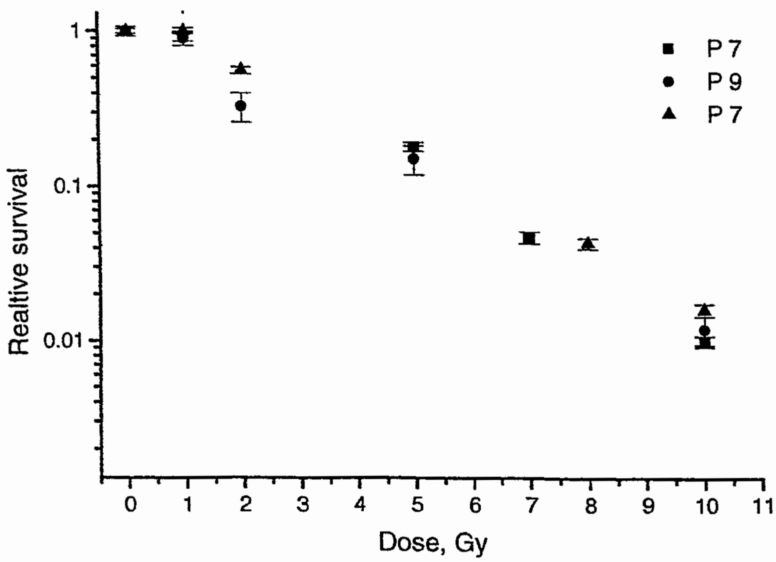

- *Irradiation with conventional X-ray tube*
- *Different passages investigated*

Data for NIH/3T3 survival from the literature

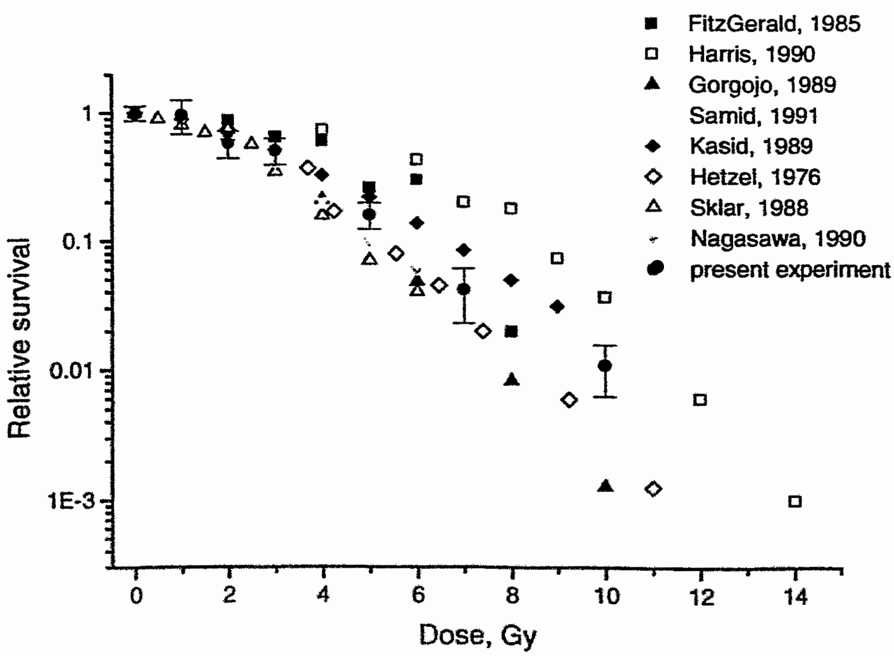

Linear-quadratic Model fit of the X-ray irradiation survival

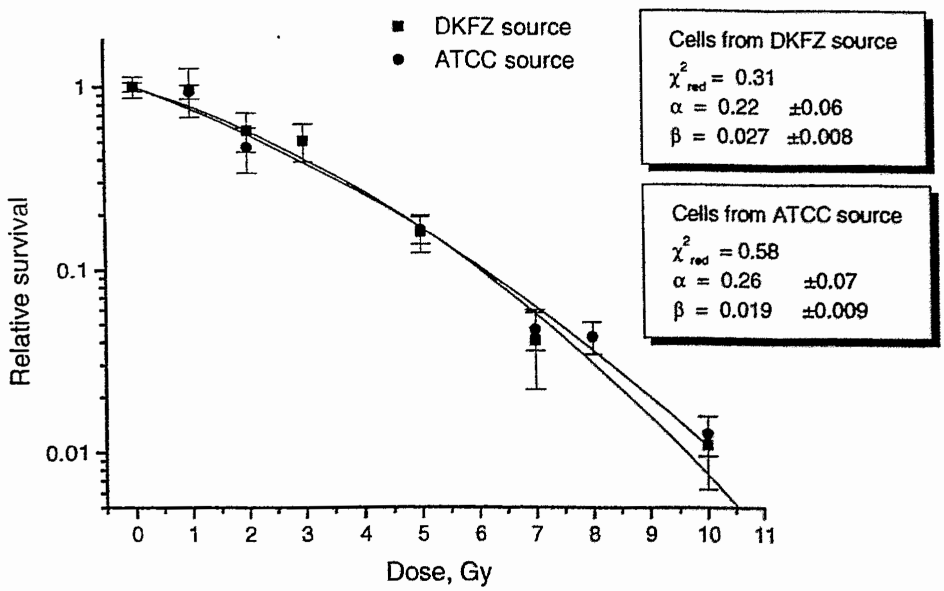

Each point represents the mean value of several experiments

Multitarget Model fit of the X-ray irradiation survival

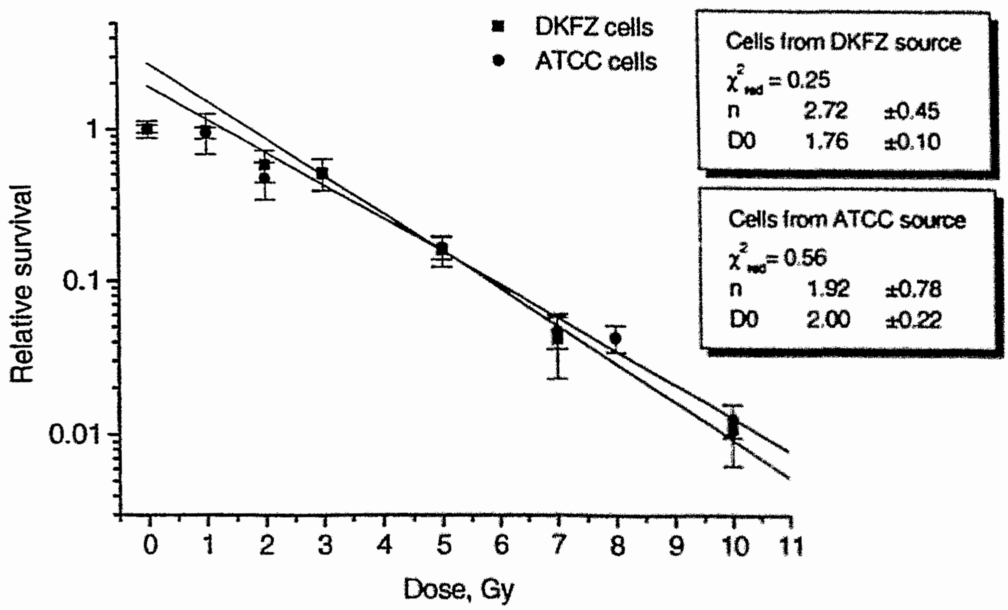

Literature data for NIH/3T3 cell line

Literature Source	Plating Efficiency, %	D_0, Gy	n
Hetzel, 1976	not reported	1.30	6.5 ± 0.4
FitzGerald, 1985	4.3	1.45	9.10
Sklar, 1988	not reported	1.41 ± 0.12	3.4 ± 0.2
Kasid, 1989	not reported	2.02 ± 0.11	3.1 ± 0.8
Gorgojo, 1989	70 -100	1.18	6.5
Harris, 1990	not reported	1.35 ± 0.09	40 ± 5
Nagasawa, 1990	not reported	1.7	2.5
Samid, 1990	not reported	1.27 ± 0.09	3
present experiment	10.5	1.8 ± 0.1	2.7 ± 0.5

Experimental design for irradiation at ELBE

Requirements for irradiation with low-energy X-rays:

- Minimal thickness of material between cells and irradiation source
- Suitable membrane material, providing cell attachment and growth
- Sufficient amount of medium covering the cell monolayer

Beamline design requirements:

- Vertical position of cells during irradiation
- Comparatively long irradiation procedure (up to 40 min)

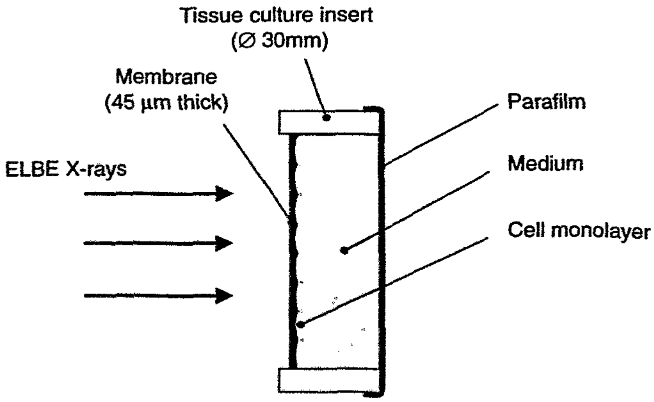

Experimental design for irradiation at ELBE

Possibilities of cell survival without medium:

By the dye exclusion assay: *Cells can survive only when covered with liquid*

Determination of membrane properties:

Membrane material	Pore size, μm	Growth of cells as monolayer	PE, %
Anopore [1)]	0.02	good	8.1
Anopore [1)]	0.2	very good	8.4
polycarbonate [1)]	3	very good	to be checked
polycarbonate [1)]	0.4	very good	to be checked
PTFE [2)]	0.4	bad	to be checked
polycarbonate [2)]	0.4	excellent	to be checked

Producer: [1)] NUNC GmbH
[2)] IWAKI corp

Conclusions

Achieved results:

- Obtaining experience in cell survival studies and determination of the special requirements to soft X-ray irradiation
- Obtaining a reference cell-survival curve at a conventional X-ray source, in a good agreement with literature data

Current stage of our research:

- Establishment of a cell laboratory at ELBE
- Design of the dose delivery system

Future plans:

- Extending the photon energy to the ultra-soft range
- Investigations with other radiation sources

J. Pawelke:

A device for cell irradiation with low energy quasi-monochromatic photons at ELBE

A Device for Cell Irradiation with Low Energy Quasi-Monochromatic Photons at ELBE

Workshop on X-rays from electron beams

Rossendorf, February 24-26, 2000

J. Pawelke, W. Enghardt, U. Lehnert, B. Naumann,
W. Neubert, A. Panteleeva, H. Prade, W. Wagner

Introduction

Radiobiological Studies with Quasi-Monochromatic X-Rays at ELBE

Generation of secondary X-rays by:

- Channeling radiation (10 keV $\leq E_\gamma \leq$ 100 keV)
- Parametric X-rays (2 keV $\leq E_\gamma \leq$ 40 keV)
- Transition radiation ($E_\gamma \leq$ 0.5 keV)
- Compton backscattering

First research project:

- Measurement of RBE of X-rays in the energy range 10-50 keV
- Cell survival studies after irradiation with channeling X-rays

ELBE Facility

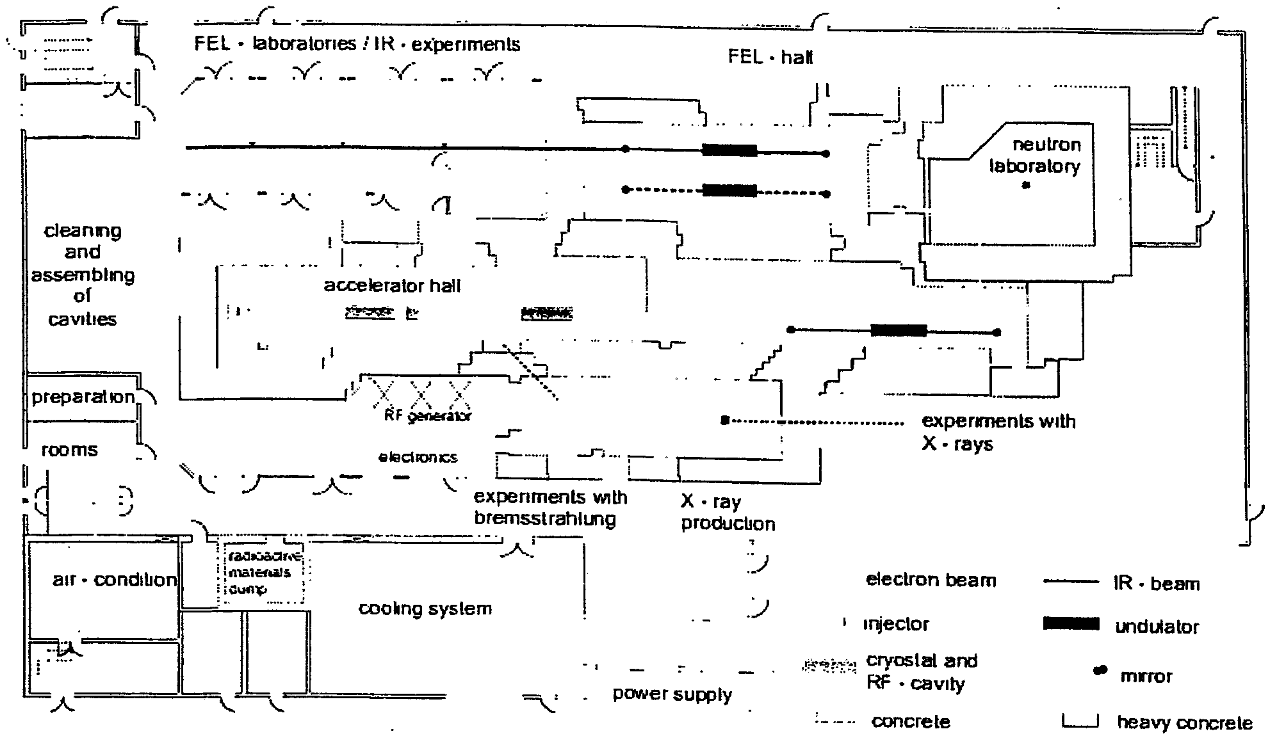

Institut für Kern- und Hadronenphysik

FZR

Beamline layout

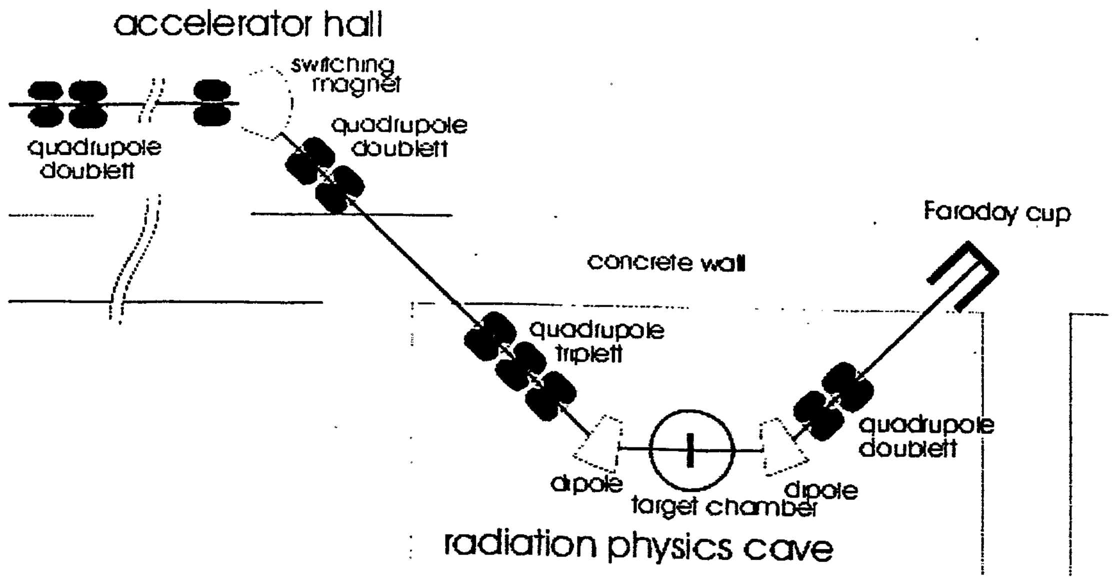

- *beam tube:* CF63 (stainless steel)
- *distance between channeling crystal and dipole magnet section:* 122 cm
- *magnet gap:* 60 mm

Institut für Kern- und Hadronenphysik

FZR

RBE determination by cell survival

Requirements:

- **Dose rate of ≳1Gy/min**
- **Homogeneous dose delivery to the irradiated field**
- **Sufficient low background radiation level**
- Absolute dosimetry with high accuracy
- A cell laboratory available

Desirable:

Calculation of spatial and spectral dose distribution for channeling as well as background radiation

Dose rate dependence on channeling photon energy

Calculations based on the experimental data

- *of photon yield for channeling in diamond (110) plane, 1→ 0 transition, 10% BW [TU Darmstadt, H. Genz et al., Phys. Rev. B53 (1996) 8922]*

and assuming:

- *100 μA electron beam (12 - 40 MeV)*
- *a 100 μm thick crystal*
- *0.5 mm water equivalent absorbing material in front of the cell monolayer*
- *20 μm cell monolayer*

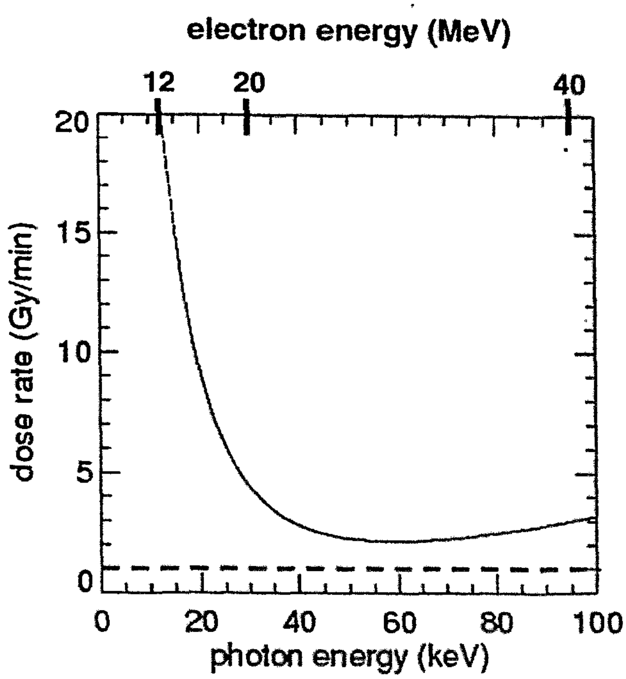

Angular distribution of channeling radiation

photon yield

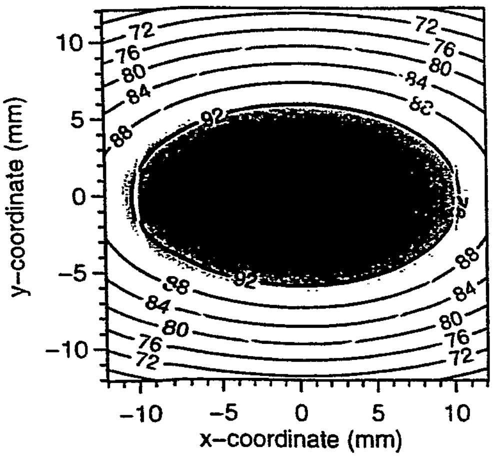

photon energy

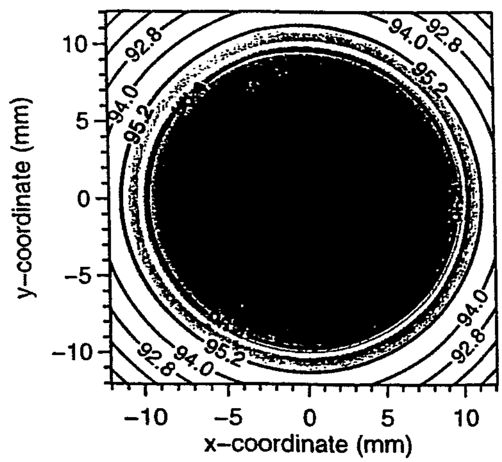

- *Dipole approximation to quantum theory of channeling radiation*
- *Relative distribution of channeling radiation at a distance 2 m from the crystal*
- *An electron beam of 20 MeV results in maximum photon energy of 30 keV*
- *The white circle represents the target area of 2 cm diameter*

Distance dependence of dose rate and dose rate spread

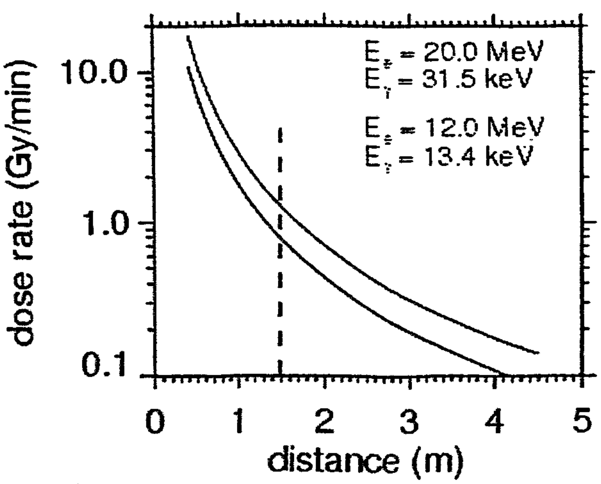

Dose rate in the target centre

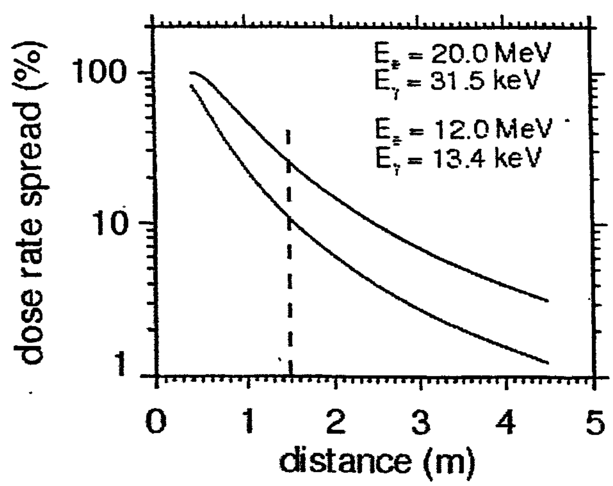

Maximal dose rate difference in the target in percentage of the maximum dose rate

Calculations are for 12 MeV and 20 MeV electron beams.

Background radiation

by

- other channeling transitions

  e.g. *20* MeV electron energy

  1 → 0 transition:

  photon energy: 30 keV
  dose rate: 1.5 Gy/min

  2 → 1 transition:

  photon energy: 17 keV
  dose rate: 1.7 Gy/min

- bremsstrahlung

- neutrons generated by (γ,n) reaction

Calculation of dose contribution by bremsstrahlung

Monte Carlo simulation by GEANT (CERN Program Library W5013) based on realistic beamline geometry

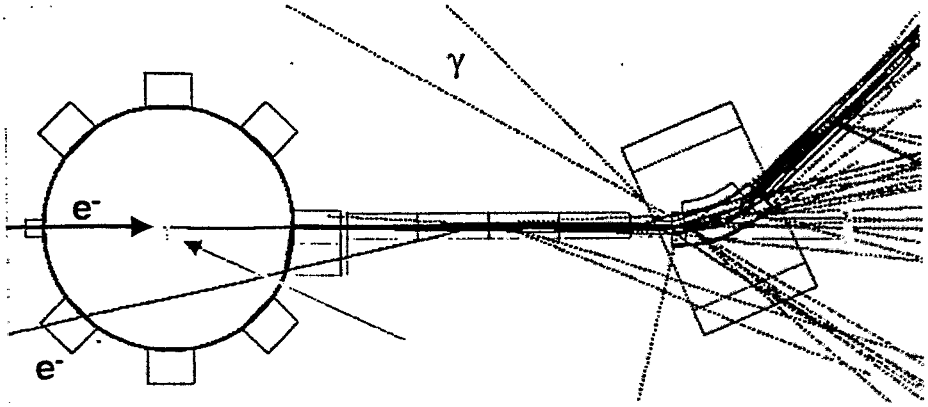

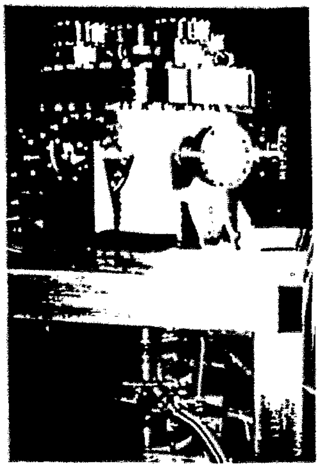

target chamber

(Distance between channeling crystal and cell monolayer: 150 cm)

<u>Sources of bremsstrahlung generation are:</u> crystal, beam tube, magnet section

Calculation of dose contribution by bremsstrahlung

20 MeV electrons on 100 μm diamond

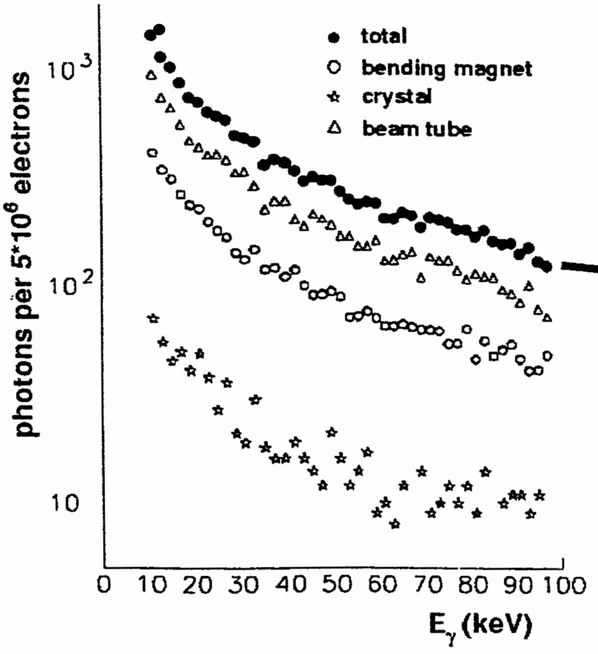

Most of the bremsstrahlung is generated by electrons which are scattered in the crystal and then hit the beam transport line

Electron beam current: 100 μA

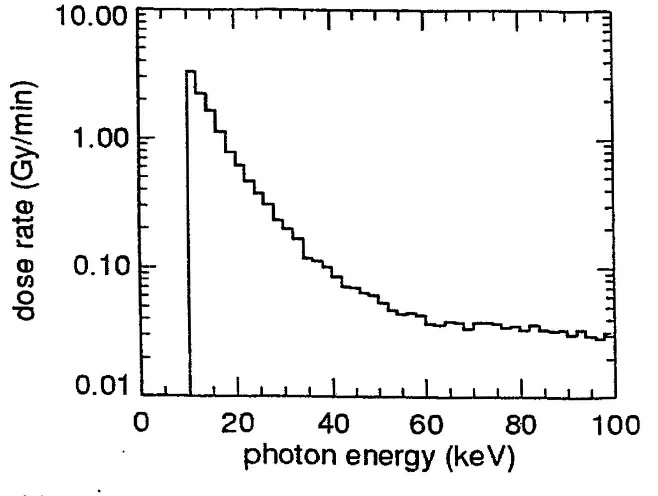

($\Delta E_i = 2$ keV)

Calculation of dose contribution by neutrons

- GEANT: calculation of photon flux $\phi(r, E_\gamma)$
- Consider: realistic beam line geometry
- Assume: all components are made from iron
- S. Costa et al., Nuovo Cimento 51B (1967) 199:
  photo-neutron reaction cross section $\sigma_{\gamma n}(E_\gamma)$
- Calculate: neutron production rate N_n
- M. Barbier, Induced radioactivity, North Holland Publ. Co., Amsterdam, 1969: neutron energy
  spectrum dN_n/dE_n for iron ($E_n \leq 6.5$ MeV)
- J. Broerse, Monograph on basic physical data for neutron dosimetry: kerma factors for water
- Consider: target geometry ($\Delta x = 20$ μm, $\varnothing = 2$ cm)
- Calculate: dD/dt integrated over neutron spectrum

$$dD/dt = 0.8 \text{ cGy/min}$$

(quality factor: ~ 10)

Conclusion

- Modification of electron optical elements of the radiation physics beamline to
  - reduce background radiation
  - be more flexible about target positioning

Current stage of our research:

- More sophisticated calculation of dose contribution by neutrons (FLUKA, MCNP)
- Monte Carlo simulation for modified beamline
- Photon background suppression by Bragg reflection (HOPG)
- Design of dose delivery and dose monitoring system

Modified beamline layout

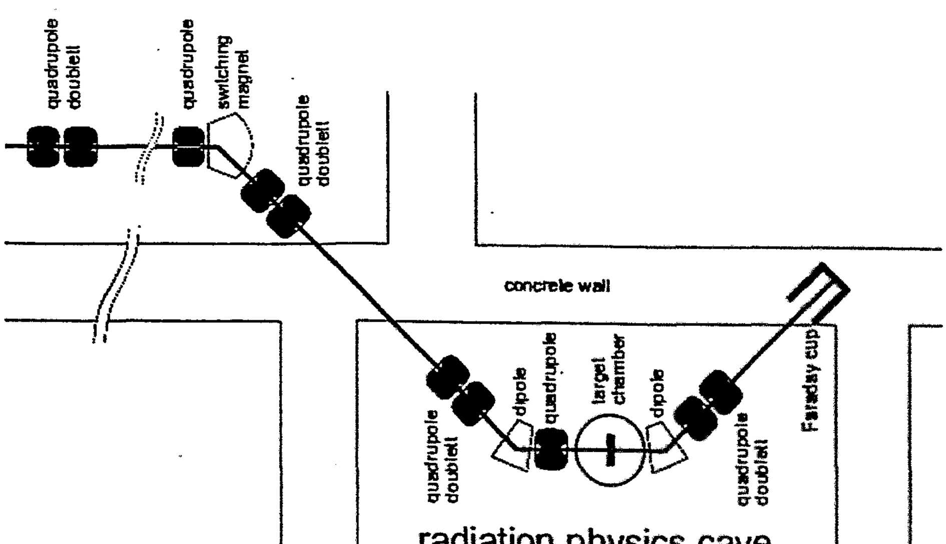

- *decreased distance between channeling crystal and dipole magnet section:* 80 cm
- *increased magnet gap:* 110 mm

Reduction of bremsstrahlung (neutron) background by about a factor of 5

List of Participant

Prof. Wenzeslaw **Andrejtscheff**
Institut of Nuclear Research and
Nuclear Energy
1784 SOFIA
BULGARIA

Phone: +359 (2) 75 00 86
Fax: +359 (2) 97 53 619
e-mail: ANDRE@INRNE.BAS.Bg

Prof. Dr. Hartmut **Backe**
Institut für Kernphysik
Universität Mainz
J.J. Becherweg 45
55099 MAINZ
GERMANY

Phone: +49 (6131) 39 55 63
Fax: +49 (6131) 39 29 64
e-mail: backe@kph.uni-mainz.de

Dr. Hans-Werner **Barz**
Institut für Kern- und Hadronenphysik
Forschungszentrum Rossendorf
Postfach 51 01 19
01314 DRESDEN
GERMANY

Phone: +49 (351) 260 3263
Fax: +49 (351) 260 3700
e-mail: H.W.Barz@fz-rossendorf.de

Dr. Ralf **Bergmann**
Institut für Bioanorgan. und
Radiopharmazeut. Chemie
Forschungszentrum Rossendorf
Postfach 51 01 19
01314 DRESDEN
GERMANY

Phone: +49 (351) 260 3097
Fax: +49 (351) 260 3232
e-mail: R.Bergmann@fz-rossendorf.de

Dr. Friedrich **Dönau**
Institut für Kern- und Hadronenphysik
Forschungszentrum Rossendorf
Postfach 51 01 19
01314 DRESDEN
GERMANY

Phone: +49 (351) 260 3372
Fax: +49 (351) 260 3700
e-mail: F.Doenau@fz-rossendorf.de

Dr. Frank **Eichhorn**
Institut für Ionenstrahlphysik
und Materialforschung
Forschungszentrum Rossendorf
Postfach 51 01 19
01314 DRESDEN
GERMANY

Phone: +49 (351) 260 3534
Fax: +49 (351) 260 3285
e-mail: F.Eichhorn@fz-rossendorf.de

Dr. Wolfgang **Enghardt**
Institut für Kern- und Hadronenphysik
Forschungszentrum Rossendorf
Postfach 51 01 19
01314 DRESDEN
GERMANY

Phone: +49 (351) 260 3653
Fax: +49 (351) 260 3700
e-mail: W.Enghardt@fz-rossendorf.de

Dr. Stefan **Fiedler**
Medical Beamline
ESRF
B.P. 220
38043 GRENOBLE-CEDEX
FRANCE

Phone: +33 (476) 88 27 62
Fax: +33 (476) 88 23 25
e-mail: fiedler@esrf.fr

Prof. Dr. Dieter **Frankenberg**
Abt. für Klinische Strahlenbiologie und
Klinische Strahlenphysik
Zentrum Radiologie
Georg-August-Universität Göttingen
Von-Siebold-Straße 3
37075 GÖTTINGEN
GERMANY

Phone: +49 (551) 39 64 84
Fax: +49 (551) 39 61 53
e-mail: dfrank@med.uni-goettingen.de

Dr. Harald **Genz**
Institut für Kernphysik
Technische Universität Darmstadt
Schlossgartenstraße 9
64289 DARMSTADT
GERMANY

Phone: +49 (6151) 16 25 21
Fax: +49 (6151) 16 43 21
e-mail: genz@ikp.tu-darmstadt.de

Dr. Inna G. **Grigorieva**
Institute of Carbon Based Materials
(NII Graphite)
111524 MOSCOW
RUSSIA

Phone:
Fax:
e-mail: inna@mikhalko.msk.su

Prof. Dr. Eckart **Grosse**
Institut für Kern- und Hadronenphysik
Forschungszentrum Rossendorf
Postfach 51 01 19
01314 DRESDEN
GERMANY

Phone: +49 (351) 260 2270
Fax: +49 (351) 260 3700
e-mail: E.Grosse@fz-rossendorf.de

Dr. Hartmut **Guratzsch**
Zentralabteilung Neue Beschleuniger
Forschungszentrum Rossendorf
Postfach 51 01 19
01314 DRESDEN
GERMANY

Phone: +49 (351) 260 3283
Fax: +49 (351) 260 3690
e-mail: H.Guratzsch@fz-rossendorf.de

Prof. Dr. Dietrich **Harder**
Medizinische Physik und Biophysik
Georg-August-Universität Göttingen
Käte-Hamburger-Weg 4-6
37073 GÖTTINGEN
GERMANY

Phone: +49 (551) 39 68 75
Fax: +49 (551) 39 79 66
e-mail: ukep@gwdg.de

Dr. Gevorg **Harutunyan**
Institute of Applied Problems
of Physics of NASRA
Hr. Nersessyan Str. 25
375014 YEREVAN
ARMENIA

Phone: +374 (2) 24 58 96
Fax: +374 (2) 28 18 61
e-mail: Hermsdorf@physik.tu-dresden.de

Dr. Dietrich **Hermsdorf**
Institut für Strahlenschutzphysik
Technische Universität Dresden
Zellescher Weg 19
01069 DRESDEN
GERMANY

Phone: +49 (351) 46 33 148
Fax. +49 (351) 46 37 040
e-mail: Hermsdorf@physik.tu-dresden.de

Dr. Mark A. **Hill**
Medical Research Council
Radiation and Genome Stability Unit
Harwell
Didcot
OXON 11 ORD
UNITED KINGDOM

Phone: +44 (1235) 83 43 93
Fax: +44 (1235) 83 47 76
e-mail: m.hill@har.mrc.ac.uk

Dr. Rainer **Hinz**
Institut für Bioanorgan. und
Radiopharmazeut. Chemie
Forschungszentrum Rossendorf
Postfach 51 01 19
01314 DRESDEN
GERMANY

Phone: +49 (351) 260 2973
Fax: +49 (351) 260 3232
e-mail: R.Hinz@fz-rossendorf.de

Dr. Gudrun **Kampf**
Zum Heiderand 30
01474 DRESDEN-WEISSIG
GERMANY

Phone: +49 (351) 269 18 07
Fax:
e-mail:

Prof. Dr. Burkhard **Kämpfer**
Institut für Kern- und Hadronenphysik
Forschungszentrum Rossendorf
Postfach 51 01 19
01314 DRESDEN
GERMANY

Phone: +49 (351) 260 3258
Fax: +49 (351) 260 3700
e-mail: B.Kaempfer@fz-rossendorf.de

Dr. Valery V. **Kaplin**
Nuclear Physics Institute
Tomsk Polytechnic University
pr. Lenina 2A
P.O. Box 25
634050 TOMSK
RUSSIA

Phone: +7 (3822) 41 79 39
Fax: +7 (3822) 42 39 34
e-mail: kaplin@npi.tpu.ru

Dr. Katsumi **Kobayashi**
Photon Factory
Institute of Materials Structure Science (IMSS)
High Energy Accelerator Research Organization (KEK)
Oho, Tsukuba
IBARAKI 305-0801
JAPAN

Phone: +81 (298) 64 56 55
Fax:: +81 (298) 64 28 01
e-mail: katsumi.kobayashi@kek.jp

Dr. Ulf **Lehnert**
Institut für Kern- und Hadronenphysik
Forschungszentrum Rossendorf
Postfach 51 01 19
01314 DRESDEN
GERMANY

Phone: +49 (351) 260 2971
Fax: +49 (351) 260 3700
e-mail: U.Lehnert@fz-rossendorf.de

Dr. Wolfgang **Matz**
Institut für Ionenstrahlphysik und
Materialforschung
Forschungszentrum Rossendorf
Postfach 51 01 19
01314 DRESDEN
GERMANY

Phone: +49 (351) 260 3122
Fax: +49 (351) 260 3285
e-mail: W.Matzf@z-rossendorf.de

Prof. Dr. Barry D. **Michael**
Gray Laboratory Cancer Research Trust
Mount Vernon Hospital
PO Box 100
Northwood
MIDDLESEX, HA6 2 JR
UNITED KINGDOM

Phone: +44 (19238) 2 8611
Fax: +44 (19238) 3 52 10
e-mail: michael@graylab.ac.uk

Prof. Dr. Alpik R. **Mkrtchyan**
Institute of Applied Problems
of Physics of NASRA
Hr. Nersessyan Street 25
375014 YEREVAN
ARMENIA

Phone: +374 (2) 24 58 96
Fax: +374 (2) 28 18 61
e-mail: malpic@iapp.sci.am

Dr. Artak H. **Mkrtchyan**
Institute of Applied Problems
of Physics of NASRA
375014 YEREVAN
ARMENIA

Phone: +374 (2) 24 58 96
Fax: +374 (2) 28 18 61
e-mail: martak@iapp.sci.am

Dr. Wim **Mondelaers**
Universiteit Gent
Department for Subatomic
and Radiation Physics
Proeftuinstraat 86
9000 GENT
BELGIUM

Phone: +32 (9) 264 65 33
Fax: +32 (9) 264 66 99
e-mail: wim.mondelaers@rug.ac.be

Dr. Victor **Morokhovskyi**
Am Europakanal 2
91056 ERLANGEN
GERMANY

Phone: +49 (9131) 79 14 33
Fax: +49 (9131) 18 63 01
e-mail: morokhovskyi@aol.com

Dr. Bärbel **Naumann**
Institut für Kern- und Hadronenphysik
Technische Universität Dresden
Adress: FZ Rossendorf
Postfach 51 01 19
01314 DRESDEN
GERMANY

Phone: +49 (351) 260 3132
Fax: +49 (351) 260 3700
e-mail: B.Naumann@fz-rossendorf.de

Dr. Waldemar **Neubert**
Institut für Kern- und Hadronenphysik
Forschungszentrum Rossendorf
Postfach 51 01 19
01314 DRESDEN
GERMANY

Phone: +49 (351) 260 3132
Fax: +49 (351) 260 3700
e-mail: W.Neubert@fz-rossendorf.de

Anna **Panteleeva**
Institut für Kern- und Hadronenphysik
Forschungszentrum Rossendorf
Postfach 51 01 19
01314 DRESDEN
GERMANY

Phone: +49 (351) 260 3657
Fax: +49 (351) 260 3700
e-mail: A.Panteleeva@fz-rossendorf.de

Dr. Jörg **Pawelke**
Institut für Kern- und Hadronenphysik
Forschungszentrum Rossendorf
Postfach 51 01 19
01314 DRESDEN
GERMANY

Phone: +49 (351) 260 3657
Fax: +49 (351) 260 3700
e-mail: J.Pawelke@fz-rossendorf.de

Dr. Melvin **Piestrup**
Adelphi Technology, Inc.
2181 Park Blvd.
94306 PALO ALTO, CA
USA

Phone: +1 (650) 328 73 37 ext. 11
Fax: +1 (650) 328 73 43
e-mail: melpie@adelphitech.com

Prof. Dr. Frank **Pobell**
Vorstand
Forschungszentrum Rossendorf
Postfach 51 01 19
01314 DRESDEN
GERMANY

Phone: +49 (351) 260 3344
Fax: +49 (351) 260 3236
e-mail: F.Pobell@fz-rossendorf.de

Prof. Dr. Alexander P. **Potylitsin**
Nuclear Physics Institute
Tomsk Polytechnic University
pr. Lenina 2A
P.O. Box 25
634050 TOMSK
RUSSIA

Phone: +7 (3822) 42 39 94
Fax: +7 (3822) 42 39 34
e-mail: pap@interact.phtd.tpu.edu.ru

Dr. Harald **Prade**
Institut für Kern- und Hadronenphysik
Forschungszentrum Rossendorf
Postfach 51 01 19
01314 DRESDEN
GERMANY

Phone: +49 (351) 260 3270
Fax: +49 (351) 260 3700
e-mail: H.Prade@fz-rossendorf.de

Heike **Rodig**
Institut für Bioanorgan. und
Radiopharmazeut. Chemie
Forschungszentrum RossendorfPostfach 51 01 19
01314 DRESDEN
GERMANY

Phone: +49 (351) 260 2959
Fax: +49 (351) 260 3232
e-mail: H.Rodig@fz-rossendorf.de

Prof. Dr. Peter **Rullhusen**
Joint Research Centre
Institute for Reference Materials
and Measurements
Retiseweg
2440 GEEL
BELGIUM

Phone: +32 (14) 571 211
Fax: +32 (14) 571 862
e-mail: rullhusen@irmm.jrc.be

Dr. Klaus-Dieter **Schilling**
Institut für Kern- und Hadronenphysik
Forschungszentrum Rossendorf
Postfach 51 01 19
01314 DRESDEN
GERMANY

Phone: +49 (351) 260 3127
Fax: +49 (351) 260 3700
e-mail: K.D.Schilling@fz-rossendorf.de

Dr. Michael **Scholz**
Adress: University Heidelberg
Dept. Clinical Radiology
Gesellschaft für Schwerionenforschung
Planckstraße 1
64291 DARMSTADT
GERMANY

Phone: +49 (6159) 71 26 27
Fax: +49 (6159) 71 21 06
e-mail: M.Scholz@gsi.de

Dr. Ronald **Schwengner**
Institut für Kern- und Hadronenphysik
Forschungszentrum Rossendorf
Postfach 51 01 19
01314 DRESDEN
GERMANY

Phone: +49 (351) 260 3332
Fax: +49 (351) 260 3700
e-mail: R.Schwengner@fz-rossendorf.de

Dr. Wolfgang **Seidel**
Institut für Kern- und Hadronenphysik
Forschungszentrum Rossendorf
Postfach 51 01 19
01314 DRESDEN
GERMANY

Phone: +49 (351) 260 3322
Fax: +49 (351) 260 3700
e-mail: W.Seidel@fz-rossendorf.de

Dr. Sonja **Selenska-Pobell**
Institut für Radiochemie
Forschungszentrum Rossendorf
Postfach 51 01 19
01314 DRESDEN
GERMANY

Phone: +49 (351) 260 2989
Fax: +49 (351) 260 3553
e-mail: S.Selenska-Pobell@fz-rossendorf.de

Prof. Dr. Nikolai F. **Shulga**
Kharkov Institute of Physics
and Technology
Akademicheskaja Street 1
310108 KHARKOV
UKRAINE

Phone: +572 (356) 462
Fax: +572 (352) 683
e-mail: shulga@kipt.kharkov.ua

Dr. Sergey **Taroyan**
Yerevan Physics Institute
Alikhanian Brothers Street 2
375036 YEREVAN
ARMENIA

Phone: +374 (2) 34 13 47
Fax: +374 (2) 35 00 30
e-mail: taroian@hermes.desy.de

Prof. Dr. William **Thomlinson**
European Synchrotron Radiation Facility
ESRF
B.P. 220
38043 GRENOBLE
FRANCE

Phone: +33 (476) 88 26 47
Fax: +33 (476) 88 21 60
e-mail: thomlinson@esrf.fr

Dr. Andreas **Wagner**
Institut für Kern- und Hadronenphysik
Forschungszentrum Rossendorf
Postfach 51 01 19
01314 DRESDEN
GERMANY

Phone: +49 (351) 2603261
Fax: +49 (351) 260 3700
e-mail: A.Wagner@fz-rossendorf.de

Dr. Wolfgang **Wagner**
Institut für Kern- und Hadronenphysik
Forschungszentrum Rossendorf
Postfach 51 01 19
01314 DRESDEN
GERMANY

Phone: +49 (351) 260 2354
Fax: +49 (351) 260 3700
e-mail: W.Wagner@fz-rossendorf.de

Dr. Rudi **Wünsch**
Institut für Kern- und Hadronenphysik
Forschungszentrum Rossendorf
Postfach 51 01 19
01314 DRESDEN
GERMANY

Phone: +49 (351) 260 3234
Fax: +49 (351) 260 3700
e-mail: R.Wuensch@fz-rossendorf.de

Dr. V. N. **Zabaev**
Nuclear Physics Institute
Tomsk Polytechnic University
pr. Lenina 2A
P.O. Box 25
634050 TOMSK
RUSSIA

Phone: +7 (3822) 41 79 39
Fax: +7 (3822) 42 39 34
e-mail: zabaev@npi.tpu.ru

Dr. Gudrun **Zwicker**
Vorstandsreferat
Forschungszentrum Rossendorf
Postfach 51 01 19
01314 DRESDEN
GERMANY

Phone: +49 (351) 260 3325
Fax: +49 (351) 260 3236
e-mail: G.Zwicker@fz-rossendorf.de
